HYDROGEN POWER: THEORETICAL AND ENGINEERING SOLUTIONS

Proceedings of the HYPOTHESIS II Symposium
held in Grimstad, Norway, 18-22 August 1997

Edited by

T. O. SAETRE
Faculty of Engineering,
Agder College,
Grimstad, Norway

Springer Science+Business Media, B.V.

A C.I.P. Catalogue record for this book is available from the Library of Congress.

ISBN 978-90-481-5029-8 ISBN 978-94-015-9054-9 (eBook)
DOI 10.1007/978-94-015-9054-9

Printed on acid-free paper

Originally published by Kluwer Academic Publishers in 1998
Softcover reprint of the hardcover 1st edition 1998

HYPOTHESIS II

SPONSORS

Andreas Ugland & Sons Co

Aust-Agder County Government

Aust-Agder Hydro Electric Power Company

Den norske bank

Elkem Fiskaa

Elkem Research

EMC Lab as

Falconbridge

Norsk Hydro

Norsk Hydro Electrolysers as

Norwegian Hydrogen Forum

Norwegian Ministry of Petroleum and Energy

Municipality of Grimstad

Statoil

The Norwegian Industrial and Regional Development Fund (SND)

The Research Council of Norway

Tinfos Jernverk

Vest-Agder County Government

Vest-Agder Energy Board

Vital Insurance Company

HYPOTHESIS II

Organising Committee

K. Andreassen, Norsk Hydro, Notodden
B. Gaudernack, Institute for Energy Technology, Kjeller
O. Hunderi, The Norwegian University of Science and Technology, Trondheim
T. Norby, The University of Oslo, Oslo
T.O. Sætre, Agder College, Grimstad (Chairman)
R. Tunold, The Norwegian University of Science and Technology, Trondheim

International Coordinators

T.N. Veziroglu, Honorary Chairman, President, International Association for Hydrogen Energy, USA
G. Spazzafumo, Coordinator of Conference Series, Italy

Conference National Advisory Committee

T. Aakvaag, Supreme Court Justice, Oslo
H. Ager-Hansen, Director, Stavanger
K.C. Gjermundsen, Managing Director, Arendal
A. Johnsen, Lawyer, Oslo
K. Kveseth, Director, Oslo
J. Lilletun, Member of Parliament, Oslo
H. Sunde, County Governor, Arendal
A.T. Svennevik (Chairman), Lillesand
A.K.L. Ugland, Owner and Manager, Grimstad

HYPOTHESIS II

Members of the International Scientific Advisory Board

PREFACE

This volume contains selected contributions to the second *Hydrogen Power, Theoretical and Engineering Solutions, International Symposium* (HYPOTHESIS II), held in Grimstad, Norway, from 18 to 22 August 1997.

The scientific programme included 10 oral sessions and a poster session. Widely based national committees, supported by an International Scientific Advisory Board and the International Coordinators, made every effort to design and bring together a programme of great excellence.

The more than one hundred papers submitted represent the efforts of research groups from all over the World. The international character of HYPOTHESIS II has been augmented by contributions coming from seven countries outside Europe.

The contributions reflect the progress that has been achieved in hydrogen technology aimed primarily at hydrogen as the ultimate energy vector. This research have already yielded mature technologies for mass production in many areas. These and future results will be of increased interest and importance as global and local environmental issues move higher up the political agenda.

In order to facilitate new contacts between scientists and strengthen existing ones, the symposium incorporated an extensive social program managed by the Conference Administrator, Ms. Ann Ystad.

A meeting of both science and industry such as HYPOTHESIS II would not have been possible without the enormous enthusiasm and hard work of many people and the support of the institutions and companies listed previously. Thus, on behalf of the Organising Committee and Agder College, I would like to extend my deepest appreciation to all these people, but especially to all the delegates and participants who came from many different countries to make this symposium a success.

T.O. Saetre

TABLE OF CONTENTS

HYDROGEN AIR FUEL CELL POWERED PASSENGER CAR

FEVER - Fuel Cell Electric Vehicle for Efficiency and Range

J.C. GRIESEMANN - D. CORGIER
RENAULT Direction de la Recherche)
9 - 11 avenue du 18 Juin 1940 - 92 500 Rueil Malmaison -FRANCE
P. ACHARD - R METKEMEYER
ECOLE des MINES
BP 207 - 06 904 Sophia Antipolis - FRANCE
B. MARCENARO - F. FEDERICI
ANSALDO Ricerche
Corso FM Perrone 25 - 16161 Genoa - ITALY
P EKDUNGE - P.PERSON
VOLVO Technological Development
Chalmers Teknik Park - 412 88 Göteborg - SWEDEN
P. SANGLAN
AIR LIQUIDE D.T.A.
BP 15 - Les Eugenieres - 38 360 Sassenage - FRANCE
G. FAITA - A. MAGGIORE
DE NORA S.p.a.
Via Bistolfi 35 - 20 134 Milan - ITALY

Various technologies are used or developed to alleviate the atmospheric pollution due to exhaust gases from the vehicles : catalytic post - treatment, gaseous fuel and electric vehicles. Renault has decided to progress one step forwards, realising a first fuel cell powered passenger car. Six teams coordinate their effort in the frame of the European Commission Program Joule.

Powered by a Solid Polymer fuel cell, supplied with hydrogen and ambient air, this vehicle will have a range comparable to classical vehicles (500 km) with a tank full of 8 kg of liquid hydrogen. Research and development have to be carried on towards *the global efficiency of the fuel cell system, towards the efficiency of efficiency of proton exchange membranes and electrode layers and toward the cost reduction of these items and the bipolar plates. The technology demonstrator FEVER will be tested in September 1997 and the technology of fuel cell powered vehicles could be economically mature between 2005 and 2010.*

T. O. Saetre (ed.), Hydrogen Power: Theoretical and Engineering Solutions, 1–11.

1. Introduction

The mankind is facing two problems related to the air quality : the increase of toxic pollutants and the greenhouse effect, mainly due to androgenic CO2 release. Although the responsibility of road transportation in the emissions of CO2 is minor (around 20%), international pressure is exerted to reduce these emissions.
Concerning the emission of toxic pollutants, it has reached such a critical state that the OCDE countries impose more and more stringent emissions limits ; in some developing countries, the quality of air in large consurbations is so poor that similar severe limitations could logically be imposed.

Solutions to these problems exist ; some of them are already implemented, others are under development. Since 1993 the generalisation of the electronic control on engines and post treatment catalysts in Europe has reduced the emissions of pollutants by a factor 20 for gasoline vehicles, without effect on CO2 emissions.

Partial solutions are presently commercialised, like L.P.G. vehicles (which bring a supplementary reduction of pollutants emissions by a factor 5, and 15 % less CO2), and batteries powered electric vehicles with zero emissions, although their range orient them mainly towards urban use.

The coming decade should witness the emergence of natural gas vehicles, with very low pollutants emissions and reducing the CO2 emissions by about 25% and, also, hybrid vehicles associating a thermal powerplant with an electric drive chain. This technology provides urban driving at zero emission and a road driving at ultra- low emissions, with a range equivalent to that of conventional vehicles.

The ultimate solution, which enables to assure an equivalent range, (about 500 km), at zero emission and independent of oil resources, could be hydrogen, used in the fuel cells at a high level of efficiency.

In 1994, the European FEVER team launched a Research and Development program aiming at realising a first passenger car powered by a hydrogen-air fuel cell. This program, FEVER*, under project management of RENAULT, results from the contribution of several Italian (ANSALDO R.I. and DE NORA), French (RENAULT, ECOLE des MINES and AIR LIQUIDE) and Swedish (VOLVO) partners .

This project is partially funded by the Commission of the European Union in the frame of the DG XII Joule Program. The demonstration vehicle is scheduled to be experimented in September 1997.

2. The Project

The demo vehicle is a Laguna break Renault. It is to be road-driven for 500 km using the 8 kg of liquid hydrogen, stored in the cryo-tank (115 liters), and external air. Its maximum speed will be of 120 km/hour for a weight of 2 200 kg with two passengers.

The vehicle is powered by an electric motor. The electric architecture is " hybrid " : that means that it associates two power sources : a main source which includes the fuel cells,

their ancilliaries and the liquid hydrogen tank (the power module) and a secondary source, the buffer battery which powers the ancilliaries at the start-up and supplies a complementary power to the motor when needed by accelerations and gradings (figure 1).

The control of the energy exchanges between the two power sources and the drive chain is ensured by a PC computer, the supervisor, which optimises these exchanges by monitoring the inputs from the two sources thanks to an controlled up-voltage converter. The elaboration of the control strategies is one of the main topics of VOLVO's action.

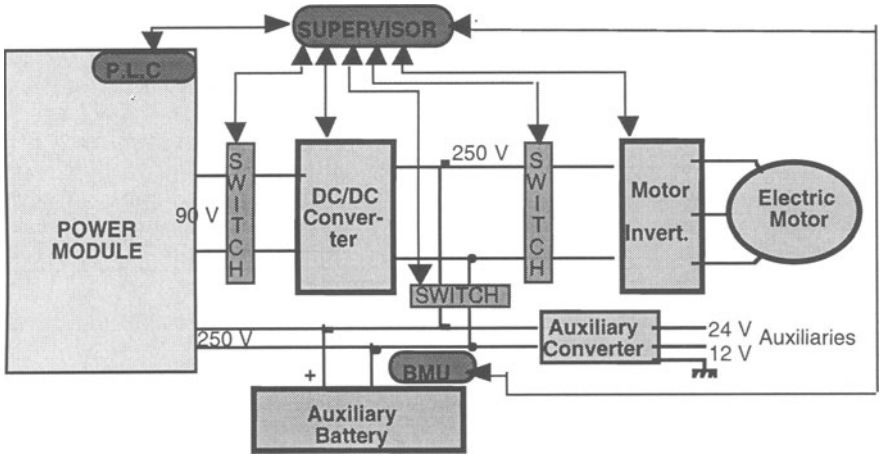

figure 1

2.1. THE ELECTRIC VEHICLE

The best energy efficiency was considered as choice criterion for the electric motor. Four technologies were tested. A numerical simulation has been realised, associating the efficiency mapping of these motors to those of several transmission systems, on European urban driving cycle.

Four motor technologies were evaluated :
- asynchronous
- synchronous with permanent magnet (internal rotor)
- synchronous with permanent magnet (external rotor
- wound rotor synchronous

The technology wound rotor synchronous associated to a fixed gear transmission (ratio 1: 9.7) gave the best energy efficiency (about 92% on the nominal operation range). It is now fitted on-board. This motor, manufactured in France, gives a maximal power of 30 kW at 3500 t/ mn, but allows transients at 50 kW for durations up to 6 mn. Its weight, including the electronic control, is about 90 kg. It is supplied with 252 volts.

The buffer battery is made of 210 leaktight elements of Ni MH cell, each one delivering 1.2 V. The whole set constitutes a reserve of energy of 2.8 kWh, air cooled. The main functions of this buffer battery are to power the fuel cell ancilliaries at the start-up and to

make available for the vehicle some complementary 10 kW power when needed by transient high loads. The choice of these elements NiMH results from the numerical simulation of the energy management in the vehicle carried out by the research teams of Volvo Technological Development. The second choice criterion was the environmental as these elements contain no Cd. One secondary function is to enable the regenerating braking, storing the electrical energy generated by the motor during braking and slopes when the inertia of the vehicle is back- transformed in electricity by the motor working as a generator.

The power module is the main power source. It contains the liquid hydrogen tank, the fuel cells, the air compression system, the flow control ancillaries and the control computer : the PLC. This power module is able to supply a nominal power of 25 kW under 90 Volts. Peak powers of about 35 kW can be obtained at lower energy efficiency.

The up-voltage converter is designed by RENAULT : It is an electronic DC/DC converter which increases the voltage supplied by the power module to the voltage required by the electrical motor : 252 Volts. The average energy efficiency on the operation range is of 90%. A secondary function of this one-way converter is to protect the power module against the electrical intensities generated backwards by the regenerative braking. Last but not least, the converter is the active organ, controlled by the supervisor which enables to monitor the energy exchanges between the power module, buffer batteries and the electrical drive chain.

The supervisor is the PC computer which helps the conductor in the management of the components of the vehicle. The driver is directly active in the starting, the driving direction, acceleration and braking. The supervisor controls the state of charge of the buffer batteries, the state of the fuel cell activity, determines the level of current supplied by each source, detects eventual failures, compensates for some failures and ensures the security on board.

2.2 THE POWER MODULE (figure 2)

The power module is designed as an autonomous rack. It contains the hydrogen tank, the fuel cells, the air compression system, the pipes and the control valves, controlled by a local control computer : the PLC. The integration of this system is realised by ANSALDO R. I. in Genoa (Italy) and its dynamic behaviour is numerically simulated by ECOLE des MINES.

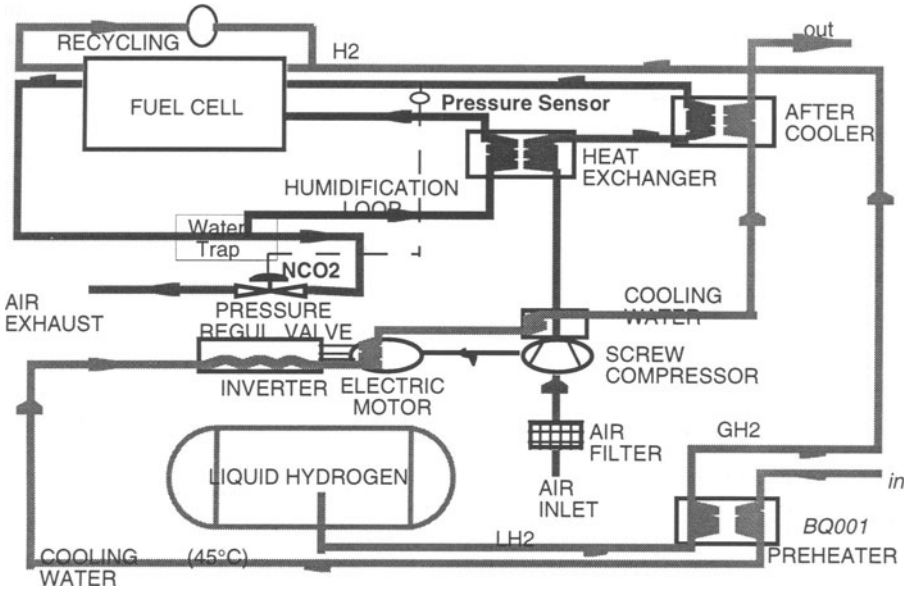

figure 2

2.2.1. Liquid hydrogen tank

The cryogenic tank has been realised by Air Liquide (France). This tank, weighting 100 kg, contains 120 liters of liquid hydrogen at 20 K, that means 8,05 kg of fuel. Composed of two thin stainless steel envelopes, the thermal insulation was improved so as to reduce the heat conduction as low as 0,7 Watts. Its cylindrospheric structure enables it not to buckle under 8 bars absolute of pressure, at this level, a safety valve releases a small quantity of hydrogen, relieving the internal pressure.

The numerical simulation predicts that a full tank could remain unused for 13 days before the first gas release. This released gas will be neutralised by a catalysator active at ambient temperature (20°C) and transforming this gas into (water) vapour. This catalytic reactor has been realised by Royal Institute of Technology, Sweden

An internal heating resistor enables to monitor the gas delivery according to the demand of the fuel cells. The gas is reheated at 30°C by an hydrogen-water exchanger before being regulated at a pressure of 2,5 bars abs. service pressure of cells.

2.2.2. Fuel cells

They are of the Solid Polymer Electrolyte type (SPFC). Three stacks are series connected to supply a power of 30 kW under 90 Volts (333 A) in nominal working conditions. Realised by the Italian Company DE NORA S.p.A., they represent a total weight of 320 kg and a volume of 225 dm3.

The fuel cells are fed, at anodic side, with hydrogen under a pressure of 2,5 bars abs. and, at cathode side, by outside air, compressed under a pressure of 3 bars abs. by the air compression system. The air flow supplied is twice the stoechiometry.

A fuel cell is a static device that converts the chemical energy of the gases directly into electrical power. At the anode side, by means of a catalyst layer, hydrogen molecules are dissociated into protons (H+) and electrons (e-) according to the reaction :

$$H2 \quad \rightarrow \quad 2H+ + 2e-$$

Protons then migrate through the membrane while the electrons flow through the external electric circuit, thus generating current. Electrons, protons and O2 react on the cathode catalyst according to the reaction :

$$2H+ + 2\,e- + 1/2\,O2 \quad \rightarrow \quad H2O$$

The most common way to evaluate the performance of the fuel cell is the polarisation curve (fig. 5), i.e. the current, voltage curve. The main parameters which affects the performances are :

- membrane and electrodes characteristics
- cell design
- operating pressure
- operating temperature
- air excess

The energy efficiency of a fuel cell depends on the current (i.e. the load) level requested by the drive chain since at high current the voltage, which affects directly the energy efficiency, decreases. This efficiency is higher at low load. If V (volts) is the voltage of a cell, the fraction of the Lower Heating Value (L.H.V.) of the fuel converted into electrical energy by the fuel cell can be calculated as follows :

$$\eta\ \% = \frac{V\ (volts)}{1{,}23}$$

where 1.23 V is the thermodynamic voltage of the reaction :

$$H2 + 1/2\,O2 \quad \rightarrow \quad H2O$$

In nominal working conditions, the cell of each elementary cell of the stacks is voltage is 0,7 volts and, therefore, the electrical efficiency about 57%. At 50% of the nominal power, the efficiency can reach 67%. Each stack is composed of 45 cells and a humidification section in which the gases are pre-treated before entering the cells. The humidification is mandatory since the membrane must be kept in the fully hydrated state, which corresponds to the highest electrical conductivity, that is to the highest voltage.
The polymer electrolyte used is the commercially available NAFION 115 from DUPONT de NEMOURS. The electrodes are supplied by E-Tek Inc. (U.S.A.) and the catalyst is platinum based, the content of which is presently 1 mg/cm3. The polarisation and power curves presented (figure 3) have been registered under the following operation conditions :

	AIR	HYDROGEN
- Pressure	4 bars abs.	3.5 bars abs.
- Over stoechiometry :	2	1.5 to 3 (close loop recirculated)

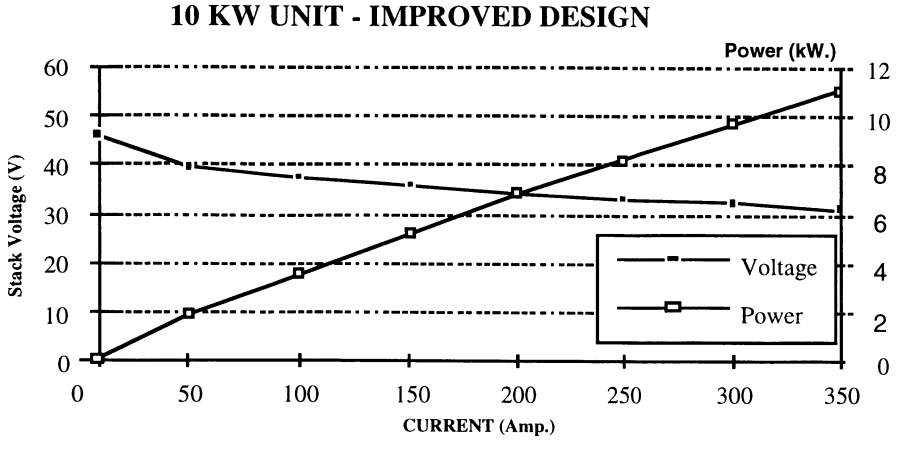

figure 3

2.2.3. The air compression system :
Apart the vehicle itself, the main power consumer on-board is the air compression system. As realised by an electrically powered compressor, the supply of 40 g of air per second under a pressure of 3 bars requires, including compression efficiencies, a consumed power about 6 kW for a power supplied by the fuel cell of 30 kW. Heat exchangers enable to increase the temperature of the humidification water up to the value experimented as optimal for the fuel cell operation.

2.2.4. The hydrogen recirculator :
To avoid the hydrogen spoil-off through recurrent purges, it was decided to investigate the benefit of a hydrogen recirculator. Realised by AIR LIQUIDE, this device was successfully tested at ECOLE des MINES and proved increased the fuel efficiency of the global system.

2.2.5. Vehicle simulation and energy management :
In the project, VOLVO T.D. was responsible for the vehicle simulation , the energy management, the auxiliary batteries and the safety study. In a series hybrid vehicle equipped with a fuel cell as an energy source, the flow of energy is complex as well as critical. Extensive simulation was needed to optimise the fuel consumption.

For this purpose, a numerical model was developed. The model is able to characterise, for a defined driving route :

- The energy requirement
- The drive chain performance
- The fuel cell operation.

It is also used to choose and size the system components (battery, electric motor...) and also the vehicle. The trade-off between fuel cell and battery pack was also studied. An overview of the model is given below (Figure 4) :

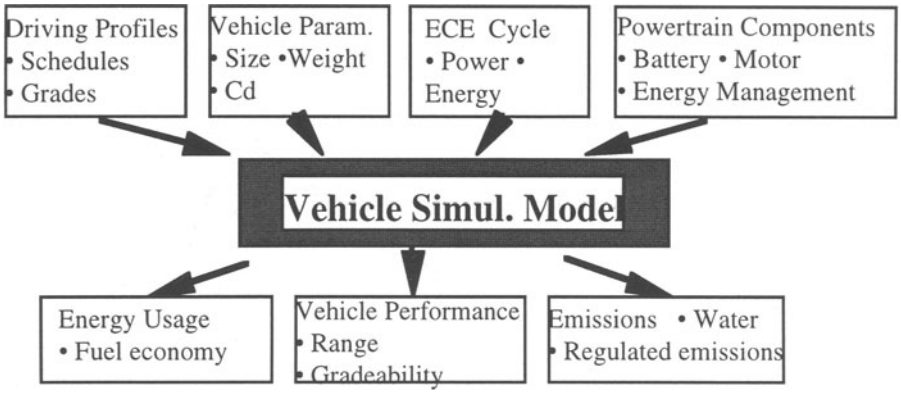

figure 4

Based on the simulation, control strategies for energy management were investigated and implemented in the vehicle supervisor. The strategy was determined not only by the overall fuel consumption but also other parameters, such as driving behaviour, safety and battery lifetime. The strategies have been derived through simulation using the vehicle simulation model. Different control strategies were evaluated.

The model was written using the Matlab/simulink simulation environment. The vehicle model is a conventional one, with a mapped model of an electric motor, models for aerodynamic and rolling resistance. The driver sends signals to the vehicle block for accelerating or braking. The output from the vehicle block is the vehicle speed and the required current to achieve this speed. The driver is modelled as a P.I. controller and takes the requested driving cycle as input and generates a torque signal to the electric motor.

The fuel cell model is one-dimensional, it includes fuel and oxidant transport into the fuel cell, transport of reactants and by-products through the porous electrolyte and water transport through the membrane as well as electrode kinetics are the electrode/electrolyte interface.

The Power Module will deliver the current demanded by the control system. It is the battery voltage that determines system voltage in the vehicle. The battery is used during the start-up phase of the Power Module, it is used, too, to supply complementary power whenever needed by the vehicle (acceleration or hill climbing...). The operating principle is given directly by the electrical system architecture : control of the SoC of the battery by current demand to the fuel cell. If the actual SoC of the battery is above the desired level, the latest is used to power the vehicle. If that SoC is below the desired level, the current reference signal to the Power Module is increased so that the Power Module recharges the battery and powers the vehicle. In normal operation, the system powers the vehicle.

Simulation results

The hereunder presented results are based on the EUDC part of the ECE 15-OA European drive cycle (400 seconds). In figure 5, are presented the speed pattern and the consequent State of Charge of the battery. The set point of the controller was fixed at 80 %.

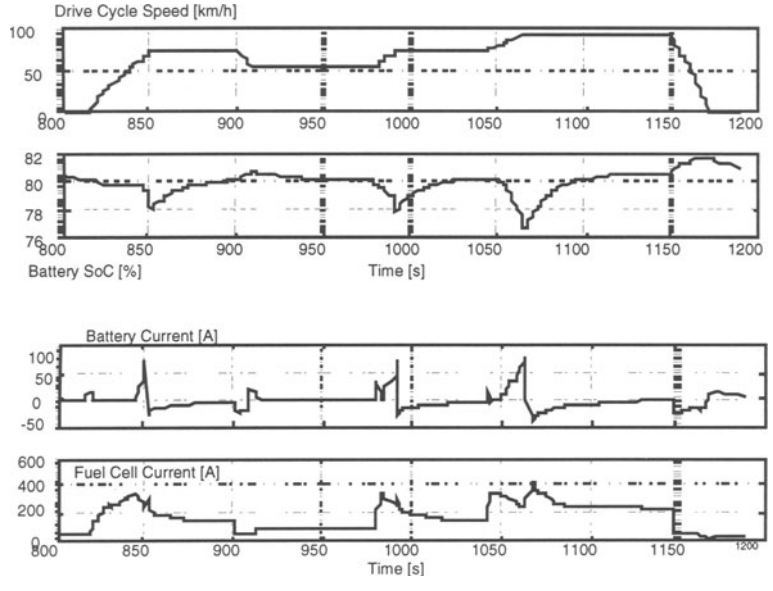

Figure 5

On the same EUDC part of the cycle, figure 5 presents the currents delivered respectively by the battery and the fuel cell. The battery supplements the fuel cell current during high accelerations in the transients where the air compressor or the hydrogen supply system suffer some response delay.

2.2.6. Safety study.

Using hydrogen as a fuel in a vehicle, a completely new element of potential safety hazard is introduced. Hydrogen, diluted in air, is detonative in the range of 4 to 76 %. In industrial sectors, this gas is currently handled according to regulated safety procedures. Nevertheless, if it is to be used in passenger cars, special considerations have to be taken into account. These new safety standards shall have to be extremely precise. To address them, a safety study was performed by the Royal Institute of Technology in Stockholm.

In this study, failure modes for the main components that cab jeopardise the safety of the entire system were identified. These failure modes make the ground for the construction of the fault/event trees in the safety study. A catalytic device, neutralising the boil-off from the liquid hydrogen tank, was developed. When the vehicle remains unused for a long period (longer than 13 days), the pressure inside the cryogenic tank increases; at the setpoint of safety pressure, a safety valve opens and releases the gas towards the catalytic neutraliser, where it is oxidised into water at ambient temperature.

The fuel cell can be periodically purged to operate continuously, thus releasing some hydrogen. At such moments, the actual gas outflow is momentaneously higher than the tank boil-off. So as to avoid a overheating of the catalytic neutraliser, a buffer balloon was designed, damping down this flow to acceptable levels.

3. Discussion

3.1. EFFICIENCY AND EMISSIONS

If one considers the efficiency chain from the fuel flow (L.H.V. is 120 MJ/kg), the global efficiency is the product of the efficiencies of each of the subsystems. For a working point at nominal power :

$$\eta \text{ global} = \eta \text{ power module} * \eta \text{ converter} * \eta \text{ drive chain}$$

For a consumption of 0,40 g/sec of hydrogen, the theoretically available power should be 52,6 kW. If the fuel cell works in its nominal conditions, the efficiency of the power module is about (30-5)/52,6=47,5%. If η converter is 0,92 and η drive chain 0,9 ; the global efficiency can be about 39%. In the phases of part load, the benefit in efficiency of the fuel cell can be obtained only if the air compression demand is consequently reduced. The emission of pollutants is zero as the vehicle produces - by electrochemical reaction at low temperatures - only water (approximately 144 g per km).

3.2 THE DIFFICULTIES

Difficulties remain to be overcome to enable the development of fuel cell vehicles. They are of different nature : firstly infrastructure, secondly economical and technical.

Concerning the infrastructure, the difficulty is of two kinds : to-day, neither a distribution network for liquid hydrogen nor a legal framework defining the homologation conditions for vehicles using hydrogen as fuel exist. Co-ordination must be undertaken at an international level in so as to define such conditions. The choice to create production plants and distribution network for such fuel remains of the political decision of States.

The technical and economical difficulties are tightly linked and must orient the research in this domain. The fuel cell technology has left the domain of space applications and is approaching the industrial stage, but important progresses remain to be done :

- The weight and volume of fuel cells working at ambient air has been notably reduced. The technology of DE NORA realises fuel cells of 108 kg and 75 dm3 for 10 kWel. The integrability in a vehicle implies goals such as 20 kg and 15 cm3 for the same power.
- The feeding of the cell with air compressed at 3 bars results in three drawbacks : a noticeable power self consumption, the necessity to cool the air overheated by compression, the contamination of the air by the lubricant oil which leads to a degradation of the electrodes' performances. This degradation is effective as soon as the content is about 0,9 ppm of equivalent CH4 of oil as analysed by ECOLE des MINES. These drawbacks orientate the research towards the design of fuel cells offering the same performance for air pressure as low as possible.

•The price of the polymer membranes (NAFION) is about 700$/m2, which means 270 $/kW. The research must therefore simultaneously concentrate its efforts towards the obtention of cheaper membranes, industrially produced, and the realisation of higher specific powers functioning with air.
•The price of precious catalysts is a significant component of the cost of this technology. At the rate of 1 mg/cm2, the induced cost is 71$/kW. In the conventional engines with catalysts, the content of precious metal of the catalyst is rather about 3,5 g of platinum for 50 kW, which means 1,4$/kW. A significant step would be to obtain performant electrodes at an impregnation rate of 0,1 mg/cm2 (anode + cathode).

4. Conclusion

The fuel cell powered vehicle realised by RENAULT and its European partners of the FEVER program is a demonstrator of technological feasibility. Fed by three stacks of fuel cell delivering an electrical power of 30 kW, it will in-house a cryogenic tank storing 8 kg of liquid hydrogen. The numerical simulation enables to forecast an autonomy of 500 km at average speed of 100 km/h. The demonstration is scheduled for June 1997.

This step of technological demonstrator is used as a basis for a program of technical and economical optimisation which will have to pursue the effort on the efficiency optimisation and the reduction of the weight, volumes and costs of this technology.

It is clear that the use of hydrogen represents the ultimate solution concerning the suppression of the carboned pollutants emissions : CO, CO2 and HC, the use of this fuel in the fuel cell rather than in the engines eliminates the formation of nitrogen oxides (NOx). This technology, very environmentally friendly will experience serious development prospects only if the technical and economical drawbacks linked to it are resolved and if the political decision is taken to promote the industrial and legal infrastructure which are necessary. Subject such decisions were taken, an opening of the market could be possible in Europe between 2005 and 2010.

HYDROGEN TECHNOLOGY FOR MOBILE APPLICATIONS

Market Launch Concept

H.BUCHNER
Konzern Service Center Technik
Daimler-Benz AG HPC 0511
D - 70546 Stuttgart

1. Introduction

Hydrogen technology has a lengthy tradition in Daimler Benz Research. As early as 1968, the world's first battery using a hydrogen-storing electrode on a titanium-nickel-hydride basis, was developed in cooperation with the Battelle Institute in Geneva [1].

This has been followed since 1972 by work on the hydrogen-powered vehicle with spark-ignition engine and hydride storage tank, comprehensive work on metal hydride development [2 - 5] and, between 1984 and 1988, a successful test (over 750,000 km) of a small fleet (10 in total) of hydrogen vehicles (cars, vans) in the hands of customers [6].Our research activities at present - in cooperation with Ballard, Canada - are concentrated on designing mobile fuel cells for generating electricity for the electromotive power train in cars, vans and buses. Industrialised and affordable products are likely here in about 10 years [7].

If we look at the wide range of international research results which have been obtained in the field of hydrogen technology during the last 30 years, the following components are of particular interest for mobile applications:

- Catalytic hydrogen burner (auxiliary heater)
- Hydride air conditioning
- Small fuel cells (0.5 - 5 kW) for the vehicle onboard power supply
- Hydrogen supply to the diesel exhaust catalytic converter (< 10 g H_2 / h) which produces a reduction of NO_x emissions by a further 60 - 90 %.

The aforementioned systems for enhancing comfort in vehicles can be operated - even with the engine switched off - with hydrogen without any pollutant emissions and can, in particular, also be used in vehicles with diesel and gasoline engines. This would enable in urban driving to save 2 - 3 l/h (30 - 50 %) of conventional fuels and to achieve corresponding reductions in emissions. The principal benefit, though, is that it is possible to introduce

T. O. Saetre (ed.), Hydrogen Power: Theoretical and Engineering Solutions, 13–24.

hydrogen technology into the vehicle market **without** having to modify the power train of the vehicle.

2. Market launch concept of mobile hydrogen technology

A fundamental prerequisite for successful marketing of hydrogen technology by the automobile industry would be a national supply infrastructure for the fuel, hydrogen. This, however, is unlikely even in the medium term (10 - 20 years). For this reason, the mobile application of hydrogen is conceivable in the best-case scenario in conurbations, in other words at those points at which the infrastructural measures can most easily be implemented and the emission reductions would achieve their greatest effect.

Such market segments, at present, represent only niche markets in which small and medium-sized firms, in particular, can be active. With a clearly definable production of hydrogen technology components and systems, it is possible to serve limited markets and thus to safeguard existing as well as to create new jobs. Such processes are currently being implemented in Thuringia.

A Working Group "Thuringia Hydrogen Technology", established in June 1996,has set itself the task of ensuring market access to mobile hydrogen technology for the participating companies in Thuringia. The principal subjects and the companies / institutes participating are listed in table 1:

TABLE 1. Thuringia Working Group

ISE / Freiburg Dr.Schaumberg;Prof.Ledjeff - Hey
- Small natural gas reformer plants
- Small electrolysers
- Small fuel cells
- Catalytic burners using hydrogen

ZSW / Ulm Prof.Garche
- Small fuel cells

PES / Rocky Hill,USA Mr.Smith
- Small,regenerative electrolysers

NET (Aisin Cosmos) / Kassel Mr.Kappes
- Hydride air conditioning systems
- Other metal hydride applications

IKE / Stuttgart Prof.Groll
- Hydride technology
- Hydride air conditioning systems

Air Products / Hattingen Mr.Schwarz
- Operative division gas distribution
- Operator of hydrogen plants e.g. small gas reformer plants,electrolysers

Blanco Med / Saalfeld Mr.Hopfe
- Operative division hydrogen technology
- Hydride air conditioning systems
- On board fuel cells
- Hydrogen stationary heating

Adapt Engineering / IMG Nordhausen Dr.Herms
- Engine conversion to hydrogen
- Vehicle construction
- H_2 - DeNOX plants
- Hydrogen two-wheeler conversion

Japan Metal & Chemicals (JMC) / Tokyo
- Hydride storage tanks Dr.Matsubara

BAM / Berlin Dr.Schmidtchen
- Savety aspects

DBAG / Stuttgart Dr.Buchner
- Concepts / coordination
- Demonstration projects

MTU / Munich Mr.Brand
- Operative division electrolysers

Industrial locations with hydrogen consumption or production are particularly suited for the market launch of mobile hydrogen technology as particularly favourable general conditions for the hydrogen supply of vehicles can, in these cases, be achieved in such catchment areas.

Table 2 shows the availability of "excess" hydrogen from the chemical industry, taking as an example a number of locations in Germany:

Table 2. Availability and costs of hydrogen [l = litre of gasoline equivalent]

~ 1 mill. l / a	Bitterfeld	80 - 100 Pf / l
~ 4 mill. l / a	Burghausen	< 50 Pf / l
~ 8 mill. l / a	Ibbenbüren	< 50 Pf / l
~ 15 mill. l / a	Degussa	30 - 40 Pf / l
~ 30 mill. l / a	Hüls	30 - 40 Pf / l
~ 700 mill. l / a	Total excess	2 - 3 % gasoline consumption p.a. (in Germany)
any desired quantities	Water electrolysis	90 - 160 Pf / l (with electricity costs < 10 Pf / kWh)

In addition, a newly developed method of Kvaerner, Norway [8] makes it possible to fractionate large quantities of hydrogen from natural gas into carbon - black and hydrogen ($C + H_2$). As about 30% by weight of every vehicle tire is composed of carbon - black (demand 4 - 5 mill. t carbon - black p.a.), it would be possible, worldwide, in this way to produce 20 billion Nm^3 hydrogen (corresponding to 6 billion l gasoline equivalent) as a coupled product in tire production at low cost (carbon - black bonus) and in addition - using electricity from hydroelectric plants, nuclear energy or regenerative energy sources - **free of CO_2**.

The costs stated relate to **untaxed** hydrogen, to enable this to be offered during an introductory period (5 - 10 years) locally, under particularly favourable economic conditions, to customers interested in mobile applications - these being primarily operators of vehicle fleets. From the point of view of fleet operators, the requirements for the conversion of vehicles to operate with hydrogen are as follows :

- No change in existing vehicle models (VW, MB, Ford, Fiat...).
- Ranges: 50 - 100 km / day
- Dual mode for spark-ignition engines (gasoline / H2)
- NOx reduction in the case of diesel engines
- Charge volume is more important than weight !!
- Service and fuelling in depots **without ex protected areas**

- Acceptable additional costs: < DM 10,000 for cars
  < DM 15,000 for vans
  (the customer expects that the costs for converting the vehicle to hydrogen are not any higher than for converting to natural gas).
- Conversion of entire fleet of diesel and gasoline vehicles initially in regional centers (development areas, cheap H_2).
  Electrolysers or natural gas reformer plants would have to be installed and operated in the depots or other vehicle locations
- Overall concept for conversion, supply and operation.
- Responsible operating company e.g. Air Products, ARAL.

3. Technical and economic conditions

3.1. Hydrogen vehicles

Spark-ignition engines operating in the H_2 lean mode have extremely low emissions (only lubricant oil emissions). Trips outside of environmentally-sensitive areas can be gasoline-based (bivalent mode with the usual ranges). The energy content of 5 litres of gasoline is contained in 1.3 kg of hydrogen (ranges depending on specific gasoline consumption of 5 - 10 l / 100 km: 50 - 100 km). This quantity of hydrogen is chemically bonded in a 100 kg hydride tank and is thus stored extremely safely and at a low pressure (< 30 bar). Standard production spark-ignition / natural gas engines can be adapted to the hydrogen lean mode at a low pressure and with a gas mixer.

Adapt Engineering at Nordhausen cooperating with IMG at Nordhausen convert vehicles with spark-ignition engines to operate on hydrogen. The most cost-effective solution for small production runs (< 100 p.a.) consists in adapting standard production vehicles designed to operate on natural gas / gasoline, as can presently be purchased on the market from various manufacturers at an added cost ranging from DM 5,000 - 7,000 compared to the gasoline model. The additional conversion costs to enable such vehicles to operate with hydrogen come to a further DM 5,000 - 7,000. Part of these costs should be borne initially by the Ministry of Economics of Thuringia to make the initial step into this market more economically attractive for the customer.
In the event of greater customer demand (500 - 1,000 cars p.a.) Adapt Engineering would be able to convert gasoline models directly to operate on hydrogen / gasoline. The conversion costs in this case would then be DM 5,000 - 7,000 in total - no subsidy from the Ministry of Economics would then be necessary.

Should the customer so wish (safety !) and/or if use is made of depot or garage electrolysers (H_2 pressure: 30 bar) for local hydrogen supplies,a hydride tank is installed in the vehicle in place of the pressurized tank (200 bar).

The corresponding additional costs compared to pressure vessels depend on the desired daily range and the number of vehicles.

JMC in Tokyo is a standard production manufacturer of economic hydride storage tanks. The initial hydrogen vehicles could be made ready by Adapt Engineering 12 - 18 months after receipt of the order; in other words, the first vehicles would be operational in early 1999.

3.2. Hydrogen auxiliary heating

The catalytic burners developed at the ISE Institute at Freiburg [9] convert hydrogen into heat, also with air, with extremely low NO_x emissions. This makes it possible to comply with an essential requirement in respect of vehicle auxiliary heating system in conurbations, namely heating the passenger compartment without burdening the environment with additional emissions. Hydrogen auxiliary heating systems can be particularly economically used at locations with a local hydrogen excess - amortization times being about 5 years. Table 3 shows a 5 kW auxiliary heater as an example:

Table 3. Design example of a auxiliary heater using hydrogen

Power output	5 kW
Operating period / Day	2 h
Energy consumption / Day	10 kWh ≡ 1l gasoline / DM 1.7
Hydrogen consumption / Day	300 g H_2
Storage weight	30 kg hydride tank
Storage costs (target)	< DM 1,200
Hydrogen costs / Day	DM 0.3 - 0.5
Savings compared to gasoline / Day	DM 1.4 - 1.2
Savings compared to gasoline / Year (150 days)	DM 210 - 180
Amortisation period	about 5 years

Such auxiliary heaters are presently being developed through to industrialisation by Blanco Med.in cooperation with ISE and JMC (from 1999).

3.3. Metal hydride air conditioning systems

In summer, the hydrogen auxiliary heater can be used for thermal powering of a hydride air conditoning system.The technical data of such a CFC-free airconditioning system, which also enables the desired cooling capacity to be offered in parked vehicles with a low noise level, low environmental impact and minimal wear-and-tear, are shown in table 4:

TABLE 4. Technical data of a hydride air conditioning system

Refrigeration capacity	3 kW
Thermal input power	7 kW
Heat supply temperature level	200°C
Heat dissipation temperature level	50°C
Refrigeration production temperature level	0°C
Weight of hydride reactors	~ 30 kg
Weight of heat exchanger	~ 20 kg
Weight of pumps, valves etc.	~ 10 kg
Total weight	~ 60 kg

Based on the present state of the art, a metal hydride air conditioner is larger, heavier and more expensive - the objectives being about DM 5,000 - than a conventional compressor air conditioner.

By exploiting the savings potential of fuel of 1.5 l gasoline / operating hour and fuel costs of DM 1.5 - 2.0 / operating hour at locations with low-cost hydrogen, good possibilities exist for developing a new market segment which could be certainly expanded as a result of increasing customer demand for a air conditioning system which is even available when the engine is switched off.

Blanco Med. in cooperation with the NET Institute / Kassel (Aisin - Cosmos / Karija) [10], JMC / Tokyo and the IKE / Stuttgart, is already developing existing prototypes of hydride air conditioning systems in small production runs for use in vehicles. The market launch is set for as early as 1999.

3.4. Fuel cell for generating on-board power

To satisfy the constantly increasing demand for electrical energy in cars, also if possible when the engine is switched off, it would be possible to supplement the conventional generator which has offered such reliable service for many years (< 6,500 operating hours) by an engine-independent power generator, particularly in the higher power range (2 - 4 $kW_{el.}$).

In view of the low overall efficiency of internal combustion engine / generator of about 5 - 15 %, use of a conventional power generator in the range from 1 kW would involve a markedly increased consumption in fuel and corresponding increase in emissions. Based on the present state of the art, the PEM fuel cell offers an interesting potential in view of its high efficiency (40 - 50 %) when operated with hydrogen. The energy savings potential compared to a conventional generator is, as shown in table 5, on average > 300 fuel / year for each kW of installed power (equals > DM 5,000 within 10 years).

TABLE 5. Comparison of fuel cell and conventional generator

Power output$_{el.}$	1 kW
Operating period	1 h
Energy$_{el.}$	1 kWh
Generator η = 5 - 15 %	
Gasoline consumption	2.0 l - 0.7 l
Costs / kWh$_{el.}$	DM 3.4 - DM 1.2
300 h operation (15,000 km) p.a.	600 l - 200 l
Gasoline costs over 10 years	**DM 10,000 - DM 3,500**
Fuel cell η = 40 - 50 %	
Hydrogen consumption	2.5 kWh - 2 kWh ≡ 0.25 - 0.2 l gasoline equivalent
Hydrogen costs over 10 years	DM 400 - DM 300 at DM 0.5 / l gasoline equivalent
Costs of fuel cell	DM 3,000
Costs of hydride storage tank	DM 750
Total costs	**approx. DM 4,000**
Weight of fuel cell	< 15 kg
Weight of hydride storage tank	15 kg / 5 kWh$_{el.}$ for 2 - 3 operating hours
Total weight	**< 30 kg**

A PEM fuel cell / hydride tank on - board power generating system with an output of 1 kW$_{el.}$ is presently being developed through to industrialisation by Blanco Med. at Saalfeld in cooperation with ISE / Freiburg [11], ZSW / Ulm and JMC / Tokyo. Costs are likely to range between DM 3,000 and DM 4,000 with small production runs (< 1,000 p.a.), while larger quantities in excess of 10,000 p.a. would cut costs to DM 2,000 - DM 3,000. A greater market potential is likely, particularly if it proves possible to develop through to industrialisation the so-called "reversible" PEM fuel cell - in other words which can also be used as an electrolyser. A development of this nature would make it possible to exploit the widely dispersed electricity infrastructure for supplying hydrogen through mobile electrolysers which can be employed as fuel cells for generating on-board electricity. Cooperation with Proton Energy Systems (PES) - the developer of the "reversible" fuel cells - and the group of companies stated above, is planned. It is likely that the on-board power generating systems will be ready for use from about the year 2000.

3.5. Hydrogen consumption in mobile applications:

Table 6 contains reference values for an average daily demand of hydrogen for use in cars. This shows that "garage" electrolysers with a small power output (2 - 5 $kW_{el.}$) operating at night (12 h, off-peak rate) would be adequate to supply throughout the country and economically with hydrogen.

TABLE 6. Hydrogen consumption for car applications

Car hydrogen / gasoline operation	10 - 20 m^3 H_2 / day
Hydrogen auxiliary heater	1 - 2 m^3 H_2 / day
Hydrogen air conditioning	2 - 4 m^3 H_2 / day
Hydrogen on-board power generation fuel cell	2 - 4 m^3 H_2 / day

This approach makes it possible to access the market also through the individual customer.

3.6. Tasks involved in commercializing H_2 vehicles:

Apart from the considerations regarding the development of the market for mobile hydrogen technology, the following steps - similar to those involved in the commercialization of natural gas vehicles - would have to be implemented within a national and international framework:

- Organising the interests of gas - and electricity supply utilities.
- Analysis of the impacts of emissions of hydrogen in vehicles.
- Evaluation of existing legal/regulatory matters.
- Development of a vehicle market profile (domestic / export)
- Marketing for vehicle and accessories conversion and sales.
- Definition of locations of fuelling points for H_2 vehicles.
- Development of the infrastructure of conversion and service centers.
- Promoting the participation and financial commitment of industry.
- Public relations work; coordination of political decision-making bodies.

These tasks which have to be solved in the medium to long term can contribute to helping mobile hydrogen technology move beyond niche markets and thus making it attractive also for the automobile industry.

In following this approach, an essential element are, in particular, projects which verify the reliability and economics of hydrogen technology in vehicles in practical applications. This is the goal which is served by the projects which are briefly outlined below and which are at present all still in the planning phase.

4. Market launch projects

4.1. Chlor - Alkali Chemie GmbH Bitterfeld (BCA)

The Bitterfeld Chlor - Alkali GmbH is in a position to make available up to 9 million m^3 of hydrogen annually (equally about 3 million liters of gasoline) with a hydrogen pressure ranging from 20 - 30 bar and costs between DM 0.8 - 1.0 / l gasoline.

This quantity would be adequate for supplying about 3,000 vehicles (cars and vans) with hydrogen propulsion or for 6,000 - 10,000 gasoline / diesel vehicles with hydrogen-powered optional equipment such as stationary heaters, air conditioning systems and fuel cells for on-board power supply. Beyond the Bitterfeld catchment area, the customer can make use of an electrolyser with a power range of 2 - 5 $kW_{el.}$. In an initial phase of the project (possibly as early as 1998) it is intended to initially fuel and operate 10 - 20 vehicles on the BCA premises. The vehicle operators will be selected according to fleet size so that it will be possible in the initial phase of the project (from 1999) to make available up to 500 vehicles for conversion. BCA is presently conducting preliminary discussions with potential operators and political decision-making bodies in Saxony-Anhalt.

4.2. Oxygen production from water electrolysis and mobile use of hydrogen

A quantity in excess of 100 million m^3 of water is processed annually with 1 g ozone (O_3) / m^3 water in drinking water treatment plants of major water supply utilities. The ozone is produced by means of electric discharge from industrial oxygen. Some 1 million m^3 of liquid oxygen is delivered annually for this pur - pose by tanker trains and evaporated.The oxygen costs are DM 250.000 p.a.

The aim of the project is to substitute the transportation of the liquid oxygen by producing oxygen locally by means of an electrolyser and marketing the by-product of this process - in other words hydrogen - for mobile applications. The technical outline data of oxygen production by means of water electrolysis are given in table 7. Consuming the hydrogen produced in mobile applications necessitates converting about 500 vehicles to operate with hydrogen in the surrounding area of the respective water plant or providing about 1,000 vehicles powered by gasoline or diesel engines with hydrogen-operated convenience systems (auxiliary heater, air conditioning, on-board power generation also when parked).
This number of vehicles has to be found in the corresponding catchment areas.

TABLE 7: Electrolytic oxygen production and by-product hydrogen

Oxygen demand	1 mill. m^3 O_2 / year	
Excess hydrogen	2 mill. m^3 H_2 / year	**equals 0.6 mill. l gasoline / year**
Operating hours	8,000 h / year	$\Rightarrow$ 250 m^3 H_2 / h
Electrolysis capacity	~ 1 $MW_{el.}$	
Oxygen costs	DM 0.25 mill. / year	+ DM 2.5 mill. over 10 years
Electrolyser power costs	DM 0.8 mill / year (DM 0.10 / kWh)	- DM 8 mill. over 10 years
Electrolyser investment (without interest on capital)	Present market price for PES electrolyser 1 MW	- DM 3 mill. over 10 years
Hydrogen bonus	DM 1.1 mill / year (DM 1.7 / l gasoline)	+ DM 11 mill. over 10 years
Profit	**DM 250,000 / year**	**DM 2.5 mill. over 10 years**

Similar concepts can also be applied to other industrial oxygen consumers, which can result in a completely new market segment for electrolysers and for mobile hydrogen technology.

4.3. Two-wheeler project at Varanasi, India

A two-wheeler with a 3 -4 kW spark-ignition engine has been successfully converted at the Banares Hindu University, India to operate with hydrogen [12]. The hydrogen is stored in an exhaust-heated metal hydride tank (30 kg). This storage tank is integrated into the seat of the two-wheeler and dimensioned so as to ensure adequate daily ranges. As forecasts in India go on the basis of an annual increase of > 100,000 two-wheelers, converting only 1% of these new vehicles to operate with hydrogen represents an interesting business for conversion companies in Thuringia. Appropriate agreements between Indian and German partners are currently being worked out. An essential element for India is also biosolar hydrogen production. Cooperation between reactor developers at the Technical University of Aachen and the Banares Hindu University, Varanasi is presently being elaborated.

5. Summary and outlook

Hydrogen is available as a by-product of the chemical industry at several locations in Germany in major quantities at an attractive price. In addition, hydrogen can be produced at any power outlet from water (electrolysis) and at any natural gas connection (with small natural gas reforming plants) and can thus be integrated into the existing energy scene (on a national basis).

In mobile applications, hydrogen permits nearly pollutant-free operation of:

- internal combustion engines (only lubricant emissions),
- fuel cells for powering electric motors

and, in vehicles with conventional gasoline and diesel engines, engine-independent and pollutant-free operation of :

- auxiliary heaters
- CFC-free air conditioning systems (hydride systems) and
- vehicle on board power generator by means of fuel cells (in addition to the alternator).

This would make it possible in urban driving to save up to 50 % of conventional fuels and to achieve corresponding reduction in emission levels.
Moreover, admixing hydrogen to the exhaust catalytic converter of a diesel engine offers the possibility of cutting its NO_x emissions by a further 60 - 90 %.

For applications in conventional vehicles, the hydrogen is stored in metal hydrides by means of chemical bonding for reasons related to safety, the compact design and adaptation to the available hydrogen supply.

A Working Group "Market Launch of Mobile Hydrogen Technology", composed of national and international research groups and companies, but, in particular, of medium-sized firms in Thuringia, is presently preparing a marketable standard production of the aforementioned components of hydrogen hydride technology for vehicles with gasoline/diesel engines, in close cooperation with the relevant public authorities.This Working Group will continue to be open for participation to all relevant companies and institutes. The primary aim of the Working Group however is to advise and to serve customers who are interested in the application of hydrogen technology in their vehicles.

In this way we can all contribute to the success of hydrogen in our vehicles, even in the short term,and thereby the extent to which the level of pollution is further reduced,especially in dense-populated areas.

6. References

1. Gutjahr,M.A.,Buchner,H.,Beccu,K.D.,Säufferer,H.: A New Type of Reversible Electrodes for Alkaline Storage Batteries Based on Metal Alloy Hydrides,*Power Sources*,Collins,D.H.(ed.) Oriel Press,Newcastle on Tyne,(1973), 79ff.
2. Buchner,H.:The Hydrogen/Hydride Energy Concept,*Proc.2nd World Hydrogen Energy Conference* Veziroglu,T.N.,Seifritz,W.(ed.),Pergamon Press,Oxford,(1978), 1749 - 1792.
3. Buchner,H.,Povel,R.:The Daimler-Benz Hydride Vehicle Project, *Int.J.Hydrogen Energy* **7**(1982), 259 - 266.
4. Buchner,H.: The Question of the Hydrogen Infrastructure for Motor Vehicles, *Int.J.Hydrogen Energy* **8**(1983), 373 - 380.
5. Buchner,H.: *Energiespeicherung in Metallhydriden,* Springer Verlag,Wien, 1982.
6. Author´s Collective : Hydrogen Drive Test,*Alternative Energy Sources for Road Transportation* Verlag TÜV Rheinland,Köln, 1990.
7. Friedrich,J.,Noreikat,K.E.:State of the Art and Development Trends for Fuel Cell Vehicles, *Proc.11th World Hydrogen Energy Conference,*Veziroglu,T.N.et al.(ed.) Schön & Wetzel,Frankfurt/Main,(1996), 1757 - 1766.
8. Gaudernack,B.,Lynum,S.:Hydrogen from Natural Gas without Release of CO_2 to the Atmosphere, *Proc.11th World Hydrogen Energy Conference,*Veziroglu,T.N.et al.(ed.) Schön & Wetzel,Frankfurt/Main,(1996), 511 - 523.
9. Gieshoff,J.,Ledjeff-Hey,K.:Hydrogen Burner with very low NOX - Emissions - Appliances for Space Heating and Cooling,*Proc.11th Hydrogen Energy Conference,*Veziroglu,T.N.et al.(ed.) Schön & Wetzel,Frankfurt/Main,(1996), 1579 - 1586.
10. Yildirim,K.-E.,Zinn,Th.,Kappes,A.,Maurer,Th.,Sakashita,H.,Klose,W.:New Generation of Metal Hydride Tube Bundle Reactors with improved Heat Transport and Examples of Applications, *Proc.11th World Hydrogen Energy Conference,*Veziroglu,T.N.et al.(ed.) Schön & Wetzel,Frankfurt/Main,(1996), 1265 - 1273.
11. Ledjeff-Hey,K.,Gieshoff,J.,Formanski,V.,Vogel,B.:7.5 kW Solid Polymer Fuel Cell with Natural Gas Processor - A Component of an Energy Project in Saxony,*Proc.11th World Hydrogen Energy Conference,*Veziroglu,T.N.et al.(ed.),Schön & Wetzel,Frankfurt/ Main,(1996), 1685 - 1693.
12. Ramakrishna,K.,Mandal,P.,Singh,A.,Singh,A.K.,Singh,B.K.,Raman,S.,Bansal,B.,Srivastava,O.N.: On the Development of Hydrogen Fuelled Two Wheeler Vehicular Intra - City Transport, *Proc.TCDC Workshop on Hydrogen Energy,*CSIR,New Delhi,(1996),S8.1.

HYDROGEN AND NATURAL GAS BUSES IN THE USA

The Cleanest Machines Ever Built

JAMES S. CANNON
Senior Fellow, INFORM, Inc.
POB 4367, Boulder, Colorado USA
jscannon@msn.com

1. ABSTRACT

In 1983, the first modern, urban transit bus powered by an alternative transportation fuel took to the roads in the USA. A little more than a decade later, about 2.5% of all USA buses are powered by alternative transportation fuels and about 20% of the new bus orders for delivery by 1998 will be powered by alternative fuels, mostly by natural gas. There are over 2,200 natural gas buses in operation or on order, plus about 600 additional buses powered by other alternative fuels. When these orders are completed, alternative fuel buses will constitute over 4.4% of the urban bus fleet in the USA. The widespread use of natural gas buses in the USA provides an important transition pathway for hydrogen vehicles because of the similarities between distribution, refueling and on-board energy storage technologies for the two fuels.

Projects demonstrating advanced hybrid-electric buses powered by natural gas or hydrogen and projects demonstrating hydrogen fuel cells in buses are also increasing in number and scale in the USA. Hydrogen buses emit virtually no air pollution and natural gas buses, especially when operating in hybrid configurations, are among the cleanest transportation machines ever built. Urban transit buses are the most promising market entry for alternative transportation fuels in the USA today.

2. ALTERNATIVE TRANSPORTATION FUEL USE IN THE USA

Approximately ten years ago the USA embarked on a national effort to begin the transition to a post-petroleum transportation age by diversifying the fuel mix used to power its 190 million cars, buses, and trucks (AAMA, 1996a; Cannon, 1989). The program has three major policy objectives:

(1) To reduce public health effects and environmental damage from motor vehicle air pollution. About 50% of all air pollution regulated under the federal Clean Air Act occurs as automotive exhausts. In many urban areas, motor vehicles account for more than 60% of the local air pollution. Nationally, about 32% of the "greenhouse" carbon dioxide emissions originate in the transportation energy sector (EPA, 1996).

T. O. Saetre (ed.), Hydrogen Power: Theoretical and Engineering Solutions, 25–35.

(2) To increase security of energy supplies. The USA now imports 50% of the oil it consumes, 68% of which is used in transportation. Nearly every vehicle is powered by a fuel refined from oil. Every second, motor vehicles in the USA burn 17,000 liters of fuel. Domestic oil production in the USA peaked in 1970 and has dropped 24% since then. Unless oil dependence in transportation is reduced, the USA will have no choice but to seek to import additional oil supplies in an increasingly competitive international market (EIA, 1996b).

(3) To develop global leadership in the transportation technologies of the 21st century. In China there is only 1 motor vehicle for every 126 people, compared to 1 vehicle for every 1.3 people in the USA (AAMA, 1996b). Nations with rapidly developing economies want the benefits of modern transportation, but they don't have oil-based fuel distribution or automotive manufacturing infrastructures in place. Duplicating the 100-year old model set by the USA, which relied on oil and perfected what is now conventional automotive technology, may not be viable. These nations may choose to build their transportation systems based on cleaner and more abundant fuels and advanced vehicle propulsion systems. Encouraging transportation alternatives in the USA can enhance the competitiveness of USA businesses in emerging international transportation markets.

During the late 1980s, the federal government and a number of state governments sponsored research and demonstration projects to test alternative fuels in conventional vehicles modified to burn them. Encouraged by the results of these early demonstrations, the federal government established the first national alternative transportation fuel use mandates and incentives in the Alternative Motor Fuel Act of 1988 and the Clean Air Act Amendments of 1990; they were greatly enhanced in the Energy Policy Act of 1992. In 1989, Texas became the first state to enact a law mandating the use of alternative fuels in select vehicle fleets. Since then more than 30 of the 50 states have enacted mandates or incentives, such as investment tax credits or fuel tax exemptions, to require or encourage the purchase of alternative fueled vehicles. According to a March 1997 survey by the National Conference of State Legislatures, more than 30 proposed alternative transportation fuel laws are actively under debate by state legislatures. Most alternative fuel laws and regulations in the USA are fuel-neutral. Each alternative fuel is given an equal opportunity to enter the market (Cannon, 1989 and 1993).

TABLE 1: ALTERNATIVE FUEL VEHICLES IN THE USA: 1992-1997

FUEL	1992	1993	1994	1995	1996	1997
Natural Gas	23,281	33,031	41,711	50,821	63,520	82,702
Methanol	5,254	10,677	15,899	19,705	19,791	19,917
Ethanol	210	468	1,020	1,663	3,916	6,200
Propane	221,000	269,000	264,000	259,000	266,000	273,000
Electric	1,607	1,690	2,224	2,860	3,306	3,925

The extensive public and private sector alternative fuel vehicle investments made over the past decade are beginning to yield important results. Table 1 shows the growth of alternative fuel vehicle use in the USA from 1992 through projections for the end of 1997 (EIA, 1996a). There are currently about 386,000 alternative fueled vehicles on USA roadways, over 90% of which are light-duty vehicles such as passenger cars, vans, andd small "pick-up" trucks.

The fastest growing alternative transportation fuel in the USA during the 1990s is natural gas. The number of natural gas vehicles has jumped nearly 400% from about 23,000 in 1992 to a projected 83,000 by the end of 1997. Most of these vehicles are powered by natural gas stored as compressed gas, although there are now about 1,000 vehicles that are fueled by liquefied natural gas. The annual growth rate of natural gas vehicles during the 1990s has been nearly 30%, compared to a growth rate for oil-powered vehicles of less than 1% per year. There are now over 1,200 natural gas refueling stations nation-wide.

Electric vehicle use is also increasing, although much more slowly than vehicles powered by the other alternative fuels. There are currently about 3,900 registered electric vehicles in the USA. Nearly all of these use batteries as the dominant electrical energy storage technology, although there are a small number of demonstration hybrid electric and hydrogen fuel cell vehicles as well. Each of the three major automotive manufacturers has announced a program and a schedule to build a prototype hydrogen fuel cell automobile by the end of the decade. A small number of hydrogen combustion engine equipped cars and several fuel cell-powered vehicles built by small companies not associated with the major automotive manufacturers are now being demonstrated in the USA.

3. ALTERNATIVE TRANSPORTATION FUEL USE IN BUSES

Despite their success over the past decade, the overall use of alternative transportation fuels in the USA remains minuscule compared to the over-arching reliance on oil-derived fuels. As shown in Table 2, the 386,000 alternative fuel vehicles are dwarfed by the 155 million gasoline-powered automobiles and the 35 million diesel powered vehicles (calculations from data in EIA, 1996a). Taken together, all alternative transportation fuel use displaces about 1.2 billion liters of oil-derived fuels annually. This is an important accomplishment. Nevertheless, it represents only 0.2% of total oil use in transportation.

TABLE 2: USA TRANSPORTATION FUEL AND VEHICLE USE - 1997		
	Annual Fuel Use (Million of Equivalent Liters)	Number of Vehicles
Gasoline	450,486	155,000,000
Diesel	104,343	35,000,000
Propane	918	273,000
Natural Gas	322	82,700
Methanol (M85)	15	19,800
Ethanol (E85)	7	6,200
Electric Battery	3	3,900
Hydrogen	<1	<20

There is one transportation application in the USA where the contribution of alternative transportation fuels is much more dramatic than the overall statistics cited above suggest. This is the urban transit bus market. The alternative fuel bus market has soared in the 1990s, far exceeding the percentage growth of alternative fuel use in the passenger vehicle market. From a bus population of zero in 1983, the number of operating alternative fuel buses now exceeds 1,500 and it will approach 2,800 when pending orders for new alternative fuel buses are completed. The growth in alternative fuel buses is shown in Table 3 (tabulations from data in APTA, 1996). Together operating alternative fuel buses and buses on order represent 4.4% of the urban transit bus fleet in the USA. This market share will undoubtedly grow. In 1996, over 20% of the orders for new buses specified an alternative fuel, most commonly natural gas.

TABLE 3: ALTERNATIVE FUEL BUSES IN THE USA 1992-1997							
FUEL TYPE	1992	1993	1994	1995	1996	1996 + New Orders	Percent of Fleet
Natural gas	116	305	634	1035	1074	2267	4.4
Methanol	61	160	351	399	230	64	<0.1
Ethanol	5	86	86	82	243	409	<0.1
Propane	15	42	42	45	43	47	<0.1
Batteries	13	18	31	37	41	51	<0.1
Traps	564	1354	2012	1520	1188	1232	2.4
All buses	51500	51600	51300	52200	50400	51000	

Natural gas currently dominates the alternative fuel bus market. The nation's first natural gas bus began testing in Orange County, California in 1986, followed two years later by two other demonstration buses in New York City. Additional demonstration buses followed and by 1992 more than 100 natural gas buses were operating in the USA. The technology for natural gas bus engines has improved immeasurably over the past decade. There are a now number of alternative fuel engine manufacturers that sell fully-warranted products that perform well, run more quiet than conventional diesel engines, and require less routine maintenance.

The number of natural gas buses increased by 500% in just two years, to 634 in 1994. A year later, natural gas buses exceeded 1,000. When the more than 1,000 natural gas buses now on order for delivery before the end of 1998 are added to those buses already on the road, there will be a total of 2,267 natural gas buses on USA roads. This number will undoubtedly go much higher as natural gas bus projects that have been announced, but not yet converted into bus orders, progress. About 20% of the natural gas buses now on the roads are fueled by liquefied natural gas; the other 80% use compressed natural gas.

TABLE 4: MUNICIPAL NATURAL GAS BUS FLEETS IN THE USA - 1996
(9 cities with more than 50 natural gas buses)

City	Buses
Houston, Texas	283
Los Angeles, California	184
Cleveland, Ohio	101
Sacramento, California	95
New York City, New York	86
Tacoma, Washington	77
Fort Worth, Texas	70
El Paso, Texas	55
Tucson, Arizona	53
Total and % of All Natural Gas Buses	1,004 (93%)

Table 4 lists the nine USA cities where natural gas bus fleets are now operating with at least 50 buses in each location (tabulations from data in APTA, 1996). Together these cities are home to 93% of all the natural gas buses operating nationwide. Some highlights from these urban bus programs include the following (Cannon, 1997):

- In 1986, Pierce Transit Company in Tacoma, Washington became the first bus operator to use natural gas buses in revenue-generating service. In 1989, it ordered 33 natural gas buses to supplement its original buses; it added 27 more in 1993 and 15 more in 1996.
- In October 1993, the Los Angeles County Metropolitan Transportation Authority voted never to purchase another bus powered by diesel fuel. It now operates 184 natural gas buses with approximately 120 more awaiting delivery from an order placed in 1994. In 1996, Los Angeles ordered another 250 natural gas buses; delivery will begin late in 1998.
- Two bus systems in New York City now operate a total of 86 natural gas buses, but this number will grow significantly. The City's Department of Transportation ordered 358 natural gas buses in 1995; most deliveries will occur in 1998. In January 1997, the New York City Transit Authority announced an initial order for 190 natural gas buses for delivery beginning in 1998. These buses will be the first of a total order for 500 alternative fuel buses to be completed over several years.

- Houston now operates the largest urban natural gas bus fleet in the country. It also owns the most buses powered by liquefied natural gas (LNG). Between 1990 and 1994, the Houston METRO purchased nearly 300 LNG buses. In 1995 and 1996, however, METRO reverted to purchasing diesel-powered buses, primarily due to the high cost of LNG fuel. In January 1997, it signaled at least a partial return to natural gas when it placed an order for 5 LNG buses and 5 buses powered by compressed natural gas. The Sun Metro bus system in El Paso, Texas also uses LNG in its natural gas bus fleet.

4. ADVANCED ALTERNATIVE FUEL BUS PROJECTS

Natural gas is by far the leading alternative fuel used in USA buses today for good reason. It burns cleaner than diesel fuel, it is domestically produced, and in most regions of the country it costs less than diesel. Natural gas also serves an important role in advanced bus technologies as well, especially as a feedstock and transitional technology for buses powered by hydrogen and as fuel in hybrid electric bus systems.

Hydrogen holds great promise as a sustainable energy carrier for transportation uses in the 21st century (Cannon, 1995). It can be produced in limitless supplies from water using renewable resources to supply the energy. It contains three times more energy per kilogram than oil or natural gas and its combustion releases no carbon dioxide. Hydrogen can also be used in fuel cells to generate electricity. Fuel cells operate pollution-free with drive-train efficiencies up to three times the efficiencies of combustion engine vehicles. Hydrogen fuel cells are much lighter and smaller than comparable battery systems in electric vehicles and they can be refueled in minutes rather the hours required for battery recharging.

The advances now being made by natural gas in the bus market can help pave the way for a sustainable hydrogen energy economy. First, steam reforming of natural gas provides a low-cost way to manufacture hydrogen until the price of renewable energy resources becomes more competitive. Secondly, much of the infrastructure for natural gas buses – including distribution pipelines, refueling equipment, and on-board fuel storage tanks – can be modified for use by hydrogen as well.

In the USA today, there are four major hydrogen bus research, development, and demonstration projects, as shown in Table 5 (Cannon, 1997). Three of these projects involve fuel cells. A project sponsored by the federal Department of Energy produced three buses between 1994 and 1996 powered by phosphoric acid fuel cells. The fuel is methanol, which is reformed on-board to produce hydrogen. These buses are undergoing tests in Maryland, California, and Illinois. The federal Department of Transportation is now sponsoring the construction of a new generation of fuel cell buses, including one powered by a phosphoric acid fuel cell and one powered by a proton exchange membrane fuel cell. These buses should be operating in 1998. In a third project, the City of Chicago has purchased three proton exchange membrane fuel cell buses manufactured in Canada by Ballard Power Systems. They are scheduled to be delivered in July 1997.

Finally, a hydrogen-powered hybrid electric bus was built and first demonstrated during the 1996 summer Olympics in Atlanta, Georgia. Electricity is generated from the power produced by a hydrogen-burning internal combustion engine. The hydrogen is stored in an metal hydride system. Additional tests are now underway in Augusta, Georgia.

TABLE 5: ADVANCED TECHNOLOGY, ALTERNATIVE FUEL BUS PROJECTS IN THE USA - 1997

Project	Fuel and Propulsion	Current Status
Department of Energy (DOE) Fuel Cell Bus	Methanol, Phosphoric Acid fuel cell (PAFC)	3 undergoing tests
Chicago Fuel Cell Bus	Hydrogen, Proton Exchange Membrane fuel cell (PEM)	3 due in mid 1997
Department of Transportation (DOT) Fuel Cell Bus	Methanol, PAFC and PEM	2 to be completed by 1998
Hydrogen Hybrid Bus	Hydrogen, Conventional combustion engine	1 completed in August 1996.
DUETS Hybrid Bus	Natural gas, Hybrid electric	1 completed in March 1997.
ATTB Hybrid Bus	Natural gas, Hybrid electric	1 built, 6 to be completed by 1998
New York Hybrid Bus	Natural gas, Hybrid electric	1 to be completed in 1997
Denver Mall Hybrid Bus	Natural gas, Hybrid electric	up to 36 to be built starting in 1998

Natural gas hybrid electric vehicles are another advanced transportation technology that is beginning to enter the bus marketplace in the USA. This technology also benefits from the extensive use of natural gas buses now underway because of the compatible infrastructures for natural gas distribution, storage, and use. There are currently several ongoing hybrid electric vehicle research and development projects in the USA. Table 5 lists four projects which involve natural gas fuel use in hybrid-electric buses.

There are two natural gas hybrid electric bus projects under primary sponsorship of the federal government, bus operators, and a number of private sector participants. The $8.0 million Demonstration of Universal Electric Transportation Subsystems (DUETS) project is jointly sponsored by the Federal Transit Administration (FTA) within the Department of Transportation and the Advanced Research Projects Agency (ARPA) within the Department of Defense. In March 1997, a prototype DUETS bus, equipped with a natural gas-powered rotary combustion engine and a 100 kilowatt electric generator, began its initial road testing in New Mexico. A second project, sponsored by the FTA, is the Advanced Technology Transit Bus (ATTB). The ATTB is a light-weight, low-floor bus built with advanced composite materials and equipped with a natural gas burning engine and electric generator. The first bus was completed in October 1996 in Los Angeles. A total of six buses will be built by the end of 1998 under this $51.2 million program. The U.S. Department of Energy has recently announced that the last of the ATTB buses will be powered by a hydrogen fuel cell in place of the natural gas combustion engine.

The New York State Energy Research and Development Authority is also funding the development of a hybrid electric bus along with several companies in New York. The first bus, completed in 1996, is equipped with a diesel-burning engine. The second bus, which will be completed in 1997, will include an engine powered by natural gas. A final project involves the construction of up to 36 natural gas hybrid electric buses for use along a 1.3-kilometer shuttle route through a downtown pedestrian mall in Denver, Colorado. In March 1997, the transit operator in Denver awarded a contract to build these buses to Columbine Bus, Inc. The first buses will be delivered in 1998.

5. ENVIRONMENTAL PERFORANCE OF NATURAL GAS AND HYDROGEN BUSES

There are many reasons for the increasing use of alternative fuels in urban buses in the USA. One of the most important is the capability of alternative fuels to meet and exceed the ever tightening air pollution control requirements facing the bus industry for particulate matter and nitrogen oxides, the two major air pollutants currently released from diesel-burning urban buses.

Particulate air pollution has long been recognized as a cause for a variety of respiratory diseases. The federal Environmental Protection Agency estimates that 70,000 people die prematurely each year in the USA due to exposure to particulate air pollution. The International Agency for Research on Cancer has identified diesel exhaust as a probable human carcinogen and the California Environmental Protection Agency in May 1997 proposed classification of diesel exhaust as a toxic air pollutant. Nitrogen oxide air pollution is also responsible for a variety of adverse environmental impacts. It combines with hydrocarbons molecules to form ozone, commonly called smog. Over one quarter of the USA populations lives in cities where air quality violates the federal public health standard for smog.

Environmental pressure in favor of alternative fuel buses is likely to increase as the result of new pollution control requirements. In January 1997, the U.S. Environmental Protection Agency proposed new public health standards limiting concentrations of fine particulate matter, including emissions from diesel-burning engines, in the air. New standards were also proposed for ozone, which correlates directly to emissions of nitrogen oxides from diesel engines. On June 25, 1997, President Clinton announced his support for these proposed standards, which are likely to be promulgated by the EPA before the end of the year.

Prior to 1988, dense clouds of noxious, black smoke from the tailpipes of urban buses were a common sight in the USA. One urban bus in that era could emit more particulate matter than the exhausts from 500 automobiles. In response to high levels of particulate and nitrogen oxide air pollution from the tailpipes of diesel-burning bus engines, the federal Environmental Protection Agency (EPA) has repeatedly tightened tailpipe emissions for urban buses. As shown in Table 6, EPA regulations began limiting bus engine emissions in 1976. Between 1988 and 1990, new EPA pollution control

regulations limited emissions to 0.8 and 8.0 grams per kilowatt-hour for particulate matter and nitrogen oxides from bus engines respectively. These standards were tightened again for both pollutants in 1991 and for particulate matter once again in 1994. One more round of nitrogen oxide emission reductions will be required in 1998, at which time particulate matter from urban bus engines will be limited to 0.07 grams per kilowatt-hour and nitrogen oxides will be limited to 5.3 grams per kilowatt-hour.

TABLE 6: FEDERAL TRANSIT BUS EMISSIONS (grams/kilowatt-hour)

Year	Carbon Monoxide	Hydrocarbons	Nitrogen oxides	Particulate Matter
1976-78	53.6	21.4 combined		None
1979-83	33.5	13.4 combined		None
1984-87	20.7	1.7	14.3	None
1988-89	20.7	1.7	14.3	0.80
1990	20.7	1.7	8.0	0.80
1991-93	20.7	1.7	6.7	0.30
1994-97	20.7	1.7	6.7	0.07
1998-on	20.7	1.7	5.3	0.07
Current natural gas	0.5	0.8	2.7	0.03

A diesel engine particulate control technology, called the particulate trap, was widely adopted by the bus industry in the face of the EPA particulate standards promulgated in the 1980s, but it failed to function properly and to consistently reduce emissions to the required levels. As shown earlier in Table 3, the use of particulate traps in conventional diesel-burning buses peaked in 1994 with 2012 buses, but it has dropped since then. The failure of particulate trap technology for conventional diesel-burning engines helped to open the door for the market entry of natural gas bus engines.

Table 6 shows that the current generation of natural gas bus engines, typically the Cummins L-10 or the Detroit Diesel Series 50 engine, achieve emission rates far below even the 1998 nitrogen oxide standard. For particulate matter, only 0.03 grams per kilowatt-hour are emitted from natural gas engines, 60% below the current standard and $1/26^{th}$ of the emission rate typical of engines under the 1988 standard.

Urban bus emission certification procedures require the testing of stationary stand-alone engines. Emissions are determined while the engine is running on a test-bed in a laboratory according to the EPA-sanctioned, heavy-duty federal test procedure (HD-FTP). The engine is operated over a specific cycle of varying torque and rpm levels on an engine dynamometer. While this simplifies the comparison of emissions from different engines, it does not indicate the actual emissions that will occur when the engine is operating in mobile applications. Conversion factors have been developed to translate engine certification results into on-road emissions in terms of grams of pollution per kilometer traveled. The EPA-developed conversion factor, which attempts to predict on-road emissions for a bus traveling at 19 kilometers/hour (the average speed assumed for an urban bus) is 4.3.

Table 7 converts the 1998 federal bus standards for particulate matter into grams/kilometer and presents data from actual tests of several alternative fuel buses operating in the USA today (Cannon, 1997). The test data are preliminary and are taken from a survey of bus projects now being conducted by the author.

TABLE 7: PARTICULATE EMISSIONS FROM BUSES IN THE USA (grams/kilometer)

Technology	Emissions
Federal standard	0.14
Conventional natural gas bus	0.05
Hybrid-electric natural gas bus	0.01
Hydrogen buses (any mode)	0.00
Electric battery bus - national power mix	0.09
Electric battery bus - California power mix	0.04

Table 7 clearly shows the attractiveness of using either natural gas or hydrogen bus technologies in order to reduce particulate air pollution. Conventional natural gas buses (e.g. those using standard mechanical drive-trains) achieve startling low particulate emission rates, 0.05 grams per kilometer. This is nearly one-third of the federal standard and considerably lower than the emission rate of the diesel-burning engines now on the market. Using natural gas as the combustion fuel in hybrid-electric bus configurations reduces particulate emissions to a mere 0.01 grams per kilometer. Hydrogen buses, operating in the conventional combustion, hybrid-electric, or fuel cell modes emit virtually no particulate matter (there is some small oil blow-by combustion and nitrogen oxide emission from hydrogen combustion, but these levels are very low).

Interestingly, not only are natural gas and hydrogen buses cleaner than the federal standards or diesel-powered buses, they are also cleaner than battery-powered buses when the pollution emitted from the power station is factored in. Using the current mix of power generation in the USA today (which is 56% coal-fired), approximately 0.09 grams of particulate matter is emitted from the power plant while generating the electricity needed to propel a battery-equipped bus one kilometer (calculations from data in EPA, 1996 and EIA, 1996b). This is nearly twice the air pollution rate compared to a conventional natural gas bus. Assuming a cleaner power mix, for example the current mix in California which is only 30% coal-fired, particulate emissions from battery-equipped buses for the entire fuel cycle are still 0.04 grams per kilometer. This is several times the particulate emission rate from a natural gas-powered, hybrid-electric bus. Thus, natural gas and hydrogen buses are among the cleanest transportation machines ever built.

6. Conclusion

The urban bus market has emerged as the most successful point of entry for alternative transportation fuels and technologies in the USA. Natural gas is the clear leader among the alternative fuels now in use to power buses. Bus projects using advanced hydrogen technologies are also on the increase. The many synergies between natural gas and hydrogen suggest that hydrogen will continue to benefit from the current trends in the expanded use of alternative fuels in buses in the USA.

7. References

American Automotive Manufacturers Association (AAMA). (1996a) ***Facts & Figures 1995***. AAMA, Detroit, Michigan.

American Automotive Manufacturers Association (AAMA). (1996b) **World Motor Vehicle Data: 1996 Edition**. AAMA, Detroit, Michigan.

American Public Transit Association (APTA). (1996). ***Transit Passenger Vehicle Fleet Inventory: Editions 1992-1996.*** APTA, Washington DC.

Cannon, James S. (1989) ***Drive for Clean Air: Natural Gas and Methanol Vehicles***. INFORM, Inc., New York.

Cannon, James S. (1993) ***Paving the Way to Natural Gas Vehicles***. INFORM, Inc., New York.

Cannon, James S. (1995) ***Harnessing Hydrogen: The Key to Sustainable Transportation***. INFORM, Inc., New York.

Cannon, James S. (1997). ***Alternative Fuel Use in Buses (forthcoming report).*** INFORM, Inc., New York.

US Energy Information Administration (EIA). (1996a). ***Alternatives to Traditional Transportation Fuels: 1995***. U.S. Department of Energy, Washington DC.

US Energy Information Administration (EIA). (1996b) ***Annual Energy Review: 1995***. EIA, Washington DC.

U.S. Environmental Protection Agency (EPA). (1996) ***National Air Quality and Emissions Trends Report, 1995***. EPA, Washington DC.

NEW OPPORTUNITY FOR HYDROGEN FUELLED VEHICLES

T. Krepec and H. Hong
Centre for Industrial Control
Department of Mechanical Engineering
Concordia University
1455 de Maisonneuve Blvd. West
Montreal, Quebec, Canada H3G 1M8

1. Introduction

New opportunities are emerging for hydrogen fuelled vehicles in pursuit of more fuel efficient and not polluting hybrid electric vehicle (HEV). The concept of such vehicle became the main goal of the FutureCar project launched by the "Partnership for a New Generation of Vehicles" (PNGV) in America. Such car should have the fuel economy of 80 miles per US gallon what corresponds to European fuel consumption measure of 3 litre per 100 km. This is three times less than fuel consumption of a mid-size family car. So, in a FutureCar three times less hydrogen would be needed for the same operating range. Furthermore, an HEV must have also electric energy stored in batteries that will complement the hydrogen energy and a smaller gas tank would be sufficient. Finally, the hybrid hydrogen electric vehicle (HHEV) would be a zero emission vehicle (ZEV). Still, the realization of such vehicle, which would also provide the customer with the required performance, driveability and comfort, requires several advanced technological solutions, which are already emerging from the R&D work initiated by the PNGV.

2. Basic Assumptions for HHEV Energy Storage

Assuming that the energy required for travelling with an HHEV through a standardized 100 km driving cycle will correspond to the lower heating value obtained from the combustion of 3 litres of gasoline, the energy for the car propulsion will be equal to:

$$3\ \text{l}/100\ \text{km} \times 40{,}000\ \text{kJ/kg} \times 0.735\ \text{kg/l} = 88{,}000\ \text{kJ}/100\ \text{km}$$

that, in turn, corresponds to the mass of consumed hydrogen:

$$88{,}000\ \text{kJ}/100\ \text{km} : 120{,}000\ \text{kJ/kg} = 0.733\ \text{kg}/100\ \text{km}$$

T. O. Saetre (ed.), Hydrogen Power: Theoretical and Engineering Solutions, 37–42.

Then, to travel the distance of 300 km, 2.2 kg of hydrogen should be stored. However, assuming that the electric energy in batteries covers 33 % of the distance, the engine fuel efficiency is 40 % and the electric motor efficiency is 85 %, the following will be the energy required to be stored in the car:

66 % x 2.2 kg = 1.452 kg of hydrogen, and
33 % x 2.2 kg x 120,000 kJ/kg x 0.4 : 3,600 s/h x 0.85 = 11.4 kw
of electric energy.

Storage of such amount of hydrogen energy in a car remains still a challenge. Using aluminium cylinders reinforced by composite windings allowing for storage pressure of 300 bar, it requires a 93 litre compressed hydrogen tank weighting 45 kg [1]. It also requires a 125 kg advanced nickel metal hydride (NiMH) battery pack [2]. The two containers can be placed in a car as shown in Fig. 1 with the total vehicle weight increase of about 100 kg, compared to gasoline fuelled vehicle.

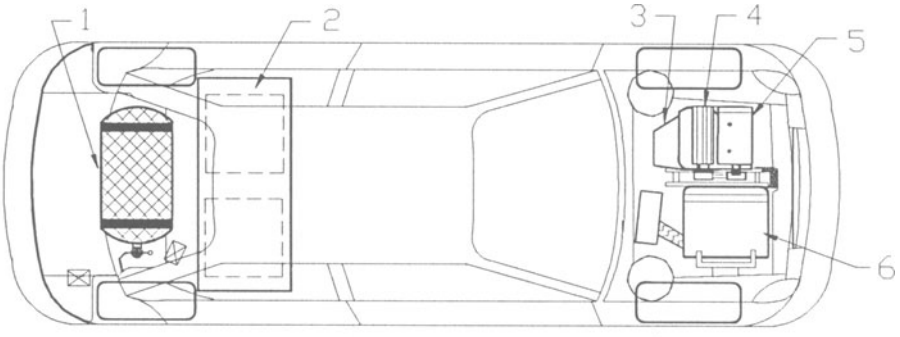

Figure 1. Schematic of the HHEV vehicle.

3. Diesel Powerplant Modification for Hydrogen Use

The recently emerging new generation of small high speed direct injected and turbocharged diesel engines offers a light (130 kg) powerplant with thermal efficiency of 40 %. It develops 60 kW at 4,200 RPM with 8,000 kJ/kWh specific energy consumption and a torque of 200 Nm in the speed range of 1,800 to 2,200 RPM. To run this engine on hydrogen, a novel gas injection system can be applied, which is discharging hydrogen directly into combustion chambers of the engine. Schematic in Fig. 2 is showing the common rail system with solenoid operated injectors in development at Concordia University for such type of diesel engines.

The tank is supplying the solenoid operated gas injectors with hydrogen at 100 bar pressure. The solenoids are installed inside the common rail for better cooling. They

are opening the injectors by moving the long rods to lift the needles of the nozzles, as per the required diesel injection timing.

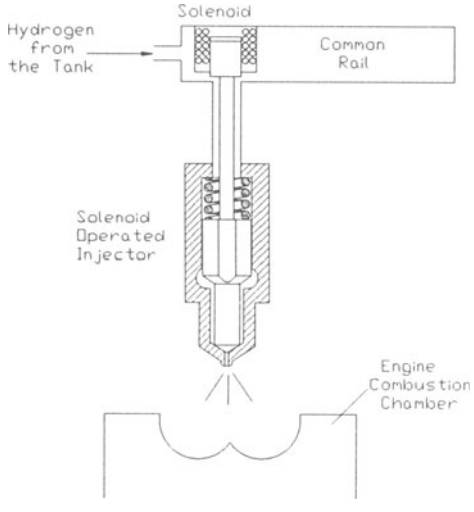

Figure 2. High pressure hydrogen injection system with solenoids installed in the common rail.

Regarding the electric powerplant, an AC 144 V Induction Permanent Magnet Electric Motor is initially chosen for the HHEV. It is combined with a controller that features smooth and powerful regenerative braking. It provides 20 kW maximum power and 58 Nm torque at 4,000 RPM and at a high efficiency of 97 %; however, in generator mode, the efficiency is 85 %. Total power of powerplants should provide HHEV with decent acceleration to 100 km/h in 15 sec.

4. Simulation of the HHEV Driving Cycles

For simulation purposes, the selection of a car had to be made to obtain all the vehicle data. A mid-size sedan shown schematically in Fig. 1, was chosen for the HHEV with following data: expected weight - 1850 kg, frontal area - 2.5 m^2, rolling resistance coefficient - 0.012, drag coefficient - 0.30.

Two different cycles have been selected: on city street and on intercity road. Each has three modes of operation: acceleration, steady speed and deceleration. They have the following features:

1) City Street Cycle; distance between lights - 1 km; maximum speed - 60 km/h, and
2) Intercity Road Cycle: distance between lights - 2 km; maximum speed - 100 km/h.

In both cycles, the engine is shut-off at the beginning of deceleration and next restarted at the beginning of acceleration. Fig. 3 shows the results of HHEV simulation for the 2 km cycle and different modes of operation. The results are tabulated in Table 1.

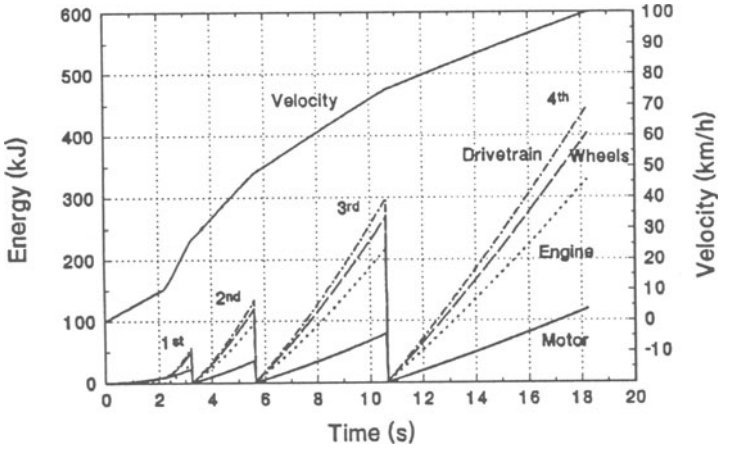

Figure 3a. Economy Mode: accumulated energy consumption during acceleration to 100 km/h.

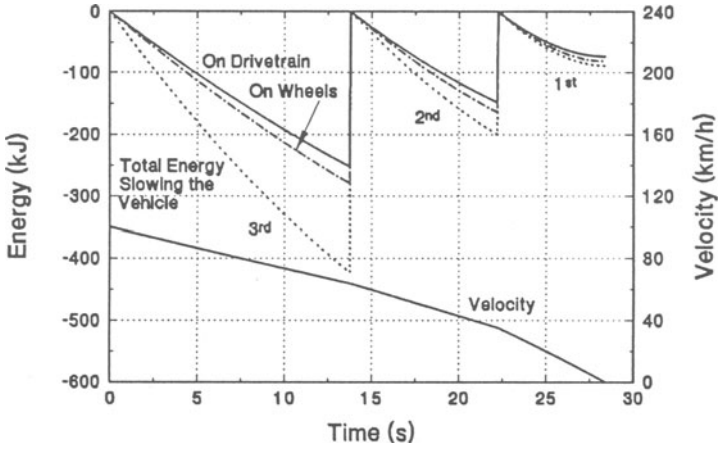

Figure 3b. Economy & Performance Mode: energy regeneration during deceleration from 100 km/h.

5. Re-evaluation of the HHEV Components After Simulation Analysis

The simulation results for the vehicle deceleration mode shown in Fig. 3b, have been drawn based on the expected capacity of two components deciding about the energy recuperation rate: the electric motor/generator and the battery pack. During deceleration, the vehicle kinetic energy decrease has to be converted by the electric generator from the mechanical energy to the electrical one, which in turn should be stored in the battery at the same rate; three questions arise:

1) is the generator capacity high enough to convert the full car kinetic energy change

to electricity ?,

2) is the battery pack large enough (at low enough state of charge) to absorb all the electric current produced by the generator ?,
3) what is the shortest deceleration distance (not using brakes) during which the full kinetic energy should be recuperated ?

TABLE 1. Performance and Economy mode simulation results.

MODE		PERFORMANCE	ECONOMY	
		100 km/h	100 km/h	60 km/h
ACCEL.	Time (s)	14.4	18.2	7.8
	Distance (km)	0.2273	0.3036	0.0658
	Fuel (l/100 km)	21.9	16.2	23.8
	from Batteries (kJ)	259.3	269.6	94.5
STEADY STATE	Time (s)	47.3	44.5	48.4
	Distance (km)	1.3133	1.2370	0.8061
	Fuel (l/100 km)	4.1		2.4
DECEL.	Time (s)	28.4		13.5
	Distance (km)	0.4594		0.1281
	to Batteries (kJ)	380.3		159.0
TOTAL	Time (s)	90.1	91.1	69.7
	Distance (km)	2.0		1.0
	Fuel (l/100 km)	5.2	5.0	3.53

To answer these questions, following analysis has to be made:

- From simulation (Table 1), the deceleration distance is 500 m, assuming the electric generator efficiency of 85 %.
- For average cars at 100 km/h, the shortest braking distance is about 100 m. However, it would not be practical to use very large motor/generator only to reduce the deceleration distance to equal the minimum braking distance; emergency braking happens very seldom and then, brakes still can be used.
- A 250 m shortest deceleration distance could be a good compromise and to achieve it, a twice more powerful 40 kW motor/generator could be used. Then, the max generated current, that should be absorbed by the battery pack at 144 V, would be 222 A.
- Regarding the battery pack charged to 75 %, the current in amperes which could be

absorbed by the 11.4 kWh battery pack was found to be about 20 times the capacity in kWh, i.e. 228 A. This is higher than 222 A current provided by the 40 kW motor/generator.

From the above analysis, it is clear that the proposed battery pack is sufficient; however, the electric motor/generator should be twice more powerful to convert the full kinetic energy to current.

6. Conclusions and Recommendations

The presented case study is showing that with recent developments in automotive technology, the concept of a hydrogen hybrid electric vehicle with a range of 300 km is feasible. To extend this range, more progress must be made in the batteries and in the gas tanks, as well as in automobile materials and structure to lower the weight of the vehicle.

Regarding a possible commercialization of HHEV, the greatest obstacles are: the cost of the fuel, the refuelling infrastructure and the public acceptance of hydrogen as the fuel for cars, taking into account some negative perception related to the past history of accidents with hydrogen. Still, the deciding factor in the acceptance of HHEV's might be the society's desire for zero emission vehicles supported by subsidies towards ZEV's from higher taxation of gasoline.

One more aspect of hydrogen car should be discussed here. It is the recently unveiled by Chrysler new fuel cell car supplied with gasoline which is scheduled for production in 2005. While it is a step in the right direction, several doubts remain:

1) it will be an LEV not a ZEV,
2) it will produce CO_2, contributing to greenhouse effect,
3) it will use a not renewable energy source,

and as such it can be considered only as a mid-solution to the environmental and energy crisis.

7. Acknowledgements

The authors are thankful to Natural Sciences and Engineering Research Council, as well as to Natural Resources Canada (CANMET) for financial support of this research.

8. References

1. DeLuchi, M.A.: Hydrogen Vehicles: an Evaluation of Fuel Storage, Performance, Safety, Environmental Impacts and Cost, *Int. J. Hydrogen Energy* **14** (1989), 81-130.
2. Ovshinsky, S.R., Fetcenko, M.A., and Ross, J.: A Nickel Metal Hydride Battery for Electric Vehicles, *Science* **260** (1993), 176-181.
3. Nikopoulos, A., Hong, H., and Krepec, T.: Energy Consumption Study for a Hybrid Electric Vehicle, SAE Paper No. 970198.

Methanol/Methyl formate Couple as a Hydrogen Storage and Carrier

K. D. Chung, M. S. Lee, O. S. Joo, S. H. Han*, S. J. Uhm
Korea Institute of Science and Technology
CheongRyang P.O. Box 131, Seoul, Korea
Fax: +822-958-5212, email: hansungh@kistmail.kist.re.kr

Introduction

Hydrogen storage has been a key issue to utilize hydrogen as a next generation energy source(1). The difficulties of hydrogen storage and transportation have limited its applications. The metal hydride and liquid hydrogen have been mainly discussed as targeting systems (2,3). Chemical hydrogen storage was regarded as a good candidate in terms of economical point of view(4). Hydrogenation of nitrogen and carbon dioxide to form ammonia and methanol, respectively, were considered for this purpose (eq. 1, 2). Those are hydrogen storage methods in molecular level, which can store large amounts of hydrogen in weight (NH_3: 17.64w% CH_3OH: 18.75w%).

$$N_2 + 3H_2 \quad <------> \quad 2NH_3 \qquad \text{(eq. 1)}$$

$$CO_2 + 3H_2 \quad <-------> \quad CH_3OH + H_2O \qquad \text{(eq. 2)}$$

However, N_2, NH_3 and CO_2 are gases at STP condition, which is a drawback for storage and transportation. Now we suggest a new chemical hydrogen storage system based on methanol and methyl formate couple which are liquid form at STP conditions (eq. 3). The another advantage of above reaction is that hydrogen can be easily separated from reaction mixture. The coupling of these two reactions makes it possible to store 6.25 w% hydrogen in total weight of methanol.

$$2\,CH_3OH \quad <-----> \quad CH_3OCOH + 2\,H_2 \qquad \text{(eq. 3)}$$

There have been efforts to develop catalytic system for the forward reaction because methyl formate is a good precursor to produce carbon monoxide. The development of methanol dehydrogenation process has not been successful due to the poor durability and selectivity of copper containing catalysts. The reverse reaction to synthesize methanol from the hydrogenation of methyl formate was relatively well understood. Herein we have investigated the deactivation mechanism of copper containing catalysts and developed a stable catalytic system for dehydrogenation of methanol to form methyl formate.

T. O. Saetre (ed.), Hydrogen Power: Theoretical and Engineering Solutions, 43–48.

Experiments

Copper containing catalysts were prepared by coprecipitation of metal acetates at pH 7. The precipitate was washed, filtered, dried in a vacuum oven and calcined at 723 K for 16 h. The composition of the resulting catalyst was 47.1 : 52.9 (CuO:ZnO in weight ratio) by Atomic Absorption Spectroscopy (Perkin-Elmer Co., 3030B AAS). The atomic ratio of Cu:Zn:M_2O_3 (M=Al. Cr) was 1:1:1. B.E.T.(Micromeritics Co., ASAP 2000) surface area of CuO/ZnO catalyst was 22.16 m^2/g, and copper surface area was 5.02 m^2/g by N_2O titration.

Methanol dehydrogenation was conducted in a stainless steel reactor (1/4" O.D. x 20 cm length, 200 mg catalyst) under the reaction conditions of temperature of 493 K, 513 K and 543 K and GHSV of methanol 3000 mL (S.T.P)/gcat.h. Methanol was introduced by passing helium carrier gas through a thermostated methanol saturator. Concentrations of reactants and products were analyzed by an on-line G.C. (T.C.D. detector, porapak Q column, 1/8" O.D. x 10 ft length). The conversion of methanol and the selectivity to methylformate were calculated based on carbon number. The catalyst was reduced in situ at 573 K for 3 h by 5 % H_2 in Ar (60 mL/min). The reactor was purged with helium until Ar was no longer detected from the purged gas, then, methanol in helium carrier gas was introduced into the reactor.

The weight change of ZnO in Cu/ZnO catalyst during methanol dehydrogenation was measured by a microbalance (Chan 2000). Catalysts of 60 mg were loaded on a sample pan and reduced in situ at 623 K for 1h by 5 % H_2 in Ar (120 mL/min). Methanol was introduced at 523 K as described above (9.2 % methanol in helium, total flow 120 mL/min). Temperature - programmed reduction (TPR) of CuO/ZnO was performed in the flow of mixture gas of helium-methanol with programmed heating up to 673 K at the heating rate of 10 K/min.

X-ray powder diffractograms (XRD) were recorded using CuKα target to examine the structure of oxide samples. Samples were packed in a cell and inserted into a sample holder.

Results and Discussion

Methanol dehydrogenation to form methyl formate over Cu/ZnO catalyst:

A typical copper containing catalyst, Cu/ZnO, was tested for the methanol dehydrogenation reaction. The concentration of methanol in feed gas was adjusted to 15 % with total flow of 67 mL/min. Conversion of methanol, 45 % at 15 min, became 15 % after 45 min at 513 K (Fig. 1). The catalyst was steadily deactivated over 20 h. The reactions at different temperature of 543 K and 493 K also showed severe deactivation within 1 h. The deactivation patterns at different temperatures were similar to each other. The selectivity to methyl formate of Cu/ZnO catalyst was about 92 % at 493 K, and lowered as temperature increased. The low selectivity to methyl formate at high temperature could be attributed to the secondary reaction of the decomposition of methyl formate into methanol and CO. The selectivity slightly increased with reaction time.

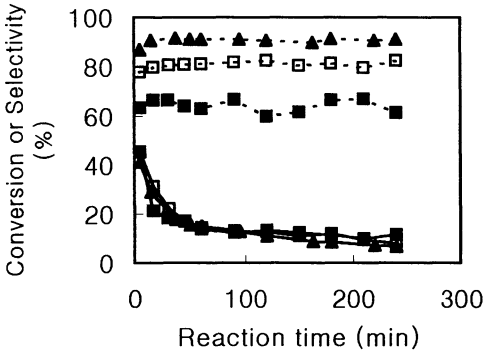

Figure 1. Deactivation of Cu/ZnO catalyst in methanol dehydrogenation at 493K (▲), 523K (□) and 543K (■): (—) conversion of methanol, (.....) selectivity to methyl formate.

Reduction of ZnO with methanol:

The reducibility of ZnO in Cu/ZnO catalyst with methanol was investigated with a microbalance. The catalyst was prereduced in situ to reduce CuO to metallic copper and purged with helium after cooling down to 523 K. As shown in Figure 2, the catalyst weight steadily decreased during the reaction with methanol at 523 K, indicating the removal of oxygen from ZnO in Cu/ZnO. After 4 h, 0.9 wt % oxygen in ZnO was depleted, equivalent to the reduction of 4.4 % ZnO. The surface to bulk atomic ratio of ZnO was calculated to be 0.034. This result meant that surface ZnO was reduced from the reaction with methanol. The weight increase at beginning of the reaction was attributed to the adsorption of methanol onto the catalyst surface.

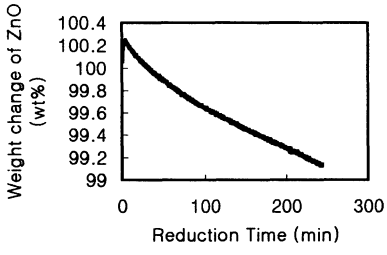

Figure 2. Weight loss of ZnO in Cu/ZnO catalyst from the reaction with methanol at 523 K after the reduction at 623 K for 1 h by 5 % H_2/Ar.

formation of spinel structure and its catalytic activity:

Thermally stable catalysts are required to improve the life time of copper containing catalysts during methanol dehydrogenation, based on above results. Catalyst with

hydrotalcite structure, which is well known to be thermally stable, were prepared at pH 9 by coprecipitation(5). The coprecipitation temperature and aging time effects on the structure and activity of catalyst were investigated. $Cu/ZnO/Cr_2O_3$ and $Cu/ZnO/Al_2O_3$ were prepared as follow: 1) 12 h aging time at room temperature (CRRT12 for $Cu/ZnO/Cr_2O_3$ and AlRT12 for $Cu/ZnO/Al_2O_3$), 2) 2 h aging time at room temperature (CRRT2 for $Cu/ZnO/Cr_2O_3$ and AlRT2 for $Cu/ZnO/Al_2O_3$), 3) 12 hr aging time at 353 K (CR8012 and Al8012). Methanol dehydrogenation reactions were conducted under the reaction conditions of 493 K and 3000 mL (S.T.P.)/gcat.h on the catalysts described above.

Fig 3 showed catalyst performances with the reaction time on $Cu/ZnO/Cr_2O_3$ catalysts. With the addition of Cr, catalysts durability was much improved. In all three cases, the conversion and selectivity did not changed significantly upto 350 min. CR8012 catalysts was very stable and highest in activity. The conversion of methanol on CR8012 catalyst rather increased from 46 % at 15 min to 50 % at 4 hr, but the selectivity was near 40 %. Meanwhile CRRT2 catalyst showed the highest selectivity and the lowest conversion among those three $Cu/ZnO/Cr_2O_3$ Catalysts. The experimental results showed that the durability were improved by the addition of Cr component in Cu/ZnO system, and the conversion and selectivity of $Cu/ZnO/Cr_2O_3$ catalysts were dependent on the precipitation temperature and aging time. The high temperature and long aging time improved catalysts activities.

Another well known hydrotalcite structure compound, $Cu/ZnO/Al_2O_3$ catalysts were compared for the dehydrogenation of methanol (Fig. 4). The durability of $Cu/ZnO/Al_2O_3$ catalysts were improved than that of Cu/ZnO.

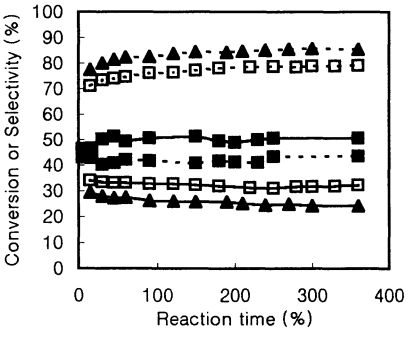

Figure 3. Methanol dehydrogenation at 493 K on $Cu/ZnO/Cr_2O_3$ catalyst prepared at pH 9: (▲) CRRT02, (□) CRRT12, (■) CR8012: (—) conversion of methanol, (....)selectivity to Methyl formate

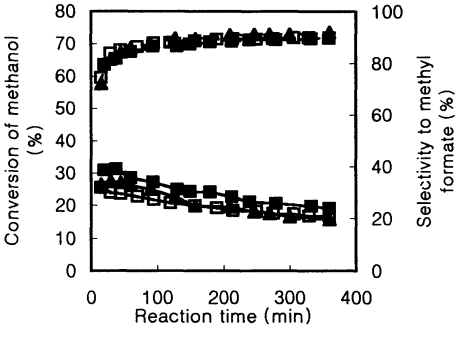

Figure 4. Methanol dehydrogenation at 493 K on $Cu/ZnO/Al_2O_3$ catalyst prepared at pH9: (▲) AlRT02, (□) AlRT12, (■) Al8012: (—) conversion of methanol, (....) selectivity to methyl formate.

However, instead of the similar spinel structure as $Cu/ZnO/Cr_2O_3$, $Cu/ZnO/Al_2O_3$ slowly deactivated as the reaction proceeded. The conversion of methanol on AlRT12

catalyst, which showed the highest activity among three samples, decreased from 31 % to 21 % after 4 hr with about 90 % selectivity to methyl formate. Both AlRT2 and Al8012 catalyst demonstrated the similar conversion and selectivity as AlRT12. It indicated that precipitation temperature and aging time did not much effect on the stability and the activity of $Cu/ZnO/Al_2O_3$ as did for $Cu/ZnO/Cr_2O_3$ catalysts.

XRD experiments for $CuO/ZnO/Cr_2O_3$ and $CuO/ZnO/Al_2O_3$ catalysts:

To understand the relationship between the structure and the activity of the catalysts, XRD studies were conducted. Fig. 5 and Fig. 6 showed the diffractograms of $CuO/ZnO/Cr_2O_3$ and $CuO/ZnO/Al_2O_3$ catalysts respecitively. Peaks at 30, 35 (main peaks), 43, 54, 57, and 63 degrees were the characteristic peaks of $CuCr_2O_3$ and $ZnCr_2O_3$ spinel structure (Fig. 5). CR8012 sample showed that aging at 353 K accelerated the formation of spinel sturcture. On the other hand, CRRT02 and CRRT12 shows ZnO peak of 32 degree and CuO peak of 39 degree with poor spinel structure. Different from $Cu/ZnO/Cr_2O_3$ XRD structure, three samples of $CuO/ZnO/Al_2O_3$ showed that the spinel structure was poorly developed with amorphous structure. Also the aging condition has little effects on the formation of spinel structure in preparation of $Cu/ZnO/Al_2O_3$ catalyst. Above experimental results indicated that the performance of catalyst could be correlated with the structure of the catalysts. Catalysts with spinel structure demonstrated high stability and high activity, while the catalyst with distinctive structure of CuO and ZnO showed low stability and low activity.

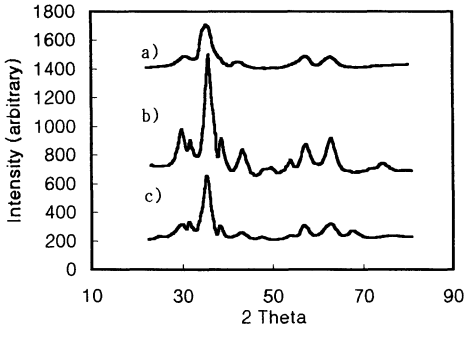

Figure 5. X-ray diffractogram of $Cu/ZnO/Cr_2O_3$oxide prepared at pH 9: a) CR8012, b) CRRT12,c) CRRT02.

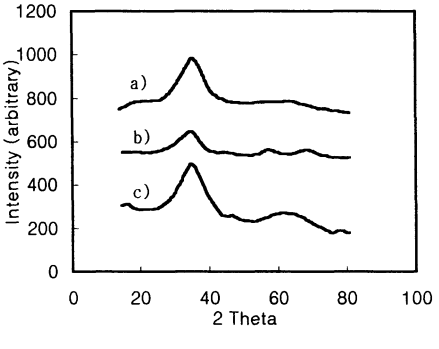

Figure 6. X-ray diffractogram of $Cu/ZnO/Al_2O_3$ Prepared at pH 9: a) Al8012, b)AlRT12, c)AlRT12.

Summary

Cu/ZnO based catalysts have been known to be good candidates for this reaction couple, but suffered from severe deactivation. It was shown that the reason of deactivation of Cu/ZnO catalyst was the reduction of ZnO in the vicinity of copper

during methanol dehydrogenation. Therefore, it was needed to modify Cu/ZnO catalysts for improving the stability of the catalysts without changing activity of methanol dehydrogenation. $CuO/ZnO/Cr_2O_3$ catalyst from precusor with hydrotalcite-like structure showed high durability in methanol dehydrogenation. The foramtion of spinel structure of zinc chromium oxide and copper chromium oxide was an essential part of the catalyst durability and promoted by the aging catalysts at high temperature.

References

1. Uehara, I., Tenth Anniversary Conference of Hydrogen Industry Counsel, Calgary, Canada, 1992
2. Hagstrom, M. T., Lund, P. D., and Vanhanen, J. P., Int. J. Hydrogen Energy 20 (1995) 897.
3. Tachtler J. and Szyszka A., Int. J. Hydrogen Energy, 19 (1994) 377.
4. Kliman, M. L. Energy, 8 (1983) 859.
5. Cavani F., Trifiro F. and Vacarri A., Catal. Today, 11 (1991) 173.

INVESTIGATION OF MIXTURE FORMATION AND COMBUSTION PROZESSES IN A HYDROGEN FUELED DIESEL ENGINE

F. DORER, P. PRECHTL, F. MAYINGER
Lehrstuhl A für Thermodynamik
Technical University München
D-85747 Garching
Germany

1. Introduction

In cooperation of two chairs of the Technical University of Munich and MAN B&W AG as the industrial client a direct-injecting hydrogen Diesel engine with high efficiency and low emissions is being developed. The investigation is founded from the Bavarian Research Foundation and concerns the conversion from diesel fuel to hydrogen of a four stroke C.I. engine with stationary 900 rpm. The piston displacement is approx. 14 l per cylinder. The problem of this research to be confronted with is to develop a hydrogen engine with direct injection and compression ignition, which has not been realized yet. The chair A for Thermodynamics investigates and optimizes the mixing and combustion processes with laser optical measurements in stationary and non stationary setups. The engine behavior investigations are done on a single cylinder test engine at the chair for combustion engines of the Technical University Munich.

2. Experimental Setups

The mixture formation, the ignition and burning processes are investigated in two different experimental setups. The aim of the first experimental setup is to get information about the highly transient concentration distribution of hydrogen during the injection process. The experimental techniques used are an application of Laser-Induced Fluorescence (LIF) on tracer molecules and the Schlieren/Schatten method. The first setup is a combustion chamber (VVK) with equivalent dimensions to the planned ship C.I. engine, that is diameter of 240 mm and a volume which represents the volume in the cylinder at top dead center (Figure 1.). This chamber has a maximum of five windows, one at the bottom and four around the diameter, to give an optimal optical access for laser measurements. The pressurized hydrogen is injected into the cold compressed air through a hydraulic controlled needle valve. The experiments done with this setup leads to an optimization of the injection system, that is the number and position of the injection holes and also the injection direction.

T. O. Saetre (ed.), Hydrogen Power: Theoretical and Engineering Solutions, 49–54.

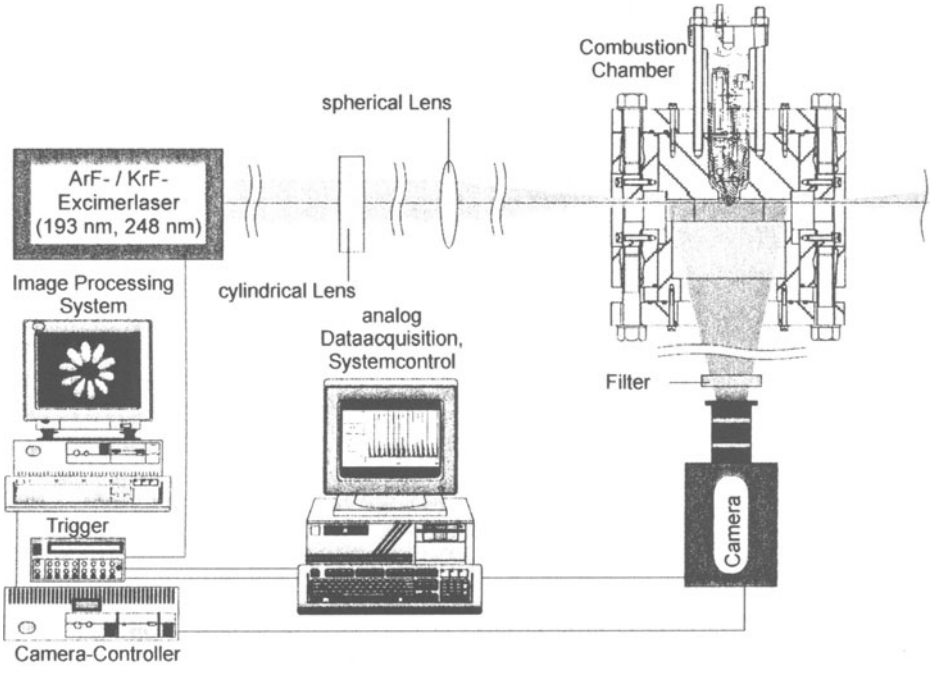

Figure 1.: Experimental setup for LIF measurements in the combustion chamber

The second setup is a single stroke rapid compression machine (EET) (Figure 2.) which simulates the compression stroke of the planned ship C.I. engine. It has an optical accessible combustion chamber and an moving piston with a quartz window. The machine has balanced masses, and allows the observation of the compression stroke with realistic piston velocities with sensitive optical measurement techniques. It has a cylinder capacity of 14 l, a compression end pressure up to 150 bar and a maximum combustion pressure up to 200 bar. The design of this setup allows a fast variation of experimental parameters, which means any compression ratios up to 25 can be adjusted. Swirl and turbulence in the combustion chamber can be induced through tangential inlets. Simple variation of experimental parameters like boost pressure, compression ratio, injection time, injection duration and nozzle geometry allow fast and effective examination of various boundary conditions.

The apparatus shown in figure 2 consists of two concentric pistons (piston 1 and 2) which are coupled through slots via hydraulic oil. The compression piston with the glass window is fixed to the piston 2. In the starting position the inner piston (piston 2) closes the connecting slots, which means both pistons are independent of each other. After opening a bypass valve the outer piston (piston 1), which is driven by compressed air, pushes the compression piston slowly into the combustion chamber. At the same time opens the inner piston the slots connecting both pistons, which leads to an acceleration of both pistons. Meanwhile compresses the compression piston with an speed up to 10 m/s the near the top dead center hydrogen is injected with 300 bar into this hot environment which leads to auto-ignition. The combustion will be observed by

conventional measurement techniques and also with self fluorescence imaging with a high speed video camera, LIF and the Schlieren/Schatten method.

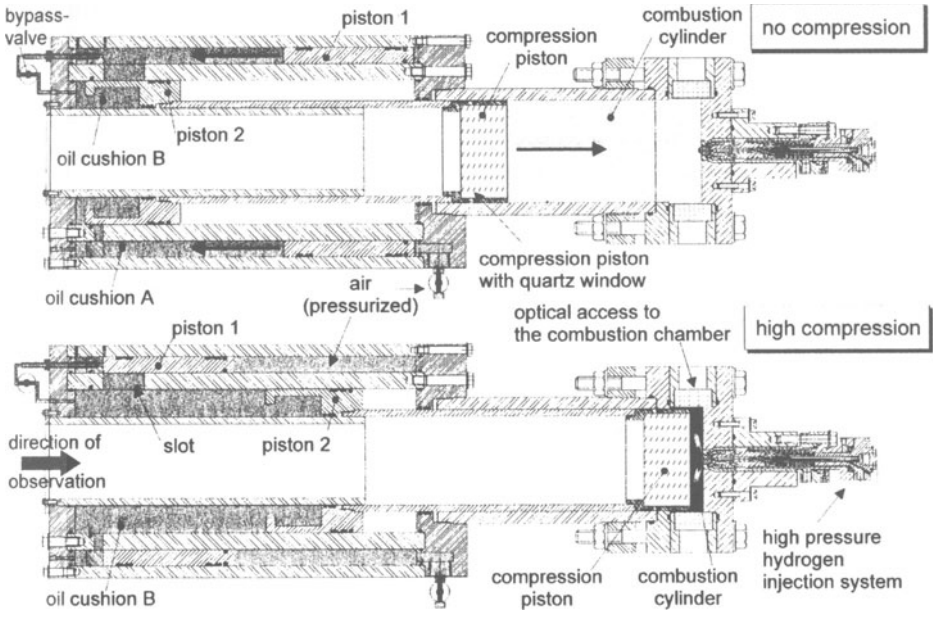

Figure 2.: Single stroke hydrogen rapid compression machine working according to Diesel's process

3. Experimental Data

The characteristics of using hydrogen instead of diesel oil or heavy oil as a fuel for large diesel engines have to be taken into consideration for adapting a combustion concept. The difference of hydrogen compared with conventional hydrocarbons lays in its wide limits of inflammability from 4 to 75 percent of volume hydrogen in air. The burning velocity of hydrogen can rise under adequate conditions to some hundred meter per second. These characteristics can be used to burn lean mixtures with low NO_x emissions nevertheless gaining a high efficiency. These properties can however lead to unwanted hard combustion or even to detonation. The fundamental knowledge of the influence of temperature, pressure, turbulence, gas composition and flow conditions is important to develop a gentle, effective and reliable combustion process.

3.1. MIXTURE FORMATION

Measurements to visualize the mixture formation of hydrogen in the combustion chamber are done in the first setup with laser induced fluorescence (LIF) on tracer molecules. These tracer molecules are unsaturated carbon bindings, which have a good cross section for excitation. This laser optical measurement technique is one of the modern contactless investigation method for gas flows. A pulsed KrF Excimer laser emits a laser beam with a wavelength of 248 nm. This laser beam is focused with a lens

setup to a small lightsheet, which travels radial through the combustion chamber. The molecules in the lightsheet layer will be excited and emit light in all directions. A intensified CCD-camera records the emitted light through the window in the bottom of the combustion chamber. This measurement technique is very capable to visualize an unburned gas mixing process and gives a quantitative image of the mixing and the concentration distribution in a combustion chamber (Figure 3.).

The experiments in the first setup leads to an optimization of the injection system, i.e. the number and position of the injection holes and the injection direction as well. Figure 3. shows the LIF images of an high pressure hydrogen injection (300 bar) into cold pressurized air (100 bar) through a hydraulic controlled needle valve with a ten hole nozzle.

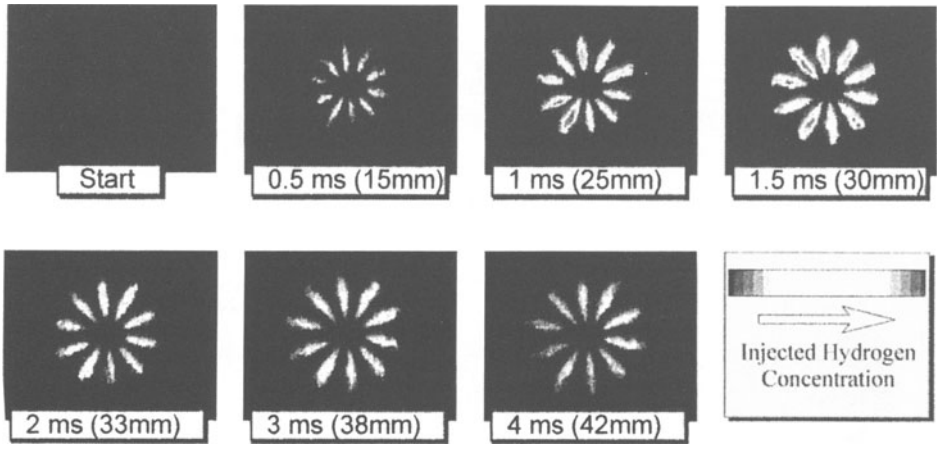

Figure 3.: Hydrogen distribution during injection visualized through LIF

3.2. COMBUSTION MEASUREMENTS

The experiments in the first setup also lead to information about the timing of the injection and the fuel mixture formation. These results were used in the experiments done in the second setup, the single stroke rapid compression machine. The effects of the mixture formation on the self ignition behavior and the combustion progress were investigated with laser optical measurements and high speed self fluorescence imaging. The injection is trigged on the piston stroke, so various points of injection around T.D.C. can be achieved. The injection system is a electronically triggered hydraulic controlled needle valve, injecting 300 bar hydrogen into the combustion chamber. It can easily be equipped with various types of nozzles, i.e. with different types and numbers of nozzles.

Figure 4. shows a characteristic combustion process with late internal mixture formation near the T.D.C. and compression ignition. The images taken with a frame rate of 13500 Hz show, that the ignition starts right after the beginning of the injection. The flame burns deflagrative along the injection jets during the hole injection duration. The

ignition delay time is short and the combustion chamber pressure rises moderately to a tolerably maximum.

Injecting hydrogen before the top dead center forms a good mixture but the combustion is detonative with maximum pressures in the combustion chamber up to several hundred bars.

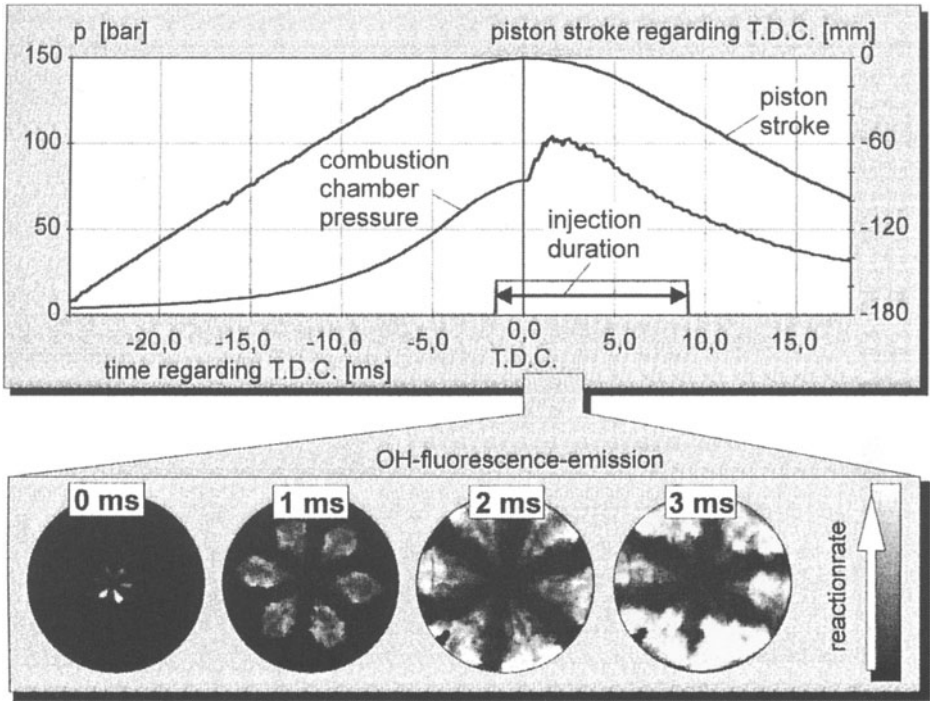

Figure 4.: Hydrogen injection near T.D.C., deflagrative combustion visualized with self fluorescence

3.3. NUMERICAL SIMULATIONS

Three dimensional numerical flow simulations with the code TASCflow from ASC are done complementary to the experimental investigations. These simulation allow a variation of different or additional parameters, which could not been easily adapted in the experiments. One of these parameters is the shape of the piston. In the experimental setups, only flat pistons are in use to allow optical access in direction of the stroke. Figure 5. shows a grid of a piece of the combustion chamber with an omega trough piston and a part of the injection nozzle with one hole. This grid has approx. 150 000 volume elements. A powerful HP workstation needs CPU time of approx. 500 hours to calculate 10 ms of simulation time of this very fine mesh. Also simulations with different kinds of swirl, different nozzle layouts and a variation of the boundary conditions have been calculated to gain information of the mixture formation and the temperature distribution. The analysis of the ignition delay has been implemented in the flow simulation with a zero dimensional simulation of the reaction kinetics, this is a

code developed from J. Warnatz. This program calculates the ignition delay dependent on the temperature and concentration of hydrogen in air at a given pressure. This method allows the definition of areas of the injection jet where self ignition conditions are present. These simulation gain information to develop an optimized injection system at given compression ratios of engines which will be converted from diesel fuel to hydrogen.

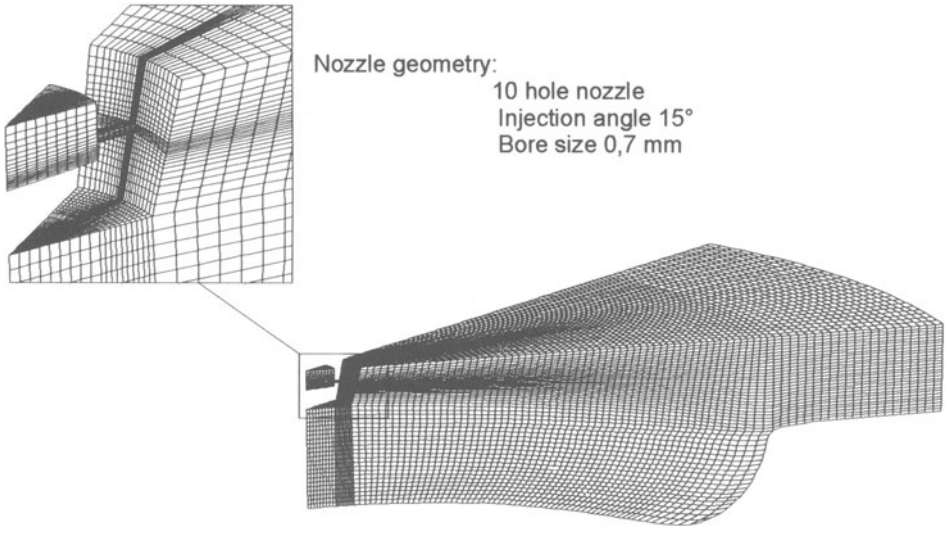

Figure 5.: Discrete geometry of the combustion chamber with utilization the rotational geometry

4. Conclusions

The developed experimental setups and the numerical simulations allow a detailed analysis of the mixture formation and of the combustion processes in a combustion ignition engine. With the experimental setups comparisons of different combustion concepts can be carried out. The results give immediate references for the improvement of nozzle layouts and combustion parameters. The experiments also show that the compression ignition with direct injection of hydrogen can be reached. The ignition delay depends on the compression ratio. With higher compression ratio a proof ignition can be realized. An injection of hydrogen near T.D.C. should be reached to avoid a good hydrogen-air mixture before the temperature for self ignition has arrived. If this can not be achieved, a hard combustion or detonation will be the result.

5. References

Eckbreth A.C. (1988) *Laser Diagnostics for Combustion Temperature and Species*, Abacus Press

Maas U. and Warnatz J. (1988) Ignition Processes in Hydrogen-Oxygen Mixtures, *Combustion and Flame* **74**, 53-69

Stephan K. and Mayinger F. (1986) *Thermodynamik*, 12. edition, Springer, Berlin

Warnatz J. and Maas U. (1993) *Technische Verbrennung*, Springer, Berlin

HYDROGEN AS AN ADDITIVE TO METHANE FOR SPARK IGNITION ENGINE APPLICATIONS

S. O. BADE SHRESTHA AND G. A. KARIM
The University of Calgary
Dept. Of Mechanical Engineering
2500 University Drive N. W.
Calgary, Canada, T2N 1N4

Abstract

It is shown that the performance of a gas fuelled spark ignition engine can be enhanced considerably when relatively small amounts of hydrogen are present with methane. This improvement in performance which is especially pronounced at operational equivalence ratios that are much leaner than the stoichiometric value, can be attributed largely to the faster and cleaner burning characteristics of hydrogen in comparison to methane. Through analytical simulation of engine performance, the addition of hydrogen is considered through its production in-situ on board the engine by electrolysis of water with the necessary energy supplied from engine power. It is shown that when the work energy required for the production of hydrogen by electrolysis is taken into account, the range of viable operation of such an engine is very narrow. This would render the whole concept of in situ hydrogen production through water electrolysis uneconomical in conjunction with engine operation, even though the presence of additional oxygen produced with the hydrogen tends, in principle, to improve engine performance beyond that observed with hydrogen addition in air.

1. Introduction

The recent ever increasing interest in operating internal combustion engines on alternative gaseous fuels has been motivated largely by the demanding regulations for cleaner exhaust emissions combined with improvements in efficiency. This is supported by the relatively cheaper cost of gaseous fuels and their abundant availability in comparison to conventional liquid fuels [1]. Moreover, the operation of engines on gaseous fuels such as natural gas, containing mostly methane, has distinct potential economic and operational benefits while retaining excellence in reliability and durability [e. g. 2].

The operation of engines on lean fuel mixtures has a number of positive features. It can, in principle, provide high thermal efficiency, low likelihood for knock, reduced emissions especially NOx and permit using higher compression ratios while reducing heat

T. O. Saetre (ed.), Hydrogen Power: Theoretical and Engineering Solutions, 55–61.

transfer. It may permit dispensing with exhaust catalytic treatment and the need for precise control of the mixture quality as usually the case with stoichiometric operation. However, there are a number of difficulties which arise primarily from the associated slower flame propagation, less complete combustion, increased cyclic variations and even the occasional flame failure. These account for the poor engine power output and excessive emissions that may be encountered with lean operation [3].

An important difficulty in the operation of engines, whether of the spark ignition or compression ignition types, on lean mixtures of methane and air is the associated low flame propagation and combustion rates. Some improvement to the burning rate in spark ignition engines is usually obtained through measures such as the employment of optimum spark timing, improved chamber design and increased turbulence. The extent of increase in the level of turbulence in engines is usually limited and there are penalties associated with the use of excessive turbulence that include excessive heat transfer and higher peak temperature and hence higher NOx emissions in optimum chamber geometry. Hence, there is a need to enhance the combustion process without bringing about some of these disadvantages. One approach is through the addition to the methane of a small amount of hydrogen, a fuel having a much cleaner and faster rates of burning than methane. The contribution of the hydrogen addition to increased preignition reaction activity is usually relatively small. This procedure is especially attractive since, due to economic and technical reasons, the operation of engines on pure hydrogen fuel remains largely a long term proposition. On the other hand, the use of hydrogen as an additive to methane, especially for engine applications, may be an attractive solution, both at present and in the near future for a reduction of the effects of some of the operational problems associated with engines fuelled with methane.

The current contribution demonstrates how the addition of some hydrogen to the methane produces notable improvements to spark ignition engine performance in comparison to when methane only is involved. It is shown while employing analytical modelling approaches that if the energy required for the production of the needed hydrogen in situ by an electrolysis process of water, the viable range of operation of such an engine becomes considerably narrowed and economically unattractive.

2. The Model

A two zone model developed to predict the performance of a gas fuelled spark ignition engine was shown by Karim et al [4,5] to be capable also of predicting the onset of knock and its intensity. In this model, the homogeneous charge of the cylinder is assumed to be divided into two zones: burned products and unburned reactants that comprise the end gas region.

An appropriate combustion energy release patten [4] is employed. This is based on formulations obtained following examination of a large number of experimental data for a variety of operating conditions. Several types of functions have been considered for such energy release in the literature [e. g. 12] such as triangular, sine or Wiebe functions. A triangular type function was adopted in the present modelling approach. The combustion energy release would take place over a certain combustion duration that would start just

beyond the spark ignition timing after an ignition lag period when a significant amount of energy begins to be released due to flame kernel development and would end as a result of the end of flame propagation. A formulation for the combustion period variations with operating conditions based on the mass of experimental data obtained with methane as well as methane-hydrogen mixtures as fuels [4,5,13] was developed. The area enclosed by the resulting energy release diagram whose base is the combustion duration would represent the known total effective energy released by combustion. This approach was shown to give good account of engine pressure temporal development and hence performance, that is in good agreement with experiment. It avoids the prediction of the detailed features of turbulent flame propagation which remain at present of questionable practical value due to their complexity and uncertainty [10,11].

The reactivity of the end gas region of the charge is evaluated throughout employing detailed reaction rates. The formation and growth of the associated reactive species are considered together with the energetic consequences of such reactions [4,5]. A reaction scheme of some 150 steps and 39 species [8,9] was developed. It considers the kinetics of combustion of gaseous fuel mixtures containing methane in air together with common gaseous fuels such as propane, ethylene, ethane, hydrogen and carbon monoxide and the diluents carbon dioxide, nitrogen and water vapour.

A knock criterion or parameter, K, was developed based on the variations with time of the calculated accumulated amount of energy released within the end gas due to the preignition reactions per unit of the instantaneous cylinder volume, relative to the total energy released normally through flame propagation over the whole cycle per unit of cylinder swept volume [4,17]. As the preignition reaction activity of the end gas becomes significantly intense, the value of the parameter increases beyond a critical value that was found experimentally to be associated with the onset of mild knocking. The composition of the burned products following flame propagation is calculated while accounting for thermodynamic dissociation [6]. Heat transfer from the two combustion zones to the outside engine walls is accounted for using formulations such as that due to Woschni [7] based on experimental observations made in engines.

For the purpose of this investigation, when a mixture of common gaseous fuels with methane was used in a spark ignition engine, the following simple approximate expression for the combustion duration was derived based on our own experimental observations made in a single cylinder variable compression ratio CFR engine;

$$\frac{1}{\Delta\theta_{c,m}} = \sum \frac{y_i}{\Delta\theta_{c,i}} \qquad (1)$$

where $\Delta\theta_{c,m}$ is the combustion duration of the fuel mixture, y_i is the molar fraction of the fuel component "i" in the fuel mixture and $\Delta\theta_{c,i}$ is the corresponding combustion duration for the same engine when operating entirely on the fuel component "i" under the same conditions.

The solution of the set of relevant simultaneous equations employing numerical methods yields values of the main properties of the two combustion zones and their variations with time. From the knowledge of the calculated cylinder pressure variation with volume changes, the corresponding indicated power output and efficiency could be evaluated. Moreover, the net rates of production and consumption of each species of the reactive end gas charge could be established. These are functions of the rates of all the simultaneous reaction steps involved [8,14] in the detailed chemical kinetic scheme for the oxidation of fuel.

The model was shown [4,5,17] to be capable of predicting engine performance parameters such as the temporal variations in cylinder pressure and the mean temperatures of the two zones for different speeds, intake temperatures, intake pressures and spark timings as well as accounting for the effects of changes in some design parameters such as compression ratio, engine size and valve timing. Good agreement with corresponding experimental data was found, as shown typically in Figure 1 for the predicted power output of a normally aspirated CFR Engine operating on methane-hydrogen fuel mixtures. The model was also capable of predicting satisfactorily the onset of autoignition of the end gas which is responsible for engine knock.

3. Result and Discussions

The model was applied to consider the performance of a S. I. Engine over a range of operating conditions consistent with those for the CFR engine. Some of the results when hydrogen-methane mixtures were employed are presented. As shown in Figure 2, the addition of hydrogen to methane improves the power output of the engine especially for very lean mixtures. This is mainly because with low equivalence ratios, the flame speed of the main fuel methane is usually quite low and the presence of the hydrogen with its superior burning rate characteristics enhances the overall burning rates of the mixture significantly. This brings with it a reduction in the cyclic variations that is especially severe at these low equivalence ratios [15]. As the equivalence ratio is increased towards the stoichiometric ratio the beneficial effects of the addition of hydrogen to the methane are diminished, since the burning rates of both fuel components are enhanced significantly. Furthermore, the increased presence of hydrogen in the main fuel starts to affect increasingly the power output adversely due to the lower heating value of the hydrogen on molar basis in comparison to that of methane. This is consistent with what is usually observed experimentally [16]. The augmentation of the power output with hydrogen addition to methane tends to drop a little as the compression ratio is increased. However, the further increase in the presence of hydrogen in the fuel mixture beyond around 20 percent by volume adversely affects the power output due to the lower heating value of hydrogen in comparison to that of methane for all compression ratios. Similarly, the effects of increased concentration of hydrogen in the fuel mixture on the power output becomes much less pronounced as the mixture initial temperature is increased. This is a reflection of the increased burning rates and reduced total energy released with increasing the intake mixture temperature for non-knocking operations. As an example, for a relatively low intake mixture temperature of 250 K with an equivalence ratio of 0.90, an increase in power

of about 7 percent can be achieved when 50 percent hydrogen is in the fuel mixture for the operating condition considered. This increase in power output becomes significantly bigger as the equivalence ratio is lowered (e.g. with an equivalence ratio of 0.70, an increase in power of 40 percent can be achieved for the same operating conditions).

One of the major problems associated with the use of hydrogen as an engine fuel is its generation and portability. Hence, the suggestion is made that the small amount of hydrogen that needs to be added to the main fuel methane may be produced continuously in situ on board the engine by the electrolysis of water using the engine output as the source for the necessary energy needed. It has been thought that the enhancement to the power production capacity with hydrogen addition may be sufficiently high to pay for the energy demand for water electrolysis. No proper evaluation of this proposition appears to have been made. Accordingly, using the simulation model described earlier it was shown that the presence of some oxygen produced with the hydrogen in the electrolysis process in general, enhances the performance of the spark ignition engine further. The slightly oxygen rich intake mixture relative to common air tends to increase the relative burning rates while affecting only very marginally the total energy input of the mixture. Thus, the increased presence of the products of electrolysis of water further augmented the power output of the engine for different equivalence ratios, compression ratios and initial mixture temperatures. Figure 3 shows the extent of variations in power for different overall equivalence ratios. The increased presence of hydrogen and oxygen in the mixture, not only replaces methane by hydrogen but also some air is replaced by oxygen. In this approach it has been assumed throughout that only hydrogen and oxygen are the products of water electrolysis and at the low temperature involved no radicals are able to survive to the engine intake charge stage.

The effects of the presence of the hydrogen or hydrogen and oxygen in their proportion in water on the incidence of knock were considered analytically using the approach described earlier. For example, at a compression ratio of 10:1 and an equivalence ratio of 0.90, the preignition reaction activity of the end gas region becomes enhanced by the increased presence of hydrogen or hydrogen and oxygen in their proportion in water indicating a greater tendency to knock than with methane for otherwise the same operating conditions.

Of course, it is essential whenever the question of hydrogen production on board is put forward that the energetic consequences of this production on the net engine power output must be fully and realistically accounted for. In Figure 4, the net energy enhancement due to the addition of hydrogen to the main fuel methane is compared with the energy required to produce the same amount of hydrogen in situ by electrolysis of water. This production energy was based on a 70 percent effectiveness of the electrolysis [18] and an overall electric generation and mechanical efficiency of 30 percent. The viable range of the operating conditions of the engine, as shown for a typical case, throughout is very narrow and limited. This would indicate, based on the work and conditions considered in this investigation that it is inadvisable to have the hydrogen produced by electrolysis despite the fact that the presence of the hydrogen with methane in moderate volumetric proportions (20 - 25%) is certainly operationally attractive.

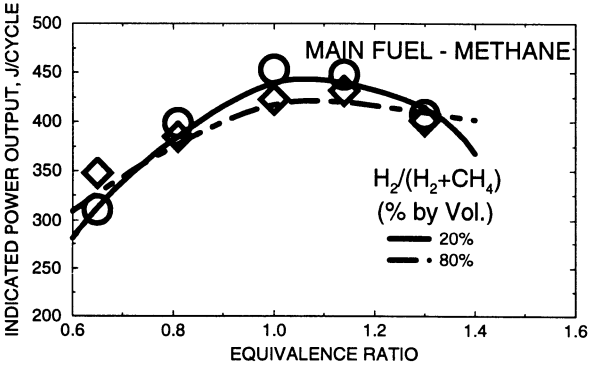

FIGURE 1. THE INDICATED POWER OUTPUT VARIATIONS WHEN OPERATING ON METHANE-HYDROGEN MIXTURES WITH EQUIVALENCE RATIO FOR COMPRESSION RATIO OF 8.5:1, SPARK TIMING OF 20 BTC AND INITIAL MIXTURE TEMPERATURE OF 298 K AT 900RPM. THE CORRESPONDING EXPERIMENTAL DATA ARE SHOWN.

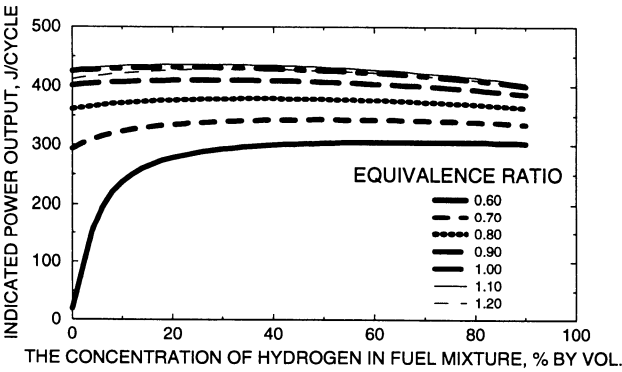

FIGURE 2. THE INDICATED POWER OUTPUT VARIATIONS WITH CONCENTRATIONS OF HYDROGEN IN A FUEL MIXTURE OF METHANE AND HYDROGEN FOR VARIOUS EQUIVALENCE RATIOS AT COMPRESSION RATIO OF 8.5:1, SPARK TIMING OF 20 BTC AND INITIAL MIXTURE TEMPERATURE OF 298 K.

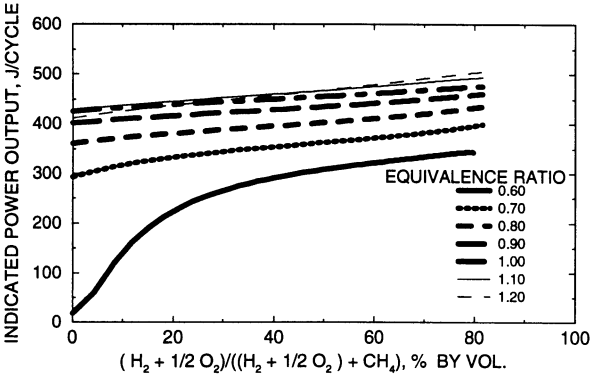

FIGURE 3. THE VARIATIONS OF INDICATED POWER VERSUS CONCENTRATION OF HYDROGEN AND OXYGEN IN THEIR PROPORTIONS IN WATER IN FUEL MIXTURES FOR VARIOUS EQUIVALENCE RATIOS AT COMPRESSION RATIO OF 8.5:1, SPARK TIMING OF 20 BTC AND INITIAL MIXTURE TEMPERATURE OF 298 K.

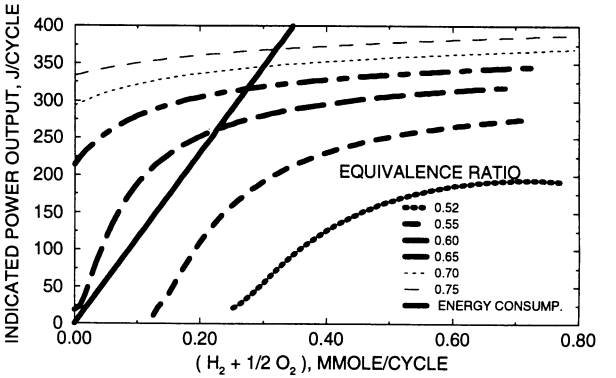

FIGURE 4. THE VARIATIONS OF INDICATED POWER OUTPUT VERSUS AMOUNT OF HYDROGEN AND OXYGEN IN THEIR PROPORTIONS IN WATER IN FUEL MIXTURES FOR COMPRESSION RATIO OF 8.5:1, SPARK TIMING OF 20 BTC AND INITIAL MIXTURE TEMPERATURE OF 298 K. THE PREDICTED ENERGY CONSUMPTION FOR THE ELECTROLYSIS IS ALSO SHOWN.

4. Conclusions

- The addition of some hydrogen to methane when used in a S. I. Engine enhances performance particularly when operating on relatively low equivalence ratio mixtures. The optimum concentration of hydrogen in the fuel mixture for producing a power gain and avoiding knock appears to be about 20 to 25 percent by volume over the range of conditions considered.

- The concept of producing the required amount of hydrogen on board the engine by the electrolysis of water while consuming some of the engine output has been shown not to be viable energetically over much of the engine operating range.

5. Acknowledgment

The contribution to this work of Mr. A. Alizadeh Atter is acknowledged. The financial support of the Natural Sciences and Engineering Research Council of Canada (NSERC) and Alternative Fuels System (AFS) is also acknowledged.

References

1. Gold, T., "Earth Outgassing of Methane", *Methane Fuel for the Future*, Editor P. McGeer and E. Durbin, Plenum Press, 1982.
2. Karim, G. A. and Wierzba, I., "Comparative Studies of Methane and Propane as Fuels for Spark Ignition and Compression Ignition Engines", SAE Trans. Vol. 92, Paper # 831196 (SP - 548), 1983.
3. Karim, G. A., Wierzba, I. and Al-Alousi, Y., " Methane-Hydrogen Mixtures as Fuels", *Intl. J. of Hydrogen Energy*, Vol. 21, No. 17, pp. 625-631, 1996.
4. Gao, J. and Karim, A. G., "A Predictive Model for Knock in Spark Ignition Engines", SAE paper # 922366 (SP - 937), 1992.
5. Karim, A. G., Gao, J. and Alizadeh Atter, A., "A Predictive Approach to Spark Ignition Engine Performance Fuelled with Common Gaseous Fuels and Their Mixtures", Proceeding of the 17th Annual Fall Technical Conference of the ASME Internal Combustion Division, Vol. 2, pp. 59-64, 1995.
6. Strehlow, R., "*Fundamentals of Combustion*", Intl. Textbook Co., 1988.
7. Woschni, G., "A Universally Applicable Equations for the Instantaneous Heat Transfer Coefficient in the Internal Combustion Engines", SAE Trans., Vol. 76, No. 670931, pp. 3065-3083, 1967.
8. Zhou, G., "Analytical Studies of Methane Combustion and the Production of Hydrogen and/or Synthesis Gas by the Uncatalyzed Partial Oxidation of Methane", Ph. D. Thesis, Department of Mechanical Engineering, The University of Calgary, 1993.
9. Karim, G. A. and Liu, Z., "A Predictive Model for the Knock in Dual Fuel Engines", SAE Trans., Vol. 101, Paper # 921550 (SP - 927), 1992.
10. Blizard, N. C. and Keck, J. C., "Experimental and Theoretical Investigations of Turbulent Burning Model for Internal Combustion Engines", SAE Trans., Vol. 83, Paper # 740191, 1974.
11. Hires, S. D., Tabaczynski, R. J. and Novak, J. M., "The Prediction of Ignition Delay and Combustion Intervals for a Homogeneous Charge Spark Ignition Engine", SAE Trans., Vol. 87, Paper # 780232, 1978.
12. Heywood, J., "*Internal Combustion Engine Fundamentals*", McGraw Hill Book Co., 1988.
13. Al-Himyary, T. J., "A Two-zone Diagnostic Combustion Model for Spark Ignition Internal Combustion Engines Based on Pressure Time Data", Ph.D. Thesis, Department of Mechanical Engineering, The University of Calgary, 1988.
14. Westbrook, C. K. and Pitz, W. J., "Complex Chemical Reaction Systems Mathematical Modelling and Simulation", J. Warnatz and W. Jager(eds.) Springer-Verlag, Heidelberg, West Germany, 1986.
15. Varde, K. S., "Combustion Characteristics of Small Spark Ignition Engines Using Hydrogen Supplemented Fuel Mixtures", SAE Paper # 810921, 1981.
16. Al-Alousi, Y., "Examination of the Combustion Processes and Performance of a Spark Ignition Engine Using a Data Acquisition System", Ph. D. Thesis, Department of Mechanical Engineering, The University of Calgary, Canada, 1982.
17. Gao, J., "A Predictive Model for Knock in Spark Ignition Engines Fuelled with Gaseous Fuels", Ph. D. Thesis, Department of Mechanical Engineering, The University of Calgary, Canada, 1993.
18. Rosen, M. A. and Scott, D. S., "Analysis of the Efficiencies of Several Hydrogen Production Process", Hydrogen Energy Congress XI, pp 479-488, 1996.

A KINETIC EXAMINATION OF THE EFFECTS OF THE PRESENCE OF SOME GASEOUS FUELS AND PREIGNITION REACTION PRODUCTS WITH HYDROGEN ON ITS AUTOIGNITION CHARACTERISTICS IN ENGINES

Y.K. WONG AND G.A. KARIM
The University of Calgary
Department of Mechanical Engineering
2500 University Drive N.W.
Calgary, Alberta, Canada T2N-1N4

Abstract

The paper describes the results of an analytical approach that models in full the reaction rate development in a motored engine of fuel mixtures of hydrogen with CH_4 and C_3H_8 in air while in the presence of exhaust gas recirculation. It is shown that the presence of these fuels with hydrogen can modify significantly the rates of reactions leading to autoignition which control the tendency of spark ignition engines to knock. It is also shown that exhaust gas recirculation can modify significantly the autoignition behaviour of hydrogen and its mixtures with methane or propane in engines.

1. Introduction

The use of hydrogen, either as the primary fuel or as an additive in a gaseous fuel mixture, in internal combustion engines has a number of attractive features. When hydrogen is used as an additive to natural gas, the wider operational mixture limits and faster flame propagation rates allow very fuel-lean operation. Consequently, such lean operation can result in higher thermal efficiencies and lower emissions. Conversely, the presence of other gaseous fuels with hydrogen such as natural gas or propane can temper the rapid rates of pressure and temperature rise associated with hydrogen operation reducing the possibility of engine knock and NO_x emissions. The operational benefits and problems associated with the use of hydrogen as an engine fuel has been described extensively in the literature [eg. 1].

The application of some exhaust gas recirculation (EGR) has so far, been employed mainly for the control of exhaust emissions, especially NO_x. EGR has the potential also to improve the fuel-lean operation of internal combustion engines and may be made to modify favourably the preignition reaction processes [2] in engines. This is achieved both thermally and kinetically by effectively 'seeding' the intake charge with some partial oxidation products from the preceding cycles that will be a source of active radicals for the following working cycle.

T. O. Saetre (ed.), Hydrogen Power: Theoretical and Engineering Solutions, 63–68.

2. Background

The preignition processes of homogeneous mixtures of gaseous fuels in air in a motored compression ignition engine are controlled by thermodynamic and transport properties, heat transfer and the preignition reactions activity of the mixture that are dependent on the type of fuel used. The preignition reactions within propane and methane-air mixtures in engines are most active on the lean side of the stoichiometric ratio while for lean hydrogen-air mixtures, the preignition reaction rates are enhanced as more hydrogen is added to the total mixture [3]. The increased presence of methane or propane in the cylinder charge would reduce the effective polytropic index of compression and lead to a reduction in the level of temperatures as mixtures are made more fuel-rich which will bring about a reduction in the overall rates of oxidation reaction. In the case of hydrogen, the corresponding reduction in the polytropic index is significantly less than for propane or methane. By increasing the concentration of hydrogen, any reduction in the peak compression temperature will have only a small effect on the overall oxidation rate in comparison to its enhancement due to the increased reactivity that comes with higher concentrations of hydrogen [4].

There has been much reported research relating to the operation of engines fuelled with mixtures of hydrogen/methane or hydrogen/natural gas and air. At around stoichiometric operation with such fuel mixtures, the power output will be reduced with increased substitution of methane by hydrogen, despite the enhancement of flame propagation rates, due mainly to the lower volumetric heating value of hydrogen compared to that of methane [5]. However, due to the wide operational limits of hydrogen, its addition to methane in engines will permit the use of leaner mixtures with reduced cyclic variations [6], higher thermal efficiencies and lower emissions, especially those of NO_x. Moreover, it speeds up both the rates of initiation and subsequent propagation of flames over the whole widened combustible mixture range [7] which will reduce the tendency to knock and lead to improved performance [1]. As more hydrogen is added to the methane, the engine will approach knocking conditions requiring remedial measures to be taken, such as changes in spark timing, that will undermine power output and thermal efficiency [8]. It is important to determine the optimal quantity of hydrogen addition such that all the benefits of hydrogen operation can be realized while maintaining the excellent knock resistant characteristics of gaseous fuels such as methane. It was shown [9] that hydrogen addition to methane in moderate concentrations will not increase the tendency to knock since although the end gas temperatures may increase somewhat, the preignition oxidation activity of hydrogen proceeds relatively slower than methane.

In this paper, the consequences of adding various quantities of hydrogen with EGR to methane-air and propane-air mixtures are examined analytically in a motored compression ignition engine in the absence of a deliberate source of ignition so as to find what mixtures are more resistant to preignition oxidation reactions that lead to engine knock. EGR, which is effected by recirculating in some way a fraction of the partial oxidation products from the preceding motored cycle into the following cycle will modify the kinetic and thermal processes and may modify favourably the preignition oxidation rates and subsequently control the tendency to knock.

The species produced by preignition reaction activity usually contain a wide range of radicals and other partial oxidation products that yield on further reactions more radicals. Boyce et al [10] found that the addition of a small quantity (around 6% of the total charge) of partially oxidized reaction products of homogeneous mixtures of n-heptane and air from an external reactor to the intake charge of a diesel engine resulted in lower ignition delays of the

main diesel liquid fuel. They suggested that the presence of some partially oxidized fuel not only augmented the local temperature by maintaining the exothermic reactions that began in the external reactor but also provided active species during the injection and pre-ignition process of the main fuel charge. Some EGR was employed to improve the cold starting of a spark-ignition and diesel engine [11,12]. Partially oxidized exhaust gases when returned to the cylinders would increase the possibility of autoignition and engine starting because of the thermal effects due to elevated charge temperatures and the kinetic effects of the partial oxidation products in the EGR gas.

3. Analytical Consideration

A one dimensional analytical model that incorporates detailed reaction kinetics described earlier by Liu and Karim [3] was modified to account for the thermal, diluting and kinetic effects of EGR on the autoignition characteristics of a homogeneous mixture of gaseous fuel and air in a motored engine in the absence of a deliberate source of ignition. For example, a fresh methane-air charge that may contain small quantities of hydrogen is assumed to be initially homogeneously mixed and ideal. A certain quantity of recirculated exhaust gas from the previous cycle is introduced and mixed adiabatically with it. The resulting mixture following intake valve closure is then compressed and subsequently expanded to the exhaust stage, ready to have a fraction of it recirculated again.

The kinetic scheme employed in the present analysis, which was developed on the basis of those reported by Westbrook et al. [13], Pitz et al. [14] and Karim and Liu [15] consisted of 137 elementary steps involving 32 chemical species. It could describe the preignition, autoignition and combustion reactions in a non-turbocharged engine with EGR when fuelled with common gaseous fuels and their mixtures such as methane, propane or hydrogen. For any set of fuel-lean operating conditions, the associated development with time of important parameters such as pressure, temperature, rates of energy release, compositions, etc., and whether autoignition is going to be encountered at any cycle or not can be established. The quantity of EGR was considered to have the same composition as that of the charge at the instant of its expansion to atmospheric pressure during the preceding cycle. When the inlet valve was opened, the fraction of exhaust gases trapped and recirculated were assumed to mix completely and adiabatically with the fresh charge at the same pressure. Convective and radiation heat transfer from the charge was accounted for throughout [16].

4. Results and Discussions

Figure 1 shows typically the effect of EGR on the time requirement to produce the first sign of autoignition (ignition delay in terms of cycles for a constant speed) for a motoring, homogeneously charged compression ignition engine fuelled with methane over a large number of calculated consecutive cycles. The ignition delay begins with the commencement of compression in the first cycle when the cylinder is filled only with the fresh intake charge having no traces of residual or exhaust gases, and it ends at the first sign of autoignition in subsequent exhaust gas recirculated cycles. It is further assumed for convenience that at t = 0, the engine immediately begins motoring at full speed with warm cylinder walls. It can be seen for the typical conditions selected that the ignition time is shortened significantly when

a fair amount of the exhaust gas in each cycle is recirculated back to be mixed with the fresh intake charge of the following cycle. These recirculated products will be the source of active radicals seeding the incoming charge of the following cycle that will enhance the reaction rate and subsequently, produce yet a greater amount of partial oxidation products that will be recirculated into the following cycle. Hence, this gradual build-up in the recirculated gas with successive cycles of partial oxidation products and active radicals will bring closer the possibility of autoignition.

It can be seen in figure 1 that hydrogen reached the autoignition stage earlier than both methane and propane even though it is generally less reactive during preignition than either of the other two gases. The cylinder charge is able to reach a higher peak temperature with hydrogen due to its higher polytropic index. The calculated adiabatic peak compression temperature of the fresh charge of the very first cycle for each of the respective fuel-air mixtures for these conditions is shown on the figure for reference. The propane-air charge had the lowest polytropic index and that resulted in a relatively low in-cylinder peak compression temperature requiring more motoring cycles for active species to build-up to obtain first autoignition, particularly at low recirculation quantities. As the amount of EGR products is increased, the number of cycles required for first autoignition is reduced since active species can build-up more quickly. As even more EGR is applied for the methane and propane cases, the number of required cycles for first autoignition increases dramatically. This is due to the cumulative heat loss without much exothermic energy release occurring in the cylinder charge during the preceding cycles. A more detailed discussion of this phenomenon by the authors can be found elsewhere [2]. In figure 2, a similar examination was made with those three fuels but at a higher intake temperature and a lower compression ratio. It can be seen that propane required less motoring cycles than methane to produce autoignition at low to moderate recirculation quantities while hydrogen did not autoignite at all. The more reactive propane led to earlier autoignition and because hydrogen is not as reactive as propane nor methane during the preignition processes, it could not produce as much partial oxidation products to lead to autoignition. Also, for all three fuels, autoignition could not be obtained at very high EGR quantities. This is mainly due to the significantly higher amounts of net heat loss that the cylinder contents endured over the cyclically repeated compression and expansion.

Figure 3 shows for operating conditions that yield similar adiabatic peak compression temperatures that the time requirements to produce the first autoignition in a motoring engine is smallest for propane at all EGR quantities, which is consistent with the higher reactivity of propane in comparison to methane or hydrogen. Hydrogen could only autoignite when the operating conditions were altered to produce significantly higher peak compression temperatures. Also, two operating conditions are shown which yield for methane the same adiabatic peak compression temperatures. The case that uses a higher compression ratio and a lower intake temperature required less time to produce first autoignition than the second case which employed a lower compression ratio and a higher intake temperature. This second case suffered from higher rates of heat loss due to its higher intake temperature.

Figure 4 shows for a typical case, the effects of varying the concentration of hydrogen in a binary fuel mixture with methane or propane on the number of successive motoring cycles required to obtain autoignition in a compression ignition engine with EGR. The quantity of EGR was set at 20% by volume while maintaining the overall equivalence ratio constant at 0.70. It is seen that when a small amount of hydrogen is added to methane, at an intake temperature of 300 K, the number of cycles required for autoignition increases significantly. In fact, when more than 10% of the fuel mixture is hydrogen, autoignition could not be

obtained for these conditions. Karim and Klat [10] also showed experimentally that the addition of small amounts of hydrogen to methane will not increase the knocking tendency since the preignition oxidation activity of hydrogen is relatively slow compared to that of the replaced methane. A similar trend was also seen when a very small amount of methane was added to the hydrogen. At methane concentrations of more than 3% in a binary fuel mixture with hydrogen, autoignition becomes very difficult mainly due to the reduction in cylinder peak compression temperatures when methane is introduced. This is an interesting result because it shows that the addition of small amounts of methane to an engine run on hydrogen can reduce the tendency to knock. This would clearly be a better alternative than the practice of using diluents such as nitrogen, carbon dioxide or water, which decreases the power output. It appears also that there is a threshold in temperature where the addition of hydrogen promotes autoignition.

It can be seen further in figure 4 the addition of moderate amounts of propane, of around 20% by volume, to an engine run on hydrogen will reduce the tendency for autoignition. However, with smaller amounts of propane addition, of up to 15%, the number of successive motoring cycles required to reach autoignition decreases substantially. Thus, the addition to hydrogen of small amounts of the more reactive propane will increase the autoignition tendencies of hydrogen but the addition of substantial amounts of propane will reduce peak compression temperature and the overall rates of oxidation reactions.

5. Conclusions

- The employment of some EGR can control and modify significantly the nature of the autoignition behaviour.
- Under certain conditions with EGR, the addition of small quantities of methane or propane to an engine fuelled with hydrogen can result in a decrease in the reaction rates leading to the onset of autoignition.

6. References

1. Karim, G.A., Wierzba, I. and Al-Alousi, Y.H.: Methane-Hydrogen Mixtures as Fuels, *Int. J. Hydrogen Energy* **21** (1996) 625-631.
2. Wong, Y.K. and Karim, G.A.: An Analytical Examination of the Effects of Exhaust Gas Recirculation on the Compression Ignition Process of Engines Fuelled with Gaseous Fuels, *SAE 961936* (1996).
3. Liu, Z. and Karim, G.A.: An Analytical Examination of the Preignition Processes within Homogeneous Mixtures of a Gaseous Fuel and Air in a Motored Engine, *SAE 942039* (1994).
4. Liu, Z. and Karim, G.A.: Knock Characteristics of Dual-Fuel Engines Fuelled with Hydrogen Fuel, *Int. J. Hydrogen Energy* **20** (1995), 919-924.
5. Nagalingam, B., Duebel, F. and Schmillen, K.: Performance Study Using Natural Gas, Hydrogen-Supplemented Natural Gas and Hydrogen in AVL Research Engine, *Int. J. Hydrogen Energy* **8** (1983), 715-720.
6. Al-Alousi, Y.H. and Karim, G.A.: Some Considerations of Cyclic Variations in Spark Ignition Engines Fuelled with Gaseous Fuels, *SAE 840232* (1984).
7. Soriano, B.: Turbulent Combustion, M.Sc. Thesis of the University of Calgary, Calgary, Alberta, Canada, (1982).
8. Karim, G.A., Al-Alousi, Y.H. and Anson, W.: Consideration of Ignition Lag and Combustion Time in a Spark Ignition Engine Using a Data Acquisition System, *SAE 820758* (1982).
9. Karim, G.A. and Klat, S.R.: The Knock and Autoignition Characteristics of Some Gaseous Fuels and their Mixtures, *J. Inst. Fuel* **39** (1966), 109-119.
10. Boyce, T.R., Karim, G.A. and Moore, N.P.W.: An Experimental Investigation into the Effects of the Addition of Partially Oxidized Reaction Products to the Intake Charge of a Compression Ignition Engine, *J. Inst.*

Petroleum **52** (1966), 300-311.
11. Gardiner, D.P., Rao, V.K., Bardon, M.F. and Battista, V.: Improving the Cold Start Combustion in Methanol Fuelled Spark Ignition Engines by Means of Prompt EGR, *SAE 910377* (1991).
12. Sun, R., Sweet, E.J., Zurlo, J.R. and Pfefferle, W.C.: Diesel Engine Cold Starting with Catalytically Ignited Recirculated Exhaust Gas, *SAE 940086* (1994).
13. Westbrook, C.K., Warnaze, J. and Pitz, W.J.: A Detailed Chemical Kinetic Reaction Mechanism for the Oxidation of Iso-Octane and N-Heptane over an Extended Temperature Range and its Application to Analysis of Engine Knock, *22nd Symposium (Int.) on Combustion* (1988), 893-901.
14. Pitz, W.J., Westbrook, C.K. and Leppard, W.R.: Autoignition Chemistry of C4 Olefins under Motored Engine Conditions: A Comparison of Experimental and Modelling Results, *SAE 912315* (1991).
15. Karim, G.A. and Liu, Z.: A Predictive Model for Knock in Dual Fuel Engines, *SAE 921550* (1992).
16. Annand, W.J.D.: Heat Transfer in the Cylinders of Reciprocating Internal Combustion Engines, *Proc. Instn. Mech. Engrs.* **177** (1963), 36-43.

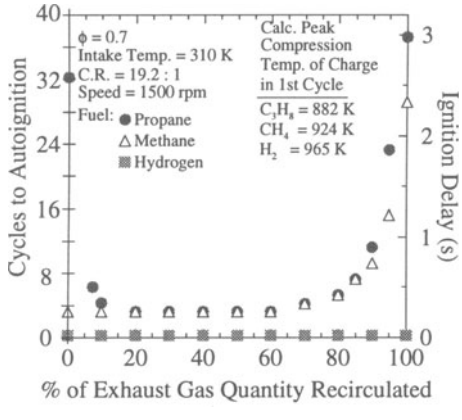

Figure 1 The Effect of EGR on the Time Reuirement to Produce First Autoignition

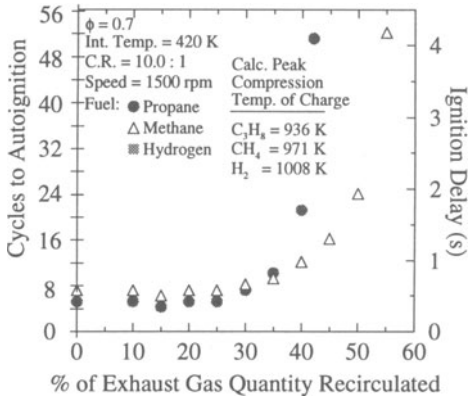

Figure 2 The Effect of EGR on the Time Requirement to Produce First Autoignition at Higher Intake Temp. and Lower C.R.

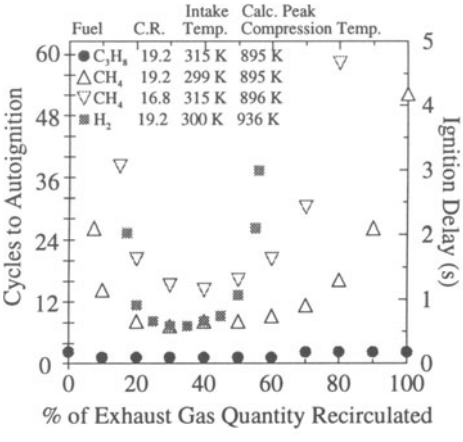

Figure 3 Effect of EGR on Time to Produce First Autoignition of Various Fuels at Conditions Yielding Similar Peak Temp. (ϕ = 0.7; Speed = 1500 rpm)

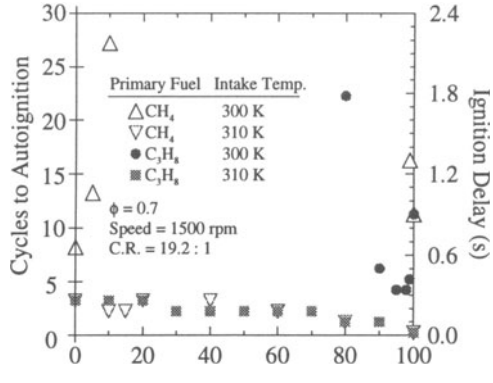

Figure 4 Effect of Varying H_2 Conc. in a Binary Fuel Mixture with CH_4 or C_3H_8 on Time to Produce First Autoignition (20% EGR)

EFFECTS OF TEMPERATURE AND TIME OF EXPOSURE ON THE FLAMMABILITY LIMITS OF HYDROGEN-AIR MIXTURES

I. WIERZBA AND B. B. ALE
Department of Mechanical Engineering
The University of Calgary
2500 University Drive, NW
Calgary, Alberta, T2N 1N4

1. Introduction

Although much research has been conducted in the field of flammability limits, there are still questions that cannot be answered adequately. For example, there are industrial processes conducted at elevated temperatures and a knowledge of the corresponding flammability limits is needed for safety considerations. Reference to the literature indicates that only very limited data are available (Coward and Jones, 1952; Zabetakis, 1965; Bunev, 1972; Hustad and Sonju, 1988). There is also the possibility that at elevated temperatures fuel-air mixtures will undergo substantial preignition reactions especially when the test fuel-air mixture is allowed to stand a while before ignition. Additionally, for some fuel and temperature combinations there is the possibility of surface reactions taking place that effectively change the composition of the mixture with time. It was shown previously (Ale and Wierzba, 1997) that the rich flammability limits of ethylene in air determined experimentally in a conventional stainless steel test tube at elevated temperatures were affected very significantly by the time of exposure of the mixture to these elevated temperatures before the spark ignition. Similar observations were reported by Bunev (1972) during experiments conducted with hydrogen-air and methanol-air mixtures in a spherical stainless steel reactor with central ignition. In both studies the observed trends were attributed to the fact that stainless steel can act as a catalyst for enhancing low temperature oxidation reaction of hydrogen and ethylene in air.

The purpose of the present work was to establish the flammability limits of hydrogen in air for upward vertical flame propagation at elevated temperatures up to 350°C and atmospheric pressure in a conventional stainless steel test tube apparatus, and to investigate the extent to which a prolonged exposure (i.e. residence time) of the mixture to elevated temperatures before spark ignition may influence the value of the flammability limits.

2. Apparatus And Experimental Procedure

The apparatus was in general similar to that developed and used by the US Bureau of Mines in their flammability limits work. The limits were established in a stainless steel smooth circular

T. O. Saetre (ed.), Hydrogen Power: Theoretical and Engineering Solutions, 69–74.

tube of 50.8 mm diameter and just over one metre in length. The tube was heated externally uniformly electrically. A set of unsheathed thermocouples (K-type) was used to monitor the wall and gas temperatures along the whole length of the flame tube. The test tube temperature was maintained at the required level for the desired residence time using temperature controller. The pressure inside the flame tube was monitored using a strain gage type pressure transducer located at the top of the tube. Ignition of the test mixture was initiated by an electric spark discharge between two horizontal conical tungsten electrodes. The electric power for ignition was supplied by a 10 kV, 23 mA centre-tapped transformer with its primary hooked to a 110 V, 60 Hz supply. The ignition system was optimized with respect to the electrode gap and the spark duration to give the widest flammability limits.

The homogeneous mixture of desired composition was prepared on the basis of partial pressures in the stainless steel mixing chamber at room temperature. It was introduced into the test tube when its temperature along the entire length was stabilized within ± 3°C of the nominal value through inlet valves located at the top and bottom ends of the tube until the pressure within the tube was slightly above atmospheric. The valves between the mixing chamber and the flame tube were then closed. The time for the gas mixture to reach thermal equilibrium with the tube wall usually did not exceed ½ minutes. The fuel-air mixture was then kept inside the test tube for the desired residence time. To allow the flame propagation at constant pressure, the valve at the bottom of the test tube was slowly opened to exhaust just prior to passing the spark. Ignition was initiated by activating the interval timer, while the top and bottom thermocouples readings were monitored. A sudden increase in the bottom thermocouple reading indicated the initiation of a flame kernel around the igniter, while a sudden rise in the top thermocouple reading marked arrival of the flame at the top of the tube.

A mixture was considered to be non-flammable if a flame kernel formed in the immediate vicinity of the spark at the bottom of the tube did not propagate the whole length of the tube in any of the repeated tests while using the same mixture composition. A number of experiments were also repeated to verify the repeatability of the results.

Using this procedure the flammability limits of hydrogen in air were determined for various initial temperatures of up to 350°C and various residence times of up to 2 hours.

3. Results

The flammability limits reported in this work relate to upward flame propagation at atmospheric pressure of 88 kPa (Calgary). The limits are quoted as the volumetric concentration of the fuel in the fuel-air mixture.

The effect of the initial temperature on the flammability limits of hydrogen-air mixtures is shown in Figure 1 for the residence time (i.e. the time interval between the time of acquiring the desirable temperature by the hydrogen-air mixture and initiation of spark ignition) of 10 minutes. Over the temperature range from 21°C to 200°C the flammability limits widened essentially linearly with increasing initial temperature. The limits were somewhat narrowed when the initial temperature was higher than 200°C showing lower rich limits and approximately constant lean limits. This behaviour of the lean limit was inconsistent with trends reported for lean flammability limit of hydrogen-air mixtures at similar elevated temperatures by Hustad and Sonju (1988).

The effect of the residence time on the rich flammability limits at different initial

temperatures is shown in Figure 2. Over the range of initial temperatures from 21°C to about 200°C, the rich limit was generally unaffected by the duration of residence time. When the initial temperature exceeded 200°C the rich limit was significantly affected by the length of the residence time. It increased for the residence time of 30 seconds, but decreased for all other residence times employed. The decrease was a function of the residence time duration. For example, an increase in temperature from 200°C to 325°C caused a drop in the value of the rich limit from 82% to 78% for a 5 minute residence time, while for a 120 minute residence time the corresponding drop was from 81% down to 47%. Similar trend was also observed for the values of the lean flammability limit of hydrogen, as can be seen in Figure 3. At an initial temperature of 300°C the lean limit of 2.6% for the 10 minutes residence time increased to more than twice this value when the residence time was increased to 6 hours.

Continuous measurements of temperature and pressure inside the test tube during the residence time showed that the temperature remained virtually constant during all tests while the pressure was decreasing with longer residence time. An example of pressure variation during the residence time for three different limiting hydrogen-air mixtures at different initial temperatures is shown in Figure 4. This may be indicative of some low temperature oxidation activity taking place during the residence time and the associated decrease in the total number of moles in the mixture.

4. Discussion

The observed behaviour of the flammability limits of hydrogen in air at initial temperatures higher than 200°C and at longer residence times is not consistent with expectation in that it shows a reduction in the limit. The rich limits are associated with oxygen deficiency. A significant drop in the measured value of this observed limit would suggest a more acute oxygen deficiency existing for the fuel available at the time of passing the spark for ignition. Some of the oxygen in the mixture must have been consumed through oxidation of some fuel during the waiting period at higher temperature. Similarly, the lean limits are associated with fuel deficiency and an increase in the value of the limit could be indicative that some fuel could have also been oxidized before spark ignition.

Detailed chemical kinetic simulation of the oxidation of hydrogen was conducted for different hydrogen-air mixtures at initial temperature of 350°C. The program involving 21 reactions with 8 species was adapted. The results of this calculation (Figure 5) showed a rather slow progress in the gas phase reactions of hydrogen oxidation at the initial temperature of 350°C at residence times up to 5 hours while a significant change in the value of the rich limit of hydrogen was observed experimentally at this temperature even for the short residence time of 10 minutes. Therefore, the observed changes in the flammability limits are most probably a result of the oxidation of hydrogen over a period of time mainly due to catalytic action on the stainless steel (316) tube surface and not through gas phase oxidation. It is known that some metals, for example, steels and iron are active catalysts for the oxidation of hydrogen and ethylene at elevated temperatures in air (Pangborn and Scott, 1979; Baker, 1974; Krishnankutty et al., 1996).

The extent of hydrogen conversion during the residence time due to the catalytic activity at the steel wall can be approximately estimated from the following considerations. It has been shown that the flammability limits are associated with a certain critical level of reaction

temperature that is assumed to be proportional to the calculated adiabatic flame temperature which has the same value under the same operating conditions (Bade Shrestha et al., 1995; Zabetakis, 1965). If all other operating conditions remain the same this temperature should remain constant for limiting mixtures irrespective of the residence time length, i.e. any catalytic activity at the wall before ignition. Such temperature can be estimated on the basis of the known flammability, L_R, measured with very short residence time, i.e. before the onset of any catalytic activity. For the rich limiting hydrogen-air mixtures the following overall reaction applies:

$$L_R H_2 + (1-L_R)(0.21 O_2 + 0.79 N_2) = [L_R 0.42 (1-L_R)] H_2 + [0.42(1-L_R)] H_2O + 0.79(1-L_R) N_2 \quad (1)$$

At the surface of the stainless steel test tube some of the hydrogen is converted to water catalytically and at the end of the residence time the overall reaction for the limiting mixture becomes the following:

$$(L_{R,res} - X) H_2 + X H_2O + 0.79(1-L_{R,res}) N_2 + [0.21(1-L_{R,res}) - \frac{X}{2}] O_2 = 0.79(1-L_{R,res}) N_2 + [0.42(1-L_{R,res}) H_2O + [L_{R,res} - 0.42(1-L_{R,res})] H_2 \quad (2)$$

where $L_{R,res}$ is the experimentally obtained rich limit at the corresponding residence time and **X** is the amount of the hydrogen converted to water (volume percent in total mixture) during the residence time. Calculated values of **X** at initial temperature of 300°C are shown in Table 1. For an ideal gas at constant volume and temperature conditions changes in pressure are proportional to changes in the number of moles of the mixture. Accordingly, the pressure at the end of the residence time, P_2, (just before ignition) is:

$$P_2 = P_1 (1 - \frac{X}{2}) \quad (3)$$

where, P_1 is the initial pressure in the test tube at the commencement of the residence time.

The values of the final pressure P_2 calculated using eq. (3) are shown in Table 1. They are close to those measured experimentally. This would support the validity and applicability of the concept used.

TABLE 1. Hydrogen conversion to water in the rich *limiting* mixtures at different residence times at T=300°C and initial pressure, P_1 = 105 kPa.

Test No.	Residence time, min	$L_{R,res}$ %	X %	Hydrogen depletion ($X/L_{R,res}$),%	Pressure, P_2 measured, kPa	Pressure, P_2 calculated, kPa
1	5	81	1.3	1.60	104.2	104.3
2	10	77	3.0	3.90	103.4	103.4
3	30	70	5.9	8.43	101.3	101.9
4	60	61	9.7	15.90	98.9	99.9
5	90	56	11.8	21.07	96.7	98.8
6	120	52	13.5	25.96	94.6	97.9

5. Conclusions

- Residence time and the type of the test tube surface should be taken into consideration when determining the flammability limits.
- At initial temperatures lower than 200°C the experimentally determined flammability limits of hydrogen in air were widened with an increase in the temperature. They were not affected by the length of the residence time before spark ignition.
- At initial temperatures higher than 200°C the values of the flammability limits of hydrogen in air when determined experimentally in a stainless steel tube apparatus were significantly affected by the length of the residence time before ignition. The longer the residence time, the smaller the rich limit and the higher the lean limit.
- The narrowing of the limits is suggested to be mainly due to catalytic reactions on the stainless steel surface of the test tube.

6. Acknowledgements

The financial assistance of the Natural Sciences and Engineering Research Council of Canada (NSERC) and Canadian International Development Agency (CIDA) is gratefully acknowledged.

The authors also acknowledge the helpful assistance of Drs. Liu and Karim on the chemical kinetic simulation.

7. References

Ale, B. B. and Wierzba, I. (1997) The Effect of Time Exposure of Ethylene-air Mixtures to Elevated Temperatures on Their Flammability Limits, paper presented at *Energy Week '97 Conference and Exhibition* organised by ASME International, Houston, Texas, 217-221.

Bade Shrestha, S. O., Wierzba, I., and Karim, G. A.(1995) A Thermodynamic Analysis of The Rich Flammability Limits of Fuel-diluent Mixtures in Air, *Journal Of Energy Resources Technology*, **117**, 239-242.

Baker, N. R.(1974) Oxides of Nitrogen Control Technologies for Appliance Conversion to Hydrogen Fuel, paper presented at *9th Intersociety Energy Conversion Engineering Conference Proceedings*, San Francisco, California, 463-467.

Bunev, V. A .(1972) Determination of The Concentration Limits of Flame Propagation at Elevated Temperatures, *Fizika Gareniya Vzryva*, **8**, No. 1, 82-86.

Coward, H. F., and Jones, G. W. (1952) Limits of Flammability of Gases and Vapors, *US Bureau of Mines*, Bulletin 503, Pittsburgh, Pennsylvania.

Hustad, J. E. and Sonju, O. K (1988) Experimental Studies of Lower Flammability Limits of Gases and Mixtures of Gases at Elevated Temperatures, *Combustion and Flame* **71**, 51-103.

Krishnankutty, N., Rodridnez, N. M., and Baker, R. T. K. (1996) Effect of Copper on The Decomposition of Ethylene over an Iron Catalyst, *Journal of Catalyst*, **158**, 217-227.

Pangborn, J., and Scott, M. L. (1979) Domestic Uses of Hydrogen, Hydrogen: Its Technology and Implications, Volume IV, *Utilization of Hydrogen*, edited by Kenneth E. Cox and K. D.Williamson, Jr., CRC Press, Inc., Boca Raton, Florida, USA, 151-188.

Zabetakis, M. G. (1965) Flammability Characteristics of Combustible Gases and Vapors, *Bulletin 627, Bureau of Mines*, Washington.

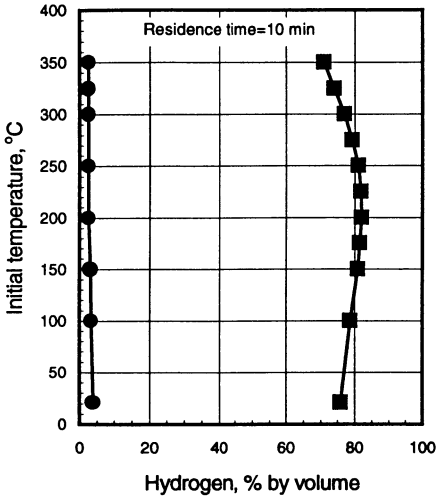

Figure 1. Flammability limits of hydrogen-air mixtures as a function of temperature at residence time of 10 minutes.

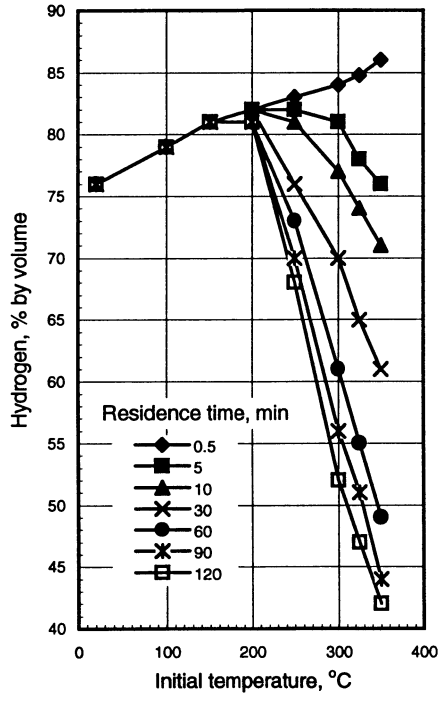

Figure 2. Rich flammability limits of hydrogen in air mixtures as a function of temperature at different residence times.

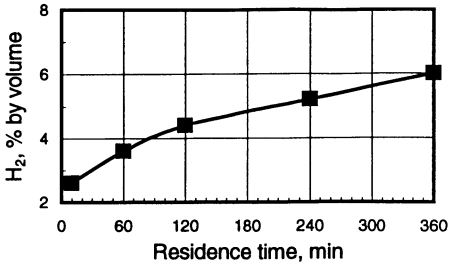

Figure 3. Lean flammability limit of hydrogen in air as a function of residence time at 300°C

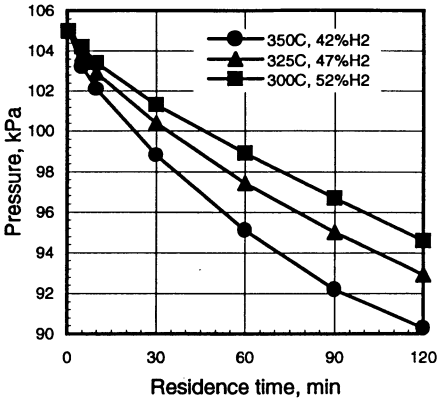

Figure 4. Pressure variation as a function of residence time for three different limiting hydrogen -air mixtures at different initial temperatures.

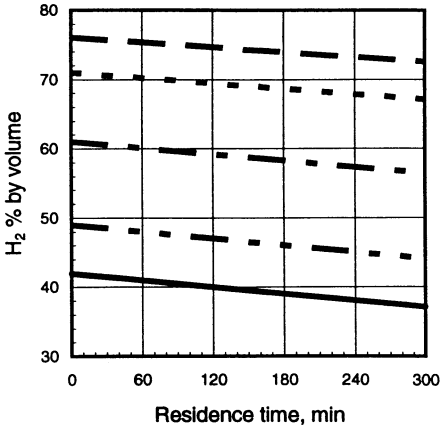

Figure 5. Hydrogen concentration variation due to gas phase reaction activity at 350°C for different initial hydrogen concentrations.

HYDROGEN PRODUCTION FROM FOSSIL FUELS

A Review

Bjørn Gaudernack
Institute for Energy Technology,
P.O.Box 40, N-2007 Kjeller, Norway

Abstract

State-of-the-art of hydrogen production from fossil sources is briefly reviewed. Production from natural gas is emphasised, some new developments and special procedures are described. The possibilities for "CO_2-free" hydrogen production are discussed. On-site production as an option for hydrogen fuel supply is also discussed.

1. Introduction

The bulk of hydrogen production today is based on fossil raw materials. Table I shows the world hydrogen production by origin. The table is based on statistics from 1988 and covers hydrogen produced both as a main product and as a by-product [1].

TABLE 1. World hydrogen production

Origin	Billion Nm^3/year	%
Natural gas	240	48
Oil	150	30
Coal	90	18
Electrolysis	20	4
Total	500	100

As we see the whole range of fossil fuels - from natural gas to coal - can be used for hydrogen production. It should be kept in mind, however, that although we talk about fossil fuel feedstock, a large proportion of the hydrogen will originate from water. This may range from ~50 % - ~ 100 %, as will be shown below.

A main disadvantage of the present practice of hydrogen production is that the carbon contained in the fossil feedstock will be released to the atmosphere as CO_2. The amounts released vary from 0,44 - 0,81 Nm^3 CO_2 per Nm^3 of H_2 produced, in the range of natural gas to coal as raw materials [1]. Globally, this corresponds to a CO_2 release of about 500 Mt/year. This is a considerable release of greenhouse gas, which should be avoided from an environmental point of view. The release can be avoided or at least substantially reduced by sequestration of the CO_2, but it has been generally thought that this would lead to prohibitive hydrogen costs. Recent studies have shown, however, that the cost increase will be moderate, at least in the case of hydrogen production from natural gas.

Another option for CO_2-free production of hydrogen from fossil fuels is pyrolytic cracking. In this case the carbon in the feedstock will appear as a pure carbon product, which may either be marketed as "carbon black", or stored as an energy carrier for future use. So far hydrogen has not been produced industrially by this method, but interesting development

T. O. Saetre (ed.), Hydrogen Power: Theoretical and Engineering Solutions, 75–89.

work is going on. Various other novel approaches to hydrogen production from fossil fuels, some of them involving use of renewable energy, are also being studied.

2. Principal processes

The main processes employed in industrial hydrogen production are steam reforming (SMR), partial oxidation (POX) and combinations of these. As mentioned above, pyrolytic cracking may also be an option. The general equations for these reactions are given below (with the special cases of methane in parentheses):

Steam reforming:

$$C_n H_m + nH_2O \rightarrow nCO + (n + m/2)\, H_2 \quad (1)$$
$$(CH_4 + H_2O \rightarrow CO + 3\, H_2)$$

Shift reaction:

$$n\,CO + nH_2O \rightarrow nCO_2 + nH_2 \quad (2)$$
$$(CO + H_2O \rightarrow CO_2 + H_2)$$

Sum reaction:

$$C_n H_m + 2nH_2O \rightarrow nCO_2 + (2n + m/2)\, H_2 \quad (3)$$
$$(CH_4 + 2H_2O \rightarrow CO_2 + 4\, H_2)$$

Partial oxidation:

$$C_n H_m + n/2\, O_2 \rightarrow nCO + m/2\, H_2 \quad (4)$$
$$(CH_4 + ½\, O_2 \rightarrow CO + 2\, H_2)$$

Shift reaction:

$$n\,CO + n\,H_2O \rightarrow nCO_2 + n\,H_2 \quad (2)$$
$$(CO + H_2O \rightarrow CO_2 + H_2)$$

Sum reaction:

$$C_n H_m + n/2\, O_2 + nH_2O \rightarrow nCO_2 + (n + m/2)\, H_2 \quad (5)$$
$$(CH_4 + ½\, O_2 + H_2O \rightarrow CO_2 + 3\, H_2)$$

Pyrolytic cracking:

$$C_n H_m \rightarrow nC + m/2\, H_2 \quad (6)$$
$$(CH_4 \rightarrow C + 2\, H_2)$$

When m goes to very small values in equation (4), the raw material is coal and we talk about partial oxidation of coal, or coal gasification. It is evident that with falling values of m, increasing proportions of the hydrogen will be provided by the water shift reaction (2). In the case of steam reforming 50-60 % of the hydrogen originates from water (50 % in the case of pure methane). With partial oxidation, the proportion is 60-100 % (100 % in the case of pure carbon) [1].

Steam reforming is the most common process and, as can be seen in Table 1, natural gas is the most common feedstock. Steam reforming may, however, be applied to heavier

hydrocarbons like LPG or naphta with end-boiling point up to 220 °C [2]. The SMR reaction (1) is strongly endothermic and is performed catalytically at high temperatures. The water shift reaction (2) is exothermic.

Partial oxidation (4) is also exothermic, it is normally performed at high temperatures without a catalyst. POX is most frequently applied to heavy oil fractions, it is commonly used in oil refineries for supply of their internal demands of hydrogen. It is, however, also possible to apply POX to methane or natural gas, and the reaction conditions may be relaxed by employing a catalyst [3]. Combinations of SMR and POX may also be of advantage, as will be discussed later.

Coal gasification is accomplished by reacting coal with oxygen and water at high temperatures. Although air-blown gasifiers exist, the common practice is to separate oxygen before applying it to the process. Various types of gasifiers, based upon fixed, fluidised or entrained beds, are in use. Data for some commonly used gasifiers are given in Table 2 below [4].

TABLE 2: Data for coal gasifiers.

Type of reactor	Pressure bar	Temperature °C	Output gas $CO+H_2$, %
Lurgi - solid-bed	20-100	400-1100	60
Winkler - fluidized-bed	1-10	850-1100	75
Texaco -entrained	30-70	1200-1600	80
Koppers-Totzek - entrained	1	1200-1800	80

All types of coal can be gasified, and also peat and biomass (an interesting example is an ammonia plant in Finland, producing 250.000 t/year of hydrogen from peat) [4].

3. Steam reforming of natural gas

Being the most common process for hydrogen production, this is well established technology. However, there are still challenges and improvement potential. Some new approaches and developments are described in the following sections.

3.1. BASIC PROCEDURE

As mentioned above, the SMR reaction is endothermic, requiring 222 kJ/mole (of CH_4). The heat is normally supplied by burning of additional natural gas and/or waste gas from the product purification unit. The process scheme is shown in figure 1.

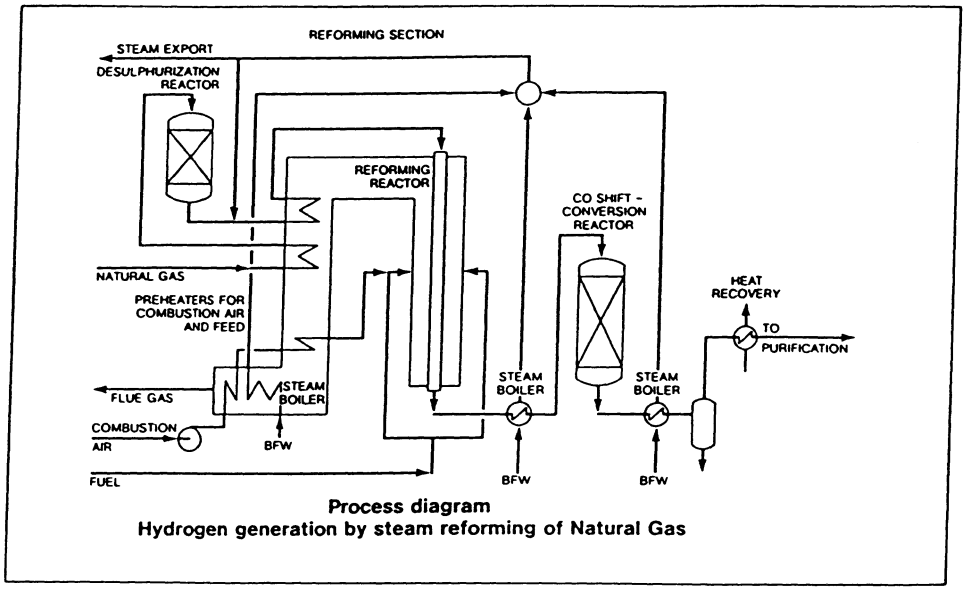

Figure 1. SMR Process Scheme.

The classical steam reformer is a large refractory-lined furnace equipped with roof or sidewall burners. Several vertical, catalyst-filled tubes run through the furnace, the reaction taking place inside the tubes at high temperature and pressure. The catalyst is usually nickel supported by alumina. Heat transfer is by radiation, and the thermal efficiency of such a reformer is around 50 %. The process conditions are strenuous, demanding high-quality steel in the tubes. Many side reactions occur, some of them leading to carbon formation. The temperature and steam: carbon ratio are important parameters to control in order to avoid coking, which would clog up the catalyst.

3.2 PRE-REFORMING

It may be of advantage to perform the reforming in two steps, i.e. add a pre-reformer upstream of the main reformer. This pre-reformer is operated at lower temperatures (350-500 °C) and with a different catalyst than the main reformer. Some of the methane and all the higher hydrocarbons will be reformed in the pre-reformer. It is claimed that the overall thermal efficiency, throughput and operating costs can be considerably improved by pre-reforming [5]. Also, the range if feedstocks for hydrogen production will be widened, up to and including kerosene.

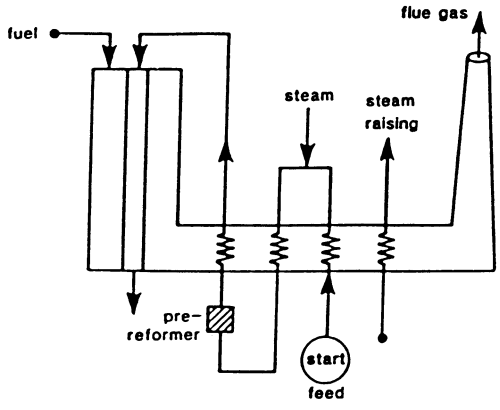

Figure 2. Pre-reforming scheme

3.3. AUTOTHERMAL REFORMING

This refers to a combination of SMR and POX applied to light hydrocarbon feedstock (natural gas, LPG, naphta). The process was originally developed by Haldor Topsøe jointly with Société Belge de l'Azote [2]. The process scheme is shown in figure 3:

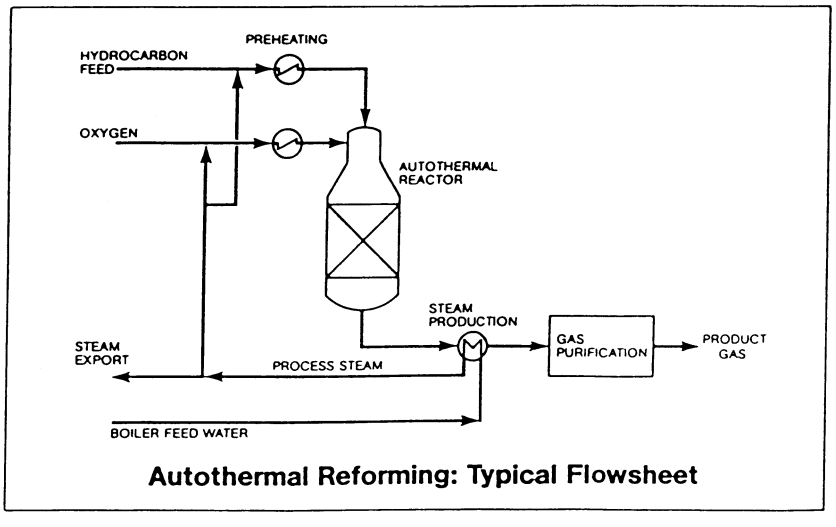

Figure 3. Process scheme of autothermal reforming

The oxygen supplied burns to extinction and provides the heat required for the SMR reaction, no additional firing is required. By adjusting the feed composition and the reactor outlet conditions, a wide range of product compositions may be obtained.

3.4. ADVANCED REFORMERS

The description of the classical steam reformer would indicate a demand for a more compact and efficient unit. In particular a more efficient heat utilisation, avoiding a large export of steam, would be desirable. A reformer designed by Haldor Topsøe, called the heat exchange reformer [2] goes a long way to meet these requirements. The reformer is schematically shown in figure 4. It is characterised by pressure combustion, convective heat transfer, and two annular catalyst beds circumjacent to the combustion chamber. The process gas flows counter-currently to the heating gases in the outer bed, co-currently in the inner bed. The design is very compact, gives a thermal efficiency of ~ 80 %, and outlet gas temperatures of ~ 550 °C (compared to 850-1000 °C in the conventional reformer). The reformer is particularly useful for small-medium scale hydrogen production.

Another novel design is the gas-heated reformer (GHR) by ICI Katalco. This is also a heat-exchange type reformer with convective heat transfer, but without a burner. Heat is supplied to the process gas by secondary gas from a second reformer, operated autothermally. The GHR is also very compact, claimed to have a volume of only 1/15 of an equivalent conventional reformer [6].

ICI Kataco has designed a hydrogen process around the GHR, and named it "Leading Concept Hydrogen Process" (LCH process). A simplified flowsheet for the process is shown in figure 6. The pre-heater for the GHR feed is gas-fired, but may be fired with purge gas from

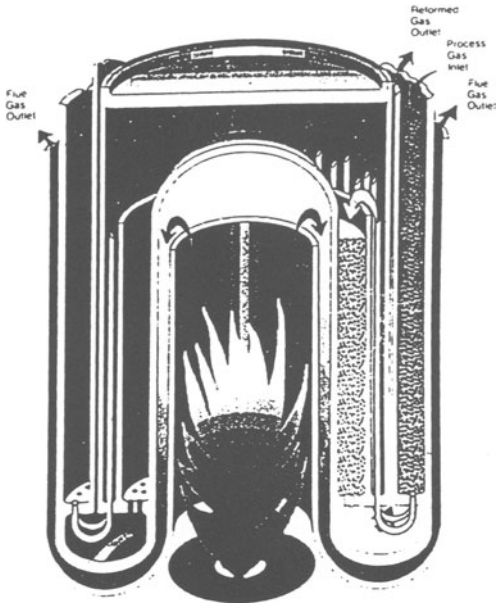

Figure 4. Heat exchange reformer by Haldor Topsøe

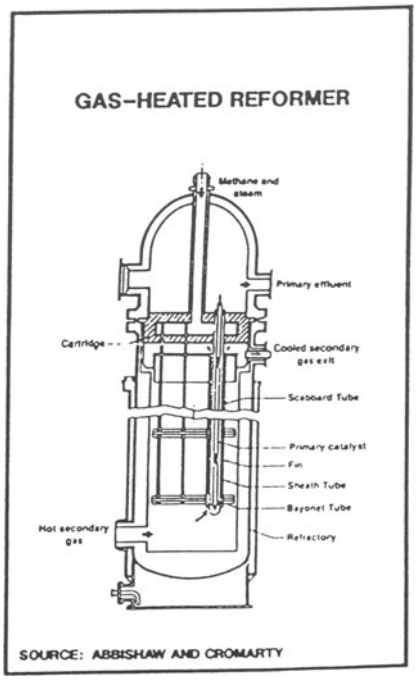

Figure 5. Katalco's gas-heated reformer

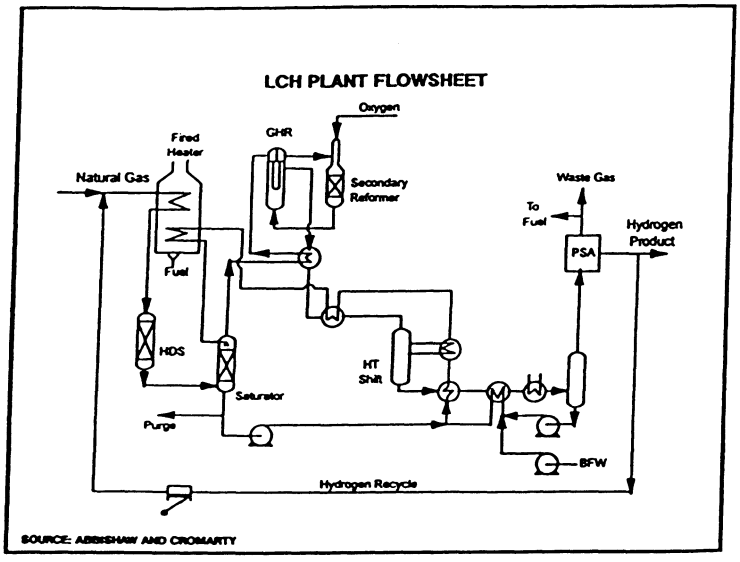

Figure 6. LCH Process scheme

the PSA unit. Higher pressures than in conventional SMR can be applied, resulting in more compact equipment. It is claimed that the area required for a LCH plant will be 25 - 30 % smaller than that of a conventional plant, and that both investments and operating costs will be considerably reduced [6].

At the MIT Plasma Science and Fusion Center, development of plasma reformers is underway [7]. These so-called plasmatrons are very compact and very light, have fast response times, high conversion efficiencies, and can be operated with a broad range of fuels. Hydrogen-rich gas (50-75 % H_2, 25-50 % CO) can be efficiently produced. Experiments with POX and pyrolysis of methane in plasmatrons are also going on [8].

3.5 IN SITU PRODUCT SEPARATION

The possibilities of incorporating selective membranes or sorbents into steam reformers or shift reactors are being investigated. Selective removal of one of the reaction products will shift the equilibrium to the product side and create more favourable thermodynamic conditions, thus permitting e.g. lower operating temperatures. The selective removal of either H_2 or CO_2 are both being investigated. One example is a concept called the water gas shift membrane reactor, being studied at ECN in the Netherlands [9]. The principle of the reactor is shown in figure 7. Hydrogen diffuses through a selective membrane to form a H_2 permeate, whereas CO_2 remains in the retentate. Various ceramic membranes, e.g. microporous silica membranes are being studied. Silica/Zirconia membranes also appear to be efficient for high temperature H_2 separation [10].

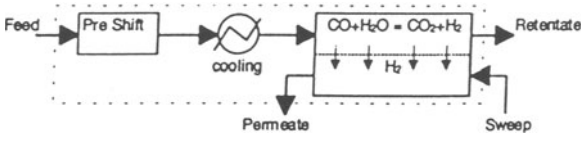

Figure 7. Membrane shift reactor system

The "classical" material for H_2-seledctive membranes is palladium or Pd alloys. Steam reforming in a Pd membrane reactor has been studied by Uemiya et al. [11], a Pd/Ag membrane reactor was studied by Jørgensen et al. at Haldor Topsøe [12]. Drawbacks of Pd membranes are the high material costs, and the fact that H_2 diffusion is rather slow. Thus, very thin films of Pd are mandatory. Thin-film membranes supported on microporous ceramic tubes have been developed and tested for separation of reformate gas [13]. A new and promising approach is a composite membrane, consisting of a relatively thick foil of a refractory metal (e.g. vanadium, zirconium) with a thin Pd coating on both sides. A remarkable increase in H_2 flowrates, compared to pure Pd membranes, has been demonstrated [14].

Alternatively, CO_2 can be removed selectively instead of H_2. The SER Process (Sorption Enhanced Reaction Process) under development by Air Products and Chemicals is an example [15]. A special CO_2 selective adsorbent (probably Ca-based) has been developed and its compatability with a suitable catalyst confirmed. A new adsorbent with higher capacity is currently being tested. The SER Process is expected to permit lower operating temperatures, less expensive construction materials, and reduce downstream purification, as compared to conventional SMR.

3.6 HYDROGEN PRODUCTION WITH CO_2 SEQUESTRATION

In the present practice of hydrogen production, most of the CO_2 is released to the atmosphere after separation from the hydrogen product. (Some CO_2 can be sold for various industrial and commercial applications, but these markets are small compared to the volumes of CO_2 produced.) The option of CO_2 sequestration, i.e. disposal in the ocean or in underground formations, is under study and consideration for reducing CO_2 emissions from fossil-fuelled power stations. This is obviously an option also for "CO_2-free" hydrogen production, but it has been thought that it would increase hydrogen costs too much to be feasible in a "hydrogen economy". Recent studies, however, indicate that the cost increase incurred by CO_2 sequestration will be quite moderate.

The concept of "CO_2-free" or "decarbonised" hydrogen production was discussed in the 11th World Hydrogen Energy Conference [17, 18] and the 3rd International Conference on Carbon Dioxide Removal [19, 20]. It is easier to separate CO_2 from H_2 in a reformate gas than from power plant flue gases, hence CO_2 sequestration will be less expensive in connection with hydrogen production. The separation may be accomplished by chemical extraction (e.g. with amines like MEA, monoethanol amine), by physical extraction, or by PSA, membranes or cryogenic methods. Ocean disposal of CO_2 is being investigated, but a more realistic option for the near-medium term is underground disposal. A large-scale demonstration of this method is being carried out by Statoil at the Sleipner field. The potential capacity for underground disposal in Europe has been thoroughly studied and evaluated to be very large [21]. (A great part of this

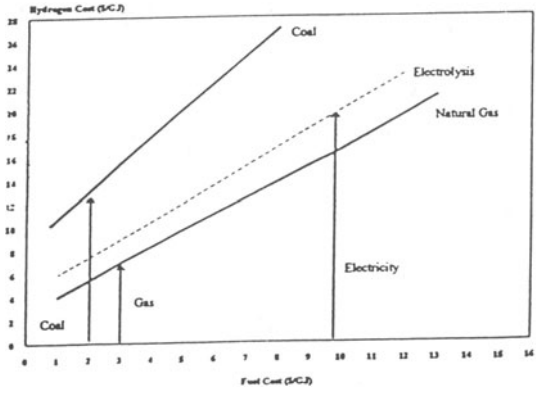

Figure 8. Costs of "decarbonised" hydrogen.

capacity is found on the Norwegian continental shelf).On contract with Statoil and the IEA Greenhouse Gas R & D Programme, the British engineering company Foster Wheeler has done a feasibility study and cost estimate of hydrogen production from natural gas and coal, with and without CO_2 sequestration. For the natural gas case, CO_2 sequestration was found to cost 20 USD/ton CO_2 (at 10 % capital return). This was found to increase the hydrogen production cost by 25 %, from 5,6 USD/GJ to 7 USD/GJ. In the coal case, the increase was considerably greater (~ 50 %). The costs are shown in figure 8 [22]. For comparison, the cost of hydrogen produced by water electrolysis, at an electricity price of 3,5 c/kWh, is also shown. This is about three times the cost of decarbonised hydrogen from natural gas. The electricity price would have to be as low as 2 c/kWh for water electrolysis to be competitive. The conclusions of the IEA Greenhouse Gas expert group are [22]:

- decarbonised hydrogen could be a potential method of obtaining deep global reductions in CO_2 emissions by replacing petroleum based fuels and direct uses of primary energy

- for the foreseeable future, this will be a cheaper source of hydrogen than renewable and other "carbon free" sources.

4. Pyrolytic cracking of natural gas

It has long been known that methane and other hydrocarbons can be cracked, i.e. split into their elemental components by pyrolysis. Until recently this method has not been considered for industrial hydrogen production. Pyrolytic cracking of higher hydrocarbons for the production of carbon black is done industrially, the process is known as the "Furnace Black Process". Heavy oil is used as feedstock and natural gas for heating. The process is characterised by low feedstock utilisation, high emissions and a gaseous by-product of low value. Recent developments aim to use lighter feedstocks, such as natural gas, and to emphasise pure hydrogen as a valuable product in addition to the carbon black. Such developments have led to the Kværner "CB & H" process, which will be described in a later presentation at this conference [23].

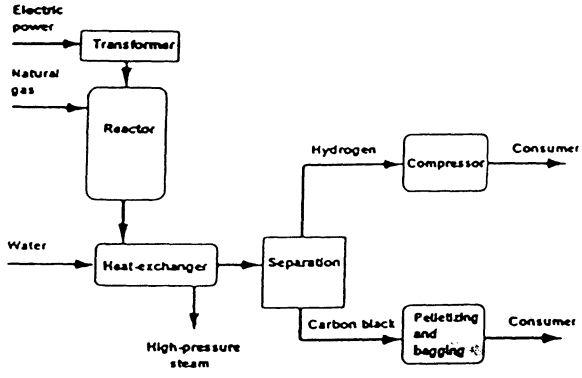

Figure 9 Process scheme of the "CB & H" process

Methane is a stable compound, it takes 75 kJ/ mole to crack it. Thus, pyrolysis of natural gas will also be strongly endothermic. In the traditional furnace, heat is supplied at high temperature by combustion of some of the gas. Modern approaches include the use of catalysts to reduce the temperature, as well as high temperature pyrolysis is plasma arcs. The catalytic approach has been studied a.o. by Kuvshinov et al. [24] in Russia and Muradov [25] in the USA. With nickel-based catalysts it is possible to operate at relatively low temperatures (500-600 °C). Problems involved are incomplete conversion to hydrogen, and the fact that carbon is deposited in the catalyst bed, implying separation problems. In

current work, Muradov is testing carbon-based catalysts to avoid this problem [26]. Also, Steinberg has found that at 900 °C, the process can proceed autocatalytically [27].

Pyrolysis of natural gas in plasma arcs has been studied several places, a.o. in France [28] and Russia [29]. The concept has been developed into an industrial process by the Norwegian company Kværner, this is the "CB & H" process to be described later [23]. The process is characterised by high efficiency, high yields of two valuable products, and no harmful emissions. A main advantage of producing hydrogen in this way is, of course, that no CO_2 is produced. There are markets for the carbon products. If these become saturated, any surplus can be regarded as an excellent energy carrier, easily stored for future use. If burnt in an IGCC plant or in a CO_2/O_2 atmosphere, CO_2 sequestration can be easily accomplished.

5. Small scale hydrogen production

Most of the world's hydrogen production takes place in large plants, and the processes for production from fossil feedstock are generally most efficient in large scale operation. Some industrial applications of hydrogen require only smaller volumes, and scaled-down versions of conventional SMR plants can be supplied for such demands (generally down to a few thousand Nm^3/day (~ 100.000 sqf/day). For smaller demands, water electrolysis or merchant hydrogen will be more economic solutions).

With the advent of fuel cells, a new market for small scale hydrogen production has started to develop. In fact a new generation of steam reformers, dedicated to fuel cells, has emerged. The heat exchange reformer by Haldor Topsøe, described earlier, was developed for fuel cell use and has indeed found such application. Later, the fuel cell suppliers have elaborated their own designs. The reformer is normally an integral part of the fuel cell plant, accounting for about 1/3 of the investment cost.

The requirements to the fuel cell reformers are different from those applying in chemical industry. Compactness and low cost are mandatory. The demands to product purity are less, since the fuel cells will tolerate appreciable contents of inactive gases like CO_2, CH_4, and N_2. The only strict limitation is for CO, particularly for PEM fuel cells. This may require a selective oxidation or another special purification step.

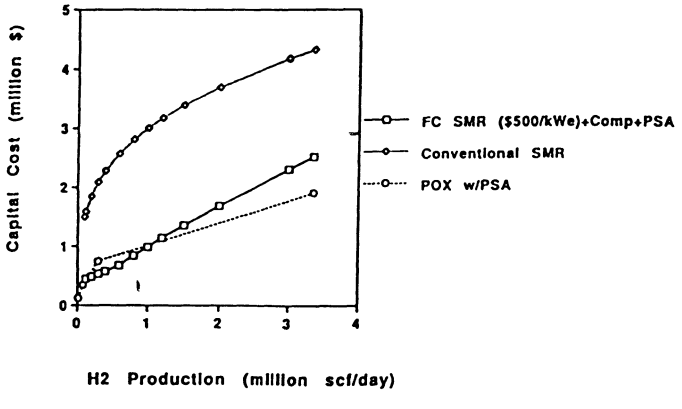

Figure 10. Capital cost of small scale reformers

The possible application of hydrogen as a vehicle fuel on a larger scale opens some interesting perspectives for small scale hydrogen production. Existing infrastructure for hydrogen distribution is limited. To establish an adequate

infrastructure for hydrogen as a fuel will be a formidable task.

On the other hand, infrastructures for natural gas distribution exist in most industrialised countries. As an alternative to distribution from large central plants, small scale decentralised hydrogen production from natural gas may be considered. For this purpose down-scaled conventional reformers, fuel cell reformers equipped with gas purification systems, or even small POX units may be used. A very interesting study of economic and other aspects of such systems has been performed by Ogden et al. [30]. Some capital and operating cost data are shown in figures 10 and 11. It is seen that the fuel cell reformers and POX units, equipped with PSA systems, will be cheaper than the down-scaled conventional reformer.

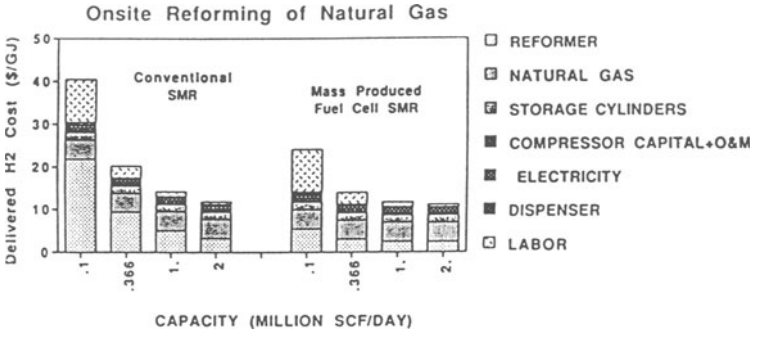

Figure 11. Delivered hydrogen costs from small scale reformers

This is reflected also in the production costs, which will be lower with the fuel cell reformers at least at the lower production rates (1 million sqf/day would supply e.g. 80 Ballard PEMFC buses or 800 automobiles per day). For on-site hydrogen production, water electrolysis may be a competitive option, if sufficiently cheap electricity can be provided. For areas without a natural gas infrastructure, this will be the only option.

For fuel cell vehicles, an alternative to carrying hydrogen on board is to carry a liquid fuel which can be converted on board to a hydrogen-rich gas. One possibility is to use methanol, which can be reformed to H_2-rich gas in small compact reformers on board vehicles. Daimler-Benz are going for this option in their new generation of fuel cell cars. Methanol is much easier to reform than natural gas or other hydrocarbons; on board reforming of such fuels is hardly feasible. But their conversion to H_2-rich gas in small compact POX units is certainly possible. Such units have the advantage to be simpler and cheaper than reformers, and to respond faster to load changes. Disadvantages are that they dilute the fuel cell feed gas with nitrogen from the combustion with air, they give lower system efficiencies and more emissions. The US company Arthur D. Little is developing compact POX units for cars, and Chrysler is building a prototype fuel cell car that will use gasoline and POX conversion. Another US company, Hydrogen Burners Technology, Inc., has developed small-scale POX converters for on-site hydrogen production; they are now on the market under the trade name of Phoenix [31].

6. Special processes

A few special concepts for hydrogen production from fossil materials, some of which involve the use of renewable energy, will be briefly described.

6.1 SOLAR REFORMING

As we have seen SMR is an endothermic, high-temperature process. This makes it a candidate for solar thermal processing. Solar energy can be concentrated to yield very high temperatures and heat fluxes. Different types of solar heated SMR reactors have been developed and tested, e.g. by DLR in Germany and the Weizmann Institute (WIS) in Israel [32]. In a 280 kW reactor tested at the WIS, 80 % conversion of methane was achieved. The solar energy contribution to the product gas can be 20-30 %.

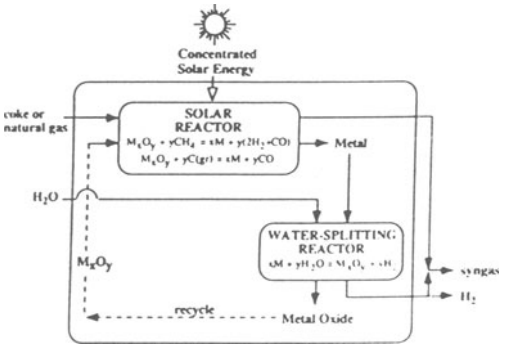

Figure 12. Solar thermal process for syngas and hydrogen

A special case is a combined reforming and metal oxide reduction process, being studied at the Paul Scherrer Institute (PSI) in Switzerland [33]. The process, schematically shown in figure 12, produces syngas in the primary step, and hydrogen in a secondary water splitting step.

6.2 HYBRID PROCESSES

In a comparison of hydrogen production processes, Rosen [34] includes some combinations of SMR with other production processes, e.g. water electrolysis. He finds that a combination of SMR and advanced water electrolysis will give better energy and exergy efficiencies than the other concepts studied. An advantage is that the oxygen produced by electrolysis can be used for autothermal reforming, improving the efficiency of the SMR part of the process.

6.3. BACTERIAL SHIFT REACTION

Some photosynthetic bacteria have the capability to shift CO into H_2. Under anaerobic, dark conditions with CO as the sole source of carbon and energy, H_2 and CO_2 are produced at nearly stoichiometric levels with CO consumption. The process is being studied at the National Renewable Energy Laboratory (NREL) in the USA [35]. A gas stream initially containing 10 % CO was shifted essentially completely into an H_2-enriched gas stream containing less than 0,1 ppm CO. Use of the bacteria as a conditioning catalyst to produce a CO-free, H_2-rich gas stream from fuel gases is considered a feasible method for generating feed gas for fuel cells.

7. Summary and conclusions

Some general conclusions may be drawn from this review of hydrogen production from fossil sources:

- Steam reforming and partial oxidation of hydrocarbons are the dominant methods for hydrogen production today.
- Although these processes are technologically mature there is potential for improvements, and promising developments are in progress.
- Steam reforming of natural gas is the cheapest method and will remain so in the near-medium term, even if CO_2 sequestration is included.
- Pyrolytic cracking of natural gas has been developed to an industrial process that appears competitive for "CO_2-free" hydrogen production.
- If hydrogen becomes a common vehicle fuel, on-site production may be a feasible alternative to central production and a large infrastructure for hydrogen distribution.
- Hybrid processes involving the use of renewable energy may be interesting options in a transition period, until hydrogen production based entirely on renewables becomes feasible.

References

1. R. Roesler, W. Zittel: *Wasserstoff als Energieträger.* Forschungszentrum Jülich GmbH (1994).

2. Topsøe Seminar on Synthesis Gas Technologies. *Haldor Topsøe A/S (1986)*

3. C. Petit, S. Libs, A. C. Roger, A. Kaddouri, A. Kiennemann: *Hydrogen production by catalytic oxidation of methane.* Hydrogen Energy Progress IX, **1**. 53 (1992).

4. B. Gaudernack, K. Andreassen, B. Arnason, P. Lund, L. Schleisner: *Hydrogen production potential in the Nordic countries.* Hydrogen Energy Progr. X, **1**, 9 (1994).

5. J. M. Foreman, J. J. Templeman: *The benefits of pre-reforming in hydrogen production plants.* Hydrogen Energy Progr. IX, **1**, 3 (1992).

6. The Clean Fuels Report, Vol 8 no. 3, 146 (1996)

7. L. Bromberg, D. R. Cohn, A. Rabinovich: *Plasma reformer - fuel cell system for decentralised power applications.* Int. J. of Hydrogen Energy, **22**, 83 (1997)

8. L. Bromberg, D. R. Cohn: *Hydrogen manufacturing using plasma reformers.* DOE Hydrogen Program Technical Review (1997).

9. M. Bracht, P. T. Alderliesten: *Water gas shift membrane reactor for CO_2 control in IGCC systems.* Proc. of 3. Int. Conf. on Carbon Dioxide Removal, **1**, 159 (1996).

10. M. Aihara, H. Ohashi, H. Ohya, Y. Negishi, S. I. Semenova: *High temperature corrosion-resistant separation membranes for thermochemical process.* Hydrogen Energy Progr. XI, **1**, 61 (1996).

11. S. Uemiya, N. Sato, H. Ando, T. Matsuda, E. Kikuchi: *Appl. Catal. 67, 223 (1991).*

12. S. Lagsgaard Jørgensen, P, E. Højlund-Nielsen, P. Lehrmann: *Steam reforming of methane in a menbrane reactor.* Catalysis Today, **25**, 303 (1995).

13. J. C. S. Booth, M. C. Doyle, S. M. Gee, J. Miller, L. A. Scholz, P. A. Walker: *Advanced hydrogen separation via thin supported Pd menbranes.* Hydrogen Energy Progr. XI, **1**, 867 (1996).

14. The Clean Fuels Report, Vol **9** no. 3, 144 (1997)

15. B. T. Carvill, J. R. Hufton, M. Anand, S. Sircar: *Sorption enhanced reaction process.* AlCheE J. **42**, 2665 (1996).

16. S. Sircar: *Sorption enhanced reaction (SER) for production of hydrogen.* DOE Hydrogen Program Technical Review (1997).

17. B. Gaudernack, S. Lynum: *Hydrogen from natural gas without release of CO_2 to the atmosphere.* Hydrogen Energy Progr. XI, **1**, 511 (1996).

18. H. Audus, O. Kaarstad, M. Kowa: *Decarbonisation of fossil fuels: Hydrogen as an energy carrier* Hydrogen Energy Progr. XI, **1**, 525 (1996).

19. B Gaudernack, S. Lynum: *Natural gas utilisation without CO_2 emissions.* Proc. of 3. Int. Conf. on Carbon Dioxide Removal, **1**, 165 (1996).

20. O. Kaarstad, H. Audus: *Hydrogen and electricity from decarbonised fossil fuels.* Proc. of 3. Int. conf. on Carbon Dioxide Removal, **1**, 431 (1996).

21. S. Holloway: *The underground disposal of carbon dioxide.* Final Report of JOULE II Project No. CT92-0031 (1996).

22. IEA Greenhouse Gas R&D Programme: *Decarbonisation of fossil fuels.* Report No. PH2/2 (1996).

23. K. Hox, S. Lynum: *More efficient, economical and environmentally friendly utilisation of natural gas - how to produce hydrogen and not* CO_2. This conference

24. G. G. Kuvshinov, Y. J. Mogilnykh, D. G. Kuvshinov, S. G. Zavarukhin, V. N. Parmon: *New ecologically sound technology to produce hydrogen and new carbon material via low temperature catalytic pyrolysis.* Hydrogen Energy Progr. XI **1**, 655 (1996).

25. N. Z. Muradov: *Hydrogen production by catalytic cracking of natural gas.* Hydrogen Energy Progr. XI, **1**, 697 (1996).

26. N. Z. Muradov: *Production of hydrogen by thermocatalytic cracking of natural gas.* DOE Hydrogen Program Technical Review (1997).

27. M. Steinberg: *Production of hydrogen and methanol from natural gas with reduced* CO_2 *emissions.* Hydrogen Energy Progr. XI, **1**, 499 (1996).

28. L. Fulcheri, Y. Schwob: *From methane to hydrogen, carbon black and water.* Int. J. of Hydrogen Energy, **20**, 3, 197 (1995).

29. V. N. Parmon, G. G. Kuvshinov, V. A. Sobiyanin: *Innovative processes for hydrogen production from natural gas and other hydrocarbons.* Hydrogen Energy Progr. XI, **3**, 2439 (1996).

30. J. M. Ogden, T. Kreutz, S. Kartha, L. Iwan: *Hydrogen energy system studies.* NREL Technical Report (1996).

31. The clean Fuels Report, Vol **8**, no. 3, 149 (1996).

32. R. Tamme, M. Abele, R. Buck, A. Wörner: *Hydrogen and synthesis gas production by solar reforming of methane and natural gas.* Hydrogen Energy Progr. XI, **1**, 691 (1996).

33. A. Steinfeld, P. Kuhn, A. Reller, R. Palumbo, J. Murray, Y. Tamaura: *Solar-processed metals as clean energy carriers and water-splitters.* Hydrogen Energy Progr. XI, **1**, 601 (1996).

34. M. A. Rosen: *Thermodynamic comparison of hydrogen production processes.* Int. J. of Hydrogen Energy, **21**, 5, 349 (1996).

35. P. F. Weaver, P. C. Maness, S. A. Markov: *Anaerobic, dark conversion of CO into* H_2 *by photosynthetic bacteria.* Proc. of BioHydrogen '97 (in press).

HYDROGEN PRODUCTION BY ELECTROLYSIS

KNUT ANDREASSEN
Norsk Hydro Electrolysers AS
P.O. Box 44, N-3671 Notodden, Norway

Abstract

Industrial electrolysers are mostly using alkaline electrolyte and are operating at about 80 ^{0}C and 1 - 30 bar. Cells based on solid electrolytes, polymers or ceramics, are developed, but have for the time being no commercial significance. The best available technology of today may have an electric energy efficiency of about 80 %. Two main types of electrolysers are in use, "tank cells" with electrodes connected in parallel and "filterpress cells" with electrodes in series. In a plant the former electrolysers are connected in series, the latter ones in parallel and eventually also in series. The hydrogen production cost is under certain assumptions about 1,40 NOK/Nm^3 or 0,40 NOK/kWh.

1. Introduction

1.1. ROUTES FOR HYDROGEN PRODUCTION

Based on various energy sources and hydrogen containing compounds as raw materials, the different routes for the production of hydrogen are illustrated in Figure 1. Chemical, thermochemical, electrical and photochemical conversion processes are used. Today steam reforming/cracking of hydrocarbons and electrolysis of water are used in an industrial large scale.

With a fossil hydrocarbon as the main energy source and raw material, and using a chemical conversion process, 30 - 50 % of the hydrogen originates from the hydrocarbon, the rest from water. Water is the main raw material in the other routes. Practically, they are based on electricity production and electrolytic water splitting. This method is therefore the most direct and general one.

1.2. WATER ELECTROLYSIS

The history of water electrolysis starts as early as the first industrial revolution. In the year 1800, Carlisle and Nicholson demonstrated splitting of water by electrolysis.

T. O. Saetre (ed.), Hydrogen Power: Theoretical and Engineering Solutions, 91–102.

In fact, it is the oldest electrochemical process known. However, nearly 100 years had to pass away before it was introduced as a useful industrial way of producing hydrogen and oxygen. In 1902 about 400 electrolysers were in operation. Norsk Hydro started its first electrolysis plant in 1928, and electrolytic generated hydrogen was the main basis for the company's fertilizer production for 50 years. The production reached a peak in the sixties, amounting to about 100 000 Nm^3/h.

Presently only 0,5 % of the total hydrogen production is generated by water electrolysis. However, in the future when the use of hydrocarbons has to be restricted as a result of limited resources and/or environmental pollution, this process may take the lead.

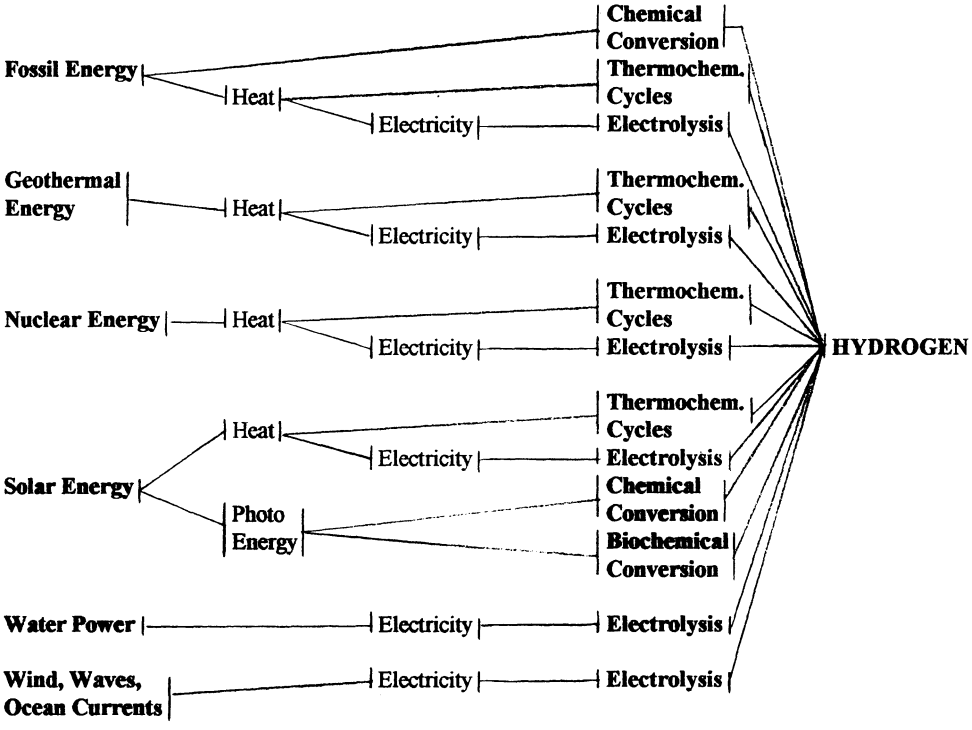

Figure 1. Hydrogen Production Routes

2. Principles

2.1. GENERAL

An electrolysis cell is composed of two electronic conductors, electrodes, in contact with an ionic conductor, electrolyte. When an electric direct current is passed through a cell containing water, the water molecule may be split into hydrogen and oxygen.

$$H_2O + \text{energy} = H_2 + 1/2\ O_2. \quad (1)$$

Water is a very poor ionic conductor, and the electrolyte has to contain also other components to obtain a reasonable conductivity. These components should not undergo any changes during the electrolysis.

2.2. ALKALINE ELECTROLYTE

The discovery of electrolytic water splitting was done in an acidic solution. Despite this fact, in industrial plants an alkaline medium has been preferred up to now, mainly because of lesser corrosion problemes.

In Figure 2 the principles of an electrolysis cell with a KOH-solution as electrolyte are shown.

The basic reactions at the two electrodes are:

$$\text{Cathode:} \quad 2\ H_2O + 2\ e^- = H_2 + 2\ OH^- \quad (2)$$

$$\text{Anode:} \quad 2\ OH^- = 1/2\ O_2 + H_2O + 2\ e^- \quad (3)$$

The net reaction is given above, reaction (1).

Between the electrodes there is a separator, a diaphragm or a membrane, to keep the produced gases apart. Hydroxylium ions migrate through the separator during the electrolysis process. The process water is generally fed to circulating electrolyte.

KOH is the most used alkaline component because of good conductivity. The concentration may be 25 - 30 % by weight. The working temperature has then to be lower than 100 ^{0}C, usually about 80 ^{0}C. The pressure could be from 1 to 30 bar.

The cathode and the anode must be corrosion resistant in the electrolyte at reducing, respectively oxidizing potentials, be good electronic conductors and have structural integrity. They should catalyze evolution of the gasses as effectively as possible.

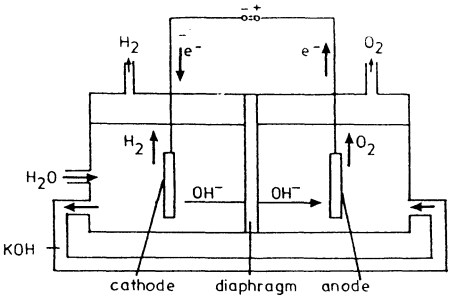

Figure 2. Alkaline Electrolyte

2.3. ACID ELECTROLYTE

Today acid solutions are not used in water electrolysis practice. However, acid membranes have been introduced as interesting electrolytes, and the technology is under continous development. The principles are shown in Figure 3.

In this case the basic reactions at the electrodes are:

Cathode: $2\,H^+ + 2\,e^- = H_2$ (4)

Anode: $H_2O = 1/2\,O_2 + 2\,H^+ + 2\,e^-$ (5)

The net reaction is of course the same as before, reaction (1) above.

Protons are migrating through the membrane during electrolysis. The membrane does not only serve as a solid electrolyte, but also as gas separator. Water may only be fed to the anode chamber of the cell.

The membrane is a so called proton exchanger. It is mostly made of polymer materials. Perfluorocarbon sulfonates are commonly used. The upper temperature limit for these is 125 - 150 °C, but in general liquid water and an operation temperature of about 80 °C is used.

Also ceramic proton conducting materials could be used as membranes. The operating temperature is then in a range where water is present as steam.

The electrodes are in these cells always placed in direct contact with the membrane. They could be thin layers of catalyst materials.

This electrolysis system allows high current densities at high cell efficiency. The drawback is high investment cost because of expensive membrane and electrode materials.

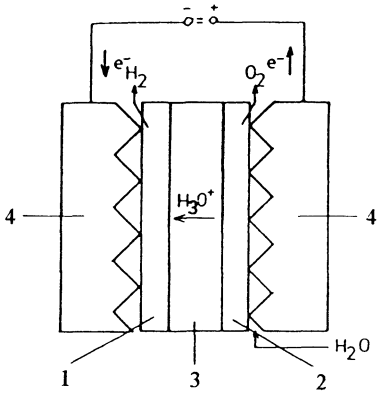

Figure 3. Acid Membrane Electrolyte

1. Cathode
2. Anode

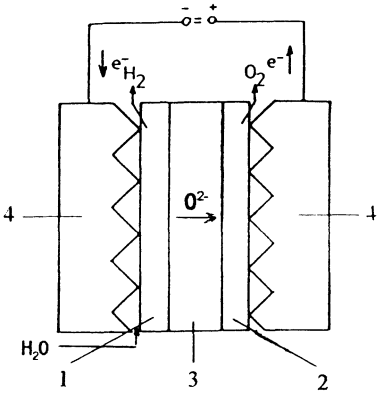

Figure 4. Oxygen Ion Conducting Electrolyte

3. Solid Electrolyte
4. Current Collector

2.4. OXYGEN ION CONDUCTING ELECTROLYTE

Electrolysis cells operating at high temperature using proton conducting ceramics as electrolyte are only tested in small laboratory scale. Much more development work is performed concerning oxygen ion conducting solid electrolytes. The principles are shown in Figure 4.

The basic reactions at the electrodes are:

Cathode: $H_2O + 2\,e^- = H_2 + O^{2-}$ (6)

Anode: $O^{2-} = 1/2\,O_2 + 2\,e^-$ (7)

The net reaction is again reaction (1) above.

In this case oxygen ions are migrating through the solid electrolyte, serving also as a gas separator. Water is fed to the cathode chamber of the cell.

The electrolyte is made of ceramic materials. The operating temperature has to be high, 700 - 1 000 ^{0}C, because only in this temperature range known ceramics have a satisfactory ionic conductivity.

The cells could operate at a high current density and have high efficiency. The drawback is that all construction materials have to be ceramics because of the high temperature used. This creates design problems, high investment and maintenance costs.

3. Energy Consumption

3.1. THERMODYNAMICS

The water splitting reaction is as stated before:

$$H_2O = H_2 + 1/2\,O_2 \quad (8)$$

Under standard conditions (component activity: 1, temperature: 273,15 K, presure: 1 bar) the Helmholtz energy (reaction enthalpy) based on liquid water is

$$\Delta H^0_{273,L} = 285{,}9 \text{ kJ/mol.}$$

This corresponds to the so called higher heating value of hydrogen.When the splitting is performed by electrolysis, the main part of the total reaction energy has to be supplied as electric energy, corresponding to the Gibbs energy. Under standard conditions we have:

$$\Delta G^0_{273,L} = 237{,}2 \text{ kJ/mol.}$$

The well known relation between Helmholtz and Gibbs energy is:

$$\Delta H = \Delta G + T \cdot \Delta S \quad (9)$$

The energy $T \cdot \Delta S$ could thermodynamically be covered by thermal energy.

The cell voltages corresponding to the two thermodynamic energies are:

The thermoneutral cell voltage: $U_{tn} = \Delta H/(2\,F)$ (10)

The reversible cell voltage: $U_{rev} = \Delta G/(2\,F)$ (11)

ΔH and ΔG and then also U_{th} and U_{rev} are functions of electrolyte composition, temperature and pressure. In Figure 5 the relationships to temperature are shown. The brake of the curves at 100 ^{0}C is of course due to the transition from liquid water to steam. It corresponds to the evaporation energy.

The energy necessary to heat the water from e.g. 25 ^{0}C to the reaction temperature T, to rise the pressure from 1 bar to the reaction pressure p, to evaporate water and to compensate for heat losses could thermodynamically be covered by thermal energy. In industrial electrolysis a greater part is however covered by electrical energy, as shown below.

The electrical energy efficiency of the electrolysis process could be defined by the equation:

$$e = U_{tn,\,273,\,I.} / U \qquad (12)$$

where U is the actual cell voltage.

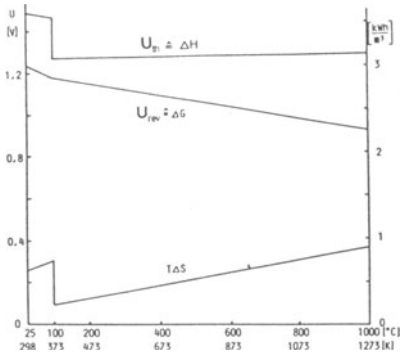

Figure 5. Voltage / Temperature Relationships

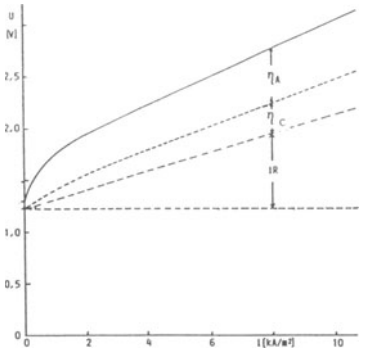

Figure 6. Voltage / Current Density Relationships

3.2. CELL VOLTAGE

Water electrolysis under technical conditions demands a cell voltage which is noticeable higher than the reversible value. The voltage has to overcome the electrical resistance in the electrodes, in the electrolyte between the electrodes and in the separator. In addition come also the overvoltages at the electrodes, which are kinetically determined. The actual cell voltage is then given by the relation:

$$U = U_{rev} + \eta_C + \eta_A + j\ R^* \qquad (13)$$

where η_C is the overvoltage at the cathode, in this case the so called hydrogen overvoltage, η_A is the overvoltage at the anode, the oxygen overvoltage, j is the current density and R^* the sum of the electrical resistances, based upon the active electrode area.

Figure 6 shows an example of the relations between voltages and current density in conventional alkaline electrolysis.

The conditions could also be illustrated as shown in Figure 7. Examples of real values are given in Table 1, refering to an industrial electrolyser using alkaline electrolyte at common conditions (25 % KOH, 80 ^{0}C, 1 bar).

The electrical resistance in the electrodes is determined by the material and design of the electrodes and the temperature. The resistance in the interface electrode/electrolyte is a function of for one thing the wetting conditions. The resistance in the electrolyte layer between the electrodes is determined by the resistivity of the electrolyte (function of composition and temperature) and the electrode gap. The resistance in the diaphragm is dependent of the material and the way it is fabricated (e.g. woven). The overvoltages are determined by the activity of the electrode surfaces, the electrolyte composition and temperature.

TABLE 1.
Ohmic Resistances and Cell Voltage Elements

Electrodes:	$R^*_A + R^*_C$	$= 2{,}0 \cdot 10^{-6}\ \Omega\ cm^2$
Electr. Surfaces:	$R_{A3} + R^*_{C3}$	$= 31{,}2 \cdot 10^{-6}$ "
Electrolyte:	R^*_E	$= 41{,}4 \cdot 10^{-6}$ "
Separator:	R^*_D	$= 36{,}0 \cdot 10^{-6}$ "
Sum	R^*	$= 110{,}6 \cdot 10^{-6}\ \Omega\ cm^2$

Rev. Cell Voltage:	$U_{rev} = U_{Al} + U_{Cl}$	$= 1{,}189$ V
Overv. (j=0,20 A/cm²):	$U_\eta = \eta_C + \eta_A$	$= 0{,}325$ "
Ohm.v.(j=0,20 A/cm²):	$U_\Omega = j \cdot R^*$	$= 0{,}221$ "
Sum:		$= 1{,}735$ V

Figure 7. Cell Voltage Elements

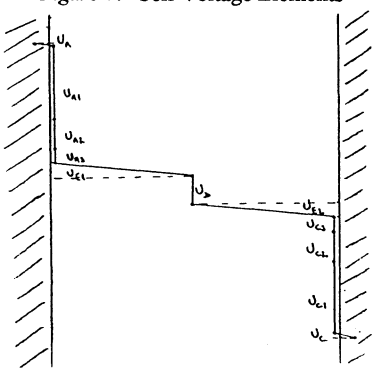

We see that the reversible cell voltage in the example makes about 68 % of the actual cell voltage, while the overvoltages and the ohmic voltage drop makes about 19 % and about 13 % of the total value respectively.

3.3. ENERGY CONSUMPTION

The energy consumed during hydrogen production is given by the following relationship:

$$E_{H2} = 2 \cdot F \cdot \rho_{H2} / (3600 \cdot M_{H2}) \cdot U / c \qquad (14)$$

where F is the Faraday constant, c the current efficiency, ρ_{H2} the density and M_{H2} the molar mass of hydrogen. Puting in the values we have for the example above:

$$E_{H2} = 2 \cdot 26{,}80 \cdot 0{,}08988 / 2{,}016 \cdot U / c = 2{,}39 \cdot 1{,}735 / 0{,}98 = 4{,}23\ kWh / m^3$$

4. Cells, Electrolysers and Plants

4.1. GENERAL

The description in this chapter will be limited to technology based on alkaline electrolytes, since for the time beeing these are the only ones used industrially, generally as KOH-solutions.

4.2. CELLS

As an example of an industrial cell configuration Figure 8 shows the elements of the Norsk Hydro design. It is made of two electrodes, two gaskets and a frame carrying the separator or diaphragm. At the bottom of the cell there are openings which form the electrolyte supply and distribution ducts. Hydrogen and oxygen respectively flow to openings at the top of the cell, forming ducts for gas and electrolyte removal. The cell is operating with 25 % KOH at 80 °C and 1 bar.

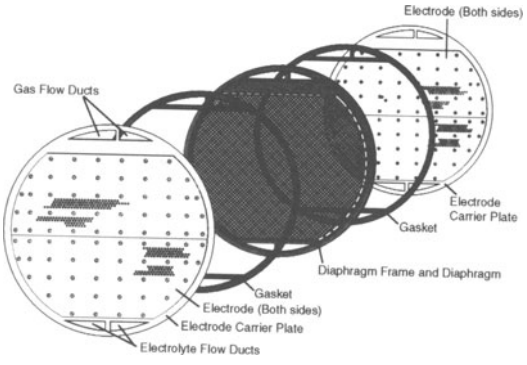

Figure 8. Norsk Hydro Cell

The gases evolving at the electrodes escape as bubbles. These are whirling around in the electrolyte and block the current paths between the electrodes. The gas/electrolyte volume ratio should therefore be low. On the other hand the gap between the electrodes should be small to minimise the ohmic resistance. Both are obtained in this case by using perforated so called fore-electrodes. Even though the gas evolution principally takes place on the front side of the fore-electrodes, the greater part of the gas bubles are rising on the back side. In some other cell designs a zero gap configuration is used. The fore-electrodes could be made of porous or extended metal sheets.

The diaphragm in the example is a woven cloth of a polymer material fixed in a frame. To act as an efficient gas separator with low electrical resistance, the cloth must be wetted by the electrolyte so that the pores are filled up. The frame and the electrodes are made of nickel plated steel. The fore-electrodes are also activated by catalytic coatings to lower the overvoltages.

4.3. ELECTROLYSERS

Industrial electrolysers are composed of many cells or electrode pairs. These may be connected in parallel or in series. Figure 9 shows the principles of a parallel connection. Each individual electrode is fed by current from outside and has only one polarity; it is monopolar, i.e. is either cathode or anode. The principles of a series connection are shown in Figure 10. Only the end electrodes are fed by current and are monopolar. The electrodes in between are bipolar, i.e. cathode on one side and anode on the other. Electrolysers having only monopolar electrodes are often called "tank cells" while electrolysers with bipolar electrodes are called "filterpress cells" due to the appearance.

An electrolysis plant have generally several electrolysers, connected in series or in series and parallel. The alternatives are shown in the Figures 11 and 12 respectively.

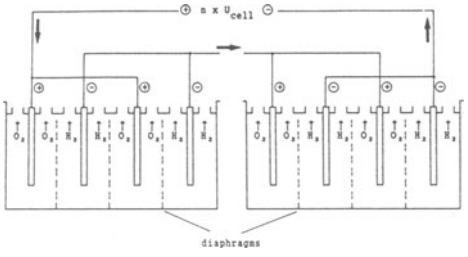

Figure 9. Parallel Connection of Cells

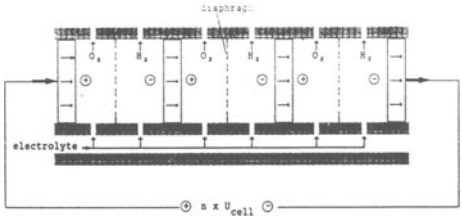

Figure 10. Series Connection of Cells

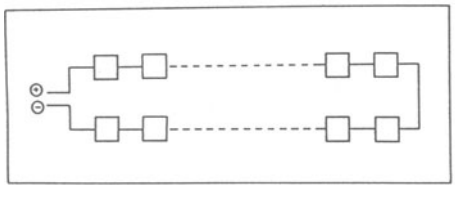

Figure 11. Series Connection of Electrolysers

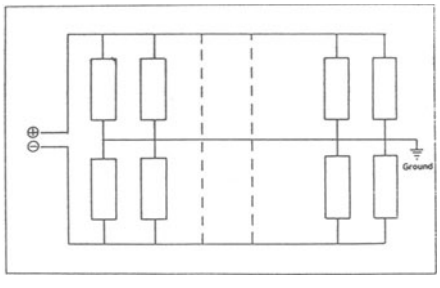

Figure 12. Parallel and Series Connection of Electrolysers

Each of the two electrolyser designs has advantages and disadvantages. The tank cell is simple and sturdy, while the filterpress cell for one thing has a lot of gaskets. The outer leeds to the tank cell cause voltage loss. The filterpress cell has channels for e.g. electrolyte supply, forming shunts to the cell stack and then causing current loss. The tank cell has a low voltage and is contingent upon a high current to give a reasonable production. The filterpress cell has a high voltage and operates with a low current. However, both are settled in a plant having several electrolysers.

As an example of a filterpress cell Figure 13 shows the Norsk Hydro design. The cell package is clamped together between rigid steel frames. The bus bars are connected to the front and rear ends.

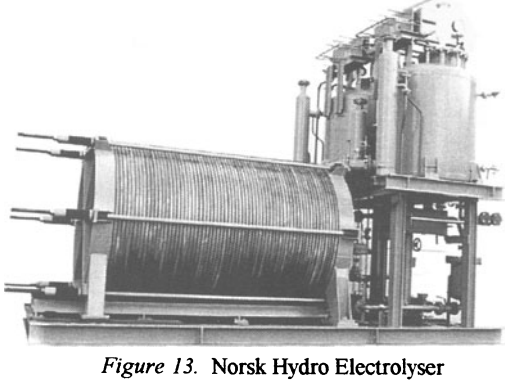

Figure 13. Norsk Hydro Electrolyser

4.4. PLANTS

The equipment around the electrolysers in a plant may vary from place to place and from provider to provider, even though the principles are not very different. As an illustration one of Norsk Hydro's systems is shown in Figure 14.

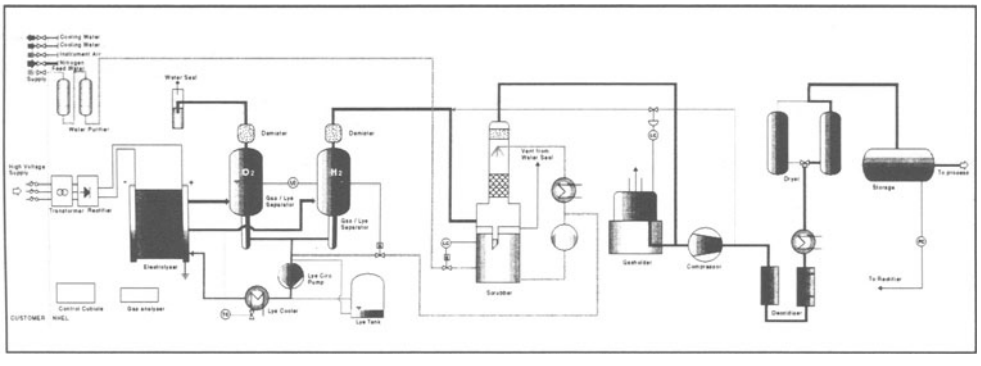

Figure 14. **Electrolyser Plant**

The produced hydrogen and oxygen gases together with some electrolyte flow through the removal ducts to the gas/electrolyte separators. The hydrogen is purified, cooled and dried and eventually compressed. Excess heat from the electrolyser is removed from the circulating electrolyte in the cooler. The feed water is purified in an ion exchanger and added to the electrolyte previous to its entry in the electrolyser's supply duct.

5. Economy

5.1. GENERAL

The economy of a hydrogen producing electrolysis plant is as usual dependent of the investment and the maintenance and operating costs, all in relation to the production rate.

5.2. COST DATA

In Table 2 are shown some characteristic data for a plant having a producing capacity of 4 000 Nm^3 H_2 / h.

TABLE 2. Cost estimates
Plant Capacity 4 000 Nm^3 H_2/h

Total investment cost:	NOK 90 000 000	
Annual capital cost:	NOK 10 500 000	
Annual maintenance and operating cost:	NOK 5 000 000	
Electricity cost:	NOK 31 500 000	
Total annual cost:	NOK 47 000 000	
Specific cost:		NOK 1,42 pr. Nm^3 H_2
		NOK 0,40 pr kWh (HHV of H_2)

The cost estimates are based on specific conditions, requirements and limitations. The most decisive are:

* The plant is located on an autonomous site equiped with its own administration, maintenance, plant control facilities and infrastructure.
* High voltage power supply and utilities such as treated and untreated water and a disposal system are readily available at reasonable cost.
* Hydrogen should be delivered at 30 bar at the plant battery limit.
* Oxygen could not be commercially used and is vented to air in plant area.
* Waste heat could not be commercialised.
* The economical lifetime of the plant is set to 15 years and the interest rate to 8 %.
* Hydrogen is produced in 8 300 h / year, the availability of the the plant is about 95%.
* Reactivation of the electrodes is done every 7 years.
* The total specific energy consumption is 4,75 kWh / Nm^3 H_2. This include the consumption in the electrolysers, the bus bars, the transformers, the compressors and other auxiliary equipment
* The electricity price is stipulated to NOK 0,20 pr. kWh.

The table shows that in this case the capital cost is about 22 % of the total production cost, the maintenance and operating costs are about 11 % and the electricity cost about 67 %.

5.3. REDUCTION OF COST ELEMENTS

In the example above the electricity cost is the dominating element in the total cost picture. It is then to emphasize that nearly 60 % of the electricity consumption is due to the Gibbs energy. Reduction of this element can practically be obtained only by rising the working temperature. The main argument for developing high temperature electrolysis processes is just to attack the thermodynamic part of the electricity consumption.

However, in the near future the research and development work seems to be centred in electrolysis at midium and low temperatures. We will here only discuss the latter, and then limit ourselves to electrolysis in alkaline solution.

5.3.1. *Energy Consumption / Energy Cost*

The energy consumption may be reduced by lowering the ohmic voltage drop, primarily in the cells themselves. The following possibilities should be valued:

* Amend the electrolysis conditions (lower the current density, rise the pressure, rise the temperature, change the electrolyte concentration)
* Reduce the resistance in the electrolyte layer between the electrodes (diminish the gap, reduce the gas/electrolyte volum ratio, secure the electrolyte circulation)
* Reduce the resistance in the diaphragm (choose another diaphragm type)
* Reduce the resistance in the electrodes (the fore an back electrodes)

The energy consumption may also be reduced by lowering/stabilizing the overvoltages. The following possibilities should be valued:

* Amend the electrolysis conditions (lower the current density, rise the temperature)
* Improve/stabilize the activity of the electrocatalysts / active coatings

5.3.2. *Investment / Capital Cost*

The specific investment may be reduced by reducing the production costs of cells, electrolysers and total plant. The following possibilities should be valued:

* Simpler cell and electrolyser design
* Cheaper construction materials
* More efficient manufacture
* More efficient installation
* Simpler design of the total plant

Some of the possibilities are more or less coupled together, especially concerning the cells, which make a greater part of the cost. By using other construction materials it may be practicable to change both the design and the manufacture.

The specific investment may also be reduced by increasing the production rate of cells and electrolysers, i.e. the current. The following possibilities may be valued:

* Enlarge the cell dimensions
* Rise the current density

Increased gas production in the cells may be contingent upon a change of the electrolyser and plant design.

5.3.3. *Economical Optimisation*

Many of the efforts pointing at reducing the energy cost may also affect the investment, and *vice versa.* As usual an economical optimisation has to be done.

5.4. POTENTIAL OF IMPROVEMENTS

As concerns electrolysis in alkaline electrolyte it should be possible to reduce the investment / capital cost by say 30 % and the energy consumption by 10 - 15 %. Based on the figures presented above the hydrogen production cost then could be lowered by about 15 %. The specific cost is then reduced to 1,20 NOK/Nm^3 or 0,34 NOK/kWh.

ELECTROCATALYTIC AND HYDRIDIC THEORY FOR HYDROGEN ELECTRODE REACTIONS AND PREDICTION OF SYNERGETIC CATALYSTS IN THE LIGHT OF FERMI DYNAMICS AND STRUCTURAL BONDING FACTORS

MILAN M. JAKSIC* AND NEDELJKO V. KRSTAJIC**
**Faculty of Agriculture, **Faculty of Technology and Metallurgy, University of Belgrade, *11080 Belgrade-Zemun, **11000 Belgrade Yugoslavia (Serbia)*

1. Introduction

The Balandin type volcano plots have been considered for the main criterion both in catalysis and electrocatalysis to estimate their fundamental properties and optimal activity: (α) The ones, when some physical feature or catalytic activity itself is plotted usually along transition series, and (β) The others, when catalytic activity arises as a function of some energetic property, the most usually of the adsorption enthalpy of intermediates bonding upon the substrate in the rate determining step (*rds*).

Pauling[1] simple quantum mechanics bonding model, being so far the basic theoretical approach in evaluating various thermodynamic, physical and chemical features, states that the interaction of the electrons with one another and with nuclei is the glue that bonds material together, which determines the strength of bonding, the configuration or structure of atoms, their electronic density of states, its Fermi surface, and their associates as a result of the bonding, and hence appears responsible for all main properties of the matter. In the same respect, ever since Hume-Rothery[2] established the relationship between numbers of electrons per atom and structures of many individual and intermetallic compounds, there has been generally accepted that there must be a strong correlation between the number of valence-bond electrons and types and the order of crystal lattice. Consequently, Brewer[3,4] employed the resonance valence bond theory, that relates the electronic state of highest multiplicity that corresponds to the electronic configuration of lowest energy level or the structure of atoms, with the corresponding phase structure in both individual metallic and multicomponent intermetallic systems (structural bonding factors) to provide the most practical simple model for predicting the relative stabilities, the structural relations, and resulting behaviour of metallic systems. Such an electronic configuration, as a bonding 'glue' that keeps the matter together and defines all its main physical and chemical properties, including hydridic behaviour, catalytic activity and electrocatalysis, in particular for hydrogen electrode reactions [(*helr*), both its cathodic evolution (*her*) and

T. O. Saetre (ed.), Hydrogen Power: Theoretical and Engineering Solutions, 103–118.

anodic oxidation (*hor*)], and the relations resulting therefrom, represent the leading idea and the aim of the present paper in an attempt to find the physical causes and roots of catalytic volcano plots.

1.1. *Physical Roots and Catalytic Consequences of Volcano Type Curves*

A broad survey of volcano plots along the Periodic Table, associated with various fundamental physical properties of elements, both of macroscopic or micro-values, such as *specific mass* (mass-density, atomic number density), *electronic and magnetic features* (surface electronic density of states, Pauling *d*-character and electronegativities, work function electrocatalytic and catalytic electron-transfer activities, cathodic separation of hydrogen isotopes, magnetic momentum, paramagnetic susceptibility), *wave characteristics* (Fermi wave-vector, cyclotron frequency), *size factor or geometrical parameters* {radius of ions, atomic volume, interatomic lattice distance, specific (atomic or molar) volume or other defining size measures, lattice parameters}, and/or *energy and related properties* (cohesive energy, melting and boiling points as its direct consequences, Fermi energy, energy of fusion and sublimation, isothermal bulk modulus, linear coefficient of thermal expansion, shear and Young modulus, surface energy, entropy and frequency of lattice vibrations, heat capacity, Debye temperature, logarithm of the exchange current density as the linear function of enthalpy of adsorption of reacting intermediaries, Arrhenius energy or enthalpy of activation, and almost all other physical and chemical parameters obeying Maxwell-Boltzmann distribution law, etc.) have been reviewed to reveal the causes of their existence, their common points, interrelations and consequences in various metallic behaviors[5-8].

Since the individual ratio between atomic mass and volume results as the effect of interaction between electrons and nuclei for each available number of protons and neutrons, their specific mass, atomic radius or volume, as a micro-cosmos, obey typical volcano plots along the Periodic Table, and determine the same feature for the mass density, atomic concentration and molar volume, as their macroscopic analogue values[7], whereas the *interatomic lattice distance* represents a further interactive relation amongst ions within a crystal lattice and the primary consequence of their defined electronic configuration, crystal ordering and bonding in the solid state, and they all together define wave properties of the lattice. One should certainly note that while atomic mass continuously grows along the whole Periodic Table, its ratio with available volume, as the result of electronic interaction with each other and with nuclei, follows symmetric bonding-antibonding volcano plots.

2. Theoretical Considerations

2.1. *The 'One Sixth Correlation' between Surface and Bulk Energy*

A typical, most characteristic and significant issue of bonding-antibonding volcano plots represents cohesive energy of elements *versus* atomic numbers along transition series (Fig. 1), in particular as compared with surface energy at their melting points in

the same dependence (Fig. 2)[9]. The same shape of volcano curves with characteristic positions of elements both in solid and liquid states clearly testifies for the electronic nature and causes of both properties. These relations as compared each with other at the same time reveal the existence of so called "one sixth correlation"[10], which as a rule associates the surface and cohesive energy of solid metals. Namely, whereas the strength of the nearest neighbour *d*-bonding is assumed to depend parabolically on the

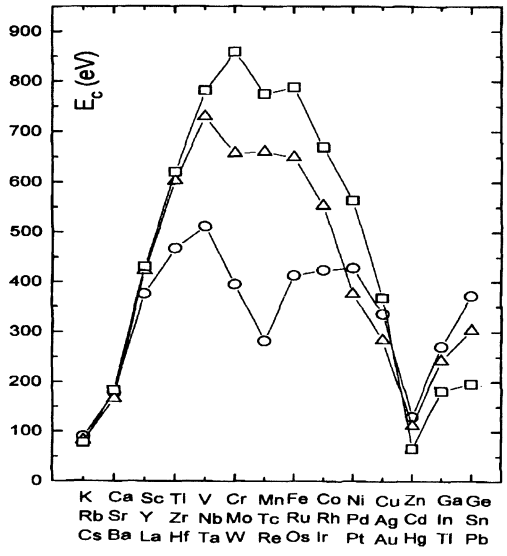

Figure 1. Cohesive energies of metals along the Periodic Table (o - 3d, Δ - 4d, and - 5d level).

number of *d*-electrons (Friedel *d-d* electronic correlations[11] or bonding-antibonding volcano plots), the main feature of surface energy could be explained by a simple bond-cutting model as a transposed projection of cohesive energy within the "one to sixth correlation". The surface energy and all correspondingly related values derived therefrom, such as the adsorption of intermediates, can thereby be simply estimated as the energy cost for cutting the bonds for one nearest neighbour atom times the number of removed nearest neighbour atoms when the surface is created. Thus, assuming that the energy for cutting a single of usually six bonds per atom within the lattice is a well defined cohesive quantity, then there exists a simple linear dependence between the surface energy and the heat of cohesion bonding. Such a simple relation between surface and bulk energy has far-reaching consequences for adsorption of intermediates in the *rds* and thereby for both hydridic behaviour and the whole catalysis and electrocatalysis of hydrogen evolution. These values are predictable from the bonding energy, while the latter stays in a straightforward relation with electronic density of states, work function, catalytic activity, or logarithm of exchange current density, etc.

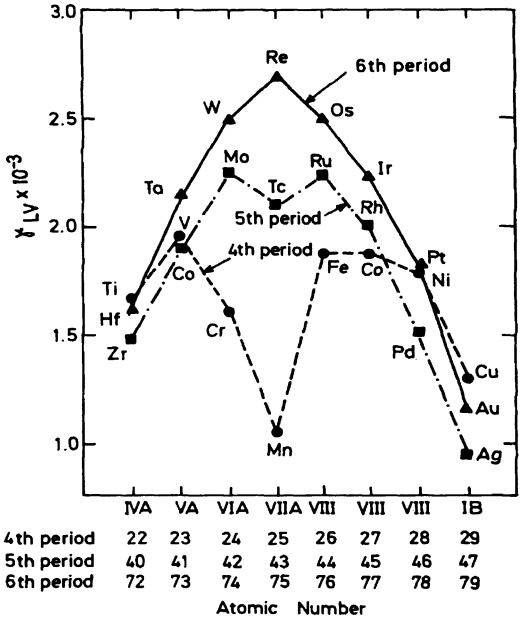

Figure 2. Surface energy of metals at their melting points along the Periodic Table (after Allen[9]).

2.2. *Cohesive versus Fermi Energy*

The plentiful evidence of akin volcanic behaviour suggests the Friedel *d-d*-electronic correlations[11] for their primary bonding-antibonding explanation, because for all reasonable forms of the finite density of states of the *d*-band (n(E)), there results much the same symmetric volcano plots as when n(E) = const. Namely, as a suitable approximation, n(E) = 10/w = const. for -w/2 ≤ E ≤ w/2, where *w* is the width of the energy band, the latter being the cause of very strong cohesion observed in transition metals. A starting point has been a simple tight bonding (Huckel) description of the band, that then includes *d-d*-electronic correlations as a perturbation. The additional assumption was that the number of *s*-electrons per atom remains constant near to unity, adding only a small constant term to the cohesion, and the model restricts to a simplified picture of the *d*-one-electron band, where all five d-semiorbitals with different orbital moments (m = 2 to -2) are supposed to be equally populated at each energy level, and the total energy band is thereby assumed symmetric with respect to the atomic energy, and approximately rectangular,

$$n_d = \int n(E)\,dE = \int_{-w/2}^{E_F} (10/w)\,dE = 10 \quad . \; . \quad (1)$$

where n_d is the number of *d*-electrons each atom possesses, so that there further follows from Eq. (1), the relation for Fermi energy,

$$E_F = (w/2)(0.2\ n_d - 1) \quad . \ . \ . \ . \ . \ . \ . \ . \ . \quad (2)$$

Cohesive energy results as the energy of state multiplied by the number of states having such an energy:

$$E_c = \int_{-w/2}^{E_F} E\ n(E)\ dE = \int_{-w/2}^{E_F} E\ (10/w)\ dE = (10/w)[(E_F)^2/2 - w^2/8] \quad (3)$$

Introducing E_F from Eq. (2), there follows a typical parabolic, symmetric volcano plot,

$$E_c = (5w/4)\ n_d\ (n_d/25 - 2/5) \quad . \ . \ . \ . \ . \quad (4)$$

with the maximum at $n_d = d^5$-electrons, exactly as the experimental evidence requires. Since the band width (w) is a linear function of the Fermi energy (E_F) (Eq. 2), the last approximate Eq. (4), clearly shows the linear dependence between cohesive and Fermi energy.

The Fermi energy itself represents the product of the Rydberg (Ry) constant (Ry = $e^2/2a_o$ = 13.6058 eV = 2.18 x 10^{-18} J, defined as the ground state binding energy of the hydrogen atom) and the dimensionless Fermi wave-vector [(k_F a_o), where a_o = ($h^2/4\pi^2me^2$) = 0.529177 x 10^{-8} cm, is the Bohr radius for hydrogen atom], so that:

$$E_F = h^2\ (k_F)^2/(8\pi^2m) = [h^2/\ (4\pi^2me^2)](e^2/2a_o)\ a_o\ (k_F)^2 =$$

$$= (e^2/2a_o)\cdot(k_F\ a_o)^2 = (e^2/2a_o)\ [(2\pi/\lambda_F)\ a_o]^2 \quad . \ . \quad (5)$$

where the Fermi wave-vector [($k_F = 2\pi/\lambda_F$)] defines the radius of sphere containing the occupied one electron levels, called Fermi sphere and the Fermi surface, as well as the Fermi *plane wave* length (λ_F). The Rydberg is as convenient a unit of atomic energy, as the Bohr radius (a_o) is of atomic distances. The Fermi energy thus has the meaning and magnitude of typical atomic binding energy with the Fermi wave-vector as the defining parameter for each individual element. The best test for the virtual elementary bonding property of the former and the common sense with cohesive and other bonding energies (fusion, sublimation, etc.), melting and boiling points as their consequences, etc., characteristic for each metal, represents typical volcanic plots of both the Fermi energy and its wave-vector along transition series[12]. Thus, volcanic plots represent by themselves classical *periodic* properties of elements along the Periodic Table.

2.3. *Physical Meaning and Significance of the Fermi Wave-Vector*

The Fermi wave-vector, in its essence interrelates both the geometric (specific mass, and/or specific volume) wave factor and the electronic density of states. Such an interdependence, for example, thereby stays in the core of the Hume-Rothery and Engel-Brewer correlations between the electronic configuration and the crystal structure of metals and intermetallic phases.

More specifically, in the ground state of a system of N free electrons, the occupied orbitals of the system fill a sphere of radius k_F, where ($E_F = \mathbf{h}^2 \cdot \frac{k_F^2}{2m}$) is by definition the Fermi energy of an electron having a wave-vector k_F[12]. Since the reciprocal lattice parameters (L_X, L_y, L_Z, the geometric factors in the **k** - space), as the specific volume, ($V = L_X \cdot L_y \cdot L_Z$, or as the average $V = L^3$) imply the atomic mass, and as the specific eigen values ($k_X = 2n\pi/L_X$, $k_y = 2n\pi/L_y$, $k_Z = 2n\pi/L_Z$, where n = 0, 1, 2, 3...) of the one electron wave function levels (the eigen state of the momentum operator of orbital, $\Psi_{\mathbf{k}}(\mathbf{r}) = A \cdot \exp(i\mathbf{k} \cdot \mathbf{r})$), define the Fermi sphere in the ground state of a system of N free electrons and at the same time the **k** - space density of levels [$\Delta\mathbf{k} = (2\pi/L)^3 = (2\pi)^3/V$][12],

$$N = 2 \cdot \frac{4\pi}{3} k_F^3 \frac{L_x L_y L_z}{(2\pi)^3} = \frac{V k_F^3}{3\pi^2} \quad \ldots . \quad (6)$$

there further follows,

$$k_F^3 = 3\pi^2 \frac{N}{V} = 3\pi^2 n \quad \ldots \ldots \quad (7)$$

In fact, each allowed k-value leads to two one-electron levels (one for each spin value, the Pauli exclusion principle), so that the electron density (n) requires multiplication by 2 in Eq. 6). Therefore, the Fermi wave-vector interrelates the geometric lattice parameters (L_X, L_y, L_Z, **k**-space) within the electronic density (n) with the system of N available electrons, and consequently all these values and/or all the other ones in a straightforward relations with them, plot typical parabolic bonding-antibonding volcano curves along transition series in the Periodic Table. In fact, such an interrelation between electronic and specific geometric lattice parameters (n = N/V), with the metallic wave features (k_F), represents a natural link between the micro- and macroscopic-world. Namely, whereas ionic radius within the lattice space defines specific atomic volume, and the nearest-neighbour interatomic distance reflects their interspace and interaction, both mostly revealing the mutual electronic and mass relation of atoms in a crystal state, and thereby the wave properties (k_F) in the micro-world, the specific volume displays macroscopic bulk characteristics of the lattice, and consequently, they all together obey typical volcanic plots[12]. Such a micro-macro world relation associated within the Fermi wave vector, in its essence corresponds to the usual multiplication of ionic charges (micro values) with Faraday (F) and Boltzmann (k_B) constants, or Avogadro (A) number to get macroscopic currents (I), molar charges (Q), universal gas constant (R), or electrochemical ($\bar{\mu}$), chemical (μ) values ($Q = e \cdot F$, $I = dQ/dt$, $R = k_B \cdot A$, $F = e \cdot A$, or $\bar{\mu} = \mu + zF\varphi$.

In fact, one often overlooks that n = N/V by definition primarily comes from the *individual* Wigner-Seitz unit cell, and as an *average* from macroscopic dimensions of larger mass (N and V usually arise undistinguished for elemental (micro-scale) and macroscopic-world space, since their ratio approximately remains the same). Similarly, one often overlooks the individual (micro fact of) bulk property of the Fermi wave-vector for specific atoms in the exposed surface, when we generalize the effect of the surface itself upon the catalytic activity. The latter actually arises as the sum or integral of all individual contributions along the whole exposed catalyst surface.

2.4. *Fermi Wave-Vector as the Universal Basic Parameter in Volcanic Plots along the Periodic Table*

Brewer[3,4] uses reliable spectroscopic data in a more quantitative manner by employing the experimental promotion energies required to achieve each of the proposed electronic configurations, together with the experimental enthalpies of sublimation, to determine the bonding energies that result from an exact Huber-Born cycle when gaseous atoms in the corresponding valence state are condensed to the solid metal (cf.[7]). Therefore, the bonding energy is obtained thermodynamically by adding the promotion energy to the enthalpy of sublimation, while the crystal structure results from the corresponding (energetically optimal) electronic configuration and implies relations within the Fermi wave-vector amongst the atomic mass, its volume and interatomic distances, electronic density of states and wave properties. In other words,

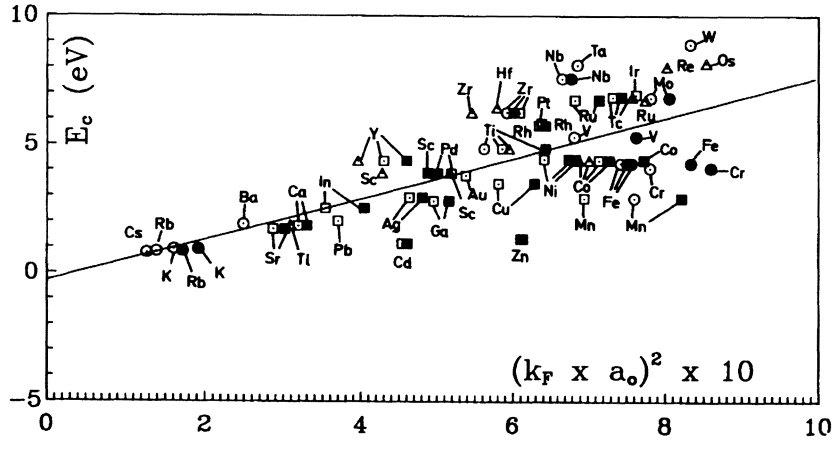

Figure 3. Cohesive energies of d-metals plotted as a function of dimensionless Fermi wave-vector[12].

one has to have a definite atomic mass and corresponding electronic configuration (or, electronic density of states) to create certain crystal structure and thereby resulting wave properties within the crystal lattice. Thus, as the consequence, the net cohesion is the result of the difference between the promotion energy required to produce an atom in its

bonding valence state and the resulting bonding energy in the solid state (thermodynamic consequences of interatomic mass-electronic interrelations as their causes with the criteria of minimum in Gibbs enthalpy of formation). Since the Fermi energy in its essence has the meaning of a typical atomic binding energy and in a straightforward manner correlates with cohesion, the latter when plotted as a function of the Fermi wave-vector, obeys a fairly well straight line dependence (Fig. 3).

In fact, whenever one takes any physical parameter, which plots parabolic volcano type curve along transition series, and correlates with the any other one obeying similar properties, there results a more or less straight line dependence. In the essence, there only imposes a logical question itself, what is the smallest common denominator for such linear plots? Since ***only*** the Fermi wave-vector interrelates the specific atomic volume (the Wigner-Seitz cell) and implies the specific mass relation, with electronic properties of ions in the metallic lattice (electronic density of states, or the electronic concentration, n), and thereby the wave features of the lattice (k_F), while the Fermi energy represents the most primitive, basic bonding energy of a lattice, such state of facts suggests the former for the basic smallest common denominator in such straight line dependencies. In other words, only these four (eigen value) properties (and the other physical features in the straight forward linear relations with them) basically create volcanic plots along transition series, while **only the Fermi wave-vector interrelates them at once**. Such state of experimental evidence and universal physical knowledge thus suggest the Fermi wave-vector, and thereby the conduction (or

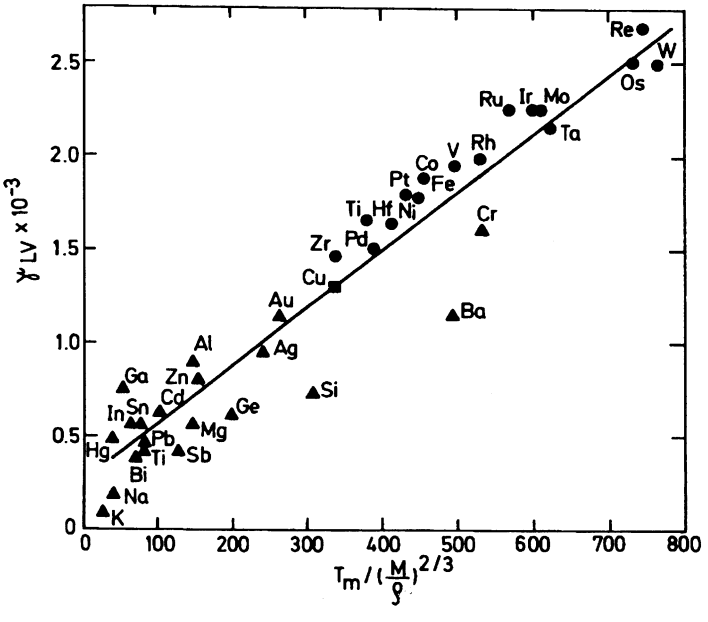

Figure 4. Surface energy (γ_{LV}) plotted as a function of macroscopic value of Fermi wave-vector (after Allen[9]).

valence) electron concentration density ($n^{2/3}$), for **the basic universal parameter** in collective metallic and intermetallic, primarily physical, and consequently chemical behaviour of transition elements. Similar linear plots have already been used for long time now in both metallurgy and crystallography (Fig. 4), but the relating parameter and resulting axis are defined on rather more macroscopic data of the same Fermi implied meaning ($T_m V^{-2/3}$).

3. Electrocatalysis for Hydrogen Evolution

3.1. *Fermi Wave-Vector and Electrocatalysis for Hydrogen Electrode Reactions*

Theoretical considerations of fundamental kinetic equations for the hydrogen evolution reaction (*her*), meanwhile, predict the existence of a Balandin-type volcano curve in the plot of the logarithm of the exchange current density *versus* the enthalpy of hydrogen adsorption for various transition metals[13,14]. In that context, Trasatti[15] was the first to confirm the existence of the parabolic volcano-type curve in the dependence of the logarithm of the exchange current density on the intermediate transition metal-hydrogen bond strengths recalculated from Krishtalik overpotential data (cf.[5]). However, more thorough Trasatti calculations have later shown that the hydrogen adsorption enthalpy links transition metals along a straight line[16]. The latter could be considered as the crucial confirmation of the present theory, though the logarithm of the exchange current density in such a plot in its essence, but indirectly, in fact relates the enthalpy of intermediate (H-adatom) adsorption *versus* itself and thence, virtually requires the straight line dependence, too. In other words, there has been emphasized that such composed energy *versus* energy volcano plots of secondary type, eventually appear ***only*** when two mutually opposing kinetic effects counteract each other along the selected axis. This might be when two reverse rate constants dramatically change along some energy axis.

Another crucial confirmation of the rightness of the present theory represents the linear plot of overpotential for oxygen evolution as a function of the enthalpy of the OH-intermediary adsorption on various transition metal substrate electrodes[17], and even more so, the correlation between the polarization (η) of cathodic hydrogen evolution and heat of H-adatom adsorption[18].

The equivalence of the Fermi level (the chemical potential of electron) to the redox potential has been demonstrated by simple thermodynamic arguments[19], while the logarithm of exchange current density in the straightforward manner correlates with the reversible redox potential of an electrode. Note also that $log\ i_0$ directly correlates with the enthalpy of hydrogen adsorption, as the bonding energy between H-adatoms and the substrate, and/or the linear part of energy of activation in the Eyring definition. The compilation of plentiful of experimental data gathered by Kita[20] from various laboratories has clearly shown that the logarithm of exchange current density for hydrogen evolution (read: the activation enthalpy of H-adatom adsorption), plot typical volcanic curves along transition series, too (cf.[5-8]). As a consequence, similar linear dependencies of electrode kinetic parameters for cathodic hydrogen evolution, as a

function of the Fermi wave-vector, electronic concentration or electronic density of states, follow on the same manner, regardless the sources of relevant parameters (bulk modulus, Fermi velocities, cyclotron frequency, paramagnetic susceptibility, specific electronic configuration, etc.)[7]. However, since the electrocatalytic $log\ i_O$ volcanic plot along transition series arises non-symmetric, with the upper most activity located at d^8-electrons, the most active elements (Pt, Pd, Ni) feature little lower values of the Fermi energy, and/or its wave-vector and, thence, require some additional kinetic correction parameter to fit better on the straight line along the electronic ($n^{2/3}$) concentration axis. In other words, such a systematic deviation of more substantial significance, meanwhile arises from the fact that electrocatalytically the most active *d*-metals (Pt, Pd, Ni) for the *her* are located on the descending part of the Fermi energy (or, symmetric bonding-antibonding) volcano plots[7], while on the corresponding Kita[20] volcanic curves they occupy the top most positions, and thereby they do not approach the upper values along the straight line plots. In fact these are the main systematic scattering points relative to the average straight line, as compared with the relation between the Fermi energy and the Fermi wave-vector.

4. Electrocatalysis along Hypo-Hyper-d-Electronic Transition Intermetallic Phase Diagrams

Kinetic studies with electrode substrates taken along some phase diagram primarily require measurements under the same equal conditions, to enable a mutual comparison of obtained data. In fact, the entire experimental evidence of electrocatalytic data in the available literature for the same (*her*) electrode reaction, while lacking in the specified actual surface areas of such electrocatalysts, prevents any relevant comparison of obtained results even for the same metallic substrate and imposes an imperative need to bring them all on the same 'common denominator' of real (exact) current densities. Thus, the main aim of the present paper has been to polish properly metallurgically produced specimens of otherwise well defined crystal structure, down to the same roughness factor (less than 1.8), or to estimate the real roughness or the actual electrode surface, and recalculate current densities on their true surface area.

The present paper represents one of the first initial approaches to study kinetic behaviour of intermetallic phases for the *her* along the phase diagrams of hypo-hyper-*d*-electronic combinations of transition elements, with two main aims: (a) To estimate the kinetics and mechanism along them, and (b) To look for the correlation between hydridic properties and electrocatalytic activity *versus* the mutual (average) electronic density of states, and compare the latter with corresponding values of individual metals along the Periodic Table[20]. Namely, any hypo-hypo- or hyper-hyper-*d*-electronic combination of transition metals leads to rather smooth phase diagrams of the melting point changes from one to another constituents, and the same features behave their other physical properties including common electrocatalytic activity; in other words, there arises no catalytic synergism or abrupt changes in between[21], but something similar to the linear dependence between individual metals along the Periodic Table. Contrary to that, the hypo-hyper-*d*-electronic combinations usually characterizes the existence of

several intermetallic Laves phases and/or stoichiometric compounds accompanied with distinct sharp changes in the melting points. The more remote are located such constituents in the Periodic Table, the more such intermetallic phases usually arise in between of them, and in fact, each such phase itself features its short range individual phase diagram between other two intermetallic constituents, and the whole main phase diagram consists from the association of the several such the smaller ones. The main aim of the present paper is to show that the same relation and the same sort of volcanic plots in all physical features above considered for individual transition metals, including electrocatalysis for the *her*, from the same reasons obey intermetallic phases and alloys of transition metals along their phase diagrams, which then should behave as the part of the Periodic Table between two pure and remote constituents, in particular for their hypo-hyper-*d*-electronic combinations.

Investigations of the *her* on individual transition metals revealed d^8-electronic configuration for the optimal in electrocatalytic activity. In other words, at least Volmer-Heyrowsky mechanism requires two empty electrons upon *d*-orbital of surface substrate atoms for recombination of two H-adatoms into an evolving molecule, while according to the general catalytic theory of Balandin, even the Volmer-Tafel mechanism certainly should easier proceed at the same exposed substrate atom, too.

Earlier Brewer[3,22] investigations in the bonding effectiveness when a hypo-*d*-electronic transition metal reacts with the right distributed hyper-*d*-electronic half of series along the Periodic Table have clearly shown the existence of well defined maximum in bonding, which coincides with maximum in electronic density of states usually of symmetric Laves phases (AB_3), and thereby, with maximum in electrocatalytic activity for the *her*[7]. At the same time Brewer multiphase and multicomponent diagrams consist from continuous isoelectronic lines, which separate various crystal structures from *bcc* over *hcp* and ending with *fcc* at the highest *d*-electron concentration. The same volcanic plot in the free enthalpy of formation arises whenever one of hypo-*d*-electronic transition metals interacts by alloying with a hyper-*d*-electronic element, and usually the latter coincides in its maximum with both the optimal (average) number of *d*-electrons already defined for individual transition metals (d^8) and, thereby, in the maximum of electrocatalytic activity for the *her*. Typical issues for the systems of Ti-Ni, Mo-Co and Zr-Ni illustrate Fig. 5, 6 and 7. In that respect, one should note that there are two type of hypo-*d*-electronic transition metals: (a) The ones, like Ti, Zr, Hf, which exhibit pronounced hydridic features because of their empty semi-*d*-orbitals, and (b) Transition elements with half-filled semi-*d*-shells, like Mo, W, Cr, which behave rather strong metallic bonding in their own lattice and thereby form hydrides only at very high pressures. Thus, the former in their combinations with hyper-*d*-electronic transition metals distinctly separate their maximal hydridic[23] from maximal electrocatalytic properties (Fig. 5 and 7), while the latter feature only electrocatalytic volcano plots (Fig. 6).

One of substantially decisive conclusions derived from kinetic measurements and analysis is that regardless the typical hydridic behaviour at higher Ti contents, all

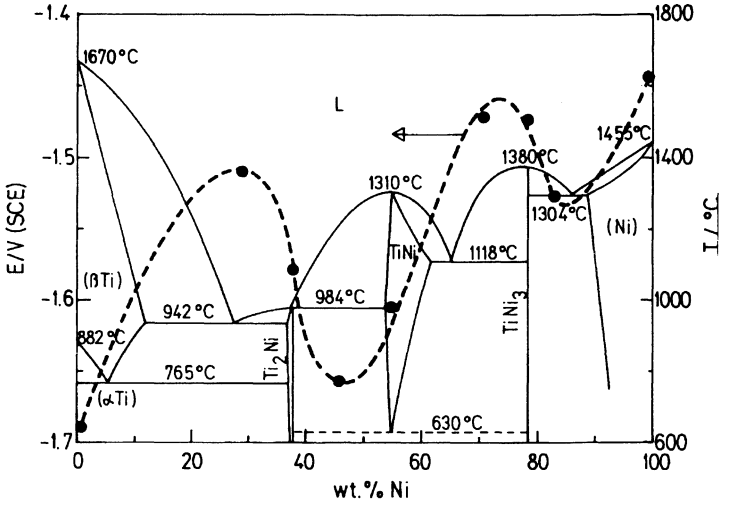

Figure 5. Relative electrocatalytic activities for the *her* along the Ti-Ni phase diagram.

intermetallic phases and alloys along the Ti-Ni phase diagram behave the same kinetics and mechanism[24], since all Tafel lines exhibit the same slope, regardless the fast hydridic diffusion in one part, and slow in another. The difference arises only in the characteristic rate constants and the effective electrode reaction rates.

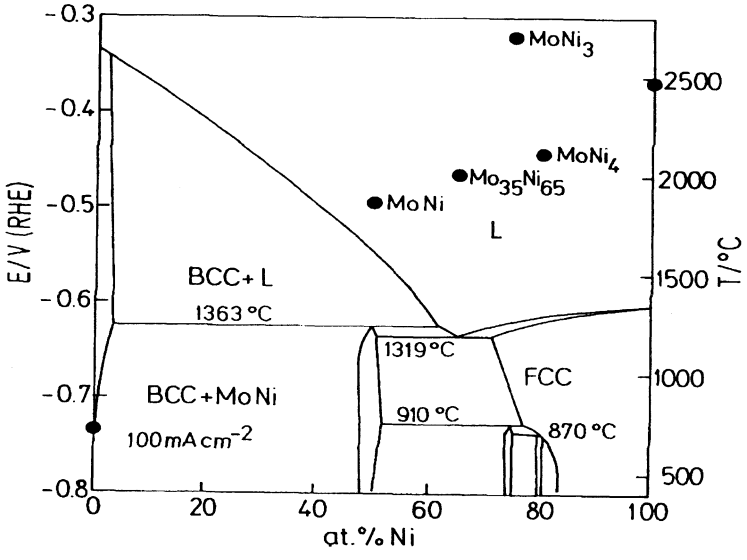

Figure 6. The same as *Fig. 5*, along the Mo-Ni phase diagram.

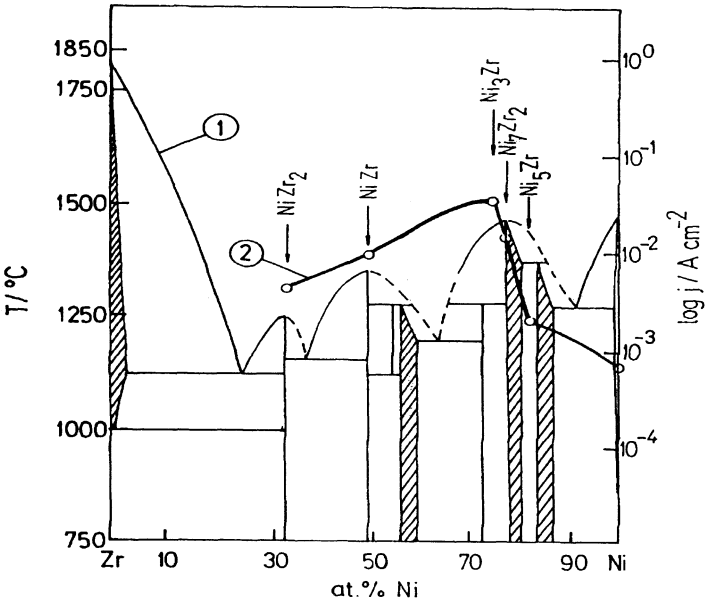

Figure 7. The same as in *Fig. 5* along the Zr-Ni phase diagram.

The TiNi electrode prepared by mechanical alloying method, after activation in the HF solution, possesses very high catalytic activity for hydrogen evolution, which is well illustrated by polarization curves obtained in 30% NaOH at different temperatures (Fig. 8). The overvoltage for *her* is only 60 mV at 300 mA cm^{-2} and 80 ^{0}C.

A rough estimation of the surface roughness is obtained from the comparison of double-layer capacities of these two kinds of electrodes at more negative potentials, where they reach constant values. Assuming that the double layer capacity of a smooth metal is 20 μF cm^{-2}, one gets surface roughness, S_r, defined as C_{dl} / 20 μF cm^{-2}, equal to 1.8 for properly metallurgically prepared TiNi electrode, and 1350 for TiNi electrode produced by mechanical alloying method.

The exchange current densities, obtained on TiNi alloy electrodes, were for ten times higher than those obtained on the polycrystalline Ni electrode[24,25]; at the some time, the rate constant values were higher for two orders of magnitude. However, comparison of the real rate constants and exchange current densities for both TiNi electrodes in 1.0 M NaOH solutions at 25 °C, recalculated on the bases of their roughness factors (S_r), shows that the above mentioned values are mutually comparable and reduce to the same order of magnitude. The much more higher activity of TiNi electrode for the *her*, prepared by mechanical alloying method, therefore, can be primarily explained by the increase in the actual surface area. However, the upper electrode surface during the HF activation certainly becomes enriched in the Ni content of otherwise developed surface

area, while the inductive effect of underneath laying Ti, as a hypo-*d*-electronic transition metal upon the activity of the former[5-8], could not be overlooked.

4.1. *Tiney-Ni versus Raney-Ni as the Catalytic Electrode Material*

So far electrodes for hydridic batteries were usually prepared from the high hydrogen storage capacity and its fast diffusion mass transfer materials, upon whose surfaces then were deposited thin layers of electrocatalysts[26,27], or from specific composite alloys featuring all these (storage, transfer, and catalytic) properties at once. In that respect, Buchner long ago suggested mixed intermetallic phases of Ti_2Ni and TiNi for hydridic fuel cells to store and both catalytically evolve and/or oxidize hydrogen[28].

The present experiments have shown that systematic activation of the TiNi intermetallics with HF solution gradually leads to and even exceeds the activity of the otherwise the most active $TiNi_3$ intermetallic phase (Fig. 8)[25]. In fact, each Ti rich intermetallic phase and alloy composed with Ni, in common with (Al removed) Raney-Ni, certainly can be activated to approach the maximal electrocatalytic activity by its partial Ti removal with HF, as already noticed for the stoichiometric compound of TiNi, but then one has to remove much more basic Ti material to face the same catalytic effect. Note the intermediate position of the TiNi intermetallic phase in both hydridic and electrocatalytic properties (Fig. 5).

In accordance with above stated measurements, there has now been developed a new advanced hydridic and catalytic material, named *Tiney-Ni*, as a counterpart to synonymous Raney-Ni. Namely, while the intermetallic TiNi phase exhibits pronounced hydridic properties and for a long time now has been considered for the one of the most promising hydridic storage and even electrode system[28], with an insurmountable obstacle of its almost impossible mechanical shaping, it turned out that its additionally activated state behaves excellent catalytic features, whereas mechanical alloying provides its easy electrode shape formation almost at will. For special electrode properties such *Tiney-Ni* certainly can be further catalytically advanced by *in situ* addition of activated species (for example, negligeable amounts of molybdate and Co-tris complex or traces of other more noble catalytic components[29]). Such an electrocatalyst immediately exhibits excellent catalytic activity for hydrogen electrode reactions (Fig. 8), rather high mechanical and chemical stability, remarkable advantages, both in its durability and activity, as compared with Raney-Ni, the latter otherwise undergoing progressive disintegration to smaller particles, and when produced by mechanical alloying, TiNi arises even as a cheaper material and ease to produce at once in any desirable shape. Thus, its bulk (which might be composed with Ti_2Ni, too) features a fast diffusing and high capacity hydrogen storage, while its simple (HF) activated surface behaves advanced electrocatalytic properties (Fig. 8). Such an advanced hydridic and catalytic material, *Tiney-Ni*, might be expect even to replace Raney-Ni both for the hydrogen electrode material and hydridic storage, as well as for various other hydrogenation reactions in chemical processes and heterogeneous catalysis.

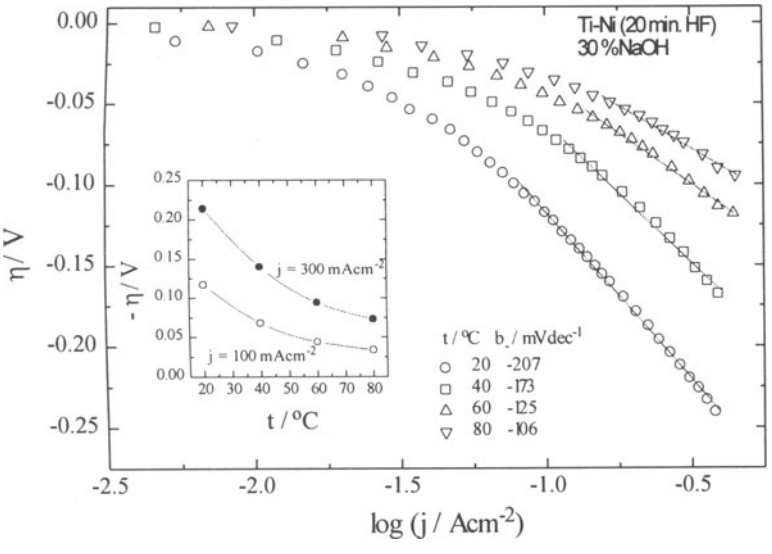

Figure 8. Polarization characteristics of *Tiney-Ni* electrode.

To clarify the basic properties of the Tiney-Ni, one should have to consider and compare the behavior of all congenial intermetallics. First, properly metallurgically prepared TiNi intermetallic phase does not undergo any dissolution and thereby any activation with HF acid. From amorphous TiNi intermetallic, HF removes oxide deposits and the initial activation is rather high, but gradually decreases within a rather short period of time. From mechanically sintered and rather porous TiNi, the HF activation has a tremendous effect. The sophisticated surface (XPS) analysis shows prevailing Ni content of rather developed surface area, partially dissolved metallic Ti besides TiO_2 oxide, and according to the theory, greatly increased electrocatalytic features. The remaining Ti keeps the matter together and induces the activity of upper parts of such an active Ni[5]. This is the main advantage as compared with Raney-Ni.

In that respect, one should have to compare hydrogen storage for the hydridic capacities of such batteries. Metallurgically prepared and crystalline TiNi has rather low capacity (about 10 mAh/g). Mechanically sintered and non-activated TiNi has much increased initial capacity (~ 80 mAh/g), which decreases with cyclization. However, the latter after HF activation exhibits dramatically increased hydridic capacity (~ 180 mAh/g, and limiting value of about 220 mAh/g), which keeps unexchanged such a value after manifold cyclizations.

References

1. Pauling, L.: '***The Nature of Chemical Bond***', 3rd Ed., Cornell Univ.Press, Ithaca, New York, 1960
2. Hume-Rothery, W.: *Structures of Metals and Alloys*, Institute of Metals, London, 1936.
3. Brewer, L.: Prediction of high temperature metallic phase diagrams, in V.F. Zackay (ed.), *High-Strength Materials*, Wiley, New York, pp. 12-103, 1965.

4. Brewer, L.: Prediction of transition metal phase diagrams, *J.Nuclear Materials* **51** (1974) 2-11.
5. Jaksic, M.M.: Advances in electrocatalysis for hydrogen evolution in the light of the Brewer-Engel valence-bond theory, *J.Mol.Catalysis* **38** (1986) 161-202.
6. Jaksic, M.M.: Brewer intermetallic phases as synergetic electrocatalysts for hydrogen evolution, *Materials Chem.Phys.* **22** (1989) 1-26.
7. Jaksic, M.M., and Jaksic, J.M.: Fermi dynamics and some structural bonding aspects of electrocatalysis for hydrogen evolution, *Electrochim.Acta* **39** (1994) 1695-1714.
8. Jaksic, M.M., and Krstajic, N.V., Electrocatalysis of hydrogen electrode reactions in the light of electronic density of states and structural bonding factors, in J.O'M. Bockris, B.E. Conway and R.E. White (eds.), *Modern Aspects of Electrochemistry*, to be published in 1998.
9. Allen, B.C.: The melting points, *Trans.Metallurgical Soc. AIME* **227** (1963) 1175-1183.
10. Methfessel, M., Hennig, D., and Scheffler, M.: Trends in the surface relaxations, surface energies, and work functions of the 4*d* transition metals, *Phys.Rev.B* **46** (1992) 4816-4829.
11. Friedel, J., and Sayers, C.M.: On the role of d-d electron correlations in the cohesion and ferromagnetism of transition metals, *J.Physique* **38** (1977) 697-705.
12. C. Kittel, *Introduction to Solid State Physics*, sixth ed., Wiley, New York, 1986.
13. Parsons, R.:The rate of electrolytic hydrogen evolution and the heat of adsorption of hydrogen, *Trans.Faraday Soc.*. **54** (1958) 1053-1063.
14. Gerischer, H.: Mechanismus der elektrolitischen wasserstoffabscheidung und adsorptionsenergie von atomarem wasserstoff, *Bull.Soc.Chim.Belgrade* **67** (1958) 506-527.
15. Trasatti, S.: The work function in electrochemistry, in H. Gerischer and C.W. Tobias (eds.), *Advances in Electrochemistry and Electrochemical Engineering*, Wiley, New York, Vol. 10, pp. 213-321, 1977.
16. Trasatti, S.: Chemical and electrochemical surface reactivity, role of the competition between solvent and reaction intermediate adsorption, in W.E. O'Grady, P.H. Ross and F.G. Will (eds.), *Proceedings of the Symposium on Electrocatalysis,* The Electrochemical Society, Pennington, N.J., Vol. 82-2, pp. 73-91, 1982.
17. Ruetschi, P., and Delahay, P.: Influence of electrode material on oxygen overvoltage: A theoretical analysis, *J.Chem.Physics* **23** (1955) 556-560.
18. Ruetschi, P., and Delahay, P.: Hydrogen overvoltage and electrode material. A theoretical analysis, *J.Chem.Phys.* **23** (1955) 195-199.
19. Trasatti, S.: The concept and physical meaning of absolute potential, a reassessment, *J.Electroanal.Chem.* **139** (1982) 1-13.
20. Kita, H.: Periodic variation of exchange current density of hydrogen electrode reaction with atomic number and reaction mechanism, *J.Electrochem.Soc.* **113** (1966) 1095-1106.
21. Brooman, E.W., and Kuhn, A.T.: Correlations between the rate of the hydrogen electrode reaction and the properties of Alloys, *J.Electroanal.Chem.* **49** (1974) 325-353.
22. Brewer, L., and Wengert, P.R.: Transition metal alloys of extraordinary stability: An example of generalized Lewis-acid-base interactions in metallic systems, *Metallurgical Trans.* **4** (1973) 83-104.
23. Bernauer, O., Topler, J., Noreus, D, Hempleman, R., and Richter, D.: Fundamentals and properties of some Ti/Mn based Laves phase hydrides, *Int.J.Hydrogen Energy* **14** (1989) 187-200.
24. Krstajic, N.V., Grgur, B.N., Mladenovic, N.S., Vojnovic, M.V. and Jaksic, M.M.: The determination of kinetic parameters of the hydrogen evolution on Ti-Ni alloys by *ac* impedance, *Electrochim.Acta* **2** (1997) 323-330.
25. Krstajic, N.V., Grgur, B.N., Zdujic, M., Vojnovic, M.V., and Jaksic, M.M.: Kinetic properties of the Ti-Ni intermetallic phases and alloys for hydrogen evolution, *J.Alloys Comp.*, (1997) in press.
26. Notten, P.H.L. and Hokkeling, P.: Double-phase hydride forming compounds: A new class of highly electrocatalytic materials, *J.Electrochem.Soc.* **138** (1991)1877-1885.
27. Preskorn, J.N., Chen.H., Chen, W., and Tornquist, W.J.: Electrochemical and infrared spectroscopic comparison of Pt, $ZrPt_3$, and $HfPt_3$ catalytic properties: Hydrogen evolution and CO adsorption, *J.Phys.Chem.* **96** (1992) 810-816.
28. Buchner, H.: The hydrogen/hydride energy concept, in A.F. Andresen and A.J. Maeland (eds.), *Hydrides for Energy Storage*, Pergamon Press, Oxford, pp. 569-597, 1978.
29. Lacnjevac, C.M., and Jaksic, M.M.: Synergetic electrocatalytic effects of *d*-metals on the hydrogen evolution reaction in industrially important electrochemical processes, *J.Res.Ins.Catalysis, Hokkaido Univ.* 31 (1983) 7-34.

STAND-ALONE SOLAR HYDROGEN PRODUCTION

"SunFuel" -- Recent Accomplishments towards a Vision

M. J. FAIRLIE, P. B. SCOTT[a], W. STEWART and A. T. B. STUART
17500 Lemarsh Street, Northridge, CA 91325 (USA)

Abstract: The Clean Air Now (CAN) Solar Hydrogen Site[b] is located at the Xerox Corporation in El Segundo, CA. It incorporates a "stand-alone" hydrogen generator, using a photovoltaic (PV) array which powers electrolysis modules. An automatic control system allows the system to operate with only periodic operator attention. The hydrogen is compressed for storage and used to fuel hydrogen powered pickup trucks. The facility and its operation are described.

Experience suggests the compression of hydrogen is one of the major concerns to be addressed in remote site design. The CAN hydrogen compression system includes the photovoltaic solar power source and an inverter which converts the 14 volt direct current power to high voltage alternating current, using programmed variable frequency to give a unique slow start capability. This three phase variable frequency current drives a 15 horsepower compressor which can run directly from the PV source and compress hydrogen to pressure as high as 35 MPa (5000 psi).

Although the CAN facility is in a metropolis (near the Los Angeles International Airport) it could just as well be on a remote island or in a remote desert site. Further, this prototype "Stand-Alone" generator could use electricity from other clean sources, such as - for instance - a wind turbine, hydroelectric, or other renewable source of electrical power.

We discuss, as an illustration, an envisioned Wind/Hydrogen Power System for a remote arctic location village. Examples of the cost of arctic electrical power are discussed. A design schematic and representative equipment are described. Operating characteristics and economics estimated using this design and energy source measurements (wind power data in combination with the generator specification) encourage development and implementation.

---

[a]Authors Fairlie, Stewart and Stuart are with the SunFuel Division of The Electrolyser Corporation, Ltd., Toronto, Canada. Correspondence is to be directed to Dr. Scott at the above address.

[b]This solar hydrogen demonstration project has been funded in part by USDOE contract DEFC36-94GO10039. The truck conversions were funded by the South Coast Air Quality Management District. Substantial cost sharing investments were also made by all members of the project team.

T. O. Saetre (ed.), Hydrogen Power: Theoretical and Engineering Solutions, 119–128.

1. The Clean Air Now/Xerox Solar Hydrogen Facility

The CAN Solar Hydrogen Facility [1] is a "stand-alone" (no connection to the electrical grid) generator with on-site storage and fueling of hydrogen vehicles. Figure 1 schematically illustrates the photovoltaic array, the electrolyzer, compressor and storage, and the final use

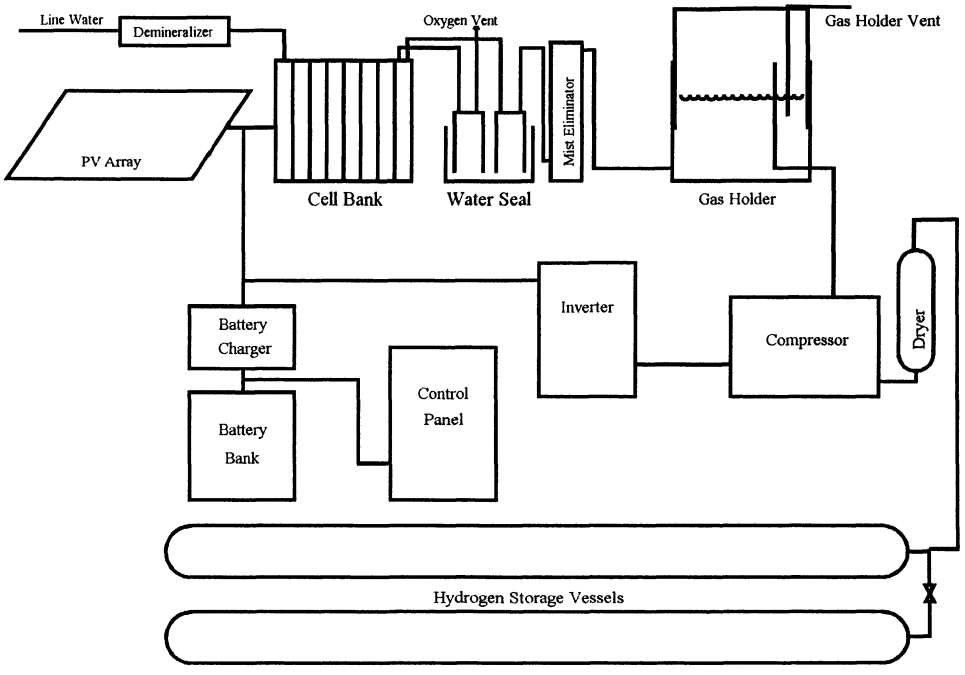

Figure 1. Schematic of the solar hydrogen generator

in a Xerox maintenance truck. The system operates at low voltages, 12-15 volts, with currents to over 2000 amperes. Oxygen generated by electrolysis is passed to the atmosphere, and the hydrogen is temporarily stored in a gasholder. When 1-2 cubic meters of hydrogen are accumulated the compressor is started and the hydrogen is compressed to high pressure - 29 MPa (4200 psi) at maximum.

The photovoltaic power derives from two arrays, one array of sun tracking Fresnel lens focused concentrators, and a smaller array of fixed plate modules. The tracking array

approaches 40 watts per square meter of land space used, including spacing required between subarrays. Due to the high currents and low voltage of the design, the voltage losses in cables and bus bars approach 8%.

The operation of the hydrogen generation system is illustrated by the plots of Figure 2, showing the insolation as seen by a global sensor mounted on one of the sun tracking Fresnel lenses, the total current I, and Iinv, the portion of that total current taken by the inverter system. The step by step increase of storage pressure, Pexit, reflects compression of approximately 2.8 MPa (400 psi), or 41 standard cubic meters (1460 SCF) hydrogen for this winter days operation.

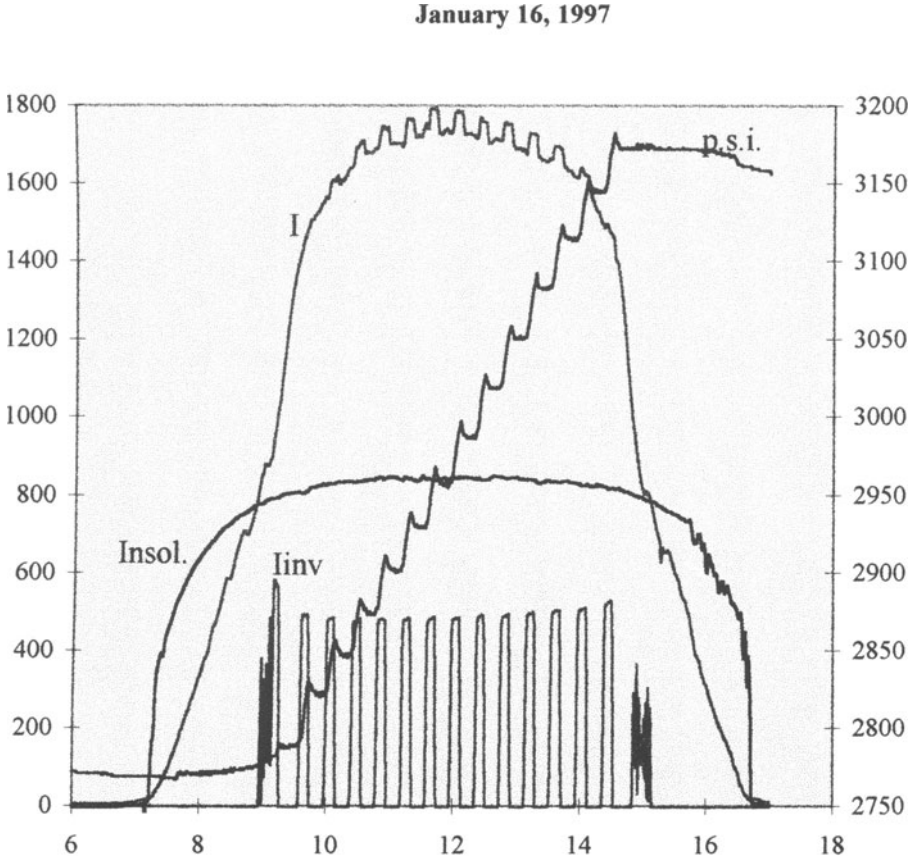

Figure 2. Operation records, showing insolation, total current I, inverter current Iinv, and storage pressure for a winter day.

The truck "fleet" is comprised of three pickup trucks modified for hydrogen use. The fuel storage, of 68 SCM hydrogen in carbon wrapped cylinders designed for vehicle storage of natural gas, occupies the forward meter of the bed of the truck. The trucks performance is

similar to that of the conventional gasoline fueled trucks, with a highway range of approximately 140 miles.

Hydrogen fuel offers notable increases in efficiency of energy use for internal combustion engines [2] as well as for fuel cells. In use with a hybrid propulsion configuration, energy efficiency increases by a factor of 2.7 and a passenger vehicle with a 500 km range becomes possible using compressed hydrogen storage.[3] Using such advanced vehicles, hydrogen production from a CAN sized facility would support approximately 300 km/day vehicle operation and up to five times that if other electrical sources allow 24 hr operation.

The CAN solar hydrogen site serves dual use as an educational facility: It aids in the engineering development of these complex technologies, and it offers an educational focal point for local schoolchildren showing the beginnings of technologies allowing motive power and clean air for their generation.

2. Renewable Hydrogen for Remote Clean Fuel Applications

Systems similar to the CAN project are of interest as a source of electrical power for remote locations. Diesel fuel shipped/flown to isolated locations is, at best, expensive - with transport cost for some sites exceeding one half dollar per liter. Danger of soil or water contamination by spills, combined with the noise, particulate and oxides of nitrogen pollution inevitable with diesel use, argue strongly for use of gaseous fuels or battery storage.

Example applications of renewable hydrogen generation, storage, and use for electrical power generation are:

A) Diesel driven generators are commonly used for electricity production in Canadian and Alaskan villages. In remote island locations, the shipment of the fuel is expensive at best and a health and environmental disaster at worst. The storage tanks have recently been subject to upgrade requirements stipulated by the federal government, as a result of the repeated occurrence of ground contamination. These locations have wind resources among the best in the world, wind-diesel systems[4] have been used, but wind- hydrogen appears much more attractive.

B) Fort Smith (a town in the Canadian North West Territories), with intermittent excess hydro-power available, is interested in hydrogen as a commercial product.[5]

Analysis suggests hydrogen production by hydroelectric or wind generation of electricity, followed by electrolysis, can - can for select sites - be a fully competitive source of fuel for a generation system.[6] The noise and fumes from the diesel, combined with increased reliability offered by a well designed hybrid electric/hydrogen system are further strong incentives. Finally, with a hydrogen system one is insured against fuel "crisis" caused price rises and unavailability.

3. Hydrogen Production/Compression Systems for Remote Operation

Available renewable hydrogen production systems use electrical power (from renewable resources such as wind, hydro, tidal action, PV ...) and electrolysis for hydrogen generation. The simplicity and lower cost of pressurized tank storage, as compared to hydride storage or liquification, make it more appropriate for the remote systems. The compression is commonly done with a multistage piston type compressor.

The renewable energy sources are [unfortunately!] prone to produce electricity at the rate dictated by nature, resulting in disadvantageous capital utilization. Clearly, photovoltaic cells lying await during the night, or worse, during the arctic winter, represent non-productive capital (at that hour). Likewise with wind, tidal, and most other forms of renewable energy generation - the capability to handle peak power production is seldom utilized. Hence the "free fuel" extracts a large capital investment cost.

The need for hydrogen compression extracts a more subtle capital investment demand, as can be illustrated by the CAN Solar Hydrogen design. During the early or late hours of the day, or during times of cloud obscuration, the hydrogen is generated at a reduced rate. As the gas holder is filled, the hydrogen must be compressed - or further generation must be vented.

Compression is done with a conventional four stage piston compressor which is driven by a 15 HP motor - with power demand reduced to about 7 KW by running at reduced rotational speed. With conventional start by use of contactors, the starting inrush would exceed double this, which would overwhelm the capability of the PV system to supply the current. This situation is compounded by the current voltage characteristic of the PV system, as illustrated in Figure 3. As more current is demanded by the load, the voltage decreases.

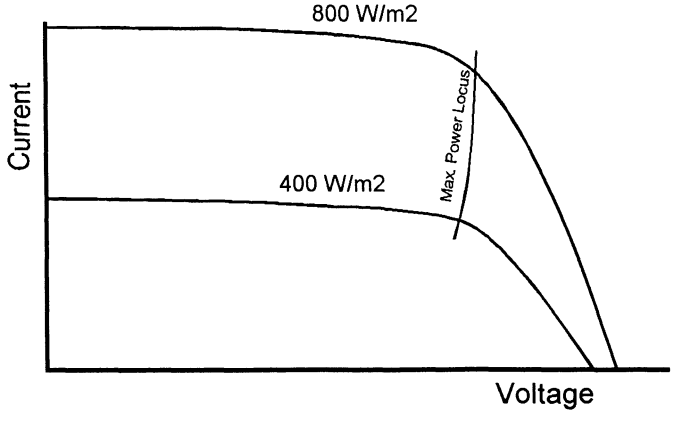

Figure 3 Current/Voltage characteristic of a photovoltaic power source.

In particular, as the upper right corner (or "knee" of the curve) is the peak power operation point for that given insolation level, further demands for current lead to increasingly large decreases in voltage, with resulting power decrease. Thus at these intermediate insolation levels it can be impossible to direct start the motor.[a]

3.1 SLOW-START OF THE CAN COMPRESSOR

The hydrogen compression is done using an air cooled four stage piston type compressor, rated for compression to delivery pressure of 350 kg/cm^2 at 8.2 Nm^2/hr at a shaft speed of 650 rpm. The three phase induction motor is run at twice the compressor shaft speed.

The motor power is provided by a specially designed inverter[b] with a microprocessor controller which is operated so as to start the compressor motor at very low rotational frequency, and then to increase the drive frequency so as to increase the motor speed. The bus bar from the PV array is split before entry to the electrolyser container, with one pair of conductors going directly to the inverter. The current is fed through a boost converter consisting of three parallel connected inductors with outputs alternately switched (at 5 khz) to ground or to a 360 volt rated capacitor bank by IGBT switches using fiber-optic driven isolated gate drivers. The high voltage DC power is converted to AC by a three phase microprocessor controlled variable frequency IGBT switched motor supply. A tachometer provides rate feedback to the microprocessor controller. The design efficiency of the inverter ranges from 70% at the 12 volt input to 80% at 18 volt input. The rated motor efficiency is 85%.

The current demand for the inverter/compressor is under 500 amperes at mid-day insolation, at which time the voltage is nearly 15 volts with no compressor operation, dropping to approximately 14 volts as the compressor runs. Early and late in the day the voltages are lower, and thus the current demand is higher. As can be seen from Fig. 2, the inverter current can approach 600 amperes during the start and end of the day, which current demand can drop the voltage to near 12 volts.

---

a) One might consider adding batteries to store the electricity and aid the motor start. A "power conditioning" unit (which includes electronics which either invert uthe DC power to AC, to run a conventional induction motor, or which provide the switching required for a brushless DC motor) would be used with the motor. If a conventional brush type DC motor (shunt, series or permanent magnet type) with voltage matching the battery is used the power conditioning may be replaced by a big current interrupter.

Batteries, however, have their own disadvantages - not least of which are cost, finite lifetime and maintenance requirements and efficiency. Due to internal resistance and electro-chemistry (including hydrogen generation if overcharged), batteries only yield part of the energy used for charging - 70% being in the vicinity of an upper limit on the storage efficiency. By assuming a battery characteristic and matching it to the CAN system, one can simulate the operation of such a system. In so doing note that the battery charges only with the higher voltages, above 14.5 volts. However, these voltages are not available at the beginning or end of the day, with low sun. Thus the batteries do not fulfill their pormise of offering full day operation.

b) The electrolysis module was supplied by The Electrolyser Corporation, including the inverter of Kennetech Windpower Power Systems manufacture and a CompAir Reavell compressor type 5409EI.

This means of motor starting has proven reliable and maintenance free in the CAN solar hydrogen system. It appears to offer multiple advantages over prior motor starting schemes.

4. Analysis of a Stand-Alone Wind/Hydrogen Village Power System

We suggest the CAN Solar Hydrogen system design may be extended for stand-alone village power systems, as illustrated in Figure 4. Here we add wind generation, a fuel cell[a]

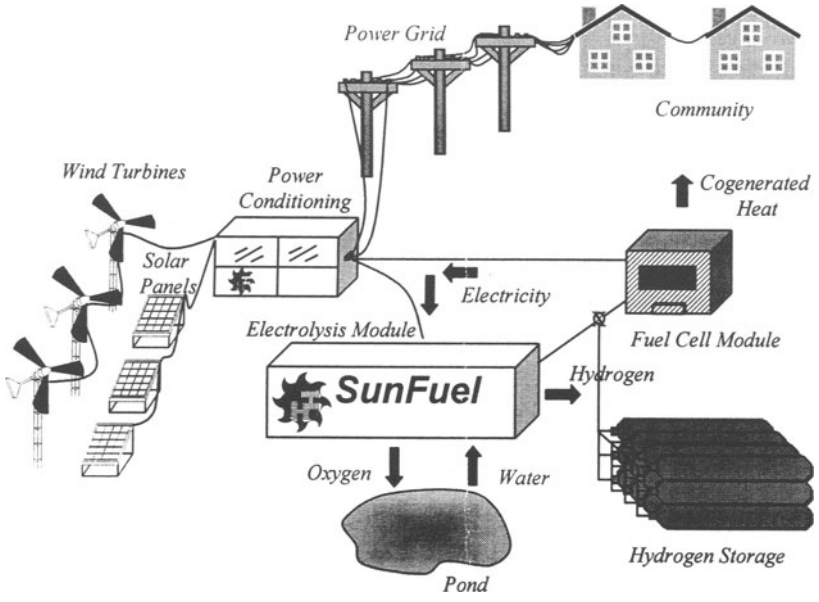

Figure 4. Stand-Alone Solar Hydrogen System powering a "Hydrogen Village".

electrical power generator, and power conditioning to provide power to a grid serving a village. Such a system has much in common with the wind-diesel systems which have become common in remote locations in recent years, but for the use of wind to generate hydrogen fuel for the electrical generation system.

The motivation is illustrated in the following table, showing the prices paid in three northern Canadian locations for fuel and electricity. Fort Smith is at 60° north latitude (as is

---

a) Until such time as fuel cells are competitively priced a hydrogen fueled internal combustion engine powered generator set can be used. Properly designed hydrogen fueled engines can match the efficiency of todays low temperature fuel cells, so only the noise and maintenance requirements of such a rotating machinery approach to electricity generation argue for the visionary advantages of the fuel cell.

Bergen, Norway), about 800 km north of Edmonton, Alberta. Cambridge Bay and Colville Lake are above the Arctic Circle, at approximately 70° north. Diesel fuel is barged in during the summer months.

	Fort Smith	Cambridge Bay	Colville Lake
Diesel Fuel Cost (Can. $, exc.of tax)	$0.26/l	$0.67/l	$0.83/l
Electricity Price	$0.11/kWh	$0.45/kWh	$2.64/kWh
Avg. electrical demand	N/A	780 kW	21 kW
Peak " "	N/A	1367 kW	77 kW
Wind speed (average)	low	21.8 km/hr	17 km/hr

Table 1 - Northwest Territories Energy Prices

Averaging over all the Northwest Territories the mean electrical energy price is $0.44/kWh, six times the North American average of seven cents per kilowatt hour.

At these arctic latitudes sun generated hydrogen is not available in the winter, but the wind resources are. The Wind/Hydrogen Power System is schematically illustrated in the following Figure 5. Recognizing that significant amounts of power are wind generated at

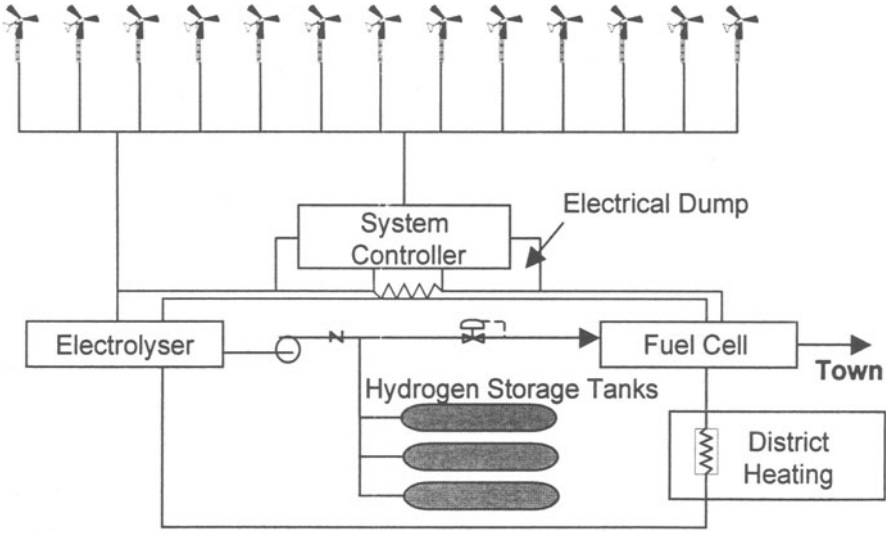

Figure 5. Schematic of the Wind Hydrogen Power System for a Remote Village

times it cannot be used, the system controller includes an electrical dump which is used for water heating, which can contribute to the village district heating requirements. The electrical generator can be in the form of hydrogen powered rotating machinery, or of a fuel cell.

Measurements of the Cambridge Bay electrical demand, wind energy measurements and a wind-hydrogen-generator control strategy have been used to derive design guidelines for the remote power system:

* Fuel cell capacity = load peak = 1.4 MW
* Energy storage = avg. demand * maximum lull = 3 million SCF hydrogen

The wind farm size is determined so as to maintain full storage but for the infrequent low wind periods, i.e., the low wind periods define the wind farm. By this means the size of the wind farm is estimated at 8 MW, with an electrolyzer of 4 MW rating but capability of acting as a controllable load to 6 MW. In those infrequent periods of operation at over 6 MW, the excess current is shunted to the electrical dump (where it heats water).

Based on present day costs, providing this renewable hydrogen power source for the Cambridge Bay community is estimated to require $25 million capital investment, with capital recovery expected from energy cost savings at a rate of $4 million per year. It is concluded that proceeding with a village wind/hydrogen system can be justified from the economic as well as from an environmental point of view.

5. New Technologies for a Renewable Hydrogen Economy

New and more effective technologies, including and in addition to the solar hydrogen project reported in the foregoing, are becoming available for these village hydrogen systems:

* Wind generation costs continue to decrease (to below the $1500/kW used to estimate the Cambridge Bay system cost) and reliability improves;

* Hydropower driven electrolysis is being installed (mid-1997) by the SunFuel Division of the Electrolyser group to fuel Ballard fuel cell buses for the city of Vancouver, B.C.

* Home and business sized electrolyzers will soon be available at modest cost to refuel small fleets of light duty vehicles overnight or at the fleet storage location. These units can be powered with off-peak electricity, and make hydrogen fuel stations easily available wherever an outlet is available.

It is appropriate at this time to carefully choose sites for one or more modest sized wind/hydrogen systems and continue the development of these renewable hydrogen sources.

1. Further detail, with photographs, is given in Provenzano, J., Scott, P.B., and Zweig, R. (1996) Demonstration of Fleet Trucks Fueled with PV Hydrogen, *HYDROGEN ENERGY PROGRESS XI, Proceedings of the 11th World Hydrogen Energy Conference, International Association of Hydrogen Energy*; to be published also in the International Journal of Hydrogen Energy.

2. Van Blarigan, P. (1996) Development of a Hydrogen Fujeled Internal Combustion Engine Designed for Single Speed/Power Operation, *Society of Automotive Engineers Paper 961690*

3. Smith, J. R. (1993) The Hydrogen Hybrid Option, *Lawrence Livermore Laboratory Report UCRL-JC-115425*

4. Hunter, R. & Elliot, G. (1994) *Wind-Diesel Systems*, Cambridge Press (1994)

5. VanCamp, J. (1996) Hydrogen and the Northern Canadian Energy System, *Proc. 11th World Hydrogen Energy Conference, International Association of Hydrogen Energy*

6. Dienhart, H. & Siegel, A. (1994) Hydrogen Storage in Isolated Electrical Energy Systems with Photovoltaic and Wind Energy, *Int. J. Hydrogen Energy,* **19**, 61-66; Kauranen, P. S. et.al. (1994) Development of a Self-Sufficient Solar-Hydrogen Energy System, *op.cit.*, **19**, 99-106

THE ADVANCED PROCESS FOR STEAM CATALYTIC CONVERSION OF HYDROCARBONS IN HYDROGEN PRODUCTION.

D.L.Astanovsky, L.Z.Astanovsky
FAST ENGINEERING LTD, P.O.Box 5, Moscow. 129110, Russia
Fax: 7 095 292 6511 BOX 18462

Abstract - Advanced technology for steam catalytic hydrocarbon conversion in a new reactor design is presented.

The influence of parameters changing of the process carrying out and catalyst activity on conversion rate are analyzed.

The example of the main characteristics of process flow diagram for steam conversion of natural gas are given.

1. INTRODUCTION

The creating in 30 years the first units for carry out steam catalytic hydrocarbon conversion opened the new way for hydrogen production. Till nowadays this method is used worldwide as most efficient and economical.

The greater demand for hydrogen in production of refinery, petrochemical, ammonia and methanol are doing actual the further advancing this process [1].

The main tasks for advancing existing hydrogen plants and new ones are as follows:

- to reduce energy consumption;
- to reduce capital investment;
- to solve environmental problems.

Many firms in the world are carrying out works for designing new and advancing existing reactors and catalysts for this process for solving this problems permanently.

2. EXISTING DIAGRAMS FOR STEAM HYDROCARBONS CONVERSION

For production of reformed hydrogen contained gas traditionally used steam hydrocarbon conversion in the tubular reactors or shift rectors using nickel catalyst. The heat supply required for endothermic reaction are carried out either by fuel gas through the walls of the reaction tubes at the expense of fuel gas burned in the intertubes space or at the expense of a part of the hydrocarbon to be burned inside the reactor above the catalyst bed combined with oxygen or air.

The heat after radiant zone of tubular reactor and heat of reformed gas are used for heating streams of process gas and steam production. The process of heat-exchange are carried out both on inner installed heat-exchange surfaces in conventional zone of reformer and on separately installed heat-exchanges [2,3].

In order to use low potential heat and reduce load on the tubular reactor pre-reforming before reformer was suggested [1,4]. In pre-reforming the conversion is carried out in adiabatic conditions.

T. O. Saetre (ed.), Hydrogen Power: Theoretical and Engineering Solutions, 129–136.

One of the main advantages of pre-reforming for steam catalytic conversion of naphtha and gas, containing hydrocarbons heavier than methane is removal of heavy hydrocarbons to methane. The pre-reformer is widely use.

With the aim of increasing process efficacy by more intensive use of heat supplied heat for carry out endothermic reaction a some diagrams and apparatuses for carrying out the process of conversion in a two stage: in the tubular reactor and shift reactor were designed and operated. So, in the tubular reactor of conversion carried out at the expense heat of gases after shift reactor [1,5].

Another way of increasing process efficacy is carrying out the process of conversion with deleting of steam and gas on two parallel flows. The first flow directed into tubular reactor heated by flue gas through the walls of the reaction tubes. The second flow directed into tubular gas heated reformer, heated by reformed gas after tubular rector [1,6].

As a rule, tubular reactors and reactors for steam catalytic hydrocarbon conversion are massive, ponderous, expensive constructions, borrowing big area.

The conversion is usually to carried out at high pressure (1,0-4,0 MPa) and high temperature (800-900°C). In the connection of above mentioned the manufacture of the reaction tubes and another parts of reactor, working in extreme conditions requires expensive heat resistant nickel alloys [2].

Tubular reformers discharge adverse gases contain such components as NOx, CO and SO_2. Taking into account the quantity of adverse gases, tubular reformers discharge tenth tons of NOx gases to atmosphere.

3. NEW SCHEME AND APPARATUS FOR CARRY OUT HYDROCARBON CONVERSION.

The process for steam catalytic hydrocarbon conversion are suggested to carry out in the new design reactor which is principally different from those currently used [7].

A new catalytic reactor features so that in annular space of a radial reactor, filled with the catalyst, the walls were placed in the form of a planar spiral (in a plane drawn perpendicularly with respect to the longitudinal axis of the reactor), forming spiral-shaped passages which have the same sections to the direction of fluid flow. So the walls are made with hollows for heat supply is necessary for carrying out conversion process. The inner space of hollow walls connected with pipes of inlet of heat-carrier.

Figure 1 shows the new design reactor comprises heat-exchanger is mounted in the lower part of reactor and the catalyst bed is placed in the upper part of reactor.

The heat-exchanger have the same design as the catalyst bed. It provides maximum surface for heat exchanging in volume unit reactor and opportunity to use heat-exchange under conditions of high temperature drops.

The advantage of a new construction reactor in comparison with used analogues are as follows:

- opportunity of use the most active fine-grained catalyst keeping low pressure drop in the catalyst bed;
- uniform spread of a fluid flow through a granular bed providing preset linear velocity;
- providing the kinetic optimum temperature conditions for carrying out a catalytic process;
- opportunity of effective heat supply to the catalyst bed;
- a high level of use of reactor volume;
- a wide range of selection of pressures and temperatures for a catalytic process;

- except of use lining materials;
- considerable reducing dimensions of apparatus and its capital investment;
- opportunity to transport reactors fully assembled by railway, road and sea transport;
- convenient for installation, easy to operate and repair.

The process scheme for natural gas conversion in the new design reactor is presented on figure 2.

Gas and steam mixture enters the reactor through the inlet pipe, then passes through the heat-exchanger, where it is heated, then goes through the central tube and through the external perforated shell in to the passages filled with the catalyst, where the hydrocarbon steam conversion reaction takes place. The converted gas leaves the passages through the inner perforated shell and goes along the annular space between inner perforated shell and the central tube and enters the heat-exchanger where it is cooled and returned the heat to gas coming to the conversion, then discharged from the reactor through the outlet pipe.

Fuel gas as heat-carrier enters the reactor and is uniformly distributed into the hollows of the spiral-shaped walls giving up the heat to the reaction zone, it then leaves the hollow walls and is collected in the annular manifold where it is then discharged from the reactor. In this case, it does not contain adverse substances. The upper part of the reactor casing where catalyst bed is placed has a special heat-resistant lining.

The converted gas and fuel gas as heat-carrier after reactor running to the boiler to utilize the heat and steam production.

The example for carry out the steam catalytic conversion of natural gas in hydrogen production are presented in Table 1.

The use of a new design reactor enable to solve two basic problems for carrying out process of conversion: to reduce pressure drop in the catalyst bed and provide heat supply required for carrying out the process.

The use of the most active fine-grained catalyst enables to reduce the volume and dimensions of reactor keeping low pressure drop in the catalyst bed.

The opportunity of creating developed surface into the catalyst bed of the new design reactor provides heat supply required for carrying out the process.

4.THE REACTOR HEAT SUPPLY.

The catalytic burner is used for production of fuel gas as heat-carrier. The diagram of catalytic burner connection to the new design reactor for natural gas conversion is presented in Figure 3.

The burner is installed directly on the reactor. The part fuel gas after boiler is mixed with air on the blower suction and goes to the burner. The fuel is running to the burner too.

The fuel gas temperature is controlled by changing the fuel gas, air and fuel ratio on the burner inlet.

The use catalytic burner for a new design reactor solves environmental problems providing discharge stack gases having no adverse components.

5. CONCLUSIONS.

The use of the advanced process for steam catalytic conversion of hydrocarbons in hydrogen production ensures:

- reduction capital investment 3-5 times in depends of unit capacity;
- reduction maintenance expenses;
- eliminate environmental pollution.

The use of catalytic burner with opportunity of continuous control of heat-carrier temperature provides optimum temperature conditions for carrying out of catalytic process. So the conditions for changing load in the reactor from 0 to maximum, without walls overheating, are created.

The catalytic reactor of new design enables to create the hydrogen production units for specific capacity in wide range of pressures.

Taking into account above mentioned the advanced process for steam catalytic conversion of hydrocarbons in hydrogen production highly perspective both for reconstruction of existing plants and construction of a new one. Positive experience of using the new design reactor for ammonia synthesis confirmed its normal operation.

6. REFERENCES.

1. Cromarty B.J. and Hooper C.W. (1997) Increasing the throughput of an existing hydrogen plant, *Int. J. Hydrogen Energy,* Vol.22, No.1, pp.17-22.
2. Nitrogen reference book (1986) Process gases production. The process gases cleaning. Ammonia synthesis, Chemistry, Moscow(in Russian).
3. Rostrup-Nielsen J.R. (1984) Catalytic Steam Reforming. Springer-Verlag Berlin Heidelberg New-York Tokyo.
4. Clark D.N. and Henson W.G.S. (1988) Opportunities for savings with pre-reformers. *AIChE Ammonia Plant Safety,* 28, 99.
5. Sosna M.H., Harlamov V.V., Semenov V.P., Kondrashenko V.D. and Alekseev A.M. (1993) Russia patent No.784148, B01J 8/04, The two stage process of catalytic hydrocarbons conversion(in Russian).
6. Panchenkov U.V., Raskin A.Y., Glauberman A.I., Sokolinsky U.A., Mukosei V.I. and Harlamov V.V. (1987) Russia patent No.1499840, B01J 8/02, The process of production hydrogen contain gas (in Russian).
7. Astanovsky D.L., Astanovsky L.Z., Raikov B.S. and Korchaka N.I. (1994) Reactor for steam catalytic hydrocarbon conversion and catalytic CO conversion in hydrogen production, *Int. J. Hydrogen Energy,* Vol.19, No.8, pp.677-681.

TABLE 1. The example of natural gas steam catalytic conversion in hydrogen production.

№	Description	Temperature, °C	Pressure, MPa	Component, % vol.
1.	Steam and gas mixture on the reactor inlet	260	2,1	H_2 - 2,16 N_2 - 0,19 CH_4 -21,38 C_2H_6 - 0,05 C_3H_8 -0,03 H_2O -76,19 Total -100,00 Steam/gas ratio 3,2
2.	Steam and gas mixture after the heat-exchanger	580	2,1	- do -
3.	The converted gas before the heat-exchanger	820	2,1	H_2 - 45,94 N_2 - 0,13 CH_4 - 3,10 CO_2 - 5,69 CO - 7,22 H_2O - 37,92 Total -100,00 Steam/gas ratio 0,61
4.	The converted gas after the heat-exchanger	530	2,1	- do -

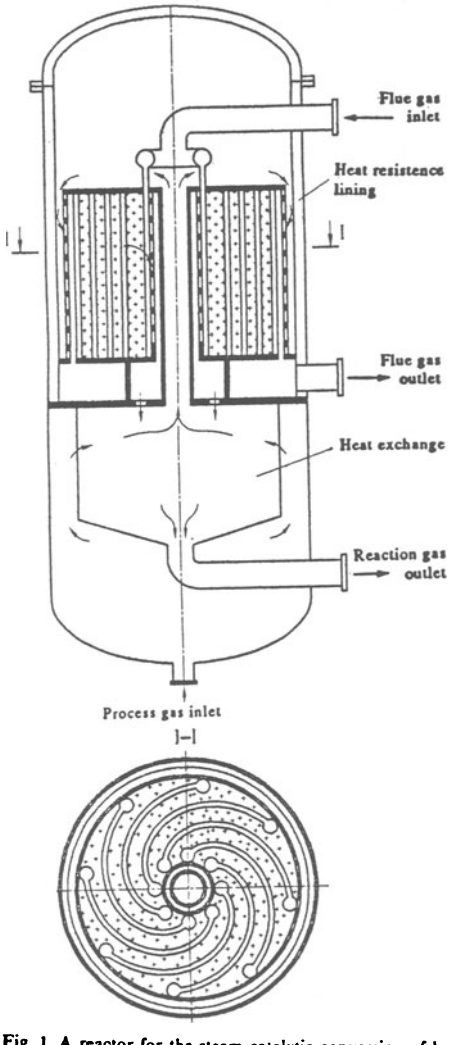

Fig. 1. A reactor for the steam catalytic conversion of hydrocarbons, shown in longitudinal section.

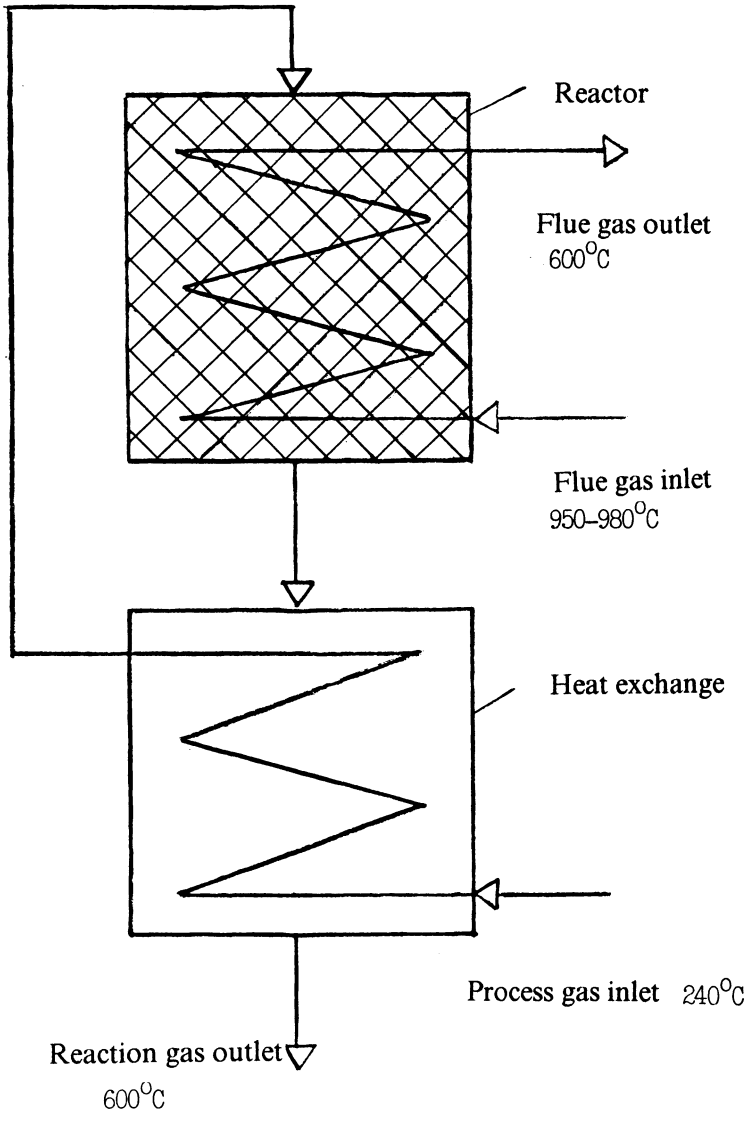

Fig.2. The process scheme for natural gas conversion in the new design reactor.

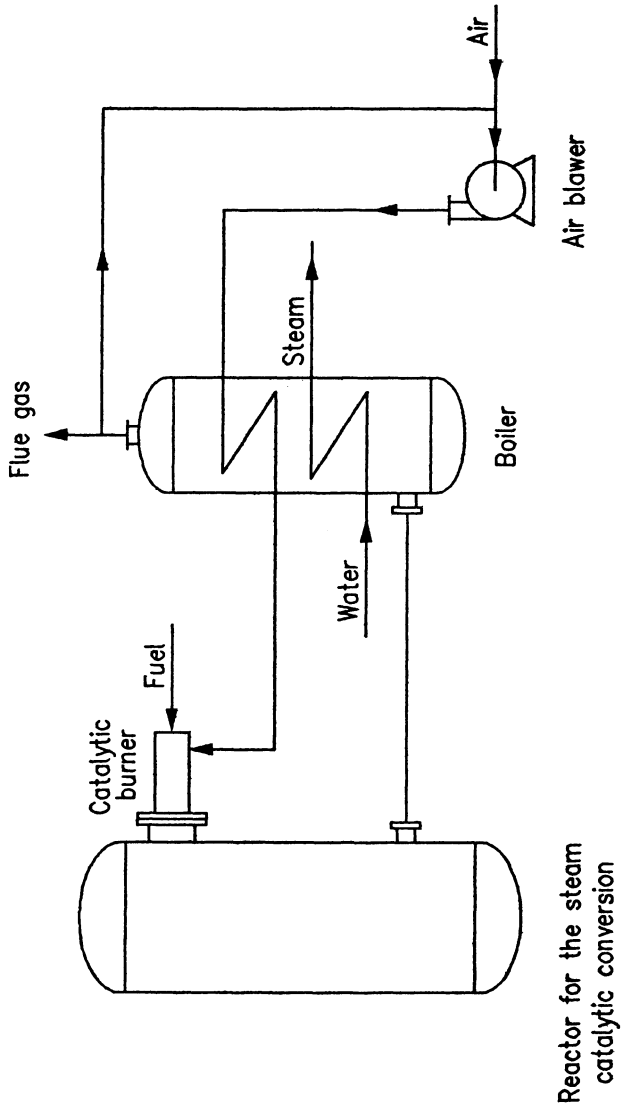

Fig.3. Diagram of catalytic burner connection to the design reactor for natural gas conversion

HYDROGEN PRODUCTION FROM METHANE VIA DIRECT HIGH-POWER IRRADIATION OF CATALYSTS

YU.YU. TANASHEV, YU.I. ARISTOV, V.I. FEDOSEEV,
V.V. PUSHKAREV and V.N. PARMON
Boreskov Institute of Catalysis
Prospekt Akademika Lavrentieva, 5, Novosibirsk 630090, Russia

1. Introduction

Taking into account the great world supply of natural gas, one of the most promising ways of hydrogen production is a catalytic processing of methane. For this aim a set of reactions, such as

$$CH_4 \rightarrow 2H_2 + C, \quad (1)$$

$$CH_4 + H_2O \rightarrow 3H_2 + CO, \quad (2)$$

$$CH_4 + CO_2 \rightarrow 2H_2 + 2CO, \quad (3)$$

has been suggested and investigated in detail. All these processes are endothermic and characterised by great deal of energy and high temperature needed for an suitable depth of methane conversion to be reached. In ordinary oven-heated catalytic reactors the delivered heat, first, is absorbed by a steel wall and then is transferred to the catalyst bed where it is converted to chemical energy. The sufficient thermal resistance between the wall and the catalyst bed together with the low thermal conductivity of the catalyst lead to a limitation of the heat flux arrived to the catalyst by the values of about 5-10 W/cm^2. Under these conditions one cannot provide the process of energy conversion with specific power loading $w = W_{chem}/V$ (W_{chem} is the enthalpy change during the energy accumulating reaction per unit time, V is the catalyst volume) larger than 5-10 W/cm^3. Therefore, the rate of hydrogen production is far lower than the maximum one because of imperfect using the resource of catalytic activity [1].

To minimise the limitation, one possible way is a direct volume heating of the catalyst by the use of highly penetrating radiation. This approach is being successfully developed at the Boreskov Institute of Catalysis (Novosibirsk, Russia). Here we summarize our experimental results on catalytic production of

T. O. Saetre (ed.), Hydrogen Power: Theoretical and Engineering Solutions, 137–142.

hydrogen from methane by the use of three kinds of penetrating radiation: accelerated electrons, concentrated light and microwaves.

2. Experimental

Three sources of radiation we used were (i) an U-12M electron accelerator with electron energy 3 MeV and electron flux 1×10^{13} - 5×10^{14} $cm^{-2}s^{-1}$; (ii) a 10 kW Xenon lamp DKSShRb-10000, the light of which was concentrated with a set of mirrors up to the heat density 5 - 200 W/cm^2; and (iii) a magnetron M-117 of 2.45 GHz frequency with generated power up to 5kW, operating under both continuos and pulse modes (pulse duration t_p = 1-100 ms and frequency ν = 0.5-125 Hz). Catalytic reactors were made from quartz or stainless steel (for accelerated electrons) and filled with commercial Ni-based (GIAP-16, GIAP-3-6N, TH-2) and Ru-based (K-3) catalysts for methane activation. For microwave experiments we also used lab-synthesized Ni- and Fe-based catalysts as well as steel and copper grids. Methane and methane containing mixtures (CH_4 + H_2O with methane volume fraction α = 0.25-0.4, CH_4 + CO_2, α = 0.2-0.25 and CH_4 + Ar, α = 0.2-0.9) were passed through the catalyst bed during irradiation. Gas - catalyst residence time τ was varied from 0.01 to 2 s. The rate of hydrogen production r, specific power loading w and energetic efficiency $\eta = W_{chem}/W_{inc}$ (W_{inc} is power of incident radiation) were calculated using the chromatographic data on dry product mixture composition and standard thermodynamic tables.

More experimental details may be found elsewhere [2-4].

3. Results and Discussion

3.1. ELECTRON BEAM IRRADIATION

It is found that in the absence of reaction a high penetrating ability of accelerated electrons provides efficient bulk heating of the catalyst up to the temperature T = 1000-1200°C. For reaction (2) there is a "threshold" effect in the chemical action of the radiation, consisting in a rapid increase of the values of r, w and η when the power supply ρ into the catalyst bed becomes larger than $\rho^* \approx 5$ W/cm^3. If $\rho > \rho^*$, the specific power loading increases almost linearly with the increase of ρ (Fig.1) reaching 50 W/cm^3 for K-3 catalyst, which is close to the theoretically predicted loading [1]. Such a tendency allows one to expect a further rise of w if the value of W_{inc} increases, the real limit for w being determined mostly by a

thermal stability of the catalysts used [2]. The rate of hydrogen production is also extremely high and may reach 20-25 Ncm^3/s per 1 cm^3 of the catalyst.

An important feature of our experiments is the non-isothermal condition of the energy conversion process, due to non-uniform absorption of radiation along the catalytic reactor. Some observed regularities of the process under study, for example, the smooth maximum of the curve ***r*** *vs* ***x*** (Fig.2), are obviously driven by this non-isothermity [2].

Among the other results it is worthy to mention a correlation between the reaction rate under radiation and the activity of catalysts used - the higher the activity measured under common heating the greater the rate. The experiments also showed the low values of ***r*** when irradiating a pure support of the catalysts (disperse Al_2O_3). Some experimental results are presented in Table 1.

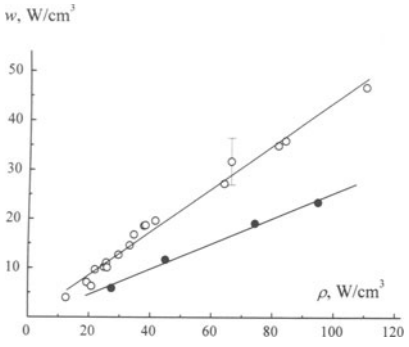

Figure 1. Experimental dependence of w value upon the average power density ρ of heat supply. Reaction (2) under electron beam, $H_2O:CH_4$ = 2.0±0.2, methane conversion x = 0.4-0.6, ○ - K-3 catalyst, ● - GIAP-3-6N catalyst.

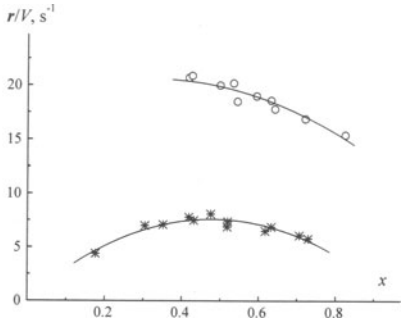

Figure 2. Experimental dependence of hydrogen production rate upon methane conversion. Reaction (2) under electron beam, $H_2O:CH_4$ = 2.0±0.2, K-3 catalyst, ○ - ρ = 110 W/cm^3, * - ρ = 38 W/cm^3.

TABLE 1. Some experimental values of the rate ***r*** of hydrogen formation, specific power loading w and efficiency η of radiation-to-chemical energy conversion for reaction (2) initiated by electron beam (V is the catalyst volume)

Catalyst	ρ (W cm^{-3})	τ (s)	x	r/V (s^{-1})	w (W cm^{-3})	η
γ-Al_2O_3	38	0.240	0.02	0.1	<1	<0.01
GIAP-16	53	0.084	0.38	5.0	14	0.26
TH-2	85	0.041	0.32	12.0	29	0.34
GIAP-3-6N	95	0.041	0.42	9.6	23	0.25
K-3	84	0.044	0.49	14.9	36	0.43
K-3	110	0.027	0.43	20.6	47	0.40

All the data obtained indicate a predominant role of the thermal mechanism in the chemical action of intensive ionizing radiation. The thermochemical action of electron beam results in intensive heating of the catalyst almost "from inside", eliminating the mentioned restrictions on heat supply into the catalyst bed, and, therefore, provides the hydrogen production with rather high values of r and w.

3.2. IRRADIATION BY CONCENTRATED LIGHT

Another way to intensify a heat supply is heating of the catalyst by highly concentrated light in reactors with transparent wall. Because of the bulk heating such reactors are named "volumetric" [5]. Under such conditions extremely high rate of hydrogen formation in reaction (2) on the K-3 catalyst is observed (Table 2). The Table 2 shows that the direct illumination of the catalyst allows to reach at $T \approx 700°C$ the specific power loading of the light-to-chemical energy conversion of about 100 W/cm^3 that is close to the maximum possible values for the catalysts tested [1].

Moreover, the light-assisted methane reforming is in many features similar to the process performed under powerful electron beam. The values of r and w appear to increase near linearly with the rise of ρ; the functions of r, w and η on the methane conversion have smooth maxims at $x = 0.5$-0.6 and $T = 600$-$700°C$, resulting from the non-isothermal conditions of the process under study [3].

It is found that the increase in the reaction rate is likely to be due to thermochemical action of the concentrated light rather than due to the photochemical one. This statement is based on the findings similar to those we have discussed above for the electron-beam-driven catalysis, namely, the similar contents of the reforming products, the low values of the reaction rate in the absence of an active metal, a distinct correlation between the rate of the light-driven reaction and the thermally-driven activity of the catalyst used.

TABLE 2. Some experimental results on methane steam reforming under heating of the K-3 catalyst by concentrated light

ρ (W cm^{-3})	τ (s)	x	r/V (s^{-1})	w (W cm^{-3})	η
39	0.027	0.18	9.1	16	0.41
44	0.063	0.67	12.4	32	0.74
95	0.024	0.47	20.7	44	0.46
172	0.023	0.83	36.7	93	0.54

3.3. IRRADIATION BY MICROWAVES

A choice of the catalyst for a MW-assisted process appears to be of great importance as it must meet some specific requirements (for instance, a good absorbency of microwave energy) in addition to the common demands of high activity, selectivity, stability, etc. Unfortunately, we have found that many commercial supported catalysts demonstrate rather poor MW-absorbency and zero rate of methane MW-conversion. On the contrary, the lab-synthesized catalysts mNi/Al_2O_3 (m >40 wt.%), tested in reaction (3), are shown to allow a combination of the demands mentioned above. They possess a high MW-absorbency and provide appreciable methane conversion (x > 0.5) under both continuos and pulse modes. Direct microwave heating of these catalysts leads to removing the limitation of heat transfer into reaction zone; the w value was measured to be as high as 40 W/cm^3. For well-absorbing catalysts the average microwave power, as in the case of electron beam and concentrated light, is found to influence strongly the rate of hydrogen production. Pulse microwave power and a structure of the pulse envelops are also of importance and give a valuable tool for management and control of the MW-driven catalysis.

Microwave power can be used for methane processing into pure hydrogen by reaction (1). Interestingly, the by-product of this reaction is filament carbon which is of high practical interest because of its prominent adsorption properties.

Another distinctive feature of the MW-catalysis is a possibility for a new channel of hydrogen production to appear due to electric gas discharges in the vicinity of the uneven catalyst surface. The discharge reaction mode can be realized at low average (but high pulse) microwave power. The experiments show a high rate of the selective methane pirolysis towards hydrogen and acetylene (>10 Ncm^3/s per 1 g of catalyst) under gas discharge in the presence of stainless steel or copper grid as "a catalyst". The rate of hydrogen formation could be further increased if argon, which is a good "discharge conductor", is added to methane at the reactor inlet in amount of up to 50 vol.% (Fig.3).

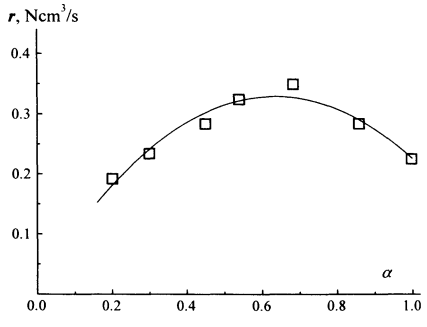

Figure 3. **Experimental dependence of MW-driven rate of hydrogen production upon methane content α in mixture CH_4+Ar at the reactor inlet. Conditions: t_p = 2 ms, ν = 1 Hz, pulse power 5 kW, gas discharge mode, MW-absorbing object is a stainless steel grid.**

Thus, application of microwave power has opened up fresh opportunities for hydrogen production via natural gas processing.

4. Conclusions

Direct radiation heating of the catalyst is shown to be able to enhance considerably the rate of hydrogen production from methane. The main reason for this is likely to be the thermochemical action of all kinds of the radiation used. We have found several common features of the occurrence of endothermic reactions under direct irradiation of catalysts regardless the reaction, catalyst or radiation nature. These are resulted from intense, volumetric and nonisothermal character of the direct catalyst heating by intense penetrating radiation. Additional advantage of suggested method of hydrogen production is formation of valuable chemical by-products (acetylene, filament carbon) in the course of catalytic methane conversion.

Basing on the results obtained one can expect that even in the near Future the development of the radiation-to-chemical energy converters will result in creation of a new generation of efficient and compact devices for hydrogen production from natural gas using solar energy, microwave power or ionizing radiation.

References

1. Aristov, Yu.I., Bobrova, I.I., Bobrov, N.N., and Parmon, V.N.: Limiting values of efficiency and specific power of thermochemical solar energy conversion, in *Proc. 7th World Hydrogen Energy Conf., Moscow, Russia, 1989*, Pergamon, N.Y., 1989, pp. 1079-1091.
2. Aristov, Yu.I., Tanashev, Yu.Yu., Prokopiev, S.I., Gordeeva, L.G., and Parmon, V.N.: ICAR-process (Immediate Catalytic Accumulation of ionizing Radiation energy) as a new promising approach to the development of cheminuclear power plants, *Int. J. Hydrogen Energy* **18** (1993), 45-62.
3. Aristov, Yu.I., Fedoseev, V.I., and Parmon, V.N.: High-density conversion of light energy via direct illumination of catalyst, *Int. J. Hydrogen Energy* (in press).
4. Aristov, Yu.I., Fedoseev, V.I., Tanashev, Yu.Yu., Pushkarev, V.V., and Parmon, V.N.: Hydrogen production via direct microwave action on heterogeneous catalysts, in *Proc.11th World Hydrogen Energy Conf., Stuttgart, Germany, 23-28 June 1996*, Schön & Wetzel GmbH, Frankfurt am Main, V.1, pp. 931-938.
5. Proc. 5th Int. Symp. on Solar High-Temperature Technologies, Davos, Switzerland, 1990, in *Solar Energy Mater. and Solar Cells* **24** (1991), 1-780.

PLASMABASED HYDROGEN AND ENERGY PRODUCTION

More efficient, economical and environmental friendly utilisation of hydrocarbons

KETIL HOX, RAGNE HILDRUM AND STEINAR LYNUM
Kværner Engineering a.s
Postboks 222
N-1324 LYSAKER

The best way to avoid a pollutant is by not producing it. Kværner's new CB&H process and PYROARC process are both characterised by being able to convert low grade hydrocarbons into clean and useful products. Both processes yield high thermal efficiency and feedstock utilisation.

The CB&H process produces hydrogen and no CO_2 from any hydrocarbon. The process does not affect the environment by producing unwanted by-products or pollution. The new process gives two valuable products, hydrogen and carbon black.

The PYROARC process converts waste and biomass to a clean fuel gas and heat.

This lecture will give a presentation of the new processes, the background for the invention and future possibilities. Some of the possibilities given by the new processes are visualised, as for the CB&H process, where interplay between various industries could significantly reduce emission of pollutants and lower power and feedstock consumption.

T. O. Saetre (ed.), Hydrogen Power: Theoretical and Engineering Solutions, 143–148.

1. Introduction

Kværner has developed several processes based on plasma technology. They are all designed for high resource economisation. The fundamental criteria for the design are;

⇒ High energy efficiency
⇒ High feedstock utilisation
⇒ High product selectivity

Two examples of processes developed are the PYROARC process and the CB&H process. They are both designed to fulfil the design criteria.

The two processes have different feedstock and product blend, but do both utilise plasma technology to produce hydrogen and energy.

2. Process Description

In order to fulfil the requirements of the CB&H process and the PYROARC process, Kværner has invented two complementary plasma generators. The plasma generator in the PYROARC process is designed for inert and oxidising atmosphere, while the plasma generator used in the CB&H process is designed for inert and reducing atmosphere.

This technology makes Kværner capable of meeting new challenges concerning process operating in both reducing and oxidising atmosphere, with different feedstocks and product specifications.

2.1 THE PYROARC PROCESS

The world's demand of energy needs alternatives to the fossil fuel based processes. An ideal process for tomorrow's energy and heat production

⇒ uses biomass or waste as feedstock
⇒ fully utilises the feedstock
⇒ has emissions close to zero

Such a process is the PYROARC process. Since 1986 this process has been tested out in a pilot plant with a capacity of 300-500 kg solid waste per hour and 50-700 kg of liquid or gaseous waste per hour. Examples of waste successfully treated in the pilot plant is, among others, spent tyres, mixtures of wood and plastic, household waste without water, chlorinated solvents, paint, batteries and simulated hospital waste.

In order to produce a clean fuel gas with emissions close to zero, the organic material has to be completely decomposed. This is achieved by using a two-stage process, consisting of a shaft gasifier and a decomposition reactor.

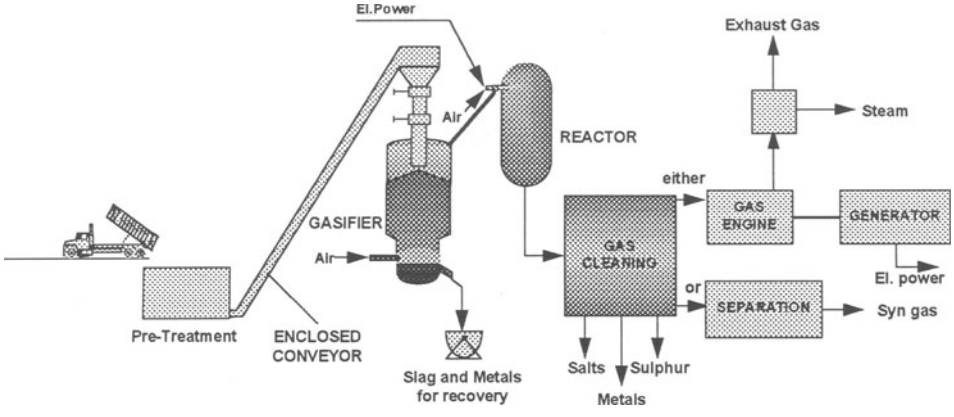

Figure 1. Flow sheet of the Kværner PYROARC process

In the shaft gasifier the organic content of the solid waste is pyrolysed and partly oxidised by use of preheated air or oxygen. If necessary, a plasma generator is used to supply energy for the gasification.

In the reactor effluent gases from the gasifier are mixed with liquid and gaseous feedstock. The plasma generator provides sufficient energy to completely decompose the organic matter. In this way, toxic hydrocarbons are eliminated. Secondary air is introduced in order to optimise the heat value of the fuel gas produced, as well as to avoid the formation of toxic gases.

The inorganic content of the feedstock is recovered as molten metal or incorporated in a glassy, non leachable slag which can be used for landfill purposes.

Secondary products from gas cleaning involves zinc-lead dust or sludge, alkaline salt and sulphur. The zinc-lead dust can normally be used for metal recovery. The alkaline salt can after proper treatment in a water treatment unit be disposed off as effluent water or dry salt. The sulphur is present mainly as H_2S which makes it possible to remove as elementary sulphur.

The fuel gas can be used as input in a gas engine for power production. It might also be feasible for synthesis gas production. The feasibility of this process application will depend on the feedstock. The process heat can be used for steam production.

2.2 THE CB&H PROCESS

The Kværner CB&H process was originally aimed at finding new ways to utilise natural gas. The process is today capable of converting any hydrocarbon, liquid or vapour, into the wanted products, carbon black and hydrogen. Since 1992 a pilot plant with capacity of 500 Nm^3 /h natural gas has been operated.

Pyrolysis of the feedstock takes place in a high temperature reactor. The necessary heat to sustain the chemical reaction is supplied by the plasma generator, where electric power is transferred to thermal energy at high efficiency. When leaving the reactor, the product is prior to being separated by filters, cooled down by heat exchange with the feedstock. Excess heat is used to produce high pressure steam for external use.

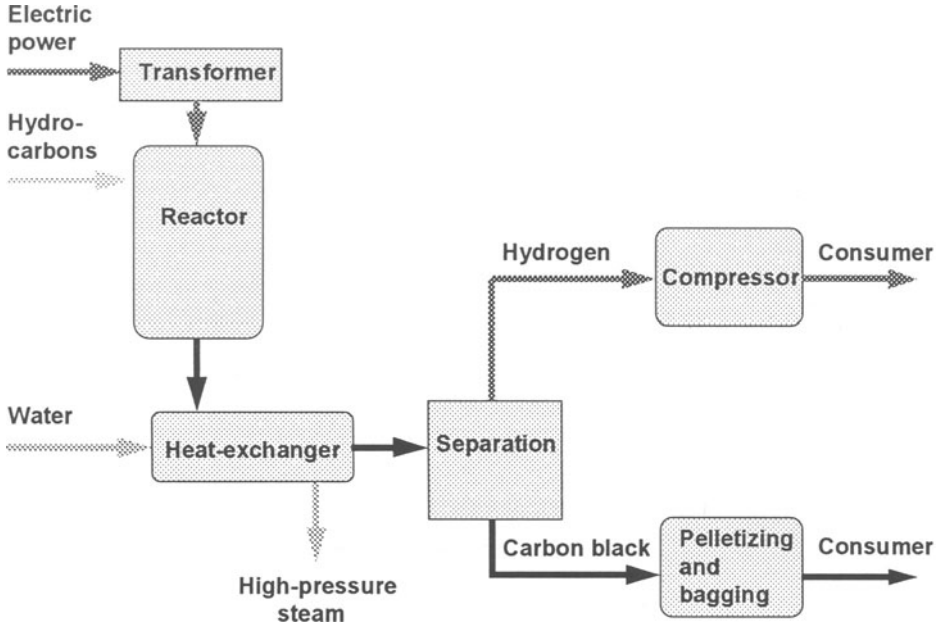

Figure 2. Flow stheet of the Kværner CB&H process

The process could also be fed by any refinery off-gases where all hydrocarbons will be converted into carbon black and hydrogen, any oxygen in the feed would be converted to CO.

Changing feedstock will affect product composition and energy consumption, but as long as the feed is a hydrocarbon, the products will still be only hydrogen and carbon black. The ratio between hydrogen and carbon in the product will reflect the ratio in the feed.

The present marked for carbon black is first of all the tire and rubber industry. Important future markets will also be the metallurgical industry. The high purity and reactivity of our carbon could improve process performance of many metallurgical processes. The replacement of more polluted carbon with our pure carbon will eliminate SO_2. The market is huge and the demand is increasing.

As an example, experiments with our carbon in SiC production gave higher yield, better product quality, reduced power consumption and reduced air pollution.

Hydrogen, being the fuel for the future, will be used in refineries and for transportation purposes. We produce hydrogen more energy efficient than other processes. These relations are visualised in figure 3.

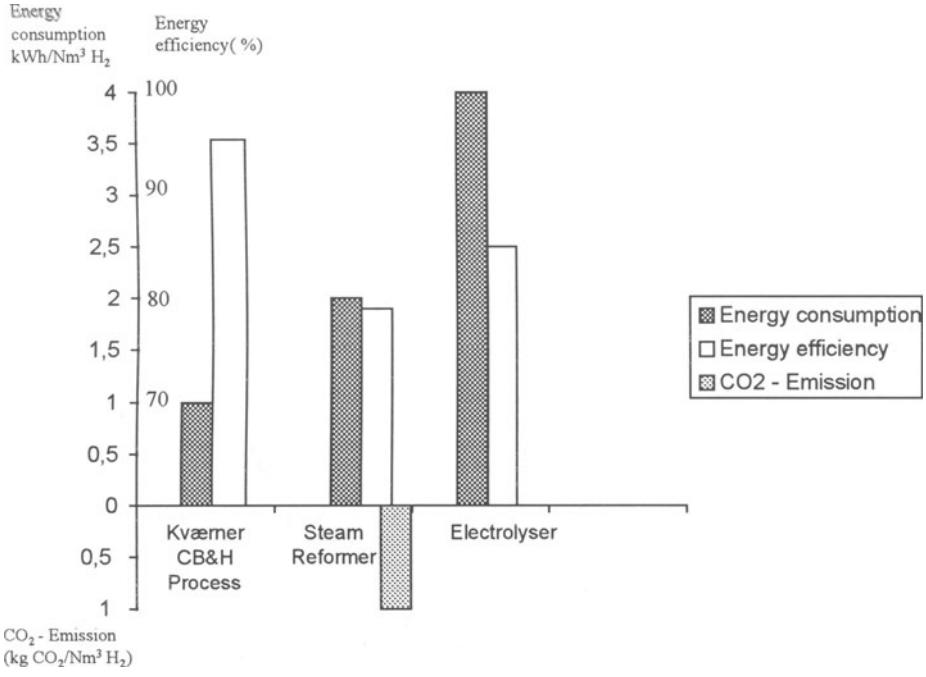

Figure 3. Kværner CB&H process compared to existing hydrogen processes

3. CO_2 Reduction by Industrial Interplay

CO_2 emission is used as a measure to compare the impact on the environment of different process plants. In the presented example the carbon black and hydrogen plant is interplaying with a natural gas fired powerstation and a silicon carbide factory. The overall heat and material balance give a large reduction in emission of CO_2, SO_2 and dust. The reductions are mainly due to better feedstock utilisation and improved energy efficiency. An even larger reduction in CO_2 emission will be achieved if the hydrogen instead is used as fuel for fuel cell powered vehicles.

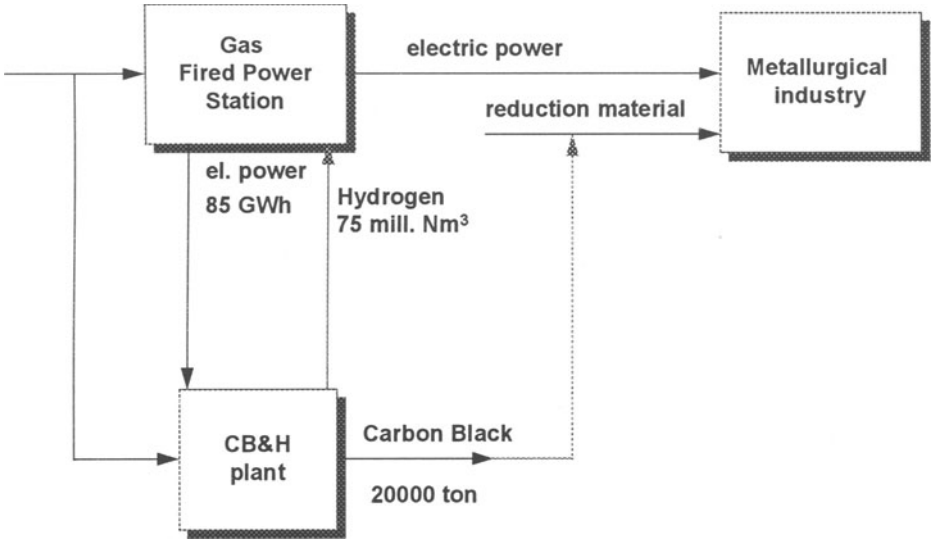

Change in CO_2 emission, tonnes per year	Cause
+ 29000	Increase caused by electric power demand from the CB&H plant.
- 45000	Decrease due to replacement of natural gas by hydrogen in the power plant.
-22000	Decrease because of increased power efficiency in SiC production.
-20000	Decrease due to enhanced feedstock utilisation.
-58000	Total reduction in CO_2 emission.

Figure 4. Interplay between a gasified powerstation, SiC production plant and the CB&H process. The calculations are based on an annual production of 75 million Nm^3 hydrogen and 20000 tonnes of carbon black.

HYDROGEN EVOLUTION AT ACTIVATED NiS_x-CATHODES IN WATER ELECTROLYSIS

B. BØRRESEN[a], A. BJØRGUM[b], G. HAGEN[a], R. TUNOLD[a] and K. ANDREASSEN[c]

[a] Department of Electrochemistry, The Norwegian University of Science and Technology, N-7034 Trondheim
[b] SINTEF Materials Technology, N-7034 Trondheim
[c] Norsk Hydro Electrolysers A/S, N-3671 Notodden

ABSTRACT

NiS_x-coated nickel cathodes are used for commercial water electrolysis in concentrated KOH solutions. Such electrodes have initially a high electrocatalytic performance. However, during operation the overpotential increases, which is also recognized by an increase of the cathodic Tafel slope. The sulphur content in the coating decreases rapidly from 25 mol% to 5 mol% during 16 days of electrolysis and to about 0.7 mol% after seven years of industrial operation. X-ray diffraction measurements indicate that the predominant sulphur containing compound is $NiS_{1.00\text{-}1.03}$. The diameter of the particles in the coating decreases from about 50-60 μm to about 10 μm during seven years of operation.

1. Introduction

An energy efficient electrolytic production of hydrogen requires low anodic and cathodic overpotentials. Due to the cost of noble metals, such as platinum, industrial electrolytic cells typically use electrodes of nickel or a nickel alloy. In general the active electrode material can either be synthesised by chemical or electrochemical processes. The nickel sulphide electrodes have shown to be catalytic active towards the hydrogen evolution reaction (HER) and has typically a cathodic overvoltage of 30-100 mV at a current density of 100 mA/cm^2 [1]. However, during years of operation the overpotential increases. Many investigations concerning the electrochemical behaviour of nickel sulphide electrodes have been reported in the literature [2,3,4]. Several investigators have found that the cathodic overvoltage decreases in the initial period of electrolysis before it starts to increase again. The length of the initial period is typically about one to two days. Vandenborre et al [5] proposed that the initial decrease of the overvoltage is due to dissolution of hydrogen in the catalytic layer.

T. O. Saetre (ed.), Hydrogen Power: Theoretical and Engineering Solutions, 149–154.

The dissolved hydrogen then gives rise to a possible formation of sulphide, which is believed to facilitate the HER. Also Sabel et al [6] noticed the initial decrease of overpotential and attributed this feature to the leaching out of sulphur of the deposited nickel sulphide layer. A subsequent increase in the overpotential was explained by poisoning of the catalytic layer by iron deposited from the alkaline electrolyte. According to De Giz et al [7] the catalytic effect is probably related to the characteristics of adsorption, which also has been claimed by Paseka [8]. Paseka also proposed that the ability to adsorb hydrogen atoms is related to the crystallinity of the nickel sulphide coating. In alkaline media the HER is often assumed to proceed by a Volmer-Heyrovsky mechanism, which implicates that the rate of step 3 in the following reaction scheme is low compared to the rate of step 2.

$$M + H_2O + e^- = MH_{(ad)} + OH^- \qquad \text{(Volmer)} \qquad (1)$$

$$MH_{(ad)} + H_2O + e^- = M + H_{2(g)} + OH^- \qquad \text{(Heyrovsky)} \qquad (2)$$

$$MH_{(ad)} + MH_{(ad)} = 2M + H_{2(g)} \qquad \text{(Tafel)} \qquad (3)$$

In this work we have investigated the long term performance of NiS_x electrodes in 25% KOH at 80°C by AC-impedance spectroscopy and steady state polarization measurements. In addition Energy Dispersive Spectroscopy (EDS) and X-ray Diffraction (XRD) measurements have been performed.

2. Experimental

The electrochemical cell was made of TEFLON and the electrode holder was made of TEFCEL. The anode was made of pure nickel (99.999%). A saturated calomel electrode was used as a reference, connected to the experimental cell by double bridging. KOH from Eka Nobel (p.a.) was dissolved in distilled and ion exchanged water. Steady state polarisation curves were recorded using a Solartron 1287 potentiostat. The electrolyte resistance, which was about 0.5 ohm, was deduced from ac-impedance spectra recorded using a Solartron 1255 frequency analyzer. EDS was performed using a micro analyser (Tracor Series II) connected to a scanning electron microscope (Zeiss DSM 940). XRD patterns were recorded using a Philips PW 1730.

3. RESULTS AND DISCUSSION

The long term performance of a NiS_x electrode has been evaluated by recording the electrode potential during galvanostatic electrolysis at an applied current density of 100 mA cm^{-2} as shown in Fig. 1. The large potential amplitudes sometimes recorded (e.g. at 110 and 300 days) are due to loss in electrical contact with the reference electrode, while the smaller amplitudes are most likely due to changes in the coverage of the electrode by hydrogen gas bubbles.

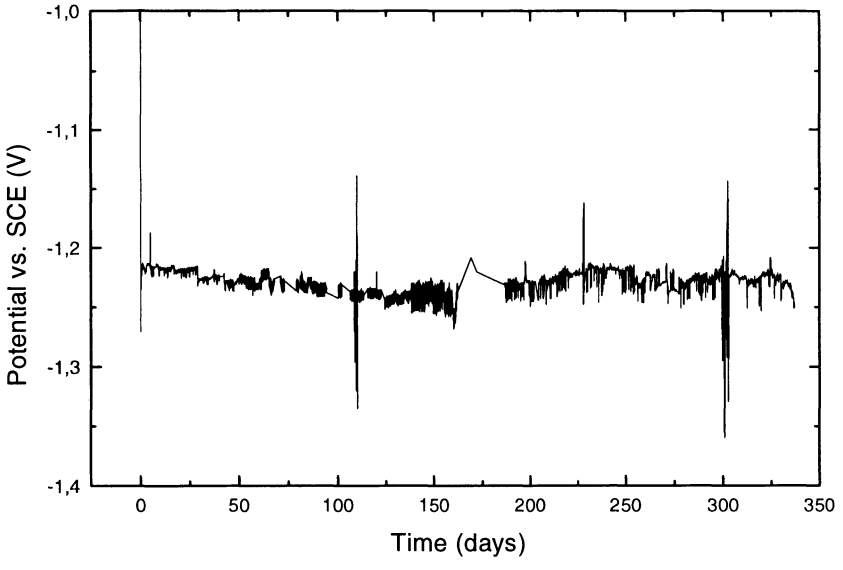

Fig. 1 Potential recorded as a function of time on a NiS_x electrode in a 25% KOH solution at 80°C.

A similar experiment was periodically interrupted in order to record steady state current-potential curves and AC-impedance spectra. The potential value of the electrode in the second experiment was found to increase somewhat more with time than in the undisturbed experiment. From the potential-current data the cathodic Tafel slope and the exchange current density was calculated and these kinetic data are given in Fig. 2. The Tafel slope was found to increase somewhat in absolute value with time, which is agreement with the observed increase in the cathodic overvoltage. The value obtained in the start of the experiment was about -32 mV/dec, which is in agreement with values obtained in a previous work [9]. Hence it is assumed that the desorption reaction (the Heyrovsky or Tafel step) is rate determining. Steady state polarization curves were also recorded for pure nickel and for an electrode which had been used in industrial water electrolysis for 7 years. The corresponding Tafel slopes were found to be about -150 mV/dec. and -104mV/dec. respectively. This indicates that the reaction becomes controlled by the charge transfer (Volmer) step with time. EDS analysis of the used cathode showed that the nickel coating contained a considerable amount of iron, which probably was deposited from the electrolyte.

The reason for the slow decrease of activity of the NiS_x electrode is not fully understood and consequently a more detailed study of the behaviour of the electrodes has been carried out. Loss of catalytic activity can be due to one of the following reasons: deterioration of the catalytic properties due to mechanical, structural or chemical changes or poisoning of the electrode by deposition of a substance which reduces the activity of the NiS_x.

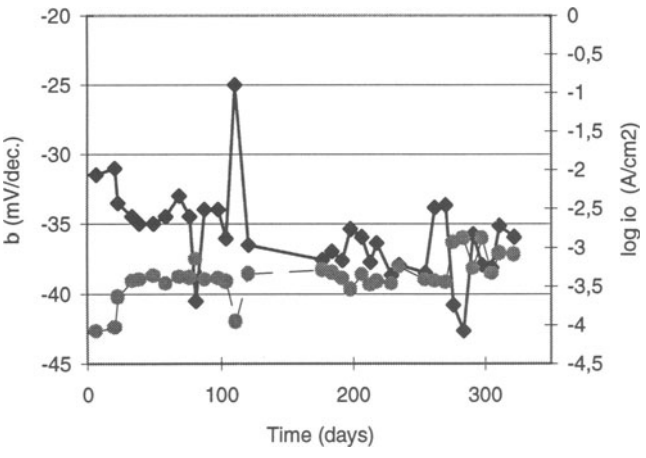

Fig. 2 Tafel slope (squares) and exchange current (circles) obtained on NiSx in 25 %KOH at 80°C.

It is well known that some of the sulphur initially incorporated in the catalytic NiS_x layer leaches out from the electrode [6,9]. It has not been investigated whether this process is a chemical or an electrochemical dissolution process. In order to determine the rate of the dissolution process, and to study the nature of process, samples of the electrolyte used for an electrolysis experiment were analyzed with respect to sulphur by atomic emission spectroscopy (ICP). In a parallel experiment a similar electrode was exposed unpolarized to the electrolyte, in which the sulphur content was analyzed. The results from these experiments are represented in Fig. 3, and it can be observed that the concentration of sulphur in the electrolyte increases rather quickly in the experiment where electrolysis were performed. After about 50 hours a value of 13 ppm was reached and the concentration increases slowly to about 16 ppm during the next 12 days. The rapid dissolution of sulphur in the first two days can be compared to the results of Sabela et al [6] who found a minimum in the overpotential after about 40-50 hours. This indicates that the electrode becomes more active as some of the sulphur leches out. However, also in the experiment with only chemical dissolution a considerable amount of sulphur was detected. This shows that at least some of the sulphur leaches out by chemical dissolution. The difference observed can be due to an increased mass transport caused by the forced convection at the cathode with gas evolution or that a parallel electrochemical dissolution takes place (e.g. $NiS + 2e^- = Ni + S^{2-}$).

The content of sulphur in the catalytic layer was determined by energy dispersive elemental analysis (EDS). These measurements show that the initial content of sulphur is about 25 mol% and decreases to about 11 mol% after 2 days and further down to 5 mol% after 16 days of electrolysis. Samples of an electrode used in an industrial electrolyzer showed that the content of sulphur had been reduced to about 0.7 mol% after 7 years. EDS analysis of the cross section of an electrode used for several days of electrolysis did not show any gradient of sulphur from the outer surface to the base substrate. This most likely shows that the diffusion of sulphur in the sulphide coating is not rate limiting for the dissolution process. The initial dissolution of a considerable amount of sulphur is apparently a fast process. It is

therefore not likely that this dissolution process is the cause of the slow increase of the overpotential with time.

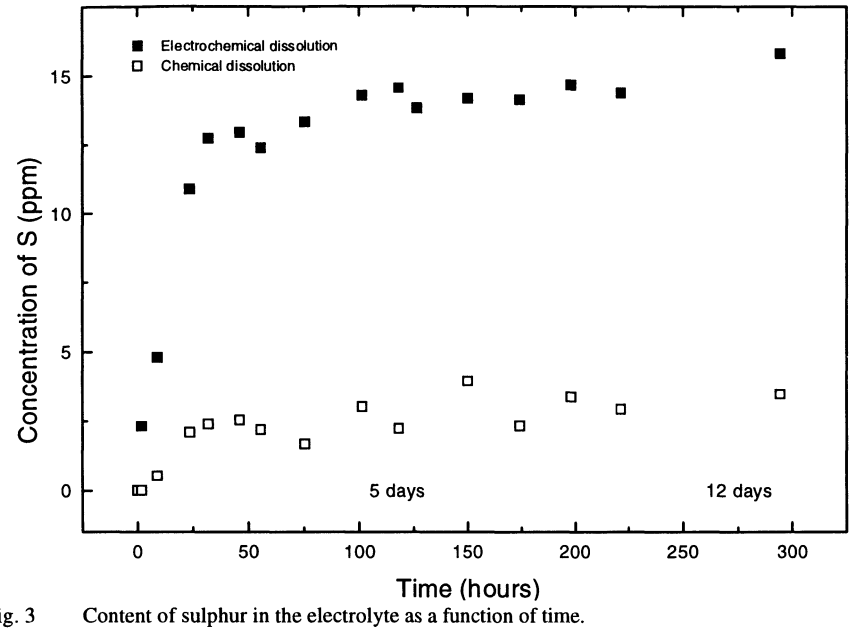

Fig. 3 Content of sulphur in the electrolyte as a function of time.

The catalytic activity of the NiS_x electrode apparently remains high even when most of the sulphur has disappeared, which is similar to observations reported by Paseka [8] who did not find significant differences in the catalytic activity of electrodes when the content of S varied between 10 and 20 wt%.

The leaching out of sulphur might lead to a recrystallization or change in structure of the NiS_x layer which again leads to a loss in activity. X-ray diffraction measurements were therefore carried out on an electrode before use and after 12, 24 and 250 hours of electrolysis. From these measurements it was found that the amorphous structure of the nickel sulphide coating on the fresh electrode crystallizes during 12 hours of operation to $NiS_{(1.00\text{-}1.03)}$ as the major structure and that this structure is maintained after 250 hours. In fact XRD measurements of an other electrode which had been used for 7 years in industrial electrolysis show that the predominant structure also for this electrode is $NiS_{(1.00\text{-}1.03)}$. From these measurements it seems evident that the predominant crystal structure appears already after a few hours of operation and that this does not change significantly during long time operation. It is however worth to notice that the half width ($\lambda_{1/2}$) of the major peak in the spectrum, at about 2.04 Å, decreases with time, which means that the domain of a regular structure grows [10], i.e. the layer becomes more crystalline with time. The change of size of the NiS_x particles has been evaluated from SEM pictures of the cross section of exposed and unexposed electrodes. These images indicate that the size of the particles decreases with time. The reason for this could be that during operation cracks develop in the coating which subsequently leads to the formation of smaller particles. It is well

known from the literature that by heating layers formed by electroless nickel plating some of the phosphorous dissolved in the coating reacts with nickel and forms nickel phosphides. In a similar way one might think that some of the "excess" sulphur forms sulphides, which due to changes in volume creates cracks in the coating. Another reason could also be that the sulphur acts as a "glue" that keeps the nickel particles together, and when the sulphur leaches out the nickel grains separate apart, or simply that leaching out of sulphur leads to a shrinkage of the solid Ni-NiS_x structure due to loss of mass. The change in particle size may result in a change of the hardness of the coating. Therefore measurements of the Vickers hardness of an unexposed and exposed catalytic layer was attempted. It was found that the hardness varied considerable of both specimen and no conclusion could be drawn in this respect.

4. Conclusion

The nickel sulphide electrodes have good and stable electrocatalytic performance, and the overvoltage did not increase significantly during nearly one year of electrolysis. A considerable amount of the sulphur initially present in the catalytic NiS_x layer leaches out during the first couple of days of operation. XRD measurements show that initially the electrodes have an amorphous structure but this changes during some hours of electrolysis to a crystalline structure. The predominant sulphur containing species in active electrodes are most likely $NiS_{(1.00\text{-}1.03)}$. After 7 years of operation small amounts (~0.7 mol%) of sulphur still remains in the cathode coating. During operation the rate determining step apparently changes from the desorption step (Heyrovsky/Tafel) to the charge transfer (Volmer) reaction.

5. Acknowledgement

This work has been supported by Norsk Hydro Electrolysers A/S (NHEL) and the Norwegian Research Council. Anita Ege (NHEL) is gratefully acknowledged for preparing the electrodes.

6. References

1) J.B. Holte, K.A. Andreassen, K. Widding and H. Harang;Norwegian patent no. 139355 (1978).
2) F. Hine, M. Yasuda and M. Watanabe; Denki Kagaku, **47** (7), 401 (1979).
3) H.E.G. Rommal and P.J. Moran; J. Electrochem. Soc. **132** (2), 325 (1985).
4) Yu.I. Kryukov, S.F. Chernyshov, A.G. Pshenichmkov, L.I. Al'tentaller, I.P. Maumov, Ya.S. Lapin and N.P. Kuznetsova; Russ. J.Electrochem. **29** (4), 446 (1993).
5) H. Vandenborre, Ph. Vermieren and R. Leysen; Electrochim. Acta, **29** 83), 297 (1984).
6) R. Sabela and I. Paseka; J.Appl. Electrochem., **20**, 500 (1990).
7) M.J.De Giz,M. Ferreira,G. Tremiliosi-Filho,E.R. Gonzales; J.Appl.Electrochem.**23**, 641 (1993).
8) I. Paseka; Electrochim. Acta, **38** (6), 2449 (1993).
9) S. Sunde, B. Johansen, G. Hagen, R. Tunold and K. Andreassen; Proc. 11th. World Hydrogen Energy Conference, Stuttgart, Germany (1996).
10) M. Sawada, K. Tsutsumi, T. Shiraiwa and M. Obrashi; J.Phys. Soc. J., **10** (6), 459 (1955)

A NOVEL HYDROGEN PRODUCTION UNIT PRODUCING HYDROGEN UNDER PRESSURE WITHOUT THE USE OF A HYDROGEN COMPRESSOR OR ASBESTOS MEMBRANES

Lars Grimsrud PhD
Norsk Process AS
Kaj Munks vei 41A
0876 Oslo, Norway

Michael Wenske
Elwatec GmbH
Oberwerder 3
04668 Grimma, Germany

1. Introduction

If no precautions are taken, the usual recovery of oil from an underground reservoir will be in the 15 - 20 % range, i.e. 80 % is left in the ground. To increase the recovery, water is pumped down into the reservoir to replace removed oil, to maintain pressure, and to flush the oil out. The water, usually seawater, must be treated before injection, so that the reservoir or injection equipment and wells are not damaged. One of the most important aspects of this treatment is the removal of oxygen. Traditionally this has been done by vacuum degassing, stripping, or a combination of these with chemical polishing to remove the last traces of oxygen.

The common denominator for all these processes is large weights and the need for chemical scavengers.

Weight becomes more and more of a problem as oil production moves into increasingly deeper waters, and scavengers may reappear in the product stream as something more nasty than what was injected, because of the conditions in the reservoir, high temperature, high pressure, and an abundance of chemical components that may react with the scavengers to produce other unwanted compounds.

To solve these problems (weight and chemicals), we went back to basic chemistry and utilized the following equation:

$$½O_2 + H_2 \rightarrow H_2O.$$

Contrary to popular belief this reaction is very slow. Bayer AG had developed a catalyst to speed up the process mainly to deoxygenize boiler feed water, to replace hydrazin, which had been classified as cancer causing. This was a "fresh water" catalyst, which had to be modified for seawater applications.

T. O. Saetre (ed.), Hydrogen Power: Theoretical and Engineering Solutions, 155–160.

For smaller, onshore applications the hydrogen is supplied from bottles or tanks. For oil field service this is not practical, because of the large amounts of hydrogen needed. Therefore, the hydrogen had to be produced "on site" with essentially no storage because of the explosion and fire danger.

It was believed that the art of producing hydrogen by electrolysis of water was well established many years ago. It was apparently so well established that nobody had examined the process and kept it up to date. There were two drawbacks with the traditional systems that made them non-acceptable for the oil industry: the use of asbestos in the electrolysis cell partition membranes and the problem with delivering hydrogen under pressure without the use of a hydrogen compressor.

For our first work with deoxygenating injection water we used a commercially available hydrogen generator, which proved to be a complete disaster. Aside from the asbestos membranes that the oil companies would not accept, the compressor proved very unreliable. A check with established suppliers showed no interest in delivering or developing a unit that could meet the stringent oil offshore requirements. This left us with the task of developing it ourselves, alone or in cooperation with other interested parties. As a result a cooperative effort was initiated between Elwatec, a German company specializing in electrolyzer cells for different purposes and Norsk Process, utilizing the cell in a complete system. The cell is described later in this paper.

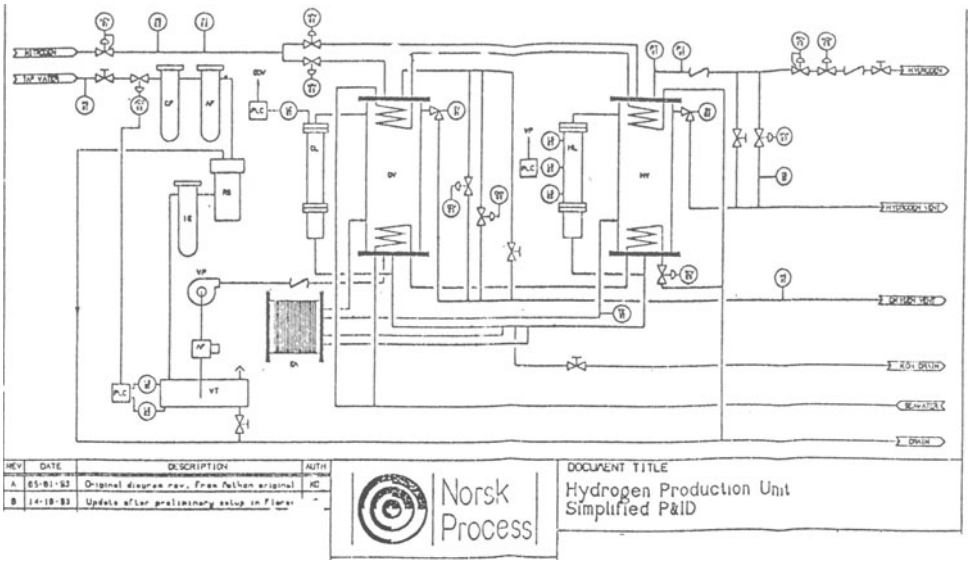

Referring to the P & ID, the hydrogen production unit (HPU) can conveniently be divided into 3 parts: The make up water treatment and supply system, the product separation and purifying system and the electrolysis cell.

2. The makeup water treatment and supply system

The make up water (to replace the water that is "split" in the electrolyzer cell) has to be treated before entering the electrolysis cell. Any contamination, mechanical or chemical, will be left in the cell as a sludge at the bottom, and will grow in thickness until it shorts out the cell and renders it useless.

Referring to the P & ID the filtering system is composed of a particle filter followed by a chlorine removal filter (activated charcoal), a reverse osmosis and an ion exchange filter. The amount of water going through the system is small, a few liters per hour, but the correct treatment is critical for the long term survival of the cell. The end result of the treatment is a particle free feed with an electrical conductivity of less than 5 microsiemens. The performance of the water treatment system is monitored by a conductivity meter situated in the feed water tank. The filter cartridges are exchanged on a set time scale unless the conductivity meter indicates failure in the system. The make up water is pumped into the hydrogen separator vessel, when the level indicator shows low level.

The water added to the system is basicly non-conducting; potassium-hydroxide is used as a medium to bring the conductivity up and to lessen the electrical losses in the cell. The concentration in the cell is 25 - 30 % and the KOH is not "used up", but is circulated from the cell to the separators and back to the cell. If the system operates as intended, the potassium hydroxide should last indefinitely. As some contamination is unavoidable, the KOH is drained and replaced with a fresh batch according to a preset maintenance schedule.

3. The electrolysis cell

The Elwatec electrolyzer is bipolar and very compact. To reach a certain production the separate modules may be connected in series or parallel or a combination of these to meet the specific requirements of the user. Every module consists of a capillary slit anode, a separator, the separator frame, o-ring seals, a capillary slit cathode and, when more moduls are stacked, also a bipolar membrane separator.

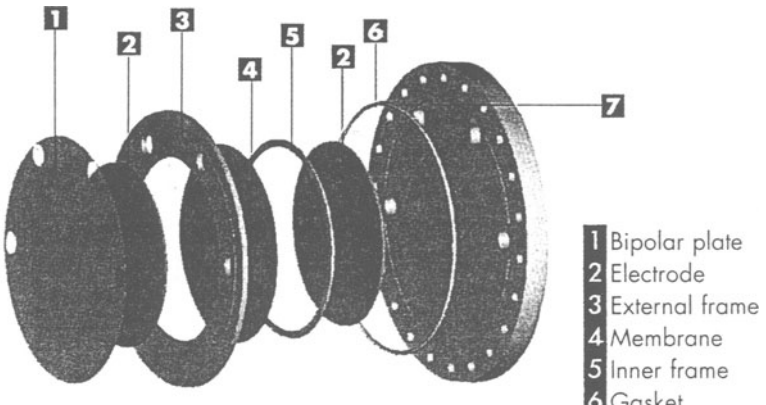

Exploded view of the electrolysis cell

In contrast to other commercially available electrolyzers the Elwatech electrolyzer can deliver hydrogen (and oxygen) up to 30 bars without the use of a compressor. This is made possible through a pressure equalizer system that assures the same pressure on both sides of the separation membranes at all times. The Elwatec cell is completely void of asbestos, the preferred membrane material in most other commercial systems. The membranes are produced by VITO and called Ziafon^{R}, a material conducive to high gas purity and with excellent electrochemical properties. The size of the Elwatec electrolyzer is also smaller by a factor of 2 - 3 compared to conventional systems. This size advantage, together with the small control and separation systems developed by Norsk Process, makes the complete system easily transportable, and well suited to be mounted for container transport.

The cells are available for 1 - 10 Nm^3 of hydrogen as standard. Other sizes are specialty items.

4. The separators

The evolved gases, hydrogen and oxygen, separated by the membranes, are led into their respective separators together with the electrolyte by means of a gas lift. (A circulation pump may also be used). Gas and liquid are cooled and separated in the separators, such that the electrolyte is returned to the cell and the gas is delivered to the consumer (hydrogen) or ejected to the atmosphere (oxygen). Cooling coils in the separators remove the excess heat (electrical losses) from the electrolyzer cell, so that the whole system operates at approx. 80°C. The separators work so efficiently that there is no need to replenish the electrolyte between replacements.

5. Instrumentation, control system and diagnostics

The control system can be either PLC based or computer based, depending on the user's preference. The amount of hydrogen produced may be manually set or determined on the basis of an external signal, (for example product stream flow rate). This signal will set the electrical current through the cell and determine the production rate. The pressure will build up in the separators and the liquid levels will drop as gas is produced. The level in the oxygen separator will be maintained by letting off oxygen, and the level in the hydrogen separator by adding water. When the pressure is built up to approx. 1 bar above the pressure in the recipient, the unit will start delivering hydrogen.

The integrity of the system is monitored by checking the purity of the evolved gases, i.e. hydrogen in oxygen and oxygen in hydrogen. A system fault will immediately result in rising impurity levels in the produced gases and lead to a shut down. The same will happen if the temperature goes above a preset limit (80°C) or the delivery of make up water should fail.

The most important control function is the level control for the separators. These are continuously monitored and controlled through conductive level controllers (no moving parts) with a back-up system of mechanical switches.

If a power failure should occur, a battery operated PLC takes over and shuts the system down and de-pressurizes it and leaves it in a standby condition (ready to start).

The whole system is continuously monitored by the computer, which will give printouts of any changes or abnormalities that have taken place, conf. example below.

ERROR.LOG

```
07:35:36 05/04/94 0 BOOT: Setting up DIO
07:35:36 05/04/94 0 BOOT: Setting up ADC
07:35:36 05/04/94 0 BOOT: Setting up channel assignments
07:35:36 05/04/94 0 BOOT: Loading configuration
07:35:36 05/04/94 0 BOOT: Installing ISR
07:35:36 05/04/94 0 BOOT: Initializing display
07:35:38 05/04/94 0 BOOT: Initializing mouse
07:35:39 05/04/94 0 BOOT: Refreshing display
07:35:39 05/04/94 0 SEAJECT controller powered up
07:36:31 05/04/94 0 Operator pushed START button
07:36:31 05/04/94 0 H2 unit started
10:32:38 05/04/94 2 High level in O2 or H2 vessel, attempting restart
```

9.0 ALARM SEQUENCE

NO	ALARM	VALUE	PLC PROCESS ACTION	REASON
2	High H2 in O2	40% LEL	Initiates stopping sequence	Possible defect membrane in electrolyzer cell
3	High KOH temp.	> 75degC	Initiates malfunction sequence	Water flood unit stopped or restriction in cooling line.
4	Low N2 pressure	<40 psi	Initiates malfunction sequence	Loss of N2 pressure
5	Fresh water conductivity high	>5 micro Siemens	Initiates malfunction sequence	Platform reverse osmosis unit stopped or malfunction.*Ion exchange filter MAJ-738 contaminated. *Active carbon filter MAJ-736 contaminated *Pleated catridge filter MAJ-737 contaminated. .
6	High hydrogen pressure	>200psi	Initiates malfunction sequence	*Restriction in H2 delivery line. *Blocked sparger in
7	Low ultra pure water pressure	<40psi	Initiates malfunction sequence	Platform reverse osmosis unit stopped.
8	Low ultra pure water tank level	zero	Initiates malfunction sequence	Ultra pure water filtration unit blocked or platform reverse osmosis unit stopped.
9	O2 level low	<20 cm	Initiates stopping sequence	Actuator valve ADV-732A malfunction. * Restriction in
10	O2 seperator high high	>80 cm	Initiates stopping sequence	Actuator valve ADV-732C malfuncion. *Restriction in hydrogen delivery line.
11	H2 seperator low low	< 20 cm	Initiates stopping sequence	Actuator valve ADV-732C malfunction. *Restriction in hydrogen delivery line.
12	H2 vessel high high	> 80 cm	Initiates stopping sequence	Actuator valve ADV-732C malfunction. *Restriction in hydrogen delivery line.
13	Low current	Out of dead	Initiates malfunction sequence	Possible weak KOH (electrolyte)
14	High current	Out of dead	Initiates malfunction sequence	Possible earth leakage
15	Low Pressure LP tank	<20 bar	Initiates compressore trip	
16	High pressure LP tank	>30 bar	Initiates malfunction sequence	
17	Low pressure HP tank			
18	High pressure HP tank	>150 bar	Initiates malfunction sequence	

PHOTOPHYSICAL AND PHOTOCHEMICAL PROPERTIES OF SOME PORPHYRINS USED IN THE PHOTOSENSITIZED REDUCTION OF WATER

RODICA MARIANA ION* and LAURENTIU FARA**
* *S.C. ZECASIN S.A. Photochem. Dept., Splaiul Independentei 202, RO - 79611 - Bucharest, ROMANIA*
** *National Agency for Renewable Energy (NARE) c/o Physics Dept., Bucharest Polytechnic University, Splaiul Independentei 313, RO-77206, Bucharest, ROMANIA*

Abstract

The photodissociation of water into H_2 and O_2 upon excitation with visible light, would be a cheap way to collect and store the solar energy in the form of a fuel (H_2).
For this purpose, we need to use an sensitizer which could absorb light in the visible range of the spectrum.
A class of substances which have the required qualities for a good photosensitizer are pophyrins: with differrent mesosubstituents and different central metals.
This paper analyzes the photophysical properties of specific porphyrins (absorption and emission properties) and at the same time, the photochemical properties of the same porphyrins (the senzitized photoreduction of methyl viologen to his radical cation which upon the catalytic action of selective platinum catalysts, will decompose the water to form hydrogen).
The structure-activity relationship for the studied porphyrins is presented, too.

1. Introduction

In the present, there are many ways of storing solar energy and its transforming into chemical potential. One of the most attractive way is the photodissociation of water into H_2, since this provides an important way to storage sunlight in the form of a fuel (H_2), [1-6].
The photogeneration of hydrogen from water in homogeneous solution requires the use of photosensitizer metallo - porphyrins appear to be the most promising candidates [7,8,16].
The metallo - porphyrins are able, in some cases, of collecting up to 45 % of the energy available in sunlight, [17].

T. O. Saetre (ed.), Hydrogen Power: Theoretical and Engineering Solutions, 161–167.

In the present study, we found that the positively-charged photosensitizer were the most suitable materials for H_2 production when methyl viologen (MV^{2+}) was used as electron relay, [2].
Because water - soluble porphyrins can sensitize H_2 evolution from water with rather high efficiencies, development of photosensitizers requires knowledge of the photophysical and photochemical properties, [10].
This paper is concerning with the photophysical (UV - VIS absorption and emission spectra) and photochemical properties (their photoreactivity) of the tetraanionic or tetracationic water-soluble porphyrins as visible-light-absorbing substrates and cationic viologens as electron - acceptor quenchers.

2. Experimental Section

2.1 MATERIALS

The tetrasodium salt of meso - tetrakis (p-sulfonatophenyl) prophyrin was prepared in the laboratory, [11]. The purity was checked by high - pressure liquid chromatography (HPLC).
(TPPS)-Pd and (TPPS)Zn were prepared according to reported procedures, [12].
Methyl viologen chloride (Aldrich) was used as received.

2.2 APPARATUS

The UV - VIS spectra were recorded with a SPECORD M 400, Carl Zeiss Jena spectrophotometer with double beam and microprocessor.
The emission spectra were obtained with a AMINCO - BOWMANN spectrophotometer.
Cyclic voltammetry was performed by using a proper installation with a platinium head working electrode, a platinium wire counter electrode, and a saturated calomel reference electrode (KCl for elevctrochemical studies in water and NaCl for those in acetonitrile).

3. Results and Discussion

To apprreciate the photochemical reactivity and efficiency of porphyrins free base or metalls - complexes as photosensitizers during the water decomposition into hydrogen is important to evaluate their absorption and emission spectra.
For this paper, we have studied and compared differently charged porphyrins which are represented in Figure 1.
Their photophysical properties (absorption and emission spectra) are shown in TABLE 1.

During the photodecomposition of water into hydrogen, the porphyrinic sensitizers can reduce methyl viologen which act as electron relay and supply the necessary electrons transfer.
The mechanism for the photoreduction of methyl viologen is:

$$
\begin{array}{ccc}
P^+ + MV^{2+} & \rightarrow & (P^+, MV^{2+}) \\
 & & \downarrow k_A \\
P^+ + MV^{2+} & \leftarrow & (P^+, MV^{2+}) \\
 & k_C \quad & \downarrow k_B \\
 & & p + MV^{2+}
\end{array}
$$

Scheme 1. The mechanism for the photoreduction of methyl viologen

It involves the formation of an encounter complex with no bonding between the reactants.
Once formed, the complex may undergo an electron transfer process to form an ion - pair (k_A) which may decay (k_B) either to the ground state or it may form separated ion products (k_C).
To have an efficient system, it is necessary that the ratio k_C/k_B be as high as possible.

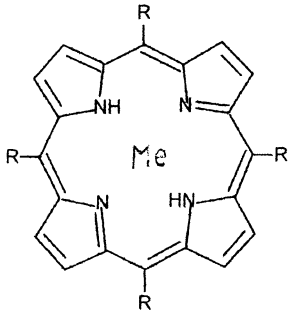

Me= Zn, Pd

$R_1 = R_2 = R_3 = R_4 = C_6H_4SO_3^-$

$R_1 = R_2 = R_3 = R_4 = C_5H_4N^+$

Figure 1 Structure of differently charged metallo - porphyrins

TABLE 1. The photophysical properties of metallo - porphyrins in aqueous solution

Metallo-porphyrins	λ_{abs} nm	$\varepsilon \times 10^{-3}$ cm^{-1}	λ_{em} nm	Φ_F	τ_S ns	K_{isc} s^{-1}	Φ_T	τ_T ns
H_2 TSPP	412 515 553	530 16.5 6.8	645 700	0.080	10.4	-	0.78	0.42
Zn TSPP	421 515 594	530 22.1 9.6	606 656	0043	1.7	-	0.84	1.4
Pd TSPP	412 520	127 10.7	690	$<10^{-4}$	200	-	1.00	0.35
H_2 TP_vP	424 520 558 584 658	 226 14.5 9.2	675 706	0.011	5.3	2.3×10^{7}	0.92	0.165
Zn TP_vP	436 562 602	180 16	625 667	0.020	1.4	6.8×10^{8}	0.90	1.30
Pd TP_vP	419 522 566	146 12.5 5.1	570	$<10^{-4}$	-	9×10^{9}	1.00	0.144

A comprehensive analysis is presented in this paper on the influence of the porphyrin ring substituents as well as metal incorporation on the photo and redox properties, as applicable to water - soluble porphyrins in aqueous media.

Positively charged substituents tend to raise the oxidation potential of the porphyrin whilst negatively charged substituents lower the oxidation potential and the thermodynamic driving force for K_A is very much lower for Zn $TPyP^{4+}$ than for Zn $TSPP^{4-}$, (TABLE 2).

TABLE 2. Redox potentials (Volts vs SCE) for TSPP, TPyP and their metallic complexes.

Porphyrin	$E^{ox}_{1/2}$ (V)	$E^{red1}_{1/2}$ (V)	$E^{red2}_{1/2}$ (V)
TSPP	1.1	-1.21	-1.60
Zn TSPP	0.87	-1.16	-
Pd TSPP	1.11	-1.23	-1.67
TPyP	1.30	-0.23	-0.43
Zn TPyP	1.18	-0.85	-
Pd TPyP	1.40	-0.63	-

If there is a strong electrostatic attraction between the ions within the ion - pair then the ion - pair will be stabilized with respect to ionic separation (k_c).
In such conditions, the yield of ions will be very low and the major decay route will involve geminate recombination (k_B).
Also, there is a strong electrostatic repulsion between the ions and the Coulomb force will assist the ions to separate which favours ionic separation over germinate recombination.
Among the free-base, Zn and Pd porphyrins, Zn porphyrins are better oxidants in the excited state. The location of the ground state oxidation potentials together with triplets having long lifetimes and good reducing properties suggests Pd porphyrins to be interesting candidates for examination as photosensitizers for water cleavage, when used with acceptor relays as methyl - viologen.
Due to their charges, tetraanionic porphyrin sensitizer (free base or metallo - complexes) may form better ion pair with the dicationic viologens added to the solution.
Evidence for such pairing is provided by absorption spectral changes that occur upon the addition of methyl viologen (0.001M) to a solution of the porphyrin, Figure 2.

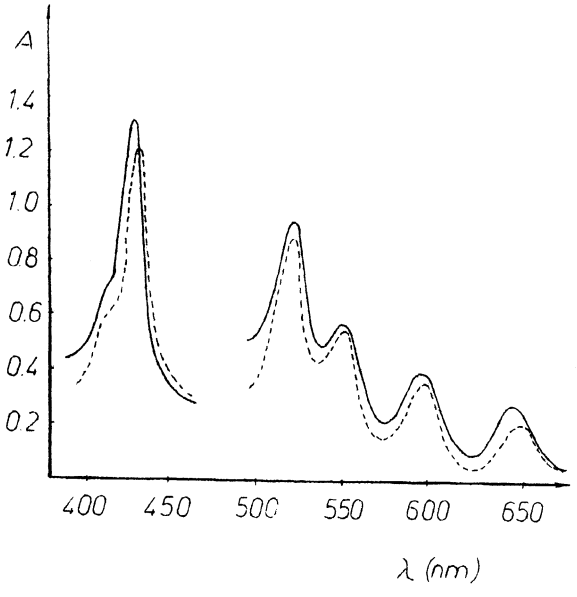

Figure.2 The spectrum of TSPP (5×10^{-6} M) in the absence (-) and in the presence of MV (0.001 M)

Attempts to determine quantitatively this association equilibrium were unsuccessful, [13,14].
The emission of all the studied porphyrins is efficiently quenched by methyl viologen in aqueous solutions. Estimates of the excited state oxidation potentials of these porphyrins based on the spectral data and the oxidation potentials suggests that

quenching by the viologens occurs by electron transfer as the viologens may be easily reduced, [15] by the excited complexes. The deviation from linearity in the Stern-Volmer plot reflects association of the porphyrin and the viologen before excitation of the chromophore. The values for the dynamics quenching constant (Table 3) shows a large association between the porphyrins and the methyl viologen.

TABLE 3 Quenching of porphyrins by methylviologen

Porphyrin	Kq ($M^{-1}s^{-1}$)
H_2TSPP	5.7×10^{8}
ZnTSPP	0.2×10^{9}
PdTSPP	3.7×10^{9}
H_2TPyP	2.1×10^{6}
ZnTPyP	3×10^{7}
PdTPyP	4.15×10^{7}

The quenching rate of the porphyrins increases with increasing the hydrophobicity of the quenching species are most probable one to Förster type energy transfer to the MV^{2+} via a triplet state process, and this is followed by migration of the oxidizing equivalent from the metalloporphyrin to MV (as it was presummed in scheme 1).

4. Conclusions

The present paper tried to develop and evaluate new efficient photosensitizers used in the photogeneration of hydrogen.
The cationic porphyrins Pd TPyP seems to be the most efficient photosensitizer used in our study.

References

1. Grätzel, M., Kayanasundaram, L. and Kiwi, J. (1982), Structure and Bonding, **49**, *Visible light induced cleavage of water into hydrogen and oxygen in colloidal and microheterogeneous systems*, Springer, New York;
2. Stefan, M. J. (1990), Ph. D. Thesis, *Photochemical conversion and storage of solar energy with fuel generation from water photolysis*;
3. Wu, G-Z. Hu, M. and Leung, H. K., (1991), *Sensitized photoredox reactions IX: Thermodynamic factors in the porphyrin - sensitized photoreduction of methil viologen*, J. Photochem. Photobiol. A.: Chemistry, **62**, 141-150;
4. Xu, H., Shen, T., Zhon, Q. Shen, S., Lin, J., Li, L., Zhon, S., Zhang, X., Yu, Q., Bi, Z., and Xiao, X., (1992), *Aspects of metal phtalocyanine photosensitization systems for light energy conversion*, J. Photochem., Photobiol. A.: Chem., **65**, 267-277;
5. Malinka, E.A., Kamalov, G.L., Vodzinskii, S.V., Melnik, V.I., and Zhilina, Z.I., (1995), *Hydrogen production from water by visible light using zinc porphyrin-sensitized platinized titanium dioxide*, J. Photochem., Photobiol. A.: Chem., **90**, 153-158;
6. Continho, P. J. G. and Costa, S.M. B., (1994), *Kinematics of the electron transfer reaction between ^{3}Zn TPP and MV^{2+} in lecithin studied by global analysis*, J. Photochem., Photobiol. A.: Chem., **82**, 149-160;

7. Ion, R.M., (1994), *Ph. D. Thesis, Spectroscopical methods used for porphyrins and metallo-porphyrins characterisation*, Bucharest;
8. Dolphin, D. (1978), *The porphyrins*, **3**, Academic Press, New York;
9. Ion, R.M., Ceafalan, L.A., Moise, F. and Iosif, A., (1992), *Photochemistry in micellar system I Photodegradation and stabilization of porphyrins*, Anal. Univ. Buc., **1**, 52-60;
10. Ion, R.M., (1996), *Photochemical production and quenching of singlet oxygen by the porphyrins*, Rom. J. Biophys., **6**, 3-4, 205-212;
11. Ion, R.M., (1993), *Porphyrinic systems used in photochemical conversion of solar energy*, Solar Energy in Romania, **2**, 1-2, 99-102
12. Harriman, A. And West, M.A. (1982), *Photogeneration of hydrogen*, Academic Press, Great Britain;
13. Harriman, A. And Richoux, M.C., (1981), *Photoproduction of hydrogen from reductive quenching of a water-soluble zinc porphyrin*, J. Photochem., **15**, 335-339;
14. Foster, R., (1969), *Organic charge - transfer complexes*, Academic Press, New York, Chapter 6, 133-152.
15. Fara, L. and Dinculescu A. (1991), *Thermal Storage of solar energy - Application in agriculture*, Ceres Publ. Press, Bucharest.
17. Ion, R.M., Teodorescu, L., Mandranel, C., Volanski, E., and Hillebrand, M., (1990), *The degradation of porphyrinic photosensitizers used in photochemical conversion of solar energy*, *Rev. Chim.*, **41**, pp. 129-132;
17. Ion, R.M. and Teodorescu, L., (1990), *New aspects about the mechanism of the photodegradation reaction of the porphyrinic sensitizers*, Rev. Chem., **41**, 312-317;

PHOTOCHEMICAL STUDIES OF In_2O_3 ADMIXED NANOSTRUCTURED TiO_2 IN REGARD TO HYDROGEN PRODUCTION THROUGH PHOTOELECTROLYSIS

R.K.KARN, M.MISHRA AND O.N.SRIVASTAVA
Department of Physics, Banaras Hindu University
Varanasi-221005, India

1. Abstract

In the present investigation, PEC solar cell based on nanostructured (ns) TiO_2 photoelectrode prepared by the hydrolysis of Titanium-tetraisopropoxide followed by deposition of thin film by spin-on method, has been developed. It has been shown that TiO_2(ns) photoelectrode bearing PEC cell exhibits higher PEC output due to improved quantum yield. Yet another improvment in TiO_2(ns) photoelectrode carried out in the present work corresponds to admixing In_2O_3 for improving the spectral response of TiO_2(ns). The PEC cell based on TiO_2(ns)-In_2O_3 photoelectrode shows PEC response (V_{oc} = 720 mV, I_{sc} = 11 mA/cm^2) under illumination of a 1000 W Xe-Hg lamp. The hydrogen gas evolution under photoelectrolysis employing TiO_2(ns) photoanode was found to be 1.4 ml h^{-1} on the other hand the In_2O_3 admixed TiO_2(ns) electrode exhibited a higher hydrogen gas evolution rate of 1.9 ml h^{-1}. Evidence and arguments have been put forward to show that the presence of In_2O_3 over TiO_2(ns) makes the system possess the advantage of a colloidal photochemical system. Better performance of the new photoelectrode is thought to be due to nanostructural nature of TiO_2 photoelectrode improved spectral response and catalytic activity of In_2O_3 in regard to the gas evolution kinetics.

Keywords : Semiconductor ; photoelectrochemical ; nanostructured ; hydrogen production

2. Introduction

The modern era of semiconducton electrodes and interest in these in photoelectrochemical devices for energy conversion, especially via the water spliting reaction can be traced to work of Honda and Fujishima on TiO_2 electrode [1]. Indeed water spliting in TiO_2 based cells can be accomplished but only with an additional electrical bais. The problem with TiO_2 is that the conduction band is too low to generate hydrogen at a useful rate [2]. Most of the small band gap oxide and non-oxide semiconductors being investigated have been

T. O. Saetre (ed.), Hydrogen Power: Theoretical and Engineering Solutions, 169–178.

found to exhibit either photocorrosion and unstable or exhibit poor spectral response. After an extensive search for suitable semiconductors during 1972-85, the interest is returning back to TiO_2 [3]. Because the bandgap of TiO_2 is larg (i.e. 3.0 eV) only a small fraction of solar light is absorbed. Several different approaches are being pursued to circumvent the poor solar spectral response of TiO_2 caused by its large band-gap. It is known in the area of semiconductor physics that the initial bandgaps can be varied through suitable alloying. The process of alloying unlike doping produces bandgap variation through the shifting of the conduction or valance band edges. In one of these, TiO_2 is doped with certain cations like Al, Cr, Y, Mo, Nb, [4,5] etc, for obtaining improved spectral response. The band-gap of TiO_2 can be reduced by alloying with VO_2 [6]. In another approach aimed to improve response through an improvement in gas evolution kinetics, loading of photoelectrodes with catalysts has been tried with TiO_2. As for example ; improved gas evolution (Hydrogen) was found when TiO_2 was loaded with RuO_2 [7]. Recently there has been attempts to improve the photosensitivity through synthesis and fabrication of nanostructured version of some oxide materials such as SnO_2, TiO_2, ZnO, CdS [8,9,10] etc. Keeping these facts in view, the present work embodies fabrication of nanostructured TiO_2 thin film and its development as photoelectrode for hydrogen production.

In the present investigation, we have synthesized and deposited TiO_2 nanostructured thin films and employed these as photoelectrode in the PEC configuration for hydrogen production. The photoelectrochemical behavior and the hydrogen evolution characteristics of nanostructured TiO_2 thin film vis a vis conventional TiO_2 film photoelectrode (e.g. deposited through anodic oxidation) has been monitored and evaluated. In addition to this the present study also spans to cover efforts on modification of TiO_2(ns) thin films to better spectral response through admixing of In_2O_3 [11]. A new technique has been followed in the present study for preparing nanostructured TiO_2 solid films by taking a sol-gel and coating through a spin-on technique. This is a modified version of the method followed by O'Regan and Michael Grätzel [12]. The motivation of following this technique was to prepare an electrode having high effective surface area and hence better quantum yield and improved hydrogen gas evolution kinetics. Surface morphology, structural and photoelectrochemical characteristics of the bare TiO_2(ns) as well as the TiO_2(ns) overlaid with In_2O_3 thin film admixtures have been investigated in relation to hydrogen evolution through photoelectrolysis.

3. Experimental Techniques

The TiO_2(ns) was prepared in the form of a sol-gel by the hydrolysis process. For preparing sol-gel $Ti[OCH(CH_3)_2]_4$ solution was added slowly to propanol drop by drop. Deionized water was slowly added under vigorous stirring for a duration of 10 minutes. Then 1ml of 70% HNO_3 was added to the mixture. The mixture was then heated at 80°C in continuously stirring condition. The propanol together with some water was allowed to evaporate during this time. In this way stable TiO_2 colloidal solution resulted. This TiO_2

solution was than concentrated by evaporation of water in vacuum at 25°C, until a viscous liquid was obtained. Carbowax M-20,000 (40% by weight of TiO_2) was added and a viscous dispersion was obtained. The chemical process can be represented as:

$$Ti[OCH(CH_3)_2]_4 \xrightarrow[80°C]{\text{Hydrolysis}} TiO_2(ns)\ \text{Sol-gel}$$

Titanium sheet which was used as the conducting substrate was ~2mm thick and ~1cm^2 area. This was cleaned by rubbing with emery paper and ultra sonically cleaned in acetone for 15 minutes. Sol-gel was kept into the ultrasonic cleaner for 15-20 minutes at a frequency of 40 KHz, so that TiO_2 particles do not agglomerate. Spin on technique employing photoresist-spinner was used for film deposition. The advantage of this technique is that one can deposit the film on the substrate almost layer by layer. Ultrasonically cleaned substrate were kept on the wheel of the photoresist spinner and spin coated at 3000 rpm for 20-30 sec. The film on the substrate was fired in air (oven) at 150°C for 5 to 10 minutes. The process of deposition and subsequent firing was repeated 5 times. The film so formed was annealed in Ar at a predetermined temperature of 700°C for achieving structural homogeneity. Finally for increasing the conductivity of the TiO_2 films, they were subjected to reduction treatment by annealing in hydrogen at 300°C for a duration of ~5 minutes. In addition to TiO_2 the photoelectrodes corresponding to $TiO_2(ns)$-In_2O_3 was also prepared for obtaining improved spectral response. To achieve this In_2O_3 was electrodeposited by cathodically polarizing the TiO_2 electrode in 0.5M $In_2(SO_4)_3$ solution at a field of 1V/cm for 2 minutes. Later on these electrodes were annealed in oxygen at 500°C ± 10°C. The surface morphology, structural and photo-electrochemical characteristics of the bare $TiO_2(ns)$ as well as $TiO_2(ns)$ overlaid with In_2O_3 thin film admixture have been investigated in relation to hydrogen evolution through photoelectrolysis. The resistance of the $TiO_2(ns)$ (~1cm^2) has been found to be $10^2\Omega$ while that of $TiO_2(ns)$ admixed with In_2O_3 is $10^{-2}\Omega$. From this it is clear that the resistance of the photoanode has decreased with In_2O_3 modification. Structural characterization of $TiO_2(ns)$/Ti and $TiO_2(ns)$-In_2O_3/Ti is performed by x-ray diffractometry using Philips PW 1710 X-ray diffractometer equipped with a graphite monochrometer. Surface morphology of the films were studied through SEM. The hydrogenation behavior of the electrode was performed by measuring the current potential (I-V) characteristics. The electrodes are connected to a pure copper wire with silver paste and sealed with pyrex polymers leaving an exposed area of 0.38 cm^2, the seal has been observed to be stable in 1M NaOH. The measurement is done employing conventional three electrode assembly a Pyrex Cell with a quartz window. A (~2cm^2) Pt was used as a counter electrode and Saturated Calomel Electrode (SCE) with luggin capillary as reference. The I-V curves of the electrodes under dark and illumination were recorded with a Princeton Applied Research (PAR) Model 173 potentiostat/Galvanostat. PAR 179 I/E converter, PAR Model 175 Universal Programmer and Houston (2000) X-Y recorder. The illumination source being 1000W Xe-Hg lamp

adjusted to an incident intensity 0.5W cm^{-2}. All the reagents are analytical grade and prepared with doubly distilled water. The evolved gas is measured by fixing inverted burettes over the electrode.

4. Results and Discussion

4.1. STRUCTURAL CHARACTERIZATION

The structural characterization of TiO_2(ns)-In_2O_3 electrode materials was carried out through XRD by employing a Philips PW 1710 diffractometer equipped with a graphite monochromator. Figs.1,2 show representative XRD patterns (Cuk_α radiation) of the as synthesized TiO_2 (ns) and TiO_2(ns)-In_2O_3 materials .Analysis of XRD patterns revealed that on admixing TiO_2(ns) with In_2O_3, does not lead to formation of any new compound material. However, a slight change in the lattice parameter (0.03Å) was invariably found for TiO_2 a=3.78Å and for TiO_2(ns)-In_2O_3 a=3.81Å. The as prepared photoelectrode materials were found to be polycrystalline. The XRD also confirmed the presence of TiO_2(rutile), TiO_2(ns)-In_2O_3. In addition to these, some diffraction peaks corresponding to Ti also appeared. These are outlined in (Fig.1,2) and presumably originate from the Ti support substrate peaks.

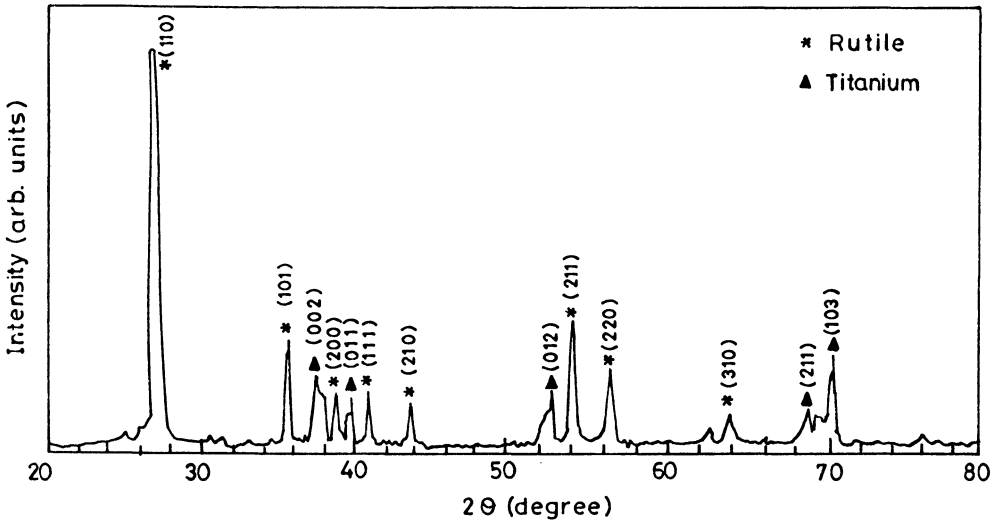

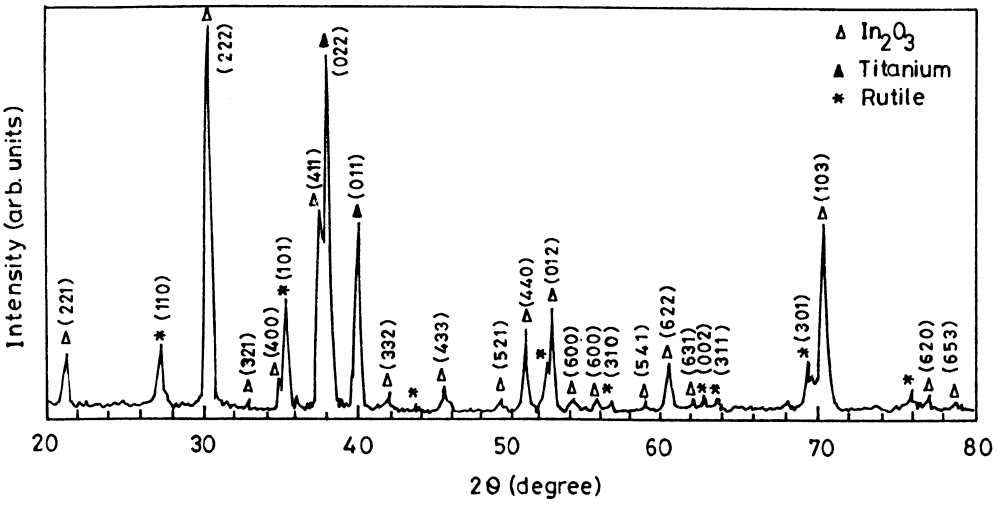

The surface characterization of the as synthesized mixed oxide TiO_2(ns)-In_2O_3 electrode was performed by employing Scanning Electron Microscope (Figs.3,4).

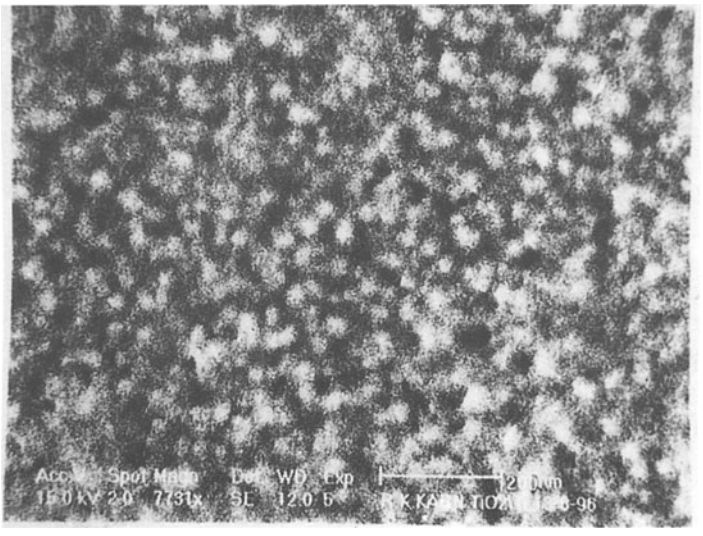

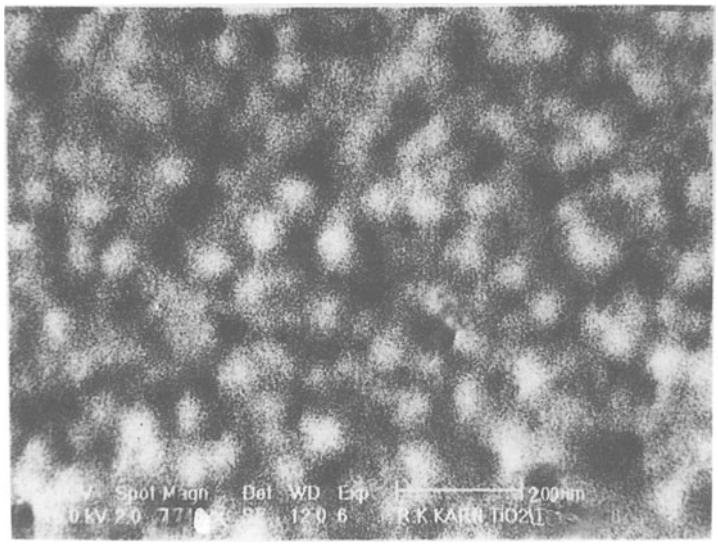

The observed microstructural characteristics reveal a fine grained structure suggestive of a nanocrystalline like matrix. Through SEM exploration the average grain size of the photoelectrode was found to be 10 to 30nm for TiO_2(ns) and for TiO_2(ns)-In_2O_3 40-120nm.

4.2. PHOTOELECTROCHEMICAL MEASUREMENTS

The photoelectrochemical characterization of TiO_2(ns) and TiO_2(ns)-In_2O_3 electrodes was performed by monitoring their current-voltage (I-V) characteristics. The measurements were done in three electrode assembly in glass cell with quartz window. Saturated Calomel Electrode (SCE) and Pt electrodes were used as reference and counter electrodes. Electrochemical measurements were performed by using Princeton Applied Research (PAR) EG & G Model, 1173 Potentiostat/Galvonostat, PAR 179 I/E convertion PAR 175 universal Pragrammer and Houston Model 2000 X-T Recorder. A 1000 W Xe-Hg lamp (oriel Corporation, U.S.A.) was used as light source. The intensity of light was adjusted and fixed at 0.5 W cm^{-2}. The I-V characteristics of TiO(ns) and TiO_2(ns)-In_2O_3 both were measured in 1 M NaOH. The TiO_2(ns) and TiO_2(ns)-In_2O_3 electrodes exhibited photovoltage and photocurrent at 640 mV 3.4 mA/cm^{-2} and 720 mV, 11 mA/cm^{-2} respectively (Fig.5,6).

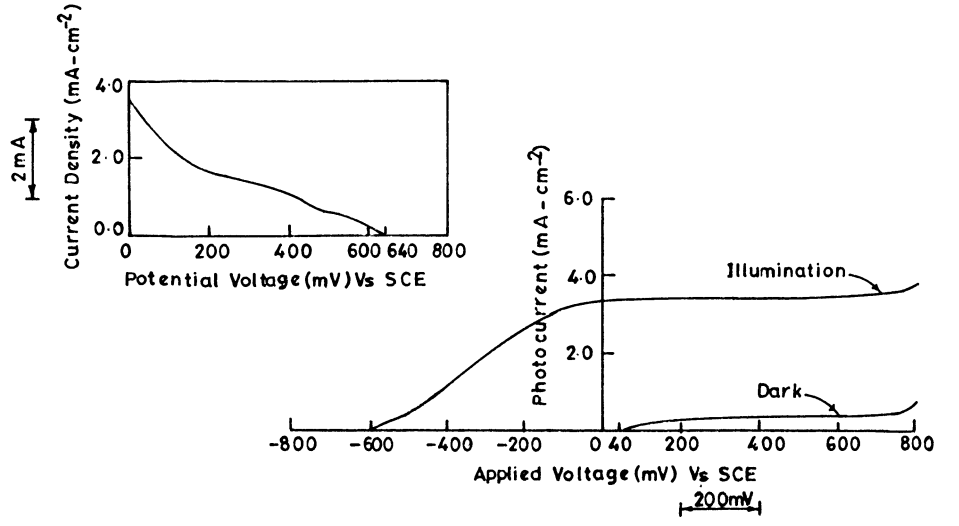
Current Density (mA-cm^{-2})
2mA
4·0
2·0
0·0
0
200
400
600 640
800
Potential Voltage (mV) Vs SCE
Photo current (mA-cm^{-2})
6·0
4·0
2·0
Illumination
Dark
-800
-600
-400
-200
0 40
200
400
600
800
Applied Voltage (mV) Vs SCE
200mV

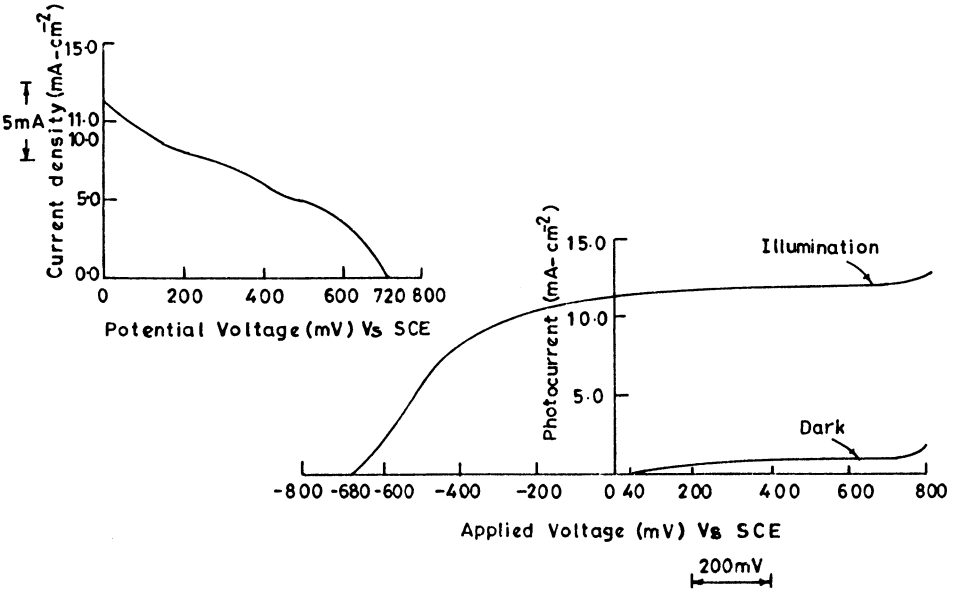
Current density (mA-cm^{-2})
5mA
15·0
11·0
10·0
5·0
0·0
0
200
400
600
720 800
Potential Voltage (mV) Vs SCE
Photocurrent (mA-cm^{-2})
15·0
10·0
5·0
Illumination
Dark
-800 -680 -600
-400
-200
0 40
200
400
600
800
Applied Voltage (mV) Vs SCE
200mV

The enhancement in the photocurrent with In_2O_3 modification is thought to be due to the improved spectral response of photoanode due to the presence of surface In_2O_3 [13]. The carrier recombination at the thin film interface is known to be low, added by high light absorption the thin In_2O_3 island on TiO_2(ns) surface cause enhancement in photoactivity of the anode. As it is clear from XRD studies, the In_2O_3 does not react with the base but forms only islands over the surface of TiO_2(ns). These photoactive islands over TiO_2 appear to act similar to Pt islands on TiO_2 or $SrTiO_3$, enhanced the activity of the anode, without forming any mixed oxide material.

4.3. PHOTOASSISTED HYDROGEN EVOLUTION STUDIES

The volume of hydrogen gas evolved under the photoassisted mode of electrolysis of the cell TiO_2(ns)-In_2O_3/1 M NaOH/Pt and the cell with TiO_2(ns) photoanode under illumination of 1000 W Xe-Hg lamp (0.5 Wcm^{-2}) was measured by using an inverted buratte over the cathode. The corresponding oxygen gas in stoichiometric quantities was evolved on the anode. The external bais applied to the cell for measurable gas evolution was varried using a potentiostat. The volumes of hydrogen gas evolved was compared for TiO_2(ns) and TiO_2(ns)-In_2O_3 electrodes. The photoelectrode was biased at fixed external bais of +0.5 V (SCE), thereby changing the corresponding electrode potentials. The mixed oxide (TiO_2(ns)-In_2O_3) photoanodes invariably exhibited higher rate of hydrogen production. A representative curve bringing out the enhanced rate of hydrogen evolution from 1 4 ml h^{-1} for TiO_2(ns) to 1.9 ml h^{-1} for mixed oxide (TiO_2(ns)-In_2O_3) is shown in Fig.7.

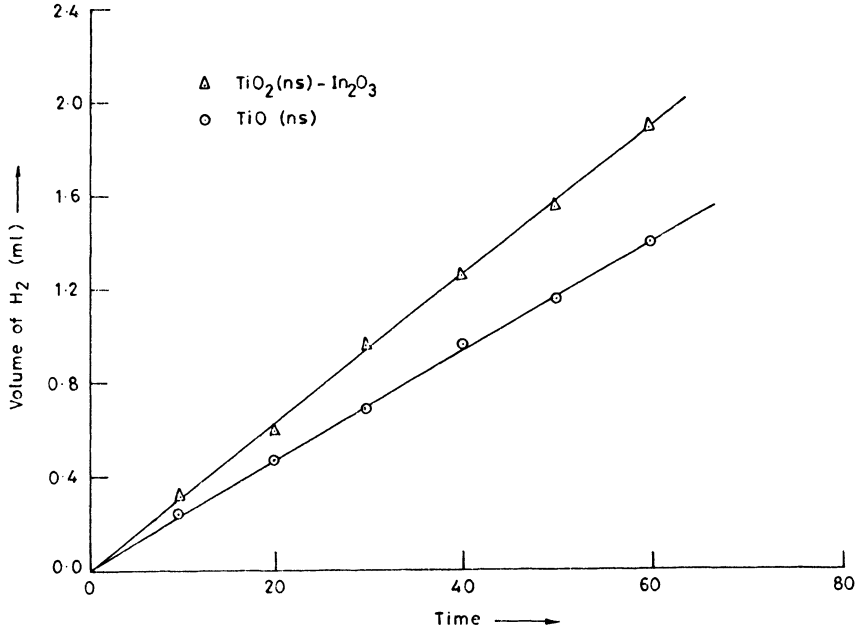

5. Conclusion

In conclusion it can be said that the nano-structured TiO_2 represents a better photoelectrode than its conventional counterpart. The hydrogen production rate for conventional TiO_2 thin film photoanode to and nanostructured TiO_2 was found to be ~1.0 ml h^{-1} and 1.4 ml h^{-1} respectively. It may be pointed out that TiO_2(ns) when admixed with In_2O_3 enhances the phototproduction of hydrogen. The hydrogen production changes to 1.9 ml h^{-1} for TiO_2(ns)-In_2O_3 as compared to 1.4 ml h^{-1} for TiO_2(ns) alone. The islands of In_2O_3 formed over the TiO_2(ns) surface appear to achieve the advantages of colloidal photochemical systems, thereby enhancing the photoactivity of the anode, leading to generation of higher density of carries. The overvoltage at the anode is thought to be reduced with the deposition of highly conducting In_2O_3 layers over the base TiO_2(ns) films, thereby increasing the gas evolution kinetics. Additional causes responsible for improved hydrogen production rates for TiO_2(ns)-In_2O_3 may be increased range of absorption and reduced energy gap. Further work on the characteristics of TiO_2-In_2O_3 and the resultant effect on hydrogen evolution are being carried out presently and results will be forthcoming.

Acknowledgment

The authors are grateful to Prof.G.V.Subba Rao, Dr.K.V.C.Rao, Prof.H.Tien, Dr.V.B.Singh and Dr.L.B.Singh for helpful discussions. The present work was financially supported by University Grants Commission (UGC) and Ministry of Non-conventional Energy Sources (MNES).

References

1. Fujishima A. and Honda K., (1972) Nature, 37, 238.
2. Chandra Babu K.S. and Srivastava O.N., (1989) Int. Journal of Hydrogen Energy, 515, 529.
3. Staldren C. and Augustynski J., (1979) J. Electrochem. Soc., 126, 2007.
4. Ghosh A.K. and Maruska H.P., (1977) J. Electrochem. Soc., 124, 1516.
5. Houlihan J.F., Armitage D.B., Hoopvkr T., Bonaquist D., Madacsi D. and Mullay L.N., (1978) Mater. Res. Bull., 13, 1205.
6. Philips T.C., Moorjani K., Murphy J.C. and Phochler T.O., (1982) J. Electrochem. Soc., 129, 1210.
7. Anpo Masakazu., Hiroki, Sukeya N.K., Yutaka K. and Harounishi T., (1980) J. Phys. Chem., 90, 1633 ; Rao K.V.C., Kumar V.G. and Gowarikar V.R., (1980) Private Communication.
8. Bedja Idriss., Hotchandani S. and Kamat P.V., (1994) J. Phys. Chem., 98, 4133.
9. Henhlein A., (1989) Chem. Rev., 89, 1861.
10. Knodler R., Sopka J., Harbach F. and Grunling H.W., (1993) Solar Energy Materials and Solar Cells, 30, 277.
11. Chandrababu K.S. and Srivastava O.N., (1990) Semiconductor Science and Technology, 5, 364 ; Schumacher L.C., Afara S.M. and Dignam M.J., (1986) J. Electrochem. Soc., 4, 133.
12. Regan O'Brain and Grätzel M., (1991) Nature, 353, 737.
13. Scot M.T., Colin M.L.and Hoffmann M.R., (1994) J. Phys. Chem., 98, 13695.
14. McCann J.F. and Bockris J.O'M., (1981) J. Electrochem. Soc., 128, 1719.

THE COMPOSITE ZIRFON® SEPARATOR FOR ALKALINE WATER ELECTROLYSIS

Ph. VERMEIREN, W. ADRIANSENS, J.P. MOREELS, R. LEYSEN
Process Technology
Flemish Institute for Technological Research (VITO)
Boeretang 200
2400 MOL
Belgium

Abstract

During the last few years, VITO has been developing a new type of microporous composite separator material for use in alkaline water electrolysis [1,2].
The separator is composed of a polysulfone matrix and ZrO_2 which is present as a powder. The manufacturing is based on the film casting technique. The Zirfon® separator is very stable in concentrated KOH solutions at elevated temperatures. Even with a high loading of ZrO_2, it is possible to produce very flexible separators with attractive mechanical properties.
As a result of a low ionic resistance and a high wettability it is possible to obtain both a low cell voltage and high gas purities.
The main challenge for this Zirfon® separator is to replace the asbestos diaphragms which are presently used in industrial alkaline water electrolysis. Different companies all over the world are testing the Zirfon® separator and excellent results have already been reported.

1. Introduction

In the conventional water electrolysis asbestos is being used as the separator material. These separators with a thickness of a few millimeters exhibit, under industrial working conditions of 90° C and 30 weight % KOH, rather high ionic resistances of 0.5 to 1 Ω cm^2 [3].
This asbestos material also suffers from extreme corrosion problems. The major drawback however is that asbestos is a carcinogenic material and its use will be forbidden in the very near future.
For these reasons VITO directed its separator development towards an alternative material having a lower ionic resistance together with a high corrosion resistance.

T. O. Saetre (ed.), Hydrogen Power: Theoretical and Engineering Solutions, 179–184.

2. Manufacturing

As already mentioned, the composite Zirfon® separator manufacturing is based on the film casting technique where the casting dope consists of a suspension of ZrO_2 in a polysulfone solution. N-methyl-pyrrolidone is used as a typical solvent, the non-solvent being either water or e.g. an alcohol. During the manufacturing, different parameters such as e.g. the amount of ZrO_2, can be adapted in order to obtain the most suitable product.
The exact and detailed manufacturing procedure has been described in a European Patent [4].
The separators are now made with a maximum diameter of 65 cm but in the very near future it will be possible to produce separators with a diameter of about 1 m.

3. Results

The results are divided in two parts starting with the general characterisation performed at VITO and followed by some results that have been obtained by different other companies.

3.1. VITO RESULTS

3.1.1. *General Characteristics*

Table 1 shows the main characteristics of a typical Zirfon® separator which is composed of 85 weight % ZrO_2 and 15 weight % of polysulfone.

TABLE 1. Main characteristics of a typical Zirfon® separator

Characteristics		Mean value
Density		1.4 g cm^{-3}
Tensile strength	• dry	2.1 MPa
	• KOH	2.1 MPa
Elongation	• dry	23 %
	• KOH	32 %
Porosity		60 %
Thickness		0.5 mm
Bubble pressure		0.4 MPa
Ionic resistance	• 30°C	0.2 Ωcm^2
	• 80°C	0.1 Ωcm^2

The Zirfon® separator from this example contains a rather high amount of ZrO_2. Indeed, it has been observed that both the wettability and the ionic resistance are being improved with increasing amounts of ZrO_2 and with this 85 weight % of ZrO_2 and only 15 weight % of polysulfone, the Zirfon® separator is still a flexible material. It is possible to further increase this amount of ZrO_2 but extremely high amounts would finally result in a worsening of the flexibility of the material. The flexibility is illustrated by the elongation values in this Table 1. The elongation values are those values that are observed at the maximum stress value of 2.1 MPa when the sample breaks. The absorption of electrolyte in the separator does not affect the tensile strength, but the flexibility, expressed as the elongation value, is being improved. The high bubble pressure of 0.4 MPa is of great importance with respect to the gas separation capability. This high bubble pressure is a result of the hydrophilic nature of the ZrO_2 together with the small surface pore diameters.
The separator from this example is made with a porous ZrO_2. The effect of the porosity of the ZrO_2 will be discussed hereafter.

3.1.2. *Type of ZrO_2*
The description of the manufacturing process already stated that different parameters can be adapted in order to obtain the desired performance and properties.
The influence of the amount of ZrO_2 has already been described [2,5].
A brief description related to the effect of the porosity of the ZrO_2 itself is given below.
The pore size distribution of two separators is illustrated in Figure 1.

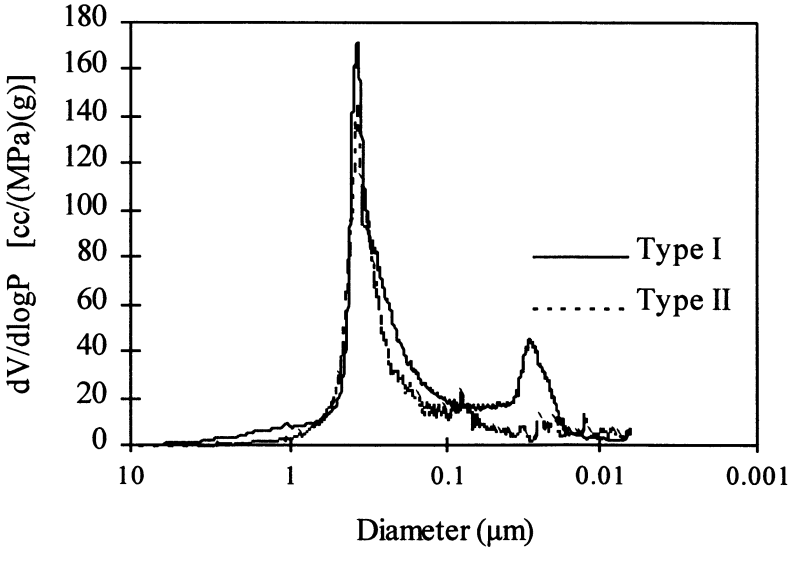

Figure 1. Pore Size Distribution (Hg-porosimetry)

Both Zirfon® separators in this Figure 1 have the same composition : 85 weight % ZrO_2 and 15 weight % polysulfone, and all manufacturing steps have been identical.
The only difference is the type of ZrO_2 that is being used. The larger peak around 0.4 μm is the same for both separators but a second smaller peak only appears for type I. This second peak in type I is induced by the porosity of the ZrO_2 which is being used. The ZrO_2 which is being used in type II is not porous itself.
The effect of the additional capillarity created by the ZrO_2 in type I on the wettability of the separator is illustrated in Figure 2.

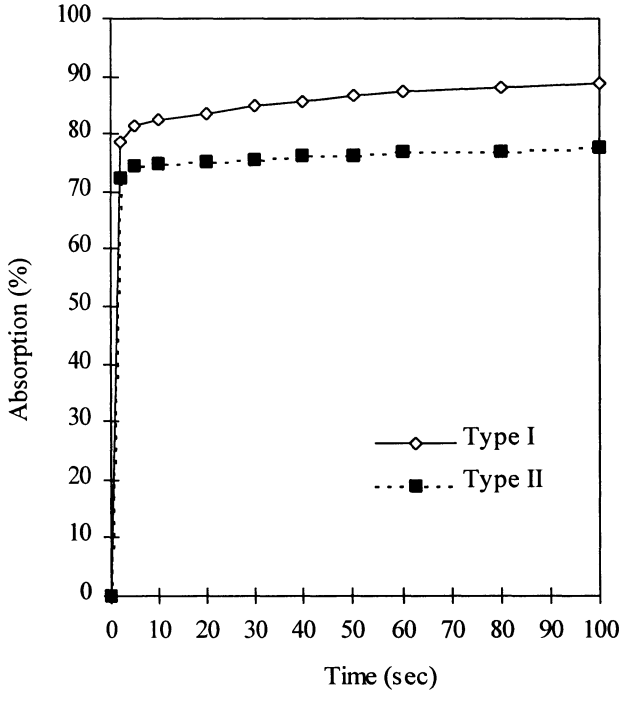

Figure 2. Absorption as a function of time (H_2O, RT)

It is clear from this Figure 2 that the additional small pores, created by the ZrO_2 in type I, result in an improved wettability of the separator.

3.2. APPLICATION RESULTS

A lot of investigation on Zirfon® is being performed worldwide. A few typical results obtained by different companies will be presented hereafter.

3.2.1. *Teledyne Brown Engineering*

Teledyne Brown Engineering has been testing the Zirfon® separator in one of their smaller size modules [2].
The Teledyne water electrolysis cell is designed on a zero-gap basis where the electrolyte only circulates in the anode compartment and reaches the cathode via the moistened separator. The separator pores must have a very small diameter so that a mixing of the gases is prevented by strong capillary forces. The cathode compartment does not contain any liquid, only hydrogen and water vapour emerge into it.
The gas pressure of the hydrogen is kept higher than that of oxygen. The electrolyte therefore does not spill over into the cathode chamber. The electrolyser is constructed as a compact bipolar unit [3].
Teledyne has already been testing the most important Zirfon® properties.
First of all the chemical stability has been tested and it was found that after several weeks in 25 weight % KOH at 90° C, no visible degradation could be observed.
The preliminary tests in a Teledyne electrolyser have been positive. It was found that the Zirfon® separator does not permeate hydrogen at pressure differences of up to ± 0.5 MPa which is excellent for their single irriguous system.
The ionic resistance was also found to be excellent, yielding voltages for a given current approximately 5 % lower than measured for asbestos.

3.2.2. *Deutsche Forschungsanstalt für Luft- und Raumfahrt e.V. (DLR)*

DLR reported that excellent electrochemical performances and high gas purities had been obtained with the Zirfon® separators [2]. The Zirfon® separators were tested in a zero-gap electrolyser equipped with DLR vacuum plasma sprayed electrodes (VPS) of 250 cm^2 size. The electrode coatings consisted of NiAl/Mo for the cathode and $NiAl/Co_3O_4$ for the anode. An in situ activation within the cell block has been performed in order to obtain very active Raney nickel electrodes. During a test period of almost 3,000 hours an excellent electrochemical performance has been observed.
For a current density of 800 mA cm^{-2}, at 90° C, a cell voltage as low as 1.68 Volts could be obtained with the Zirfon® separators.
The gas purity has also been measured in a zero-gap electrolyser with 2 separate electrolyte circuits. The gas purity has been determined by gas chromatography.
The gas purities, measured in 5.3 N KOH at 70° C, were higher than 99.9 % for both the H_2 and the O_2 gas (for current densities ranging between 100 and 400 mA cm^{-2}).

3.2.3. *ELWATEC Elektrolyse- und Wassertechnik GmbH*

Elwatec in Germany confirmed the excellent properties that have been obtained elsewhere. The ELWATEC Electrolysis System features an electrolysis cell with a very compact bipolar design. Unlike other electrolysis systems operating at atmospheric pressure, the ELWATEC system can deliver hydrogen at up to 3 MPa

without the use of a compressor. If pressures exceeding 3 MPa are required, a simple compressor can be used.
The ELWATEC electrolysis cell uses Zirfon® as the separator material.
The hydrogen production capacity of the standard ELWATEC system is variable up to 10 m^3h^{-1} where the simple modular design allows the stacking of additional units in parallel. Without the use of a catalyst, the energy consumption ranges between 4.5 and 5.1 kWh^{-1} and the hydrogen is produced with a purity of 99.7 %.
The ELWATEC electrolysis plant, developed in cooperation with Norsk Process AS, is fully automatic and has a record of proven reliability and performance. Originally developed for use on offshore oil platforms, the design meets or exceeds all requirements for quality, safety and reliability in the harsh offshore environment.
The ELWATEC Electrolysis System equipped with the Zirfon® separator is the only hydrogen electrolysis system certified for offshore use, and is designed and built to operate in a Zone 1 location.

4. Conclusions

An increasing demand for this new Zirfon® separator has been observed during the last few years. This is the result of the growing experience at different companies.
The main advantages, as they are described by those companies, are : asbestos free, good conductivity, good gas separation, KOH resistance, long-term stability under relatively high electrical load, easy handling and mechanical stability.
A further positive development of the market is therefore expected.

References

1. Vermeiren, Ph., Adriansens, W., and Leysen, R. (1996) Zirfon® : A new separator for Ni-H_2 batteries and alkaline fuel cells, *Int. J. Hydrogen Energy* **21**, 679-684.
2. Vermeiren, Ph., Adriansens, W., Moreels, J.P., and Leysen R. (1996) Evaluation of the Zirfon® separator for use in alkaline water electrolysis and Ni-H_2 batteries, in T.N. Veziroglu and C.J. Winter (eds.), *Hydrogen Energy Progress XI,* Published on behalf of the International Association for Hydrogen Energy, pp. 2103-2111.
3. Divisek, J. (1990) Water electrolysis in a low- and medium-temperature regime, in H. Wendt (ed.), *Electrochemical Hydrogen Technologies*, Elsevier, Amsterdam, pp. 137-212.
4. Vermeiren, Ph., Doyen, W., Adriansens, W., and Leysen, R. (1995) Preparation of a membrane and its use in an electrochemical cell, European Patent No. 0624283.
5. Vermeiren, Ph., Moreels, J.P., and Leysen, R. (1996) Porosity in composite Zirfon® membranes, *Journal of Porous Materials* **3,** 33-40.

INVESTIGATION OF THE STEADY STATE AND TRANSIENT OPERATING BEHAVIOUR OF A 20 kW PRESSURE ELECTROLYSER

Frank Menzl
Fachhochschule Stralsund
Große Parower Straße 145
D-18435 Stralsund
-GERMANY-

Michael Wenske
ELWATEC GmbH
Oberwerder 3
D-04668 Grimma
-GERMANY-

1. Introduction

A 20 kW alkaline pressure electrolyser has been operated in Complex Laboratory Alternative Energy at the College of Stralsund for two years. This electrolyser was manufactured by MAG Grimma GmbH. Than it was developed further and is now maintained by ELWATEC GmbH Grimma. The purpose for operating the electrolyser is the use of hydrogen as an energy carrier. Different kinds of renewable sources of energy like solar radiation and wind energy are used in the Complex Laboratory Alternative Energy. In addition to the electrolyser the Laboratory consists of a wind power plant, a solar installation, a solar simulator, a block-type thermal power station and a catalytic heating system. The disadvantage of renewable sources of energy is that they are not available continuously. Therefore an energy storing system is necessary. Hydrogen produced by electrolyses from renewable sources of energy could be used as such an energy carrier. But there are special requirements for an intermittently operated electrolyser. Structural arrangements of the electrolyser, especially the new cell design and experiences in operating the electrolyser in different operating regimes are presented in this paper. The ELWATEC electrolysis system comprises two 10 kW cells. These cells feature a very compact bipolar design. Furthermore, the use of capillary electrodes results in a number of advantages. For instance, the system can be run at partial capacity without any difficulties. It also eliminates the need to supply the system with a support current at shut down mode. The ELWATEC electrolysis system delivers hydrogen at up to 30 bars without the use of a compressor. Two different operating regimes of the electrolyser were considered. The first one was the steady state behaviour of the electrolyser. The steady state curve and the efficiency depending on the power input were determined. The second one is the operation of the electrolyser with changing loads. First results have been presented in [1]. Another system was investigated in [2]. The electrolyser was connected to the wind power station indirectly and was operated in an intermittently operating regime. The power input of the electrolyser was controlled by the power output of the wind power plant via the central switching cabinet.

T. O. Saetre (ed.), Hydrogen Power: Theoretical and Engineering Solutions, 185–190.

2. The Installation of Electrolyser and Hydrogen Storage Tank

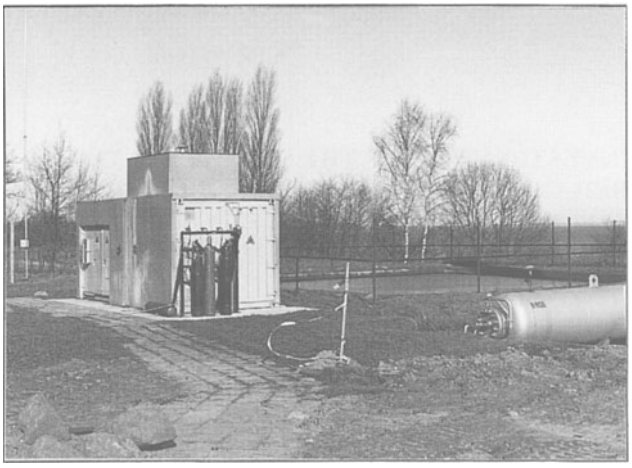

Fig. 1 : Installation of Electrolyser and Hydrogen Storage Tank

Fig. 1 shows the installation of the electrolyser and the hydrogen storage tank in the Complex Laboratory. The electrolyser was developed further and is now maintained by ELWATEC GmbH Grimma. Unlike other electrolysis systems operating at atmospheric pressure, the ELWATEC system can deliver hydrogen at up to 30 bars without using of a compressor. If pressures exceeding 30 bars are required, a simple compressor can be used. Simplification of the compressor and reduction of compressor stages, greatly reduces maintenance costs and down-time of the system. The electrolysis cells do not utilise asbestos partition membranes common to other systems. That it is not a hazard to its users or the environment. Other similar electrolysis systems typically require two to three times more space than the complete ELWATEC system. In fact, the electrolyser is so compact that it can easily be made portable by fitting it in a suitable container. Table 1 shows the technical data of the electrolyser. The hydrogen storage tank has a geometrical volume of 8 m^3. The pressure limitation of the tank is 115 bars. Since the system works without a compressor, the tank is only used to the maximum pressure of electrolyser, that is 30 bars. The tank contains then 240 Nm^3 hydrogen and is filled within 60 hours. If a higher output of the electrolyser is needed, the simple modular design allows additional units to be stacked in parallel while retaining all their individual design advantages and performance. The electrolysis system in the Complex Laboratory comprises two 10 kW cells (Fig. 2). The cells feature a very compact bipolar design.The cell design is shown in Figure 3. To increase the electrical conductivity of the liquid in the cell, potassium hydroxide (KOH) is added to the water

Table 1. Technical data of Electrolyser

Capacity H_2	4	[Nm^3/h]
Capacity O_2	2	[Nm^3/h]
Gas purity H_2	99,7	[%]
Energy consumption	20	[kW/h]
Operating pressure	30	[bars]
Number of cells	80	
Operating temperature	80	[°C]
Weight	450	[kg]
Geometrical dimensions	[mm*mm*mm]	
Electrolyser	700*1150*1890	
Transformer	800*400*700	
Switchboard	800*300*1000	

as an electrolyte. The water consumed in the process is replaced with demineralized (low conductivity) water on a continuous basis. The end-product gases, oxygen and hydrogen, are separated in the cell by special membranes, and are led to a gas/liquid separator through built-in channels. Furthermore, the use of capillary electrodes results in a number of advantages. For instance, the system can be run at partial capacity without any difficulty. It also eliminates the need to supply the system with a support current at shut-down mode. Therefore the system is suitable for island solutions. The integrated control and safety system controls the electrolysis plant by processing data relating to electrolyte level and temperature, power, voltage, operating pressure, differential pressure and output gas quality. Safety parameters are controlled by a separate PLC, operating independently of the instrumentation and control system and independent of the external power supply. The entire electric system is designed and built to meet with Zone 1 specifications and requirements.

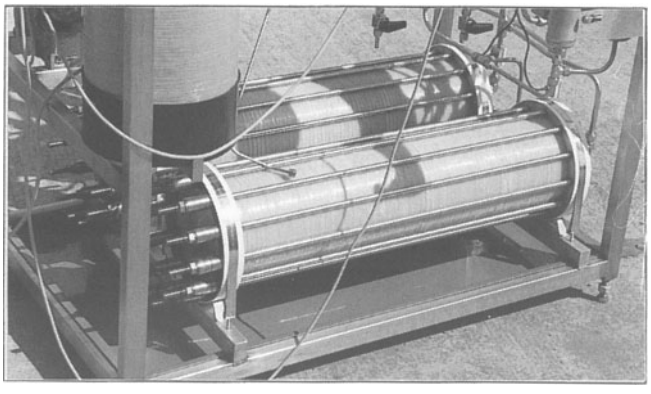

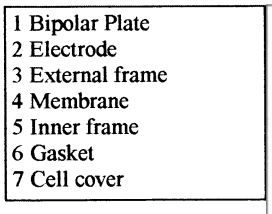

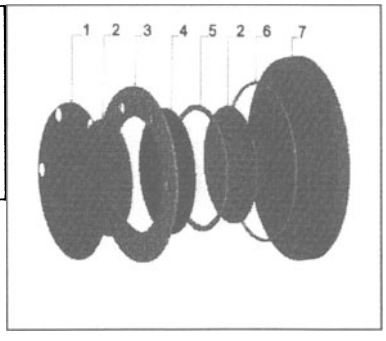

Fig. 3: Cell design

3. Static and Transient Behaviour of the Electrolyser

The static and dynamic behaviour of the electrolyser was investigated in the Complex Laboratory. The aim was to control the electrolyser depending on the power output of the windmill.

3.1. START OPERATION OF THE ELECTROLYSER

During the start operation the whole operating range of the electrolyser is used. The electrolyte temperature is 20 °C and the pressure is 0 bars. The reference current is set to 120 Amps. The actual current is limited by the control system depending on the actual pressure. After achieving a pressure of 13 bars the current limitation is switched

off and the actual current is only limited by the temperature. The hydrogen production for consumers starts at that point. The requirements to the pressure differential control system are very high in this phase. Since the temperature limits the current, the actual current does not achieve the reference current and the converted power is also limited. An excess power of the windgenerator is fed into the network. After achieving the operating temperature of 75 °C the current difference disappears. The starting operation is shown in Fig. 4.

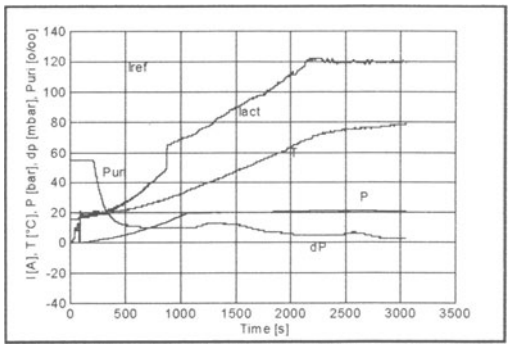

Fig. 4: Start Operation

3.2. STATIONARY OPERATING REGIME

Secondly, the power consumption and the hydrogen production of the electrolyser have been measured. A defined volume of 34.06 l was filled with hydrogen and the required time was determined. The results are shown in table 2. Figure 5 illustrates the hydrogen production curve versus the actual current. The dependence is highly linear as expected. The negative offset of the hydrogen production curve results from a non-measured gas flow through a bypass for the gas quality sensor. This value amounts to 0.32 m^3/h and is independent of the operating point, since the pressure in the bypass is controlled to a constant value. The current density amounts up to 4 kA/m^2.

Table 2: Steady State Operating Points

Current [A]	Voltage [V]	Power [kW]	Pressure [bar]	Temperature [°C]	Volume Flow [Nm^3/h]
24	114	2,7	14,8	62	0,47
24	114	2,7	14,8	62	0,45
48	131	6,3	15,7	70	1,25
48	131	6,3	15,7	70	1,2
71	144	10,2	15,8	76	2,05
71	144	10,2	15,8	76	1,95
96	158	15,1	15,9	78	2,83
96	158	15,1	15,9	78	2,82
121	170	20,5	16,3	77	3,52
124	171	21,2	16,3	77	3,70

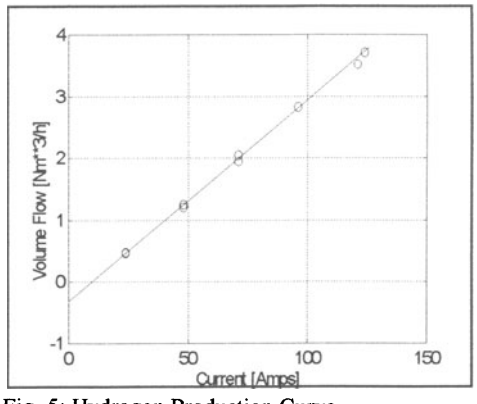

Fig. 5: Hydrogen Production Curve

3.3. INSTATIONARY OPERATING REGIME

Since the electrolyser should be coupled with the windmill, an investigation of the transient electrolyser behaviour is necessary. The electrolyser has been equipped with a

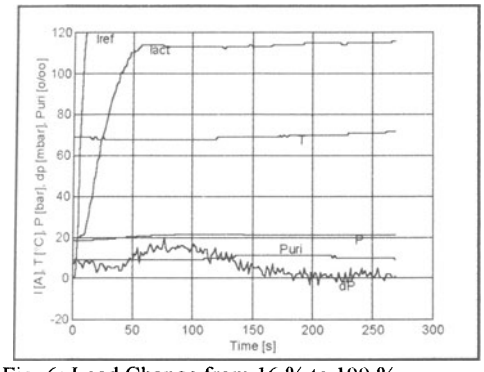

Fig. 6: Load Change from 16 % to 100 %

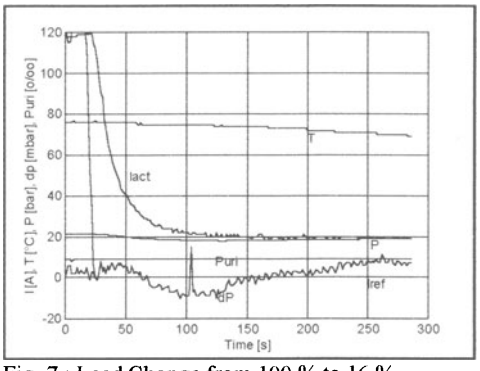

Fig. 7 : Load Change from 100 % to 16 %

load control input and the system was exited by a load change from 16 % to 100 % (Fig. 6, stage 2 to stage 10) and a load change from 100 % to 16 % (Fig. 7, stage 10 to stage 2) nominal power output. It can be seen that the actual current follows the reference current with a delay time of round about 40 s. The pressure differential doesn't exceed the limit of 25 mbar. In the case of a load change to 100 % (Fig. 6), the actual current is limited by the electrolyte temperature. Figure 8 shows a load change of 100 % caused by the temperature limit reached at 80 °C. This load excitation led to a current limitation and a connected power consumption saturation. This effect was not caused by electrolyses cells, it was caused by exceeding the differential pressure limit. The control system has been improved in later electrolyses plants.

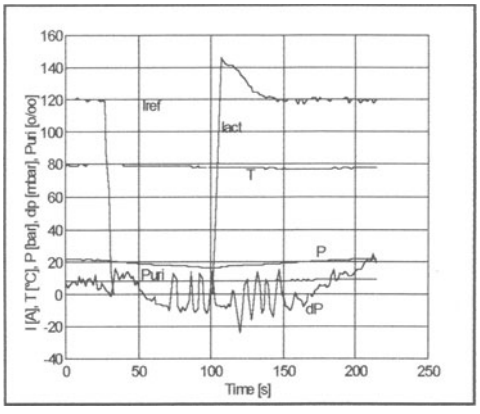

Fig. 8 : Load Change of 100 %

3.4. INTERMITTENT OPERATING REGIME

The suitability of a 100 kW electrolyser as a control system for a mains supply has been investigated in [3]. At first in the Complex Laboratory the power input of the electrolyser was controlled by the measured wind speed. The minimal load is saturated to 20 % rated power output. The sample rate for changes of the control input was 5 minutes. The sample rate for measurements was 1 second. Fig. 9 shows the values of

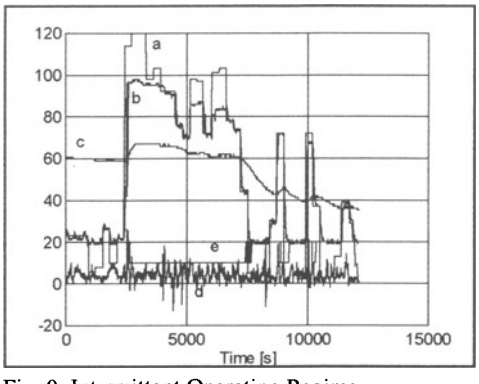

Fig. 9: Intermittent Operating Regime

of reference current (a), actual current (b), temperature (c). The values for pressure differential (d) and gas purity (e). The elctrolyser operates well, but detailed measurements show that a large load-change as shown in Figure 9 leads to a reduction of actual current, due to a pressure differential near the limit. Secondly the electrolyser was controlled by the power output of the windmill as shown in Fig. 10. The power output signal (100 kW equates 100 %) was scaled down to an input signal (100 % equates 120 A) of the electrolyser. Fig. 11 shows the result. The [c1]actual current follows the reference current with a time delay. An energy excess is fed into the network. An energy demand is satisfied from the network.

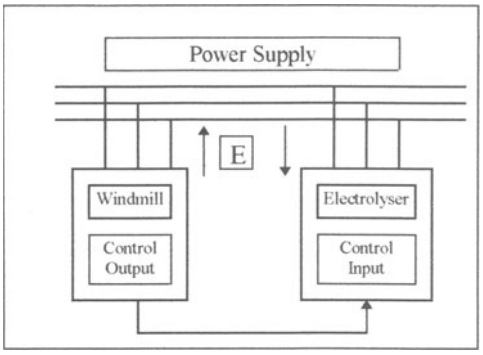

Fig. 10: Windmill-Electrolyser-System

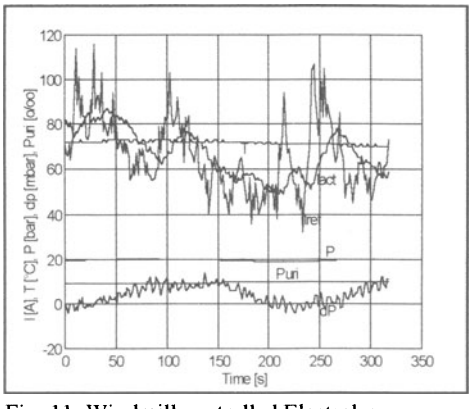

Fig. 11: Windmill controlled Electrolyser

4. Summary

The present paper describes the investigation of the static and dynamic behaviour of an 20 kW pressure electrolyser. The suitability for a coupled operating regime with a wind power plant has been investigated. At first the static behaviour has been analysed. The share of oxygen in hydrogen gas is lower than 0.5 Vol%. But reaching the temperature limit of 80 °C leads to a switch off of the electrolyser, accompanied by an increase of the oxygen share in hydrogen gas up to 1.3 Vol%. Therefore, an improvement of the cooling system is necessary. Secondly, the electrolyser was excited by different step signals for load changing and finally, the electrolyser has been controlled by the power output signal of the windmill. The investigation shows that the development of a direct coupled wind-hydrogen system will be only a small step.

References

[1] F. Menzl, J. Lehmann
Modelling of a Hybrid Energy Supply System with Hydrogen as an Energy Carrier in a Sewage Treatment Plant, *European Union Wind Energy Conference,* Goteborg, Sweden 1996

[2] A. G. Dutton, A. J. Ruddell, H. Dienhart, W. Hug, W. Seeger J.A.M. Bleijs
Electrolyser and System Operation in Wind/Hydrogen Electrolysis Systems,
European Union Wind Energy Conference, Goteborg, Sweden 1996

[3] Chr. A. Schug, G. Newi
Elektrolyse als Regelkomponente, VDI Berichte, Nr. 1201, 1995

HYDROGEN EVOLUTION ON NI-P ALLOYS. THE EFFECT OF DEPOSITION CONDITIONS.

T. BURCHARDT , T. VÅLAND, T.O. SÆTRE
Agder College
Groosevg. 36, N-4890 Grimstad
NORWAY

Abstract- The hydrogen evolution reaction (HER) was studied on Ni-P_x electrodes containing 8 to 16 weight percent P prepared by potentiostatic deposition. The amount of P in the alloy varied with deposition potential. The activity of the electrodes was dependent on the P concentration, and the formation of a passive film. Cyclic voltametry was used to study the removal of this film.

INTRODUCTION

The hydrogen evolution reaction (HER) has been extensively studied. For the use in alkaline water electrolysis, a mechanically and chemically stable active electrode is required. Because of their chemical inertnes, nickel-based electrodes are among the most often used electrode materials for the hydrogen evolution reaction. Electrolytically prepared amorphous Ni-P_x layers, containing a low amount of P, have been reported to show catalytic effects on the hydrogen evolution reaction in alkaline solutions [1]. In this work the Ni-P_x layers have been formed by electrolytic deposition on a Ni substrate. By varying the deposition potential, the amount of P could be varied between 8 and 16 wt. %. The activity of the electrodes was studied in 1 M KOH solutions using electrochemical techniques.

EXPERIMENTAL

The Ni-P_x electrodes were prepared by potentiostatic electrodeposition on a Ni-plate with an exposed area of $3cm^2$. Prior to deposition, the Ni plate was polished with 1000 Mesh SiC, etched in concentrated HNO_3 and washed in distilled water. The deposition was conducted in a glass cell with volume of 0.3 liter. A three electrode set-up was used, with a Ni counter electrode and a saturated calomel reference electrode. For all the experiments the temperature was monitored with a ETS-D2 probe, which also served as an input for the temperature control system - a hot plate combined with a

T. O. Saetre (ed.), Hydrogen Power: Theoretical and Engineering Solutions, 191–196.

magnetic stirrer. The temperature could then be kept stable at 25 ± 1 °C. To attain an inert atmosphere, the cell was continuously bubbled with N_2 (g). The electrolyte consisted of 0.1 M $NiSO_4$, 0.3 M NaH_2PO_2, 0.15 M H_3BO_3 and 0.1 M NaCl, giving a solution with pH in the range 4-5. The electrodeposition time was 1 hour for all samples producing Ni-P_x layers with thicknesses from 1 μm to 8 μm depending on the deposition potential. The HER was performed in a glass cell, using a 1 M KOH solution at 25 °C . The counter electrode was a wire of Pt. As reference electrode a saturated calomel electrode was used.

RESULTS AND DISCUSSION

The amount of P in an electrodeposited amorphous NiP_x layer can be effectively controlled by varying the deposition potential. This has previously been studied [2]. It is probably due to a difference in the reaction mechanisms. The P deposition becomes diffusion controlled while the Ni deposition still remains charge transfer controlled. In the present experiments, the P content in the NiP_x alloy was varied between 8 and 17 wt.%. This was achieved by changing the deposition potential in the range from -725 mV to -900 mV vs SCE. As can be seen from Figure 1, the P content in the alloy decreases when the potential is decreased.

The hydrogen evolution reaction on electrodeposited amorphous NiP_x electrodes was studied in a 1 M KOH solution. Potentiostatic experiments were performed at -1.3 V vs. SCE. The first 30 minutes of polarization caused a pronounced increase in the current density. After the samples had been activated the current density stabilized. Figure 1 shows the stable current densities obtained for the various samples after 1 hour of polarization.

The hydrogen evolution reaction is significantly increased when the P content in the alloy is in the range around 10 wt. %. This can be more clearly seen from Figure 2 were the current density is given on a linear plot. A distinct peak occurs, with a maximum current density of 0.032 A/cm^2 at 9.8 wt% P. This value being over 200 times larger than the lowest current density (0.00028 A/cm^2 at 16.4 wt% P). Figure 3 shows potentiodynamic polarization sweeps taken with the various electrodes. A remarkable active surface for the hydrogen evolution reaction can be seen when the amount of P is in the range around 10 wt%.

An etched pure Ni electrode was polarizing at -1.3 V vs SCE in 1 M KOH. A hydrogen evolution current density of 0.001 A/cm^2 was obtained. As can be seen from Figure 1 this indicates that the presence of a large amount of P in the alloy causes an inhibition of the hydrogen evolution reaction. On the other hand, small amounts of P catalyses the reaction. The catalytic effect is reduced as the P concentration in the alloy moves towards 0 wt%. The current density will then probably move towards the value for pure Ni deposition.

An activation of the NiP_x electrodes during polarization occurs. This can be seen as an increase in the hydrogen evolution reaction with time before it stabilizes. This is probably due to the removal of passive layers on the NiP_x electrodes. The characterization of passive layers on NiP_x in alkaline solutions has been studied by Wronkowska [3].

Figure 4 shows Tafel sweeps taken on a NiP_x electrode with 10 wt% P. Two Tafel lines are presented, one taken before polarizing the sample, the other after 30 minutes of polarization. The Tafel line obtained before polarization is probably due to the removal of a passive $Ni(OH)_2$ layer. After the passive layer has been removed, a Tafel line that is characteristic for the hydrogen evolution reaction is obtained.

Figures 5, 6 and 7 show cyclic polarization sweeps using a NiP_x electrode containing 10 wt% P, but with different cycle numbers. They show that the cycles result in removal of the passive layer whereby an active electrode is obtained. Figure 5 shows the first sweep. The cathodic polarization removes the passive film. When polarizing in anodic direction the reversible potential for the hydrogen evolution reaction is obtained. Figure 6 shows the last cycle. At this stage, most of the passive film has been removed. The reversible potential for the hydrogen evolution reaction is higher when sweeping in cathodic direction due to a lower partial pressure of H_2. Figure 7 show 4 cyclic sweeps. A gradual activation of the NiP_x electrode can be observed in that case for each sweep.

The stability of the NiP_x electrodes was tested by polarizing the samples at -1.3 mV vs SCE in a 1 M KOH solution over a period of 14 days. Figure 8 shows the polarization of a NiP_x electrode with 8.5 wt% P. The polarization of the sample does not seem to affect the efficiency of the electrode. A reduction in the current density can be seen during the start of the experiment, and after exposing the electrode to air and reintroducing it into the cell. This is probably due to absorption of hydrogen into the alloy. This will, however, be treated further in another publication [2].

CONCLUSION

Large variations in the current density for the hydrogen evolution reaction were observed when changing the amount of P in amorphous NiP_x electrodes. The catalytic effect was largest around 10 wt% P, increasing the hydrogen evolution reaction over 200 times.

A gradually activation occurred when the electrodes were polarized cathodic. This was due to the removal of a passive film formed on the electrode surface. After an initial activation, the current density of the hydrogen evolution reaction was stable. Only an insignificant reduction in the current density could be observed after 14 days of polarization.

REFERENCES

1. Paseka, I. (1995) Evolution of hydrogen and its sorption on remarkable active amorphous smooth Ni-P(x) electrodes, Electrochimica Acta, Vol.40, No.11, p. 1633-1640.

2. Burchardt,T. Unpublished results.

3. Wronkowska, A. (1993) In situ and ex situ characterization of passive layers on $Ni_{1-x}P_x$ in alkaline solution, The Electrochemical Society, Vol.140, No.4, p.995-1005.

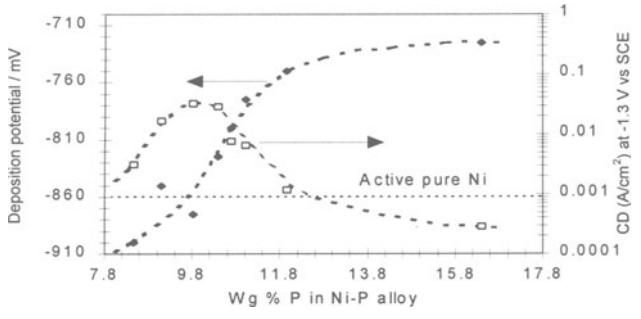

Figure 1. The effect of deposition potential and current density for the hydrogen evolution reaction on the P concentration in an amorphous NiP alloy.

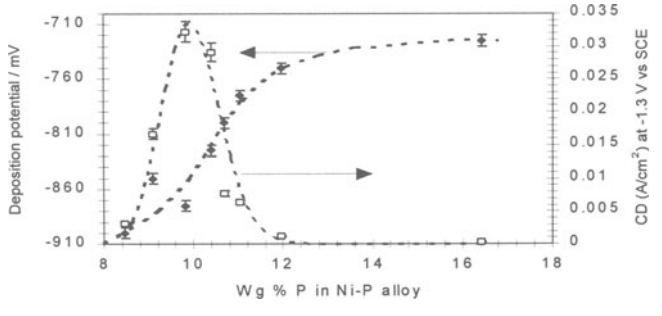

Figure 2. The effect of deposition potential and current density for the hydrogen evolution reaction on the P concentration in an amorphous NiP alloy.

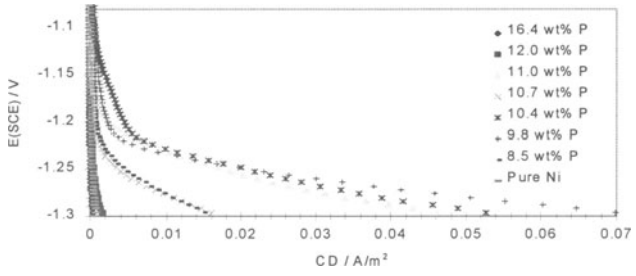

Figure 3. Tafel sweeps on amorphous NiP electrodes in 1 M KOH at 25 °C.

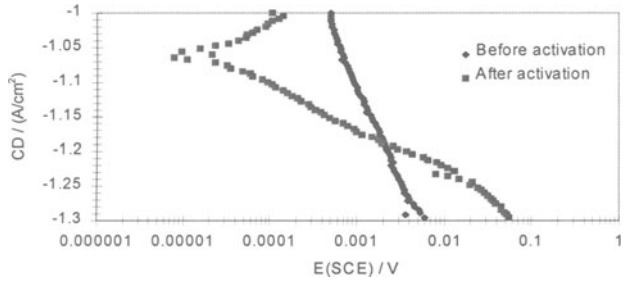

Figure 4. Tafel sweeps on a passive and active amorphous NiP electrode with 9.8 wt% P in 1 M KOH at 25 °C.

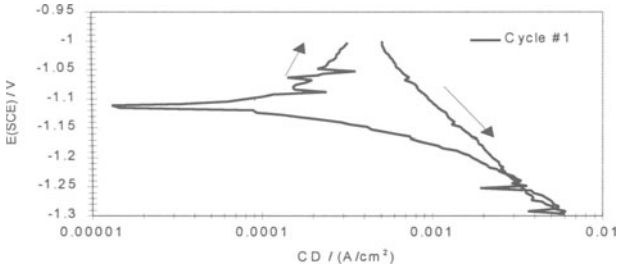

Figure 5. Cyclic sweep on an amorphous NiP electrode with 9.8 wt% P in 1 M KOH at 25 °C (sweep nr. 1).

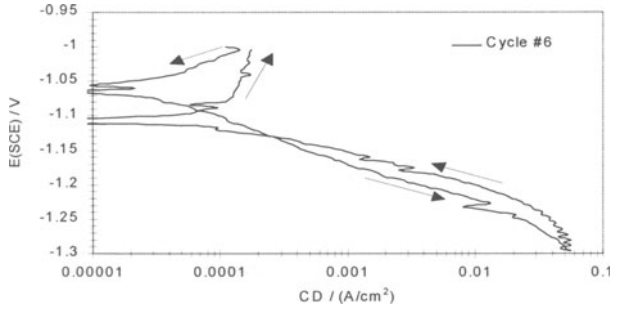

Figure 6. Cyclic sweep on an amorphous NiP electrode with 9.8 wt% P in 1 M KOH at 25 °C (sweep nr. 6).

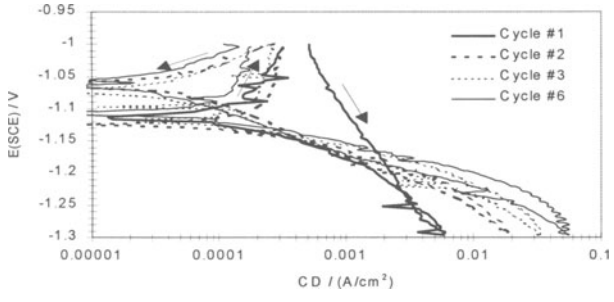

Figure 7. Cyclic sweep on an amorphous NiP electrode with 9.8 wt% P in 1 M KOH at 25 °C (sweep nr.1,2,3,6).

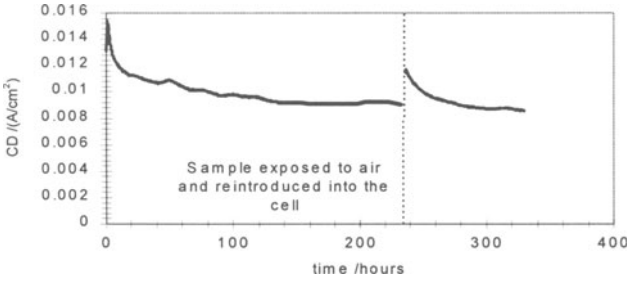

Figure 8. Hydrogen evolution current density for NiP electrode with 8.5 wt% P in 1 M KOH at 25 °C. Potentiostatic experiment at -1.3 V vs SCE.

PRODUCTION OF HYDROGEN BY RADIOLYSIS

R.I.Garber, I.M.Neklyudov, B.V.Borts, A.I.Voloshchuk, L.P.Rekova

National Science Centre "Kharkov Institute of Physics and Technology", Kharkov , Ukraine

Introduction

Hydrogen is a valuable source material for many processes of chemical industry and metallurgy. Being made cheaper, it can also be used as fuel. Pipelining of hydrogen over great distances is competitive in economical efficiency with electric power transmission. Moreover, water can be used as an initial material for hydrogen production. Nowadays, there are three types of the processes that are being developed to produce hydrogen through the use of nuclear energy.

1. The nuclear energy is transformed into the vapor (or gas) energy, which, in its turn, is transformed into the electric energy and, eventually, hydrogen is produced in electrolyzers. Decomposition of water in electrolyzers is now the only technique being used in practice to produce hydrogen.

2. It is expected that the nuclear energy will be transformed into thermal energy, which then will be used to decompose water with an aid of multistep thermochemical processes.

3. The penetrating radiation of nuclear reactions is supposed to be used for radiolytic decomposition of water.

Each of the above processes has its advantages and drawbacks. One of the most important characteristics of this or that technology is the efficiency which is defined as the ratio of the heating power of products to the energy consumed for their production. In electrolysis, the efficiency typically makes 20 to 25%; the thermochemical cycles under design are characterized by similar efficiency values. Until recently, the efficiency of radiolysis was considered to be lower. However, as demonstrated by the studies reported here, the radiolysis of powder-like hydroxides offers a possibility of producing hydrogen with an appreciably higher efficiency. This is achieved owing to the fact that on escaping from powder granules the radiolysis products are quickly molized, neutralized and loose

T. O. Saetre (ed.), Hydrogen Power: Theoretical and Engineering Solutions, 197–205.

their capability for regeneration. If the products are gaseous, e.g., hydrogen or carbon oxide, then they can easily be extracted through the pores of a powder-like mixture, pellets, granules.

If water is irradiated in order to obtain radiolysis products, then the process can be characterized by the parameter G(x) , which is equal to the number of molecules x that have escaped from the water as it absorbed 100 eV of the penetrating radiation energy. Our interest here is with the yield of hydrogen as certain quantities of penetrating radiation energy are consumed; it is characterized by the paramenetr $G(H_2)$, i.e., the number of hydrogen molecules leaving the water during absorption of 100 eV of penetrating radiation energy. The $G(H_2)$ value depends on many factors, including the nature of penetrating radiation, too. Table 1 lists the $G(H_2)$ values for some kinds of radiation that penetrate water according to [1].

Table 1

	X-rays	Gamma - rays	β-tritium source	32 MeV deuterons	α -particles
G(Í $_2$)	0.65	0.45	0.5...0.6	0.7...1.05	0.07...1.65

It seems likely that the data on radiolysis of water under the action of fission fragments were not published. The authors of refs.[2, 3, 4] suggested that $G(H_2) = 1.6$ might be obtained by the action of fission fragments. In [3, 4] there are indications that higher yields of hydrogen can be obtained if water solutions of acids or alkalis rather than water are irradiated.

The highest efficiency in the radiolysis of water vapor was obtained in ref. [5], where a combined action of heating and irradiation with 3 MeV electrons was investigated. At a temperature of 500°C and a pressure of 760 mm Hg an efficiency of about 20%, i.e.,$G(H_2) \sim 8$, was obtained.

We have used a disperse uranium-calcium hydroxide mixture formed so that the fission fragments escape from fuel particles (FP) and give their energy for dissociation of the matrix material. Uranous-uranic oxide (natural enrichment) was used as a FP substance.

To provide the initial material, a chemically pure CaO sample was filled with water and after the reaction was completed the required portion of U_3O_8 was added. The mixture containing $Ca(OH)_2$ and U_3O_8 was subjected to irradiation. The procedure was performed using high energy electrons from the linear accelerator. The hydrogen yield was determined by methods of chemical and mass-

spectrometry analyses. Radiation doses and fission fragment yields were determined by calculations, using the following formula:

$$\beta = \frac{\sigma \Phi N}{S} \quad , \qquad (1)$$

where β is the number of fission events, $\sigma = 10^{-23}$ cm^2 is the ^{238}U fission cross section for photonuclear reactions, Φ is the fluence of electrons that have passed through the specimen, N is the number of ^{238}U atoms in the specimen, ½is the sectional area of the specimen. To experimentally determine the number of fissions, the ^{131}I content in the ampoule was defined by the gamma-spectrometry method.

Calculation of energy absorbed during irradiation of the mixture

To calculate the radiolytic yield of hydrogen, it was necessary to determine the amount of radiation energy absorbed by calcium hydroxide crystals.

Table 2 gives the ratios of the numbers of hydrogen, oxygen and calcium atoms to the number of uranium atoms in the specimens under study.

Table2.

Element	Number of specified element atoms per uranium atom
Hydrogen	8.4
Oxygen	11.0
Calcium	4.2

The energy transferred to calcium hydroxide per fission event was calculated as follws. The FP shape is approximated by spheres of diameter equal to a typical linear size of FP. Direct calculation of the number of FP, whose typical linear size is within the given range of lengths, shows that the sizes of the overwhelming majority of FP do not exceed the fragment ranges. Therefore, the radii of all the spheres simulating a uranium-containing material should be considered to satisfy the inequality

$$2R < \lambda\,, \qquad (2)$$

where **R** is the spherical radius and $\lambda = 10$ μm is the fragment range in the FP material with all the fission fragments leaving the FP. Since the total energy of the incident electron is low as compared to the rest energy of the $\mathbf{U_3O_8}$ molecule-target, the uranium nuclei disintegrating under the action of photonuclear reactions can be assumed to be at rest. Then an almost obvious assumption that all equal volumes of FP material comprise the equal number of uranium atoms is also valid.

All the above-given considerations allow us to think of each element of the bulk of the sphere that simulates the FP as an isotropic source of fission fragments whose kinetic energies will be denoted by $\mathbf{E_{01}}$ and $\mathbf{E_{02}}$. In this case, the number of fragments of each kind escaping to the element of solid angle α_0 is given by

$$d_n = \frac{n_0 \alpha_0}{4\pi} = \frac{n_0}{2} \sin\theta d\theta\,, \qquad (3)$$

where $\mathbf{n_0}$ is the number of fission events in the unit volume, θ is the polar angle of emission in spherical coordinates.

Let us assume that the disintegration of the uranium nucleus has taken place at a distance r from the centre of the sphere. We consider the fragment escaping at an angle θ. From the triangle OAB (fig. 1) we can easily find the path **x** travelled by the fragment until it escaped from the sphere

$$x = -r\cos\theta + \left(r^2\cos^2\theta + R^2 - r^2\right)^{1/2} \qquad (4)$$

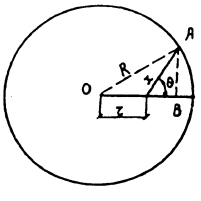

Fig. 1.

By the commonly used relation $E_i(x) = E_0 e^{-\frac{x}{\lambda_i}}$ on setting $\frac{x}{\lambda_i} << 1$, we have

$$E_i = E_{oi}\left(1 - \frac{x}{\lambda_i}\right) . \qquad (5)$$

This assumption does not distort the interpretation of experiment, because the energy of fission fragments decreases with distance nonlinearly. Combining of the last two formulas results in

$$E_i \le E_{oi}\left\{1 + \frac{r\cos\theta}{\lambda_i} - \frac{\left(r^2\cos\theta + R^2 - r^2\right)^{1/2}}{\lambda_i}\right\} . \qquad (6)$$

Multiplying expression (6) by the number of particles flying into the element of angle $d\theta$ at an angle θ, we obtain the energy carried away by the **i**-th-sort fragments at an angle θ :

$$d\varphi_i = E_i d_n < \frac{E_{oi} n_o}{2}\left\{1 + \frac{r\cos\theta}{\lambda_i} - \frac{(r^2\cos^2\theta + R^2 - r^2)^{1/2}}{\lambda_i}\right\}\sin\theta d\theta . \qquad (7)$$

Integration over the angle gives the energy carried away by the ***i*** th-sort fragments from the unit volume of the spherical layer with the radial coordinate ***r***

$$\Phi_i \le \frac{E_{oi} n_o}{2}\int_0^{\pi}\left\{1 + \frac{r\cos\theta}{\lambda_i} - \frac{\left(r^2\cos^2\theta + R^2 - r^2\right)^{1/2}}{\lambda_i}\right\}\sin\theta d\theta =$$

$$= E_{oi} n_o \frac{E_{oi} n_o R}{2\lambda_i}\int_{-1}^{1}\sqrt{z_2 - \frac{R^2 - r^2}{r^2}}\, dz =$$

$$= E_{oi} n_o - \frac{E_{oi} n_o R}{2\lambda_i} - \frac{E_{oi} n_o}{2\lambda_i r}\left(R^2 - r^2\right)\ln\frac{R+r}{R-r} . \qquad (8)$$

Multiplying Φ_i by the spherical layer volume $\mathbf{4\,\pi\,r^2dr}$ and integrating the result between **0** and **R** we obtain the expression for the total energy carried away by the ***i***-th-sort fission fragments beyond the sphere:

$$W_i \le \int_0^R 4\pi r^2 \Phi_i \, dr = \frac{4}{3}\pi R^3 n_0 E_{oi}\left(1-\frac{3}{4}\frac{R}{\lambda_i}\right) . \qquad (9)$$

Averaging the result over the radius, we arrive at the expression for the mean energy

$$\overline{W}_i \le \frac{4}{3}\pi \overline{R}^3 n_0 E_{oi}\left(1-\frac{3}{4}\frac{\overline{R}^4}{\overline{R}^3\lambda_i}\right) \qquad (10)$$

The mean energy carried away by all the fragments out of the sphere is found by summing with respect to sorts of fragments:

$$\overline{W} = \sum \overline{W}_i \le \frac{4}{3}\pi\, \overline{R}^3 n_0 \sum_i \mathrm{E}_{oi}\left(1-\frac{3}{4}\frac{\overline{R}^4}{\overline{R}^3\lambda_i}\right) . \qquad (11)$$

The factor before the summation sign in eq. (11) is the average number of fission events that have taken place inside the sphere. Hence, the mean energy carried away beyond the sphere per fission event is

$$\omega \le \frac{3\sum_i \overline{W}_i}{4\pi \overline{R}^3 n_0} = \sum_i \mathrm{E}_{oi}\left(1-\frac{3}{4}\frac{\overline{R}^4}{\overline{R}^3\lambda_i}\right). \qquad (12)$$

We assume the fission fragment energies to be 100 and 66 MeV, and the ranges to be 10.3 and 9.6 μm, respectively. Then, by formula (12), the mean energy carried away to the matrix material and related to one fission event is $\varpi < 116.1$ MeV.

Calculation of radiolytic yield of hydrogen

To calculate the radiolytic hydrogen yield, we have used the following formula

$$G_{H_2} = \frac{V_{H_2} \ell 100}{\beta \varepsilon_g}, \qquad (13)$$

where G_{H2} is the radiolytic hydrogen yield (molecules per 100eV); V_{H2} is the volume of hydrogen evolved (norm. cm^3); L = 2.68 x 10^{19} is the number of hydrogen molecules in 1 cm^3 at atmospheric pressure.; β is the number of fission events; ε_g is the energy released from FP in each particular ^{238}U fission event.

Irradiator design

The design of the irradiator is shown in fig. 2. Ampoule 1 charged with pellets was placed in the output electron beam of the accelerator LU-300. The ampoule was connected by service lines to the gas extraction system 4. The gas extraction system consisted of a distributing gear and several flasks which could be connected to the gear during the exposure. The tightness of the system and pressure variations in the course of the experiment were controlled by means of a vacuume gauge 3. The temperature of the ampoule heated by the electron beam was measured by thermocouples T_1 and T_2 fixed at ampoule ends. The water vapor was supplied from the boilder 5 via a capillary tube 6 to the ampoule end, and flowing around the mixture under irradiation, it came together with the gas entrained to the gas extraction system. The vapour was condensed in the trap7.

The data from experiments on hydrogen release are listed in Table 3.

Table 3

Experiment	Overheating temperature, ^{0}Ñ	Electron dose õ10^{-17}	Fission events x10^{-13}	H_2 yields, norm. cm^3				$G(H_2)$ molecules per 100 eV of absorbed fragment energy	.% efficiency(total hydrogen combustion energy related to the absorbed
				overheating	under electrons	under fission fragments	total yield		

									fragment energy)
1	550	1.5	2.28	6.2	1.8	31.2	39.3	30.41	90.31
2(1)	500	1.082	1.32	6.2	3.0	9.9	19.1	16.61	49.33
3(1-3)	300	4.015	5.5	--	11.0	60.3	71.3	24.28	72.11
3(4-5)	550	2.628	3.6	6.2	7.2	18.5	31.9	11.38	33.80
								20.67	61.39

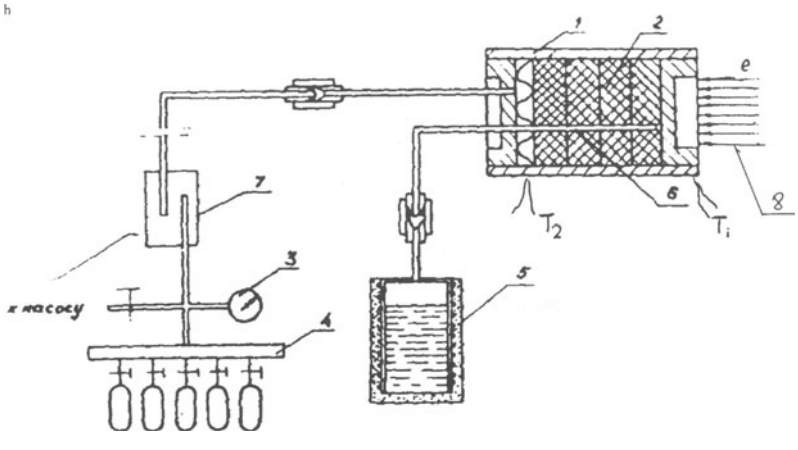

Fig. 2. An irradiator variant with water vapor and working mixture supply: 1-ampoule body (stainless steel); 2 - working mixture pellets; 3 - vacuum gauge; 4 - distributor with flasks to sample the gas evolving under irradiation of the working mixture (glass); 5 - vessel with distilled water and a heater (boiler);- 6 - capillary tube-vapor guide line; 7 - trap to condense water vapor; 8 - high-energy electron beam.

Conclusions

The possibility of obtaining high yields of hydrogen through the exposure of calcium hydroxide to natural uranium fission fragments is confirmed experimentally. The amounts of hydrogen obtained in some experiments were determined not only from the mass-spectrometry data, but also with the use of standard chemical analysis methods.

The radiolytic hydrogen yield averaged over six independent experiments comprises 20.41 hydrogen molecules per 100 eV of absorbed fission fragment energy. The corresponding energy efficiency makes up to 60.62.

Since on interaction with water or water vapor calcium hydroxide enters into the exothermal reaction to liberate 15.6 kcal/mole, it can easily be regenerated; this was attested to by one of irradiation experiments. Therefore, in the long run, we are dealing with a radiolytic decomposition of water at low temperatures or at temperatures readily available woth modern reactor engineering techniques.

Comparison of the present data with the characteristics of the facilities now in service or being under design, devised to produce hydrogen with the use of nuclear fuel, shows good prospects for the proposed method. This motivates the performance of more extensive studies in order to develop technical projects on the use of the radiolysis of crystal hydrates or hydroxides in nuclear energetics.

References

1. Vladimirova M.V., Atomnaya Ehnergiya 1964, v.17, is.3, pp. 222-224.

2. Legasov V.A., Belousov I.G., Vopr. At. Nauki i Tekh., ser. Atomno-vodorodnaya ehnergetika, 1977, is. 2(3), pp.19-25.

3. Kerr W., Majumdar D.P., Hydrogen Energy, 1974, ptA, , pp 167-181.

4. Majumdar D.P., Reyes H., Kerr M., Hydrogen Energy, 1975, ptA, pp 1-81.

5. Dzantiev B.T., Ermakov A.N., Popov V.N., Atomnaya Ehnergiya 1977, v.46, is.5, p.359.

DECOMPOSITION OF WATER OVER ZEOLITES WITH POSSIBILITIES FOR MEASURING MASS VARIATION OF ZEOLITE DURING IRRADIATION

Magdalena Momirlan
Institute of Physical Chemistry "I.G.Murgulescu"
Romanian Academy
Spl. Independentei 202,
Bucharest 77208, Romania

Abstract

An experimental device for catalytic decomposition of water over zeolites with possibilities of measuring the mass variation of zeolite during UV radiation was built.

By means of an electronic microbalance to which an irradiation system of zeolites was added, mass variation of samples and temperature rise of zeolites during irradiation were measured.

Microgravimetric measurements of mass variation of zeolite during irradiation were accomplished at the same time with the study of the temperature increase during irradiation. The decrease in weight of zeolites during irradiation, assigned to the elimination of water molecules from zeolite was noticed.

Introduction

The dissociation of water using light quanta represents a nonconventional method of hydrogen generation. The use of light energy for water dissociation is possible because water vapor absorb light (ultraviolet radiation photons of 194 9Å.)

Zeolites and zeolite like materials are based essentially on tetrahedral networks which encompass channels and cavities (Anpo et al.,1993)

Sorbate molecules of various size can be accomodated in these intecrystalline voids and undergo chemical reactions subject to stereochemical constraints. According to common views zeolites are based

T. O. Saetre (ed.), Hydrogen Power: Theoretical and Engineering Solutions, 207–212.

on open and fully crosslinked framework structures of corner-sharing SiO_4 and AlO_4 tetrahedra. (Murakami et al. 1986 and Meier, 1992)

$$M_{m/z}[mAlO_2 \cdot nSiO_2] \cdot qH_2O$$

Mordenite is one of the siliceous zeolites and typical formula of syntetic mordenite is : $Me_{2/z}O[Al_2O_3 \cdot (9-10)SiO_2] \cdot 6H_2O$

In our experiments the acid form mordenite was used :

$H_8[Al_8Si_{40}O_{96}] \cdot 24H_2O$ FeH- mordenite

obtained from Na form :

$Na_8[Al_8Si_{40}O_{96}] \cdot 24H_2O$ through ionic exchange of Na^+ with H^+ .

Experimental

An experimental device for decomposition of water over zeolites with possibilities for measuring the mass variation of zeolite during UV radiation was built up (fig.1).

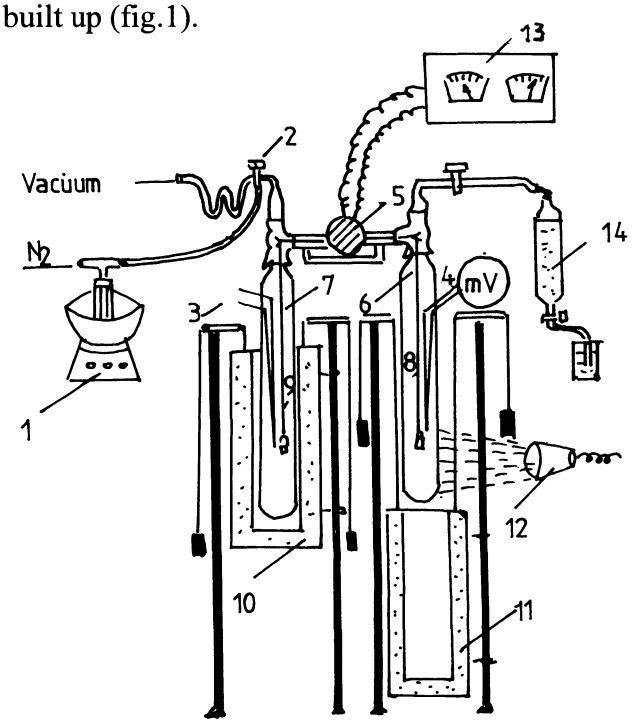

Figure 1- Experimental unit for catalytic decomposition of water over zeolites with possibilities for measuring mass variation of zeolite during irradiation:1.- electrical bath; 2.- vacuum valve; 3,4 - thermocouple Pt- Pt Rh; 5 - microbalance; 6,7 - quartz tubes; 8,9 -threads for hanging of sample and counterweight; 10,11 - furnaces; 12 - irradiation lamp; 13 - continous current amplifier; 14 - hydrogen collecting vessel.

Results

Zeolite is active in vacuum and when is taken out in atmosphere is deactivated, gaining the same weight lost in vacuum. Starting from the performed researches, we can conclude that a zeolite is activated considering when the maximum decrease in weight was registered, proving the complete elimination of water from intercrystalline channels.

In the case of irradiations with ultraviolet light, the distance between zeolite and irradiation source is important. The temperature of sample was increased from room temperature up to 70°C.

Microgravimetric measurements of mass variation of zeolite during irradiation were accomplished at the same time with the study of the temperature increase during irradiation. The decrease in weight of zeolites during irradiation, due to elimination of water molecules from zeolite was noticed. (fig. 2.)

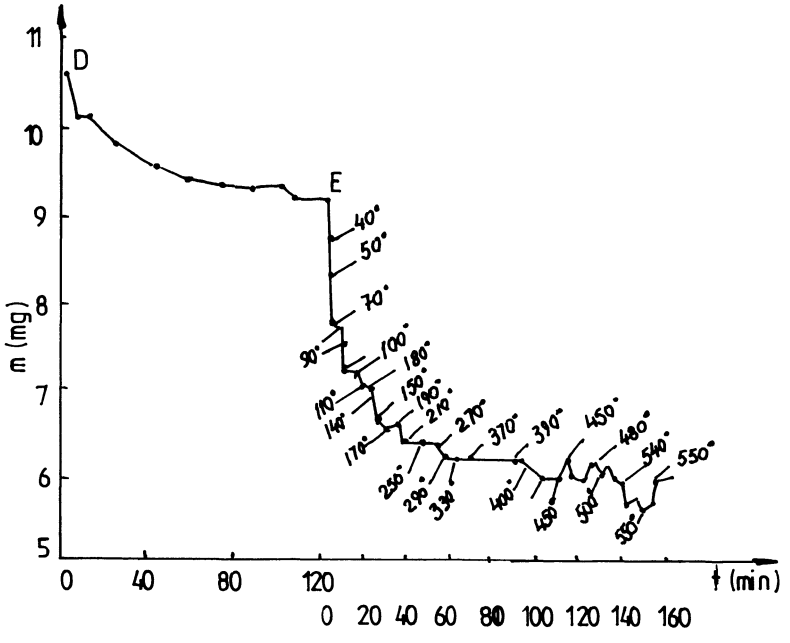

Figure 2.- Behaviour of the catalyst to heating with temperature programing to 550°C, in air, after iradiating with UV radiations.
DE - decrease in weight of the catalyst during irradiation.

Zeolites modified with Ag can be used at water dissociation in hydrogen and oxygen :

$$2Ag^{+} + 2ZO^{-} + H_2O \xrightarrow{h\gamma} 2Ag^{0} + 2ZOH + \frac{1}{2}O_2$$

zeolite with Ag^{+} ions

The OH groups are lost after a thermal treatment and H_2 is evolved. (Zamaraev et al, 1980)

$$Ag^{0} + ZOH \xrightarrow{t^{o}} Ag^{+} + ZO^{-} + \frac{1}{2}H_2$$

The results of hydrogen evolution by decomposition of water in presence of Fe-H mordenites are given in table 1.

After effecting one experiment of succesive H_2 generation the catalyst undergone a second process of activation, followed by the reaction. The steps generation stages of H_2 are refer to hydrogen volumes collected succesevely in a reaction cycle.

Table1.Hydrogen volumes generated over FeH- mordenites according to the process.

Activation no.	H_2 generating stage	Produced H_2 (ml)	
		on stages	total after activation
I	1	0,210	0,390
	2	0,165	
	3	0,012	
	4	0,003	
	5	0,001	
II	1	0,140	0,388
	2	0,126	
	3	0,090	
	4	0,030	
	5	0,002	
III	1	0,185	0,387
	2	0,102	
	3	0,083	
	4	0,012	
	5	0,005	

IV	1	0,163	0,410
	2	0,127	
	3	0,088	
	4	0,021	
	5	0,011	
V	1	0,209	0,390
	2	0,102	
	3	0,059	
	4	0,013	
	5	0,007	
VI	1	0,199	0,370
	2	0,099	
	3	0,046	
	4	0,020	
	5	0,006	
VII	1	0,213	0,390
	2	0,101	
	3	0,061	
	4	0,011	
	5	0,004	
VIII	1	0,234	0,462
	2	0,082	
	3	0,073	
	4	0,064	
	5	0,009	
IX	1	0,201	0,390
	2	0,104	
	3	0,063	
	4	0,016	
	5	0,006	
X	1	0,203	0,338
	2	0,084	
	3	0,042	
	4	0,009	
	5	0,000	

The 2nd and 3rd columnes of table 1 suggest that the hydrogen volume collected in the last stage of one reaction cycle is much less than in the first, which denotes a deactivation of the catalyst during the reaction. This finding imposed the catalyst activation by another cycle. From the table 1 it is noticed that after 10 activations, the catalyst does not present any tendency of weaking its efficiency.

Conclusion

A low degree of water conversion in hydrogen in a cyclic process was developed, use has been made of an experimental device which affords the measuring the mass variation of zeolites during irradiation with UV light.

Acknowledgement

The author is much indebted to dr.Gr. Pop for the synthesis of zeolites.

References

Anpo,M., Negishi,N., and Nishiguchi,H. ,(1993) Critical Reviews in Surface Chemistry, 3(2), 131-169.

Murakami,Y.,Iijina,A., and Ward, J.W.,(1986) *Proceedings of the 7th International Zeolite* Conference, Tokio.

Meier,W.M., and Olson,D.H.(1992) *"Atlas of Zeolite Structure Types"*, Third Revised Edition, Ed. Butterworth-Heinemann.

Zamaraev,K.I. and Parmon V.N.(1980) Catal. Rev. 22(2), 261-324.

RUTHENIUM CATALYSTS FOR HIGH TEMPERATURE SOLAR REFORMING OF METHANE

A. BERMAN and M. EPSTEIN
Weizmann Institute of Science,
Solar Research Facilities Unit,
Fax : (972) 8 9344117;
E-mail : jhberman@wis.weizmann.ac.il

1. Introduction

The reforming of CH_4 with CO_2 is a the highly endothermic reaction (1) :

$$CO_2 + CH_4 = 2CO + 2H_2 \qquad \Delta H = -247 \text{ kJ/mole} \qquad (1)$$

The process can be a promising energy carrier and a method to produced chemicals. When the energy required to drive the reaction comes from renewable source, such as solar, the CO_2/CH_4 reforming has potential to play a significant role in reducing CO_2 emissions (Edwards et al, 1995). Catalysts based on Rh metal were used previously for reforming reactions in Solar Chemical Heat Pipe at Weizmann Institute (Levy et al.,1993). The reforming of methane with CO_2 was investigated on Ru catalysts supported on alumina. The kinetics of the CO_2/CH_4 reforming on the $1\%Ru/Al_2O_3$ catalyst was studied. The appropriate kinetic models were developed. The results of long term tests show that $1\%Ru/\gamma\text{-}Al_2O_3$ (Engelhard) catalyst was the most suitable for a pilot 350 kW tube reactor (Berman et al.,1996).

Solar volumetric reactors are capable of higher rates of heat transfer, are operated at high temperatures (above 1000 °C), and higher conversions can be reached. In the vicinity of 1000 °C and in the presence of water, the specific area of the gamma form of alumina is strongly decreased. This phenomena is associated with the transformation of γ-alumina into alpha phase. The thermal stability of the metallic catalysts can be improved by decreasing the rate of diffusion and phase transformation. Rare earth based promoters and alkaline-earth metal ions have been described in the literature in connection with this matter (Beguin et al., 1991). In the present paper the reforming of methane with CO_2 on Ru/Al_2O_3 catalysts promoted with Ceria is described. Effects of Ce on the activity and thermal stability of the catalysts were studied. Data for unpromoted Ru catalysts are given for comparison.

2. Experimental

The Ru catalysts (supported on alumina) promoted by Cerium Oxides were tested in flow system. The following Ru catalysts were prepared in our laboratory:

T. O. Saetre (ed.), Hydrogen Power: Theoretical and Engineering Solutions, 213–218.

1) Ru/Al_2O_3 catalysts containing 0.25, 0.5 , 1 and 2%Ru
2) Ru/Al_2O_3 catalysts containing 2%Ru and 2, 5, 7 ,10, and 20% Ce
3) Ru/Al_2O_3 catalysts containing 1%Ru and 0.5, 1, 2, and 5% Ce

The Ru catalysts were prepared by impregnation of support (gamma alumina Harshaw, A1-3438 T1/8", surface area 180 m^2/g) with ruthenium nitrosyl nitrate solution, followed by drying at 120 ^oC for 10 h and reduction at 375-450 ^oC under hydrogen/argon mixture. The Ru-Ce catalysts were prepared by two stage impregnation : first stage- with ruthenium nitrosyl nitrate solution, followed by drying at 150 ^oC for 10 h and second stage-impregnation with ammonium ceric nitrate (BHD) solution.

A flow setup was used for catalyst testing at high temperatures (900-1200 ^oC).

Active surface of Ru catalysts and size of Ru particles were measured by method of hydrogen thermal desorption. The results are given in Table 1.

TABLE 1. Hydrogen adsorption on Ru/ Al_2O_3 catalysts

Catalyst	Adsorption, H_2 ncc/g	Dispersion, H/Ru	Particle size, nm
0.25%Ru/Al_2O_3	0.16	0.58	1.56
0.5%Ru/Al_2O_3	0.14	0.5	1.8
1%Ru/Al_2O_3	0.33	0.3	3.0
2%Ru/Al_2O_3	0.57	0.26	3.4
2%Ru+7%Ce on Al_2O_3	0.84	0.4	2.2

3. Activity of Ru catalysts

The Ru/Al_2O_3 catalyst containing 0.25, 0.5, 1 and 2% Ru were tested for CO_2 reforming of methane at pressure 4 ATM in the temperature range of 450-1050 ^oC.

Fig.1 shows that the rate of total methane conversion increased with the increase in

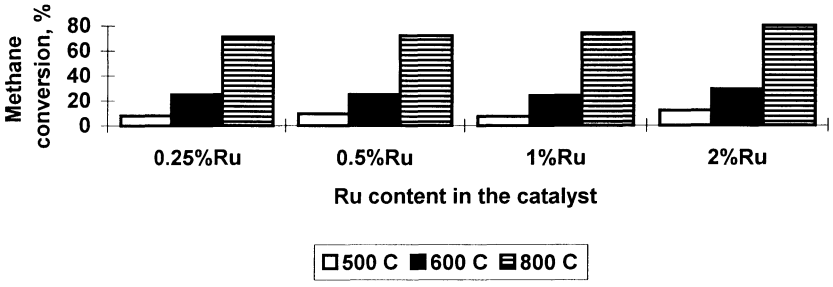

Figure 1. Methane conversions in reforming with CO_2 for different metal loading at temperatures of 500, 600, 800 ^oC and at a pressure of 4 ATM.

loading over the range of 0.25-2% wt. However, although the increase in the overall rate of reforming of methane was observed, the activity per 1 mg of metal decreased with the

increase in Ru loading. The Ru/Eu_2O_3, Rh/Al_2O_3, Rh/SiO_2, Rh/TiO_2 catalysts also showed the same trend (Zhang et al.,1996). Dispersion of the Ru metal on Al_2O_3 decreases (from 0.58 to 0.25) and particle size increases (from 1.6 to 3.4 nm) with increase in Ru loading (Table 1). It can be suggested that CO_2/CH4 reforming on Ru catalysts is a structure- sensitive reaction, where the specific rate of reaction (per Ru atom) decreases with increasing Ru particle size. The higher the dispersion, the higher is the metal-support interaction, which results apparently in an enhanced rate of reaction.

4. Activity of the Ru catalysts promoted with Ceria.

The activities of the Ru/Al_2O_3 catalysts promoted with Ceria were investigated in flow system. The 0.25- 2% Ru catalysts supported an alumina with different content of promoter were prepared and tested in laboratory. The results for catalysts containing 2% Ru and 2,5,10 and 20% wt Ce are shown in Fig. 2

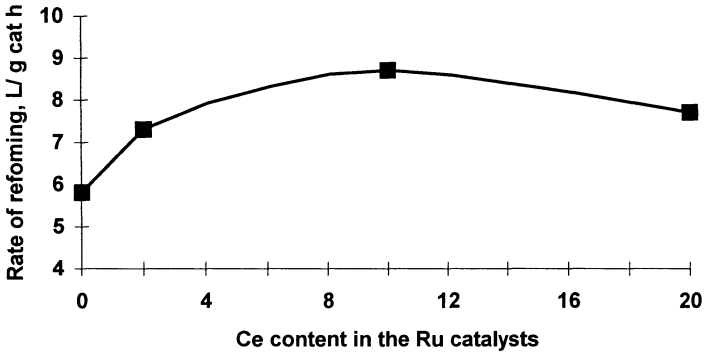

Figure 2. Plot rate of CO_2/CH_4 reforming- Ce content in the 2%Ru /Al_2O_3 catalysts, obtained at temperature of 800 °C and pressure of 3 ATM. CO_2 /CH_4 ratio = 1.2.

It can be seen that rate of reaction has a maximum at about 10 % of Ce content. Ce/Ru molar ratio in the sample with maximum activity is 3.6. The dispersion H/Ru is increased (from 0.26 to 0.4 for the 2%Ru+7%Ce sample) by the addition of Ce (Table 1.). The catalysts containing 1%Ru and 0.5-5% wt Ce were also tested. The results are shown in Fig. 3. It can be seen that maximum activity was obtained on 1%Ru+0.5%Ce/Al_2O_3 catalyst with Ce/Ru molar ratio = 0.36. It can be concluded that the effect of Ceria in Ru/Al_2O_3 catalysts depends not only on Ce/Ru molar ratio but on the Ru content in the catalyst.

For explaining the data obtained , the model proposed for ammonia synthesis (Murata et al., 1992) can be used. It can be assumed that lanthanide nitrate is decomposed into oxide over Ru surface.

$$2M(NO_3)_3 + 24H_2 \xrightarrow{Ru} M_2O_3 + 6NH_3 + 15H_2O \qquad (2)$$

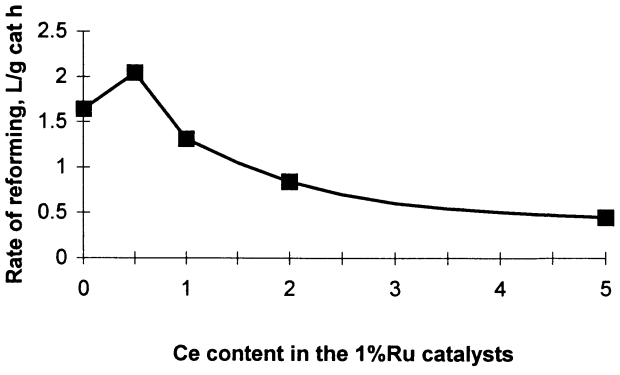

Figure 3. Rates of CO_2/CH_4 reforming on 1%Ru /Al_2O_3 catalysts containing Ce at 600 °C.

The oxide is considered to be the final state, as suggested by XPS results. The oxide is quite stable . The melting point of Ce_2O_3 is high (1965±50K) and its mobility at least at temperatures 500-700°C must be low . So, lanthanide oxide formed on the Ru surface or on the Ru-Al_2O_3 boundaries cannot spread easily to the support. Lanthanide ions have a large ionic radius in spite of their high valence (+3). Under the reducing conditions of this reaction, the Ru atom might be negatively charged through contact with lanthanide oxides.

$$Ru - -Ru - M \Leftrightarrow Ru^- - Ru^- - Ru^- - M^{3+} \cdot$$

This can increase in catalytic activity of the promoted Ru catalysts at low Ce content. It can be assumed that high content of Ceria can block the active centers and decrease the catalytic activity .

5. Deactivation of Ru catalysts at high temperatures

Fig.4. show effect of Ru content in the catalysts on deactivation after high temperature test (reaction at 1050 °C for 5 h). It can be seen that the rate of deactivation of Ru/Al_2O_3 catalysts decreased with an increase in Ru loading. So, a reduction of Ru particle size results in an enhanced rate of deactivation. Experiments were carried out to estimate rate of deactivation of 1%Ru catalysts supported on alumina at temperature of 1100°C. The activity of the fresh samples were measured in the temperature range of 500- 1100°C at pressure 4 ATM, CO_2/CH_4 ratio was 1.3. These experiments were repeated at 1100 °C for t hours (t = 0.25; 3 and 8 h) followed by cooling to room temperature. The results are presented in Fig. 5. . It can be seen that the Ru/Al_2O_3 catalysts are deactivated sharply after reaction at 1100 °C. Carbon deposition was observed after the reaction at high temperature.

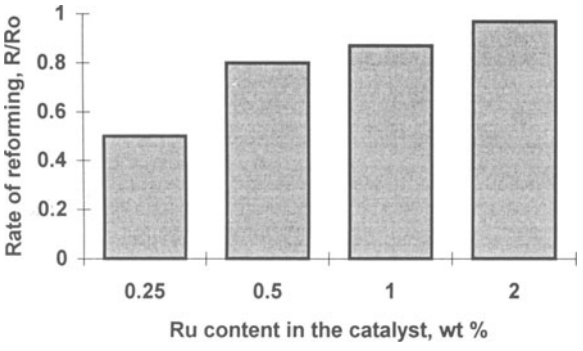

Figure 4. Rate of hydrogen formation (related to the rate for fresh sample) measured at 600 °C after reaction at 1100 °C for 5 hours as a function of the Ru content in the catalyst supported on alumina..

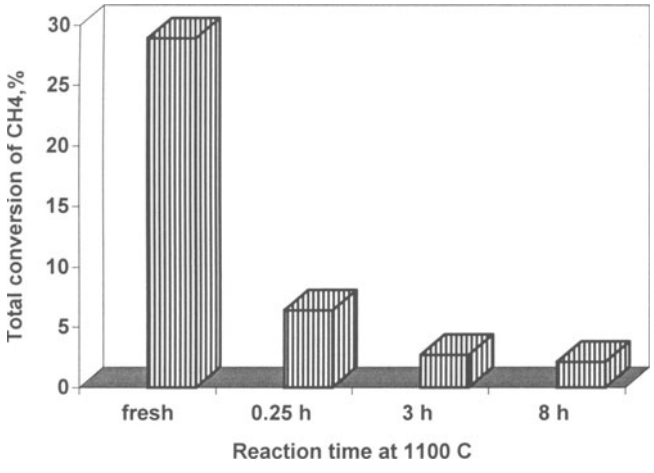

Figure 5. Deactivation of the 1%Ru/γ-Al_2O_3 catalyst after reaction at 1100 °C ; CO_2/CH4 ratio=1.3. The methane conversions were measured at 600 °C.

6. Deactivation of Ru catalysts promoted with Ceria

High temperature stability test was carried out on 1%Ru+5%Ce catalyst under the conditions mentioned above (reaction at 1100 C for 8 hours). The results were presented in Fig.6. It can be seen that activity is increased several-fold after reaction at temperature 1100 °C for 0.5 h followed by slow deactivation. Comparison of Fig.5 and

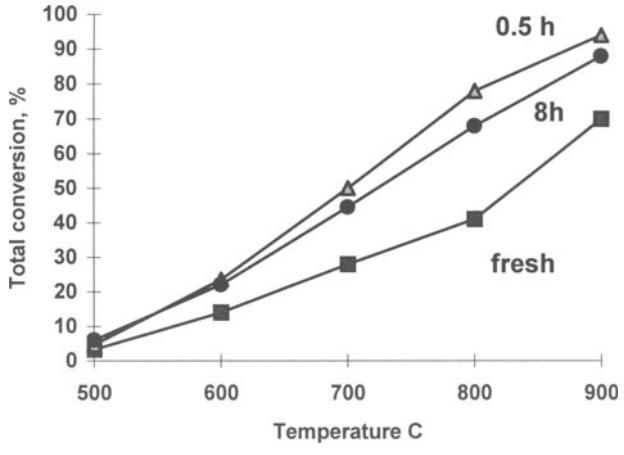

Fig 6. Reforming of methane with CO_2. High temperature test of 1%Ru+5%Ce/Al_2O_3 catalyst. The total CH_4 conversion as a function of temperature for the fresh sample and after reaction at 1100 °C for 0.5 and 8h. Pressure was of 4 ATM.

Fig. 6 show that addition of Ce increases substantially the thermal stability of Ru catalysts supported on alumina.

The following explanation is suggested. Ceria can slow the sintering by anchoring small Ru particles on the support and decreasing rate of diffusion. Mobility of Ceria increases when temperature increases. Ceria can migrate at high temperatures from the Ru surface to the Ru-alumina boundaries. At high Ce content this could reduce blocking of the active centers and increasing the catalytic activity.

It can be concluded that the active centers of the promoted Ru-Ce catalyst supported on alumina have a dynamic structure which can be changed in the course of reaction.

7. References

Beguin, B., Garbovski, E. and Primet, M. (1991) Stabilization of alumina toward termal sintering by silicon addition, *J. Catalysis* **127,** 595-604.

Berman, A., Levitan, R., Epstein, M. and Levy, M (1996) Ruthenium methanation and reforming catalysts for solar chemical heat pipe, *Proc. of the ASME 1996 Int. Solar Energy Conference*, San Antonio, Texas, 1996, pp.61-69.

Edwards, J. H. and Maitra, A.M. (1995) The chemistry of methane reforming with carbon dioxide and its carrent and potential applications, *Fuel Processing Technology* ***42***, 269-289.

Levy, M., Levitan, R., Rosin, H. and Rubin, R. (1993) Solar energy storage via closed loop chemical heat pipe, *Solar Energy* **50,** 179-189.

Murata, S. and Alka, K. (1992) Preparation and characterization of chlorine-free ruthenium catalysts and the promoter effect in ammonia synthesis, *J. Catalysis* **136,** 118-125.

Zhang, Z.L., Tsipouriari, V. A., Efstathiou, A. M. and Verykios, X. E. (1996) Reforming of methane with carbon dioxide to synthesis gas over supported rhodium catalysts, *J. Catalysis* **158**, 51-63.

HYDROGEN PRODUCTION FROM HYDROGEN SULFIDE USING MEMBRANE REACTOR

HARUHIKO OHYA, HIROFUMI OHASHI,
MASAHIKO AIHARA and YOUICHI NEGISHI
Department of Material Science and Chemical Engineering
Yokohama National University
79-5 Tokiwadai, Hodogaya-ku, Yokohama 240, JAPAN

1. Abstract

For the purpose of separating hydrogen from the thermal decomposition process of hydrogen sulfide using membrane reactor at high temperature, zirconia (90mol%)-silica (10mol%) composite membranes coated on porous ceramic tubing were investigated from 298K to 1023K.

Using the composite membrane for the thermal decomposition of hydrogen sulfide at 1023K, it was found that the maximum hydrogen conversion in the permeation side was 22.6[%] and that of feed side was 5.0 [%].

2. Introduction

One of the components of air pollution is sulfur dioxide produced by combustion of oil containing organic sulfur, therefore this problem demands the removal of sulfur from crude oil. Nowadays, it is done by hydrosulfurization which produce hydrogen sulfide as an unavoidable by-product in a petroleum refinery. In general, hydrogen sulfide is partially oxidized by the Claus process where valuable product is only elementary sulfur. As an alternative process, hydrogen recovery from the thermal decomposition of hydrogen sulfide to hydrogen and elementary sulfur using membrane reactors, has been proposed[1].

$$H_2S = H_2 + 1/2\ S_2 \qquad (1)$$

The recovery of hydrogen from the thermal decomposition of hydrogen sulfide enables to recycle hydrogen for hydrosulfurization without supplying hydrogen.

Kameyama et al. [2,3] reported that the use of a microporous Vycor type glass membrane and a new microporous alumina membrane, at the thermal decomposition of

T. O. Saetre (ed.), Hydrogen Power: Theoretical and Engineering Solutions, 219–223.

hydrogen sulfide has increased the yield of hydrogen continuously by about two times of equilibrium one. And a study using a composite metal membrane reactor for thermal decomposition of hydrogen sulfide has been reported by Edlund et al.[4].

In this study, zirconia-silica composite microporous membrane, which might withstand a highly corrosive gas, H_2S, were prepared in order to investigate the possibility of separating hydrogen from the gaseous mixture which is produced from the thermal decomposition process of hydrogen sulfide.

3. Experimental

3.1. MEMBRANE PREPARATION

A thin microporous ZrO_2-SiO_2-Y_2O_3 layer was coated on the surface of a porous ceramic tubing, the dimensions of which were 5.5mm o.d. and 3.5 mm i.d., and the average pore diameter was 0.5 μ m (supplied by Toto Co. Ltd.), using the same method as reported earlier [5].

3.2. APPARATUS

A schematic flow diagram of the experimental apparatus is shown in Fig. 1. All tubing were made of 316 stainless steel and the cell was made of 310S stainless steel. The dimensions of cell containing the composite membrane were 27mm i.d. and 350mm in length.

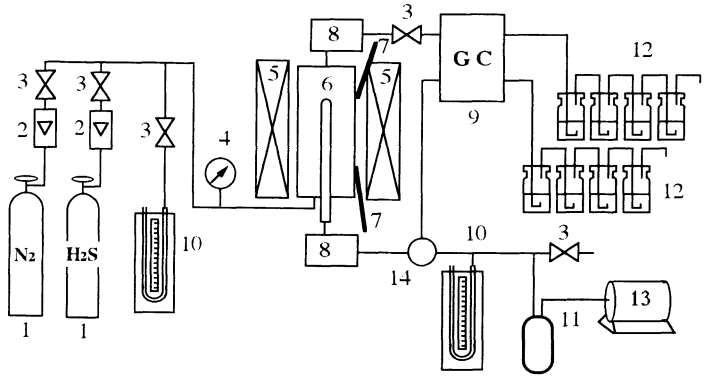

1 GAS CYLINDER
2 FLOW METER
3 PRESSURE CONTROL VALVE
4 PRESSURE GAUGE
5 ELECTRIC FURNACE
6 MEMBRANE
7 THERMO COUPLE
8 SULFUR CONDENCER
9 GAS CHROMATOGRAPH
10 MANOMETER
11 COLD TRAP
12 GAS WASHING BOTTLE
13 VACCUME PUMP
14 6-WAY COCK

Fig. 1 A schematic flow diagram of the experimental apparatus.

3.3. EXPERIMENTAL METHOD

3.3.1 Permeation of Pure Gas

Before introducing pure gas into the system, the whole system was kept evacuated for 10h, and then each feed pure gas of H_2, N_2, H_2S was introduced from each gas cylinder into the cell. The pressure of the cell was controlled by the pressure-control valve. The pure gas permeation rates were measured by the soap-bubble flowmeter.

3.3.2 Separation of H_2 - H_2S Gaseous Mixture

The permeation characteristics of H_2 - H_2S gaseous mixture (approximate feed composition were 5 and 95 mol% respectively) were measured at room temperature. In the separation experiment of H_2 - H_2S gaseous mixture, pure H_2 and H_2S were introduced from each gas cylinder into the cell, feed composition were controlled by adjusting the feed rate. The operating pressures of feed side were controlled the range of 0.1 to 0.2 MPa absolute and that of permeation side was kept 5.3 kPa absolute using the pressure-control valve and vacuum pump. The composition of gaseous mixture at the feed side and permeation side were analyzed with gas chromatography (GC-8A, Shimadzu Co., Ltd.) using Porapak Q column (GL Sciences Inc.).

3.3.3 Reaction Experiment

Reaction experiment of H_2S was carried out under the condition as follow: reaction temperature 923-1023K, operating pressure of feed side 0.1-0.25 MPa absolute and that of permeation side 5.3 kPa absolute, superficial space velocity 0.05 and 0.10 s^{-1}. A product sulfur was removed continuously using a trap cooled by a ice. The composition of gaseous mixture at the feed side and permeation side were analyzed with gas chromatography.

4. Results and Discussion

4.1. PURE GAS PERMEANCE

The results and discussion of the pure gas permeation experiment is to be published.

4.2. SEPARATION OF H_2-H_2S GASEOUS MIXTURE

The results and discussion of the separation experiment of H_2-H_2S gaseous mixture is to be published.

4.3. REACTION EXPERIMENT

4.3.1 Effect of the Transmembrane Pressure

Figure 2 shows the relationship between H_2 conversion (defined as the following equation) and T.M.P. at 1023K and at 0.05 s^{-1} of superficial space velocity.

$$H_2 \text{ conversion } [\%] = \frac{J_{H2}}{J_{H2S} + J_{H2}} \times 100 \quad (2)$$

As shown in Fig. 2, the H_2 conversion at the permeation side decreased with increase of T.M.P.. And H_2 conversion at the feed side decrease slightly with increase of the T.M.P.. This decrease is caused by the fact that the equilibrium constant of decomposition of H_2S decrease with increase of the T.M.P.

4.3.2 Effect of the Reaction Temperature

Figure 3 shows the relationship between H_2 conversion and the temperature at 0.105 MPa of T.M.P. and at 0.10 s^{-1} of superficial space velocity. As shown in Fig. 3, H_2 conversion at permeation side were higher than the equilibrium conversion for each temperature.

4.3.3 Effect of the Superficial Space Velocity

Figure 4 shows the relationship between H_2 conversion and the superficial space velocity at 0.105MPa of T.M.P. and at 1023K.

As shown in Fig. 4, H_2 conversion of 22.6 [%] were obtained at permeation side compared to 5.0[%] at feed side under the condition of superficial space velocity 0.05s^{-1}.

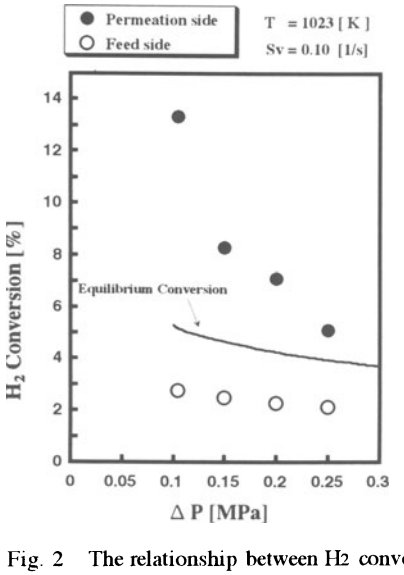

Fig. 2 The relationship between H_2 conversion and T.M.P. at 1023K and at 0.05 s^{-1} of superficial space velocity.

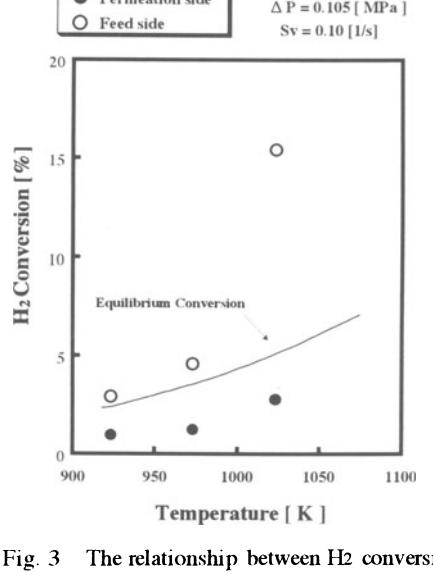

Fig. 3 The relationship between H_2 conversion and the temperature at 0.105 MPa of T.M.P. and at 0.10 s^{-1} of superficial space velocity.

5. Conclusion

It was found that the membrane reactor integrated by zirconia composite membrane gave H_2 conversion of 22.6 at permeation side under the reaction condition of T.M.P. 0.105MPa, temperature 1023K, superficial space velocity 0.05 s^{-1}.

6. Nomenclature

J_i flux of component i [mol / m^2 · s]

7. References

[1] M.E.D.Raymont (1975) Make hydrogen from hydrogen sulfide, Hydrocarbon Processing **July**, 139-142.

[2] T.Kameyama, M. Dokiya, M. Fujishige, H. Yokokawa and K. Fukuda [1981] Possibility for effective production of hydrogen from hydrogen sulfide by means of a porous Vycor glass membrane, Ind. Eng. Chem. Fundam. **20**, 97-99.

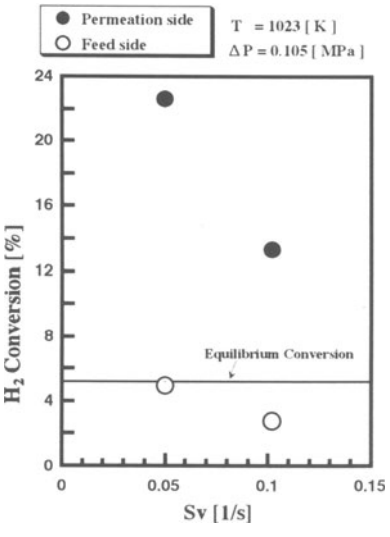

Fig. 4 The relationship between H_2 conversion and the superficial space velocity at 0.105 MPa of T.M.P. and at 1023K.

[3] T.Kameyama, K. Fukuda, M. Fujishige, H. Yokokawa and M. Dokiya (1983) Production of hydrogen from hydrogen sulfide by means of selective diffusion membrane, Int.J.Hydrogen Energy **8** (1), 5-13.

[4] D. J. Edlund and W. A. Pledger (1993) Thermolysis of hydrogen sulfide in a metal-membrane reactor, J.Memb.Sci. **77**, 255-264.

[5] H. Ohya, H. Nakajima, N. Togami, M. Aihara and Y. Negishi (1994) Separation of hydrogen from thermochemical processes using zirconia-silica composite membrane, J. Memb. Sci. **97**, 91-98.

THE BEHAVIOUR UNDER VACCUM AND UV IRRADIATION OF SOME Ag ZEOLITES USED IN HYDROGEN GENERATION

GR. POP* and MAGDALENA MOMIRLAN**
* Zecasin,Spl. Independentei 202 cod 77208 Bucharest, Romania
** Institute of Physical Chemistry "I.G.Murgulescu"
Spl. Independentei 202 cod 77208 Bucharest, Romania

Abstract

Microgravimetric measurements of zeolite mass variation zeolite during irradiation were carried out at the same time with a study on the temperature increase during irradiation.

The diagrams of Ag zeolites mass variation versus time over temperature range 40-550°C in vacuum under UV irradiation were plotted.

This characterization aims at selecting the activation method of the zeolit before every experiment of hydrogen generation.

Introduction

In the process of hydrogen generation over zeolites, their pretreatment before reaction plays an important role.

Silver zeolites can be used for water decomposition in hydrogen and oxygen. The process consists in a photochemically induced reduction of the Ag^+ from zeolite, followed by an oxidative thermal desorbtion of hydrogen at 600°C and $1 \cdot 10^{-5}$mm Hg:

$$2Ag^+ + 2ZO^- + H_2O \xrightarrow{h\nu} 2Ag^0 + 2ZOH + \frac{1}{2}O_2$$

$$Ag^0 + ZOH \xrightarrow{600°C} Ag^+ + ZO^- + \frac{1}{2}H_2$$

There are no indications regarding the utilization of this process at a larger scale than in laboratory. [1]

The technical literature describes a cyclic process for hydrogen evolution from water according to which water steam is fed at over 500°C and over 10 at in a vessel containing a hydrated mordenite with big pores (cylindrical channels with a cross-section of 7...7.3 Å) and the Si/Al of 5...30 ratio; the mordenite contains the metal cation (in a higher oxidation state) selected from the group : Cu, Cr, V, Fe, Co, Ni, Ho, Pm, Yb, Eu, In,

T. O. Saetre (ed.), Hydrogen Power: Theoretical and Engineering Solutions, 225–230.

Ti, Ru and Rh. Oxygen is produced and the metal cation is reduced to an lower valence; mordenite is not dehydrated; the solid reaction product from the first vessel is transferred to a second reaction vessel at 200°....400° and a pressure of over 10 at in order to induce the hydrogen generation and the cation oxidation from the mordenite to a higher valence. The cycle thus achieved can be repeated several hundred times. [2]

However, this process operates at high pressures in order to avoid the zeolite dehydration and to determine the cation reduction at a lower valence. Pressure is obtained by help of steam, the partial hydrogen pressure representing only an extremely small fraction in this atmosphere, corresponding to the very low degree of conversion of water in hydrogen; technically, obtaining of this pressure rises difficulties amplified by the degradation of the metallic materials by steam.

The process established by us eliminates the above mentioned disadvantages by effecting continuos water decomposition in moderate vacuum up to 10^{-2} mm Hg, and temperatures up to 500°C. [3]

Experimental

Measurements were effected both in vacuum as well as under UV irradiation.

The Ag zeolites weight variation has been determined with a Sartorius type electronic microbalance connected to a vacuum line [4]. By help of on electronic microbalance to which an irradiation system of Ag zeolites was added, the mass variation of samples and the temperature rise of zeolites during irradiation were measured.

Results and discussion

Three Ag zeolites were used:
HZSM-5 with 4% Ag(Z1), HZSM-5 with 6% Ag(Z2) and HY with 20% Ag (ZY_{Ag-1}).

Measurements of the evolution of zeolites weight variation were effected both in vacuum as well as during irradiation.

The diagrams of zeolites weight loss were plotted versus time.

It was noted that at vacuum outgasing, the weight loss is more advanced if the reaction was occurred at a temperature higher than room temperature .

Fig.1 shows the weight loss at room temperature in case of zeolite Z1. (4% Ag) while in fig.2 is represented the weight loss of the same zeolite at outgasing in vacuum at 300°C.

Figures 1 and 2 suggest that, at vacuum outgasing, the weight loss is stronger in the former ten minutes. This behaviour is not dependent on the temperature at which vacuum outgasing takes place.

At vacuum outgasing the proportion of weight loss depends on the type of zeolite, and on the metal modified. Figures 2 and 3 present mass variation diagrams for two different zeolites. The weight decrease is different and depends on the quantity of silver percentage. In zeolite Z2 (6% Ag) the weight loss at vacuum outgasing at 300°C is higher than in zeolite Z1 (4%Ag).

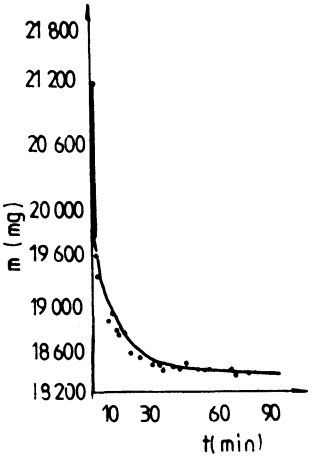

Figure 1. Weight decrease of zeolite Z1 as a function of time during vacuum outgasing at room temperature.

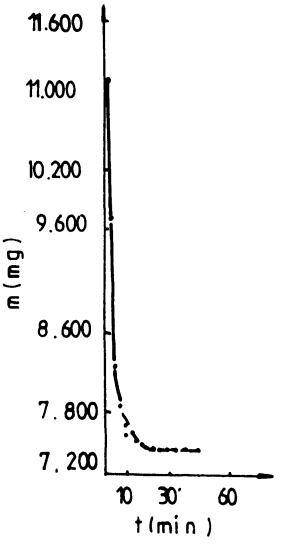

Figure 2. Weight loss of zeolite Z1 as a function of time during vacuum outgasing at 300°C.

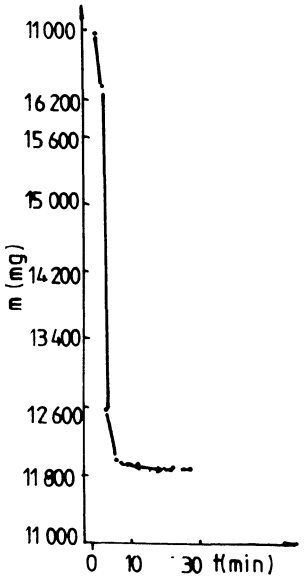

Figure 3. Time dependence of Z2 weight loss during vacuum outgasing at 300°C

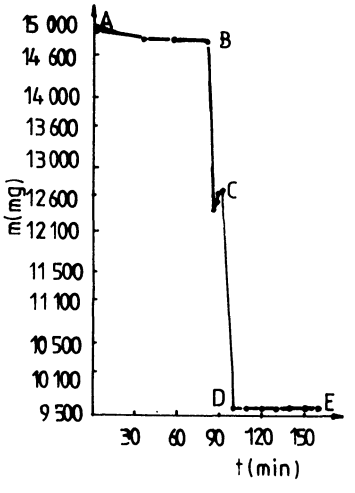

Figure 4. Weight decrease of zeolite Z2 in air (AB), vacuum (BC) and nitrogen (DE) at 400°C

The behaviour of zeolite Z2 in vacuum and nitrogen at 400°C was examinated (fig. 4). In this case an insignificant weight loss was observed in air at solar light (AB) in the first 80 minutes. At vacuum outgasing an instantaneous weight loss was noted (BC) and in nitrogen atmosphere with heating at constant temperature, 400°C, a strong, decrease of zeolite weight was noted.

The experiments on zeolite ZY_{Ag-1} (20% Ag) were as follows: carried out the zeolite was subjected to vacuum outgasing and heated increasing temperature up to 550°C; the sample was taken out from the unit area kept in air in order to recover the initial weight and again subjected to heating up to 550°C. Another sample of the same type of catalyst was weighed, applied the same treatment , except that, this time, the zeolite, after being outgased, in vacuum , heated by temperature programming to 550°C and maintained in air in order to recover the initial weight. It was then subjected to UV irradiation for two hours and only afterwards subjected to programmed heating up to 550°C.

Fig. 5 and 6 represent the behaviour of zeolite ZY_{Ag-1} at programmed heating up to 550°C. The weight loss in programed temperature regime is higher than without.

The weight of Ag modified zeolite decreases during UV irradiation less than in case of its vacuum outgasing.

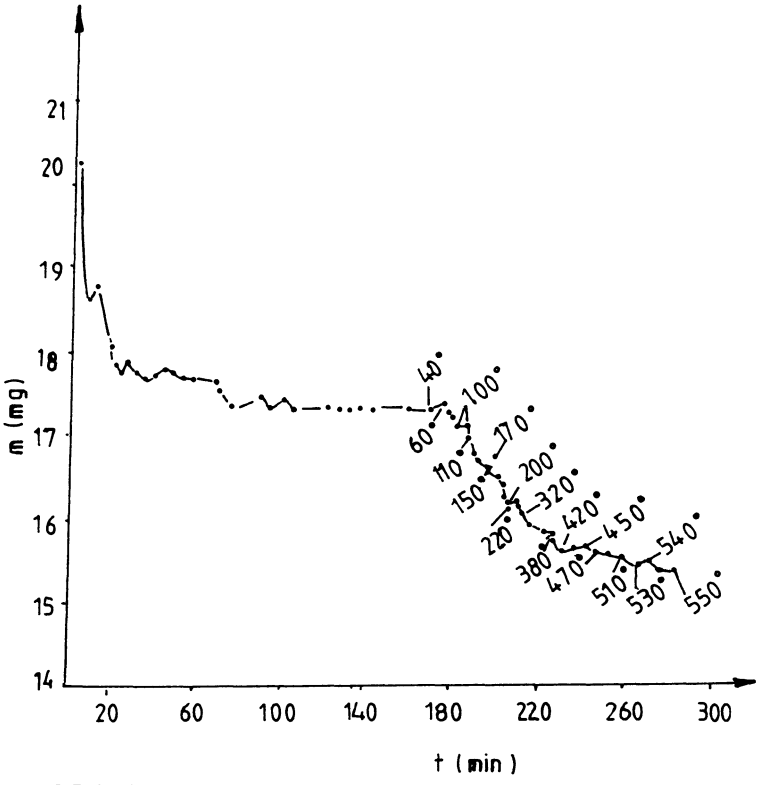

Figure 5. Behaviour of the catalyst ZY_{Ag-1} at heating up to 550°C in atmosphere. Cycle I.

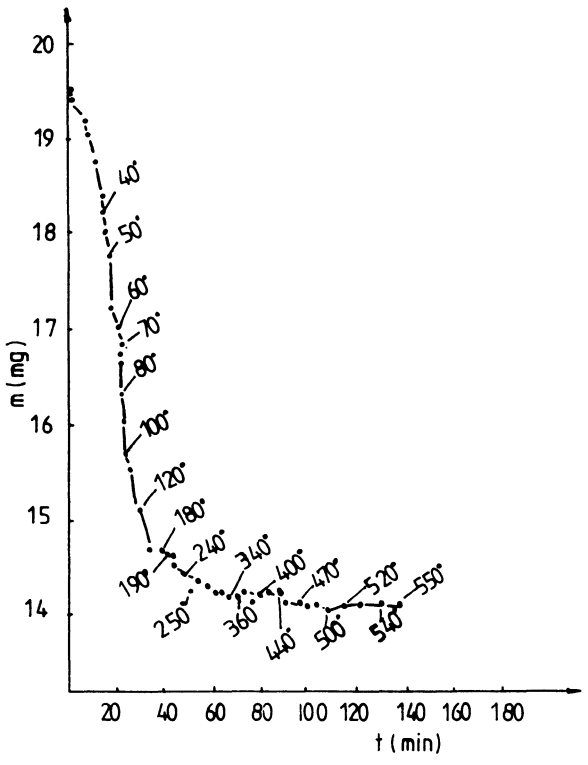

Figure 6. Behaviour of the catalyst ZY_{Ag-1} at programmed heating up to 550°C in atmosphere. Cycle II.

Conclusions

The characterization of some Ag zeolites with different Ag content (4%, 6% and 20%) is intended to select the activation method of zeolite before every experiment of hydrogen generation.

A zeolite is considered activated when the maximum decrease in weight is recorded, proving the complete elimination of water from intercrystalline channels.

In case of vacuum outgasing the weight loss is more important if temperature is higher than room temperature. The percentage of weight loss in vacuum depends on the type of zeolite. At the same type of zeolite, the weight loss depends on silver percent in the modified zeolite. The weight loss depends on Ag zeolites ranged within 5% -14%.

Microgravimetric measurements of zeolite mass variation during UV irradiation were carried out at the same time with the monitoring of temperature increase during irradiation. The weight loss of zeolites during irradiation should be assigned to the elimination of water molecules from zeolite.

In case the zeolites are subjected to ultraviolet radiation the distance between the sample and the irradiation source increases the temperature from room temperature to 70° C.

References

1. Jacobs P.A., Uytterhoeven J.B. and Beyer H.R., *J. Chem. Soc.*, **4**, 77, (1977)
2. Dorrance W.H., *USA Patent* nr. 4, 278- 650/ 14 Jul. 1981, Int. Cl. COL B1/08:COL B13/06
3. Pop Gr., Wohl A, Momirlan M., Musca G. and Georgescu S., *Romanian Patent* no. 95468 (1988).
4. Momirlan M., *Renewable Energy*, vol. **5**, p. 2588-2592, Ed. Pergamon Press. (1992)

PRESSURE AND TEMPERATURE EFFECTS ON WATER DISSOCIATION REACTION FOR HYDROGEN PRODUCTON OVER ZEOLITES

Magdalena Momirlan* and N. Boriaru**
* Institute of Physical Chemistry "I.G.Murgulescu"
Spl. Independentei 202,77208 Bucharest , Romania
** Politehnica University Thermotech. Dept.
Spl. Independentei 313, 79590 Bucharest, Romania

Abstract

Hydrogen was produced in a quartz reactor from overheated steam of water using zeolites activated at 500°C under a vacuum of 10^{-2}mmHg.

The pressure and temperature influences on hydrogen molar fraction evolved by water dissociation have been illustrated using a mathematical model based on Gibbs potential minimisation.

Introduction

In order to establish the mechanism of hydrogen evolution from water over zeolites the influence of reaction parameters on hydrogen generation was studied.

The main parameters of the reaction are: pressure and temperature.

The degree of water steam dissociation under the work conditions of the experimental equipment and the chemical equilibrium composition at constant pressure and temperature are important to be determined.

Experimental

Zeolite modified by impregnation with salts of some non-noble metals with variable valences, is introduced in a quartz weighing nacelle suspended in a quartz reactor. The reactor is equipped with a tube for introducing overheated steam, as well as with a tube for evacuation of the resulted gases and water steam; the latter is condensed by water cooling and the non condensable gases reach a collection phial; the collected gases are analysed periodically by gas chromatograph. In order to remove the air from the system (reactor and catalyst) the reactor is purged with an inert gas; collection of the whole quantity of hydrogen generated in reactor is also guaranteed by purging.To be heated, the reactor is introduced in an electric adjustable furnace. Temperature of catalyst is controlled by a Pt-PtRh thermoelement, whose warm welding is in the immediate vicinity of the nacelle with catalyst. After nitrogen or argon purging, the catalyst is activated by its gradual heating for 2 hours at 500°C under a vacuum of 10^{-2} mm Hg and by maintaining the temperature of 500°C and the mentioned vacuum, for 2 hours.

T. O. Saetre (ed.), Hydrogen Power: Theoretical and Engineering Solutions, 231–235.

The reactor is left to cool at room temperature under vacuum, after which it is gradually heated, by steam introduction starting from 200°C. Within 2 hours the temperature rises to 500°C. This temperature is maintained for 4 hours. The reactor is purged in the end with nitrogen or argon at 500°C.

Zeolites are porous crystalline solids and their formula are based essentially on tetrahedral networks which include channels and cavities.

Results and discussions

It's a well-known fact that the work conditions can influence on the chemical equilibrium in reactive systems.

To illustrate this influence on hydrogen production through water dissociation, a system with 6 constituent species (H_2O, H_2, O_2, OH, O, H) has been considered.

For each of the implied species, the molar free enthalpy in pure state is given by:

$$g_i^\circ = - R\ T \ln K_p \qquad (1)$$

so that the molar free enthalpy of one mixture component becomes:

$$g_i = g_i^\circ + R\ T \ln p_i \qquad (2)$$

and, consequently, the molar Gibbs potential of the system is :

$$g = \sum x_i\ g_i \qquad (3)$$

with ν_i the stoichiometric coefficient of i species in the given equation.

Searching for the solution minimising the Gibbs potential of the reacting system at the given conditions, and satisfying also the conservation law for the implied species, the adopted mathematical model (Rand [6]) permits, using the Lagrange multipliers method, to determine the chemical composition at equilibrium on the base of equilibrium constant ($K_p(T)$). [7].

The results presented in Table 1 show the temperature and pressure influence on the molar fraction of the hydrogen at equilibrium, at pressures varying between 0.35 and 2.45 bars and temperatures of 1800-2100 K.

Table 1. Molar fraction of H_2 evolved by water dissociation (p=0.35-2.45 bars, T=1800-2100 K)

pressure	Temperature [K]						
bars	1800	1850	1900	1950	2000	2050	2100
0.35	0.003	0.004	0.005	0.006	0.008	0.010	0.013
0.7	0.002	0.003	0.004	0.005	0.007	0.008	0.011
1.05	0.002	0.003	0.003	0.004	0.006	0.007	0.009
1.4	0.002	0.002	0.003	0.004	0.005	0.007	0.008
1.75	0.002	0.002	0.003	0.004	0.005	0.006	0.008
2.1	0.001	0.002	0.003	0.003	0.005	0.006	0.007
2.45	0.001	0.002	0.003	0.003	0.004	0.006	0.007

The diagrams from fig.1 are making this effect more evident.

In order to test the precision of the obtained solutions, a possible system of 6 parallel reactions has been considered[5]:

$$H_2 + 1/2\ O_2 = H_2O \quad (R1)$$
$$OH + 1/2\ O_2 = H_2O \quad (R2)$$
$$H_2 + O = H_2O \quad (R3)$$
$$H + OH = H_2O \quad (R4)$$
$$2\ O = O_2 \quad (R5)$$
$$2\ H = H_2 \quad (R6)$$

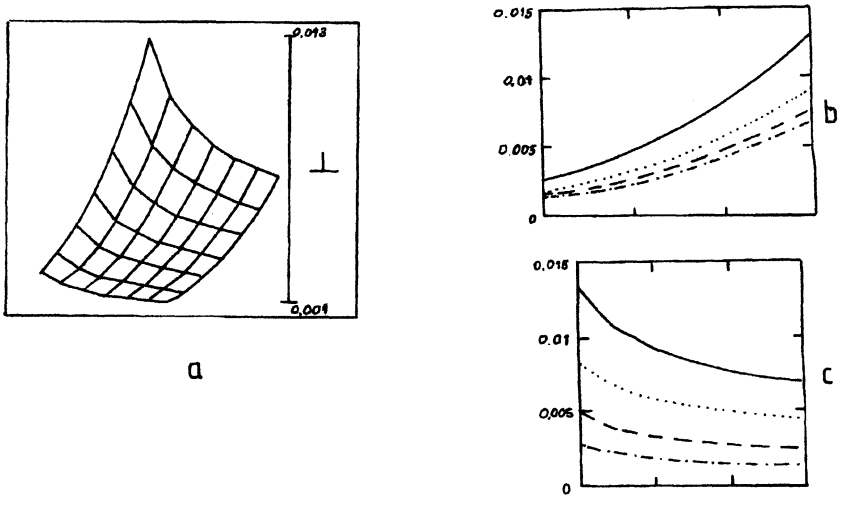

Figure 1 Pressure and temperature influence on molar fraction of H_2 at p=0.35-2.45 bars and T=1800--2100 K: a) combined effects; b) effect of temperature; c) effect of pressure

For each chemical reaction, the value of the equilibrium constant (K_p) calculated as function of the resultant partial pressures of the component species at equilibrium:

$$K_p = \prod p_i^{\nu_i} \quad (4)$$

has been compared to its value resulting from the Gibbs potential change through the same reaction:

$$K_G = \Delta G/RT \quad (5)$$

with:

$$\Delta G = \sum_{RH} \nu_i g_i - \sum_{LH} \nu_i g_i \quad (6)$$

For the solutions presented in Table 1, the coincidence between K_p values calculated in both ways, goes until the fourth-sixth decimal. As the molar fraction of the minor species diminishes at lower temperatures or higher pressures, the precision of the results tends to decrease also. To improve it, additional conditions have been imposed permitting the extension of the domain well reproduced by the mathematical model. As an illustration, Fig.2 shows the computed effect of the work conditions on the molar fraction of the hydrogen generated by water dissociation, between 0.35-1.75 bars and 1100-1400 K.

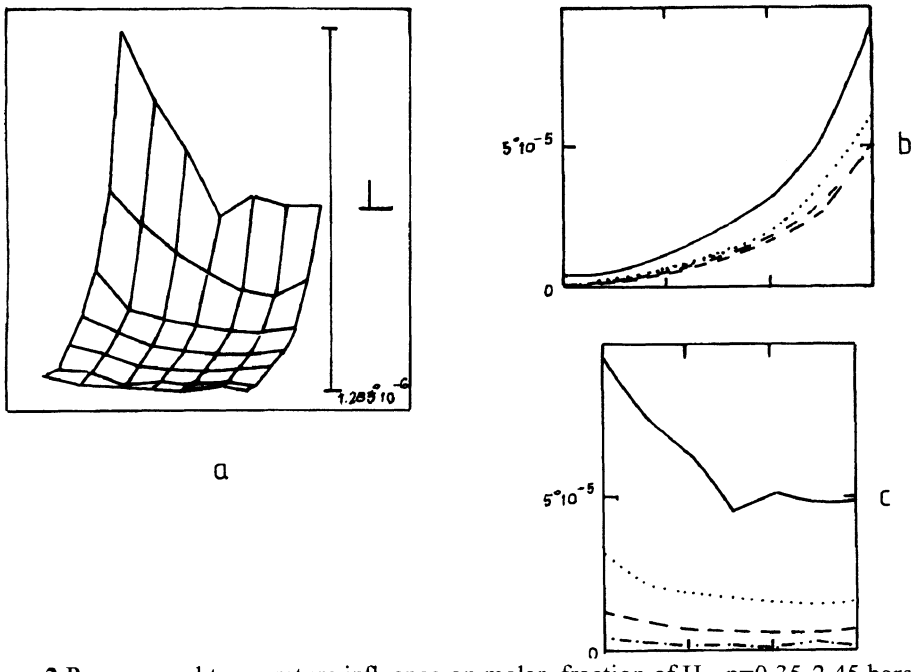

Figure.2 Pressure and temperature influence on molar fraction of H_2 p=0.35-2.45 bars, T=1100--1400 K a) combined effects b) effect of temperature c) effect of pressure

Nomenclature

ΔG [J] - Gibbs potential (free enthalpy) change through reaction
g_i [J/mole] - molar Gibbs potential of component i
g_i° [J/mole] - molar Gibbs potential of i species in pure state
ν_i[moles] - stoichiometric coefficient of component i for the given reaction equation
χ_i - molar fraction of i species
R [J/mole.K] - molar constant of the ideal gas
T [K] - absolute temperature
p_i [bar] - partial pressure of component i
K_G - equilibrium constant, as function of Gibbs potentials
K_p - equilibrium constant, as function of partial pressures

LH (RH) -left hand (right hand) of the chemical reaction equation

Around 800 K, the obtained results (Table 2), even if satisfactory as order of magnitude, were not good enough to give a proper representation of the pressure or temperature influence on the equilibrium composition.

Table 2. Molar fraction of H_2 $*10^{10}$, evolved by water dissociation, p=0.35-1.75 bars, T=800-860 K

pressure	Temperature [K]						
bars	800	810	820	830	840	850	860
0.35	0.595918	0.466159	0.732525	0.380824	0.408189	0.409435	0.320116
0.7	0.893662	0.540620	0.552001	0.508463	0.487409	0.445852	0.526549
1.05	1.397642	0.820794	0.747521	0.770890	0.738734	0.734550	0.858157
1.4	2.200459	1.190508	1.183685	1.294849	1.009653	1.008106	1.333342
1.75	3.237569	1.945206	1.688166	2.267602	1.612733	1.556945	2.033965

Further refinements of the calculation procedure will try to bring its precision at the requested level.

Conclusions

As expected the best molar fraction of H_2 obtained from water dissociation corresponds to the highest temperature and lowest pressure possible to be reached in the reaction vessel

The influence of pressure seems to be more effective under 1 bar as well as that of temperature over 2000K.

The mathematical model describes well these tendencies at higher temperatures (over 1800K). However further refinements of the calculation procedure are expected to bring a better precision at temperatures around 1000 K.

References

[1] Pop, Gr., Wohl, A., Momirlan, M., Musca, G., Georgescu, S. (1988). Romanian Patent no.95468.

[2] Momirlan, Magdalena. (1992). *Revue Roumaine de Chimie*, 37, 9, 1001-1006.

[3] Momirlan, Magdalena, Birjega, Ruxandra. (1996). *Hydrogen Energy Progress XI-Proc. 11th World Hydrogen Energy Conf., Stuttgart, Germany*, 3, 2631-2638.

[4] Greisinger, A., Spindler, K., Hahne, E. (1996). *Hydrogen Energy Progres XI-Proc. 11th World Hydrogen Energy Conf., Stuttgart, Germany,* 3, 2513-2522.

[5] Grunwald, B., Apostolescu, N. (1975). The Thermal and Chemical Inhomogeneity of the gases from the Internal Combustion Motors, E.A. Bucharest, 124.

[6] Murgulescu , I. G., Valcu, Rodica. (1982). Introduction in Chemical Physics, III-rd vol. Chemical Thermodynamics, E.A. Bucharest, 482-498.

[7] JANAF Thermochemical Tables. (1965). Daw Chemical Midland, 547-586.

[8] Momirlan, Magdalena (1992). *Renewable energy, technology and the environment-Proc. 2nd World Ren.Energy Congres*, 5, 2588-2592.

ELECTROCHEMICAL PERFORMANCE OF ZR-MN-V-NI BASED AB_2 LAVES PHASE ALLOYS AS THE NEGATIVE ELECTRODES OF NI/MH BATTERY

A. HUANG and T. -P. PERNG
National Tsing Hua University
Department of Materials Science and Engineering
Hsinchu, Taiwan

Abstract

The effects of composition modification on the electrochemical discharge properties were explored for the nonstoichiometric $ZrMn_{0.6}V_{0.2}Ni_{1.2}M_{0.05}$ (M= Fe, Ni, Cu, Al) C15 Laves phase alloy electrodes. Modification of $ZrMn_{0.6}V_{0.2}Ni_{1.2}Co_{0.1}$ by addition of a small amount of La was also made. The gas-phase hydrogenation pressure-composition-temperature (P-C-T) curves were used to evaluate the possible electrochemical performance. Among them, the Al-added composition exhibited the best discharge performance and the least pulverization after the cyclic test. The better performance is explained based on the electrochemical characteristic and particle morphology.

1. Introduction

The electrochemical performance of Ni/MH battery hinges on what negative electrode material is adopted. Two types of hydrogen storage alloys are frequently utilized as the electrode materials, namely, AB_2 and AB_5 alloys. Generally speaking, the AB_5 type alloys are recognized to have 250-300 mAh/g discharge capacity, whereas the discharge capacities of AB_2 alloys in the initial stage could reach as high as 300-400 mAh/g. Whether AB_5 or AB_2 alloys are selected, multicomponent alloys have been developed to satisfy the severe requirements as better electrode materials. For example, Wakao et al. proposed that the AB_2 type alloy $Zr(V_{0.33}Ni_{0.5}Mn_{0.17})_{2.4}$ exhibited a high capacity of 366 mAh/g [1]. $ZrMn_{0.3}Cr_{0.2}V_{0.3}Ni_{1.2}$, devised by Moriwaki et el., was reported to show a remarkable capacity of 360 mAh/g [2].

Previously, Hsu explored the effect of composition variation in Zr-Mn-Ni based C15-type alloys on the electrochemical performance and found that the composition $ZrMn_{0.6}V_{0.2}C_{0.1}Ni_{1.2}$ had high capacity and fast activation rate, but the life-time performance was not satisfactory [3]. In the present study, modification of the composition $ZrMn_{0.6}V_{0.2}Ni_{1.2}$ with addition of other elements was conducted. Modification of $ZrMn_{0.6}V_{0.2}Ni_{1.2}Co_{0.1}$ by adding a small amount of La was also made. The electrochemical properties were measured and compared to those of the host alloys, in an attempt to further improve the electrode performance of AB_2 alloys.

T. O. Saetre (ed.), Hydrogen Power: Theoretical and Engineering Solutions, 237–242.

2. Experimental

A series of Zr-Mn-V-Ni based alloys were prepared by arc melting under an argon atmosphere. The ingots were annealed in vacuum at 1000°C for 10 hr to get homogeneity. For electrochemical test, Ni-P electroless coating was made on the alloy powders. The amount of coating was about 21wt%. Crystallographic characterization of the alloys was carried out by X-ray diffraction (XRD). Scanning electron microscopy (SEM) was used to inspect the electrode morphologies before and after the cycle life test.

A Sievert's type apparatus was used for the pressure-composition-temperature (P-C-T) measurements. The pressure range was controlled at 0.01-50 kgf/cm^2. The charge-discharge test of the sample electrodes was performed using an automated battery cyclic test system. The charging was controlled at 100mA/g for 10^4 seconds. The charging current was then cut off for 1.8×10^3 seconds. Following this, discharging at a current of 50 mA/g was made until the voltage of the battery dropped to below 900 mV. A stirred water bath was used to keep the operating temperature at 25°C.

3. Results and Discussion

3.1. $ZrMn_{0.6}V_{0.2}Ni_{1.2}M_{0.05}$ (M=Fe, Ni, Cu, Al) Alloys

The X-ray diffraction patterns for this series of alloys indicated that the major phase was the C15-type Laves structure. In some cases some unknown tiny peaks were also observed. The existence of the unknown peaks implied that the homogeneity of the samples was affected by the deviation from stoichiometry.

When Cu, Al, Fe or Ni was added to the composition $ZrMn_{0.6}V_{0.2}Ni_{1.2}$ to form $ZrMn_{0.6}V_{0.2}Ni_{1.2}M_{0.05}$, the lattice constants were changed from 7.064 to 7.040, 7.040, 7.058 and 7.057A, respectively, based on the (311) peak of the XRD patterns. Non-transition metals Al and Cu were more effective in reducing the lattice constant. As for the P-C-T curves, the hysteresis was reduced for all four nonstoichiometric compositions. For the Ni- and Fe- added alloys, both the hydrogenation capacity and the slope of the plateau remained nearly unchanged. For the Al- and Cu- added compositions, not only the hydrogenation capacity but also the flatness of the plateau region was decreased. Figures 1 compares the P-C-T curves at 30°C for the alloys $ZrMn_{0.6}V_{0.2}Ni_{1.2}M_{0.05}$ (M=Cu, Al) with that of the host alloy. The Cu-added alloy, had higher and steeper plateau and less capacity than those of the Al-added one, although the lattice constants were both 7.040A for the two compositions.

Figure 2 compares the electrochemical behaviors for these alloys. The peak capacities were 330, 326, 333 and 266mAh/g for the Ni-, Fe-, Al- and Cu-added alloys, respectively. Compared with the host composition, they all had better discharge performance. After 100 cycles, the Al-added sample had the highest capacity. Based on the P-C-T curves, the theoretical discharge capacities of the Cu- and Al- added alloys would be smaller than that of the host composition. The better performance of these two electrodes was probably duo to better electrochemical characteristics in the alkaline solution, especially for the Al-added alloy.

Significant improvement in the cycle life due to the addition of a very small amount of aluminum was observed by Willems [4]. For the composition $LaNi_{2.5}Co_{2.5}$ modified to $LaNi_{2.5}Co_{2.5}Al_{0.1}$, the charge retention after 500 cycles of test was 80%. The beneficial effect was attributed to the formation of a passive oxide film on the surface. T. Sakai et al. also studied the substitution of Al for Ni in the $LaNi_5$ based alloys [5]. They found an increase in the overpotential for the Al-substituted alloys and suggested a denser oxide film formed on the surface which effectively shielded the hydride from reaction with water and oxygen. The dense oxide film also hindered the diffusion of hydrogen from the bulk to the surface. For AB_2 alloys, S. Wakao et al. observed shortening in cycle number for activation and elongation of cycle life induced by addition of a small amount of aluminum to the composition $Zr(V_{0.33}Ni_{0.67})_{2.4}$ [1]. They proposed that aluminum accelerated oxidation-induced activation and aluminum oxide inhibited excessive oxidation.

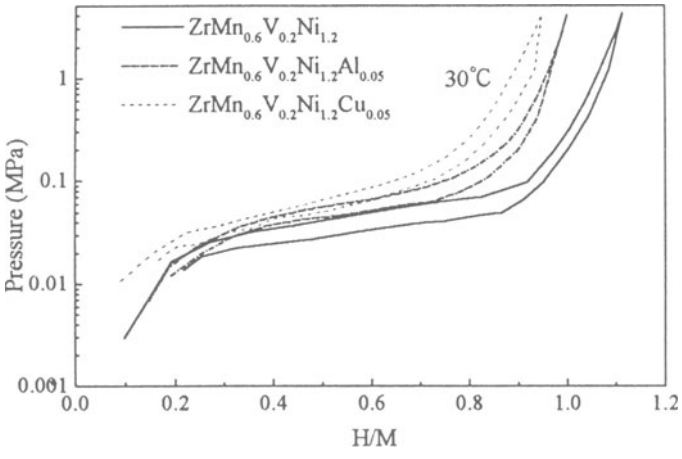

Fig. 1. P-C-T curves of $ZrMn_{0.6}V_{0.2}Ni_{1.2}$ modified with Al and Cu.

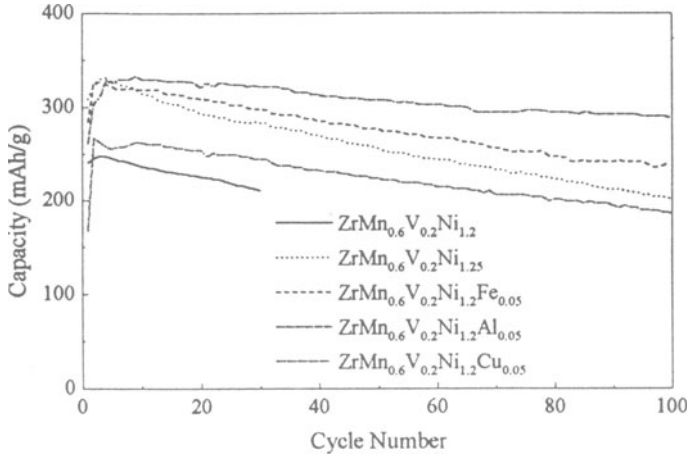

Fig. 2 Discharge capacity curves of $ZrMn_{0.6}V_{0.2}Ni_{1.2}M_{0.05}$ (M=Fe, Ni, Cu, Al) alloys.

3.2. $ZrMn_{0.6}V_{0.2}Ni_{1.2}Co_{0.1}$ and La-added Alloys

Besides the addition with Al or 3d-transition metals, Bernauer and Halene have recommended addition of lanthanum and misch metals as deoxidation agents [6]. It was proposed that deoxidation agents could enhance the homogeneity of the microstructure of the Laves phase. Kim et al. studied the electrode performance of Zr-Cr-Ni-La C14 Laves alloy. They found that the electrode could be easily activated because hydrogen atom could easily penetrate through the oxide or hydrated oxide of La and hydride phase was formed at the sub-surface layer [7]. In this study, the hydrogenation properties of $ZrMn_{0.6}V_{0.2}Ni_{1.2}Co_{0.1}$ and $ZrMn_{0.6}V_{0.2}Ni_{1.2}Co_{0.1}La_{0.03}$ were compared. After the addition of La, in the P-C-T curve the hysteresis became slightly larger but the hydrogenation capacity remained the same [8]. As for the electrochemical performance, the La-added alloy exhibited higher capacity, as shown in Fig. 3. The peak capacity increased from 305 to 335 mAh/g. However, the charge retention after 100 cycles was 67.5%, less than that of $ZrMn_{0.6}V_{0.2}Co_{0.1}Ni_{1.2}$, which was 73.1%.

3.3. Effect of Addition with Al or La

From Figs. 2 and 3, the peak discharge capacities for the two compositions $ZrMn_{0.6}V_{0.2}Co_{0.1}Ni_{1.2}La_{0.03}$ and $ZrMn_{0.6}V_{0.2}Ni_{1.2}Al_{0.05}$ were higher than 330 mAh/g. However, after 100 cycles of charging/discharging, the La-added alloy showed considerable decay in capacity while the Al-added one retained 86% of its peak value. The mechanism for the decay in electrode performance could be explored by comparing the morphologies of the powders and the electrochemical behaviors. Fig. 4 shows the SEM micrographs of the two electrodes after 100 cycles of test. The pulverization was more severe for the La-added alloy. The addition of aluminum probably endowed the alloy with a higher tenacity and reduced the degree of pulverization. In the process of repeated charging/discharging, pulverization of the particles caused exposure of the active surface to the alkaline electrolyte and loss of electric contact of the particles with the substrate, resulted in the decay of discharge capacity.

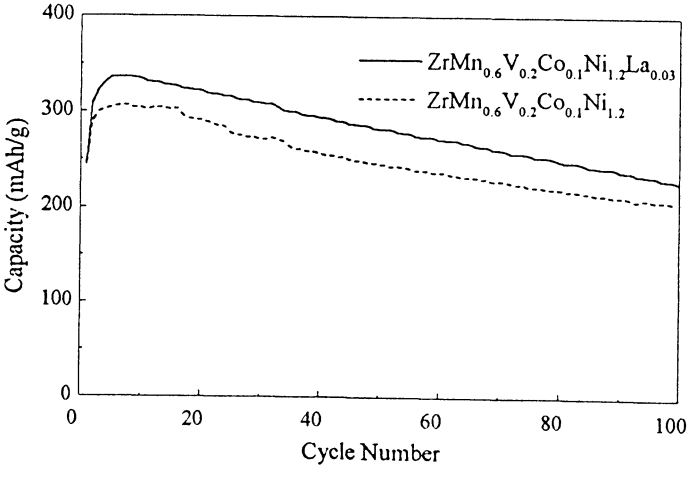

Fig. 3 Discharge capacity curves of $ZrMn_{0.6}V_{0.2}Ni_{1.2}Co_{0.1}$ and La-added alloys.

Fig. 5 compares the polarization behaviors of the two electrodes after they have been fully activated. The La-added composition showed a lower value of overvoltage than the Al-added one. The overvoltage at 200 mA/g of current density for the former one was 0.133V, and for the latter one was 0.180V. The evaluation of electric conductivity for the two compositions were also undertaken. The $\Delta i/\Delta V$ value for the La-added alloy was 1.482 A/gV, being higher than that for the Al-added composition, 1.064 A/gV. All these might imply that a denser oxide film was formed on the surface of the Al-added alloy. The denser oxide film might either hinder the hydrogen permeation or protect the sub-surface from oxidation.

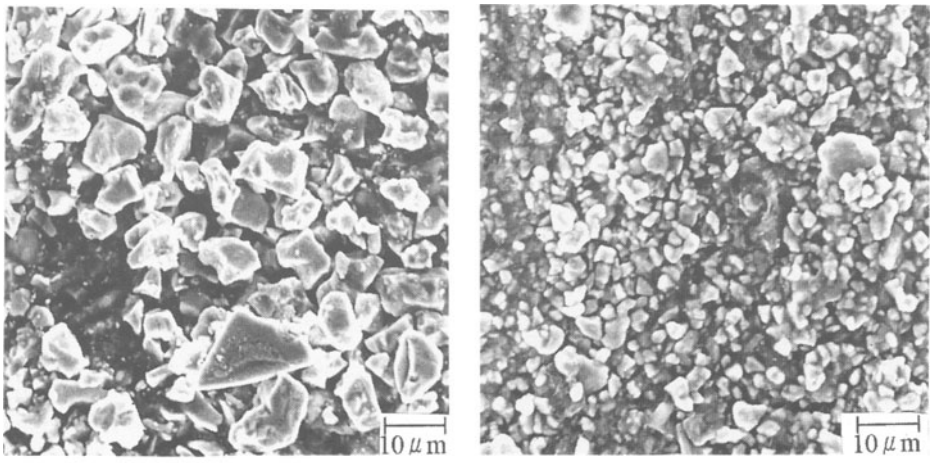

Fig. 4 SEM micrographs of the alloy particles after 100 cycles of discharge test. (a) $ZrMn_{0.6}V_{0.2}Ni_{1.2}Al_{0.05}$, (b) $ZrMn_{0.6}V_{0.2}Ni_{1.2}Co_{0.1}La_{0.03}$.

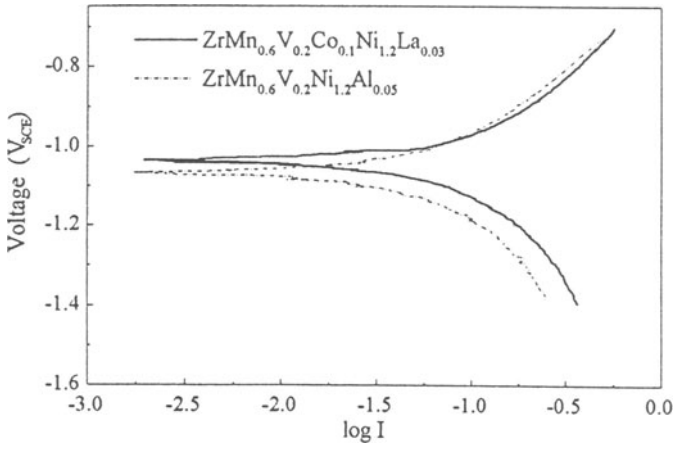

Fig. 5 Electrochemical polarization curves of $ZrMn_{0.6}V_{0.2}Ni_{1.2}Al_{0.05}$ and $ZrMn_{0.6}V_{0.2}Ni_{1.2}Co_{0.1}La_{0.03}$.

4. Conclusions

1 For the nonstoichiometric compositions $ZrMn_{0.6}V_{0.2}Ni_{1.2}M_{0.05}$ (M= Fe, Ni, Cu, Al), they all had better discharge performance than the host alloy. A small amount of addition of La to $ZrMn_{0.6}V_{0.2}Ni_{1.2}Co_{0.1}$ enhanced the charge capacity but decreased the cyclic stability.

2 The best discharge performance of the Al-added alloy was ascribed to the higher tenacity and the formation of a dense oxide film.

Acknowledgments

This work was supported by the National Science Council of ROC under Contract NSC 84-2216-E007-031 and National Tsing Hua University Fellowship 82-3-1.

References

1. Wakao, S., Sawa, H., and Furukawa, J. (1991) Effect of partial substitution and anodic oxidation treatment of Zr-V-Ni alloys on electrochemical properties, *J. Less-Common Met.*, 172-174, 1219-29.
2. Moriwaki, Y., Gamo, T., Seri, H., and Iwaki, T. (1991) Electrode characteristics of C15-type Laves phase alloys, *J. Less-Common Met.*, 172-174, 1211-18.
3. Hsu, Y.-S. (1994) Hydrogenation properties and electrochemical performance of substitutional Zr-(Mn-Ni) based alloys, M. S. Thesis, National Tsing Hua University.
4. Willems, J. J. G. (1984) Metal hydride electrodes stability of $LaNi_5$ related alloys *Philips J. Res.*, 39, 1-94.
5. Sakai, T., Miyamura, H., Kuriyama, N., Kato, A., Oguro, K., and Ishikawa, H. (1990) Metal hydride anodes for nickel-hydrogen secondary battery, *J. Electrochem. Soc.*, 137, 795-99.
6. Bernauer, O. and Halene, C.(1987) Properties of metal hydrides for use in industrial applications, *J. Less-Common Met.*, 131, 213-24.
7. Kim, S.-R., Lee, J.-Y., and Park, H.-H. (1994) A study of the activation behavior or Zr-Cr-Ni-La metal hydride electrodes in alkaline solution, *J. Alloys Comp.*, 205, 225-29.
8. Hsu, Y.-S. and Perng, T.-P. (1995) Hydrogenation of multicomponent Zr-base C15 type alloys, *J. Alloys Comp.*, 227, 180-85.

APPLICATION PROPERTIES OF AB_2-TYPE HYDROGEN ABSORBING ALLOYS.

S.V.MITROKHIN, V.N.VERBETSKY, A.G.FRIDMAN*

Department of Chemistry, Moscow State University, 119899, Moscow, Russia.
** - All-Russian Institute of Light Metals, Moscow, Russia.*

1. Introduction

Use of hydrogen absorbing alloys in various practical applications is always connected with the problem of production of starting alloys. The transition from laboratory samples to small-scale production involves the change of furnace and its operation mode and this has an effect on the preparation method of mixture of starting metal. Also, for some applications such as thermosorption compressors the exact values of thermodynamical parameters of reaction are needed. In the present work we present the results of investigation of series Laves phase hydrogen-absorbing alloys which can be promising in for use in different devices.

2. Experimental Part

Alloys were prepared by conventional arc melting. Manganese was taken in an excess of 3 (Alloys 3, 6-12 according to Table 1) or 7 mass.% (Alloys 1, 2, 4, 5) to the calculated quantity to reduce the loss due to fugacity while melting. Obtained samples were analysed by X-ray, atomic absorption spectroscopy, and energy dispersion X-ray analysis (EDXA). Hydriding and isotherm measurements were carried out in a standard Sieverts type apparatus. Hydrogen was of 99.999% purity obtained from $LaNi_5$ hydrogen accumulator.

Chemical analysis was performed by atomic absorption method according to following schedule:

1. Investigation and choice of a way of dissolution for alloy with the purpose of creation of optimum conditions of atomic absorption determination of elements;
2. Choice of a way of graduation of used AA spectrometers;
3. Development of a course of the alloy analysis in view of peculiarities of its chemical probe preparation and atomic absorption analysis of multicomponent alloys;

The measurements were carried out on one-beam atomic AA spectrometer "Hitachi". The prospective unified way of dissolution for multicomponent alloys, namely in a mixture of saturated nitric and hydrochloric acids with the subsequent addition of hydrofluoric and nitric acids corrected depending on structure of analysed samples and on element to be determined by AA method.

For the analysis of titanium and iron the most expedient way of alloy dissolution for this type of alloys type for simultaneous definition of the specified elements in a

T. O. Saetre (ed.), Hydrogen Power: Theoretical and Engineering Solutions, 243–249.

solution of a sulphuric acid (1:3) or (1:4) was chosen, since it was necessary to avoid using HBF_4 acid.

Graduation solutions should contain the same quantity of chromium (for titanium) and titanium (for iron) and should be used through the whole course of the analysis. Check of correctness was carried out by a method "entered - found ".

3.Results and Discussion

The composition of starting alloys according to alloying mixture of metals in presented in Table 1. The results of chemical analysis of some alloys are presented in Table 2. Comparing the data it is clear that the actual composition of some of the obtained samples (1, 3 and 6) differs from that of the alloying mixture. The reason for this is at first the fugacity of manganese during melting which leads to some loss of these metals and conformably to the change of the composition. Since the excess of manganese was always the same the data shows that it is necessary to determine the exact amount of metal excess in every case.

TABLE 1. Composition of starting alloys.

Alloy No.	Ti	Zr	Mn	Cr	Fe	V	Ni	Co	Al	Cu
1	0.95	0.05	1.35	0.45	0.2					
2	0.95	0.05	1.2	0.3	0.5					
3	0.9	0.1	1.5	0.1	0.05	0.25	0.05	0.05		
4	0.9	0.1	1.5	0.1	0.05	0.25	0.05	0.05		
5	0.9	0.1	1.5	0.4	0.1					
6	0.9	0.1	1.2	0.6		0.2				
7	0.85	0.15	1.5	0.1	0.05	0.25	0.05	0.05		
8	0.8	0.2	1.8			0.1			0.1	
9	0.8	0.2	1.7	0.1		0.2				
10	0.8	0.2	1.5	0.1	0.05	0.25	0.05	0.05		
11	0.8	0.2	1	0.9						0.1
12	0.7	0.3	1.5	0.1	0.05	0.3	0.05			

TABLE 2. Chemical analysis of alloy composition.

Alloy No.	Ti	Zr	Mn	Cr	Fe	V	Ni	Co
1	1.36	0.06	0.70	0.51	0.37			
2	1.26	0.06	0.74	0.38	0.56			
5	1.07	0.11	1.39	0.42	0.01			
10	0.683	0.288	1.523	0.096	0.051	0.304	0.055	
12	0.781	0.201	1.535	0.088	0.069	0.227	0.046	0.052

According to X-ray analysis all alloys are multiphase samples with phase of hexagonal structure typical of Laves phases being the main one. In fact the same result for other AB_2 alloys was obtained in [1]. Comparison of X-ray patterns of our samples with those presented in [1] shows that they are very much alike. This proves our assumption that the minor phases in our case are also $(Ti,Zr)(Mn,Cr,Fe)O_3$ oxide phase and unidentified cubic phase with cell parameter a = 2.43 Å. This results is confirmed by the data obtained by EDXA which shows that all samples contain at least two different phases (Table 3). The main phase is represented on the images like a bright field having inclusions of dark and black colour. Its composition differs considerably from that according to chemical analysis. On the other hand the overall composition as measured by EDXA well enough coincides with the latter. And all of them differ from the initial metal ratio of the melting schist. This is mainly due to the fact that the fugacity of chromium and especially manganese plays the leading role in the process of preparation of alloys and should be thoroughly controlled.

TABLE 3. Composition of phases in alloys according to EDXA and chemical analysis.

Alloy No.	Composition	Overall	Main phase	Dark phase	Black phase	Chemical analysis
2	Ti	1.10	1.57	1.01		1.26
	Zr	0.07	0.07	0.07		0.06
	Mn	0.98	0.73	0.98		0.74
	Cr	0.34	0.21	0.40		0.38
	Fe	0.51	0.44	0.54		0.56
5	Ti	1.05	1.46	0.93	1.94	1.07
	Zr	0.12	0.13	0.14	0.08	0.11
	Mn	1.39	1.16	1.40	0.85	1.39
	Cr	0.44	0.25	0.53	0.13	0.42
	Fe	0.00	0.00	0.00	0.00	0.01

The desorption isotherms for investigated systems are shown in Fig.1-5. Hydrogen sorption properties are presented in Table 4. All alloys begin hydriding rather easily without preliminary activation at pressure about 50 atm. However, for those systems when the dissociation pressure is higher complete hydriding requires pressures about 100 atm. Still for the Alloy 2 this maximum experimental pressure is not enough to form hydride phase at ambient temperature even after cooling the sample to the liquid nitrogen temperature (curve 2, Fig.5) to eliminate the influence of the hysteresis effect. In fact the hysteresis factor $ln(P_{abs}/P_{des})$ is about 1.3 in this case.

The value of the dissociation pressure at ambient temperature varies in a wide range from 0.3 to 60 atm. Hydrogen content is rather high for this type of alloys and reaches a value of 2 mass.% in some cases.

TABLE 4. Absorption properties of investigated alloys

Alloy No.	T_e (K)	P_{diss} (atm)	Absorption capacity H/AB_2	Mass.%	ΔH, kJ/mole	ΔS, J/K·mole
	253	5.6	3.08	1.90		
1	273	10.9	2.72	1.68	19.2	90.2
	293	20.2	2.42	1.50		
	253	19.7	3.8	3.06		
2	273	34.9	3.19	2.56	16.4	89.6
	293	57.2	3.10	1.88		
3	293	5.2	3.01	1.83		
4	293	5.6	2.57	1.55		
	253	1.8	3.72	2.25		
5	273	3.4	3.29	2.00	18.3	77.1
	293	5.8	2.93	1.79		
6	293	6.5	3.02	1.86		
7	293	2.6	2.98	1.78		
8	293	7.0	2.76	1.66		
9	293	3.0	2.74	1.63		
10	293	1.4	2.95	1.75		
11	293	6.0	3.07	1.83		
12	293	0.3	3.29	1.94		

4. Conclusions

The results of the present work show that one of the main problems for the application of AB_2-type hydrides in metal-hydride technology is the preparation of alloys and unlike the $LaNi_5$-type alloys the expenditure of some components particularly manganese and chromium should be thoroughly controlled. The investigated alloys are characterised by good sorption properties and can be proposed for use in such systems as thermosorption compressors and refrigerators.

5. Acknowledgement

This work was supported in part by the Russian Foundation for Basic Research Grant No.95-03-08787.

6. Reference

1. Huot, J., Akiba, E., and Ishido, Y. Crystal Structure of Multiphase Alloys (Ti,Zr)(Mn,V)$_2$, *J. of Alloys and Compounds,* **231**, (1995), 85-89.

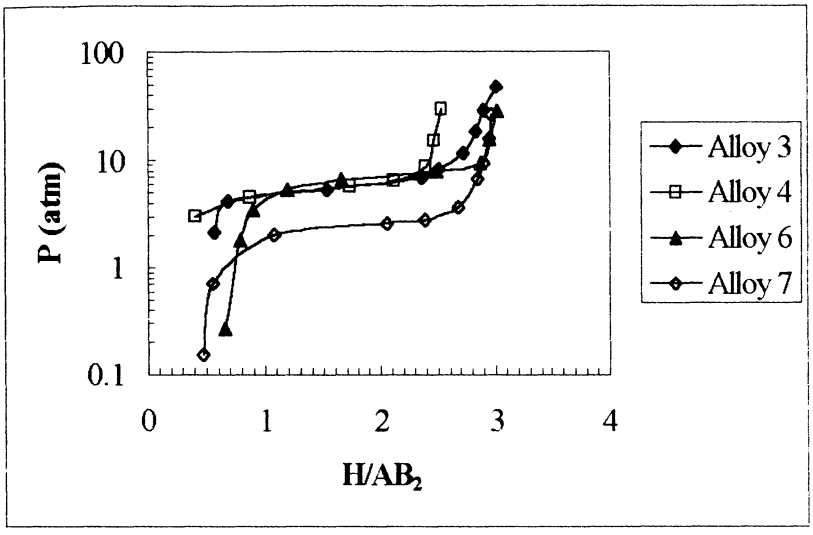

Figure 1. Desorption isotherms for alloys 3, 4, 6 and 7 at 293 K.

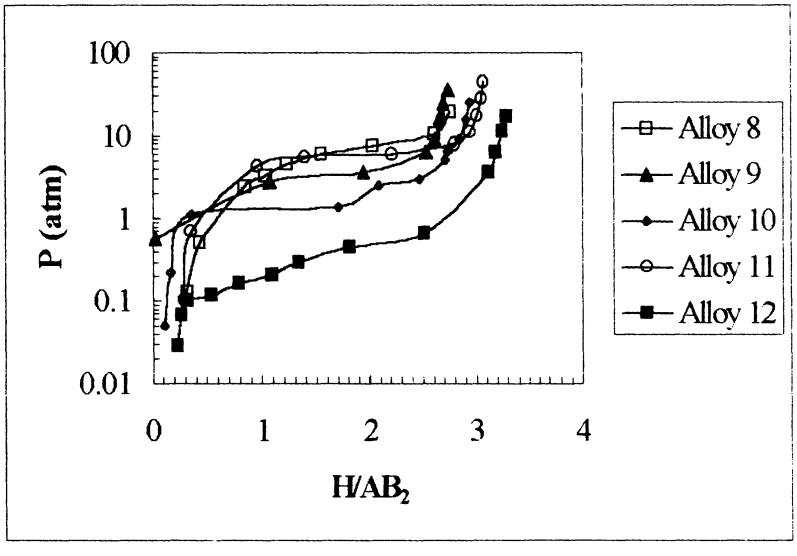

Figure 2. Desorption isotherm for alloys 8-12 at 293 K.

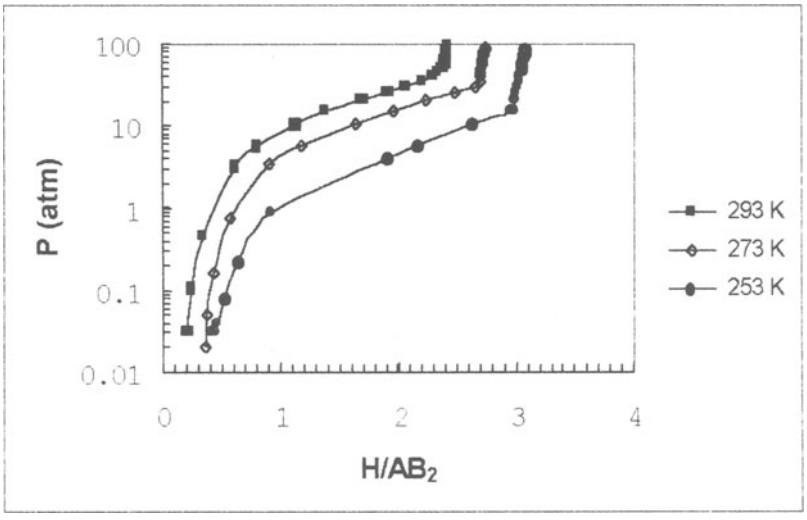

Figure 3. Desorption isotherms for the system Alloy 1 – H_2.

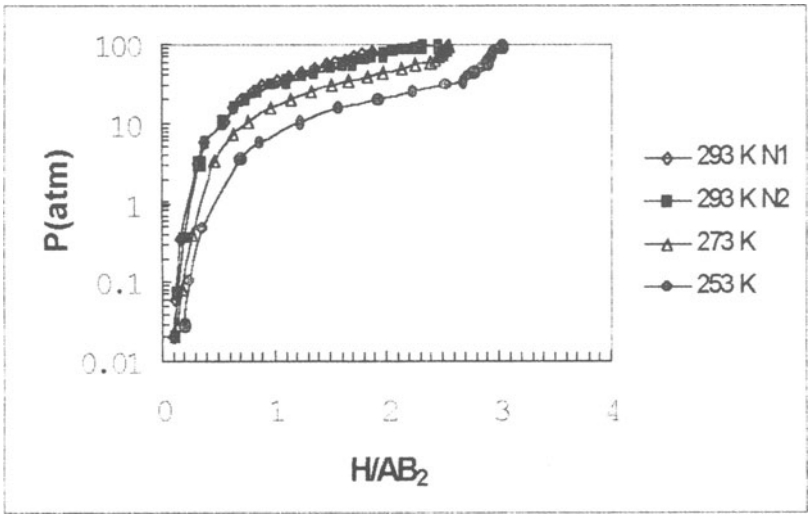

Figure 4. Desorption isotherms for the system Alloy 2 – H_2.

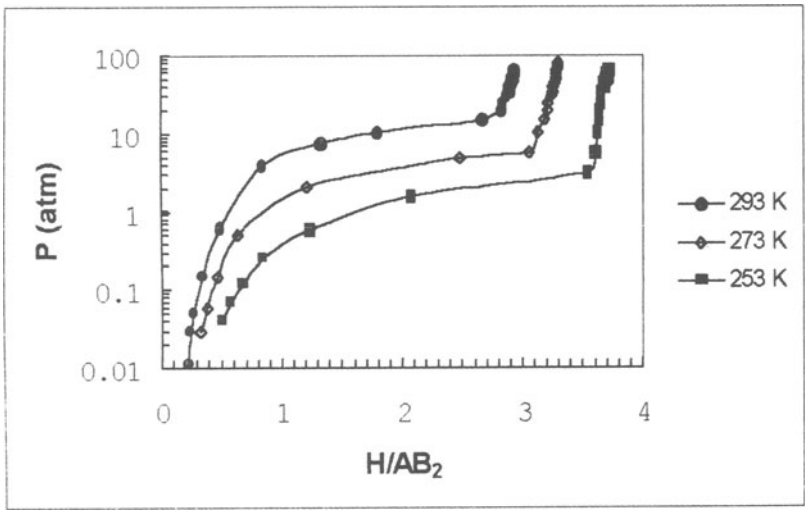

Figure 5. Desorption isotherms for the system Alloy 5 – H_2.

ON-BOARD HYDROGEN STORAGE SYSTEM USING METAL HYDRIDE

L. K. HEUNG
Westinghouse Savannah River Company
773-A, Savannah River Site, Aiken, SC 29808, USA
Phone: 803-725-3161 Fax: 803-725-2756

Abstract. A hydrogen-powered hybrid electric bus has been developed for demonstration in the city of Augusta, Georgia, USA. The hydrogen is stored in a solid form using an on-board metal hydride storage system. The system performs better than the design requirements.

1. Introduction

Hydrogen is widely considered to be the fuel of the future, mainly because it is renewable and burns cleanly. Metal hydrides store hydrogen in a solid state which has a safety advantage over gas or liquid hydrogen. For this reason, metal hydrides have been studied for on-board hydrogen storage since the early seventies[1,2]. Due to the large number of metal hydrides available and the different requirements for different applications, the challenge has been to select the best metal hydride and to design the best storage vessel for a specific application.

After the Cold War, the US Department of Energy (DOE) initiated a technology transfer effort. As part of this effort, a team named H2Fuel was formed to utilize the hydrogen technology developed at the Savannah River Site. The team involved DOE, its contractor, industry, academia and local government. A battery powered, 10-meter transit bus was converted into a hydrogen-powered hybrid bus. The bus would be used by the city of Augusta, Georgia, in its transit system.

Figure 1. The H2Fuel hydrogen-powered bus

2. The H2Fuel Bus

The original electric bus was powered by four 28-battery packs and had a driving range of about 130 km. Two of the four battery packs (approximately 1,000 kg per pack) were replaced with hydride hydrogen storage vessels. An internal combustion (IC) engine and an electric generator were added. The hydride storage system stores and feeds hydrogen to the combustion engine. The engine-generator set produces

T. O. Saetre (ed.), Hydrogen Power: Theoretical and Engineering Solutions, 251–256.

electricity to power the electric drive motor and to charge the batteries. The batteries serve as a reservoir for the excess energy of the generator, to be charged when the power demand is low and to be drawn down when the power demand is high. This arrangement allows the use of a small generator (70 kW) and a large electric drive motor (170 kW). This hybrid power system permits the IC engine to run most efficiently and is expected to extend the driving range of the original electric bus from 130 km to 200 km. A photo of the bus and a schematic of the hybrid power system are shown in Figures 1 and 2, respectively.

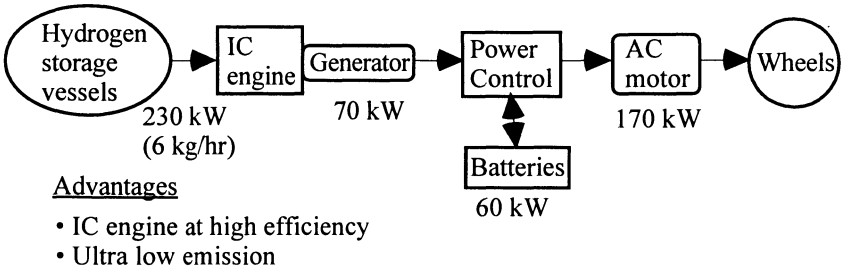

Figure 2. Schematic of the hydrogen-powered hybrid power system

3. On-Board Hydrogen Storage System Design Requirements

When serving in the Augusta city transit system, the bus is expected to be started up in the morning and run for the day. At the end of the day it will be refueled and charged. To fulfill this operation plan, the hydride storage system must meet the following design requirements:

- Hydrogen storage capacity is for a full day's scheduled operation of the bus.
- The storage system does not add more weight to the original electric bus.
- Hydrogen pressure and flow rate meet the fuel requirements of the engine.
- Refueling time to be compatible with the operation schedule.
- Engine coolant is used to provide heat for hydrogen desorption.
- Water is used for cooling during refueling via an external heat exchanger.
- Refueling hydrogen is from a tube trailer or an electrolyzer.

To meet the above requirements, different metal hydrides and hydride vessel designs were considered. The chosen metal hydride and vessel design are described below.

4. Metal Hydride Selection

Lanthanum-nickel-aluminum type material has been used at the Savannah River Site for more than 15 years in various applications[3,4]. This type of material has been shown to have excellent chemical stability and was chosen to be the starting material for the bus project. To reduce the cost of the material, lanthanum was replaced with "lanthanum rich mischmetal" (designated symbol Lm). The general formula was $Lm_xNi_{(5-y)}Al_y$. A value of x slightly larger than 1 was used to improve the material's performance[5]. The value of y is adjusted for the required hydrogen pressure, since the hydrogen pressure

increases with the decrease of the y value[6]. Three specific formulations were tried before the selection criteria were met. The final material has the following properties:

Formula: $Lm_{1.06}Ni_{4.96}Al_{0.04}$
(Lm = La 55.7% Ce 2.5% Pr 7.7% Nd 34.1%)
Absorption pressure at 60°C and 0.5 H/M: 18.5 atm
Desorption pressure at 60°C and 0.5 H/M: 13.5 atm
H_2 capacity at 40°C and 20 atm: 0.92 H/M; 1.27 wt%
van't Hoff equation at 0.5 H/M: $\ln P=\Delta H/(R*T)+\Delta S/R$
(P=pressure, atm; ΔH=enthalpy, 6580 cal/mol for absorption, 6577 cal/mol for desorption; ΔS=entropy, 25.56 cal/mol/°K absorption, 24.91 cal/mol/°K desorption; R=gas constant, 1.987 cal/mol/°K)

5. Hydride Vessel Design

General technical issues encountered in the design of metal hydride vessels for on-board hydrogen storage include:

- Hydride particles expand upon hydrogen absorption and contract on desorption, this can cause compaction, swelling and consequent damage to the vessel.
- Metal hydride powder is a poor heat transfer medium causing slow hydrogen absorption and desorption.
- Filters used to confine the hydride powder can impede the flow of hydrogen.
- Metal hydrides are heavy and require light weight vessels.

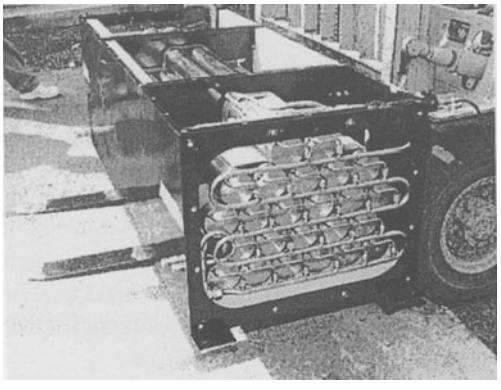

Figure 3. "Box" of the on-board hydrogen storage vessels

With the above issues in consideration, the final design of the on-board hydrogen storage system consists of two "boxes" of metal hydride vessels. Each "box" contains 24 horizontally installed cylindrical vessels. The vessels are 9-cm in diameter and 152-cm long. They are assembled inside an aluminum box to form a stack of 6 vessels wide and 5 layers high. The aluminum boxes are 66-cm wide, 53-cm high, and 173-cm deep. All 24 vessels in a box are connected in parallel. The photo of a partly assembled box is shown in Figure 3. The boxes are installed below the bus floor on both sides of the chassis.

The cylindrical hydride vessels are made from thin wall, stainless steel tubes. The components inside each vessel include a porous stainless steel filter, aluminum divider plates, cylindrical aluminum foam pieces, and a U-shaped water tube. The filter permits hydrogen to flow freely in and out of the vessel but confines the metal hydride powders in the vessel. The divider plates separate the vessel into short sections to prevent the

metal hydride powders from shifting among the sections. The aluminum foam pieces with metal hydride particles in their pores improve the heat transfer between the hydride and the water tube. The engine coolant flows through the water tube to provide heat during desorption and to remove heat during absorption of hydrogen. A schematic of the hydride vessel is shown in Figure 4.

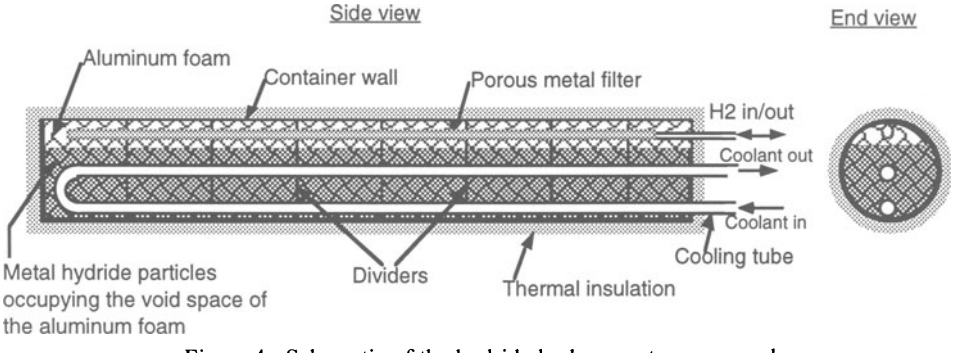

Figure 4. Schematic of the hydride hydrogen storage vessel

Limited by weight, only 2 boxes of vessels, or 48 of the originally planned 80 were installed on the bus. The total weight of the two boxes of hydride vessels is 1900 kg, about the same as the two packs of batteries which they replaced. The metal hydride weight is 1250 kg, or 66% of the total weight. The hydrogen capacity is 15 kg compared to the bus gross weight of 15000 kg.

6. Hydrogen Feed Rate and Heat Transfer

When running at full power, the hydrogen combustion engine requires a hydrogen feed rate of 6 kg/hr at 10 atm pressure. At this rate the heat required for hydrogen desorption is calculated to be 19800 kcal/hr. The hydride storage system must be able to transfer this much heat from the coolant to the metal hydride during operation. It can be shown by calculation that the main resistance to heat transfer is in the metal hydride powder. Based on previous work, the heat transfer coefficient of a metal hydride bed is solely dependent on the hydrogen pressure and is 72 kcal/hr/m^2/°C at 10 atm hydrogen pressure.[7] With this heat transfer coefficient, the coolant can only transfer 8003 kcal/hr to the metal hydride, which is only 0.4 of what is required. The heat transfer coefficient must be increased to 180 kcal/hr/m^2/°C to meet the required heat transfer rate.

Aluminum foam pieces were added to the vessel to improve the heat transfer in the metal hydride bed. To evaluate the effectiveness of the aluminum foam, a 14-cm single section experimental bed was first fabricated and tested. The results showed that the aluminum foam increases the heat transfer coefficient of the metal hydride bed by a factor of approximately 5. That gives an overall heat transfer coefficient of 360 kcal/hr/m^2/°C, which is two times the required value of 180 kcal/m^2/hr/°C. With this higher heat transfer coefficient, a single box of 24 hydride vessels can support the required hydrogen feed rate of 6 kg/hr. Two boxes together can double the design goal.

7. Performance

The H2Fuel bus has undergone driving tests in the streets of Augusta since April 1997, accumulating more than 1000 km of travel distance at the time of this writing. The on-board hydrogen storage vessels have been refueled over 20 times.

7.1 ACTIVATION

Activation of the on-board metal hydride was accomplished at ambient temperature using flowing water for cooling. The hydride vessels were evacuated and purged with hydrogen, then exposed to 20 atm hydrogen. The hydride began to absorb hydrogen after an incubation time of about 15 minutes. Once started, the hydrogen was absorbed as fast as it could flow into the vessels.

7.2 HYDROGEN FEED RATE

Operational data collected to date have shown that the hydrogen storage system can supply hydrogen to the engine at a rate exceeding the design goal. This was demonstrated by a set of data collected during a test operation in which only one box of 24 hydride vessels was used to feed the engine. Using the average values of coolant temperature, hydride temperature and hydrogen consumption rate, and the water coolant tube surface area, one can calculate the heat transfer coefficient. The calculation yielded a heat transfer coefficient of 426 kcal/hr/m^2/°C. See Table 1. Note that the value calculated from the 14-cm single section was 360 kcal/hr/m^2/°C, and the required value for 6 kg/hr hydrogen feed was 178 kcal/hr/m^2/°C. The actual heat transfer coefficient is the highest among the three. This higher value allows the engine to operate with only one box of hydride vessels on line.

TABLE 1. Heat transfer and hydrogen feed rate data

Coolant temperature in coolant tube	inlet=65.5 °C, outlet=54.4 °C average=60 °C
Average hydrogen feed rate from one box (24) of the vessels over a one hour engine operation	3.4 kg/hr
Hydride temperature in equilibrium with 10 atm hydrogen pressure (average)	51 °C
Average heat transfer rate from coolant to hydride =3.4 kg/hr*6.6 kcal/mole*(1000 mole/2 kg)	12540 kcal/hr
Overall heat transfer coefficient =12540 kcal/hr/(60 °C -51 °C)/2.93 m^2	426 kcal/hr/m^2/°C

7.3 REFUELING

Presently, hydrogen from a tube trailer is used to refuel the bus. The connection between the hydrogen supply and the hydride storage system is accomplished by using a Sherex fueling nozzle and receptacle. The heat of absorption during refueling is removed via a water-cooled external heat exchanger. With a supply hydrogen pressure set at 18 atm, the hydride can be charged to 75% full in about 60 minutes; another 60

minutes are needed to charge the remaining 25%. The refueling time meets the original target time of 2 hours.

8. Conclusions

An on-board hydrogen storage system using metal hydride has been successfully developed, fabricated and demonstrated on a city transit bus. Road testing to date has shown that the original design goals have been reached or exceeded. The use of metal hydride for on-board hydrogen storage gives a safety advantage and has a high potential to be successfully used in applications where weight is not a prohibitive factor. The hydrogen storage system in this project was developed for an IC engine, but it can be applied to a fuel cell powered system as well. When the fuel cell technology becomes more economical, the IC engine can be replaced with a fuel cell to further increase the energy efficiency.

Acknowledgments

This paper was prepared in connection with work done under Contract No. DE-AC0996SR18500 with the U. S. Department Of Energy. The hydride storage vessels were fabricated by Hydrogen Components Inc. through a procurement order from the Westinghouse Savannah River Company. My colleagues, T. J. Warren conducted the hydride activation test, T. Motyka and W. A. Summers gave me helpful reviews.

References

1. Topler J. and Feucht K.(1988) Results of a Test Fleet with Metal Hydride Motor Cars, *Metal-Hydrogen Systems*, vol. II, 1451-1461, Edited by R. Kirchheim, E. Fromm, and E Wiche, Stuttgart.
2. Das L. M. (1996) On-Board Hydrogen Storage System For Automotive Applications, *Int. J. Hydrogen Energy,* vol. 21, No. 9, 789-800.
3. Ortman M. S., Heung, L. K., Nobile A., and Rabun R. L. III (1990) Tritium Processing at the Savannah River Site: Present and Future, *J. of Vacuum Science & Technology* A 8 (3), 2881-2889.
4. Motyka, T. (1992) The Replacement Tritium Facility, *Fusion Technology*, vol. 21, 247-252.
5. Marmare R. W. and Lynch F. E. (1991) Investigation of Long Term Stability in Metal Hydrides, Final Report to NASA, NAS9-18175.
6. Diaz H., Percheron-Guegan A. and Achard J. C. (1979) Thermodynamic and Sturctural Properties of $LaNi_{5-y}Al_y$ Compounds and Their Related Hydrides, *Int. J. of Hydrogen Energy*, vol. 4, 445-454.
7. Heung L. K. (1988) Heat Transfer and Kinetics of a Metal Hydride Reactor, *Metal-Hydrogen Systems*, vol. II, 1451-1461, Edited by R. Kirchheim, E. Fromm, and E Wiche, Stuttgart.

THERMODYNAMIC AND STRUCTURAL CHANGES OF AN AB_2-LAVES-PHASE ALLOY ($Ti_{0,98}Zr_{0,02}V_{0,43}Fe_{0,06}Cr_{0,05}Mn_{1,52}$) DURING EXTENDED THERMAL CYCLING

M. WANNER, G. HOFFMANN, M. GROLL
Institut für Kernenergetik und Energiesyteme (IKE),
University of Stuttgart,
Pfaffenwaldring 31, D-70569 Stuttgart, Germany

Abstract

The investigated alloy $Ti_{0.98}Zr_{0.02}V_{0.43}Fe_{0.06}Cr_{0.05}Mn_{1.52}$ (HWT 5800) underwent about 10^5 thermally driven hydrogen absorption/desorption cycles (between 45 and 120°C) and exhibited an excellent stability against prolongued cycling. The capacity losses after 10^5 cycles are below 10%. At the beginning and after the end of cycling additional experimental techniques were employed in order to determine possible structural, stoichiometric and thermodynamic changes. Among others, X-ray powder diffractometry, Thermal Desorption Spectroscopy and PCI-measurements were utilised. These experiments reveal interesting changes like additional phases after degradation and again after regeneration treatment of the cycled alloy.

1. Introduction

Metal hydrides used in periodically working thermodynamic machines undergo several 10^5 absorption-desorption cycles during the lifetime of the device. This might cause changes in materials properties such as reaction enthalpy, equilibrium pressure, hysteresis and plateau slope. Most investigations of the stability of the thermodynamic properties against prolongued cycling [1-13] deal with AB_5-alloys. Only few work [14, 15] has been done on AB_2-Laves-Phase materials. The numbers of cycles in these experiments do not exceed 10^4 which is less than 10% of the number that will occur during the lifetime of a metal hydride sorption machine. So the present work where the alloy $Ti_{0.98}Zr_{0.02}V_{0.43}Fe_{0.06}Cr_{0.05}Mn_{1.52}$ was cycled 85,100 times is an important contribution to the knowledge about cyclic stability of AB_2-alloy hydrides.

T. O. Saetre (ed.), Hydrogen Power: Theoretical and Engineering Solutions, 257–262.

2. Experimental Details

2.1. CYCLING DEVICE

In [16] the cycling device is described in detail. Six different materials, one of them was $Ti_{0.98}Zr_{0.02}V_{0.43}Fe_{0.06}Cr_{0.05}Mn_{1.52}$, can be cycled independently at different cycling conditions. The cycling device contains four reactors for each material. This makes it possible to remove individual reactors in order to thoroughly investigate the cycled samples outside the apparatus.
The alloy was delivered as a fine powder with a medium particle diameter of 17 µm. 20g were filled in the annular gap of each cylindrical reactor. The four reactors and a 2ℓ-gas-vessel are coupled to a closed system. Its pressure is detected with a piezoresistive pressure transducer. The desorption is forced by heating the sample up to the maximum temperature T_{des} = 120°C with an electrical heater located in the axis of the reactor. The following absorption is caused by air cooling down to the minimum temperature T_{abs} = 45°C. From the pressure difference between the maximum pressure p_{des} after desorption and the minimum pressure p_{abs} after absorption the system related reversible hydrogen capacity Δx_{sys} can be calculated. One complete absorption-desorption-cycle lasts 15min. As the cycling lasted three years some hydrogen was lost (Fig. 1) as a consequence of diffusion or very small undetectable leakage. After 72,660 cycles the lost hydrogen was refilled.
After the end of cycling one reactor was regenerated (at 400°C and 1hPa for 24h).

2.2 PRESSURE-COMPOSITION-ISOTHERMS AND THERMAL DESORPTION SPECTROSCOPY

The PCI-apparatus used for this work is already described elsewhere [17]. The hydride composition is determined volumetrically. The hydrogen is supplied at a constant flow rate between 1.5 and 3 cm_n^3/min. This dynamic measuring method is regarded to be most representative for the conditions in metal hydride sorption machines [17]. The liquid cooling of the PCI-reactors guarantees constant temperatures ($\Delta T \leq 0.3K$).
PCI-measurements were taken from the as delivered alloy (after activation), from the degraded sample (after 85,100 cycles) and from the regenerated sample. Three isotherms (-20°C, 0°C, 20°C) were determined for each sample. The sample masses varied between 3g and 4g.
For the Thermal Desorption Spectroscopy (TDS) we used the same apparatus. The degraded sample was heated up to 650°C at a constant heating rate of 3K/min. The evolved hydrogen was gathered in a gas vessel. Its pressure is determined by a piezoresistive pressure difference transducer. The hydrogen evolution rate is measured by a BROOKS mass flow controller. In addition the results were verified by comparing them to the deviation of the rising hydrogen pressure.

2.3. OTHER EXPERIMENTAL TECHNIQUES

X-ray powder diffraction (XRPD) was applied to detect phase changes or the appearance of additional phases in the three samples. Diffraction Patterns were taken on a SIEMENS D 5000 Diffractometer with Cu-K_α radiation.
The particle size distribution of as delivered, degraded and regenerated material was determined by an HR850 CILAS ALCATEL Laser Granulometer.

3. Results and Discussion

At the given cycling temperatures (45/120°C) about 65% of the total hydrogen storage capacity (1 H/M) can be reversibly ab-/desorbed (Fig. 1). This value decreased only slightly to a final value of 61%. One part of the decay was due to the loss of hydrogen. That was shown by refilling hydrogen at cycle no. 72,660. The other part originates from the changes of the thermodynamic properties of the material.

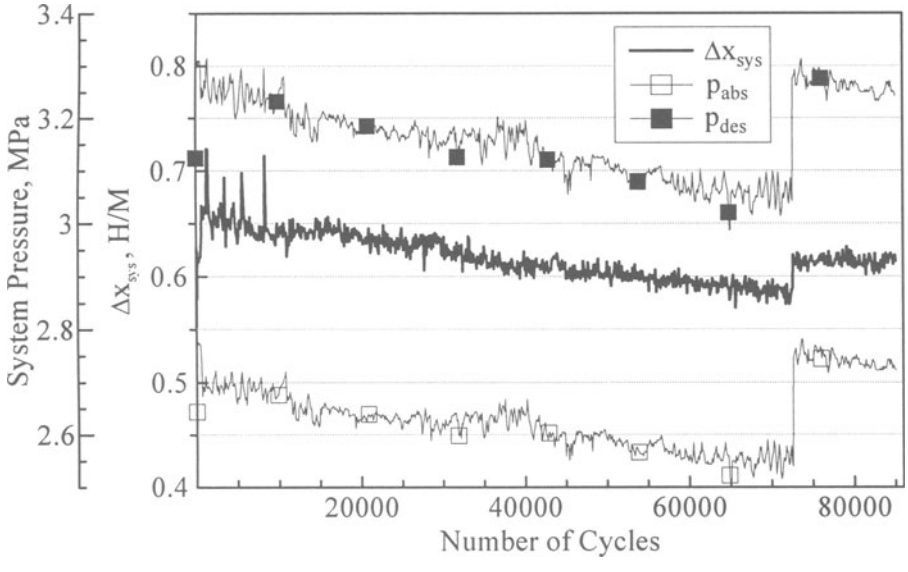

FIGURE 1. Capacity losses during cycling

Fig. 2 shows three absorption PCI's at 20°C. The degraded sample exhibits a steeper and shorter plateau region. The total hydrogen capacity has decreased during cycling. The regeneration brought the initial capacity back even though the plateau is not as flat as before the long-term cycling. From the Van't-Hoff-plots of each sample the values for the reaction enthalpy ΔH and entropy ΔS were derived. Table 1 compares the values of the as delivered sample to the degraded alloy and shows that only small changes occur.

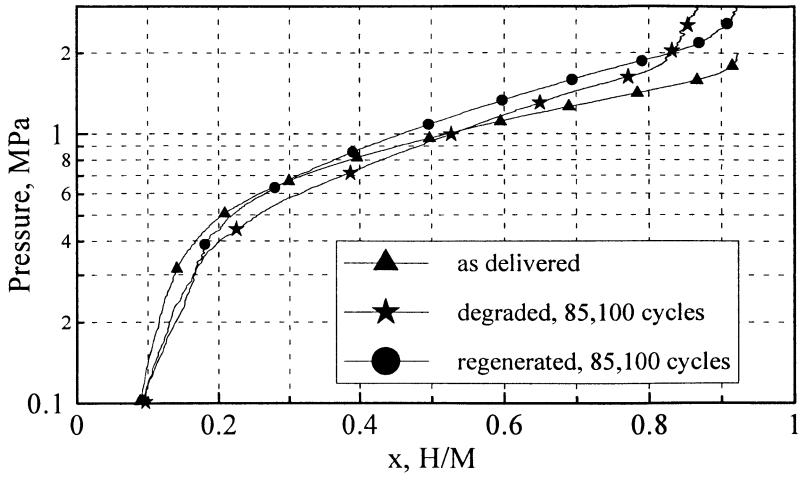

FIGURE 2. Absorption PCI's of of three different samples at 20°C

TABLE 1. Reaction enthalpy and reaction entropy of two samples

	Absorption		Desorption	
	ΔH [kJ/mol]	ΔS [J/(mol·K)]	ΔH [kJ/mol]	ΔS [J/(mol·K)]
as delivered	-22.1	97	28.4	-116
degraded	-21.9	94	27.3	-107

During the TDS-experiment 0.061 H/M hydrogen were evolved (see Fig. 3). The evolution started above the upper cycling temperature (120°C). Around 600°C it came to a standstill. The maximum of the evolution rate was reached between about 250°C and 450°C. The results indicate that other hydrides than AB_2H_3 might have been formed during the long-term cycling and that these more stable hydrides dissociate between about 250°C and 450°C.

Besides the Laves-Phase pattern that is indicated by the dashed lines in Fig. 4 the XRPD of the as deli-

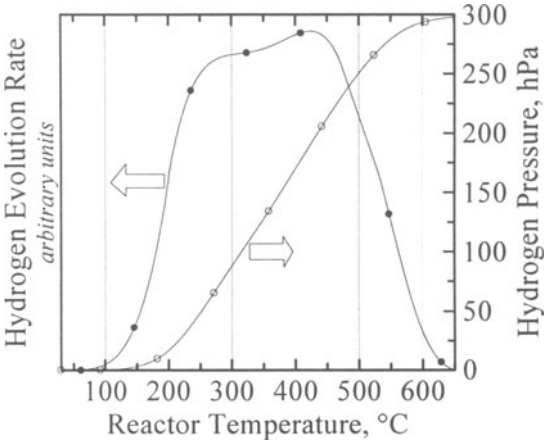

FIGURE 3. Thermal desorption spectrum

vered alloy shows the three most important lines of elementary Zr. The degraded sample exhibits broadened peaks of the AB_2-phase. The Zr-pattern is weakened but still present while it is completely disappeared in the spectrum of the regenerated sample. None of the spectra gives a hint to the presence of additional hydride phases.

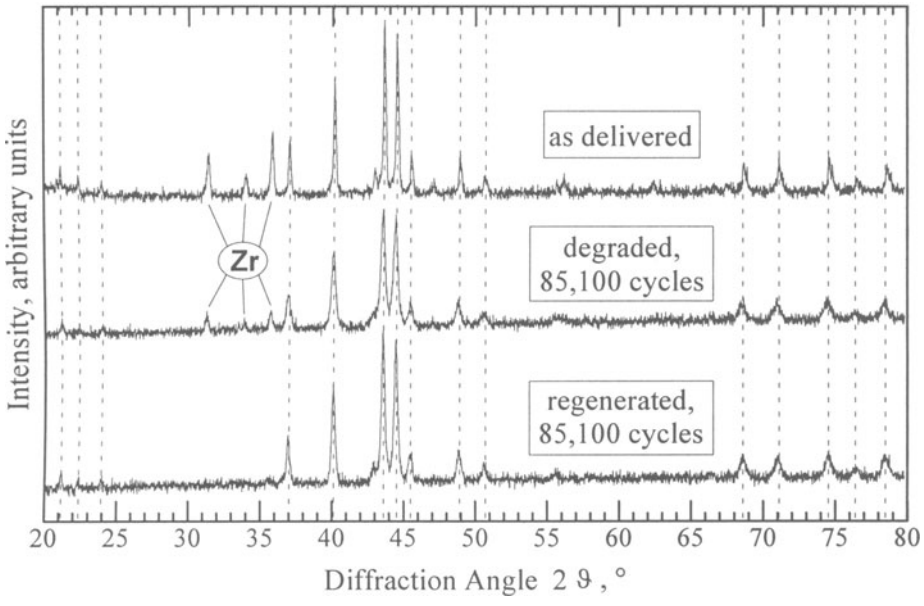

FIGURE 4. X-ray diffraction patterns of $Ti_{0.98}Zr_{0.02}V_{0.43}Fe_{0.06}Cr_{0.05}Mn_{1.52}$

The medium particle size of the as delivered alloy was 17µm. During cycling it decreased to a value of 6µm. As expected the regeneration procedure had no further influence on the particle size distribution.

4. Conclusions

The investigated alloy $Ti_{0.98}Zr_{0.02}V_{0.43}Fe_{0.06}Cr_{0.05}Mn_{1.52}$ (HWT 5800) is well suited for the application in metal hydride sorption machines because of its extraordinary stability during long-term cycling. Furthermore small changes in its thermodynamic properties can be regenerated by heating the alloy under vacuum to at least 400°C.
The importance of the Zr surplus in the as delivered sample could not be elucidated.
The degradation might be based on the formation of hydrides besides AB_2H_3 that are too stable to be dissociated under the normal cycling conditions. XRPD did not show such additional phases but the degradation was so small that such phases probably cannot be resolved by the diffractometer.

Acknowledgements

The authors are very grateful to various laboratories of the Max-Planck-Institut für Metallforschung in Stuttgart (especially to M. Thomas) for their support with XRPD and laser granulometry experiments.
This work was supported by the Deutsche Forschungsgemeinschaft (DFG) in the frame of Sonderforschungsbereich 270 "Hydrogen as an Energy Carrier".

References

1. Cohen, R.L., West, K.W., Wernick, J.H.: Degradation of $LaNi_5$ by Temperature Induced Cycling, *J. Less-Common Met.*, **73** (1980), 273-279
2. Cohen, R.L., West, K.W.: Intrinsic Cycling Degradation in $LaNi_5$, *J. Less-Common Met.*, **95** (1983), 17-23
3. Goodell, P.D.: Stability of Rechargeable Hydriding Alloys During Extended Cycling, *J. Less-Common Met.*, **99** (1984), 1-14
4. Park, J.M., Lee, J.-Y.: The Intrinsic Degradation Phenomena of $LaNi_5$ and $LaNi_{4.7}Al_{0.3}$ by Temperature Induced Absorption-Desorption Cycling, *Mat. Res. Bull.*, **22** (1987), 455-465
5. Chandra, D., Bagchi, S., Lambert, S., Cathey, W., Lynch, F., Bowman, R.: Long-Term Thermal Cycling Studies of $LaNi_{5.2}$, *J. Alloys Comp.*, **199** (1993), 93-100
6. Kim, G.H., Lee, J.-Y.: The Changes of Hydrogenation Properties Induced by Thermal Cyclings in $MmNi_{4.5}Al_{0.5}$ and $MmNi_{4.15}Fe_{0.85}$, *J. Less-Common Met.*, **132** (1987), 123-132
7. Han, J.I., Lee, J.-Y.: An Investigation of the Intrinsic Degradation Mechanism of $LaNi_5$, *Int. J. Hydrogen Energy*, (1988), 577-581
8. Ahn, H.J., Lee, J.-Y.: Intrinsic Degradation of $LaNi_5$ by the Temperature Induced Hydrogen Absorption-Desorption Cycling, *Int. J. Hydrogen Energy*, **2** (1991), 93-99
9. Wang, Q. D.,Wu, J.: The Cycling Behavior of Multi-Component Mischmetal-Nickel Hydrogen Storage Alloys on Cycling with Industrial Hydrogen, *Z. Phys. Chem. NF*, **164** (1989), 1305-1311
10. Mordkovich, V.Z., Korostyshevsky, N.N., Baychtock, Y.K., Dudakova, N.V., Mordovin, V.P., Sosna, M.H.: $LaNi_5$ and $Ce_xLa_{1-x}Ni_5$ Changes in the Course of Thermobaric Cycling in Hydrogen and Nitrogen/Hydrogen Mixture, *Int. J. Hydrogen Energy*, **10** (1990), 723-726
11. Josephy, Y., Bershadsky, E., Ron, M.: Investigation of $LaNi_5$ after prolongued Cycling, *J. Less-Common Met.*, **172-174** (1991), 997-1008
12. Lambert, S.W., Chandra, D., Cathey, W.N., Lynch, F.E., Bowman, R.C.: Investigation of Hydriding Properties of $LaNi_{4.8}Sn_{0.2}$, *J. Alloys Comp.*, **187** (1992), 113-135
13. Zhu, H.Y., Wu, J., Wang, Q.D.: Disproportionation of $LaNi_5$ and TiFe in 4 MPa H_2 at 300°C, *J. Alloys Comp.*, **185** (1992), 1-6
14. Gamo, T., Moriwaki, Y., Yanagihara, N., Iwaki, T.: Life Properties of Ti-Mn Alloy Hydrides and their Purification Effect, *J. Less-Common Met.*, **89** (1983), 495-504
15. Bernauer, O., Töpler, J., Noréus, D., Hempelmann, R., Richter, D.: Fundamentals and Properties of some Ti/Mn Based Laves Phase Hydrides, *Int. J. Hydrogen Energy*, **3** (1989), 187-200
16. Friedlmeier, G., Manthey, A., Wanner, M., Groll, M.: Cyclic Stability of Various Application-Relevant Metal Hydrides, *J. Alloys Comp.*, **231** (1995), 880-887
17. Friedlmeier, G., Schaaf, M., Groll, M.: How to Measure Pressure Concentration Isotherms Representative for Technical Application, *Z. Phys. Chem. NF*, **183** (1994), 185

OPTIMIZATION OF FABRICATION CONDITIONS OF METAL-HYDRIDE ELECTRODE RECHARGEABLE WITH HYDROGEN GAS

N. KURIYAMA, T. SAKAI, H. TANAKA, H. T. TAKESHITA,
I. UEHARA, AND T. IWASAKI*
Osaka National Research Institute, AIST, MITI
Midorigaoka 1-8-31, Ikeda, Osaka 563, Japan
*Osaka Electro-Communication University
Hatsu-machi 18-8, Neyagawa, Osaka 572, Japan

1. Introduction

An air-metal hydride (Air-MH) battery has been studied as one of energy conversion systems with a high energy density for electric vehicles (theoretical capacity: 458 $Wh \cdot kg^{-1}$ for Air-$LaNi_5H_6$) [1,2]. The metal-hydride negative electrode of this battery is recharged by exposing it to hydrogen gas (H_2-recharge), and also electrochemically recharged by use of an additional electrode for oxygen evolution. Therefore the Air-MH battery is suitable for the use in the future community in which both hydrogen gas and electricity are available. We have developed a metal hydride electrode for this battery, and showed that the electrode was recharged with hydrogen gas at the rate comparable to usual electrochemical recharging [3].

In this paper, we will report optimization of fabrication conditions of the electrode (surface treatment, activation method of the electrode, content of binder, and diameter of alloy particles) to improve H_2-recharge rate, dischargeability, and longer cycle life than our first electrode.

2. Experimental

2.1 H_2-CHARGE/DISCHARGE EXPERIMENT

The testing system for H_2-rechargeable electrodes is shown in *Figure 1a*. The electrode holder with an electrode was placed in a polyethylene vessel filled with 6M KOH aqueous solution. The vessel was immersed in a water bath, and equipped with a nickel plate as a counter electrode and a Hg/HgO (6M KOH) reference electrode. Discharge and electrochemical charge were controlled by a Hokuto Denko HJ-201B charge/discharge controller. Pressure of hydrogen gas was manually controlled by a mass-flow meter and a strain-gauge manometer.

H_2-recharge of an electrode and determination of its capacity were carried out at 40 °C as follows: (1) The valves 1, 2, and 3 in *Figure 1a* are opened, and electrolyte in the cell is removed by flowing H_2 gas for 30 s. (2) The valve 3 is closed, and the pressure in the cell is kept at 0.118 MPa for a given period. (3) The valves 1, 2, and 3 are closed, and electrochemical capacity of the electrode are determined by electrochemical discharging to -0.8 V (vs. Hg/HgO). Discharge current are

T. O. Saetre (ed.), Hydrogen Power: Theoretical and Engineering Solutions, 263–268.

decreased down to 20 mA step-by-step during discharging, when electrochemical capacity of the electrode is measured.

Electrochemical capacity of an electrode after H_2-recharge for 0.5 hours ($C_{0.5}$) was measured to estimate rate of H_2-absorption. Since the electrochemical capacity of our electrodes without any treatment were saturated with H_2-recharge for over 12 hours [3], electrochemical capacity of the electrode after H_2-recharge for 15 hours (C_{15}) was also measured to determine its maximum electrochemical capacity. A ratio, $100 \cdot C_{0.5}/C_{15}$, was calculated as a measure of H_2-recharge rate of electrodes.

Dischargeability of an H_2-rechargeable electrode was also tested at 40 °C with the cell shown in *Figure 1a*. The electrode was discharged at a given current, I, after H_2-recharge of half of C_{15}. Dischargeability of the electrode was shown as a ratio of electrochemical capacity at I, C(I), to that at 0 $mA \cdot g^{-1}$, C(0), where C(0) was determined by extrapolation of C(I) to 0 $mA \cdot g^{-1}$.

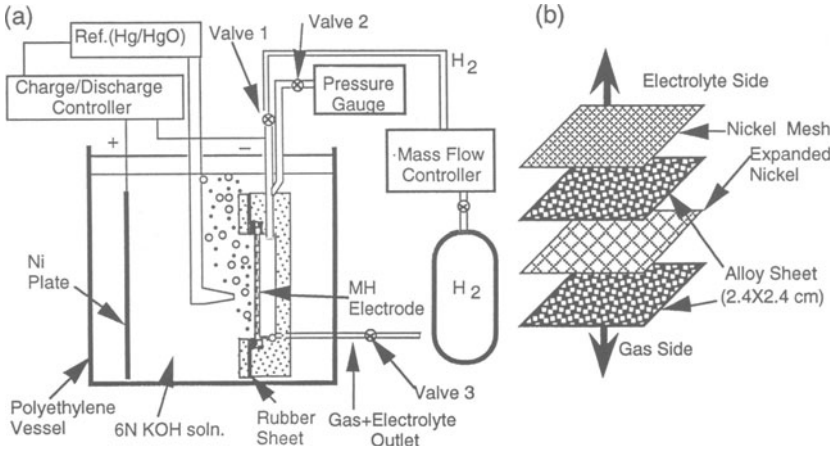

Figure1. (a) Half-cell testing system for the H_2-rechargeable electrode. The vessel is placed in a water bath at 40 °C. (b) Structure of a H_2-rechargeable electrode.

2.2 ELECTRODE PREPARATION

An AB_5-type alloy, $MmNi_{3.5}Co_{0.7}Al_{0.8}$, was purchased from Santoku Metal Industry, where Mm indicates mishmetal (La: 25%, Ce: 54%, Pr: 5%, Nd: 16% in atomic ratio). The alloy was used without any heat treatment. An ingot was crushed into powder and sieved. The alloy powder was chemically coated with copper (20 wt% of alloy) [4]. The powder was mixed well with PTFE dispersion (Daikin Industry, POLYFLON D-2) as binder, and the mixture was shaped into two sheets. A H_2-rechargeable electrode consists of the alloy sheets, a fine nickel mesh, and an expanded nickel sheet. Those were stacked as shown in *Figure 1b*, and pressed at 100 $kgf \cdot cm^{-2}$ at 300°C *in vacuo*. The electrode was cut into a 24×24 mm square (net alloy weight : 1.70 g), and held by a electrode holder with a 20×20 mm square window, when H_2-recharge/discharge experiment was carried out.

Two different surface treatments, acid treatment and reduction treatment, made for the alloy powder under 150 μm. For the acid treatment, 8 g of the alloy powder before copper coating was stirred in 300 cm^3 of 0.06 M hydrochloric acid. For the reduction treatment, 10 g of the alloy powder after copper coating was kept at 80 °C

for 16 hours in 50 cm^3 of a alkaline reducing agent, 6 M KOH aqueous solution containing 1 g of $NaPH_2O_2$. The effect of the surface treatments was examined for the electrodes adding 5 wt% of PTFE for weight of alloy powder. The surface of the alloy powder without copper coating was analyzed with a XPS spectrometer (Shimazu ESCA-750) before and after the surface treatments. Ar^+ ion sputtering at 2 kV was used to measure depth profiles of XPS spectra.

Influence of particle size of alloy was examined for alloy powder under 63 μm, 105 μm, 150 μm, and between 63 μm and 150 μm after the reduction treatment. 2 wt% or 5 wt% of PTFE for weight of alloy was added to the test electrodes. Distribution of particle size was determined by light scattering method. Influence of binder content was also examined for the electrodes containing 2 wt%, 5 wt%, and 10 wt% of PTFE to weight of alloy. The alloy powder for this test was sieved under 63 μm or 150 μm, and treated with the reducing agent. In this paper, 'wt%' means the percentage to the weight of alloy in the electrode.

3. Results and Discussion

3.1 EFFECT OF SURFACE TREATMENT

Discharged capacities of the electrodes after H_2-recharge for 0.5 hours and 15 hours ($C_{0.5}$ and C_{15}) are shown in *Figure 2*. The electrodes using alloy powder without treatment and with acid treatment showed similar discharged capacities, that is, similar H_2-recharge rate. On the other hand, the electrode with reduction treatment exhibited larger discharged capacities than the other electrodes. 45% increase in $C_{0.5}/C_{15}$ of this electrode relative to the untreated electrode shows appreciable improvement of the H_2-recharge rate through the reduction treatment. Depth profiles of relative concentrations of elements determined by XPS shown in *Figure 3* indicate disappearance of Al and enrichment of La and oxygen for the alloy with reduction treatment with respect to the others which show similar depth profiles. In the decomposed region, Ni was metallic, and La was oxidized. These results suggest that the alloy surface coexisting metallic Ni and oxide of rare earth elements should lead to active surface for absorption of H_2.

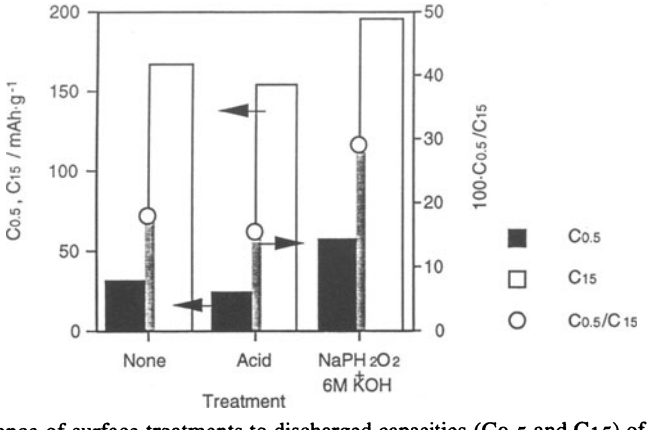

Figure 2. Influence of surface treatments to discharged capacities ($C_{0.5}$ and C_{15}) of the electrodes and the ratio, $C_{0.5}/C_{15}$, as a measure of H_2-recharge rate of electrodes.

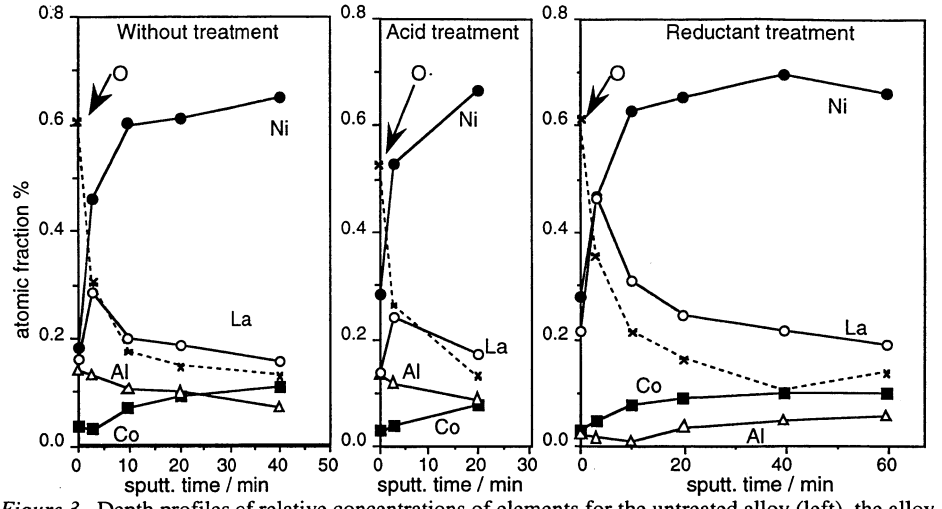

Figure 3. Depth profiles of relative concentrations of elements for the untreated alloy (left), the alloy with acid treatment (center), and the alloy with reduction treatment (right). ○:La, ●:Ni, ■:Co, △:Al, ✖: O, where concentration of La is multiplied by 4.0.

3.2 INFLUENCE OF PARTICLE SIZE AND BINDER CONTENT

The reduction treatment which exhibited the fastest H2-recharge rate in the previous section was applied to alloy powder used in the electrodes in this section.

Influence of particle size of alloy to H_2-recharge is shown in *Figure 4*. Discharged capacity after 0.5 hours H_2-recharge of the electrodes increased with decreasing maximum particle size of alloy powder, and the electrode (<63μm-5wt%) recharged 40% of C_{15} for 0.5 hours. (In this section, for example, 'electrode (<63μm-5wt%)' is abbreviated as the electrode using the alloy powder smaller than 63 μm and containing 5 wt% of binder (PTFE) to 1 part of alloy.) On the other hand, quite slow H_2-recharge was observed for the electrode (63~150μm-5wt%) without particles smaller than 63 μm, and this electrode was not saturated with hydrogen even after H_2-recharge for 48 hours.

$C_{0.5}/C_{15}$ values estimated from particle size distribution of alloy powder and $C_{0.5}/C_{15}$ for the electrode (<150μm-5wt%), $S/S_{(<150\mu m)} \times \{C_{0.5}/C_{15}\}_{(<150\mu m)}$, were also calculated, where spherical particles of alloy was assumed. The estimated values agrees well with the measured $C_{0.5}/C_{15}$ values as shown in *Figure 4*. Therefore, H_2-recharge rate is concluded to be proportional to surface area of alloy powder in an electrode, and particles smaller than 63 μm are required for effective H_2-recharge.

Figure 5 shows influence of content of binder and particle size of alloy powder to H_2-recharge of the electrodes. For both the electrodes using powder smaller than 63 μm and 150 μm, the electrodes (<150μm-2wt%) and (<63μm-2wt%) indicated better $C_{0.5}$ and H_2-recharge rate than the electrodes containing more binder, respectively, for the same particle size distribution of alloy. Better dischargeability was also observed for the electrode containing smaller amount of binder as shown in *Figure 6*. These results suggest that excess binder should cover alloy particles and interfere diffusion of H_2 and electrolyte to an alloy surface. Since the mixture of alloy powder and PTFE binder less than 2 wt% was difficult to shape a sheet for an electrode, 2 wt% of binder is the best content for the H_2-rechargeable electrode.

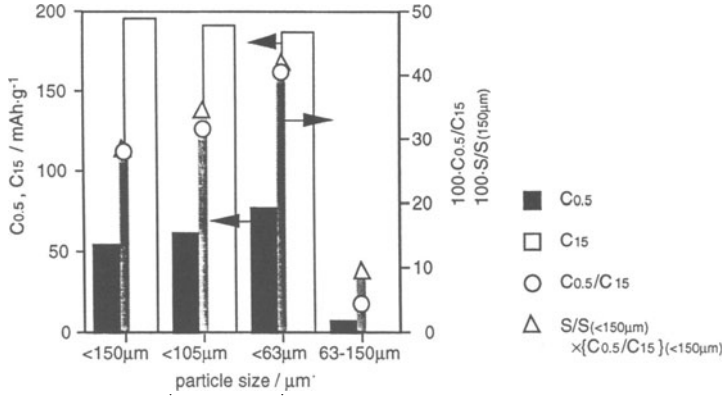

Figure 4. Influence of particle size to H_2-recharge of the electrodes. Open triangles indicate relative surface area, $S/S_{(<150\mu m)}$, assuming spherical shape of the alloy particles. '$C_{0.5}/C_{15}$' for the electrode '63~150μm' was evaluated by using average of C_{15} of three other electrodes.

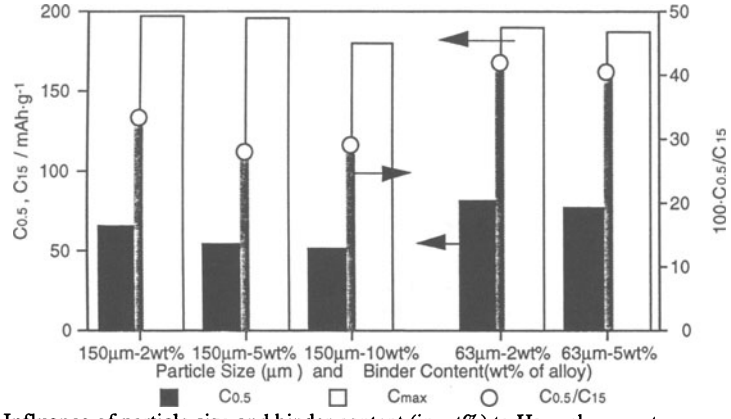

Figure 5. Influence of particle size and binder content (in wt%) to H_2-recharge rate.

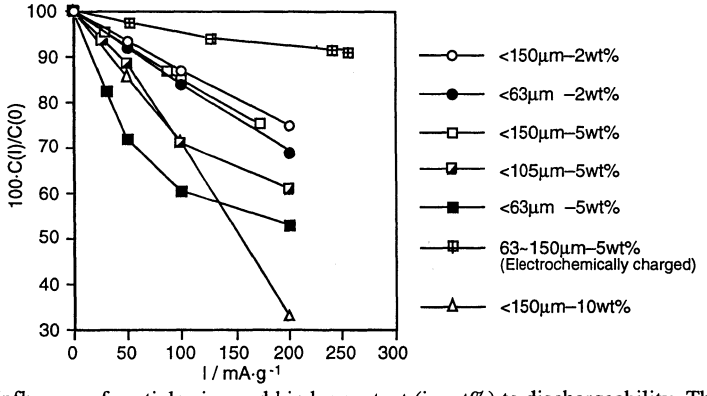

Figure 6. Influence of particle size and binder content (in wt%) to dischargeability. The electrode (63~150μm-5wt%) was electrochemically charged.

Based on the comparison of H_2-recharge rate, the electrodes containing finer alloy powder and smaller amount of binder is more suitable to effective H_2-recharge. However, as shown in *Figure 6*, the electrodes (<63μm-2wt%) and (<63μm-5wt%) containing fine alloy particles indicated worse dischargeability and maximum electrochemical capacity, C_{15}, than the electrodes (<150μm-2wt%) and (<150μm-5wt%) containing large particles, respectively. This result shows that fine particles interfere discharge process, probably because of increase of resistance in the electrode due to increase in particle-to-particle contact. This speculation would be supported by better dischargeability of the electrode (63~150μm-5wt%) without fine alloy particles.

3.3 THE OPTIMIZED ELECTRODE AT THE PRESENT STAGE

According to the results of influence of particle size of alloy and binder content to H_2-recharge and dischargeability, at the present stage, the best preparation conditions of the electrode for an H_2-rechargeable air-MH battery is :

surface treatment : reduction treatment
(16 hours in 6 M KOH containing $NaPH_2O_2$ at 80 °C)
particle size of alloy powder : <150 μm
binder content : 2 wt% of alloy powder.

This optimized electrode absorbed hydrogen of 34% of its capacity for 30 min. H_2-recharge at 40 °C, and showed fairly good dischargeability. This recharging rate is higher by 80%, and the dischargeability is higher by about 5%, than those of the original electrode [3].

4. Conclusion

Fabrication conditions of the electrode (surface treatment, content of binder, and particle size of alloy) were optimized in order to obtain higher H_2-recharge rate and dischargeability than our first electrode. The alloy, $MmNi_{3.5}Co_{0.7}Al_{0.8}$, was adopted in this study in order to show the effect of preparation method. The optimized electrode absorbed hydrogen of 34% of its capacity for 30 min. H_2-recharge at 40 °C. This recharging rate is higher by 80% than that of the original electrode. The dischargeability of the optimized electrode was also increased by 25%. These results show the possibility of an Air-MH battery rechargeable with hydrogen gas.

5. References

[1] Folonari, C., Iemmi, G., Manfredi, F., and Rolle, A.: Metal hydride fuel cells: a feasibility study and prespectives for vehicular applications, *J. Less-Common Met.*, **74** (1980), 371-378.

[2] Sakai, T., Iwaki, T., Ye, Z., Noréus, D., and Lindström, O.: Air-metal hydride battery construction and evaluation, *J. Electrochem. Soc.*, **142** (1995), 4040-4045.

[3] Kuriyama, N., Sakai, T., Miyamura, H., Uehara, I., and Ishikawa, H.: Development of an metal-hydride electrode rechargeable by mean of gaseous hydrogen, *Hydrogen Energy Progress X*, (Proc. 10th World Hydrogen Energy Conf., Cocoa Beach, FL, June 20-24, 1994), (1994), 1713-1718.

[4] Ishikawa, H., Oguro, K., Kato, A., Suzuki, H., and Ishii, E.: Preparation and properties of hydrogen storage alloy-copper microcapsules, *J. Less-Common Met.*, **107** (1985), 105-110.

ABSORPTION AND CAPACITY OF HYDROGEN WITH A La-Ni ALLOY PARTICLE BED

N. MITSUISHI*, S. FUKADA**, S. SATO*, Y. MIYAIRI*
* *Department of Mechanical Engineering, Kyushu Kyoritsu University, Jiyugaoka, Yahatanishi-ku, Kitakyusyu, 807, Japan*
** *Department of Nuclear Engineering, Kyushu University, Hakozaki, Fukuoka 812-81, Japan*

Deuterium and tritium have to be recovered from mixtures of hydrogen isotopes and inert gas in the fuel cycle of a fusion reactor, since the hydrogen isotopes have to be used as fuel and helium also has to be removed as ash or sweep gas. The high recovery efficiency at the low concentration of hydrogen is of great concern in the fuel cycle because tritium is radioactive and valuable. A metal particle bed is one of the most useful ways of the separation of hydrogen isotopes and inert gases. In this study the capacity and absorption rate of hydrogen at low concentrations were experimentally investigated using the particle bed of La-Ni alloys such as La_3Ni and La_2Ni_3. H_2-Ar mixtures containing 1% to 10% H_2 were used, and the flow rate of the mixture was 116 NTP ml/min. In order to obtain the temperature dependence of hydrogen capacity (hydrogen atoms/alloy molecule) and absorption rates, the experiments were carried out in the temperature range 25-200 °C.
It was found that the breakthrough curves after more than 20 absorption and desorption cycles of hydrogen by these alloys coincide with the first breakthrough curve. It means that these La-Ni alloys are promising hydrogen absorbing alloys that may keep their activities. These alloys may be used to absorb hydrogen at room temperature to 50°C. The hydrogen capacity was values among 1 and 4 at the concentrations of hydrogen 1 to 10%. The results obtained of each alloy are discussed.

1. Introduction

In recent years recovering only hydrogen isotopes from hydrogen isotopes and inert gas mixtures in the fuel cycle of a D-T fusion reactor has gained interest. Especially, the storage of tritium and the removal of hydrogen isotopes from gas mixtures have been of great importance in the loops of the plasma exhaust gas and the blanket sweep gas in the fuel cycle. A recovery method using a metal particle bed is considered to be one of the most useful ways because of the reversible absorption and desorption of hydrogen. Many candidates of elementary metals such as uranium [1] yttrium [2,3] zirconium alloys [4,5], and titanium[6] have been proposed as hydrogen absorption materials. Any of those metals has a large capacity of hydrogen absorption, enough to be used as the storage material, whereas many metals except uranium and some other metals cannot effectively absorb hydrogen at temperatures lower than around 400°C. On the other hand, uranium has been used as a storage material at room temperature in the field of nuclear engineering. However, the elutriation of fine particles is a serious

T. O. Saetre (ed.), Hydrogen Power: Theoretical and Engineering Solutions, 269–274.

problem on its use, since uranium is used in the form of fine particles with a diameter of a few microns and is an internationally regulated material.
In this paper, an experimental study was carried out for the separation of a single component from hydrogen-argon mixtures using a La_3Ni or La_2Ni_3 particle bed.

2 Experimental

2.1 MATERIALS

TABLE 1 shows analytical data for lanthanum and nickel used. Lanthanum and nickel were taken into an argon glove box, washed with a mixture of hydrofluoric acid and nitric acid in order to remove oxides on metal surfaces. They were then washed with distilled water and acetone , weighed and melted in an arc melting furnace. The alloys were crashed and screened in an argon glove box, and packed in a column.

TABLE 1 Analytical data for La and Ni

Elements	La
Production by	Bauton steel & R.E.Co. in China
T.Re	98.5% min
La/T.Re	99.5% max
Ce+Pr+Nd +Sm+Y	1% max
Fe	0.5% max
Si	0.07% max
P	0.01% max
S	0.02% max

Elements	Ni
Production by	Inco.Co.
Co	0.0005% max
Cu	0.0005% max
Fe	0.0025% max
Pb	0.0005% max
Zn	0.0005% max
Al	0.0005% max
Si	0.0005% max
Ca	0.0005% max
As	0.0005% max
Mo	0.0005% max
W	0.0005% max
Ni	Bal (99.0%min)

2.2 APPARATUS

Figure 1 is a schematic diagram of the experimental apparatus. The part labeled "11" is a column packed with La-Ni alloy particles for selective hydrogen absorption from argon-hydrogen mixtures. The bleed system was maintained at an atmospheric pressure during absorption. *Figure 2* shows the details of the packed column. The packed column is a quartz pipe with an inside diameter of 10mm, heated using an electrical furnace or kept at around room temperature using a waterbath. The temperature was kept at a constant value by means of a temperature controller.
TABLE 2 shows packed conditions of La-Ni alloys.

TABLE 2 Packed beds of La_3Ni and La_2Ni_3 particles

	La_3Ni	La_2Ni_3
Analytical data of atomic ratio	$La_3Ni_{1.06}$	$La_2Ni_{3.10}$
Alloy weight (g)	5.005	5.005
Tungsten weight (g)	15.000	15.000
Particle dia.(mesh) (Alloy and W)	125~180 μ m (83~119mesh)	125~180 μ m (83~119mesh)
Weight ratio (Alloy :Tungsten)	La_3Ni : W= 1 : 3	La_2Ni_3 : W= 1 : 3
Packed height (mm)	50.0	47.0

2.3 PROCEDURES

The activation procedure was as follows; For La_3Ni 100% H_2 gas flows at a temperature of 470°C for 6 hours, and for La_2Ni_3 100%H_2 gas flows at a temperature of 610°C for 6 hours. These were repeated 3-5 times.
After the activation, the hydrogen absorption experiment was performed as follows. After the degassing of the particle bed at a temperature of 470°C for La_3Ni or 610°C for La_2Ni_3, and at a pressure of 4×10^{-4} Pa, highly purified argon gas was introduced into the bed and the bed was kept at the desired temperature and pressure. The H_2-Ar gas mixture was fed in, and the gas composition at the column exit was measured by a gas chromatograph. The experiments on hydrogen desorption were conducted with flowing argon because it was found to give the same results as that obtained by evacuating the column. Table 3 shows the experimental conditions.

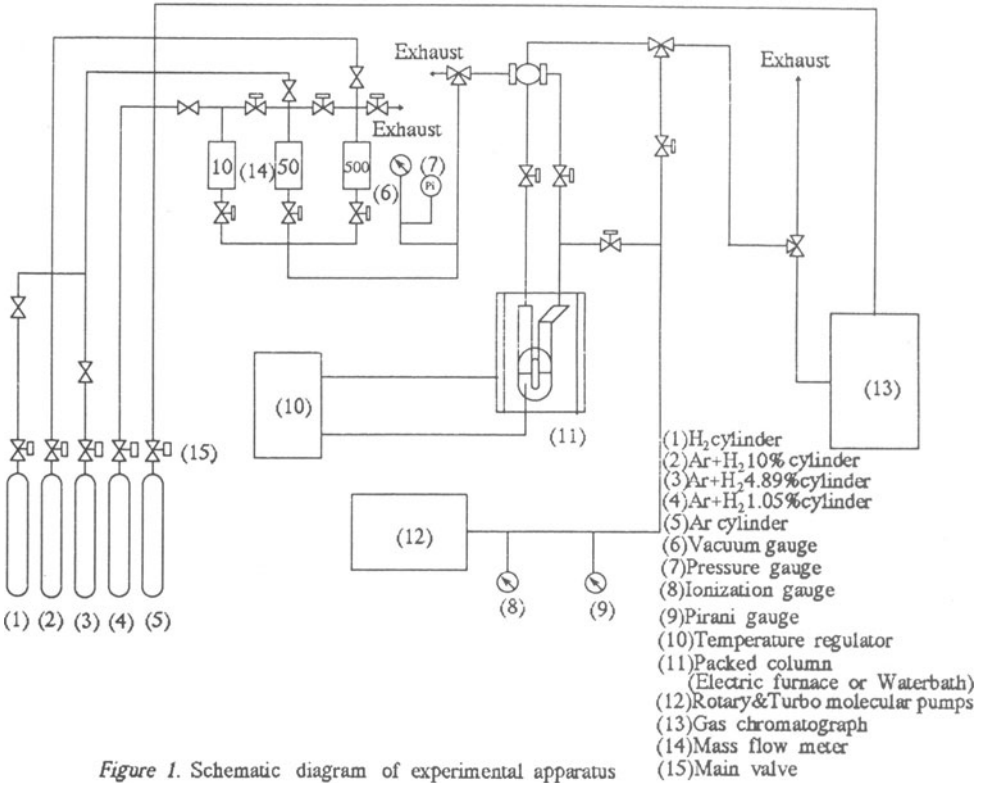

Figure 1. Schematic diagram of experimental apparatus

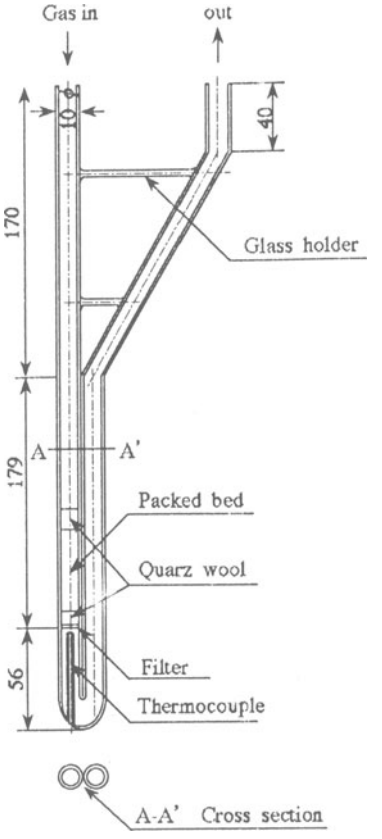

Figure 2. Packed column

TABLE 3 Experimental conditions

	La_3Ni		La_2Ni_3	
	Absorption	Desorption	Absorption	Desorption
Bed temperature (℃)	25,50,100,150	470	25,50,100, 150,200	610
Gas flow rate ml(NTP)/min	116	116	116	116
Gas composition	1.05,4.89,10% H_2+Ar	Ar	1.05,4.89,10% H_2+Ar	Ar

3. Results and Discussions

Figure 3 (a) shows an example of the effluent curve (this is called a breakthrough curve) for absorption of hydrogen. Unfortunately we can not determine the rate of mass transfer because there is no isotherm reported for these alloys and hydrogen. However, the slope of S shape is very steep. Therefore the rate of mass transfer is to be considered very high.

Figure 3 (b) shows also a typical example of hydrogen desorption by pure argon gas flowing. After more than 100 minutes almost all hydrogen was removed.

Figures 4 and 5 show hydrogen capacity that means hydrogen atoms/alloy molecule. In the case of La_3Ni, the dependence of temperature is very small, on the other hand, for La_2Ni_3 hydrogen capacity decreases with increasing temperature. These results may be considered to be very useful for engineering application.

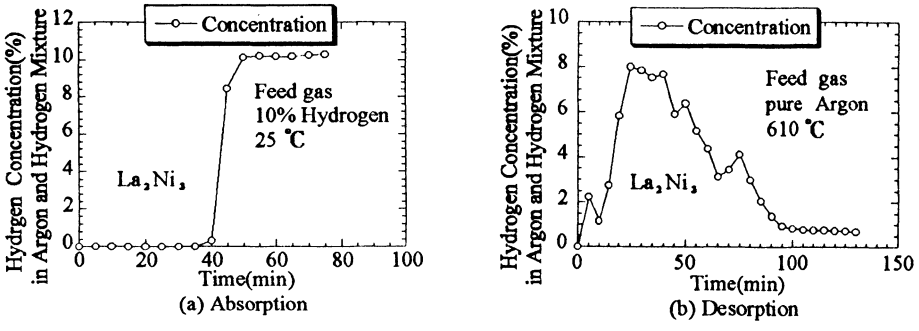

Figure 3. An example of absorption and desorption curves for La_2Ni_3

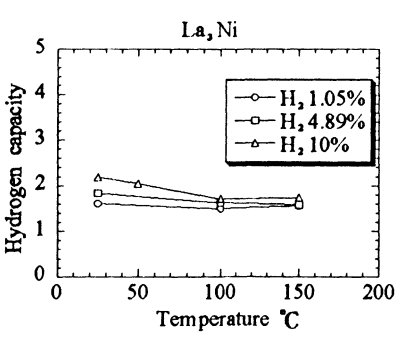

Figure 4. Relation between hydrogen capacity and temperature for La_3Ni

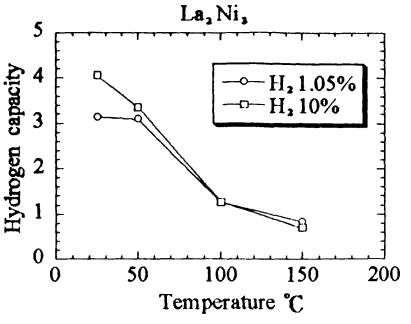

Figure 5. Relation between hydrogen capacity and temperature for La_2Ni_3

4. Conclusions

The selective absorption and desorption of hydrogen in an inert gas were experimentally investigated using La-Ni alloy particle packed bed. The results obtained are as follows:

(1)The La_3Ni and La_2Ni_3 can absorb comparatively large amounts of hydrogen in the temperature range 25-150 °C. The values of hydrogen capacity (hydrogen atoms/alloy molecule) are 1-4 at the hydrogen concentrations of 1.05 to 10%.

(2)The hydrogen concentrations at the outlet of the bed were less than 1 ppm.

(4)For almost complete hydrogen desorption, temperatures of 470°C for La_3Ni and 610°C for La_2Ni_3 are required.

References

1. Bokwa, S.R., Miller, J.M., Holtslander, W.J., and Johnson, R.E.: Handling high specific activity tritium, *Nucl. Instrum. Methods* **SA257**(1987), 52-56
2. Fukada, S., Kitajima, S., and Mitsuishi, N.: Effects of mass transfer resistance on hydrogen absorption in yttrium particle bed, *J.of Nuclear Sci., and Tech.* **25-11**(1988), 895-897
3. Fukada, S.,Nakahara, T.,and Mitsuishi, N.:Experimental and computational studies on absorption and desorption and multicomponent hydrogen isotopes from inert gas mixtures in a yttrium particle bed, *J.of Nuclear Material* **171** (1990), 399-407
4. Mitsuishi, N.,and Fukada, S.:Absorption and desorption of hydrogen with particle bed of some zirconium alloys , *J. ofNuclear Material* **175** (1990), 209-217
5. Mituishi, N., and Fukada, S.:Comparison of hydrogen absorption and desorption characteristics for zirconium and zirconium alloys, *Proc of 10th World Hydrogen Energy Conf., Cocoa Beach* , USA(1994), 1079-1088
6. Fukada, S., and Mituishi, N.:Effects of nitrogen on hydrating of a titanium particle bed, *Int . J. Hydrogen Energy* **18.8**(1993), 647-651

ON THE DEVELOPMENT OF NEW HYDROGEN STORAGE MATERIALS FeTi(Zr), Mg-xwt.% $CFMmNi_5$ AND Mg_2Ni (NANOPARTICLE) FOR IMPROVED HYDROGENATION CHARACTERISTICS

B.K.SINGH, S.S.SAI RAMAN, ARVIND KUMAR SINGH
Department of Physics, Banaras Hindu University, Varanasi-221005, INDIA

B.B.BANSAL
Department of Mechanical Institute, Institute of Technology, Banaras Hindu University, Varanasi-221005, INDIA

O.N.SRIVASTAVA
Department of Physics, Banaras Hindu University, Varanasi-221005, INDIA

1. Abstract

FeTi is one of well known state of the art hydrogen storage material. However its activation is rather difficult and research needs to be done to make the activation amenable. We have therefore undertaken a systematic study to find out the most appropriate elemental substitution which can turn the material readily activated. The basic idea behind them is to provide catalytic decomposition of hydrogen and reduce the activation temperature of FeTi. The $Fe_{1-x}Zr_xTi_{1+y}$ (x=0.2, y=0.3) alloy has been successfully synthesised using R.F.induction furnace (12 KW) under argon atmosphere in a previously outgassed graphite crucible. The structural characterisation (XRD) revealed that the as synthesised sample is multiphasic in nature and it exhibit the phases FeTi, Fe_2Ti, $FeTi_2$ and Ti respectively. P-C. isotherms was experimentaly determined and showed the storage capacity ~1.20 wt% at 200°C. The activation as well as desorption kinetics of FeTi is found to be significantly improved by addition of Zr corresponding to $Fe_{0.8}Zr_{0.2}Ti_{1.3}$. In search of new high hydrogen storage (>1.5wt%) capacities, alloys with general formula Mg-xwt% $CFMmNi_5$ (x=20, 30, 40 and 50) have been successfully synthesised. The as-synthesised composite materials have been activated at 550° ± 10°C under a hydrogen pressure of ~34 Kg cm^{-2} and their hydrogen storage capacities and desorption kinetics have been evaluated. The new composite hydrogen storage materials, in contrast to the native ingredient $CFMmNi_5$ [cerium free Mischmetal pentanickellide] have been found to possess much higher storage capacity (e.g. ~5.6. wt% for Mg-30wt% $CFMmNi_5$ as compared to ~1.4wt% for $CFMmNi_5$ alone) and to exhibit favourable absorption-

T. O. Saetre (ed.), Hydrogen Power: Theoretical and Engineering Solutions, 275–290.

desorption kinetics, typified to be about ~140 cm^3 min^{-1}. The structural, micro-structural characteristics have been explored using XRD, TEM, SEM and EDAX techniques. The synthesis of the hydrogen-storage alloy Mg_2Ni has been carried out through a single-step mechanical alloying and energy ball mill. The synthesised ball-milled Mg_2Ni alloy has been found to exist in the form of fine (nano) particles with sizes to about 40Å. The nanoparticle form has been found to lead to easy activation for hydrogenation by annealing at 300°C (about 10^{-4} torr vacuum) for 30 min. and hydrogen uptake has been found to commence from the first cycle itself.

Keywords : Hydrogen storage alloys ; Storage capacity ; Nanoparticle ; Magnesium rare earth nickel composite ; Desorption kinetics.

2. Introduction

Harnessing Hydrogen embodies two important ingradients, namely hydrogen production and storage. As regards to production, hydrogen is being routinely produce through any of the present on-hand technologies. For e.g. naptha cracking, steam reforming of natural gas, elctrolysis including off-peak power electrolysis. However the storage technologies cannot be said to have matured. The high pressure gaseoues storage has the problem of safety and storage efficiency and the storage in the form of liquid H_2 suffers from poor economic viability and sensitive handling problems. The storage in the form of reversible hydrides even though in its nascent stage as the foremost possibility of being successful in large scale application. The present known hydrides even though viable have the perrennial problems related to limited rather low storage capacities. For e.g. the present state of the art hydrides (FeTi ~1.7 wt.%), ($LaNi_5$ ~1.5 wt.%), (Mg_2Ni has comparitively high storage capacity of ~3.8 wt.% operate at high temperatures 300-400°C). The other desirable properties like desorption kinetics, recyclability, dormancy, poissonning effect due to impurity in the hydrogen gas, hysteresis etc., which is also have to be optimised. Because the foregoing factor, there is an ever on going search to find better hydride materials. To achieve this to prominent routes are being followed ; first to modify and optimise the present storage material. For e.g. development of composite and nanoparticle version and second to develop altogether new materials such as new carbon forms : (Fullerenes C_{60} and other higher versions) and graphitic tubules.

The present paper describes and discus the investigations dealing with the development of viable hydrogen storage system through the modification of the known storage materials. In particular this paper deals with the synthesis, characterisation and hydrogenation/ dehydrogenaion studies of FeTi(Zr), Mg-xwt% $CFMmNi_5$ and Mg_2Ni (in the nano particle form obtained through ball milling).

3. Experimental Details

3.1. SYNTHESIS OF $Fe_{1-x}Zr_xTi_{1+y}$ HYDROGEN STORAGE MATERIAL

Pure iron powder (purity 99.99 wt%), titanium and zirconium (purity 99.99 wt%) was used as a starting material. The compound of $Fe_{1-x}Zr_xTi_{1+y}$ (x=0.2, y=0.3) was taken in the right stoichiometric proportions, pressed into a pellet form (1 x 0.5 cm) and melted employing on R.F.induction furnace (12 KW) under an argon atmosphere in a previously outgassed graphite crucible which was kept inside the silica tube. The as-prepared alloy ingot was melted repeatedly (5-6 times) to achieve homogeneity. The agglomerate produced in this way was removed from the graphite crucible, crushed and a powder of ~0.1-1.0 mm was selected for hydrogenation experiments. Before the experiment, the compound was analysed by X-ray diffraction characterization employing a Philips X-ray diffractometer (PW-1710) using CuK_α radiation.

The hydrogen absorption and desorption behaviour were investigated using a sievert's type apparatus fabricated in our laboratory and utilized earlier for hydrogenation studies of other hydrogen storage material [1]. A known quantity of the alloy powder was placed in a reactor and was evacuated upto 10^{-4} torr. About 40 kg/cm^2 of hydrogen was introduced from a high pressure gas cylinder. Since the as-synthesized alloy does not absorb hydrogen at room temperature, this was activated at high temperatures(100-500°C) was attempted for the as-synthesized and powder forms of $Fe_{1-x}Zr_xTi_{1+y}$ (x=0.2, y=0.3) alloy phases. It was found that the most favourable activation process correspond to that where the alloy was heated to 400 ± 5 °C in approximately 40 kg/cm^2 hydrogen pressure. In order to activate the alloy, the reactor was heated at temperature of 400 ± 5 °C for 3-5 h continuously and then cooled to room temperature over 10 h duration. The hydrogen desorption characteristics of the alloy were monitored at room temperature, it was found that desorption did not take place of room temperature. Several absorption runs at different temperatures (100, 150 and 200 °C) were monitored. Finally, the hydrogen desorption chraracteristics of the activated sample were then evaluated at 400°C by monitoring the pressure composition-isotherm (P-C-T) through volumetric method.

3.2. SYNTHESIS OF Mg-x wt.% $CFMmNi_5$ COMPOSITE MATERIAL

The $CFMmNi_5$ alloy was synthesized through a solid state diffusion process by melting the stoichiometric mixtures of individual elements. High purity nickel (99.99%) and cerium-free misch-metal were taken in the correct stoichiometric proportions and pressed into a pellet form (1x 0.5 cm^2) to obtain an alloy with stoichiometry $CFMmNi_5$, and melted by employing a radio frequency (r.f.) induction furnace (12 KW) under an argon atmosphere in the silica tube containing the material. During the melting process, water was circulated in the outer jacket around the silica tube to suppress contamination of the silica by the alloy constituents, particularly magnesium. The initially prepared alloy ingot was melted

repeatedly (five or six times) to achieve homogeneity [2]. The agglomerate produced in this way was removed from the silica tube, crushed and subjected to X-ray diffraction characterization.

The composite alloys Mg-x wt.% $CFMmNi_5$ with x = 20, 30, 40 and 50 were prepared using the encapsulation method by taking a stoichiometric amount of $CFMmNi_5$ alloy and magnesium (99.99% purity), pressed into a pellet form. As the melting (boiling) point of Mg is lower than that of $CFMmNi_5$, and also taking into account the fact that Mg sublimes, a somewhat modified method was employed to avoid evaporation of Mg during the reaction to form pellets. In the encapsulation method, the lower melting or subliming component (e.g. Mg) is essentially first made in the form of a small pellet. It is then surrounded by an appropriate quantity of powder of the second ingredient (e.g. $CFMmNi_5$) and pelletized. The resulting pellet then has a low melting/subliming component in its core (i.e. Mg) and a high melting component (e.g. $CFMmNi_5$) surrounding the core from all sides. The superiority of the method is demonstrated by the negligible probability of escape of magnesium from the pellets when melted [3]. This leads to the nearly correct stoichiometric formations of Mg-x wt.% $CFMmNi_5$. The pellets were melted in a silica tube under an argon atmosphere with the help of the r.f. induction furnace, in the same was as employed for the synthesis of $CFMmNi_5$ alloy.

A Philips X-ray powder diffractometer PW-1710 equiped with a graphite monochromator was used for the structural characterisation studies of the as-synthesized as well as the hydrogenated composite materials Mg-x wt.% $CFMmNi_5$. Elemental compositions were checked through energy dispersive X-ray analysis using a PV-9900 EDAX analyser attached to a Philips EM-CM-12 electron microscope. The surface characteristics of the samples were monitored through scanning electron microscopy (SEM) to obtain microstructural features. After activation, the hydrogen was desorbed and the P-C-T charactersitics were monitored by a volumetric method after outgassing of the reactor vessel, employing the experimental system fabricated in this laboratory.

3.3. SYNTHESIS OF Mg_2Ni HYDROGEN STORAGE MATERIAL

The synthesis of Mg_2Ni was accomplished by ball milling of a stoichiometric mixture of Mg (99.8% pure) and Ni (99.9% pure). The magnesium and nickel powders were sieved to achieve a particle size of abount 100 μm. The mixture was ball milled for 100 h, at room temperature in an argon atmosphere with milling speed of 40 rev min^{-1}. The high energy ball mill used here was fabricated indigenously and was based on a somewhat modified version of the mill designed by Benjamin [4]. It has a cylinder of inner diameter about 5.6 cm, volume about 400 ml having an impeller and 40 steel balls of diameter about 0.95 cm. The volume fraction of the balls with reference to the tank was approximately 0.35.

4. Results and Discussion

4.1. $Fe_{1-x}Zr_xTi_{1+y}$ (x=0.2, y=0.3)

4.1.1. *Hydrogenation/Dehydrogenation Characteristics*

The hydrogen desorption kinetics (hydrogen concentration vs time) for the optimized hydrogen storage alloy $Fe_{0.8}Zr_{0.2}Ti_{1.3}$ was measured at 200°C under pressure 30 kg/cm^2. Fig.1 shows the rate of desorption of $Fe_{0.8}Zr_{0.2}Ti_{1.3}$ material, a comparison between Fig.1 with the known desorption characteristics of FeTi reveals that the initial hydriding rate was much faster but the total absorption capacity was lesser than the native $FeTi_{1.3}$.

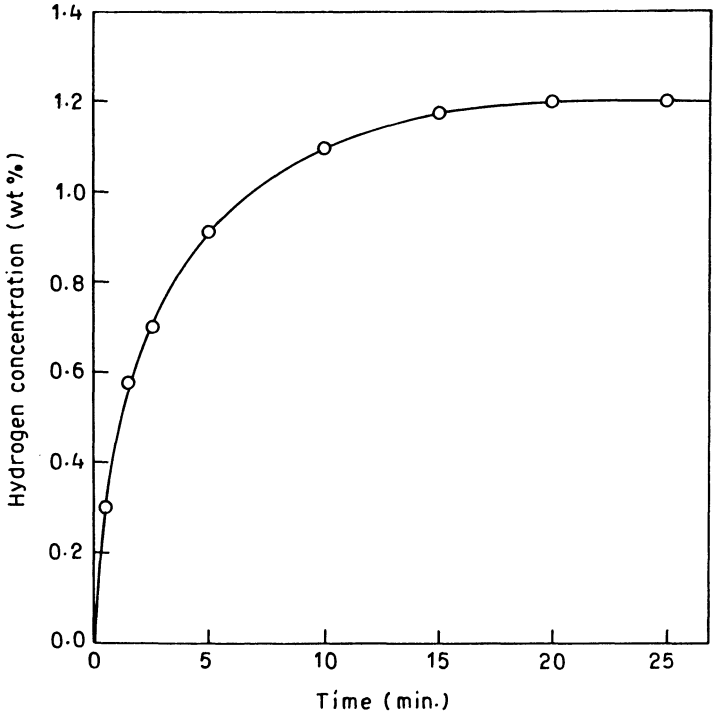

Fig.1. The amount of hydrogen desorbed vs time (kinetic curves) during the dehydriding process of the $Fe_{0.8}Zr_{0.2}Ti_{1.9}$ hydrogen storage alloy.

The Desorption of hydrogen to about 80% of the saturation value was accomplished within 6 minutes. However, the total time required for complete hydrogenation has been found to be about 20 minutes. The representative P-C-T curve of $Fe_{1-x}Zr_xTi_{1+y}$ (x=0.2, y=0.3) alloy is shown in Fig.2. The maximum storage capacity obtained for $Fe_{0.8}Zr_{0.2}Ti_{1.3}$, corresponds to ~1.20 wt% at 200°C.

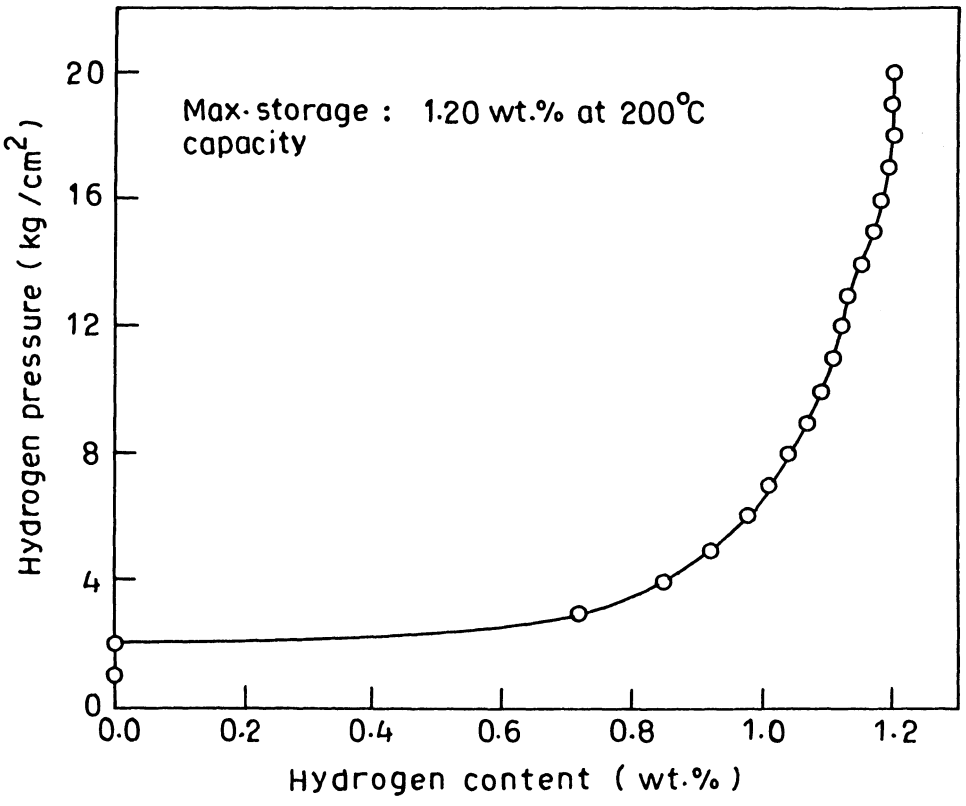

Fig.2. Pressure-Composition Isotherm of $Fe_{1-x}Zr_xTi_{1+y}$ (x=0.2, y=0.3) alloy at 200°C.

4.1.2. *Structural Characterization - (XRD) Exploration*

In order to unravel and understand the reason for the interesting hydrogen storage capacity of $Fe_{1-x}Zr_xTi_{1+y}$ (x=0.2, y=0.3), structural (XRD) characterization of as-synthesized sample was carried out.

Fig.3 shows the representative XRD pattern of the as-synthesized $Fe_{0.8}Zr_{0.2}Ti_{1.3}$ alloy. The analysis of XRD pattern revealed that the as-synthesized sample is of multiphasic in nature. It exhibits FeTi, Fe_2Ti, $FeTi_2$ and Ti phases, where FeTi is the dominant phase, Fe_2Ti, $FeTi_2$ and Ti are the minority phases.

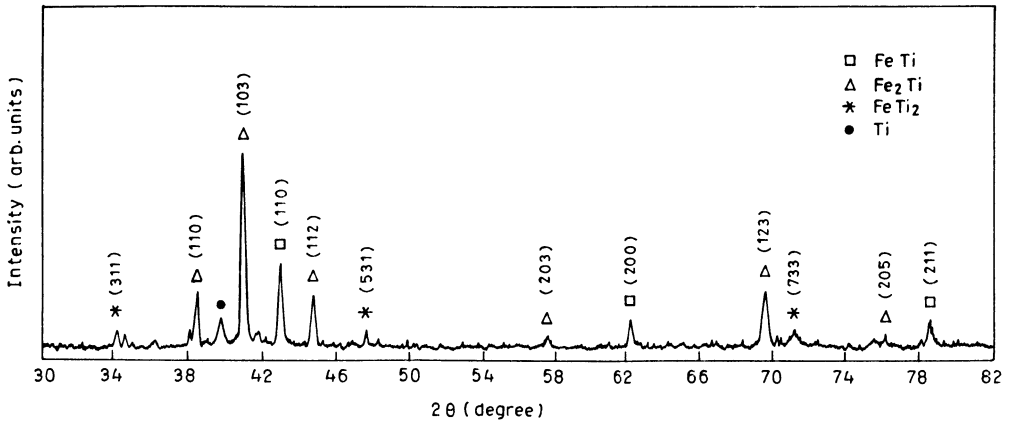

Fig.3. X-ray powder diffraction patterns of the as-synthesized $Fe_{0.8}Zr_{0.2}Ti_{1.3}$ alloy ; the formation of several phases have been outlined.

4.2. Mg-x wt.% CFMmNi$_5$ (x = 20, 30, 40 and 50)

4.2.1. *Hydrogen Dehydrogenation Characteristics*

The viability of the composite materials Mg-x wt.% CFMmNi$_5$ as high storage capacity materials (up to about 5.6 wt.%) has been elucidated in the present investigation. However, for composite materials including Mg-x wt.% CFMmNi$_5$, an important characteristic relates to the fact that they are multiphasic and have a high density of interfaces. Both features would make the details of desorption kinetics, and the related 'hysteresis' effect, hydrogenation characteristics, is essential for judging the viabillity of a hydrogenation material in practical system, e.g. vehicular transport, heat pumps, etc. Motivated by these considerations, the present investigations were carried out. In this paper. We describe and discuss these aspects for the composite materials Mg-x wt.% CFMmNi$_5$ appear to be one of the important forms of hydrogen storage material, with highest storage capacity around 5.6 wt.%.

The dehydriding behaviour of the composite alloys Mg-x wt.% $CFMmNi_5$ was evaluated and analysed for several values of x (20, 30, 40 and 50) at a temperature ranging from 400 to 500°C. Fig.4. represent desorption kinetic curves under different isothermal temperature conditions and at a pressure P of about 4 kg cm^{-2} for the optimised composite materials Mg-x wt.% $CFMmNi_5$ with x.

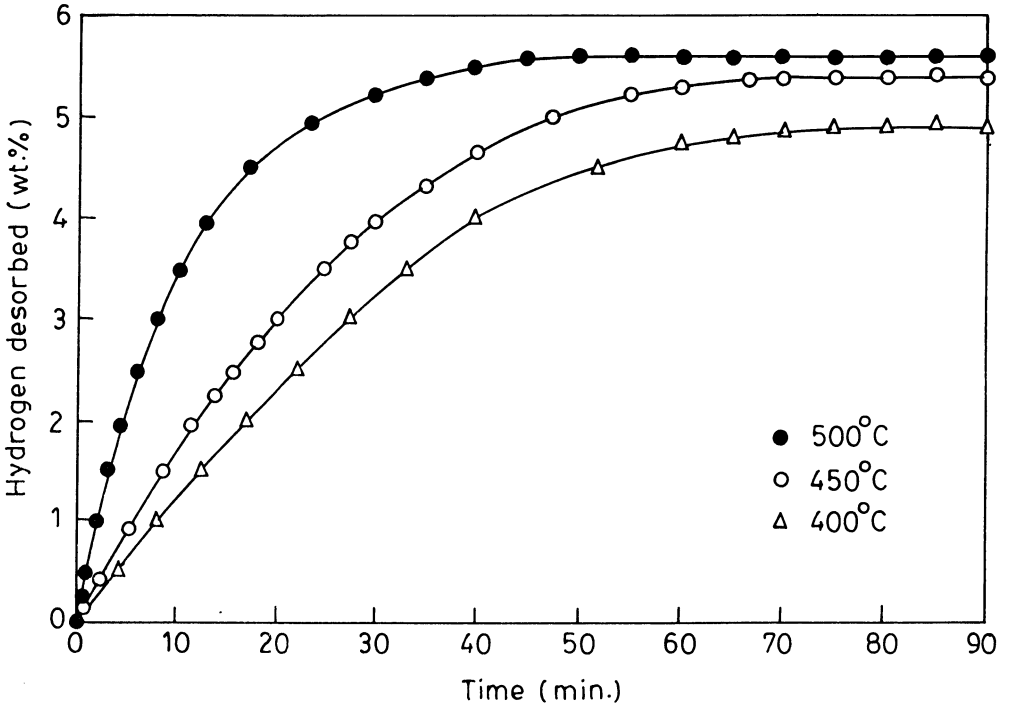

Fig.4. The amount of hydrogen desorbed vs time (kinetic curves) during the dehydriding process of the Mg-30wt% $CFMmNi_5$ composite alloy at different temperatures (400, 450 and 500 °C).

The results reveal that the desorption was strongly affected by temperatue and concentration of the intermetallic alloy $CFMmNi_5$. The initial release of hydrogen from the materials was linear with time, and this decreased at longer times. From the hydrogen desorption vs. time curves (see Fig.4), it may be inferred that the initial hydriding-dehydriding rate is much faster, and about 3 to 4 times better than the host material (say $CFMmNi_5$).

The hydrogen storage characteristics of the activated samples were then evaluated by monitoring the P-C-T isotherm for every cycle of hydrogenation of the material at three different temperatures, 400, 450 and 500 °C. The pressure-comosition isotherm of Mg-x wt% $CFMmNi_5$ for various of x have been evaluated. Representative P-C isotherms for the as-prepared composite optimised alloy is shown in Fig.5.

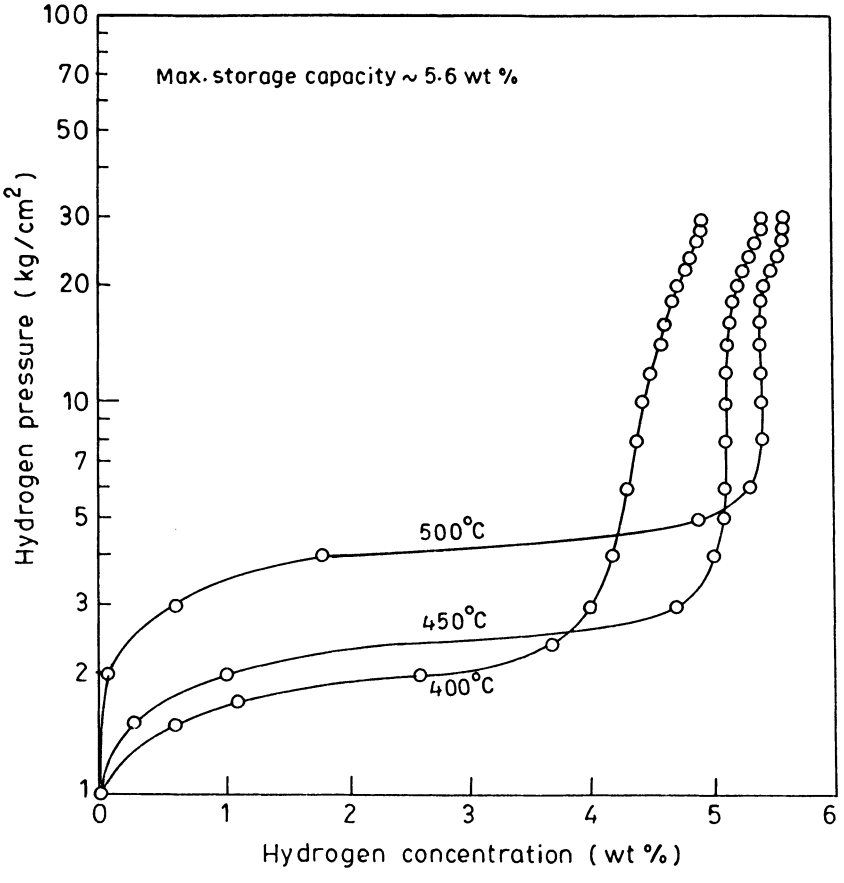

Fig.5. Pressure composition isotherms of the optimised composite alloys Mg-30 wt% $CFMmNi_5$.

It is clear from the P-C isotherms that the maximum weight percentage of hydrogen desorbed from the material is ~5.6 wt% for x=30 at 500 ± 10°C. It was noticed that after ten hydrogenation dehydrogenation cycles, the sample corresponded to fine particle-size (1-5μ) powders without any deterioration in hydrogenation characteristics. The storage capacity is, however, about 3.5 times greater than the cerium free mischmetal pentanickelide system and it makes this storage system attractive. Thus, the present

material can be said to correspond to a new exotic hydrogen storage material with viable hydrogen storage characteristics.

4.2.2. *Structural and Microstructural Characteristics-XRD and SEM Explorations*
In order to unravel the curious hydrogenation behaviour of Mg-x wt.% $CFMmNi_5$, structural (X-ray diffraction (XRD)) and microstructural (Scanning electron microscopy (SEM)) were carried out. It was found that hydrogenation capacities are closely correlated with the alloys. Figs.6(a)-6(d) show a representative X-ray diffraction pattern of the as-synthesized Mg-x wt.% $CFMmNi_5$ for x = 20, 30, 40 and 50 respectively.

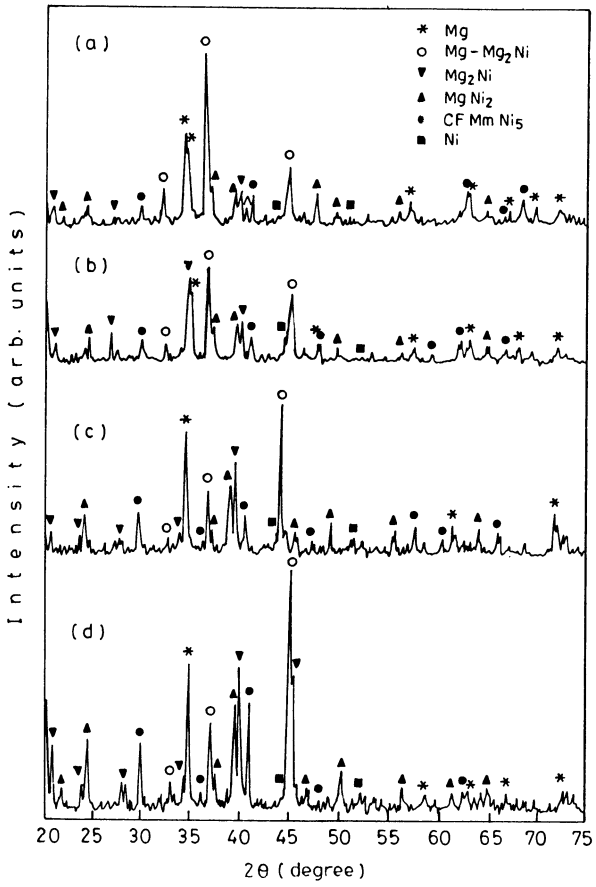

Fig.6. X-ray powder diffractions of the as-synthesised Mg-xwt% $CFMmNi_5$ composite alloys for various values x = (a).20, (b) 30, (c) 40 and (d) 50 ; the formation of several phases have been outlined.

These results reveal that the as-synthesized composite alloys are multiphasic in nature ; the majority and minority phases are free Mg, Mg-Mg_2Ni, $CFMmNi_5$ ($LaNi_5$) and $MgNi_2$, free Ni, $NdNi_5$ and $PrNi_5$ respectively. XRD patterns taken from the hydrogenated materials showed broadly similar features to those exhibited by the as-synthesized alloys with regard to the observed phases.

It is expected that an important parameter influencing hydrogenation-dehydrogenation is the presence of Ni on the surface. The hydriding and storage capacity are probably dependent on the Ni-bearing phases which form sites favourable for hydride reaction, and may also serve as channels by which the hydrogen can enter and exit the bulk of the main phase.

Fig.7(a) represents a scanning electron micrograph with secondary electrons of the as-synthesized composite material Mg-30 wt.% $CFMmNi_5$. The micrograph demonstrates the multiphasic nature of the material, in accordance with the XRD results already described.

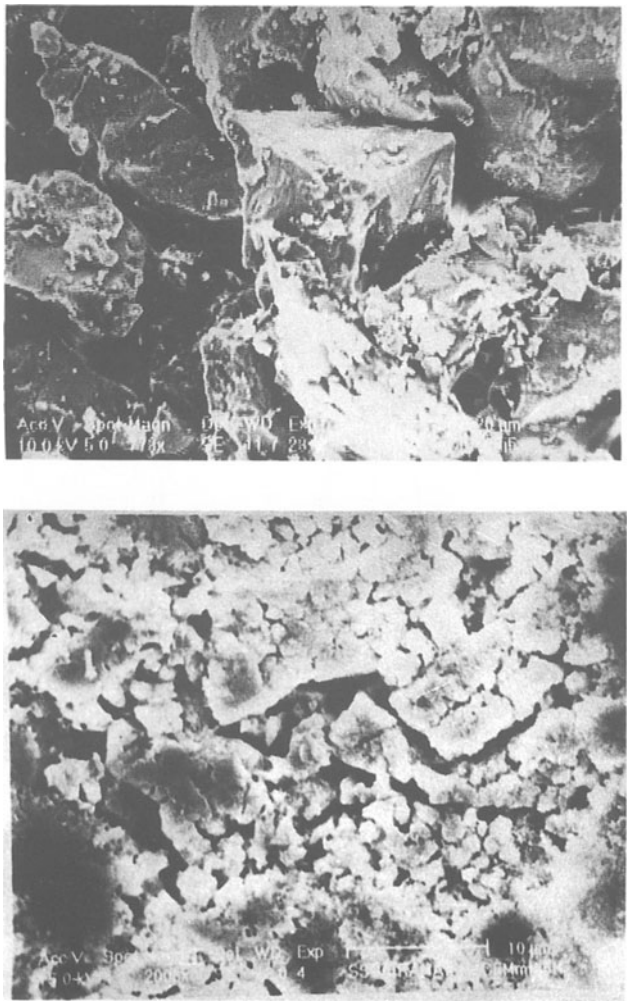

Fig.7. Represeutative scanning electrone micrograph of (a) the as-synthesized composite material Mg-30wt% $CFMmNi_5$ showing a magnesium matrix surrounded by $CFMmNi_5$ grains and (b) the hydrogenated (around to 10 cycles) composite materials Mg-30 wt% $CFMmNi_5$.

A micrstructure of the composite material Mg-30wt.% CFMmNi$_5$ exhibiting extensive cracking, obtained after activation and several hydrogenation-dehydrogenation cyclings, is shown in the SEM image of Fig.7(b).

4.3. Mg_2Ni ALLOY BY MECHANICAL ALLOYING

4.3.1. *Structural Characterisation - XRD Exploration*

In order to monitor the possible alloy formation, a small amount (0.5 gm) of the ball-milled material was intermittently taken out from the ball mill at time intervals of 50, 80 and 100 h. These small quantities were subjected to XRD characterization employing a Philips PW 1710 X-ray diffractometer equipped with graphitic monochromator and working with CuKα radiation (λ=1.5418 Å).

Fig.8 is a representative XRD pattern of the sample ball milled for 100 hours. This pattern reveals the clear and prominent peaks of Mg_2Ni with some free nickel. Thus the XRD characterization revealed that the Mg_2Ni alloy formation resulted after about 100 h of ball milling the elemental mixtures.

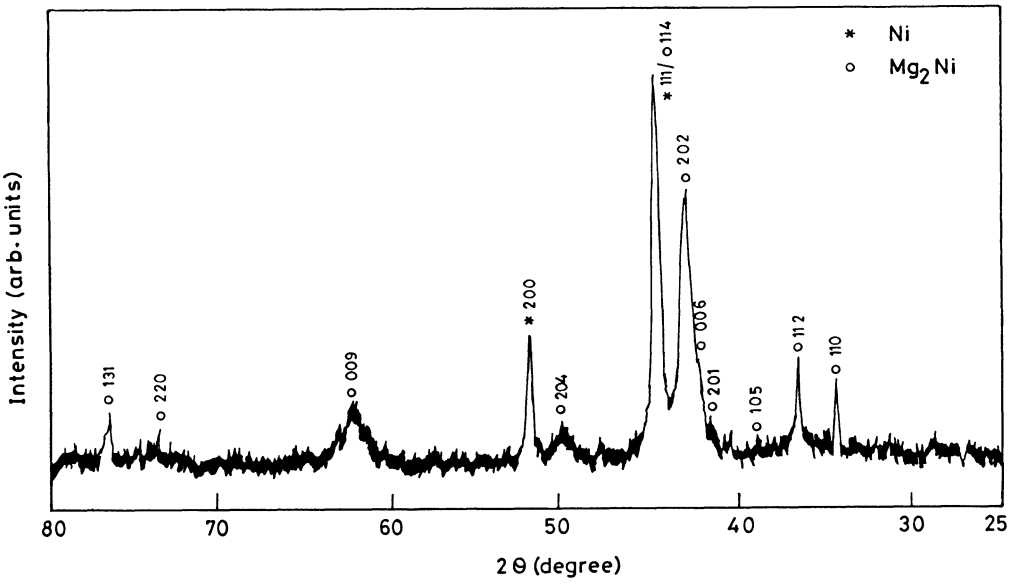

Fig.8. X-ray diffractograph of the mixture ball milled for 100 hours ; XRD peaks corresponding to well developed Mg_2Ni indication nearly complete alloy formation have been outlined and can be clearly seen.

4.3.2. *Hydrogenation/Dehydrogenation Characteristics*

The powder ball milled for 100 h was characterized for its hydrogenation dehydrogenation behaviour by monitoring the P-C-T curves. The alloy was activated by heating up to 300 ± 1 °C in vaccum of 10^{-4} torr for 30 min. Thereafter hydrogenation was carried out at the same temperature at a pressure of 30 kg cm^{-2}.

Fig.9 represents a typical P-C desorption curve at a temperature of 300°C from the Mg_2Ni ball milled powder in its fifth cycle which corresponds to 3.2 wt.%.

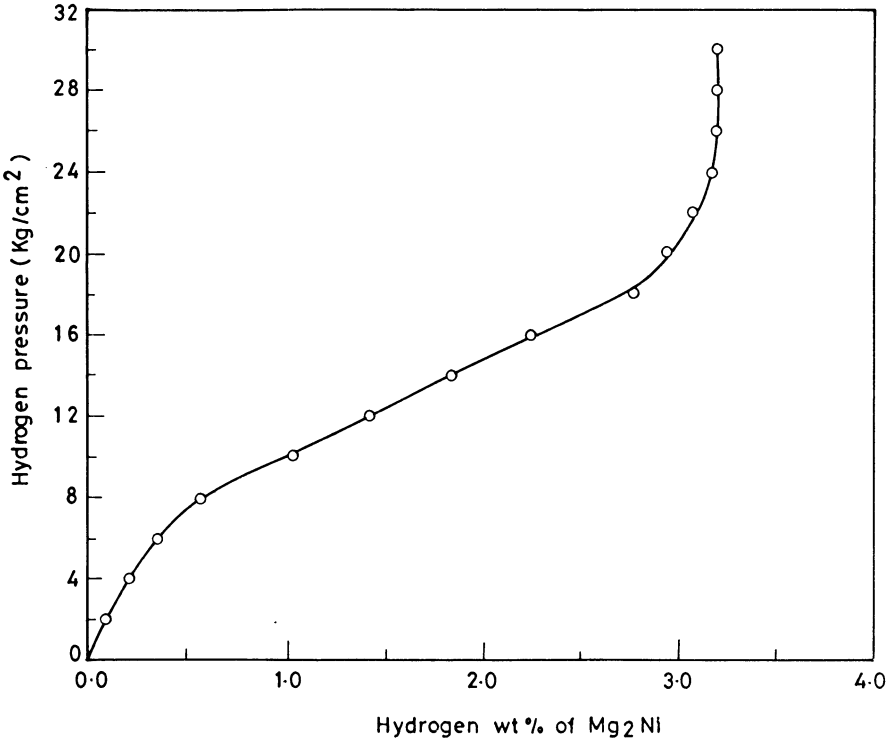

Fig.9. P-C desorption curves for activated sample which had been milled for 100 hours after fifth cycle.

Although the mechanically alloyed powder shows only 0.81 wt.% of hydrogen desorption in the first cycle, this in comparison to other versions of mechnically alloyed Mg_2Ni corresponds to a higher storage capacity. The excellent hydrogen desorption of the mechanically alloyed Mg_2Ni (ball milled for 100 h) may be attributed to the increased surface area corresponding to small particles (or isolated grains) resulting from continuous fragmentation in the ball milling process. In addition to this, the effect of the Mg_2Ni-Ni biphasic nature of the material may also lead to the improved hydrogenation characteristics.

4.3.3. *Microstructural Characterisation of Mg_2Ni - TEM Investigations*

The mechnically alloyed Mg_2Ni was also subjected to microstructural characterization using the transmission electron microscopic technique. Fig.10 shows the dark field image of the mechanically alloyed material exhibiting particle (isolated grains) size of about 40Å.

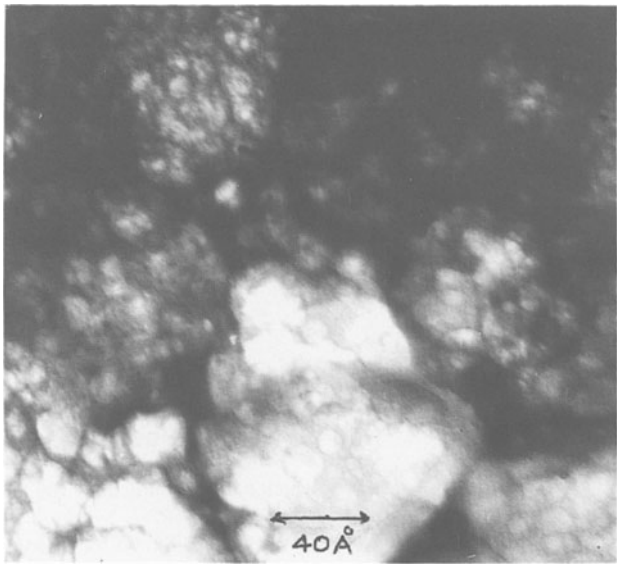

Fig.10. TEM image the sample ball milled for 100 hours . showing the presence of Mg_2Ni particle size of about 40Å.

It may be suggested that in the process of mechnical alloying the continuous fragmentation of particles leads to occurrence of isolated grains and owing to their small size,they become capable of absorbing and desorbing right from the first cycle.

Conclusion

In conclusion, it can be said that the present investigations have resulted in the development of several types of hydrogen storage materials namely $Fe_{0.8}Zr_{0.2}Ti_{1.3}$, Mg-xwt.% $CFMmNi_5$ (x = 20, 30, 40 & 50) and Mg_2Ni nanoparticle version obtained through ball milling. We have described and discussed the specific relevance of each of the materials in regards to synthesis, characterisation and their relevance of hydrogenation behaviour. As for e.g. FeTi(Zr), the important characteristics regards to the fast kinetics in comparision to the known hydrogen storage material (say FeTi) have been studied. For the case of composite materials Mg-xwt.% $CFMmNi_5$, the hydrogenation behaviour has been found to correspond to multiphasic system exhibits extraordinarily high storage capacity of ~5.6 wt.% ; however it operated on high temperature (300-400°C). This mateiral however can taken to be better than the presently known highest hydrogen storage capacity material Mg_2Ni (3.8 wt.%). As regards the nanoparticle version of Mg_2Ni as prepared through mechanical alloying, the most interesting feature corresponds to the higher storage capacity in the 3rd or 4th hydrogenation cycle and also shows better desorption kinetics.

Acknowledgement

The authors are grateful to Prof.T.N.Veziroglu (President, IAHE), Prof.M.Groll (Universitat Stuttgart, Germany), Dr.E.Willers and Prof.H.P.Gautam for encouragement. We are pleased to acknowledge Dr.S.Venkatesan and Dr.K.Sapru of ECD devices, USA for helpful discussions during the INDIA-UNDP Workshop on Hydrogen Energy (Nov. 29 - Dec.1st, 1996). The financial support from Council of Scientific Industrial Research (CSIR) and Ministry of Non-conventional Energy Sources (MNES), New Delhi are gratefully acknowledged.

References

1. Singh,S.K.,Singh,A.K.,Ramakrishna.K.,and Srivastava,O.N. (1989) Investigation on the hydrogenation/dehydrogenation characteristics of hydrogen storage alloys, Int.J.Hydrogen Energy, 14,105.

2. Singh,S.K.,Singh,A.K.,Ramakrishna.K.,and Srivastava,O.N. (1985) Investigation on the structural and hydrogenation characterisation of $LaNi_5$ ..... Thin Films, Int. J.Hydrogen Energy, 10,523-529.

3. Dutta,K., and Srivastava,O.N. (1990) Synthesis,Characterisation and hydrogenation behaviour of the La_2Mg_{17} intermetallic, Int. J. Hydrogen Energy, 15, 341-344.

4. Benjamin,S. (1976), Fabrication of ball mill for the investigation of intermetallic hydrides, Sci Ame., 40,234.

Thermodynamic Properties and Cyclic-Stability of the System Mg_2FeH_6

B. Bogdanović , K. Schlichte and A. Reiser
Max-Planck-Institut für Kohlenforschung,
Kaiser-Wilhelm-Platz 1,
45470 Mülheim a. d. R., Germany

1. Introduction

The demand for energy has increased continuously since the beginning of the industrial revolution. At the moment, the supply of energy can still be satisfied from fossil sources, however, these are limited and cause environmental problems. In contrast, thermal solar energy based power stations offer the possibility of clean and less expensive energy. To make these more effective and independent of the variable input of the sun, thermal energy-storage systems are needed which operate at temperatures between 400°C and 550°C. Although at the present no economical thermal energy storage systems are available, magnesium and its alloys in the form of the hydrides are potential candidates. The energy density of these systems is much higher (1080 kJ/kg) [1] than comparable systems such as latent heat storage systems (174 kJ/kg at 308°C) [2]. For commercial use, high reversibility of the storage material must be guaranteed at a minimum cost. To enhance the efficiency of a thermo-electric power plant it is necessary to use as high a working temperature as possible. Over the years we have been trying to develop high temperature storage systems having a good cyclic stability and report here that the Mg_2FeH_6 system is eminently suitable for this task. To add iron to a Mg system is not a new idea: before the common hydride-phase of Mg and Fe was discovered, various groups used iron as a catalyst for the hydrogenation reaction or as a medium to hinder agglomeration. These investigations were, however, restricted to a limited number of hydrogenation and dehydrogenation cycles [3, 4, 5]. In these early investigations, the Mg_2FeH_6-phase was not identified and this was first explicitly synthesized and characterised in 1984 by Yvon and Didisheim et al. [6, 7] by using a sintering technique employing stoichiometric Mg / Fe pellets under high pressure 2-12 MPa and temperatures of 450°C-520°C for 2 to 10 days. The yield was about 50% and purification was necessary. In further studies by Konstanchuk et. al. [8, 9, 10], the conditions of formation and the kinetic behaviour of mechanically alloyed mixtures of Fe and Mg have been investigated. Mechanical alloying has also been reported by Mitov, Khrussanova et. al.[11] and Huot and Akiba et.al.[12] and the latter reported a yield of 84% [13]. Although the system has received some attention, the available data, especially for technical application, are not satisfactory.

T. O. Saetre (ed.), Hydrogen Power: Theoretical and Engineering Solutions, 291–296.

2. Experimental Details

For the syntheses of the ternary species Mg_2FeH_6, Mg powders from Norsk Hydro, Sample C having a particle size 25-70 nm, 99.9% pure and Mg from Eckard-Werke Fürth Germany, PK31 having a particle size 25-100 nm, 98.5% pure and 99.95% pure, have been used. The iron powder is from Merck, particle size < 10 nm, 99% pure. We have used hydrogen of 99.999 % purity. The hydrogenation/dehydrogenation reactions have been carried out in a Sievert Apparatus as described in ref. [14]. The high-pressure experiments were performed in special stainless steel autoclaves (Nicrofer 7216). The high pressure differential scanning calorimetry was carried out with a DSC 27HP Mettler Toledo and X-Ray powder diffraction measurements with a Stoe diffractometer STUDI 2P with a PSD and using CuK_α- radiation. The SEM investigations and the TEM pictures were obtained with an ISI-60 and Hitachi HF 2000 respectively.

3. Results and Discussion

3.1. SYNTHESIS

The methods so far used to synthesize Mg_2FeH_6 are based on sintering, melting or mechanical alloying procedures. We have found that the direct formation from the elements is possible. A convenient synthetic approach involves a cyclic procedure. Approximately 20 cycles with a pressure of 8-9 MPa and temperatures between 480-545°C are necessary. In the initial cycles the observed capacity of around 3.7 wt% is presumably associated with the intermediate formation of MgH_2. The H-content subsequently increases to 5.27wt%, and approaches the theoretical value of 5.47wt%. Powder diffraction analysis of the sample shows only signals from the Mg_2FeH_6 phase and no peak is observed which can be associated with MgH_2 or Fe. This is underlined by the high hydrogen content from chemical analysis. The fast formation of the ternary hydride is presumable the result of the small particle size of the starting materials. (Fig.1a,b). A further acceleration is possible if MgH_2 is used.

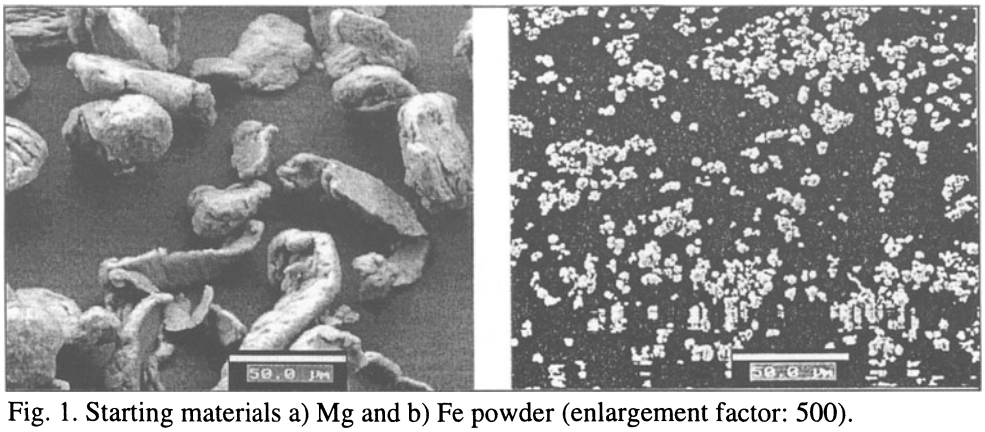

Fig. 1. Starting materials a) Mg and b) Fe powder (enlargement factor: 500).

3.2. ELECTRON MICROSCOPE INVESTIGATIONS

Fig. 2 shows a SEM picture of Mg_2FeH_6 (enlargement factor: 500) after 800 cycles. A sponge like structure of Mg_2FeH_6 particles can be seen which is totally different from that of the starting materials. Fig. 3a shows a TEM-picture of the same material with the single crystalline structure of a Mg_2FeH_6 plane (enlargement factor: 500,000). Additional EDX-analyses also show a homogeneous Mg / Fe distribution. The same material in a dehydrogenated state is shown in Fig. 3b (enlargement factor: 200,000): small Fe agglomerations are surrounded by Mg, which is transparent in this picture. The metal crystallites formed vary in size from 10 nm to50 nm. EDX-analyses show that the crystallites consist either of pure Fe or of pure Mg. This result shows that a total separation of the two metals takes place during decomposition of the hydride. This result is expected since Mg and Fe are only marginally soluble in each other [15]. During the hydrogenation procedure, the metals then recombine in the presence of hydrogen.

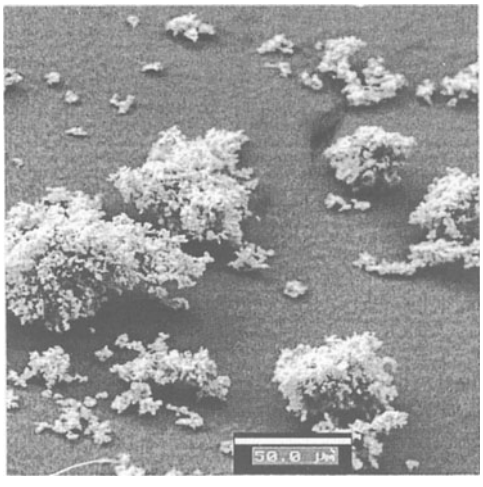

Fig. 2 SEM $MgFeH_6$ enlargement factor: 500

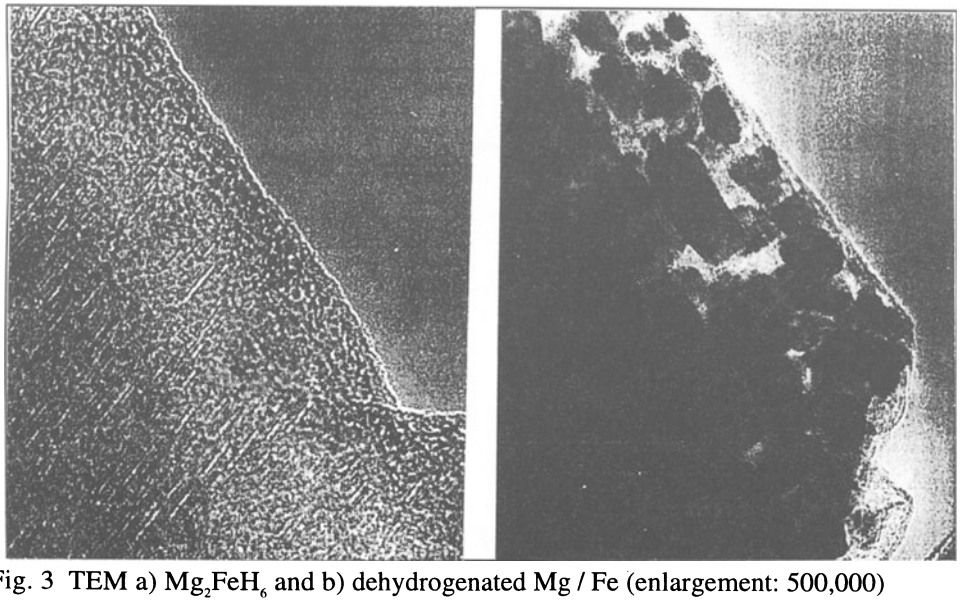

Fig. 3 TEM a) Mg_2FeH_6 and b) dehydrogenated Mg / Fe (enlargement: 500,000)

3.3 THERMODYNAMIC PROPERTIES

Desorption and absorption PCI-measurements have been carried out at 350°C, 450°C and 502°C after the Mg_2FeH_6 material has been formed in an initial 20 cycles (temperature 480°C to 547°C and pressure between 83-90 bar H_2). The resulting hydrogen capacity is 5.27wt%. The PCI curves yield a hydride-system having a small hysteresis and a low plateau-slope compared to MgH_2 (Fig. 4). No second phase (MgH_2) can be seen. Each isothermal line shows a capacity of more than 5wt%. The data for the heat of formation (ΔH_F) have been calculated from the desorption curves at 50% H_2 capacity and are compared with values given in reference [9]:

ΔH_F (350-501.9°C)	= -79.5 kJ/mol	± 3 kJ/mol	
ΔH_F (352-427°C)	= -86 kJ/mol	± 6 kJ/mol	Ref.[9]
ΔS_F (350-501.9°C)	= -137.3 J/mol K	± 5 J/mol K	
ΔS_F (352-427°C)	= -147 J/mol K	± 9 J/mol K	Ref:[9]

From these data, the equilibrium pressure curve of Mg_2FeH_6 has been determined: Ln p (bar) = -9561.1/T+16.5. This function proved to be both valid and useful for measurements carried out at elevated temperatures.

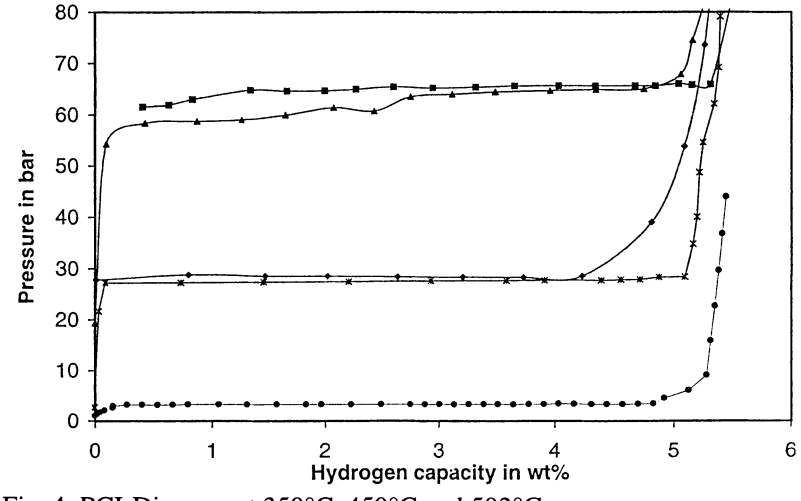

Fig. 4. PCI-Diagram at 350°C, 450°C and 502°C

3.4. CYCLIC TESTS

Testing the cyclic stability was the primary aim of this investigation and therefore several samples have been studied and subjected to 1200 hydrogenation and dehydrogenation cycles. The data for more than 800 cycles are shown Fig. 5 whereby the hydrogenation and dehydrogenation phases have a duration of 90 minutes. Hydrogenation has

been performed at 470°C and 8 MPa and the dehydrogenation at 535°C and under 8,8 MPa H_2 pressure. No decrease in the hydrogen capacity could be observed: the Mg_2FeH_6 system remains stable with a capacity of ca. 5 wt%. The observation that the purity of the Mg has no effect upon the stability is of obvious commercial importance.

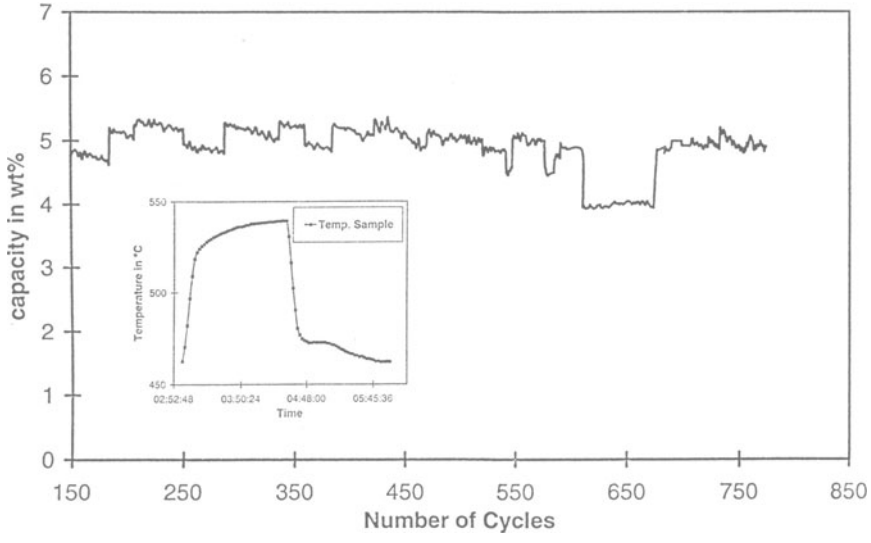

Fig. 5. a) Cyclic stability diagram for Mg_2FeH_6 and b) Temperature curve of one cycle

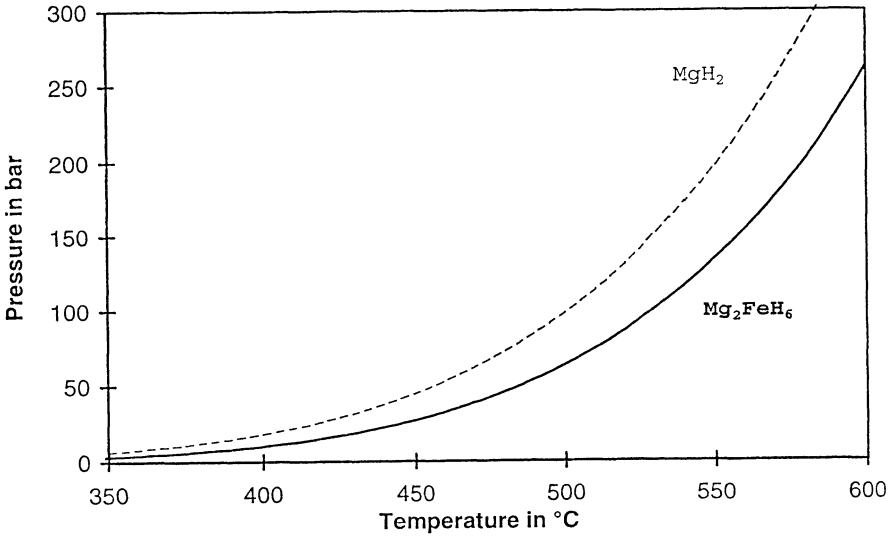

Fig. 6. Dissociation- pressure-diagram for Mg_2FeH_6 compared to MgH_2

If we take a closer look at the reaction curve shown in Fig. 5b, we can see that the

rehydrogenation / dehydrogenation steps are mirrored in the temperature curve. The starting point for both reactions are retarded in respect to the equilibrium conditions. In particular the rehydrogenation reaction takes place at a much higher pressure. This is a result of the high activation energy of the reaction [10]. The same behaviour could be observed in the pressure DSC-device measurements. The rehydrogenation takes place under conditions typical for the formation of MgH_2. These measurements do not allow us to decide whether MgH_2 is formed initially and then reacts to Mg_2FeH_6. The formation of Mg_2FeH_6 without the intermediate formation of MgH_2 is possible and can be tested by carrying out the reaction under conditions in which the formation of MgH_2 is thermodynamically impossible (Fig. 6, pressure: 12.8 - 13.3 MPa, temperature 530-573°C). Under these conditions, the hydrogen uptake over 90 minutes is reduced, suggesting that Mg_2FeH_6 can be formed directly but at a significantly reduced rate. This is in agreement with the results in ref. [9, 10] in which the energy of activation for the direct formation of Mg_2FeH_6 is determined to be much higher than that for MgH_2.

4. Summary

We have shown that Mg_2FeH_6 is an excellent material for hydrogen and thermal heat storage. We have also demonstrated the technically important cyclic stability of the system and observe a constant hydrogen storage capacity over 1200 cycles. The method of preparation is both simple and cheap and no further purification is necessary. Dissociation pressure curves have been measured at elevated temperatures (up to 500°C) and have been used to derive more accurate thermodynamic data. The results show that it is possible to increase the working temperature of a heat storage system based on Mg to above 450°C and this material could be used to give a more efficient and economical heat-storage unit of the type described in ref. [16]. Further investigations are in progress.

References:

[1] Straßburger K., Ph. D. Thesis, Fachbereich 13 Universität Gesamthochschule Essen (1992)
[2] Michels H, 8th Int. Symp. On Solar Thermal Concentrating Technologies Köln (6-11.10.1996)
[3] Battelle Mem. Institute, Genf, Germ. Off. DE 2945981 (1979)
[4] Welter J. M., Scripta Metallurgica, 16, 285-286 (1982)
[5] Kernforschungsanlage Jülich, Germ. Off. DE 3147839 (1983)
[6] Didisheim J. J., Yvon K. et al., Inorg. Chem., 23, 1953-1957 (1984)
[7] Selvam P., K. Yvon, Int. J. Hydrogen Energy, 16, 9, 615-617, (1991)
[8] Konstanchuk I.G., et al. Izv.Sib. Otd. Akad. Nauk. SSSR, Ser. Khim., Nauk, (3)29 (1986)
[9] Konstanchuk I.G., et al., J. Less-Common Metals, 131, 181-189 (1987)
[10] Konstanchuk I.G., Stepanov A.A., Russ. J. Phys. Chem., 63, 11, (1989)
[11] Mitov I., Khrussanova et. al., Mat. Res. Bull. 27, 905-910, (1992)
[12] Huot J., Hayakawa H., Akiba E., J. Alloys and Compounds 248, 164-167, (1997)
[13] Huot J., Hayakawa H., Akiba E., Abstract of ISMANAM-95, Quebec, July 24-28, (1995) P-A7.1.
[14] Neuy A., Ph. D. Thesis, Ruhr Universität Bochum (1995)
[15] Burylev B. P., Liteinoe Proizvod, (10)27-8 (1966)
[16] Bogdanović B., Straßburger K., Int. J. Hydrogen Energy, 20, 811-822, (1995)

CHARACTERIZATION OF THE ELECTROCHEMICAL PROPERTIES OF METAL HYDRIDES BY AC IMPEDANCE

Variation in the properties with state of charge

LARS OLE VALØEN AND REIDAR TUNOLD
Department of Electrochemistry
Norwegian University of Science and Technology
N-7034 Trondheim, Norway

AND

SVEIN SUNDE
IFE, N-1750 Halden, Norway

Abstract. Results from impedance measurements fitted to a model of granular metal hydride electrodes intended for battery use, are presented. The results show rather large variations in the kinetic parameters for the charge/discharge process at different states of charge of the hydride material. The optimum energy efficiency for a battery electrode of the material used is obtained in the range of 40 to 95% depth of discharge. The results confirm the usefulness of the impedance method for in situ characterization of hydride electrodes.

1. Introduction

The electrochemical properties of metal hydrides are interesting due to the possibility of using these as electrodes in rechargeable batteries (Sakai *et al.*, 1995). Knowledge of the charging and discharging processes and their rates, is important for the development and optimization of electrode materials. Impedance measurements appear especially promising for electrochemical in situ characterization. Impedance characterization of MH_x electrodes for battery purposes generally makes use of equivalent circuits for interpretation of data (Kuriyama *et al.*, 1993; Zhang *et al.*, 1995). Impedance measurements have also been used to obtain variations of the polarization resistance as a function of depth of discharge (DOD) (Popov *et al.*, 1996). The work of Zhang *et al.* (1995) contains analytical expressions for the impedance derived based on a proposed reaction mechanism. In that

T. O. Saetre (ed.), Hydrogen Power: Theoretical and Engineering Solutions, 297–302.

work, however, hydrogen diffusion in the electrode is neglected. Durand *et al.* (1994) proposed an impedance model for intercalation of hydrogen in a thin film with linear diffusion. Lim and Pyun (1993) have done the same for a thin metal membrane under permeable conditions.
The scope of this work is to show that the properties of metal hydride electrodes can be investigated in a systematic way using electrochemical impedance measurements combined with a theoretical impedance model for such electrodes. The model used in this work (Valøen *et al.*, 1997) is developed for granular metal hydride electrodes and includes the rate of hydrogen exchange at the hydride-electrolyte interface, and absorption and diffusion of hydrogen into the bulk of the alloy. The exchange reaction is assumed to occur in several steps: discharge and adsorption of hydrogen at the interface and interfacial transfer and absorption of hydrogen atoms with hydride formation. The subsequent and parallel transport process is approximated as spherical diffusion in the particles.

2. Theoretical considerations

A mathematical model can be a useful tool to distinguish and understand causes to and roles of various coupled phenomena. In our model we have assumed that the electrode reactions at the metal hydride surface can be associated with three distinguishable processes (Valøen *et al.*, 1997). The first of these is a charge transfer reaction given by

$$H_2O + \square_M + e \rightleftharpoons H_{ad} + OH^- \tag{1}$$

where $\square_M$ is an active site on the surface of the metal hydride forming alloy. The adsorbed hydrogen then reacts with the alloy to form interstitial hydrogen in the surface layer of the particle

$$H_{ad} \rightleftharpoons H_i + \square_M \tag{2}$$

The interstitial hydrogen subsequently forms a hydride phase

$$xH_{i,r_H} + M_{r_H} \rightarrow MH_{x,r_H} \tag{3}$$

where r_H is the radius of the reaction zone for the hydride formation. Parallel to this, hydrogen diffuses through both the hydride phase and the metal phase

$$H(MH_x)_{r=a} \rightarrow H(MH_x)_{r=r_H} \tag{4}$$

$$H_{i,r=r_H} \rightarrow H_{i,r<r_H} \tag{5}$$

Equations 3 to 5 are written for the charging of a hydride particle, with radius r=a, where the reaction zone for hydride formation, with radius r_H,

is moving inward. In the further development we have assumed that Eq 3 is in equilibrium and that the diffusion coefficient, D_H, is the same in the two phases. This means that formally the diffusion takes place in a continuum. The diffusion is further modelled by assuming particles with spherical symmetries.

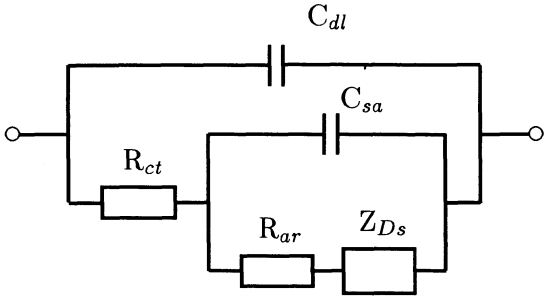

Figure 1. Equivalent circuit representation of the impedance model (Valøen *et al.* 1997).

The faradaic impedance, Z_f, is now calculated as the ratio between the Laplace-transformed potential and current (Valøen *et al.*, 1997). By arranging the mathematical model as an equivalent circuit, the model can be verified by ac impedance measurements. By use of this equivalent circuit, it will also be possible to monitor variations in the circuit elements as the experimental conditions are varied.

3. Experimental

Electrodes were made of $MmNi_{3.5-3.7}Co_{0.7-0.8}Mn_{0.3-0.4}Al_{0.3-0.4}$ (GfE), a misch metal based AB_5 type alloy, mixed with fine copper powder (Merck, p.a.,64μm), and cold-pressing this mixture at $4{\cdot}10^8$ Pa (Willems, 1984). The mixture was pressed together with a layer of copper powder and a copper plate in a sandwich construction. This alloy was chosen because it showed no degradation with cycle life for the number of cycles needed to perform the measurements. The electrolyte was 6M KOH (Merck, p.a.) in deionized water at 25°. Charging was carried out at the 1.25C rate, 338 mA/g for the current alloy, with 10 % overcharge. Discharging was carried out at the same current density to a cutoff voltage of -600 mV vs Hg/HgO. Before measurements, the electrodes were activated during 30 charge/discharge cycles. The electrodes were kept at the steady state open circuit potential of the electrode after discharging it to the actual depth of discharge (DOD). The impedance was obtained in the frequency range from 10 kHz to 0.1 mHz with an amplitude of 5 mV, using a computer-controlled Solartron 1250 frequency response analyzer coupled directly to a Princeton EGG 273 potentiostat.

4. Results

A complex plane and a Bode plot for a metal hydride electrode are shown in figures 2 and 3 respectively. For the high frequency part the model fits the experimental points rather well. The fit to the low frequency part is less evident. In this range, however, one might expect a rather large distribution of the diffusion time constant due to the variation in the particle size. The Bode plot shows a surprisingly smooth fit for the imaginary part vs frequency.

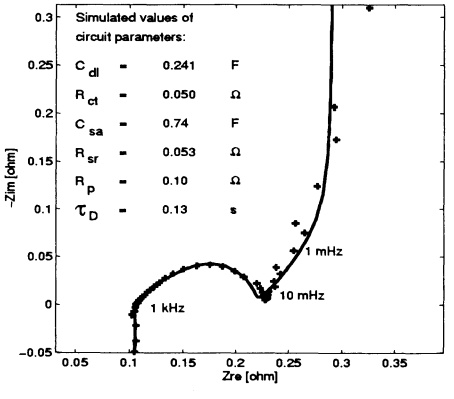

Figure 2. Complex plane plot, hydride elecrode, 60% DOD. Measured values (+) compared with model (-).

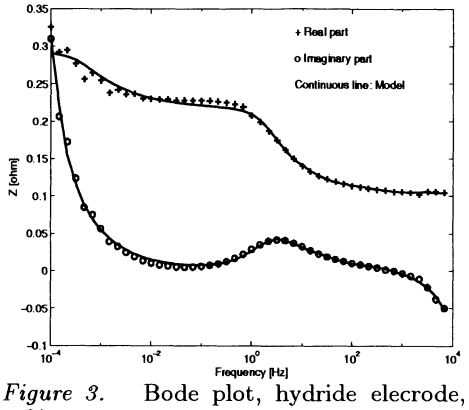

Figure 3. Bode plot, hydride elecrode, 60% DOD. Real part values (+) and imaginary part values (o) compared with model (-).

A plot of the polarization resistance as a function of depth of discharge (DOD) is shown i fig 4. As seen from the figure, the polarization resistance varies considerably with DOD. The resistance is relatively high for completely charged electrodes (low DOD), and decreases to a shallow minimum between approximately 40 and 95 % DOD. Then the resistance increases due to the increase in the absorption resistance, R_{ar}, cf Fig 7.

A plot of the diffusion time constant as a function of DOD is shown i fig 5. As seen from the figure, the diffusion time constant for hydrogen diffusion shows no significant variation up to 95% DOD where the time constant suddenly increases. This increase may very well be due to the increased α-phase content This may slow down the diffusion process as the interaction between the metal (α) phase and the hydrogen (proton) becomes stronger as the hydride phase decreases and disappears and the remaining hydrogen is absorbed in the metal (α) phase. The slightly higher time constant for fully charged electrodes may be due to the reduced number of unoccupied sites as the hydrogen content in the electrodes has reached its maximum.

Plots of the charge transfer resistance, R_{ct}, and the absorption resistance, R_{ar}, as functions DOD are shown i fig 6 and 7.

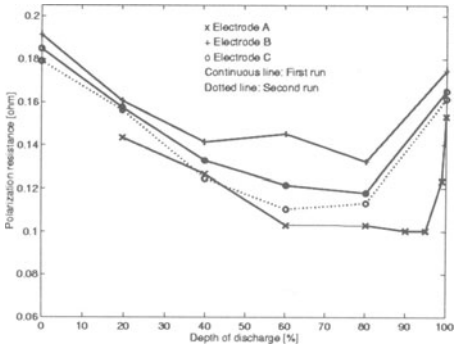

Figure 4. Polarization resistance, R_p, as a function of depth of discharge (DOD).

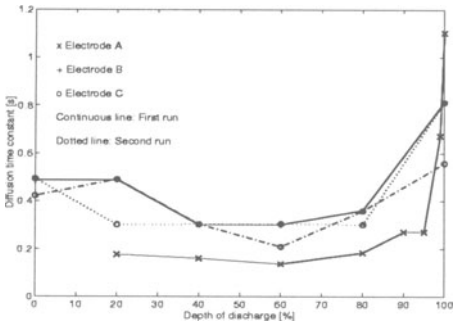

Figure 5. Diffusion time constant, τ_D, as a function of depth of discharge (DOD).

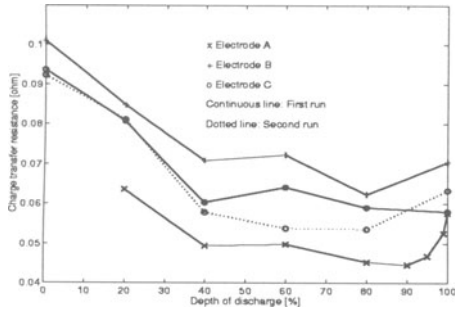

Figure 6. Charge transfer resistance, R_{ct} as a function of depth of discharge (DOD).

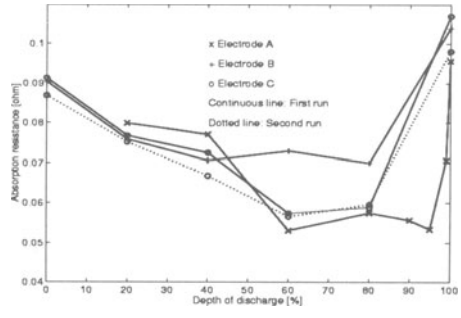

Figure 7. Absorption resistance, R_{ar}, as a function of depth of discharge (DOD).

As seen from the figures, the charge transfer step and the interfacial transfer (absorption) step are closely related to each other and therefore not independent. However, some information can be extracted from the figures 6 and 7. First, the absorption resistance is higher than the charge transfer resistance for all DOD. The sudden increase for high DOD is also more well defined for the absorption resistance.

5. Discussion

Mathematical modeling of misch metal based hydride electrodes is a complex process due to the fact that the electrode consists of several metal hydride forming alloy components and particles pressed together with a binder material or pasted into a foam material.

In spite of the fact that the metal hydride particles are not uniform in size and also not spherical, the experimental data agrees quite well with the proposed model in the whole frequency region.

The fit of the low frequency part is best when the diffusion processes are

fast and of less importance, i.e. at medium DOD, cf. fig 5. As one can see from the expression for the diffusion time constant, $\tau_D = \frac{a^2}{D}$, it is strongly dependent on the length of the diffusion path. The diffusion path will be unique for each particle, as the electrode consists of a mixture of particle sizes.
It will be very difficult to perform measurements with a constant particle size throughout the entire electrode, as the metal hydride particles crack down to smaller units during cycling (Boonstra and Bernhards, 1990). A sign of this is that the interfacial capacitances (not shown) increase during cycling, and that this increase most likely is a result of an increased active electrode area.

6. Conclusion

The calculated impedance based on the proposed electrochemical model agrees well with experimental findings. The results show rather large variations in the kinetic parameters for the process at different states of charge of the hydride material. The optimum energy efficiency for a battery electrode of the material used is obtained in the range of 40 to 95% depth of discharge. The results confirm the usefulness of the impedance method for in situ characterization of hydride electrodes.

7. Acknowledgements

The authors wish to acknowledge the Norwegian Research Council for financial support through the NYTEK programme, and R. Edwards for performing some of the impedance measurements.

References

T. Sakai, M. Matsuoka, and C. Iwakura. In K.A. Gschneider Jr. and L. Eyring, Ed., *Handbook on the Physics and Chemistry of Rare Earths*, vol. 21, pp 133–178. Elsevier Science B.V., (1995).
N. Kuriyama, T. Sakai, H. Miyamura, I. Uehara, H. Ishikawa, and T. Iwasaki. *J. Alloys and Compounds*, **202**, 183–197, (1993).
W. Zhang, M.P. Sridar Kumar, S. Srinivasan, and H.J. Plohen. *J. Electrochem. Soc*, **142**(9), 2935–2943, (1995).
B.N. Popov, G. Zheng, and R.E. White. *J. Applied Electrochemistry*, **26**, 603–611, (1996).
R. Durand, J.C. Chen, J.P. Diard, and C. Montella. In B.E. Conway and G. Jerkiewicz, Ed., *Electrochemistry and materials science of cathodic hydrogen absorption and adsorption*, vol. 94-21, pp 207–219. The Electrochemical Society, Inc, (1994).
C. Lim and S-I. Pyun. *Electrochim. Acta*, **38**(18), 2645–2652, (1993).
L.O. Valøen, S. Sunde, and R. Tunold. *J. Alloys and Compounds*, **253-254**, 656–659, (1997). In press.
J.J.G. Willems. *Philips J. Res. Suppl.*, **39**(1), (1984).
Boonstra and Bernhards. *J. Less-Common metals*, **161**, 355–368, (1990).

HYDROGEN-INDUCED PHASE TRANSFORMATIONS IN H-STORING ALLOYS OF ZIRCONIUM

V.A.YARTYS[1,2], I.Yu.ZAVALIY[1], A.B.RIABOV[1], P.W.GUEGAN[3], J.C.CLARKE[3], I.R.HARRIS[3], B.C.HAUBACK[2] and H.FJELLVAG[2]
[1]*Karpenko Physico-Mechanical Institute of the National Academy of Sciences of Ukraine, 5, Naukova Str., Lviv, 290601, UKRAINE*
[2]*Department of Physics, Institute for Energy Technology, P.O.Box 40, N-2007, Kjeller, NORWAY*
[3]*School of Metallurgy and Materials, The University of Birmingham, Edgbaston, Birmingham, B15 2TT, U.K.*

1. Introduction

Zirconium-based Zr-V and Zr-Fe alloys are known to be highly efficient absorbers of low pressure hydrogen. Their working performance is structure-dependent and can be improved by modifying the composition of the basic alloys with doping elements. Particularly promising in this respect are modifications of oxide materials where both H-sorption capacity and hydrogenation activity can be increased substantially, especially when boron or rare earth oxides are introduced into the matrices of Zr-V and Zr-V-Fe [1-3].

Zr-Fe-based ST 198 alloy (SAES Getters) is one type of hydrogen getter alloy. This alloy contains the Zr_2Fe intermetallic compound as its major constituent. A disproportionation of Zr_2Fe, when loaded with deuterium gas in the pressure region of 10^{-5}-10^{-3} bar and temperature above 300 °C was indicated in reference [4] leading to the formation of $ZrFe_2$ and ZrD_{2-x} and, possibly, α-Fe and ZrD_{2-x}. The irreversibility of the disproportionation was pointed out by the authors [4], thus limiting the performance of the material.

At higher hydrogenation pressures, up to 0.5 bar H_2, this compound was even found to disproportionate around room temperature. However, on cooling the sample down to -23 °C, only with sufficient thermal conductivity between the sample and the sample holder, could the disproportionation of Zr_2Fe be avoided successfully [5]. The $Zr_2FeH_{4.5}$ interstitial-type saturated hydride formed in this way possesses the same $CuAl_2$ type crystal structure as the initial intermetallic compound.

The thermodynamic stability of the Zr-Fe metal lattice can be modified substantially by a partial substitution of zirconium by hafnium (as in the $Zr_{1.6}Hf_{0.4}Fe$ [6]) or by the introduction of oxygen into the Zr-Fe metal lattice, leading to the formation of the $Zr_4Fe_2O_{0.6+x}$ oxide [6-8]. In this case, no signs of a H-induced disproportionation were indicated with the same hydrogenation conditions as those applied in reference [4].

In addition, isostructural Ni- and Co-containing Zr_2Fe intermetallics were studied extensively as hydrogen sorbing materials [9-16]. These studies showed that, under "mild" hydrogenation conditions, the crystalline hydrides with anisotropically

T. O. Saetre (ed.), Hydrogen Power: Theoretical and Engineering Solutions, 303–314.

($Zr_2CoH_{\sim 5}$) or isotropically ($Zr_2NiH_{\sim 5}$) expanded unit cells are formed with hydrogen atoms filling the Zr_4 and Zr_3Me tetrahedral interstices, preferentially ($Zr_2NiH_{\sim 5}$) or in an ordered way ($Zr_2CoH_{\sim 5}$) [14,16]. However, when more "severe" hydrogenation conditions were applied (Zr_2Co at 873 K/30 kbar H_2)[13], Zr_2Co after hydrogen combustion or Zr_2CoH_5 at 500 °C [15, 16], Zr_2Ni at 40 bar H_2 [9]), a disproportionation of the metal matrix occurred, leading to the formation of ZrH_2 and $ZrCoH_3$ [13], ZrH_2 and $ZrCo_2$ [15, 16], $ZrNiH_3$ and ZrH_2 [9]. Under special conditions, the metallic glass state can be obtained in Zr_2Ni, which is followed by a significant modification of the hydrogenation behaviour [17].

Hydrogenation-Disproportionation-Desorption-Recombination is an elegant hydrogen metallurgical process, in which the reversibility of the disproportionation step is achieved providing a full recovery of the virgin metallic material, with a substantially refined microstructure. The HDDR-processing of material giving submicron grains has been achieved in NdFeB (for example, [18]) and SmFeN (for example, [19]) alloys resulting in the appearance of significant coercivities related to the much refined grain sizes.

The *HDDR* route has not yet been studied for the zirconium-containing H-sorbing alloys. However, it is clear that its use could lead to new advanced properties for H-storage applications, due to the expected refined microstructure in the fully recombined state.

In this work, the ability of a number of Zr-containing intermetallic compounds with the Zr_2Me stoichiometry, including Zr_2Fe, Zr_2Ni, Zr_2Co and $Zr_4Fe_2O_{0.6}$, to participate in the Hydrogenation-Disproportionation-Desorption-Recombination process was investigated, revealing for the first time that the HDDR route can be employed successfully for all these compounds.

2. Experimental Details

The alloys were prepared from high purity metals by arc melting in an argon atmosphere. Fe_2O_3 oxide was used in order to introduce oxygen into the $Zr_4Fe_2O_{0.6}$ alloy. Subsequent annealing was applied where necessary to homogenise the alloys (1000 °C for 7 days for $Zr_4Fe_2O_{0.6}$; 800 °C for 28 days for Zr_2Ni and Zr_2Co). The Zr_2Fe alloy was studied in the as cast condition.

X-ray diffraction studies (Philips PW 1012/10 diffractometer with Cu-Kα radiation) revealed that the alloys crystallise in the $CuAl_2$ (Zr_2Fe, Zr_2Ni and Zr_2Co) and Fe_3W_3C structure types ($Zr_4Fe_2O_{0.6}$), with the values of unit cell constants close to those reported in the literature.

The hydrogenation and desorption properties were studied at the University of Birmingham by Temperature Pressure Analysis (TPA) and Hydrogen Differential Thermal Analysis (HDTA) techniques. In both cases the samples were heated at a rate of 5 °C in hydrogen (TPA) or in vacuum (HDTA). Details of the experimental equipment used may be found elsewhere [20, 21].

Powder neutron diffraction studies of $Zr_2NiD_{2.16}$ were performed at JEEP II reactor , Kjeller and at Risø, Forsøgsanlag, Denmark, using neutrons of wavelengths 1.825 Å and 1.4305 Å, respectively. Refinements of the structure were carried out using the multi-phase Rietveld programs MPREP and MPROF.

3. Results and Discussion

3.1. HYDROGENATION AND DISPROPORTIONATION

On heating in hydrogen gas up to 940 °C, the multistage phase transformations have been found to occur for all the compounds studied. A complete disproportionation, revealed by X-ray diffraction studies (see Fig.1), took place in the case of the Zr_2Fe compound only:

$$2\,Zr_2Fe + (3\text{-}3x/2)\,H_2 \rightarrow ZrFe_2 + 3\,ZrH_{2-x}$$

Under the same hydrogenation conditions, two hydrogen absorption events starting at 380 °C (initial hydrogenation) and 665 °C (disproportionation) are indicated for the $Zr_4Fe_2O_{0.6}$ η-oxide (Fig.2). X-ray diffraction studies showed that the disproportionation was only partial and that $ZrFe_2$ and δ-oxyhydride $ZrO_{1-x}H_y$ are formed on the second H-absorption event (Fig.3). At the same time, the main constituent phase was identified as $Zr_4Fe_2O_{0.6}H_x$ hydride formed upon H desorption from the initially formed $Zr_4Fe_2O_{0.6}H_{7.5}$ (a = 12.862(3) Å [6]). It can be concluded from the rather close values of the cell constants for the virgin $Zr_4Fe_2O_{0.6}$ η-oxide (a = 12.180(1) Å) and for the hydride (a = 12.236(5) Å), that η-oxyhydride $Zr_4Fe_2O_{0.6}H_{7.5}$ loses most of the hydrogen on heating to 940 °C.

On H-loading in the HDTA rig, the Zr_2Ni compound also exhibits two absorption effects. The main one on initial hydrogenation takes place at 255 °C (Fig.4).

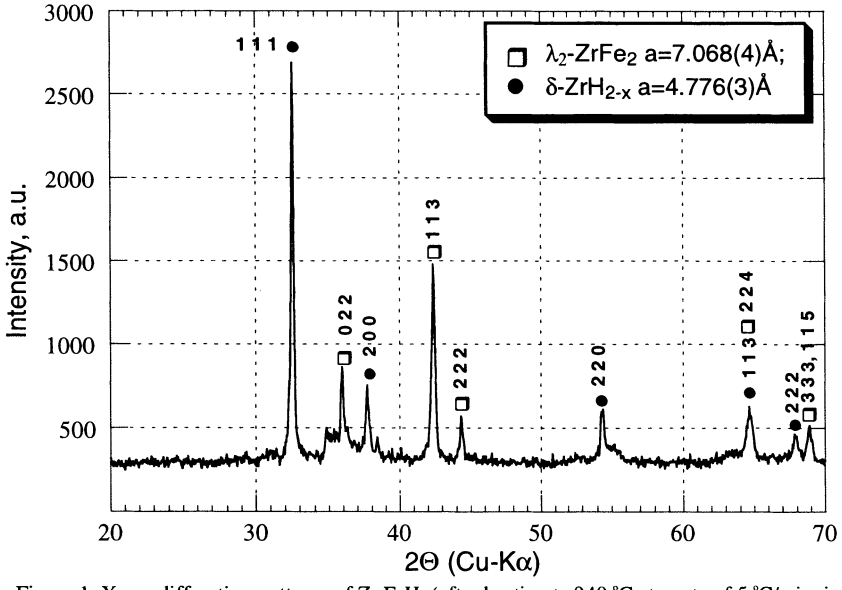

Figure 1. X-ray diffraction patterns of Zr_2FeH_x (after heating to 940 °C at a rate of 5 °C/min in the TPA-rig) indicating a full disproportionation.

A second exothermic effect, presumably due to the disproportionation of the material, was observed at 535 °C. On further heating, a small endothermic peak was seen at 655 °C which can be attributed to H-desorption from the constituent hydrides.

X-ray diffraction studies indicated nearly complete disproportionation of the initially formed Zr_2NiH_5 hydride. On heating this hydride in hydrogen, a partial hydrogen desorption occurred with the formation of $ZrNiH_x$ ($x \rightarrow 0$; CsCl structure type) and ZrH_{2-x} hydrides. Only one very weak peak corresponding to Zr_2NiH_{5-x} was

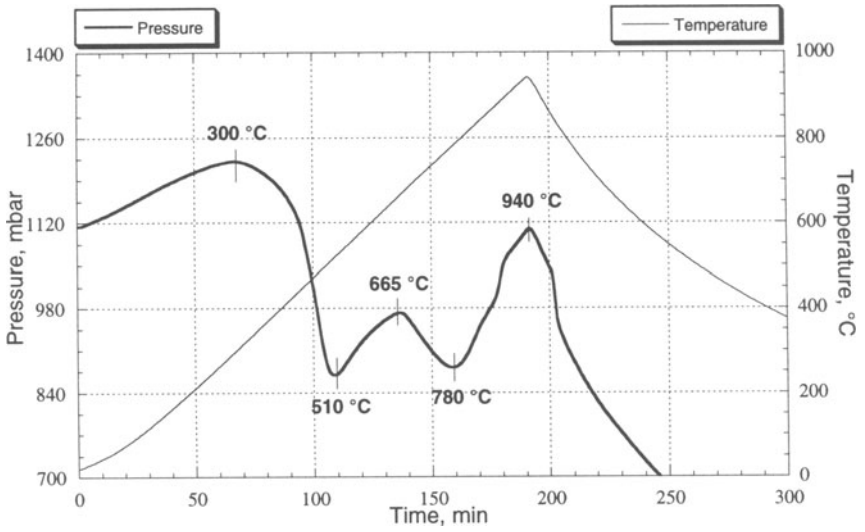

Figure 2. TPA traces for $Zr_4Fe_2O_{0.6}$ (heating to 940 °C).

seen as addition to the peaks from two other phases. Rather broad X-ray diffraction peaks indicated that a partial amorphisation of the alloy takes place following the heating-cooling cycle in hydrogen gas. It should be pointed out that the measured value of the cell parameter of $ZrNiH_x$ a = 3.192(4) Å is close to those of the CsCl type ZrCo intermetallic compound (a = 3.181-3.198 Å [22]). However, in the Zr-Ni binary system, a CrB-type intermetallic compound is normally formed [23]. The observed stabilisation of the CsCl type structure can be attributed to the influence of hydrogen dissolved in the metal matrix.

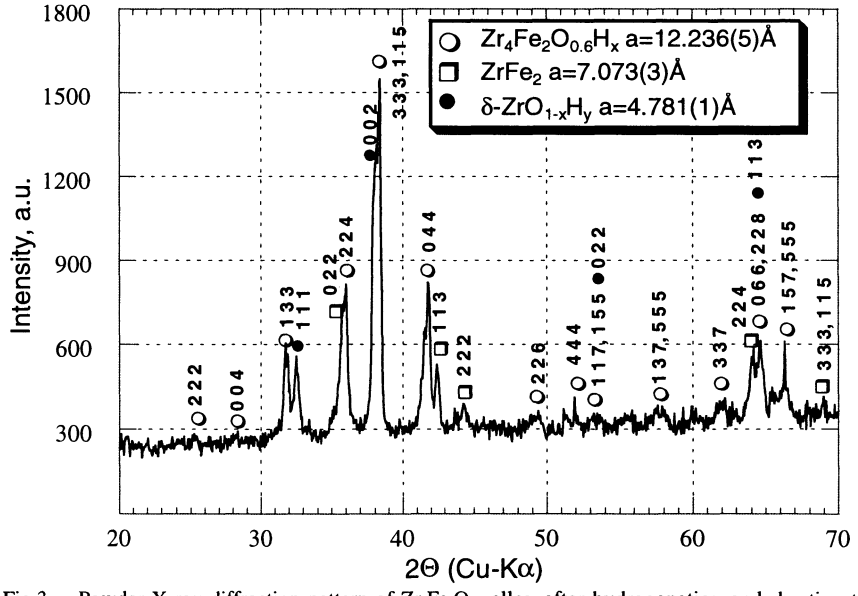

Fig.3. Powder X-ray diffraction pattern of $Zr_4Fe_2O_{0.6}$ alloy after hydrogenation and heating to 940 °C in the TPA rig.

A very similar hydrogenation behaviour was observed in the Zr_2Co-H_2 system upon the completion of the HDDR process. Here the formation of $ZrCoH_x$ ($x \rightarrow 0$; CsCl structure type; a ~ 3.18 Å) and ZrH_{2-x} was indicated by the presence of their strongest diffraction peaks only, possibly reflecting a certain degree of amorphisation of the metal matrix.

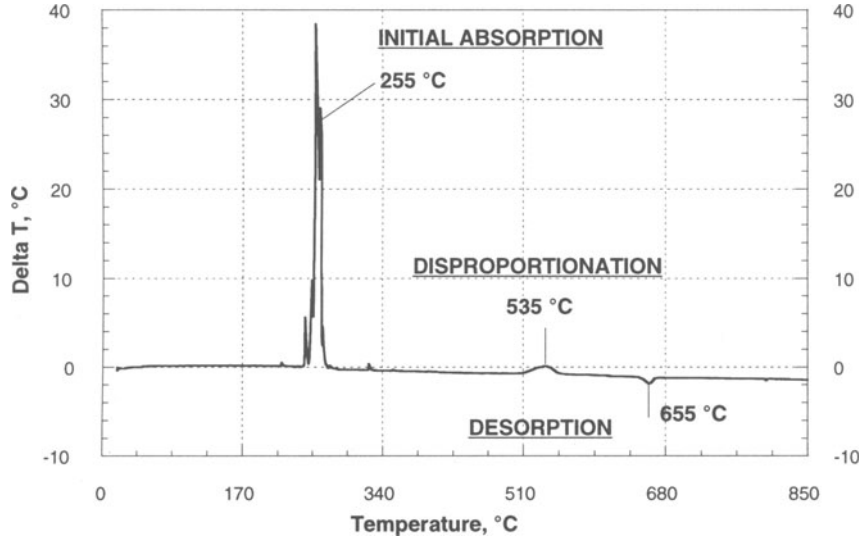

Figure 4. Hydrogenation of Zr_2Ni in the HDTA rig (1 bar H_2; heating rate 5 °C/min).

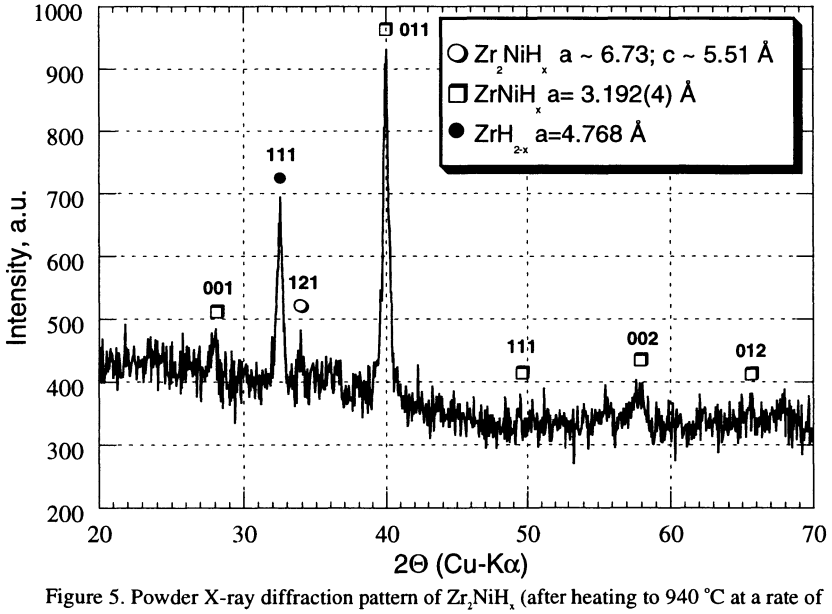

Figure 5. Powder X-ray diffraction pattern of Zr_2NiH_x (after heating to 940 °C at a rate of 5 °C/min in the TPA rig).

3.2. DESORPTION AND RECOMBINATION

These studies indicated that the desorption behaviour of the hydrogenated alloys are significantly different and depend on the phase composition.

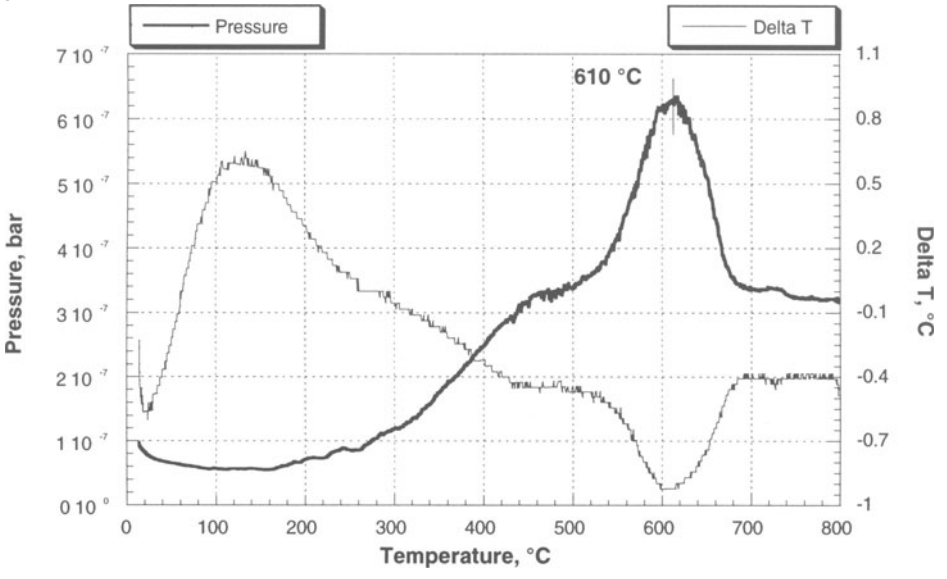

Figure 6. HDTA traces of hydrogen vacuum desorption from the disproportionated Zr_2FeH_{4-x} hydride.

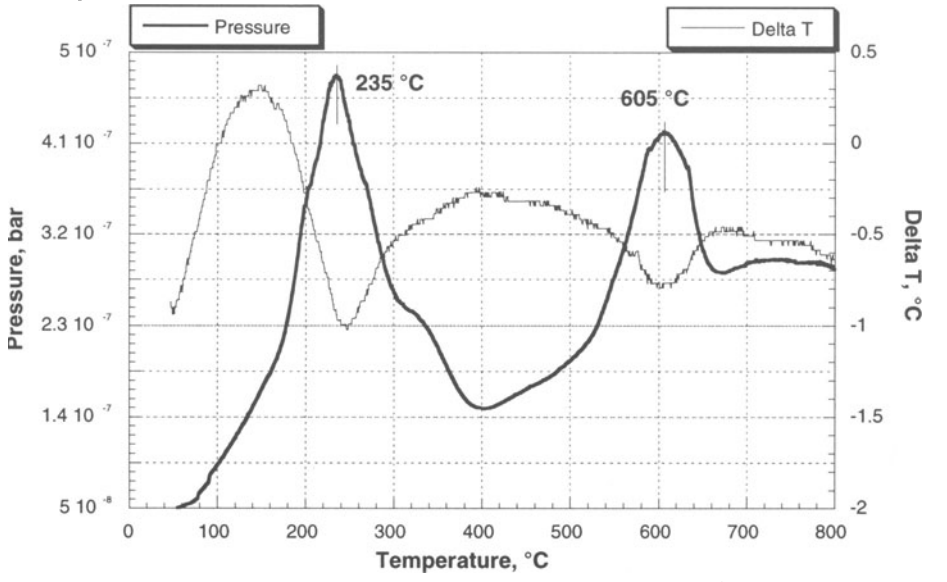

Figure 7. HDTA traces of hydrogen desorption from the partially disproportionated Zr_2NiH_{4-x} hydride.

For the completely disproportionated Zr_2Fe hydride, containing only one constituent hydride (ZrH_{2-x}), a single high temperature event of hydrogen desorption with a maximum around 610 °C was observed (see Fig.6). As expected, the temperature of

this event coincides well with the corresponding temperature for the ZrH_2 binary hydride [24]. The initial low temperature peak which occurs in all the ΔT traces (Figs 6,7,10,11) is a characteristic of the HDTA system and hence, at present, it is not possible to confidently discern any small thermal events in the low temperature region.

When the material was only partially disproportionated, particularly when it contains some amount of amorphous hydride phase (Zr_2NiH_4), an additional low temperature H-desorption event appears in the HDTA traces originating from the decomposition of the non disproportionated interstitial type hydride (see Fig.7). Here the desorption peak corresponding to the $ZrH_2 \rightarrow Zr$ transition at 605 °C is preceded by a stronger desorption peak at 235 °C which was identified as hydrogen release from the amorphous Zr_2NiH_x.

The hydrides of the alloys studied were found to desorb hydrogen completely on vacuum heating in the temperature range up to 700 °C. This desorption was accompanied by full recombination of the intermetallic crystal lattices for all the materials under investigation, including Zr_2Fe, $Zr_4Fe_2O_{0.6}$, Zr_2Ni and Zr_2Co. This conclusion is based on the X-ray diffraction studies of both recombined alloys (see Fig.8 containing the data for the $Zr_4Fe_2O_{0.6}$ as a typical example) and their hydrides synthesised in a "mild" synthesis mode from the recombined materials (Fig.9 contains the data for the $Zr_2FeH_{4.5}$ "cycled" material synthesised as the insertion type hydride after completing several HDDR cycles).

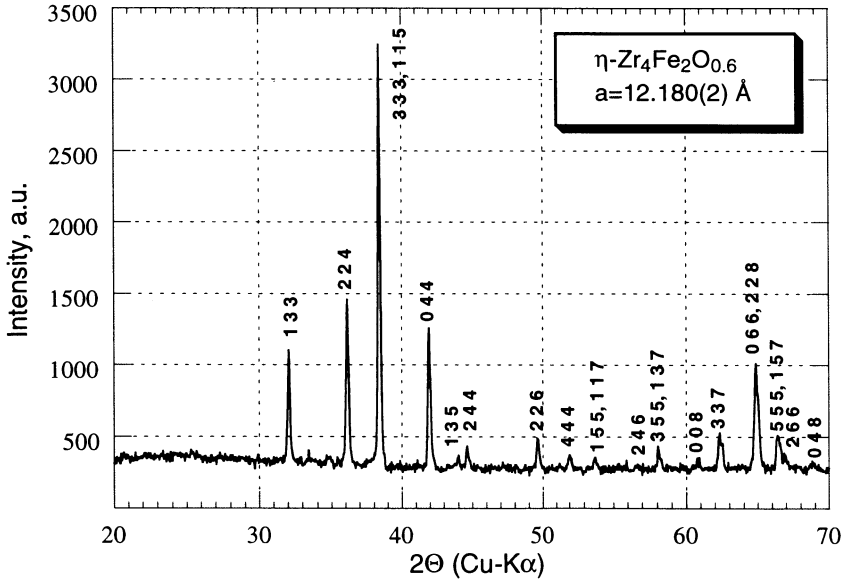

Figure 8. Powder X-ray diffraction pattern of recombined $Zr_4Fe_2O_{0.6}$ alloy after completing the HDDR cycle.

In contrast to the material that contained ZrH_{2-x} binary hydride, the insertion-type Zr_2MeH_x and $Zr_4Fe_2O_{0.6}H_{7.8}$ hydrides exhibited much lower thermal stability. Hydrogen desorption started just above room temperature and, in the case of Fe-containing hydrides, hydrogen desorption was complete before 300 °C, with a peak in the vicinity of 215 °C. The shape of the HDTA trace which is not symmetrical (see Fig.10 where the data for the Zr_2FeH_4 hydride are shown), indicates that two rather near overlapping H-desorption events take place for these hydrides. However, more detailed studies of

the H-desorption properties are necessary in order to distinguish whether additional "lower" hydrides are separated in the phase diagram by two-phase region, or a continuous reduction of H content proceeds within a region of extended solid solution of hydrogen in the metal matrix.

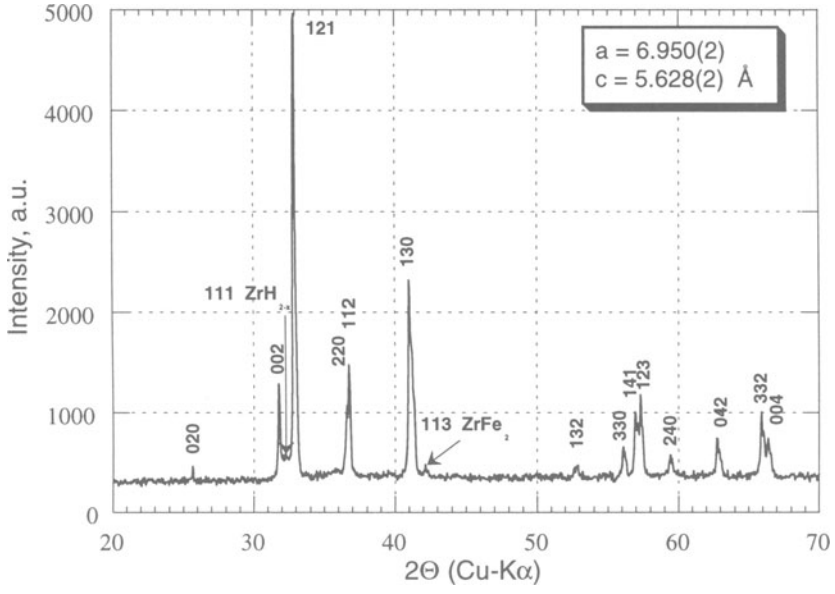

Figure 9. Powder X-ray diffraction pattern of the $Zr_2FeH_{4.5}$ hydride ($CuAl_2$ type) synthesised from the recombined alloy. The minor traces of ZrH_{2-x} and $ZrFe_2$ originate from a small inhomogeneity of the initial alloy.

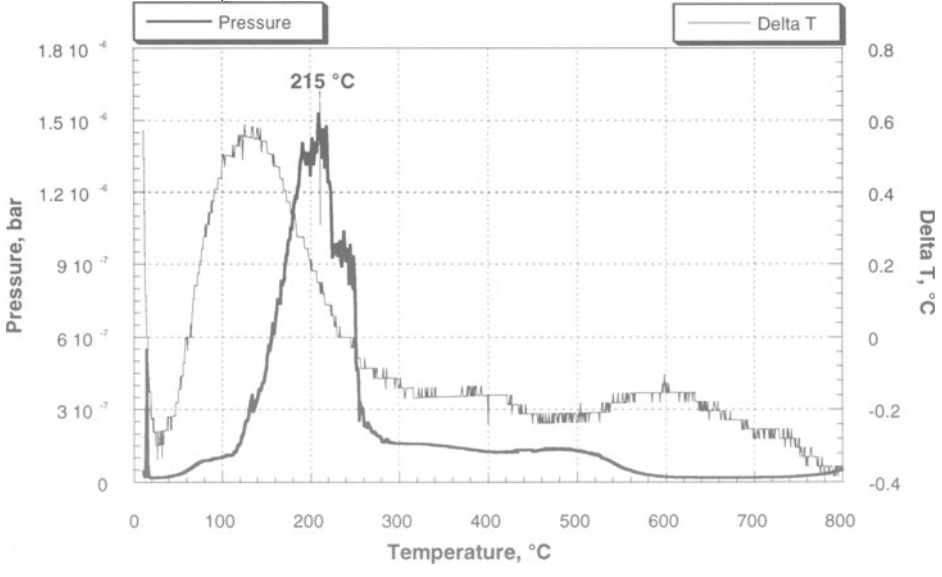

Figure 10. HDTA hydrogen desorption from the $Zr_2FeH_{4.5}$ hydride ($CuAl_2$ type) synthesised from recombined alloy after completing several HDDR cycles.

X-ray diffraction studies showed that on the hydrogenation of Zr_2Fe and Zr_2Ni, the initial tetragonal symmetry of the unit cells remains unchanged. The increase in unit cell volume has similar values in both cases, 19.3 (Fe) and 20.5 (Ni) %. However, for the Fe-containing compound, the lattice expansion is strongly anisotropic and is provided mainly by unit cell enlargement in the basal plane ($\Delta a/a$ = 9.0 %; $\Delta c/c$ = 1.5 %). In contrast, on formation of the Zr_2NiH_4 hydride the expansion of the unit cell proceeds in both [100] (5.5 %) and [001] (8.3 %) directions. The differences probably indicate filling of different types of interstices in the crystal structures of Zr_2NiH_4 and Zr_2FeH_4.

In this study two well resolved H-desorption events were observed in the HDTA spectrum of $CuAl_2$-type, Zr_2NiH_4 hydride with maxima around 215 and 450 °C (see Fig.11). The desorption from the Ni-containing hydride was completed at 600 °C indicating its higher thermal stability compared to that of the Fe-containing counterpart.

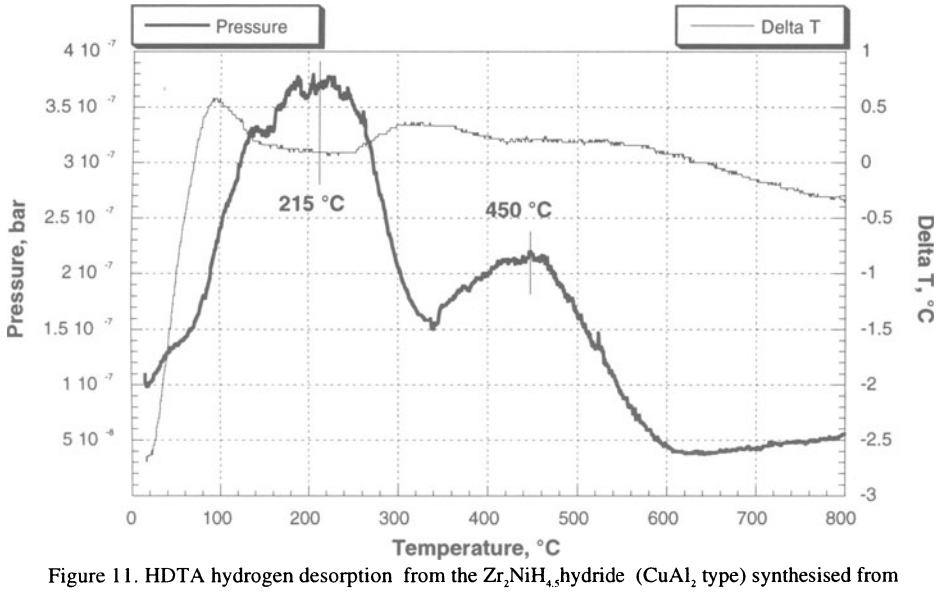

Figure 11. HDTA hydrogen desorption from the $Zr_2NiH_{4.5}$hydride ($CuAl_2$ type) synthesised from the recombined alloy after completing several HDDR cycles.

In order to produce an intermediate Zr_2Ni-based hydride, H vacuum desorption was terminated at the point where the first evolution event was completely finished (340 °C). An X-ray diffraction study of this hydride showed that its cell constants (a = 6.637(3); c = 5.389(5) Å) agree well with literature data (a = 6.6573(2); c = 5.3862 Å) for the $Zr_2NiD_{2.1}$ deuteride [14], which was synthesised in the "absorption" mode. This observation confirms the identification of the synthesised hydride as the dihydride Zr_2NiH_2.

3.3 NEUTRON DIFFRACTION STUDIES OF $Zr_2NiD_{1.84}$

In order to characterise the distribution of hydrogen atoms in the crystal lattice of the intermediate type Zr_2NiD_{4-x} hydrides, neutron diffraction studies of the deuterated Zr_2Ni alloy with the nominal composition $Zr_2NiD_{1.84}$ were performed. The hydride was obtained from a powdered alloy at pressures less then 1 bar D_2 and temperatures below

250 °C. Profile refinement of the neutron powder data indicated that this material contained two hydride phases. Its main constituent (~ 82 %) has been identified as $Zr_2NiD_{2.21}$ deuteride. As expected, the values of the cell constants for this hydride (a = 6.7169(6); c = 5.4530(7) Å) are in the region between those for the $Zr_2NiD_{2.1}$ dihydride and trihydride $Zr_2NiH_{2.9}$ (a = 6.7357(2); c = 5.4742(2) Å [14]). The second phase constituent (~ 18 %) was found to be the α-solid solution of D in Zr_2Ni containing 0.18 at.D/f.u.Zr_2Ni. Its cell constants are increased slightly (a = 6.5301(12); c = 5.2958(17) Å) in comparison to those of the Zr_2Ni intermetallic compound (a = 6.4875(2); c = 5.2656(2) Å [14]).

Refinements showed that the Zr_4 tetrahedron (16l sites) is the only type of interstice occupied by D atoms in α-$Zr_2NiD_{0.18}$. The results are summarised in Table 1. Crystal structure of $Zr_2NiD_{0.18}$ is shown in Fig.12.

Table 1.

Atomic coordinates and occupation numbers for two-phase mixture of $Zr_2NiD_{2.21}$ and $Zr_2NiD_{0.18}$. Space group I4/mcm. R_{prof} = 8.5 %; R_{wprof} = 11.1 %. Occupation numbers n = D/Zr_2Ni. For D atoms in $Zr_2NiD_{2.21}$ B was constrained to be equal. B_D = 0.7(1).

	$Zr_2NiD_{2.21}$	$Zr_2NiD_{0.18}$
8 Zr in 8h: x; x+½; 0	x = 0.1667(4); B = 0.22(5)	x = 0.1650(15); B = 0.22(5);
4 Ni in 4a: 0, 0, ¼	B = 0.26(6)	B = 0.26(6)
D1 in 8g: ½; 0; z	z = 0.770(12); n = 0.24(2)	-
D2 in 16l: x; x+½;z	x = 0.3749(6); z = 0.8833(10); n = 1.88(4)	x = 0.372(23); z =0.849(5); n = 0.15(8); B = 0.7(1)
D3 in 32m: x; y; z	x = 0.171(7); y = 0.929(18); z = 0.934(1); n = 0.09(4)	-

The metal-deuterium distances in the structures studied are in a range: Zr-D = 1.801(3)-2.161(3) Å, Ni-D = 1.600(1) Å ($Zr_2NiD_{2.21}$) and Zr-D = 1.88(1)-2.09(11) Å ($Zr_2NiD_{0.18}$).

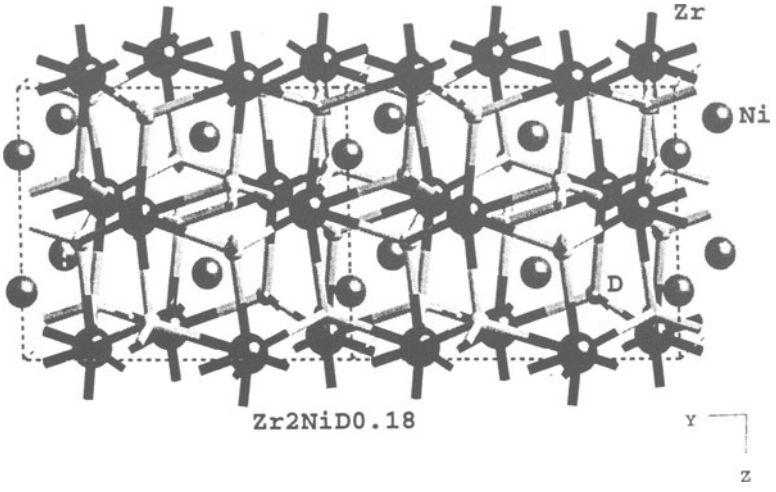

Figure 12. Crystal structure of $Zr_2NiD_{0.22}$ hydride (YZ projection).
Zr_4 interstices filled by D atom are indicated.

Following the increase of deuterium concentration up to $Zr_2NiD_{2.21}$, the 16l sites remain the favourable positions for H atoms, accommodating 1.88 of the total 2.21 at.D/f.u. In addition, two more types of interstices are occupied, namely the Zr_4 tetrahedra 8g (0.24 at.D/f.u.) and the Zr_3Ni tetrahedra 32m (0.09 at.D/f.u.). A comparison of the results of the refinement for $Zr_2NiD_{2.21}$ with the literature data for $Zr_2NiD_{2.1}$ and $Zr_2NiD_{2.9}$ shows that the same three types of interstice are occupied by D atoms in all three structures and that the occupation numbers for the D atoms in $Zr_2NiD_{2.21}$ are intermediate between those for $Zr_2NiD_{2.1}$ and $Zr_2NiD_{2.9}$.

These results indicated that, despite the observed separation of the two H-evolution events in the HDTA trace, formation of a solid solution of hydrogen in Zr_2Ni, at least between $H/Zr_2Ni = 2$ and 3, can be achieved by choosing the appropriate P-T synthesis conditions for the loading of the intermetallic material.

4. Conclusions

Despite numerous studies of the disproportionation behaviour of Zr-containing H-sorbing materials which frequently accompany their hydrogenation, no reports on the possibility of recovering the starting alloys after the removal of hydrogen from the metal lattice have yet been published.

In this work the Hydrogenation-Disproportionation-Desorption-Recombination process was applied successfully for the first time to intermetallic compounds of zirconium.

Zr-Fe, Zr-Ni and Zr-Co having 2:1 stoichiometry, including those containing oxygen ($Zr_4Fe_2O_{0.6}$) were found to be amenable to HDDR processing. Their stability with respect to disproportionation depends both on the behaviour of the constituent elements and on the crystal structure of the metal lattice. A transition from Fe- to Co- and Ni-containing compounds gives a change from the $CuAl_2$ structure type to the Ti_2Ni- and Fe_3W_3C-types, thus increasing the stability of the material.

The recombination step for the disproportionated intermetallics occurs in the vicinity of 600-620 °C, where a decomposition of zirconium dihydride, formed for each compound studied, took place.

The Hydrogenation-Disproportionation-Desorption-Recombination process which allows not only the restoration of the initial properties, but also the possibility of a favourable modification of the material into a desired metallurgical condition (refined grains, amorphous, improved homogeneity, etc.) opens new ways to study further the application of hydrogen metallurgy routes in zirconium-based (and other) alloys as H-storage, H-getter and battery electrode materials.

Acknowledgements

The authors would like to thank the Royal Society for the provision of research grant supporting a collaborative research programme between the Physico-Mechanical Institute of the NAS of Ukraine and the School of Metallurgy and Materials at the University of Birmingham. Financial support from the Research Council of Norway is also highly appreciated (VAY + BCH). The opportunity to collect neutron diffraction data at Risø, Denmark is gratefully acknowledged.

References

1. Yartys, V.A., Zavaliy, I.Yu., Lototzky, M.V., Riabov, A.B., and Shmal'ko, Yu.F. (1994) Oxygen-, boron- and nitrogen-containing zirconium-vanadium alloys as hydrogen getters with enhanced properties, *Z.Phys.Chemie*, **183**, 485-489.
2. Yartys, V.A., Zavaliy, I.Yu., Lototzky, M.V., Bulyk, I.I., Novosad, P.B., and Shmalko, Yu.F. (1991) Zr-V-Fe alloys as effective hydrogen storage materials, *Physicochemical Mechanics of Materials*, **27**, No. 2, 26-36.
3. Yartys, V.A., Zavaliy, I.Yu., and Lototzky, M.V. (1992) Low pressure hydrogen absorbers based on the oxide-doped Zr-V and Zr-V-Fe alloys, *Koordinatz.Khim. (Soviet Journal of Coordination Chemistry)*, **18,** No. 4, 409-423.
4. Nobile, A., Mosley, W.C., Holder, J.C., and Brooks, K.N. (1994) Deuterium absorption and materials phase characteristics of Zr_2Fe, *J.Alloys and Compounds,* **206**, 83-93.
5. Raj, P., Suryanarayana, P., Satnyamoothy, A., Shashikale, H., and Iyer, R.M. (1992) Zr_2FeH_x system hydrided at low temperatures - structural aspects by Mossbauer and x-ray diffraction studies, *J.Alloys and Compounds,* **178**, 393-401.
6. Zavaliy, I.Yu., Riabov, A.B., Yartys, V.A., Wiesinger, G., Michor, H., and Hilscher, G. (in press) $(Hf,Zr)_2Fe$ and $Zr_4Fe_2O_x$ alloys and their hydrides: phase equilibria, crystal structure and magnetic properties, *J.Alloys and Compounds*.
7. Aubertin, F., Gonser, U., and Campbell, S.J. (1984) Hydride formation by zirconium iron alloys and by η–phase $Zr_4Fe_2O_{0.6}$, *J.Phys.F,* **14**, 2213-2223.
8. Zavaliy, I.Yu., Riabov, A.B., and Yartys, V.A. (1995) Oxide-modified Zr-Fe alloys: thermodynamic calculations, X-ray analysis and hydrogen absorption properties, *J.Alloys and Compounds*, **219,** 38-40.
9. van Essen, H.M., and Buschow, K.H.J. (1979) Hydrogen absorption in various zirconium and hafnium-based intermetallic compounds, *J.Less-Common Metals,* **64,** 277-284.
10. Aubertin, F., Campbell, S.J., Pope, J.M., and Gonser, U. (1987) Nuclear magnetic resonance (NMR) studies of hydrogen diffusion in Zr_2Ni hydrides, *J.Less-Common Metals,* **129,** 297-303.
11. Aubertin, F., Campbell, S.J. (1990) Phase separation in hydrides of Zr_2Ni, *Hyperfine Interactions,* **54**, 767-773.
12. Asif, M., Havill, R.L., Titman, J.M., and Frick, B. (1995) Neutron quasi-elastic scatterting measurements of hydrogen diffusion in the $NiZr_2$ intermetallic phase, *J.Alloys and Compounds,* **231,** 243-247.
13. Verbetzky, V.N., and Movlaev, E.A. (1997) Synthesis and transformations of hydrides under high quasihydrostatic pressures, *J.Alloys and Compounds,* **253-254**, 38-40.
14. Chikdene, A., Baudry, A., Boyer, P., Miraglia, S., Fruchart, D., and Soubeyroux, J.L. (1989) Neutron-diffraction studies of $Zr_2NiH(D)_x$ hydrides, *Z.Phys.Chem.N.F.,* **163,** 219-224.
15. Dolukhanyan, S.K. (1997) Synthesis of novel compounds by hydrogen combustion, *J.Alloys and Compounds,* **253-254**, 10-12.
16. Bonhomme, F., Yvon, K., and.Fischer, P. (1993) Tetragonal Zr_2CoD_5 with filled Al_2Cu-type structure and ordered deuterium distribution, *J.Alloys and Compounds,* **199** (1-2), 129-132.
17. Libowitz, G.G., and Maeland, A.J. (1984) Interaction of hydrogen with metallic glass alloys, *J.Less-Common Metals,* **101,** 131-143.
18. Ragg, O.M., Keegan, G., Nagel, H., and Harris, I.R. (1997) The HD and HDDR processes in the production of Nd-Fe-B permanent magnets, *Int.J.Hydr.Energy,* **22**, 333-342.
19. Okada, M., Saito, K., Nakamura, H., Sugimoto, S., and Homma, M. (1995) Microstructural evolutions during HDDR phenomena in $Sm_2Fe_{17}N_x$ compounds, *J.Alloys and Compounds,* **231**, 60-65.
20. Book, D., and Harris, I.R. (1995) Hydrogen absorption/desorption studies on $Nd_{16}Fe_{78}B_8$ and $Nd_{11.8}Fe_{82.3}B_{5.9}$, *J.Alloys and Compounds,* **221**, 187-192.
21. Yartys, V.A., Wiesinger, G., and Harris, I.R. (1997) Hydrogenation behaviour and structure of $R_5Fe_2B_6$ (R = Ce, Pr, Nd, Sm, Gd and Tb) borides, *J.Alloys and Compounds,* **252**, 201-208.
22. Buschow, K.H.J. (1982) Crystallisation of amorphous $Zr_{1-x}Co_x$ alloys, *J.Less-Common Metals,* **85,** 221-231.
23. Kirkpatrick, M.E., Bailey, D.M., and Smith, J.F. (1962) The structure of $NiZr_2$, NiZr and their hafnium analogues, *Acta Crytsallographica*, **15,** 252-255.
24. Riabov, A.B., Yartys, V.A., Guegan, P.W., Clarke, J.C., and Harris, I.R. (1997) Microstructural characterisation and hydrogen absorption-desorption behaviour of Zr-V and Zr-V-O-based alloys, Int.Conference "Hydrogen Materials Science and Chemistry of Mteal Hydrides", Katsiveli, Crimea, Ukraine, to be published in *International Journal Hydrogen Energy.*

EFFECT OF HYDROGEN THERMO-SORPTIVE ACTIVATION BY METAL HYDRIDES: MAIN LINES OF INVESTIGATIONS AND PERSPECTIVES

YU.F.SHMAL'KO
Institute of Mechanical Engineering Problems of National Ukrainian Academy of Sciences. 2/10 Pozharsky St., Kharkov 310046, the Ukraine

1. Introduction

The problem «Hydrogen in Metals and in Intermetallic Compounds» is the subject of intensive investigations in quite a number of field both of fundamental character (solid state physics, inorganic, physical and structural chemistry, and others) and applicative character (hydrogen power and engineering, materials science, chemical current sources, etc.). During the past two decades this problem has been treated in hundreds of works, whose most exhaustive reviews were published in monographs [1,2]. To date investigated most exhaustively were the physico-chemical aspects of the given line of studies connected with obtaining of new hydride-forming materials, investigation of their structure and hydrogen sorption properties. Problems connected with the influence of hydrogen on the electron structure of metals and alloys, and elucidation of the essence of the metal-hydrogen bond in different hydrides are being intensively studied. A great number of works deal with investigation of the catalytic and electrochemical properties of metal hydrides.

The results obtained allowed to establish and further develop a number of promising fields of application of metal hydrides, viz. hydrogen treatment (storage, extraction and purification, compriming and controlled supply); technology of hydrogen treatment of materials (e.g. production of permanent magnets); chemical technology (hydrogen transfer reaction catalysts); developments connected with storage and conversion of energy (electric storage cells and fuel elements, thermo-compressors, etc.).

At the same time, some aspects of interaction in hydride-forming material-hydrogen systems have been studied insufficiently fully yet. For instance, this concerns the mechanisms of elementary processes in the skin surface layer of the gas phase of the mentioned systems accompanying hydrogen sorption-desorption. Analysis of some phenomena connected with these aspects was performed by our group in the review [3], with account of available information about hydrogen state in metal hydrides. It allowed to draw the following conclusions:

T. O. Saetre (ed.), Hydrogen Power: Theoretical and Engineering Solutions, 315–322.

1. The mechanism of reversible interaction of hydride-forming materials with hydrogen includes the reversible elementary processes of «dissociation ↔ recombination» and «ionization ↔ neutralization» proceeding on the solid phase surface.
2. The elementary processes mentioned in item 1 lead to the appearance on the metal hydride surface of participating therein hydrogen particles in the thermodynamically non-equilibrium state: atomic and molecular ions, excited atoms and molecules.
3. Depending on the external conditions, there may appear the possibility of emission of one or other kind of particles mentioned in item 2 into the gas phase in the course of hydrogen sorption-desorption by hydride-forming materials (effect of thermo-sorptive hydrogen activation by metal hydrides).
4. The effect mentioned in item 3 should primarily manifest itself in a change of the electric transfer characteristics of the gas phase.

On the basis of the aforesaid, we developed an approach to the set-up of experiments aimed at investigating the effect of thermo-sorptive hydrogen activation by metal hydrides. This approach provides for a detailed investigation of the gas phase physical properties during sorption-desorption of hydrogen by hydride-forming materials, and first of all the characteristics of electric transfer in gaseous hydrogen.

2. Preliminary studies

In 1987 we published the results of our first investigation of the anomalies of electric transfer of the gas phase in metal hydride-hydrogen systems which allowed to speak about the existence of the effect of thermo-sorptive hydrogen activation by metal hydrides [4]. It was shown that the characteristics of glow discharge ignition in hydrogen desorbed from a composite material sample based on $LaNi_5H_x$ under the pressure of 1-2 kPa essentially differs from the same for usual (equilibrium) molecular hydrogen under the same conditions. In particular, the relative potential gradient (E/P_{H_2}) for desorbed hydrogen of the gas gap corresponding to break-down was by 1.5 to 2 times lower than that of the equilibrium one. It was found also that even in the absence of external ionization sources, hydrogen desorbed from metal hydrides (composite materials based on $LaNi_5H_x$ and YNi_2H_x) under the pressure lower than 10 Pa contains a significant fraction of positive ions, and in the range of pressures lower than 10^{-3} Pa these ions are identified by mass spectrometry methods as protons.

In the course of more detailed studies of gas discharge characteristics in hydrogen desorbed from the metal hydride $LaNi_5H_x$ [5] it was established that a change of the glow discharge characteristics is primarily due to a change of the gas phase properties, and not to some other side effects (e.g. influence of the electrode material). Mass spectrography analysis of the discharge plasma demonstrates that during the passage from equilibrium molecular hydrogen to hydrogen desorbed from a metal hydride the plasma ion composition changes, viz. the fraction of atomic (H^+) and complex (H_3^+) ions grows with respect to the molecular (H_2^+) ones. At this, the hydrogen being desorbed from the

metal hydride has an increased ionization efficiency as compared to equilibrium hydrogen (upon ignition of the gas discharge or at electron impact).

The experimental mass spectrometry estimates of the ionization potential and section for hydrogen desorbed from metal hydrides (ionization method: electron impact; investigated process: $H_2 + e \rightarrow H_2^+ + 2e$) carried out in [6] have shown that in the region of energies of ionizing electrons corresponding to the ionization cross-section maximum (70-100 eV) the ratio of ionization cross-sections of hydrogen desorbed from metal hydrides (e.g. getter alloy Zr-V-Fe saturated by hydrogen) and that of equilibrium hydrogen is within 1.3 to 1.5 (Fig.1). At this, the potential of appearance of H_2^+ ions in the case of hydrogen desorbed from the sample $(Zr\text{-}V\text{-}Fe)H_x$ is 0.3 to 0.5 eV lover than in the case of equilibrium molecular hydrogen. This value is close to energy of the first vibrational level of the hydrogen molecule in the ground electron state (0.55 eV). This fact allowed the authors to assume that one of the manifestations of the effect of thermosorptive hydrogen activation is excitation of the vibrational levels of the H_2 molecule formed during recombination of H atoms on the hydride surface.

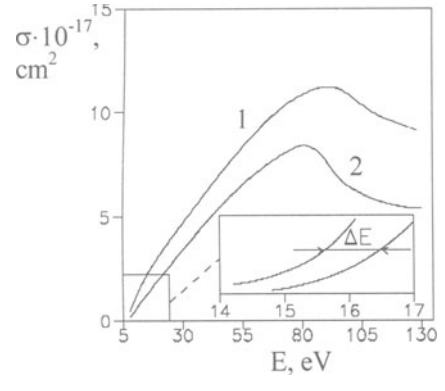

Figure 1 - Cross-sections of hydrogen molecular ionization by electron impact:
1 - H_2 desorbed from $(Zr\text{-}V\text{-}Fe)H_x$
2 - Equilibrium H_2 from a cylinder

In works [7,8] we made an attempt to practically use the effect of thermosorptive hydrogen activation by metal hydrides to increase the efficiency of a hydrogen ion source. The characteristics of an experimental brassboard gas-discharge ion source were investigated. The metal hydride element made of a composite material containing a zirconium alloy saturated with hydrogen and a copper binder was installed in the anode of the gas-discharge chamber. In the test experiments this element was replaced by a copper sample of the same shape and size. The obtained results have shown that the introduction of a metal hydride into the anode of the ion source gas-discharge chamber substantially increases its gas and energy efficiency both in the regime of generation of H^- and H^+. In particular, the discharge ignition voltage in the gas-discharge chamber or the hydrogen pressure at which the discharge is ignited drops. At this, a growth of the ion yield is observed, which makes up 15-20% in the regime of H^- generation and more than 30% in the regime of H^+ generation. In the presence of a metal hydride the discharge in the gas-discharge chamber burns more stable, noises decrease and ion beam quality increases.

The results obtained stimulated the authors to set up more refined investigations of the change of the charge and energy states of particles of the gas phase in the «hydride-forming material - hydrogen» system. To date we have developed a mass-spectrometry method of identifying the vibrationally-excited states of hydrogen and deuterium molecules desorbed from metal hydrides and deuterides. For samples of hydrides and deuterides based on the alloys Zr-V and Zr-V-Fe preliminary results were obtained, accord-

ing to which hydrogen (deuterium) desorbed therefrom may be considered as a combination of H_2 (D_2) molecules in their ground and first vibrationally-excited states [9-11].

Continuation of experimental studies along these lines would allow, on the one hand, to extend our knowledge of the nature of the effect of thermo-sorptive hydrogen activation by metal hydrides, and, on the other hand, to find new ways of its practical application, primarily in energy conversion systems.

3. Perspectives of further investigations

We propose a detailed further investigations of the effect of thermo-sorptive hydrogen activation along three main lines. The most important features of their realization are considered in the following subsections.

3.1. DETERMINATION OF THE COMPONENT COMPOSITION OF THE GAS PHASE OF THE HYDRIDE-FORMING MATERIAL - HYDROGEN SYSTEMS, INCLUDING THE DISTRIBUTION OF ITS PARTICLES OVER THE VIBRATIONALLY- AND ROTATIONALLY-EXCITED STATES.

Here we chose mass-spectrometry of hydrogen desorbed from different metal hydrides as the basic experimental method. In so doing, ionization efficiency curves can be obtained and their fine structure can be determined by means of the respective mathematical treatment. The shift of the vertical ionization potentials obtained by this procedure, as compared to similar characteristics of equilibrium hydrogen, will yield information about the vibrationally-excited states of molecules of hydrogen desorbed from a metal hydrides.

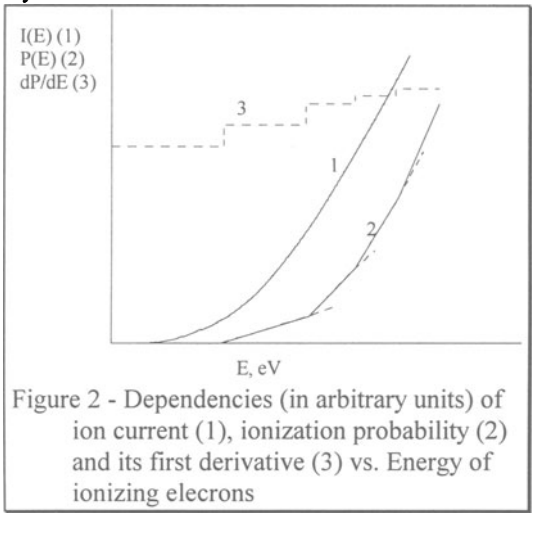

Figure 2 - Dependencies (in arbitrary units) of ion current (1), ionization probability (2) and its first derivative (3) vs. Energy of ionizing elecrons

The ionization potentials are measured by plotting the ionization efficiency curves (IEC). The latter represent the dependence of the current of ions of respective mass on the energy of ionizing electrons. The presence of an initial IEC section smoothly increasing from zero is on the one hand due to the energy spread of the ionizing electrons (0.5 - 1 eV), and on the other hand it results from the distribution of the initial neutral molecules over the vibrational-rotational states and molecular ions formed by their ionization. By eliminating in one or other manner the smoothening effect of the ionizing electrons energy spread on the shape of the IEC initial section one can obtain the ionization probability curve whose fine structure (threshold, bends and jumps) is

used directly to determine the set of vertical ionization potentials of neutral hydrogen molecules (Fig.2).

Our group have developed a method of mathematical treatment of IEC plotted with the use of a standard mass-spectrometer. The method allows to reveal the IEC fine structure.

In the given approach the dependence of the detected ion current **i** on the ionizing electron energy **V** is presented in the form of the ionization probability convolution $\mathcal{P}$, being a function of the full energy of ionizing electrons **E** and the distribution of ionizing electrons **m($\mathcal{U}$)** over the thermal energies $\mathcal{U}$:

$$i(V) = \int_0^\infty \mathcal{P}(\mathcal{U} + V) \cdot m(\mathcal{U})\, d\mathcal{U} \qquad (1),$$

where $\mathcal{U}$ **+ V = E** - the full energy of an ionizing electron.

The problem of reconstruction of the ionization probability dependence on the ionizing electrons energy **$\mathcal{P}$(E)** consists in solving integral equation (1). Such a solution is usually obtained by the inverse convolution method with the use of fast Fourier transform (FFT) algorithms. In so doing, it is possible to reconstruct the ionization probability **$\mathcal{P}$(E)** at an arbitrary energy distribution **m($\mathcal{U}$)** of ionizing electrons. However, in the case of Maxwellian energy distribution of electrons it is possible to develop algorithms corresponding to the convolution transform without using FFT [12]. The feature of this group of methods is the application of some finite-difference operator to the points of the experimentally plotted IEC.

As analysis done by the authors has shown, in case of Maxwellial energy distribution of ionizing electrons, equation (1) allows for an exact solution in the form of a differential operator which effects the non-homogeneous term **i(V)** in the initial integral equation (1):

$$\mathcal{P}(E) = \beta^2 \left\{ i(E) - \frac{2}{\beta}\frac{di(E)}{dE} + \frac{1}{\beta^2}\frac{d^2 i(E)}{dE^2} \right\} \qquad (2),$$

where β **= 1/kT**; **T** is the temperature of ionizing electrons.

Using different methods of approximating differential operator (2) by finite-difference operators makes it possible to derive approximate methods of solving equation (1) which correspond to necessary accuracy requirements.

Using analytical expression (2), a trinomial difference operator was derived:

$$\mathcal{P}(E) = \frac{\exp(2\beta \cdot \Delta E)}{(\Delta E)^2}\left[i(E) - 2\exp(-\beta\Delta E) \cdot i(E + \Delta E) + \exp(-2\beta\Delta E) \cdot i(E + 2\Delta E) \right. \qquad (3),$$

where Δ**E** is the energy shift step **i(E)**. Expression (3) is derived in the assumption $\beta\Delta$**E**<<**1** which is usually satisfied.

The common drawback of the group of methods based on applying finite-difference operators of kind (3) to experimentally plotted IEC points is their increased sensitivity to experimental errors. The presence of even small noise as low as fractions

of a percent leads to an oscillating resulting curve unsuitable for obtaining quantitative data on the energy states of the particles being analyzed.

Using different methods of smoothening the initial curves before applying the convolution procedure leads not only to smoothing out of IEC features, but in a number of cases it results in the appearance of a false fine structure [13].

We have developed a method allowing to overcome this obstacle [9]. The essence of the approach being proposed consists in the following. On the basis of a set of values of the detected ion current $\bar{I}_k$ ($k=1,2,...,n$) corresponding to the points of the experimentally plotted IEC, curve I_k is built, which after application of operator (3) is transformed into a broken line having rectilinear sections between the bends and a specified number of bends. The location of bends is selected so that quantity

$$S = \sum_{k=1}^{n} (\bar{I}_k - I_k)^2 \qquad (4)$$

acquires a minimal value corresponding to the most probable set of vertical ionization potentials. Minimization of the sum of squares of residuals S is performed by the coordinate-to-coordinate descent method.

In the described method of IEC mathematical treatment it is intended to use additional information (besides the initial experimental IEC) which may obtained both in the course of experiments and from other sources. In particular, for hydrogen one may theoretically calculate the vertical ionization potentials corresponding to transition of the given vibrationally-excited state of a neutral molecule into some vibrationally-excited state of a molecular ion.

In addition to mass spectrometry investigations, the method of UV photoelectron high-resolution gas spectroscopy can be used. This method will allow to measure the ionization potentials of hydrogen desorbed from metal hydrides with resolution of the vibrational structure of the electron spectrum, and the relative intensities of the photoelectron spectrum peaks. For molecules of desorbed hydrogen, the obtained results will allow to find the binding energy and identify the character of molecular orbitals. Systematic measurements of the rotational structure of the photoelectron spectra of hydrogen and its isotopes can also be carried out.

3.2. INVESTIGATION OF THE MANIFESTATIONS OF THE EFFECT OF THERMO-SORPTIVE HYDROGEN ACTIVATION BY METAL HYDRIDES CONNECTED WITH A CHANGE OF THE ELECTRIC TRANSFER CHARACTERISTICS IN THE GAS PHASE.

The investigations are planned to be carried out in two stages. At the first stage we can plot the ignition curves of a glow discharge (Paschen's curves) in a medium of hydrogen desorbed from metal hydride samples of different composition under the pressure of 1-1000 Pa.

In the course of these experiments the sample temperature, the gas pressure and composition above it, and the current hydrogen content in the metal hydride are monitored (the latter parameter is determined indirectly by the amount of hydrogen evacuated from the working volume).

The gas gap break-down characteristics are measured in two regimes, viz. at constant pressure and variable voltage across the discharge gap, or at constant voltage and variable hydrogen pressure. In both cases the moment of break-down is detected by the appearance of a current in the discharger circuit. According to the value of the relative discharge ignition voltage (**U/P**, where **U** is the voltage drop across the discharge gap, and **P** is hydrogen pressure), and depending on the reduced pressure value (**P/d**, where **d** is the value of the gap between the electrodes) Paschen's curves are plotted for equilibrium hydrogen (in absence of a metal hydride sample) and for hydrogen desorbed from different metal hydrides. A change of the shape of Paschen's curve as well as of the position of its minimum carry information about the degree of activation of hydrogen by metal hydrides.

At the second stage it is planned to carry out investigations of gas discharge parameters in hydrogen activated by metal hydrides, viz. the volt-ampere characteristics of the discharge in the Penning-type cell with a metal hydride electrode, and the discharge plasma parameters (electron temperature, plasma density, its ion composition and emission characteristics).

The obtained information will allow to specify the influence of the effect of hydrogen activation by metal hydrides on the character of elementary process in the gas discharge, and to evaluate the variation of emission of hydrogen positive and negative ions (its isotopes) due to the influence of the effect of hydrogen activation. In particular, due to anomalous excitation of vibrational levels of hydrogen molecules an increase of the rate of formation of hydrogen negative ions in the plasma volume is anticipated.

3.3. INVESTIGATING THE CATALYTIC ACTIVITY OF METAL HYDRIDES IN HYDROGEN TRANSFER REACTION

The catalytic properties of metal hydrides in solid-phase reactions of saturation of hydride-forming materials by hydrogen (effect of improvement of hydrogen sorption properties in multiphase polymetallic compositions) can be investigated. For this, comparative experiments in studying the kinetics of hydrogen sorption-desorption by such compositions can be carried out. The details of such investigations are reported elsewhere [14].

The results of investigations along this line will serve as a basis for carrying out experiments along the two above-mentioned remaining lines, viz. investigation of ionization potentials of activated hydrogen and of electric transfer characteristics in its medium.

4. Conclusion

The implementation of investigations proposed in this paper will allow to detect the elementary processes on the interface surface and in the skin surface layer of the «hydride-forming material - hydrogen» systems gas phase; establish the regularities of the interrelation of the hydrogen-sorption, catalytic and some other characteristics of hydride-forming materials with the energy and charge states of particles of the gas phase

coming into contact with these materials. On the other hand, the results obtained in the course of these experiments will allow to improve the existing processes of energy conversion and develop the physico-chemical foundations of new effective processes in which hydrogen and its isotopes are used as the working medium.

References

1. *Hydrogen in Metals* (in 2 volumes), Ed. by G.Alefeld and J.Volkl, Springer-Verlag, 1978.
2. *Hydrogen in Intermetallic Compounds* (in 2 volumes), Ed. by L.Schlapbach, Springer-Verlag, 1992.
3. Shmal'ko, Yu.F., Lototsky, M.V., Klochko, Ye.V., and Solovey, V.V.: The formation of excited H-species using metal hydrides, *J. Alloys and Compounds* , 231 (1995) 856-859.
4. Podgorny, A.N., Solovey, V.V., Shmal'ko, Yu.F., Lototsky, M.V., Prognimak, A.M., Pitul'ko, S.Ye., and Valuiskaya, S.B.: Hydrogen activation in hydrogen-intermetallide hydride systems, *Probl. in Nuclear Science and Engineering, Ser. Nuclear-Hydrogen Power and Technology,* 1 (1987) 68-72 (in Russian).
5. Galchanskaya, S.A., Dorokhov, V.V., Lazarev, N.F., Lototsky, M.V., Solovey V.V., and Shmal'ko, Yu.F.: Investigating the process of hydrogen activation by metal hydrides. I. Mass spectrometry analysis of gas-discharge plasma, *Ibid., Ser. Nuclear Engineering and Technology,* 1 (1989) 55-58 (in Russian).
6. Valuiskaya, S.B., Lototsky, M.V., Skripal', L.P., Solovey, V.V., and Shmal'ko, Yu.F.: Investigating the process of hydrogen activation by metal hydrides. II. Mass spectrometry determining of the hydrogen ionization potential and section, *Ibid.,* 58-61 (in Russian).
7. Shmal'ko, Yu.F., Lototsky, M.V., Pitul'ko, S.Ye., and Solovey, V.V.: Investigating the hydrides of zirconium-containing hydrogen-getter alloys for increasing the efficiency of hydrogen ion sources, *Ibid, Ser. Nuclear-physical Investigations (theory and experiment),* 1 (1992) 6-8 (in Russian).
8. Shmal'ko, Yu.F., Lototsky, M.V., Solovey, V.V., Yartys', V.A., and Strokach, A.P.: Application of metal hydrides in hydrogen ion sources, *Z. Phys. Chem.,* 183 (1994) 479-483.
9. Shmal'ko, Yu.F., Solovey, V.V., Lototsky, M.V., and Klochko, Ye.V.: Mass-spectrometry determination of vibrationally-excited states of molecules of hydrogen desorbed from the surface of metal hydrides, *Int. J. Hydrogen Energy,* 20 (5) 1995 357-360.
10. Klochko, Ye.V., Lototsky, M.V., and Shmal'ko, Yu.F.: Influence of isotopic effect on the shift of the ionization potentials for hydrogen desorbed from the metal hydride surface, In: *NATO International Conference «Hydrogen Material Science and Chemistry of Metal Hydrides», 2-8 Sept. 1995, Katsiveli, Crimea, Ukraine,* p.150.
11. Klochko, Ye.V., Lototsky, M.V., and Shmal'ko, Yu.F.: Mass spectrometry method of investigating vibrationaly-excited states of molecules of hydrogen desorbed from the surface of metal hydrides, In: *«Cold Nuclear fusion and new energy source», Minsk, Belarus, May 24-26, 1994,* p. 72-78 (in Russian).
12. Vogt, J., and Pascual, C.: Inverse convolution applied to the evaluation of electron impact ionization efficiency curves, *Int. J. Mass Spectrom. Ion Phys,* 5 (9) (1972) 441-448.
13. Raznikov, V.V., Dodonov, A.F., and Zelenov, V.V.: Revealing of the fine structure of ionization efficiency curves for molecules, radicals and excited particles ionized by electrons having thermal energy distribution, In: *«Mass Spectrometry and Chemical Kynetics»,* Ed. by V.M.Tal'roze, Moscow, «Nauka», 1985, p.129-137 (in Russian).
14. Lototsky, M.V.: The effect of improvement hydrogen-sorption properties in multiphase polymetallic compositions, HYPOTHESIS II, Rep. No. 422

INDUSTRIAL METAL-HYDRIDE CONTINUOUSLY-OPERATED COMPRESSOR

YU.F.SHMAL'KO*, A.I.IVANOVSKY*, M.V.LOTOTSKY* AND D.V.VOLOSNIKOV**

* *Institute of Mechanical Engineering Problems of National Ukrainian Academy of Sciences. 2/10 Pozharsky St., Kharkov 310046, the Ukraine*

** *Joint-Stock Company «Lviv Chemical Plant». Lviv 290070, the Ukraine*

1. Introduction

Metal-hydride thermosorption compressors (TSC) are expediently differ from conventional mechanical hydrogen compressors by that they have not moving parts working in hydrogen environment. Thus they have not moving seals. The given advantage is to the greatest extent exhibited at high pressure hydrogen force-pumping - 15.0 MPa and above. Besides, TSCs do not require the lubrications and characterised by dynamic steadiness and high purity of delivered hydrogen.

For a number of years our laboratory is engaged in development and creation of metal-hydride engineering for hydrogen compression. During fulfilment of these activities a series of metal-hydride TSCs was created which have found the application in various research and production centres of Ukraine and abroad [1,2]. However, these were rather small, laboratory scale systems with hydrogen productivity no more than $4 \cdot 10^{-2}$ g/s (1.6 m^3/h).

In 1995-1997 we have developed, created and first entered into maintenance a pilot sample of the KM-1510 industrial scale compressor intended for filling by hydrogen of standard 40-liter gas cylinders. The works were carried out by the order of Joint-Stock Company «Lviv Chemical Plant» (Ukraine), for providing the deep argon purification technological assembly by compressed hydrogen.

The main specifications of the customer to development were the following ones:

- hydrogen output - up to 10 m^3/h;
- hydrogen supply operating mode - continuous;
- heat supply - electrical;
- cooling - forced air convection;
- suction pressure - from 0.3 MPa;
- discharge pressure - up to 15.0 MPa.

T. O. Saetre (ed.), Hydrogen Power: Theoretical and Engineering Solutions, 323–326.

In the given paper the brief description of results of development, creation and industrial tests of mentioned pilot sample of the metal-hydride hydrogen compressor is presented.

2. Compressor's structure and operation

The general view of metal-hydride hydrogen compressor KM-1510 is shown in Figure 1.

Figure 1. A general view of the compressor KM-1510

Compressor has overall dimensions 2350×1150×1050 mm at weight of 700 kg. It consists of:

- the frame containing two units of heat exchangers with fans, support of the control block, the thyristor unit;
- the set of generators-sorbers (60 items) built into the heat exchanger's units;
- gas-distributing system;
- electric equipment and control system.

The functional scheme of the compressor is shown on Figure 2.

The compressor consists of two two-stage compressing modules (Im and IIm). The modules include compressing stages: the first stage of the first module (IsIm), second stage of the first module (IIsIm), first stage of the second module (IsIIm) and second stage of the second module (IIsIIm). Each stage represents the battery of fifteen generators-sorbers (GS 1... 15) with built-in tubular heaters (TH) isolated from high pressure. The compressor also includes gas-distributing line with branch pipes of suction (H_2 input) and forcing (H_2 output), pressure gauges (are not indicated) and reverse valves

(RV1...RV6), system of air cooling based on fans (FI, FII), as well as the control block (CB).

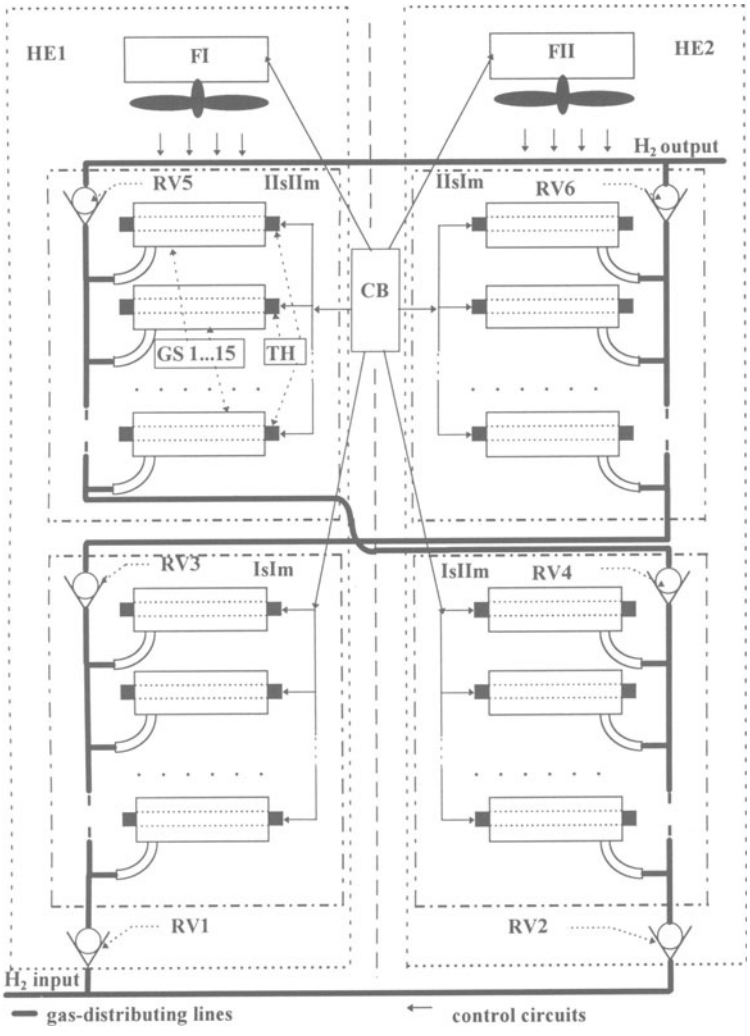

Figure 2. The functional scheme of the compressor KM-1510

Structurally compressing modules are located in two heat exchangers. The first heat exchanger (HE1) contains GSs of compressing stages IsIm and IIsIIm, second (HE2) - GSs of stages IsIIm and IIsIm. The generators-sorbers of each heat exchanger are joint in a unified package and are located horizontally.

Thus, each module integrates its first and second stages on gas, and each heat exchanger - first and second stages of different modules on thermal effect.

Main functional elements of the compressor are the generators-sorbers (GS) representing filled by a hydride-forming material heat-transport devices of a regenerative type. The generators-sorbers of the first stages (IsIm, IsIIm) are filled by a «high-

temperature» hydride-forming intermetallide $LaNi_{4,5}Mn_{0,5}$. The generators-sorbers of the second stages (IIsIm, IIsIIm) are filled by a «high-temperature» hydride-forming intermetallide $LaNi_5$.

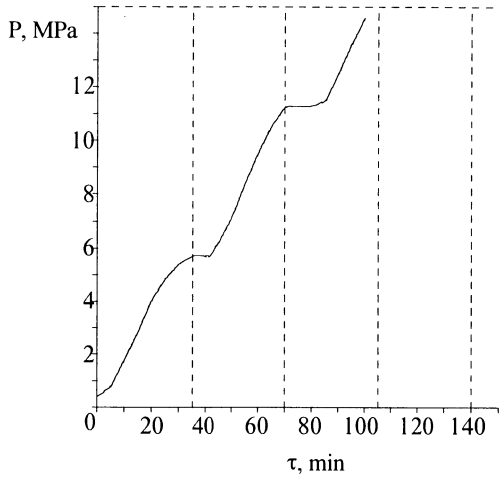

Figure 3. Compressor's operating cyclogramm.

The operation of the compressor is implemented by periodic forced heating and cooling of GS batteries heat exchangers. The first and second stages of different heat exchangers (or the same compressing modules) work in phase opposition providing a continuity of hydrogen compression.

The switching of modes of hydrogen suction and forcing implements by switching of the power supply from electro-fans to THs, with the help of control block (CB). The gas flows thus are switched automatically, with the help of systems of reverse valves (RV1...RV6).

In Figure 3 the cyclogramm of compressor's operating in a mode of filling two parallel jointed gas cylinders with a capacity of 40 l the each is shown. The vertical dashed lines in a Fig. 3 correspond to switching heat exchangers' heating or cooling. The specific output on force-pumped hydrogen is provided at consumed electrical power up to 27 kW.

3. Conclusion

The pilot sample of metal-hydride hydrogen compressor KM-1510 was transferred to the customer in May, 1997 and now it is successfully maintained on industrial base of Lviv Chemical Plant.

The calculation of an economic efficiency of the described compressor leaves for frameworks of the present paper. However, the fact that the given development was financed by an industrial firm in conditions of a deep economic crisis in Ukraine, testifies to high competitiveness of this class of metal-hydride compressing engineering.

References

1. Solovey, V.V., Ivanovsky, A.I., Kolosov, V.I., and Shmal'ko, Yu.F.: Series of metal hydride high pressure hydrogen compressors, *JALCOM* **231** (1995) 903-906.
2. Ivanovsky, A.I., Kolosov, V.I., Lototsky, M.V., Solovey, V.V., Shmal'ko, Yu.F., and Kennedy, L.A.: Metal hydride thermosorption compressors with improved characteristics, *Int. J. Hydrogen Energy* **21**(11/12) (1996) 1053-1055.

CRYO-HYDRIDE HYDROGEN COMPRESSOR FOR PRESSURE UP TO 4 KBAR

YU.F.SHMAL'KO*, A.I.IVANOVSKY*, M.V.LOTOTSKY*,
L.V.KARNATSEVICH** AND YU.YA.MILENKO**
* *Institute of Mechanical Engineering Problems of National Ukrainian Academy of Sciences. 2/10 Pozharsky St., Kharkov 310046, the Ukraine*
** *National Research Centre «Kharkov Physical-Technical Institute». 1 Akademicheskaya St., Kharkov, 310108, Ukraine*

1. Introduction

Compression of gaseous hydrogen up to high pressure by conventional methods represents a difficult technical problem. The main problem here consists of a reliability of seals of moving parts. In this connection it would be tempting to use such engineering solutions which generally eliminate availability of mobile elements working in hydrogen medium.

Calculations carried out by us, as well as the preliminary experiments have shown that for reaching hydrogen pressure more than 100 MPa such a solution can be cryogenic compression of hydrogen. It consists of supply of intermediate pressure (30-40 MPa) hydrogen into cooled by liquid nitrogen high-pressure vessels, switching-off these vessels from a supplying hydrogen line, and then - their warming up to room temperature. At an appropriate selection of ratios of volumes of such vessels and operation temperatures it is possible obtaining hydrogen pressure up to 400 MPa.

The difficulty of a realization of the given solution at an exit for frameworks of laboratory experiments consists of a problem of hydrogen compression up to intermediate pressure 30-40 MPa. The use of conventional mechanical compressors for this purpose is complicated their cumbrousness, low efficiency and reliability, as well as availability of impurity of air and vapors of lubrication in compressed hydrogen. These impurities are condensed at cooling and litter the pipeline and locking fittings.

The actual way of the solution of the given problem represents implementation of preliminary compression of hydrogen with the help of metal-hydride thermo-sorption compressing stage which is characterized by absence of moving elements and high purity of hydrogen being supplied[1,2].

In the present work the implementation of such an approach is described. Here the experimental sample of combined cryo-hydride compressor providing hydrogen compression from 1.5 up to 250-400 MPa is created.

T. O. Saetre (ed.), Hydrogen Power: Theoretical and Engineering Solutions, 327–329.

2. Description of compressor's design

2.1. METAL-HYDRIDE STEP

The first, metal-hydride step of the compressor represents metal-hydride module (generator-sorber) filled by hydride-forming intermetallic compound **$MmNi_5$** in quantity of 1.6 kg. The module provides a reception of low-pressure (1.5-2.0 MPa) hydrogen, its intermediate storage (reserve not less than 240 l at normal conditions), purification (the contents of impurities is not higher than 10^{-2} %) and force-pumping into cryogenic steps under the pressure up to 40 MPa.

Structurally metal-hydride module is made as a cylindrical stainless steel vessel with an axial filtering collector of hydrogen. Taking into account high barothermical loads, the module is made without welded joints, with face lens-type seals. The outside and internal frame diameters make 47 and 33 mm respectively, its length is 580 mm. For acceleration of heat transfer the module is equipped with internal transversal copper ribs having thickness of 0.5 mm with a pitch of 4 mm. Hydrogen reception (absorption) is carried out at room temperature, it output (desorption) under increased pressure - at T=500-600 K. Heating the module is realized with the help of outside electric heater by power 1 kW, heating temperature is controlled by the thermocouple. Metal-hydride module, using the system of valves, is connected with a source of low-pressure hydrogen and cryogenic part of the compressor. The time of filling metal-hydride stage by hydrogen makes 1-1.5 hours, the time of maximum pressure developing in a stage makes 30 minutes.

2.2. CRYOGENIC PART

Cryogenic part of the compressor consists of two stages, e.g.: pressure vessels of volumes 60 and 30 cm^3 which can, being connected with the previous stage by hydrogen, be cooled by liquid nitrogen up to T=77 K and, being isolated from gas lines, to be warmed up to room (or higher) temperature. The initial pressure 30-40 MPa in both cooled stages is provided with metal-hydride stage of the compressor. When cryogenic stages are warmed up to room temperature, in last of them the pressure up to 250-400 MPa is generated.

The pressure vessels, connective pipelines, needle-shaped or membrane valves [3] and specially developed capacitive pressure transducers with small own volume are mainly made of thermal-treated beryllium bronze.

The time of implementation of one cycle of obtaining maximum pressure makes about 1 hour.

Our calculations show that by increase of number of cryogenic stages of the compressor it is possible to achieve the higher pressure, up to 500 MPa.

3. Conclusion

The testing results of the compressor described above have shown its functionality and higher reliability, on a comparison with conventional mechanical hydrogen compressors. The combined design of the compressor allows to simplify and to speed up process of hydrogen compression up to high pressure and to provide it high purity. Except above-listed, essential advantage of the compressor are minimal (in the perspective, practically zero) losses of working gas that is especially important at implementation of compression of heavy isotopes of hydrogen (deuterium and tritium). It is achieved by implementation of return of compressed gas from the last cryogenic step to first metal-hydride one.

The results of the present work show a basic capability of creation of high-effective and reliable hydrogen compressors or gasostats based on above-described engineering solution providing the pressure of hydrogen or its isotopes up to several kilobars. Such devices can find application in laboratory practice, for example testing various materials and designs on resistance to hydrogen corrosion. The other application of such compressors can be synthesis of hydrides, deuterides and tritides of a number of elements (nickel, cobalt, iron, etc.) which can be obtained only at high pressure of gaseous hydrogen (deuterium, tritium), as well as purposeful change of plastic and magnetic properties of a number of metallic materials.

References

1. Solovey, V.V., Ivanovsky, A.I., Kolosov, V.I., and Shmal'ko, Yu.F.: Series of metal hydride high pressure hydrogen compressors, *JALCOM* **231** (1995) 903-906.
2. Ivanovsky, A.I., Kolosov, V.I., Lototsky, M.V., Solovey, V.V., Shmal'ko, Yu.F., and Kennedy, L.A.: Metal hydride thermosorption compressors with improved characteristics, *Int. J. Hydrogen Energy* **21**(11/12) (1996) 1053-1055.
3. Milenko, Yu.Ya., and Karnatsevich, L.V.: Membrane high-pressure valve, *PTE (Devices and Technique of Experiment)* **5** (1996) 145-146.

FRACTURE MECHANICS IN HIGH PRESSURE HYDROGEN FOR THE THERMOMECHANICALLY TREATED STEEL X70

P. Deimel, H. Fischer, E. Sattler, M. Hoffmann
Staatliche Materialprüfungsanstalt (MPA) Universität Stuttgart, Pfaffenwaldring 32, D 70569 Stuttgart, Germany

1. Introduction

An important aspect in the transportation of gaseous energy carriers like natural gas or hydrogen in long-range pipelines is the economy. To achieve this goal not only the price for production is decisive, but also the costs for the pipeline. In consequence the transported volume per time unit should be increased by higher gas pressure and larger diameter of the pipes. The realization of these demands depends on the availability of suitable steels of high strength and toughness as well as good weldability. One class of steels having these characteristics are the thermomechanically treated steels used in modern long-range transport pipelines for natural gas [1,2]. With respect to high pressure hydrogen the operation pressure should be higher than 10 MPa for a competitive economy [3]. In this context the question whether existing modern pipelines for natural gas can be used for hydrogen transport and distribution or not is to be considered also [4- 6]. A further aspect is the interaction of high pressure hydrogen at ambient temperature with the pipe material and the measures to mitigate hydrogen embrittlement, if present, by e.g. admixtures to the hydrogen gas. A survey on hydrogen embrittlement of ferritic steels is given in [6] and on the inhibiting characteristics of special admixtures with respect to material properties in [7]. In order to clarify this situation also for thermomechanically treated steels first qualitative results on the amount of hydrogen embrittlement were received by the constant extension rate test for the steel StE 480.7 TM (X70) [8]. Thereby the inhibiting influence of oxygen admixture was investigated. A quantitative statement on the toughness behaviour in presence of high pressure hydrogen with admixtures of oxygen received by fracture mechanics J-integral tests was not available for the steel X70. Therefore it was the aim of the present investigation to close this gap also in view of materials related safety considerations.

2. Results

2.1 CHEMICAL COMPOSITION AND MECHANICAL PROPERTIES OF THE STEEL X 70

The material used for the fracture mechanics tests was the thermomechanically treated steel StE 480.7 TM (X70). The chemical composition is given in Table 1. The tensile

T. O. Saetre (ed.), Hydrogen Power: Theoretical and Engineering Solutions, 331–336.

properties for two different orientations of the tensile specimens are compared with the specification in Table 2. For the upper shelf the Charpy-V-notch impact energy for the transverse direction was 180 J.

TABLE 1. Chemical composition of the steel X70 in weight percent

StE 480.7 TM		C	Si	Mn	P	S	Al	V	Nb
Specification for ladle analysis DIN 17172/1978	min.			1,10					
	max.	0,16	0,55	1,70	0,035	0,025	[1]	≤0,12	[1]
Check analysis		0,16	0,47	1,48	0,013	<0,003	0,04	0,06	0,03

[1] Sum of Al, V and Nb ≤ 0,20

TABLE 2. Characteristic data of tensile test and Charpy impact test for the steel X70

StE 480.7 TM	Position of specimen	Yield strength $R_{t0,5}$ (MPa)	Tensile strength R_m (MPa)	Elongation at fracture A_5 (%)	Reduction of area Z (%)	Impact Energy T = 0°C C_v (J)
Min. requirements DIN 17172/1978	Transverse	480	600-750	18	-	31
Experimental values	Transverse	467	662	25	67	154
	Longitudinal	484	654	25	63	169

2.2 EXPERIMENTAL PROCEDURE AND RESULTS

The fracture mechanics behaviour was investigated by using 20 mm thick compact tension specimens CT 20 taken in C-L orientation from the original tube with an outer diameter of 1067 mm, a wall thickness of 25.4 mm and a length of 4000 mm. The 20% side grooved specimens were tested in a high-pressure hydrogen test cell integrated into a servohydraulic load unit. The testing facility and the necessary evacuation and flushing procedure are described in [9]. The tests were performed at room temperature and a pressure of 9 MPa in different gaseous environments like pure hydrogen (quality 6.0), hydrogen with admixtures of 10 vpm oxygen and 150 vpm oxygen respectively as well as in argon (quality 6.0).

The fracture mechanics test procedure was the single specimen technique with partial unloading according to ASTM E 813-89 with a crack opening displacement rate at the front face of the specimen of 0.003 mm/s. The actual J-integral and the corresponding crack advance Δa was calculated for each partial unloading. The crack resistance or J-R curve is obtained by fitting these J-Δa-points by a polynomial approximation. Comparing the resulting J-R curves for the different environments, Figure 1, shows that for the total range of crack extension the highest J-values were obtained for the test in argon and the lowest ones for the test in pure hydrogen. The J-R curves for the tests with oxygen admixture are situated between these two borderlines. The J-R curve for the fracture

mechanics behaviour in 150 vpm oxygen is oriented towards the J-R curve for inert environment, whereas the J-R curve for 10 vpm oxygen admixture lies only slightly above the J-R curve for pure hydrogen.

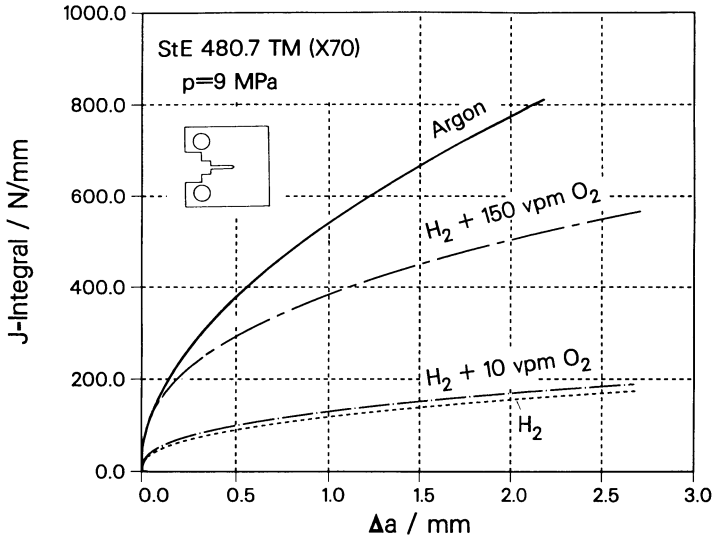

Figure 1. J-R curves derived from fracture mechanics tests in different environments

Only for the test in argon the investigation of the fracture surface by means of a scanning electron microscope (SEM) revealed a distinct continuous stretched zone with a width of 101 µm. The value $J_{i,phys}$ of the J-integral at physical crack initiation was determined from the J-R curve as the intersection point of a line drawn parallel to the ordinate axis at the abscissa $\Delta a=\Delta a_{str}$ according to the German standard DVM 002. For the specimen tested in hydrogen with 150 vpm oxygen only a few small stretched areas but no continuous stretched zone was found whereas on the fracture surface of the specimens tested in hydrogen with 10 vpm oxygen and in pure hydrogen no stretched zone existed. Because a quantification of the influence of the environment on $J_{i,phys}$ was not possible, two other characteristics were determined, the critical value J_{Ic} of the J-integral near the onset of stable crack extension according to ASTM E 813-89 and the J-integral $J_{0,2}$ at a crack extension of 0.2 mm according to DVM 002. The results of the fracture mechanics tests are given in Table 3. In all environments the $J_{0,2}$-values were smaller than the J_{Ic}-values. The highest values of J_{Ic} and $J_{0,2}$ are obtained in argon environment, the lowest ones in pure hydrogen. The admixture of 10 vpm oxygen has almost no inhibiting effect on the J_{Ic}- and $J_{0,2}$-values, whereas 150 vpm oxygen admixture causes a remarkable restoration of both values compared to argon environment.

For quantitative information on special features of the fracture surfaces scanning electron micrographs were taken from the fracture surfaces originated in argon as well as in pure hydrogen atmosphere, Figure 2, showing the transition from the fatigue precracked

TABLE 3. Results of fracture mechanics tests at a pressure of 9 MPa on the steel X70 in different environments at room temperature

Environment	ASTM E 813-89	DVM 002	
	J_{Ic} (N/mm)	$J_{0,2}$ (N/mm)	$J_{i,phys}$ (N/mm)
Argon	311	178	106
H_2 + 150 vpm O_2	281	176	-
H_2 + 10 vpm O_2	79	73	-
H_2	70	67	-

region to the region of the stable crack growth. A stretched zone has developed only in argon. The profile of the fracture surface was determined along the lines marked on the micrographs using an automatically operating image processing system connected to a SEM. The profile of the specimen tested in argon shows a pronounced blunting as transition region between the precrack and the stable crack advance, a typical indication of a stretched zone.

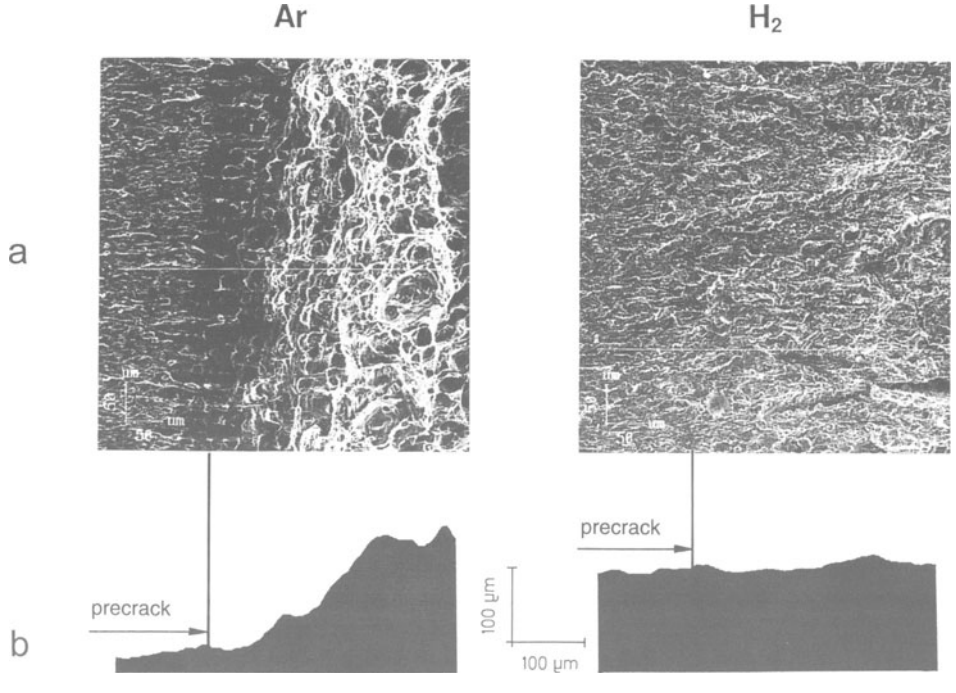

Figure 2. Influence of environment on the details of crack advance in the steel X 70 for a pressure of 9 MPa
a) Top view b) Height profile

The formation of the fracture surface in the region of the stable crack growth is also influenced by the composition of the gaseous environment, Figure 3. Dimples typical for ductile fracture behaviour, completely cover the fracture surface developed in argon whereas the fracture surface developed in pure hydrogen shows quasi-cleavage fracture without any dimples. Adding oxygen to pure hydrogen results in fracture surfaces of a mixed mode. As can be expected from the J-R curve in the case of 10 vpm oxygen the nearly quasi-cleavage fracture surface included only a few dimples, whereas in the case of 150 vpm oxygen only small quasi-cleavage regions were found in the dimpled fracture surface.

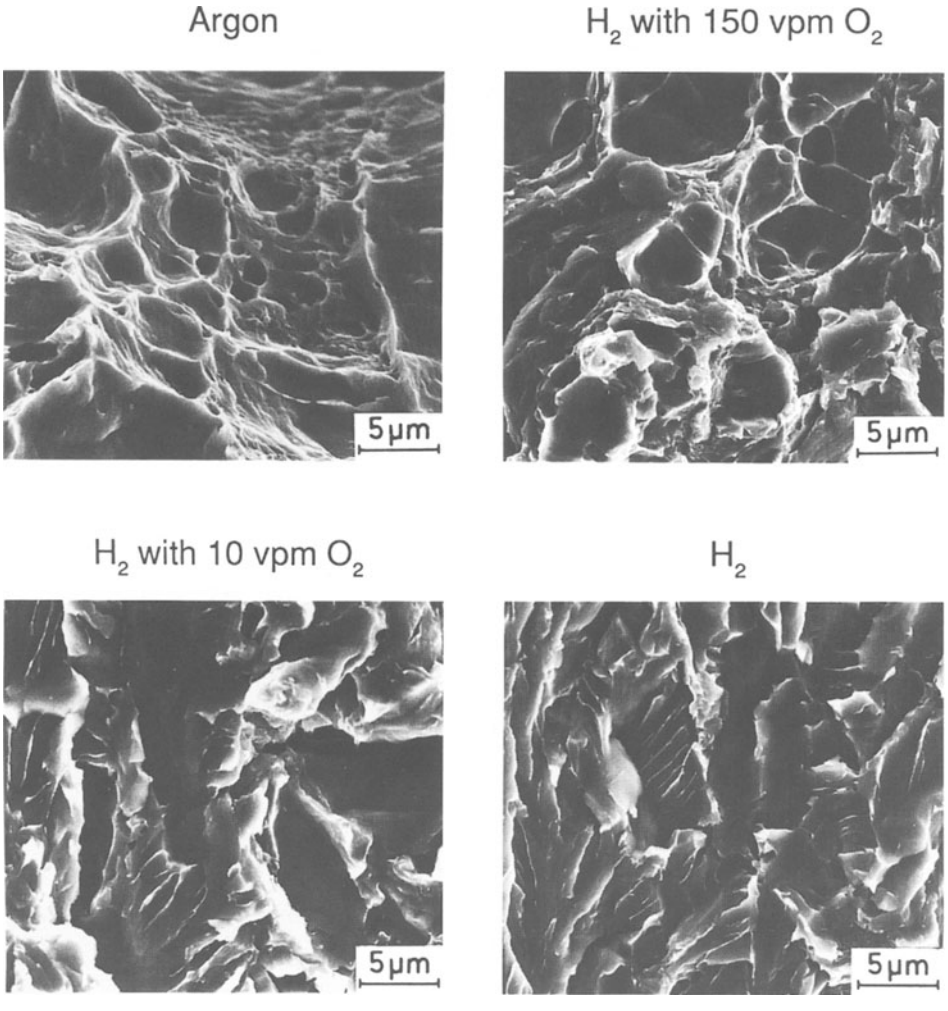

Figure 3. Microscopic fracture behaviour of the steel X 70 in different environments - micrographs of the fracture surface

3. Conclusions

The fracture mechanics behaviour of the thermomechanically treated steel X70 in a high pressure hydrogen environment is influenced by the admixture of oxygen to the hydrogen gas.

An amount of 10 vpm oxygen admixture has almost no beneficial influence, whereas 150 vpm oxygen admixture leads to a J-R curve oriented towards that received for inert environment. Since a stretched zone was not detectable in high pressure hydrogen up to 150 vpm oxygen admixture the value $J_{i,phys}$ for physical crack initiation could not be determined. To compare the materials behaviour two other standardized values, J_{Ic} and $J_{0,2}$, had to be used. They show a pronounced effect of 150 vpm oxygen, so that both values are almost comparable to those for argon environment.

The investigations were financed by the Deutsche Forschungsgemeinschaft (DFG) and realized within the Collaborative Research Center 270 "Hydrogen as an Energy Carrier" of the Universität Stuttgart.

References

1. Käding, G., Bleilebens, H., Fix, W., Wolhard, D. and Wünnenberg, K.: Innovationsprozesse in der Stahlindustrie, *Stahl und Eisen* **113**, Heft 3 (1993), 39-47.

2. Hillenbrand, H.G., Amoris, E., Niederhoff, K.A., Perdix, C. Streißelberger, A. and Zeislmair, U.: Manufacturability of linepipe in grades up to X 100 from TM processed plate, in Denys, R. (ed.), *Pipeline Technology*, Volume II, Elsevier Science B.V. (1995), 273-285.

3. Steyer, H., Diplomarbeit, DFVLR (1982).

4. Fasold, H.-G.: Wasserstoffgas - ein potentieller Energieträger des 21. Jahrhunderts ?, *gwf-gas/erdgas* **129** (1988), 281-291.

5. Deimel, P., Fischer, H. and Hoffmann, M.: EQHHPP Supplementary Task Program, WP 480 Final Report, MPA-Report 871 700, Stuttgart, September 1991.

6. Deimel, P. and Hoffmann, M.: Materialfragen beim Einsatz von Wasserstoff in gasförmiger und flüssiger Form, in Studie *"Gefährdungspotential bei einem verstärkten Wasserstoffeinsatz"* im Auftrag des Büros für Technikfolgenabschätzung des Deutschen Bundestages (TAB), DLR Stuttgart, (Februar 1992), 78-174 and literature cited therein.

7. Kussmaul, K., Deimel, P. and Sattler, E.: Einfluß von gasförmigem Wasserstoff unterschiedlicher Reinheit auf die Eigenschaften ferritischer Rohrleitungsstähle, in *Kolloquium 1994 des Sonderforschungsbereichs 270, "Wasserstoff als Energieträger"*, VDI-Verlag, Düsseldorf, (1994), 267-286.

8. Kussmaul, K., Deimel, P. and Sattler, E.: Tensile properties of the steel X70 in high pressure hydr o-gen gas with admixtures of oxygen at different strain rates, in Block, D.L. and Veziroglu, T.N. (eds.) *Proc. 10th WHEC*, June 20-24, 1994, Cocoa Beach, Vol.1 (1994), 285-294.

9. Kussmaul, K., Deimel, P., Fischer, H. and Sattler, E.: Fracture mechanical behaviour of the steel 15 MnNi 6 3 in argon and in high pressure hydrogen gas with admixture of oxygen, in Veziroglu, T.N. et al. (eds.), *Proc. 11th WHEC*, June 23-28, 1996, Stuttgart, Vol.3 (1996), 2113-2122.

NEUTRON DIFFRACTION STUDIES OF THE Ti_3Al/D SYSTEM

A.J. MAELAND, B. HAUBACK, M. SØRBY, and H. FJELLVÅG
Institutt for energiteknikk N-2007 Kjeller, Norway

1. Introduction

Complex hydrides of the light elements ($LiAlH_4$, $NaAlH_4$,Na_3AlH_6) are attractive storage materials based on their high hydrogen content. However, they have not been given serious attention as such in the past due to the apparent problem of formation from the elements and the reversible recovery of hydrogen. Bogdanovic and Schwicardi recently reported on Ti-doped alkali metal aluminum hydrides results which suggest these compounds may indeed be potential novel reversible hydrogen storage materials when combined with certain catalysts [1] as illustrated in reactions (1) and (2)

$$NaAlH_4 \text{ (Ti-doped)} <=====> 1/3Na_3AlH_6 + 2/3Al + H_2 \quad (1)$$

$$1/3\ Na_3AlH_6 <=======> NaH + 1/3Al + 1/2\ H_2 \quad (2)$$

3.7 weight percent hydrogen is available in reaction (1) and a total of 5.6 percent if the reaction proceeds through (2). The hydrogen contained in NaH is very tightly bound and is not recoverable in a practical storage material. From hydrogen dissociation measurements at 484 and 353K the two pressure plateaus corresponding to reactions (l) and (2) were extrapolated to lower temperatures by Van't Hoff plots; it was estimated that the dissociation pressure of the first plateau is 1 bar below room temperature and that of the second plateau becomes 1 bar between 373 and 423K [1]. These values put these materials in the categories of low and medium temperature reversible hydrides, respectively [2].Similar reactions may be envisioned for other alanates having even higher hydrogen contents:

$$Zr(AlH_4)_4 \text{ (catalyst)} <====> ZrH_2 + 4Al + 7H_2 \quad (6.6\%) \quad (3)$$

$$Mg(AlH_4)_2 \text{ (catalyst)} <====> MgH_2 + 2Al + 3H_2\ (7.0\%) \quad (4)$$

$$LiAlH_4 \text{ (catalyst)} <===== > LiH + Al + 3/2H_2 \quad (7.9\%) \quad (5)$$

T. O. Saetre (ed.), Hydrogen Power: Theoretical and Engineering Solutions, 337–342.

The mechanism by which the dopant or catalyst works is not known, but the suggestion has been made that a titanium aluminide (or its hydride) may be involved [1] and with this possibility in mind, we have begun a study of the titanium aluminides and their hydrides.

Four titanium aluminide phases have been identified as stable at room temperature: Ti_3Al (hex. $D0_{19}$) and TiAl (tetragonal $L1_0$) both with large compositional existance ranges,22to 39 and 48 to 69.5 atomic percent Al, respectively, $TiAl_2$ (ordered f.c.c.) with a narrow existance range from 65 to 68 percent Al, and $TiAl_3$ (f.c.c. $D0_{22}$) which is essentially a line compound [3]. Our focus in this study is the Ti_3Al phase. From hydrogen absorption isotherms and x-ray data Rudman et al [4] reported two ternary hydride phases in the Ti_3Al/H system at temperatures below 473K; a b.c.c. phase for $0.4<x<0.5$ and a f.c.c. phase for $x > 1.5$ where x refer to the hydrogen to metal ratio, (H/M).The phases were said to be metastable and transformed to TiH_2 on heating above 473K. The f.c.c phase has been observed by others, but the existance of the b.c.c. phase has been questioned [5]. The structure of a new hydride phase with $x = 0.25$, i.e. Ti_3AlH, was recently determined by neutron diffraction to be that of the cubic $E2_1$ type [6]. In this structure the aluminum atoms occupy the corners of the cube while the titanium atoms are in the face centered positions (cf. $AgCu_3$) and hydrogen is located at the center of the cube surrounded by a perfect octahedron of titanium atoms. We report here the structure of the f.c.c. phase determined by x-ray and neutron diffraction studies. Because of the much more favorable ratio of coherent to incoherent cross-section of deuterium as compared to that of hydrogen, the deuteride rather than the hydride was used in our study.

2. Experimental

Ti_3Al was prepared by a reactive sintering technique in which well mixed elemental powders of titanium and aluminum in the appropriate stochiometric ratio were heated to a temperature suffieiently high to initiate the exothermic reaction between aluminum and titanium [7]. The mixed powders were packed into 15cm long, 1.3cm diameter stainless steel cans to which a 8mm diameter tube had been welded.The filled can was carefully evacuated while heating to 875K After cooling to room temperature the tube was crimped and welded shut. The sample was then isostatically hot pressed at 1220K for one hour at a pressure of 204Mpa.The heating rate to maximum temperature was about 50K/min. After cooling to ambient temperture the steel can was removed and x-ray and neutron diffraction patterns were obtained on the sample. Deuteriding of the sample was done by first degassing at 725K, then admitting deuterium to a pressure of 9.3Mpa and cooling quickly to below 473K; this temperature was then maintained while the absorption very slowly took place. The amount of deuterium absorbed was calculated from the drop in pressure and the known volume of the system. The neutron diffraction patterns of the deuterium free sample, a solid piece,machined into a more or less cylindrical shape, 6cm long, were made with the sample in air using a neutron wavelength of 1.825 A. The deuterated sample, pulverized during the absorption process, was further ground to a fine powder under an

argon atmosphere and transferred to a 5mm vanadium cylinder and sealed. The powder pattern was recorded using a neutron wavelength of 1.5380 Å.

3. Results

X-ray diffraction patterns of filings of the as prepared Ti_3Al sample showed only the Ti_3Al phase, but a neutron diffraction pattern of the bulk sample (4 grams) showed clearly the presence of a fair amount of TiAl as well, Figure 1. The amount of TiAl

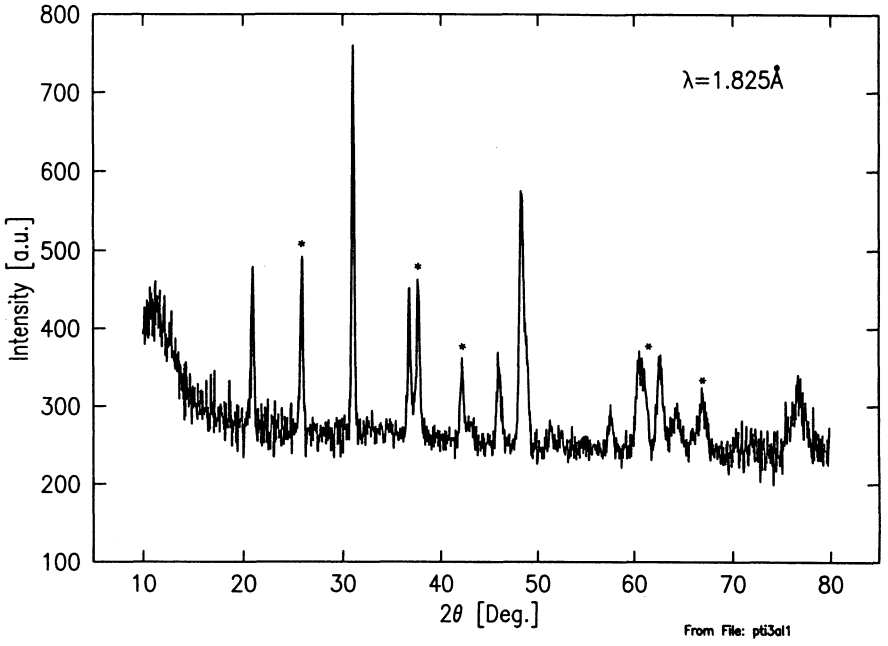

Figure 1. Neutron Diffraction Pattern of as prepared Ti_3Al. Starred reflections are due to the TiAl phase.

was reduced substantially following a three day vacuum anneal at 1200K as seen in Figure 2, and TiAl was barely discernable after an additional anneal for one week. The amount of deuterium absorbed by the sample corresponded to an H/M ratio of 1.46(i.e. $Ti_3AlH_{5.9}$). The neutron diffraction data were analyzed using the General Stucture Analysis System (GSAS) [8]. The computer program is based on the Rietveld method [9] and is capable of extracting structural information and analysis from diffraction data obtained on multiphase systems. The neutron diffraction data recorded for the deuterium free sample after the first anneal was refined and the results are summerized in Table I. The results of the refinement on the deuterated sample is also shown in Table I. Diffraction patterns generated from the refinements are compared to the experimentally obtained patterns in Figures 2 and 3.

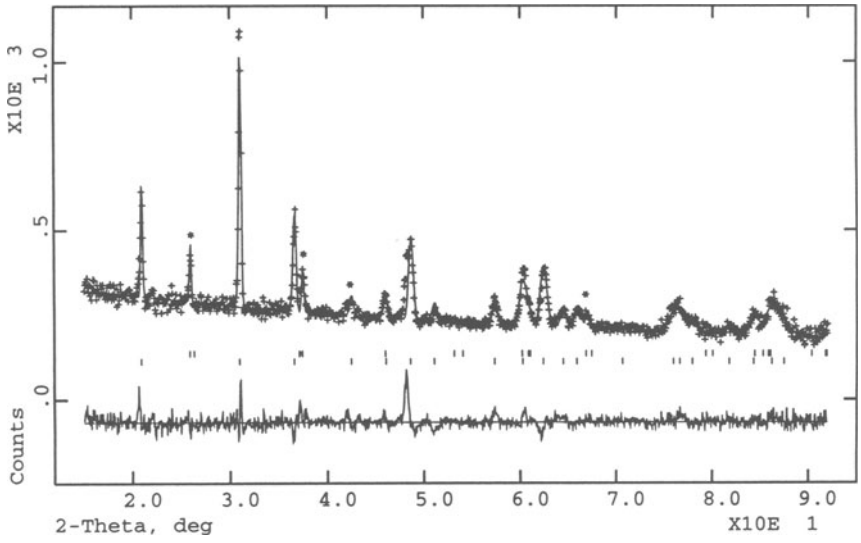

Figure 2. Calculated and Observed Neutron Diffraction Pattern of Annealed Ti_3Al Sample. Starred reflections are due to TiAl phase.

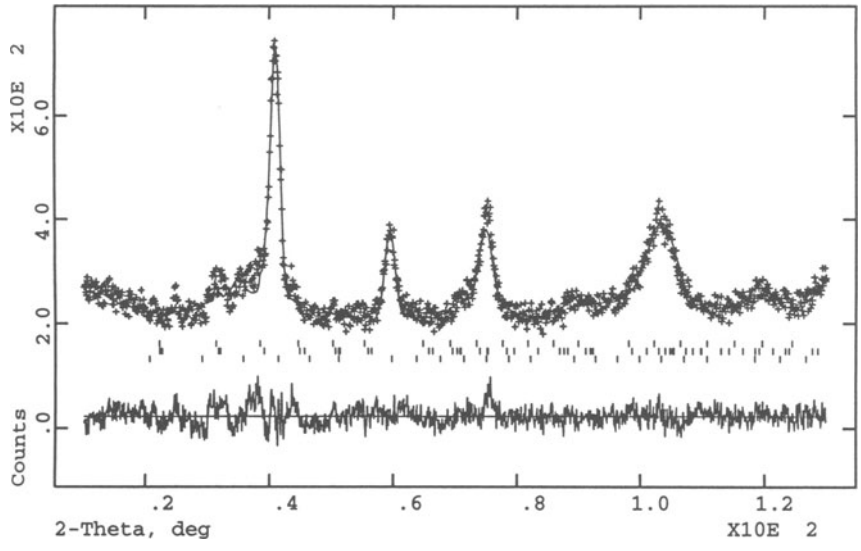

Figure 3. Observed and Calculated Neutron Diffraction Patterns of Ti_3AlD_x (Nominal Composition $Ti_3AlD_{5.9}$.

Table I. Results of Structure Analysis

Sample	Phases and structure	Cell parameters	Fract.(wt%)	R_{wp}
D free Ti_3Al(an.3da.)	Ti_3Al	a=5.8072, c=4.6582	90.7	0.0643
	TiAl	a=4.0145, c=4.0772	9.3	
$Ti_3AlD_{5.9}$	Ti_3AlD72, f.c.c	a=4.3977	86.5	0.0669
	TiAl, tetrag.	a=4.0145, c=4.0772	6.2	
	Ti_3AlD,cubic	a=4.0879	7.3	

4. Discussion

There is very good agreement between the calculated and observed patterns for the deuterium free Ti_3Al sample. The additional intensity in the observed pattern at the 100, 101, and 201 reflections may be due to preferred orientations, although the additional intensity near the 201 reflection appears to be different and may be caused by a reaction intermediary. It should be noted that the intensity of the peak near the 201 reflection decreased very much during the annealing process, cf. Figures 1 and 2. The refinement indicated that, in addition to a weight fraction of 90.7% Ti_3Al and 9.3% TiAl, the composition of the Ti_3Al phase was slightly titanium rich, i.e. Ti had sustituted for Al on some of the Al sites.The calculated Al site coccupation is 0.86 Al, 0.14 Ti. Following the second anneal, the amount of TiAl was reduced to an estimated 1-2 weight percent and the Al site occupation in Ti_3Al presumably approached the ideal value of 1 for Al and 0 for Ti.

There is also good agreement with the calculated and observed patterns for the deuterated sample as well. It is noteworthy that a small amount of the Ti_3AlD phase is present in the sample. This is probably due to loss of deuterium from the sample during handling which of course involved temporarily exposure to vaccum when going into the glove box. The major phase is of course the f.c.c. phase which we have listed as $Ti_3AlD_{7.2}$ in Table I. The ideal composition is Ti_3AlD_8 and the structure of the metal atom lattice for this phase is the same as for the Ti_3AlD phase, i.e. Al atoms on the corner of the cube with Ti atoms at the center of the faces. The deuterium atoms, however, occupy different sites in the two phases; octahedral sites in Ti_3AlD and tetrhedral sites in Ti_3AlD_8. The structure refinement, however, indicate that not all the deuterium positions in the lattice are occupied. The refinement, however, revealed an even more interesting feature, namely that titanium atoms have substituted for aluminum on aluminum sites in the lattice; in fact, we find a titanium atom in approximately 3/4 of the aluminum sites. This means of course that the phase is richer in titanium than the composition $Ti_3AlD_{7.2}$ indicates. The more accurate formulation would be $Ti_3Al_{0.25}Ti_{0.75}D_{7.2}$. If the substitution were to be carried out to completion, i.e. until all the aluminum sites were occupied by titanium, the result would be TiD_2. Our view is that the Ti_3AlD_{8-z} phase is metastable and nonstoichiometric with respect to hydrogen c«tent and will disproportionate at a rate which will depend on temperature. The disproportionation, if carried out to completion, is suggested to occur as in equation (6):

$$Ti_3AlD_{8-z} < ======= > 2TiD_2 + TiAl + [(4-z)/2]D_2 \qquad (6)$$

In the intermediary stages we would expect the precipitation of TiAl from Ti_3AlD_{8-z} leading to an enrichment in titanium and an increase in D/M as aluminum is removed from the lattice.We believe the value of the lattice parameter supports this view. The value for our sample, 4.3977Å, is less than that of TiD_2 which is 4.440Å [10], reflecting the presence of some aluminum on Ti sites in the TiD_2 lattice (atomic radius for Al is a little smaller than for Ti). The presence of Al on Ti sites in TiD_2 is of course similar to having Ti on Al sites in the Ti_3AlD_{8-z} structure.

Assuming a disproportionation reaction as in equation (6) should lead to an increase in the TiAl fraction of the sample. Under the conditions of deuterium absorption in ourstudies, the TiAl phase would not be expected to absorb appreciable amounts of deuterium. While there is some increase in the TiAl fraction when compared to the deuterium free sample (from an estimated 2% to 6.2%), the increase is far from enough to account for the expected increase based on mass balance estimates. The reason for this we believe is that TiAl formed at these low temper atures and reacti on conditions is amorphous or nanocrystalline and is therefore not easily detected in the neutron diffraction pattern. There is in fact some indications of very broad, underlying intensity in the pattern at positions which may suggest amourphous TiAl. Further studies to clarify this question is underway. Another possibility is that the disproportionation reaction leads to amorphous Al and not TiAl.

5. Conclusions

Ti_3Al reacts with hydrogen under appropriate conditions of temperature and pressure to form a hydride of composition Ti_3AlH_{8-z}. The hydride is metastable and disproportionates at relatively low temperatures (approx. 473K). The final product of the disproportionation reaction is TiH_2. At intermediate stages the disproportionation results in an enrichmnet of titanium in the phase resulting from susbtitution of titanium on aluminum sites. The hydrogen content, (H/M), simultaneously increases as hydrogen sites become energetically more favorable due to the greater attraction of titanium for hydrogen.

6. Acknowledgement

This project is supported by the Research Council of Norway and is part of a project sponsered by the International Energy Agency (IEA) Hydrogen Implementing Agreement, Task 12 - Metal Hydrides for Hydrogen Storage.

7. References

[1] Bogdanovic, B. and Schwicardi, M. (1997) Ti~oped alkali metal alurninum hydrides as potential novel reversible hydrogen storage matcrials,J. Alloys and Compounds **253 - 254,1 - 9**

[2] Buchner, H. Energiespeicherung in Metallhydriden, 1982, Springer - Verlag, Wien

[3] Murray, J. L. (1987) Al-Ti (Aluminum-Titanium) in Phase Diagrams of Binary Titan ium, 225 - 227

[4] Rudman, P. S., Reilly, J. I. and Wiswall, R: H. (1978) The forn3ation of metastable hydrides $Ti_{0.75}Al_{0.25}H_x$ with $x < 1.5$, J. Less-Common Met. **58**, 231 -240

[5] Xiao, H. Z., Robertson, 1. M.,and Bimbaum, H. K. (1996), Effects of hydrogen on the microstructure and microchemistry of Ti_3Al intermetallics, J. Mat. Res. **11**, (91 2186-2197

[6] Schwartz, D. S., Yelon, W. B., Berliner. R B., Lederich. R. J. and Sastry, S. M. L.(1991), A novel hydride phase in hydrogen charged Ti_3Al, Acta metall. mater..**39**, (11), 2799 - 2803

[7] Maeland, A. J. and Narasimhan, D (1989) Preparation of Ti_2CuAl_5 by reactive sintereing, in "High Temperature Ordered Intermetallic Alloys", Koch, C. C., Liu, C. T., Stoloff, N. S., and Taub, A. I., eds., Materials Research Society, **133**, Pittsburg, PA

[8] Larson, A. C. and Von Dreele, R. B., GSAS General Structure Analysis System, LANSCE, MS -H805 LosAlarnos National Laboratory, Los Alamos, NM 87545

[9] Rietveld, H. M., (1969) J. Appl. Cryst., **2**, 65 - 71

THE EFFECT OF IMPROVEMENT HYDROGEN-SORPTION PROPERTIES IN MULTIPHASE POLYMETALLIC COMPOSITIONS

M.V.LOTOTSKY
Institute of Mechanical Engineering Problems of National Ukrainian Academy of Sciences. 2/10 Pozharsky St., Kharkov 310046, the Ukraine

1. Introduction

Traditionally laboratory researches of the hydrogen-sorption characteristics of hydride-forming materials (individual metals and the intermetallic compounds) are carried out using the samples which are homogeneous on their composition and structure. Thus high purity metals are used, compound's stoichiometry is maintained carefully, a homogenising annealing is done, etc. As a result, the «pure» experimental data which have been not complicated by influence of various side effects is received during consequent researches of interaction of obtained compositions with hydrogen [1,2].

Proceeding to industrial-scale hydride-forming alloys the above mentioned uniformity of composition and structure, as a rule, is not observed. From economic reasons the requirement to purity of initial metals here are lower, except for rigid limitations to the contents of non-metallic components reducing hydrogen-sorption capacity. Thus the additional importation of technological additives, for example, calcium is possible [3]. Besides, the industrial hydride-forming materials are usually cast alloys which were not subjected to a homogenising annealing. As a result, alongside with basic intermetallic phase, in commercial hydride-forming materials there are additional phases which can change hydrogen-sorption properties of an alloy on a comparison with laboratory samples of appropriate intermetallides. The contents of such impurity phases in a final yield can be up to 5-10 % [3].

From an applied point of view, the non-uniformity of composition and structure of hydride-forming materials has both positive and negative aspects. The latter mainly include the deviations in a behaviour of P-C-T-diagrams of industrial alloys from «ideal» for homogeneous laboratory samples - the plateau pressure varies and its slope increases, sorption-desorption hysteresis grows, etc. [2]. On the other hand, the inhomogeneous samples are often characterized by less severe activation conditions, best hydrogen absorption kinetics and, in a number of cases, the higher hydrogen sorption capacities, than their homogeneous laboratory analogs. For a number of applications (for example, hydrogen getters [4]) this circumstance is decisive for the benefit of use just of multiphase, inhomogeneous hydride-forming compositions.

T. O. Saetre (ed.), Hydrogen Power: Theoretical and Engineering Solutions, 343–352.

In the basis of improving hydrogen-sorption properties of such compositions, probably, the effect experimentally opened at the end of 60-th - middle of 70-th lies [5-7]. This effect consists that if hydride-forming metals are saturated with hydrogen at the presence of additional phases characterized by high speeds of interaction with gaseous hydrogen, the process of hydride formation takes place in softer conditions, with the best kinetics and, as a rule, results in reaching higher hydrogenation degrees, than in case of the same metals taken as individual.

Up-to-date the rather large volume of experimental data on a manifestation of described effect in various hydride-forming alloys and compositions is accumulated. Therefore, in this work the attempt of systematization of the main literature data on this problem was undertaken with the purpose of determining a working hypothesis about the mechanism (mechanisms) of the effect and definition of possible ways of its further researches.

2. The review of experimental data for various hydride-forming materials

In this section we shall consider experimental observations of the effect of improving of hydrogen-sorption properties in multiphase hydride-forming compositions. The greatest number of activities on the given line was carried out using compositions on the base of magnesium and zirconium. Therefore, we have born the data devoted to these compositions in separate subsections (2.1 and 2.2). The subsection 2.3 is devoted to compositions based on other, less systematised by corresponding experimental data metals or intermetallides.

2.1. MAGNESIUM-BASED COMPOSITIONS

In the literature there are enough many data under the hydriding characteristics of a magnesium and compositions based thereon. The rather full review of these data as of a 1985 was made by Selvam e.a. [8]. The more late information can be found in the papers included into the book [1].

The main shortage constraining creation of hydrogen accumulators based on MgH_2 are the low speeds of interaction of pure metal with hydrogen, especially at the first hydriding. According to the data of the different authors surveyed in the work [9], time of a complete hydriding of magnesium (the first cycle) at the temperature of 613 K and pressure up to 3 MPa makes from 6 till 336 hours. Such significant divergences are probably caused by high sensitivity of reaction of magnesium with hydrogen to purity, particle size and surface state of initial metal, conditions of its activation, purity of hydrogen used, etc. The reaction can be accelerated by increase of temperature and pressure (650-720 K, 10-20 MPa) in a combination with application of gas-phase catalysts (iodine vapours, carbon tetrachloride, etc.) and milling of the solid during the process [10,11]. As to repeated hydridings of a pure magnesium, here the data of the different authors are more reproducible: at hydrogen pressure of 2-4 MPa and temperature of 550-670 K the time of 80-90% hydriding of a magnesium makes from 2 till 20 hours (the reason of discrepancies is, probably, the same, as for the first hydriding), then the reaction practically stops [12-15].

In the case of hydriding of polymetal compositions based on magnesium the dynamics of hydrogen sorption is cardinally improved. Still Reilly and Wiswall [5,6] indicated that the hydride-forming intermetallides Mg_2Cu and Mg_2Ni present alongside with a phase of a magnesium in its alloys with copper and nickel catalyse the hydriding of magnesium. The similar effect was discovered a little earlier by Mikheeva and her colleagues. [16,17]. They showed a possibility of the formation of magnesium hydride during interaction of alloys Ce-Mg and Ce-Mg-Al with gaseous hydrogen in extremely soft conditions - at room temperature and atmospheric pressure, without any preliminary activating processing. At this, the cast alloys showed the more good hydrogen-sorption characteristics (best hydriding dynamics and higher hydrogen sorption capacities), than annealed ones [16].

In the Figure 1 the most typical results illustrating change of hydrogen sorption dynamics for magnesium in polymetal compositions based thereon are presented. The appropriate characteristics of the samples, as well as their hydriding conditions are given in the Table 1.

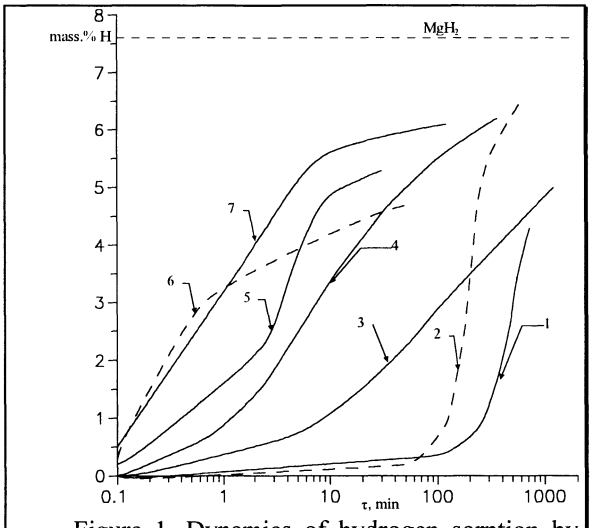

Figure 1. Dynamics of hydrogen sorption by magnesium and magnesium-based compositions

As it can be seen from the data of Fig.1, the introduction of conventional gas-phase catalysts (CCl_4) into hydrogen (the curve 2) essentially accelerates the hydriding of magnesium (curve 1), however hydrogen absorption dynamics still remains slow. The speed of hydrogen absorption is increased in some extend when the alloying components are introduced into magnesium, within the limits of formation of the diluted solid solution (curve 3). The authors [24] note that with increasing the concentration of a solid solution of an alloying element (Al, Ga, In) in magnesium the effect of improving hydrogen sorption dynamics disappears. However, in the case of highly-concentrated solid solutions containing hydride-forming components, it is exhibited again even in the more pronounced form. It is illustrated by the data [14] obtained for industrial magnesium alloy of a type MA-15 (curve 4). The alloys of this type are characterised by a mesh size of a grain (due to the presence of zirconium), besides they, depending on a mode of heat treatment, can represent either over-saturated magnesium solid solutions, or inclusions of small quantities of intermetallic phases into magnesium matrix [25].

The effect of improving hydrogen-sorption properties have much more pronounced character if one adds to magnesium the hydride-forming intermetallides characterized by high hydrogen sorption properties. It is illustrated with curve 5, which corresponds to compacted mechanical mixture of magnesium with 20 % $LaNi_5$. Here is practically observed a complete hydriding of a magnesium up to MgH_2 for 30-60 minutes [18,19].

The best hydrogen-sorption properties have magnesium alloys containing rare earth metals. They are represented by magnesium-rich intermetallides (RMg_2, R_2Mg_{17}, R_5Mg_{41}, RMg_{12} etc.) which disproportionate yield MgH_2 and RH_3 during the interaction with gaseous hydrogen (curve 6) [20,21]. In other cases these are multiphase alloys containing, apart from a phase of magnesium, intermetallic phases which, as a rule, are hydride-forming ones. Such compositions have the highest hydrogen sorption dynamics (curve 7), and hydrogen absorption takes place even at room temperature.

Table 1. Hydriding characteristics of magnesium and compositions based thereon

Curve No. (Fig.1)	Sample composition		Hydriding conditions		Notes	Ref.
	Component	Phase	T, Ê	P, MPa		
1	Mg	Mg	683	40		[14]
2	Mg	Mg	683	40	Hydrogen contained the admixture of CCl_4 (~2%)	[14]
3	$Mg_{0.99}In_{0.01}$	Mg (solid solution)	543	80	Alloy	[15]
4	Mg-94.11 Zn-4.01 La-1.24 Cd-0.52 Zr-0.12 (mass.%)	Mg (solid solution) The traces of intermetallic phases	613	30	Industrial magnesium alloy of the type MA-15	[14]
5	Mg-80 $LaNi_5$-20 (mass.%)	Mg + $LaNi_5$	618	30	Compacted mechanical mixture of Mg and $LaNi_5$ powders	[18, 19]
6	RMg_{12} (R-La,Ce)	RMg_{12} (initial and after dehydriding in vacuum at T>700 K); Mg+RH_2	598	30	Alloy; phase composition of hydriding products is MgH_2+RH_3	[20, 21]
7	$Mg_{75}Y_6Ni_{19}$	Mg+Mg_2Ni+YNi_2	473	30	Alloy; phase composition of hydriding products is MgH_2+Mg_2NiH_4+YH_2	[22, 23]

The main explanations of the mechanism of improving hydriding characteristics of magnesium-based compositions are reduced to surface deoxidation at the boundaries of magnesium grains with catalysing hydride phase [26], facilitation of internal diffusion of hydrogen due to increasing the concentration of lattice defects in the solid phases [24], or its external diffusion via microcracks and grains boundaries [9]. In some works it is also mentioned about the role of hydrogen state in course of improving magnesium hydrogen-sorption properties by the metal components. So, the availability of a hydride-forming intermetallide in the system Mg-Mg_2Cu [26] results that to the Mg-Mg_2Cu interface from the side of Mg_2Cu monatomic hydrogen is continuously supplied. The latter can also be formed during dissociative adsorption of hydrogen molecules on clusters of transition metals - this makes it's possible to explain the acceleration of hydriding in mixtures Mg + $LaNi_5$ [18,19] and in «mechanical alloys» of magnesium with various metals [27]. The fine illustration of this mechanism is described in [10] where the synthesis of magnesium hydride from a shaving of pure metal and active hydrogen which was obtained immediately during the synthesis by interaction of zinc with hydrochloric acid. The hydriding of magnesium in this case takes place at room temperature and atmospheric pressure.

2.2. ZIRCONIUM-BASED COMPOSITIONS

The reaction of gaseous hydrogen with a zirconium with formation of ZrH_2 takes place in severe conditions: pressure till 7-10 MPa and temperature of the order 500 K. Reaction duration thus makes some hours [28, 29]. At the same time, the hydriding of majority of zirconium intermetallides, as a rule, takes place already at room temperature and hydrogen pressure of the order 0.1 MPa. Thus the hydriding speed is extremely high - in the case of ZrV_2 it is 2-3 order of magnitude higher than for individual zirconium at 500-600 K [29].

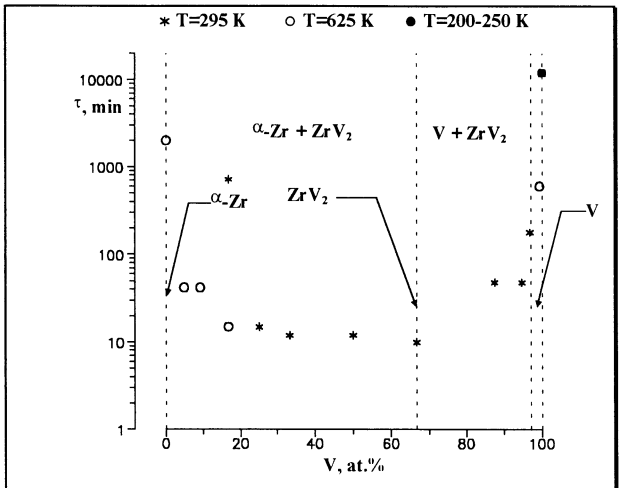

Figure 2. Hydriding characteristics of Zr-V alloys [10, 31]

In zirconium-based alloys and compositions where hydride-forming intermetallides are formed the hydriding proceeds practically in the same (or little bit more rigid) conditions, as in case of appropriate intermetallic compounds. Thus, apart from hydriding of an intermetallide, it is observed practically complete hydriding of a zirconium with ZrH_2 formation. So, according to data [30] the compacted mechanical mixture of zirconium with 20 % of ZrV_2 absorbs hydrogen with quantitative formation of ZrH_2 at P = 1 MPa and room temperature for 2 hours, and at the same pressure and T = 523 K only for 15 minutes.

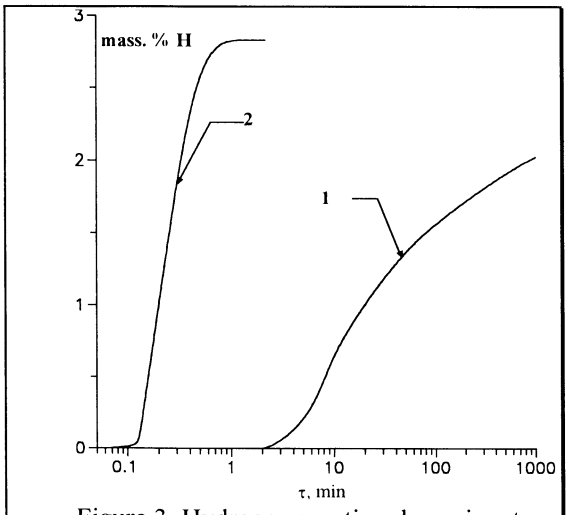

Figure 3. Hydrogen sorption dynamics at P=0.05 MPa by the samples of alloys $Zr_{55}V_{40}Fe_5$ (1) and $Zr_{55}V_{40}Fe_5$ + 3% B_2O_3 (2)

The Figure 2 illustrates a behaviour of Zr-V alloys during their hydriding. The ordinate axis represents the time of complete hydriding of an alloy at P = 3-4 MPa. It can be seen in Fig.2 that the alloys of the composition α-Zr + ZrV_2 have still best hydrogen sorption dynamics [29] than appropriate mixtures [30]. The similar effect of improving the hydrogen-sorption properties is exhibited in alloys of a system Zr-V-Fe (α-Zr + $Zr(V,Fe)_2$) [31, 32].

At modifying of alloys Zr-V and Zr-V-Fe by the oxide components they, apart from α-Zr and

Laves phase $Zr(V,Fe)_2$, include oxygen-containing hydride-forming intermetallide η-$Zr_3(V,Fe)_3O$. Such modified alloys have the higher hydrogen-sorption characteristics (Fig. 3) intensively absorbing hydrogen at room temperature and pressure lower than atmospheric one [32,33]. The similar behaviour is exhibited by oxygen-modified alloys Zr-Fe having the phase composition of α-Zr + Zr_2Fe + η-Zr_2Fe_4O [34, 35].

The improvement of hydrogen-sorption properties in zirconium-based multiphase compositions can be explained by a number of factors, first of all:

- Hydrogen activation during its sorption-desorption by hydride-forming intermetallic phases [32, 36].
- Change of surface state for difficult to hydriding phase α-Zr - either its deoxidation or, in the case of oxygen-containing alloys, formation of oxygen-containing intermetallic layers permeable for hydrogen [32].
- The availability of a developed grid of microcracks providing the intensive hydrogen entry into the bulk of an alloy [35].

2.3.THE OTHER COMPOSITIONS

The effect being considered in this work, apart from compositions based on Mg and Zr, is peculiar to a lot of similar compositions in which the individual metal or intermetallic compound acts as a «difficult to hydriding» component.

The adding of hydride-forming intermetallides to vanadium or niobium [7,29,30,37,38] allows to obtain VH_2 or NbH_2 at room temperature and hydrogen pressure of several MPa during less than 1 hour. The relation of time of a hydriding to vanadium contents in alloys V+ZrV_2 is shown in Figure 2. At the same time the dihydrides of pure vanadium and niobium can be synthesized only at reduced (200-270 K) temperatures, the time of a hydriding thus makes about 10 days [7,10,29]. It is marked in [37] that with increase of vanadium purity the speed of its hydriding is essentially decelerated.

In a number of works devoted to interaction of titanium-based alloys and compositions with gaseous hydrogen was shown that the presence of hydride-forming intermetallides essentially increases hydriding speed and depth. Examples are the alloys of a system Ti-V-Ni in the region of phase compositions β-Ti+Ti_2Ni [39,40], Ti-V-Fe (β-Ti + λ_1-$Ti(V,Fe)_2$) [41], mechanical mixtures of alloys Ti-V-M (where M - Cr, Mn, Fe, Co, Ni, Cu and Al) with $LaNi_5$ [42], etc. In [40] the original and rather probable explanation of acceleration of a hydriding in alloys β-Ti+Ti_2Ni is given: the increase of Ti_2Ni volume during hydrogen absorption results in mechanical destruction of a sample and increases the total reaction surface.

In some works [30] it is mentioned about catalytic activity of hydride-forming intermetallic compounds in the processes of obtaining ScH_2 and YH_3 from individual R.E.M. and gaseous hydrogen.

The effect of improving hydrogen-sorption properties is exhibited also for some hydride-forming intermetallides. As a rule, it is observed on mechanical mixtures of intermetallic compounds one of which is a highly effective reversible hydrogen absorbent. Examples of such compositions are TiFe+$LaNi_5$ [43, 44], $Ti_{0.8}Zr_{0.2}Cr_{0.8}Mn_{1.2}$+ $LaNi_5$ [45], etc. In such mixtures the «difficult to hydriding» component is characterised by high speeds of hydrogen sorption - desorption even during the first hydriding cycle, at less hard preliminary activation conditions.

In a number of cases the hydride-forming intermetallides as component parts of multiphase alloys containing other intermetallic hydride-forming phases which are characterized by highly effective hydride formation, show much higher degrees of a hydriding, than observed in single-phase samples. So, for η-phases in alloys α-Zr+ZrV_2+η-Zr_3V_3O and α-Zr+Zr_2Fe+$ZrFe_2$+η-Zr_2Fe_4O the degree of hydriding determined proceeding from known concentration relations of hydrides lattice periods, was more than twice above achieved at a hydriding single-phase η-Zr_3V_3O and η-Zr_2Fe_4O [32-35].

3. Discussion and Conclusions

3.1. MECHANISMS OF THE EFFECT

The results presented in Section 2 give the basis to assert that the effect of improving hydrogen-sorption properties in multiphase hydride-forming compositions has universal character and it is peculiar to various compositions which essentially differ on a chemical nature of a basic hydride-forming component (Mg, Zr, Ti, V, Nb, rare earth metals, etc.).

The analysis of the adduced data allows to allocate some possible mechanisms which can underlie the effect being considered.

3.1.1. Hydrogen activation in gas phase

In a series of works [26,29, etc.] a catalytic effect of hydride-forming intermetallides on hydrogenation of difficult to hydriding metals is explained by appearance of monatomic hydrogen formed either as a result of the H_2 molecules dissociation on active metal clusters, or during hydrogen output from the bulk of intermetallic hydride. The elementary stage of hydrogen dissociative chemisorption is thereby bypassed. This stage is often limiting one in the total hydriding process [9].

In our opinion, it is necessary to treat little bit wider this mechanism, as appearance in a near-surface layer of a gas phase of hydrogen particles in thermodynamically non-equilibrium state. Apart from H atoms, it there can be hydrogen atomic or molecular ions, as well as exited atoms and molecules. The appearance of such particles is a result of hydrogen sorptive activation [36,46]. It can explain practically all cases of improving the hydrogen-sorption characteristics in multiphase polymetal compositions. In this respect large interest is represented by cross correlation between improving hydrogen-sorption properties of zirconium multiphase alloys and «degree» of hydrogen activation by them [32].

3.1.2. Surface effects

The improving hydrogen-sorption properties can also occur in consequence of change of surface state of difficult to hydriding phase. If this phase is characterized by the formation of protective oxide layers, then the surface deoxidation, or other effects causing to destruction of such layers can take place in multiphase alloys [8,26,32]. Besides, in a number of cases the transformation of a surface oxide to hydrogen-permeable oxygen-containing intermetallic phase [32] is possible.

This mechanism has more particular character, being exhibited only in alloys under phase boundaries. At the same time, for components forming on air strong surface oxide layers (first of all it concerns to magnesium), its contribution can be determining.

3.1.3. Microstructure factors

It is necessary to relate to the microstructure factors promoting the hydriding of multiphase alloys the availability (or appearance during hydriding) of microcracks in the bulk of an alloy, as well as increasing the concentration of lattice defects. It facilitates hydrogen supply into hydride-forming material that, in turn, results in acceleration of nucleation and growth of hydride phases grains, especially when the rate-limiting factor becomes internal diffusion of hydrogen [8,9,24,35,40]. This mechanism can take place only when the hydride-forming material is either the cast alloy, or polymetal composition obtained by a sintering. At the same time, probably just it is responsible for differences in the hydriding characteristics of cast and annealed samples.

3.2. THE PERSPECTIVES OF FURTHER INVESTIGATIONS

Despite of an abundance of a published experimental material on study of the effect of improving hydrogen-sorption properties in multiphase polymetallic compositions, the data about its nature in many respects remain not clear. The attempts of explanation of the effect considered in the previous subsection, as a rule, affect particular cases and do not give convincing explanation of the mechanism of the effect as a whole. The exception represents the mechanism 3.1.1 (hydrogen sorptive activation) which under our opinion is exhibited in all hydride-forming compositions, including mechanical mixtures of various metals and intermetallides. However, its contribution into total effect can be rather different in various compositions, and even the attempt of its rough estimation can become a subject for further, already systematic, researches. As a first step in this direction it is possible to recommend comparative study of phase-structural and hydrogen-sorption properties for multiphase polymetallic compositions in the following series: the multiphase alloy → the mixtures of phases composing an alloy, → the same mixtures with inert filler → individual phases. In addition, it would be also interesting to carry out parallel measurements of energy-state characteristics of hydrogen during its reversible interaction with samples of these compositions. The appropriate express-testing technique based on measurement of the electrotransfer characteristics in a gas phase of «hydride-forming material - hydrogen» systems, is developed in our laboratory [32,36,46].

On the basis of results obtained it can be essentially extended the existing conception about a nature of considered effect, and the general principles of development of highly effective hydrogen absorbents for various metal-hydride technological systems can be determined - beginning from hydrogen accumulators and finishing hydrogen getters and metal-hydride systems for increasing the efficiency of the physical-energy installations

References

1. *Hydrogen in Intermetallic Compounds (in 2 volumes)*, Ed. by L.Schlapbach, Springer-Verlag, 1992.
2. Percheron-Guegan, A. and Welter, J.-M.: *Preparation of intermetallics and hydrides,* In [1] (vol.1), pp.11-48.
3. Shmal'ko, Yu.F., Lototsky, M.V., e.a.: The new production technology, structure and hydrogen-sorption properties of hydride-forming alloys based on systems mischmetal-nickel and zirconium- titanium-manganese, In: *Noble and Rare Metals. Proc. Int. Conf. «BRM-94»,, 19-22 Sept., 1994, Donetsk, Ukraine,* vol.3, pp.95-96 (in Russian).
4. Yartys', V.A., Zavaliy, I.Yu., and Lototsky, M.V.: Material science aspects of new high-effective hydrogen getters creation, In: *Second All-Union School on Non-Sputtering Getters (Researches and Technology). 4-7 March, 1991,* Ed by Yu.M.Pustovoit, I.V.Kurchatov Nuclear Energy Institute, Moscow, pp.28-31 (in Russian).
5. Reilly, J.J., and Wiswall, R.H.: Reaction of hydrogen with alloys of magnesium and copper.- *Inorg. Chem,* **6**(12) (1967), 2220-2223.
6. Reilly, J.J., and Wiswall, R.H.: The reaction of hydrogen with alloys of magnesium and nickel and the formation of Mg_2Ni, *Ibid.* **7**(11) (1968), 2254-2256.
7. Carstens, D.H.W., and Farr, G.R.: The formation of niobium dihydride from niobium catalysed by $LaNi_5$, *J. Inorg. Nucl. Chem.* **36**(2) (1974), 461.
8. Selvam, P., e.a.: Magnesium and magnesium alloy hydrides, *Int. J. Hydrogen Energy* **11**(3) (1986) 169-192.
9. Gerard, N., and Ono, S.: Hydride formation and decomposition kinetics, In [1] (vol.2), pp.165-195.
10. Antonova, M.M. and Morozova, R.A.: *Preparation Chemistry of Hydrides. A Manual*, «Naukova Dumka» Publ., Kiev, 1976 (in Russian).
11. Dymova, T.N., e.a.: Synthesis of magnesium hydride from inactivated metal, *Russ. J. Inorg. Chem.* **6**(1963), 763-767 (in Russian).
12. Stander, C.M.: Kinetics of formation of magnesium hydride from magnesium and hydrogen, *Z. Phys. Chem.* **104**(1977), 229-238.
13. Vigeholm, B., e.a.: Hydrogen sorption performance of pure magnesium during continued cycling, *Int. J. Hydrogen Energy* **8**(10) (1983), 809-817.
14. Burnasheva, V.V., Verbetsky, V.N., Lototsky, M.V., and Semenenko, K.N.: Interaction of magnesium-based alloys with hydrogen, *Protection of air pool against contamination by transport toxic exhausts. Kharkov, 20-22 Oct., 1981. Collected Abstracts,* Published by Institute for Problems in Machinery of NAS Ukraine, Kharkov, 1981, pp.142-143 (in Russian)
15. Mintz, M.H., Gavra, Z., and Hadari, Z.: Kinetic study of the reaction between hydrogen and magnesium, catalysed by addition of indium, *J. Inorg. Nucl. Chem.* **40**(1978) 765-768.
16. Mikheeva, V.I., e.a.: Hydrogen absorption by cerium alloys with magnesium. *Russ. J. Inorg. Chem.* **8**(6) (1963) 1314-1319 (in Russian).
17. Mikheeva, V.I., e.a.: Hydriding of cerium alloys with magnesium and aluminium, *Ibid.* **8**(7) 1715-1721(in Russian).
18. *Patent No. 2324980 (France)*, 1977
19. Song, M.Y., and Lee, J.Y.: A study of the hydriding kinetics of Mg - (10-20 w/o) $LaNi_5$, *Int. J. Hydrogen Energy* **8**(5) (1983) 363-367.
20. Darriet, B., e.a.: Les alliages terre rare - magnesium riches en magnesium et leur application au stockage de l'hydrogene, *Mat. Res. Bull.* **14**(1979) 377-385.
21. Semenenko, K.N., e.a.: Interaction with hydrogen of intermetallic compounds containing a magnesium, *Bull. Moscow Univ., Series 2, Chemistry* **24**(1) (1983) 16-27 (in Russian).
22. Klyamkin, S.N., and Kuliev, S.I.: Interaction of magnesium alloys with hydrogen, The deposited manuscript, VINITI, No. 7085-83 Dep., 1983 (in Russian).
23. Kuliev, S.I.: Interaction of magnesium alloys and composite materials based thereon with hydrogen, Ph.D. Thesis Abstract, Publ. By Moscow State Univ. (Chemical Faculty), 1989 (in Russian).
24. Mintz, M.H., Malkiely, S., Gavra, Z., and Hadari, Z.: Effect of group IIIa metal additives on the kinetics of magnesium hydride formation, *J. Inorg. Nucl. Chem.* **40**(1978) 1949-1951.
25. Rokhlin, L.L.: *Magnesium alloys containing rare earth metals*, «Nauka» Publ., Moscow, 1980 (in Russian).

26. Genossar, J., and Rudman, P.S.: The catalytic role of Mg_2Cu in the hydriding and dehydriding of Mg, *Hydrogen in Metals. Int. Meet. Mem. Carl Wagner. Münster, 1979, Prepr. Pap. and Program.* Vol.2, pp.624-634.
27. Ivanov, Ye.Yu., e.a.: Mechanical alloys of a magnesium - new materials for a hydrogen power engineering, *Reports of USSR Academy of Sciences* **286**(2) (1986) 385-388 (in Russian).
28. Kost, M.Ye., and Mikheeva, V.I.: Hydrides of transition metals, *Russ. J. Inorg. Chem.* **22**(11) (1977) 2910-2924 (in Russian).
29. Burnasheva, V.V., e.a.: Hydriding of zirconium alloys with vanadium, *Bull. of USSR Academy of Sciences, Inorganic Materials* **20**(5) (1984) 799-803 (in Russian).
30. *Author's Certificate No.958317 (USSR)*, 1982.
31. Yartys', V.A., Zavaliy, I.Yu., Lototsky, M.V., e.a.: Alloys based on Zr-V-Fe as effective hydrogen absorbents, *Physical-Chemical Mechanics of Materials* **27**(2) (1991) 26-36 (in Ukrainian).
32. Lototsky, M.V.: Hydride-forming alloys of a zirconium and their use as getters and sources of hydrogen, Ph.D. Thesis, L'vov State Univ., Chemical Faculty, 1992 (in Russian).
33. Yartys', V.A., Zavaliy, I.Yu., Lototsky, M.V., e.a.: Oxygen-, boron- and nitrogen-containing zirconium-vanadium alloys as hydrogen getters with enhanced properties, *Z. Phys. Chem.* **183**(1994) 485-489.
34. Zavaliy, I.Yu., Lototsky, M.V., e.a.: Oxide-modified Zr-Fe alloys: thermodynamic calculations, X-ray analysis and hydrogen absorption properties, *JALCOM* **219**(1995) 38-40.
35. Riabov, A.B.: Hydrogen-sorption oxygen-containing zirconium-based alloys and phase-structural transformations induced by hydrogen, Ph.D. Thesis (in press), L'vov State Univ., Chemical Faculty, 1997 (in Ukrainian).
36. Shmal'ko, Yu.F., Lototsky, M.V., e.a.: The formation of excited H species using metal hydrides, *JALCOM* 231(1995) 856-859.
37. Semenenko, K.N., e.a.: The influence of $LaNi_5$ on sorption characteristics of vanadium, *Bull. Moscow Univ., Series 2, Chemistry* **25**(3) (1984) 320-321 (in Russian).
38. *Author's Certificate No. 1063775 (USSR)*, 1983.
39. Verbetsky, V.N., and Zontov, V.S.: Hydrogen interaction with alloys of titanium-vanadium-nickel system, *Russ. J. Inorg. Chem.* **30**(3) (1985) 589-592 (in Russian).
40. Zontov, V.S.: Hydrogen interaction with alloys of Ti-V-M systems, where M - Al, Ni, Co, Ph.D. Thesis Abstract, Publ. By Moscow State Univ. (Chemical Faculty), 1985 (in Russian).
41. *Author's Certificate No. 849706 (USSR)*, 1980.
42. Mitrokhin, S.V.: Interaction of alloys and intermetallic compounds of titanium and zirconium with hydrogen, Ph.D. Thesis Abstract, Publ. By Moscow State Univ. (Chemical Faculty), 1985 (in Russian).
43. *Patent Application No. 53-90183 (Japan)*, 1978.
44. Semenenko, K.N., Verbetsky, V.N., e.a.: Hydrogen absorption in TiFe-$LaNi_5$-H_2 system, *Bull. Moscow Univ., Series 2, Chemistry* **22**(5) (1981) 513-515 (in Russian).
45. Suda, S., and Uchida, M.: Mixing effects of different types of hydrides, *Hydrogen Energy Syst. Proc. 2-nd World Hydrogen Conf. Zürich, 1978*, Oxford e.a., 1979, vol.3, pp.1561-1573.
46. Shmal'ko, Yu.F.: Effect of hydrogen thermo-sorptive activation by metal hydrides: main lines of investigations and perspectives, HYPOTHESIS II, Rep. No. 426

COMPARATIVE STUDY OF SURFACE STATE AND ELECTROCHEMICAL PROPERTIES OF TiFe HYDROGEN STORAGE ALLOY AS WELL AS $TiFe_2$ ALLOY BY XPS AND POLARIZATION CURVES METHODS

V.A.LAVRENKO, V.Z.MORDKOVICH, V.A.SHVETS, and T.V.KHOMKO
Institute for Problems of Materials Science
3 Krzhyzhanovsky str., Kiev, 252142 Ukraine

1. Introduction

In this work the surface state and parameters of chemical bond were determined by XPS method for two intermetallic compounds of Ti - Fe system - TiFe and $TiFe_2$. As it is known, TiFe has a cubic structure of CsCl type and as a result of hydrogen absorption forms γ-$TiFeH_2$ hydride with monoclinic lattice while $TiFe_2$ has a hexagonal structure and does not form a hydride phase at its interaction with hydrogen [1].

2. Results and discussion

The corresponding XPS spectra [2] were obtained for TiFe and $TiFe_2$ powders, deposited on a gold holder with the aid of carbon adhesive coating at vacuum of 1.10^{-8} mm Hg using device of Shimazu Japanese firm with MgK_α radiation for the sounding depth of 10-40 A° before and after removal of thin surface layer (~ 0.01 μm) by the bombardment with Ar^+-ions. As a standard the gold lines are used. The atomic ratios of elements on the surfaces were calculated from the values of area under corresponding characteristic electron binding energy peaks of elements, also taking into account their chemical displacements in XPS spectra as to standard and peaks shape.

First of all, the results obtained for specimens after Ar^+ treatment testify to a strong enough metallic binding in both compounds, largely for the account of generalization of titanium atoms electrons. Besides, these results give the reference data concerning E_b values for

T. O. Saetre (ed.), Hydrogen Power: Theoretical and Engineering Solutions, 353–358.

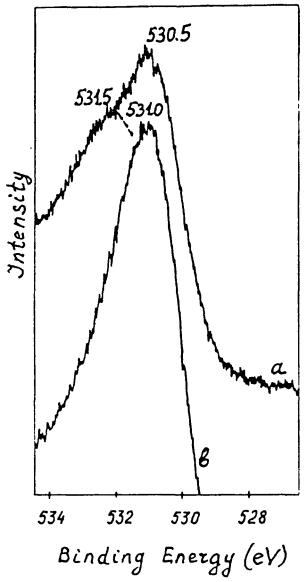

Figure 1. XPS O(1s) profiles for TiFe: a - after 50 h treatment in vacuum at 1200°C, b - after Ar^+-ions bombardment during 50 h at 1200° C.

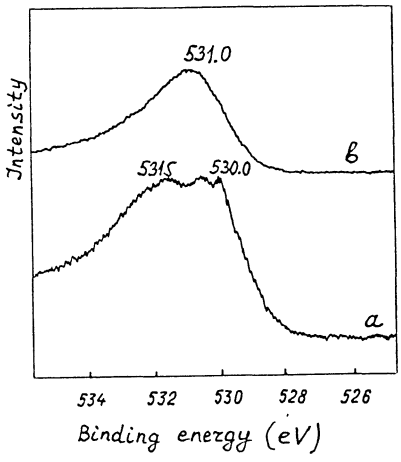

Figure 2. XPS O(1s) profiles for $TiFe_2$: a - after 50 h treatment in vacuum at 1200°C, b - after Ar^+-ions bombardment during 50 h at 1200°C..

$2p_{3/2}$ binding electron levels of Ti and Fe atoms in both intermetallic compounds as well. It was established that the initial outer layer (before Ar^+ treatment) for TiFe specimen is enriched by iron up to composition appropriate to relation Ti : Fe = 1 : 2. However, it also contains 8 % of free Ti atoms. Herein the oxygen is present in this layer in chemisorpted state (two peaks: the main, sharp E_b = 530.5 eV and washed out E_b =531.5 ones, Fig.1).

Unlike TiFe, the analysis of XPS spectra for the outer layer of $TiFe_2$ specimen showed that the free Ti atoms are absent, and here the surface is enriched with iron in a significantly more extent: Fe content exceeds Ti one already by 17.5 times. The binding energy peak for 1s-electron of oxygen in this case (Fig.2) corresponds to a wide enough range of 530 - 532 eV. Probably, it is a combination of three different states of oxygen on the initial surface of $TiFe_2$ specimen: 1/ O_2, more weak-binded (it corresponds to an energy level of spectrum stripe of 531.5 - 532 eV), 2/ chemisorpted O_2 (530.5 eV), and 3/ chemically binded oxygen (530 eV), the last one, maybe, as a result of long enough preliminary contact of Fe atoms of $TiFe_2$ specimen outer layer with an air. Namely it could lead to formation of FeO(OH) surface monolayer and give a XPS signal corresponding to chemically binded oxygen [2]. It must be noted that in both Fig.1 and 2 the XPS O(1s) profile after argon ions bombardment has more symmetrical E_b =531 eV peak which corresponds only to solid solution of O_2 into the lattices of intermetallic compounds.

Electrochemical polarization investigation carried out using P-5848 Soviet apparatus in the potentiodynamic regime (the second electrode was Pt) in 30 % KOH solution at 25°C showed that despite a nearness of stationary potentials of both TiFe and $TiFe_2$ electrodes (-0.65 and -0.66 V, correspondingly), their cathodic behaviour was significantly different, especially for the reverse motion of cathodic polarization curves (Fig.3). All the potentials were given in the relation to a chlorine-silver electrode. At first, at the potential region from -0.65 to -1.2 V the electroreduction of chemisorpted oxygen takes place on the surface of both electrodes:

$$O_{2ads} + 4e^- + 2H_2O = 4\ OH^- \qquad (1)$$

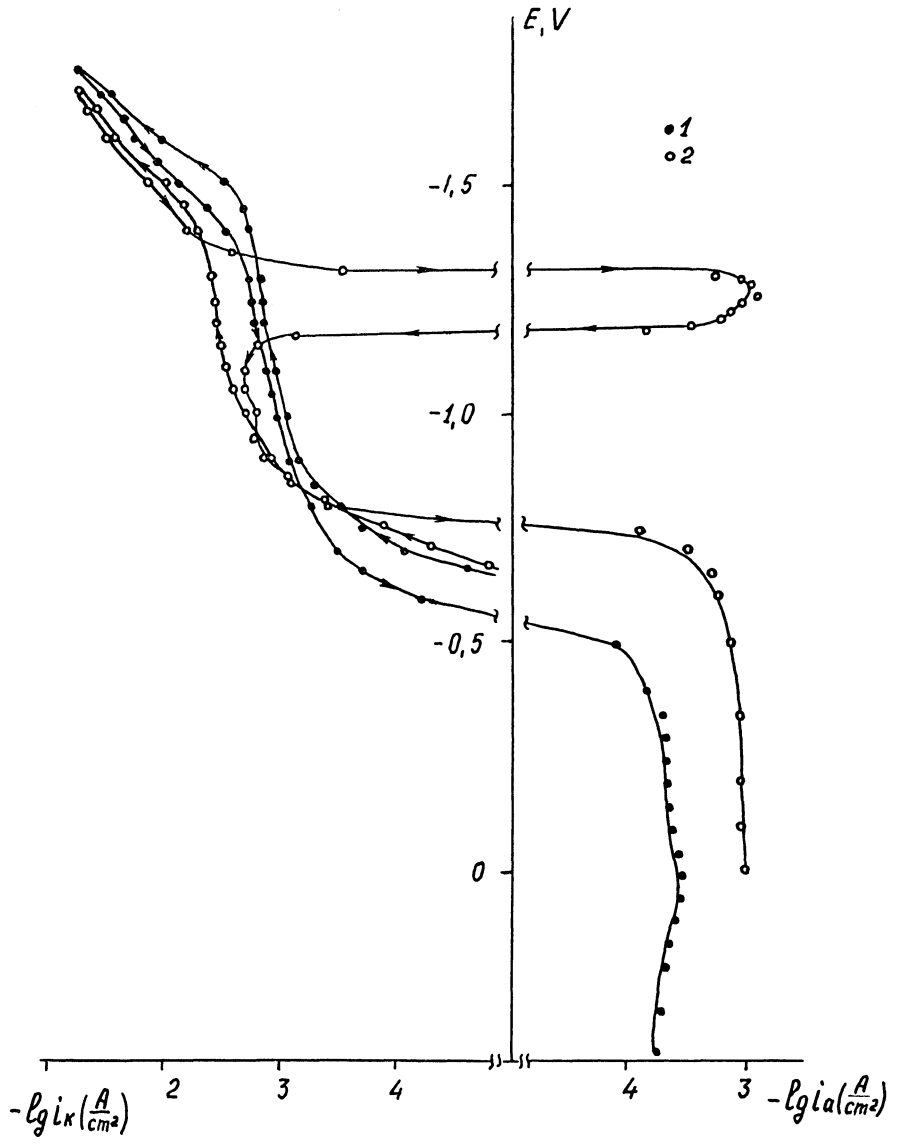

Figure 3. Cathodic and anodic polarization curves for TiFe (1) and $TiFe_2$ (2) electrodes in 30 % KOH.

Then the limiting currents for this process are achived and, beginning from -1.4...-1.45 V, the hydrogen evolution is observed, according to the summary reaction

$$2H_2O + 2e^- = H_2 + 2\,OH^- \qquad (2)$$

For the TiFe specimen the reverse motion of cathodic curve does not coincide with the straight one. Obviously, the corresponding hysteresis (its maximum value is 0.12 V) is conditioned by change of electrode surface composition, the reaction (2) being realized through two stages.

The first one leads to atomic hydrogen formation:

$$H_2O + e^- = H + OH^- \qquad (3)$$

and then there are two ways for hydrogen atoms expenditure:

$$H_{ads} + H_{ads} = H_2 \qquad (4)$$

and

$$TiFe_{surf} + H = TiFeH_{surf} \qquad (5)$$

The latter leads to β -TiFeH formation when the hydrogen atoms fill in the octahedral interstitial positions in a TiFe structure, evoking a rhombic distortion of its cubic lattice. In the case of $TiFe_2$ electrode the reverse motion of cathodic curve on the section of water electroreduction, in accordance with reaction (2), coincides with the straight one. But then, at -1.35 V, the electrode surface is suddenly recharged (Fig.3), and in the potentials region down to -1.15 V, apparently, the primary provisional surface passivation occurs:

$$2\,Fe_{surf} + O_{2dissolved} + 2H_2O = 2\,FeO(OH)_{surf} + 2H^+ + 2e^- \qquad (6)$$

It becomes possible because the $TiFe_2H$ cannot form, and up to this moment the released H atoms cleans out the $TiFe_2$ electrode surface from the adsorpted oxygen according to chemical reaction:

$$4\,H + O_{2ads} = 2H_2O \qquad (7)$$

However, at the potentials from -1.1 to -0.8 V the cathodic reaction (1) takes place again because the O_2 molecules are capable to adsorpt on $TiFe_2$ surface, covered up by FeO(OH) surface complexes, as well.

The transition to anodic sections of polarization curves occurs at the potentials of -0.56 and -0.75 V for TiFe and $TiFe_2$ electrodes, respectively. In both cases at potentials up to + 0.4 V the only reaction takes place:

$$4\,OH^- = O_2 + 2H_2O + 4e^- \qquad (8)$$

The limiting currents of this reaction are observed in the region of - 0.3...+0.3 V for the TiFe specimen and -0.55...+0.1 V for $TiFe_2$ nonhydrided electrode, correspondingly.

3. Conclusion

The peculiarities of electrochemical behaviour of TiFe and $TiFe_2$ electrodes at their polarization in an alkali solution confirm the results of XPS investigation of surface state of these intermetallic compounds. The different electrochemical properties of alloys above are, mainly, explaned by very large content of Fe in the surface layer of $TiFe_2$ and different character of oxygen adsorption on the initial specimens.

4.References

1. Kolachev B.A., Shalin R.E., Ilyin A.A.: Hydrogen storage alloys, Metallurgy ed., Moscow, 1995 (in Russian).
2. Nefedov V.I.: XPS in chemical compounds, Chemistry ed., Moscow, 1984 (in Russian).

STUDY ON THE HYDROGEN EMBRITTLEMENT AND CORROSION OF STAINLESS STEELS USED AS NI/MHX BATTERY CONTAINERS

H.J. CHUANG[a], S.Y. CHEN[b] AND S. L.I. CHAN[a]
[a] *National Taiwan University, Taipei, Republic of China*
[b] *Chung Shan Institute of Science and Technology, Lung-Tan, Republic of China*

Abstract

Stainless steels are used as the containers for Nickel-metal hydride (Ni/MHx) batteries. In this work stainless steel 304 、304L 、316 、316L 、17-4PH and 430 were selected to study their relative susceptibility to hydrogen embrittlement and alkaline corrosion under battery environments. Comparisons were made by immersion test under different hydrogen pressure over the electrolyte, U-bend tests and slow strain rate tensile test with cathodic H_2 charging. The results showed that high strength 17-4PH suffered severe corrosion after long time immersion in the electrolyte solution and were sensitive to hydrogen embrittlement after hydrogen charging. Ferritic 430 performed better than 17-4PH during immersion test but lost its ductility after hydrogen charging. All the austenitic steels (304 、304L 、316 、316L) were found to be suitable as the materials for Ni/MHx battery container, and the present tests can not discriminate their relative resistance to the corrosion and hydrogen embrittlement in the electrolyte.

Introduction

The development of Nickel-metal hydride (Ni/MHx) batteries is gaining speed in the last twenty years. In addition to be used as the power sources in many handy type equipment, these heavy duty batteries also find applications in electric vehicles. The batteries usually contain a strongly alkaline electrolyte with 30~40 wt% KOH. During charging/discharging reactions, hydrogen pressure within the battery may increase, and there may be stray current inside the battery because of these reactions. The high pressure of hydrogen, together with the electric current, increase the chance of hydrogen absorption into the metal and hydrogen embrittlement of the metal may resulted. All these impose strict requirements on the materials chosen for battery container, which should withstand this aggressive environment much longer than the life of the battery. This is particularly true when Ni/MHx batteries are used as the high density power sources for electric vehicles. In addition, hermetic seal is also required for the container, so that welding is necessary. As welding can change the microstructure of a material dramatically, it is important to study on the possible damage of battery container during such situations, so as to choose a right material to meet those requirements. Stainless

T. O. Saetre (ed.), Hydrogen Power: Theoretical and Engineering Solutions, 359–364.

steels can normally be used in caustic environment [1,2], but stress corrosion cracking might occur under stress, or when a susceptible microstructure is present [3]. The situation is further complicated by the presence of hydrogen pressure and stray currents encountered in the Ni/MHx batteries. Although the corrosion resistance of stainless steels in acid is well-documented, there were relatively few literature regarding the behavior of stainless steel and their weldments in the Ni/MHx batteries. In this work, stainless steels 304 、304L 、316 、316L 、430 and 17-4 PH were selected to evaluate their performance in battery environment. These six stainless steels belong to three types: austenite (304 、304L 、316 and 316L) 、ferrite(430) and precipitate hardening martensite (17-4PH). Among the austenitic stainless steels, 304L and 316L were included so as to study the possible effect of carbon content on corrosion resistance. To stimulate the conditions in the batteries, plastically strained stainless steels in the form of U-bend specimens were immersed in the electrolyte under different hydrogen pressures. This provides information regarding the degree of pitting and cracking of the materials after different duration of immersion. Cathodic charging is one of the effective ways to force hydrogen penetrate into the metal, this was carried out on the materials studied in both acid and alkali solution. Slow strain rate tensile testing after hydrogen charging was used to differentiate their relative susceptibility to hydrogen embrittlement.

Experimental Details

All specimens were obtained from commercial 1mm thick plates and their compositions are listed in Table 1. Hardness of each material was measured and is included in Table 1. Laser welding was employed to make a weldment on the base materials with an heat input of 464 J/cm.

Stress corrosion of the stainless steel was determined by U-bend immersion method as described in ASTM G30. The specimens were in the form of 1.5 cmx15cm coupons, and polished up to #2000 SiC abrasive paper. They were then bent plastically to form U-shaped specimens. In the case of the welded specimens, the weld was situated at the center of the specimen. The U-shape was maintained by fixing the specimens with ABS bars. Immersion test was carried out in an environment simulating that in Ni/MHx batteries. That is, a solution made out of 30 wt% KOH +1 wt% LiOH. After degreasing with acetone, the U-shaped specimens were completely immersed in the test solution . The specimens were at least 5 mm apart in the chamber. The solution, together with the specimens, were kept in a hermetically sealed chamber filled with either air(1 atm, 4 months), 5 atm H_2 (3 weeks) or 20 atm H_2 (2 weeks). It should be noted that the duration of immersion was different according the severity of the environment. After immersion, the coupons were cleaned with water and acetone, dried and examined under optical microscope for the extent of pitting and cracking on the coupons.

The preparation of tensile test specimens were followed ASTM E8. The gage length of the tensile specimens is 2.00±0.05 inch . The welded region of welded specimen were arranged at the middle of the gage length. Tensile testing was first performed on specimens in air. To study the effects of corrosion and hydrogen charging on the stainless steels, the specimens were subjected to either immersion test or hydrogen charging before the slow strain rate testing : (a) immersion in electrolyte for 21 days, with a 5 atm hydrogen over the electrolyte. (b) Cathodic charging of hydrogen on the gage length of

tensile specimens in acidic solution (4 vol% H_2SO_4 +20 mg As_2O_3) and (c) Cathodic charging of hydrogen on the gage length of tensile specimens in an alkali solution with a composition similar to that in the immersion test. In the charging, the specimen acted as the cathode, and a Pt mesh as the anode. A charging current density of 40 mA/cm^2 was imposed on the specimen for 2 hours. To avoid excessive escape of hydrogen from the specimen during slow strain rate testing, the specimens were cleaned immediately after charging, and electrolessly coated with Cu. The tensile test was performed with a strain rate of $3.3*10^{-4}$/sec. The fracture morphology has been analyzed by optical microscopy and scanning electron microscopy.

Results and Discussion

1. IMMERSION TEST

The degree of pitting and cracking of the U-bend specimens after immersion test can be evaluated as 17-4PH >> 430 > 316L ~ 316> 304L ~ 304. Stainless steels are good in resisting corrosion in alkaline solutions. To be a battery container, stainless steel plates will be deformed to required shape, which induced tensile and compressive stresses. U-bend test gave similar effects on the specimens, thus the results obtained from these specimens after immersion can give us an indication of what to expect on the material in the service condition. 17-4PH, especially those after welding, suffered severe pitting and cracking on the surface. Most pits located on the deformed area (Fig.1). With an increase in hydrogen pressure over the electrolyte the amount of pitting, as well as the average size of pits, also increased. For specimens with laser welding, pitting was enhanced. Microcracks have also been found in the specimens immersed in electrolyte under H_2 atmosphere, which was an evidence of hydrogen embrittlement. Although laser welding produced a relatively narrow heat affected zone (HAZ) next to the weldment, the cooling rate was too fast that it produced a residual stress and a microstructure more susceptible to hydrogen embrittlement. For 430 stainless steel, pitting was mostly found at the edge of specimen, but on the whole the amount of pitting was much less than that in 17-4PH. Some very fine cracks, however, were found in the cross-section of the coupons. A few pits were found on the top of U-bent area of 316 specimens. No difference can be detected between welded specimens and that without welding. Low carbon content stainless steel 316L did not give good results. Severe pitting corrosion as compared to that in 316 was found after 2-weeks immersion in 20 atm H_2/electrolyte(Fig.2). When immersed in electrolyte under a hydrogen atmosphere, microcracks in addition to pitting were observed on the welded specimens and those without welding. It is possible that with a higher sulfur content in this materials, there was more non-metallic inclusions available for pitting or crack initiation. Molybdenum is good to in resisting pitting in acid[5], but may not be that efficient in an alkaline solution. The above suggestion is only speculative and more work has to be done to clarify the effect of chemical composition on the pitting and cracking in alkaline solution. Our work here indicated that 304 has the best corrosion resistance in the battery environment. Only a small amount of pitting was found on the specimens, and most of them were located along the scratch marks of specimen(Fig.3). An extended immersion test of 13 months was done on these specimens, and even in this case the degree of pitting was insignificant. No cracking was found in 304 stainless steel. For the 304L specimens,

the extent of pitting and cracking was marginally higher than that in 304, suggesting the low carbon content of 304L did not provide any beneficial effect over the 304. It is reasonable here because all the specimens have not been sensitized, and it is expected that the chromium was still remained in the solid solution for effective corrosion resistance. However, if sensitization does occur in these steels, it is quite possible that the low carbon stainless steels will have a much better resistance to pitting and intergranular corrosion.

2. SLOW STRAIN RATE TENSILE TEST (S.S.R.T.)

The results of slow strain rate testing are given in Tables 2. The ductility is represented in Fig.4. It is obvious that the austenitic stainless steels have a lower tensile strength and a higher ductility. The 17-4 precipitation hardened stainless steel has a much higher tensile strength and consequently a very low ductility. After hydrogen charging or immersion in the electrolyte, all specimens suffered different degrees of ductility loss. Their tensile strength, on the other hand, remained mainly unchanged. On account of the strength of materials, the higher the tensile strength (such as 17-4PH), the more susceptible it is to hydrogen embrittlement. In many cases, the 17-4PH tensile specimens failed prematurely as soon as the tensile testing began. This indicated a high susceptibility of 17-4PH to hydrogen embrittlement. The 430 stainless steel was better in that it retained some ductility after immersion test or hydrogen charging. All austenistic stainless steels performed satisfactorily in both the immersion test and hydrogen charging conditions. It is difficult to differentiate them with respect to the susceptibility to hydrogen embrittlement in above conditions. Austenitic stainless steel are known to have a better resistance to hydrogen embrittlement then their ferritic counterpart. It is also possible that since the hydrogen diffusion in austenite was many orders lower than that in ferrite, the two-hour charging did not pose any significant damage on the austenitic stainless steels.

Laser welding seems to have little effect on the strength and ductility of uncharged tensile specimens. When tested after immersion test or hydrogen charged, the welding did not have a pronounced effect on the tensile properties. However, for 304L and 316 specimens where the fracture was located in the weldments, the lost in ductility was generally larger. When the effects of hydrogen charging in acid and in alkali are compared, it was found that 3xx series stainless steels performed equally well in acid and alkali. But for 430 and 17-4 , the elongation after hydrogen charging in alkali solution was definitely better. This may be due to the passive film formed on specimen's surface in the alkali solution during hydrogen charging, which acted as an effectively barrier for hydrogen entry. Moreover, the addition of As_2O_3 in the acid solutions promoted atomic hydrogen formation, assisted the hydrogen entry into the metal, which would otherwise recombined to form H_2 and escape from the solution . For the austenistic stainless steel, on the other hand, the hydrogen diffusion in the metal is so slow, which renders the effect of passive film formation insignificant. Immersing the specimens in the electrolyte for a long period of time has the same effect on the elongation as hydrogen charging in acid. It is possible that pitting or cracking was initiated during immersion, and this may assisted further crack growth or aiding hydrogen transfer.

The 3xx stainless steels were very ductile and typical microvoid coalescence was found on the fracture surface of tensile specimens tested in the air. After immersion

under H_2 or hydrogen-charged, the dimples became larger, but the fracture morphology remained ductile. Most of the tensile specimens measured fractured at the base material except 316, which broke in the weldment in all three environments. The high strength 17-4 PH failed in a dimple manner in air, but with hydrogen charging or immersion in the electrolyte, pores started to formed on the fracture surface (Fig.5), which agglomerated to form cracks in the tensile testing.

Conclusion

In this work, hydrogen embrittlement and alkaline corrosion were both concerned. According to the results obtained, austenitic stainless steels (304 、304L 、316 、316L) were good choices as the materials for Ni/MHx battery container. Among the four candidates, 304 is recommended for its low costs and good workability. To be a long life container, the compositions of material and surface treatments after deformation are also very important. Because of laser welding and without sensitization, the variation of carbon content in these six stainless steels did not show different results. However, when the welding processes changed or sensitization occurred, carbon content should add into consideration.

References

1.Fontana M.G. *Corrosion Engineering* (1986) McGraw-Hill International Editions, pp134-135.
2.Johns D.A. (1992) *Principles and Prevention of Corrosion*, Maxwell Macmillan , p.52 and p.58.
3.Ke R. and Alkire R. (1995) *J. Electrochemical Soc.*, vol 142, no.12, p.4056
4.Fast J.D. (1971) *Interaction of Metals and Gases*, vol. 2, p.134.
5.Greene N.D. and Fontana M.G. (1959) *Corrosion*, 15:25t

TABLE 1 : Composition and hardness of stainless steels

	C	Si	Mn	P	S	Cu	Ni	Cr	Mo	V	Hv
304	0.077	0.50	1.28	0.017	0.005		8.34	18.04		0.07	196
304L	0.029	0.40	1.41	0.017	0.008	0.26	9.01	18.03	0.32	0.08	175
316	0.058	0.64	1.65	0.024	0.005		11.79	17.59	1.93	0.09	168
316L	0.030	0.60	1.65	0.024	0.011		10.75	16.60	2.27	0.10	165
430	0.056	0.69	0.26	0.021	0.013	0.06	0.1	18.54	0.65	0.06	182
17-4PH	0.032	0.43	0.61	0.018	0.001	3.31	4.28	15.58	0.01	0.28	373

TABLE 2 : Environmental effects on stainless steels by slow strain rate tensile test

	Tensile Strength σ_{UTS} (MN/m^2)				Elongation ε (%)				Reduction Area R.A.(%)			
	normal	immersion *	H_2 charging		normal	immersion *	H_2 charging		normal	immersion *	H_2 charging	
			acid	alkali			acid	alkali			acid	alkali
304	690	651	641	627	71	74	80	76	59.9	61.2	60.4	58.2
304W	686	673	639	656	72	64	75	77	60.5	62.9	61.1	59.1
304L	642	631	630	635	55	50	57	60	61.5	56.8	58.8	59.7
304LW	640	626(w)	616	631	59	56	52	60	62.5	49.8	49.8	60.4
316	648	638	611	617	63	67	69	63	62.1	60.3	67.6	59.0
316W	647(w)	631(w)	630(w)	623(w)	47	50	52	47	38.0	42.9	39.1	37.7
316L	626	623	608	603	63	62	69	43	61.4	62.5	60.2	57.0
316LW	621	613	616	605	63	63	49	44	64.1	59.3	49.8	59.6
430	455	445	480	442	33	31	13	28	53.8	49.4	9.2	32.2
430W	456	449	453	448	30	28	6.5	27	56.1	49.3	9.1	33.1
17-4	1158	1131	210	1123	5	4	0	4	18.1	25.1	0	8.8
17-4W	1152(w)	1128(w)	77	1123	3	3	0	4	12.2	9.6	0	8.8

(w): the specimen broke down at welded part
* : immersed in electrolyte under 5 atm H_2 for 3 weeks

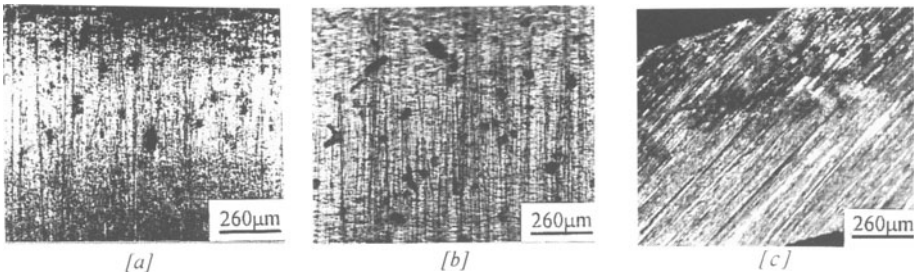

Figure 1. Pittings on 17-4PH [a] Surface near welding after 4 month immersion.[b] Surface near weldingafter immersion in 20atm H2/electrolyte for 2 weeks. [c] Side view of [b].

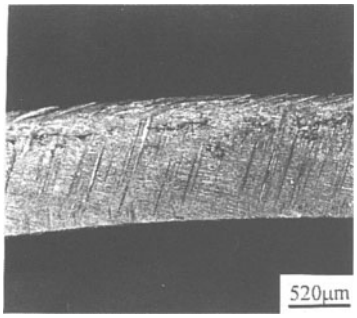

Figure 2. Pittings on deformed part of 316L after immersed in 20 atm H2/electrolyte for 2weeks

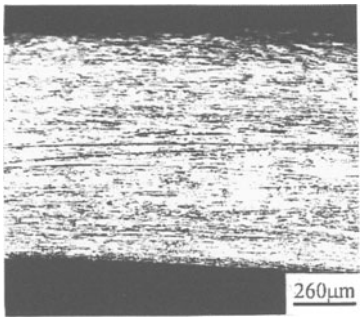

Figure 3. Less pittings found on 304 after immersed in 20 atm H2/electrolyte for 2weeks.

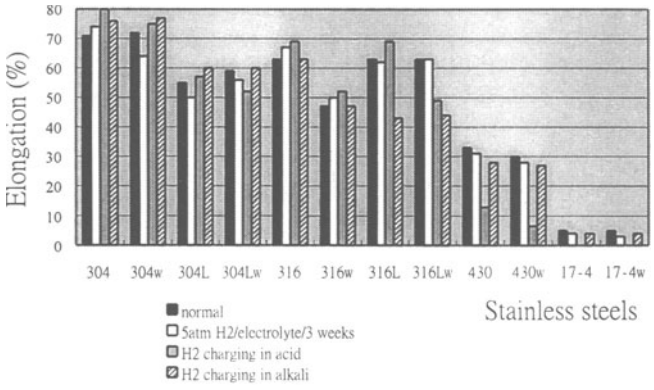

Figure 4 Environmental effects on ductility of stainless steels by slow strain rate tensile test

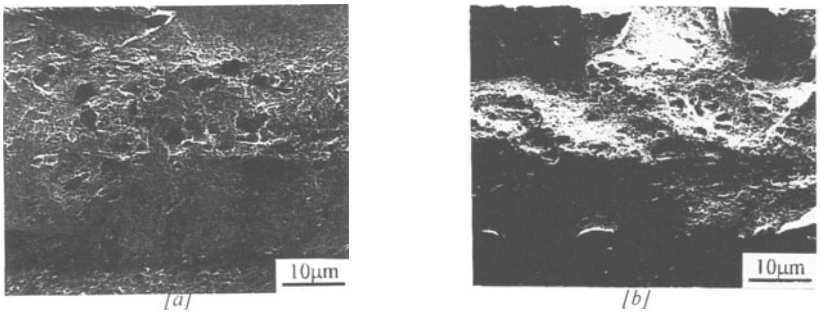

Figure 5. Fracture surface morphology of 17-4PH by S.S.R.T. after H2 charging [a]edge [b]center

METAL HYDRIDES FOR A COMPRESSOR WITH STRICT BOUNDARY CONDITIONS

M.T. HAGSTRÖM, P.D. LUND AND J.P. VANHANEN
Helsinki University of Technology
Department of Engineering Physics and Mathematics
P.O.Box 2200
FIN-02015 HUT, Finland

1. Introduction

A potential application of metal hydrides in self-sufficient solar hydrogen energy systems is to compress the electrolytically produced hydrogen with a metal hydride compressor (MHC), in order to reduce the volume of the seasonal gas storage. Compared to the use of metal hydrides as the hydrogen storage media, far less of often rare and expensive alloy materials are needed. In addition, MHC integrates very well into the overall energy system if the waste heat of the electrolyzer can be used as the heat source for the thermally driven compressor.

The main challenge in this application is the narrow working temperature interval of the MHC which is set by the precondition of self-sufficiency: if no other heat source but a low-temperature solid polymer or alkaline electrolyzer is available and the only source of cold is the ambient, the working temperature of the MHC will be constrained between about 20 and 60 °C. If cold water is available for cooling, the lowest achievable temperature may be close to 10 °C; and if the thermal coupling between the electrolyzer and the MHC can be made especially effective, maybe 70 °C can be reached. Nevertheless, the boundary conditions are very strict and that is why the materials characteristics, such as hysteresis and pressure-composition-isotherm (PCI) plateau slope, play an utmost important role.

Quite a lot of studies on MHCs have been carried out (e.g. [1-9]) and mainly small scale prototypes have been constructed but relatively little attention has been paid to finding high pressure alloys with minimal hysteresis which is necessary if the heat source temperature is the limiting factor. Such materials are looked for in this study.

2. First stage alloy

The inlet pressure to the first stage of the projected multi-stage compressor is approximately 20 - 30 bar which is determined by the outlet pressure of a state-of-the-

T. O. Saetre (ed.), Hydrogen Power: Theoretical and Engineering Solutions, 365–370.

art electrolyzer. An alloy with fairly good characteristics for this stage does not seem to be a problem: $Mm_{0.75}Ca_{0.20}Cu_{0.05}(NiAl)_5$ [7] or some other Mm-based AB_5 alloy [3,4] could be used. Also, e.g. $Ce_{0.6}La_{0.4}Ni_4Co$ seems to have suitable properties [10]. On the other hand, AB_2 alloys offer good choices, too, such as $Ti_{0.9}Zr_{0.1}MnCr_{0.9}V_{0.1}$ [11].

3. Second and higher stage alloys

On the contrary to lower pressure alloys, higher pressure alloys usually show an unacceptably large hysteresis effect for practical purposes [12-16], or substantially reduced capacity or considerable PCI-plateau slope [17]. Since published experimental data on substitutional effects of high pressure hydrides is limited and unsatisfactory, it was decided to synthesize new materials and to study their hydrogen sorption properties. The emphasis was put on the search for substitutional elements that would most effectively reduce hysteresis and keep PCI-plateaux wide and flat, and not so much yet on the actual pressure levels of the PCIs.

4. Experimental

In the AB_2 group, the approach presented by Bernauer & al. [18] was applied to produce hexagonal C14 alloys with *d*-electron concentration (DEC) of 4. This value should keep the α-phase (solid solution) to the narrowest possible and the hydrogen storage capacity to about H/M = 1.0 (hydrogen to metal atom ratio). Purity of the starting materials was 99 % or more. Samples were prepared by arc melting in a water cooled Cu crucible under an argon atmosphere of 0.5 bar and then annealed at 1200 °C for 24 h under an argon atmosphere of 1 bar. The chemical composition of the samples was analyzed by ICP (Inductively Coupled Plasma) spectrometer and powder XRD measurements were done using Cu Kα radiation. Below 0 °C, PCIs were measured after initial activation of the samples (at 50 bar and decreasing temperature from 80 °C down to -60 °C) and several hydriding-dehydriding cycles. Above 0 °C, PCIs of two selected samples were measured after activation at 140 - 150 bar and 20 °C and a few absorption-desorption cycles using different apparatus and different samples than in the low temperature measurements. The composition of the target alloys and the ICP analysis results are presented in Table 1.

In the AB_5 group, $Ce_{0.7}La_{0.3}Ni_{4.5}X_{0.5}$ samples (X = Al, Cu or Co) were prepared by melting the elements in an RF induction furnace at 1500 °C under an argon atmosphere of 200 mbar. Purity of the starting elements was generally 99.98 %. X-ray analysis was made using Siemens D-500 diffractometer. PCIs of the Co-substituted sample were measured using the same procedure as for the AB_2 samples above 0 °C, except for the activation pressure which was 200 bar. Al- and Cu-substituted samples were studied only by PDSC (Pressure Differential Scanning Calorimeter). This equipment has been used previously e.g. to determine dynamic van't Hoff plots of candidate alloys for

hydrogen storage [19] and to study dynamic and reversible changes in the absorption behaviour of $LaNi_5$-H_2 system [20].

TABLE 1. The target composition of the AB_2 samples and the results of the chemical analysis (ICP).

Target composition	Ti	Zr	Cr	Mn	Fe	V
TiCrMn	1.00		0.97	1.01		
$TiCrMn_{0.85}Fe_{0.1}V_{0.05}$	1.00		0.99	0.87	0.11	0.04
$TiCrMn_{0.7}Fe_{0.2}V_{0.1}$	1.00		0.97	0.67	0.21	0.10
$TiCrMn_{0.55}Fe_{0.3}V_{0.15}$	1.00		0.97	0.56	0.30	0.14
$TiCrMn_{0.4}Fe_{0.4}V_{0.2}$	1.00		0.99	0.42	0.40	0.19
$Ti_{0.95}Zr_{0.05}CrMn$	0.95	0.05	0.97	1.01		
$Ti_{0.95}Zr_{0.05}Cr_{1.2}Mn_{0.8}$	0.95	0.05	1.17	0.81		
$Ti_{0.85}Zr_{0.15}CrMn$	0.85	0.15	0.97	1.01		
$Ti_{0.85}Zr_{0.15}Cr_{1.2}Mn_{0.8}$	0.85	0.15	1.17	0.77		

5. Results and discussion

X-ray spectra of the synthesized AB_5 alloys showed no evidence of impurity phases. The calculated lattice parameters and unit cell volumes are shown in Table 2. X-ray spectra of the AB_2 alloys were not analysed in detail but they appeared to be fine, too.

TABLE 2. Lattice parameters and unit cell volumes of the synthesized AB_5 alloys.

Alloy	a [Å]	c [Å]	V [Å^3]
$Ce_{0.7}La_{0.3}Ni_{4.5}Al_{0.5}$	4.9491 (0.0007)	4.0397 (0.0009)	85.69 (0.02)
$Ce_{0.7}La_{0.3}Ni_{4.5}Cu_{0.5}$	4.9409 (0.0004)	4.0123 (0.0004)	84.83 (0.02)
$Ce_{0.7}La_{0.3}Ni_{4.5}Co_{0.5}$	4.929 (0.0002)	3.9993 (0.0002)	84.144 (0.008)

Dynamic (PDSC based) and static (PCI based) van't Hoff plots of the studied AB_5 alloys (Fig. 1) showed that Al is the most effective substitution element for Ni in the group of Al, Cu and Co to reduce hysteresis effect. On the other hand, PDSC absorption and desorption peak widths increased significantly compared to Cu-substituted alloy (Fig. 2) which indicates sloping PCI plateaux. The possibility of a kinetic effect was eliminated by varying heating rates (between 5 and 80 °C/min): the shape of the curves was the same in all cases. In Fig. 1, the absorption and desorption curves of Al-substituted alloy cross each other which is due to the difference in reacted fraction (H/H_{max}) at the peak position of PDSC absorption and desorption curves. If taken at the same hydrogen concentration (which is easy to do with PCIs but not with PDSC curves), these curves do not, of course, cross each other. Co-substituted alloy showed wide and flat PCI plateaux but large hysteresis effect (Fig. 1).

Figures 3a and 3b show the low temperature van't Hoff plots of the studied AB_2 alloys. Substituting Mn by Fe and V (Fig. 3a) was found to be effective in hysteresis reduction, mainly through lowered absorption pressures. Increasing V content or temperature decreases hysteresis. Although a practically hysteresis free alloy with reasonably flat PCI plateaux was found ($TiCrMn_{0.4}Fe_{0.4}V_{0.2}$), it could not be considered a true candidate for our purpose because its PCI plateaux lengths were considerably

shortend with increasing temperature. On the other hand, $Ti_{1-x}Zr_xCr_{2-y}Mn_y$ alloys (Fig. 3b) showed better hydrogen storage capacity persistence with increasing temperature but clearly worse hysteresis and plateaux slopes. Two alloys, $TiCrMn_{0.55}Fe_{0.3}V_{0.15}$ and $Ti_{0.95}Zr_{0.05}Cr_{1.2}Mn_{0.8}$, were selected for PCI measurements above 0 °C, in order to find guidelines for further studies. The PCIs are shown in Fig. 4.

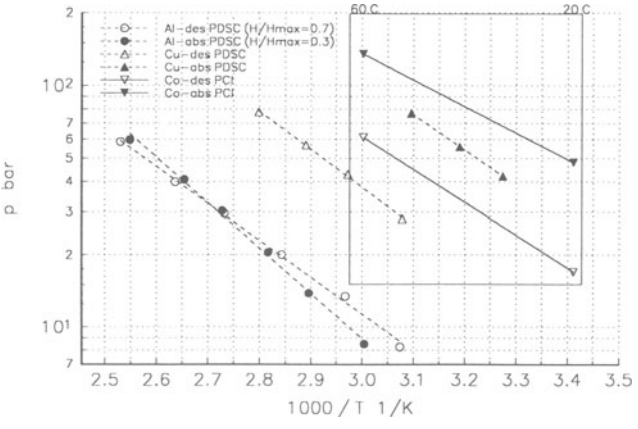

Figure 1. van't Hoff plots of the $Ce_{0.7}La_{0.3}Ni_{4.5}X_{0.5}$-$H_2$ system (X = Al, Cu or Co).

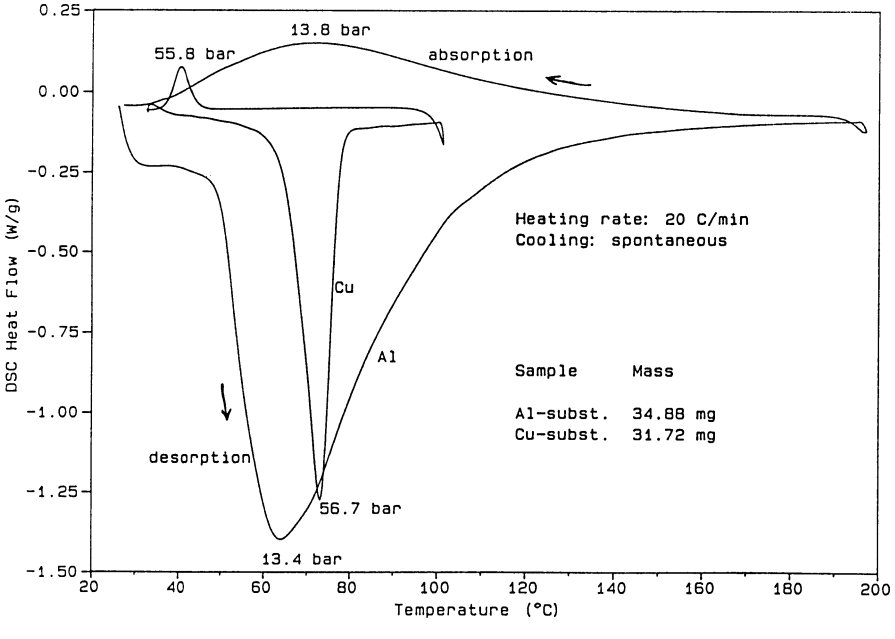

Figure 2. Typical thermal absorption-desorption cycles of $Ce_{0.7}La_{0.3}Ni_{4.5}X_{0.5}$-$H_2$ system (X = Al or Cu).

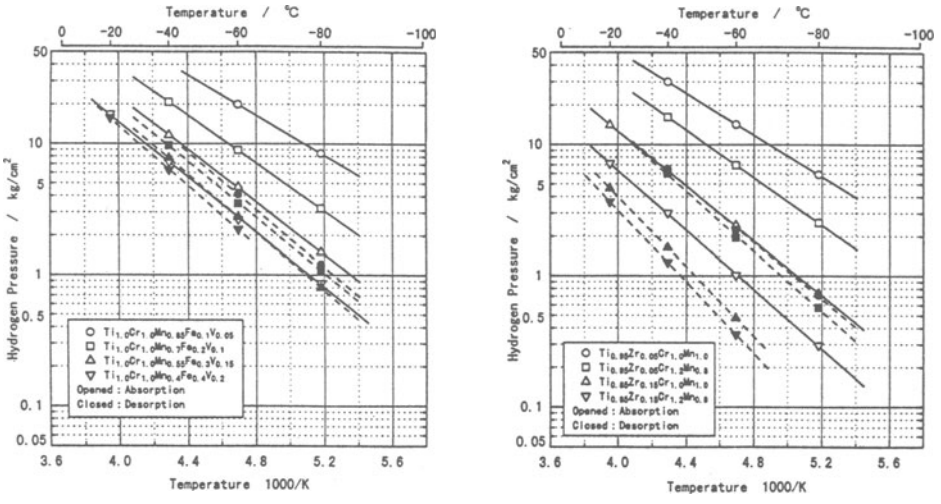

Figure 3a. Low temperature van't Hoff plots of $TiCrMn_{1-3x}Fe_{2x}V_x$-H_2 system (x=0.05,0.1,0.15 or 0.2).
Figure 3b. Low temperature van't Hoff plots of $Ti_{1-x}Zr_xCr_{2-y}Mn_y$-H_2 system (x=0.05 or 0.15;y=0.8 or 1.0).

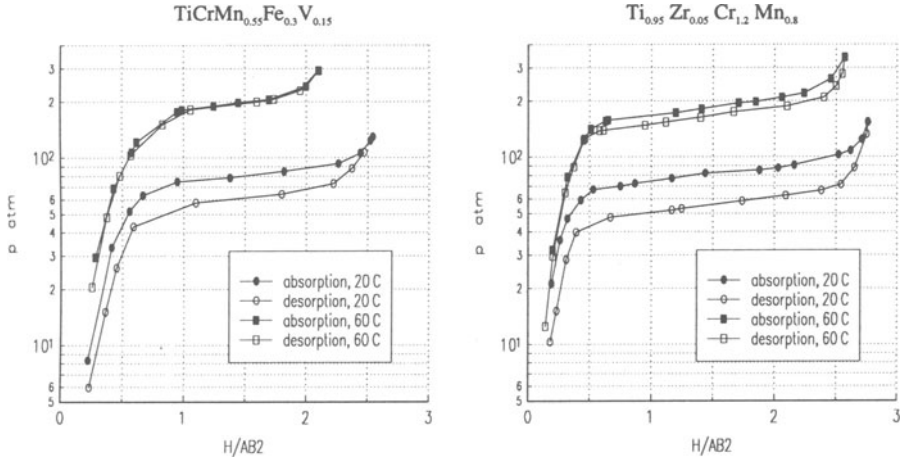

Figure 4. PCIs of $TiCrMn_{0.55}Fe_{0.3}V_{0.15}$-$H_2$ and $Ti_{0.95}Zr_{0.05}Cr_{1.2}Mn_{0.8}$-$H_2$ systems at 20 and 60 °C.

6. Conclusions

Since Al reduced hysteresis effectively in the $Ce_{0.7}La_{0.3}Ni_{4.5}X_{0.5}$-$H_2$ system (X=Al, Cu or Co), and Cu and Co maintained good PCI-plateaux, it could be reasonable to study combined substitution (Ce,La)(Ni,Al,Co)$_5$ (e.g.). It should also be studied whether AB_5 alloys with other single substitution elements, such as Sn, showed better characteristics than the ones synthesized so far.

$Ti_{0.95}Zr_{0.05}Cr_{1.2}Mn_{0.8}$ has promising PCI characteristics which should, nevertheless, be further improved in regard to hysteresis and plateaux slope. For that purpose, partial substitution of Mn by V is going to be studied.

Acknowledgements. Dr. T. Kabutomori at JSW (Japan) is gratefully acknowledged for preparing the AB_2 samples and carrying out all experimental work below 0 °C. Big thanks are also due to Dr. S. Klyamkin at Moscow State University for measuring the PCIs above 0 °C. Further, Dr. A. Züttel and Dr. K. Gross at University of Fribourg are thanked for preparing the AB_5 samples and characterizing their XRD spectra.

References:

1. Nomura K., Akiba E. and Ono S., Development of a metal hydride compressor, *J. Less-Common Met.* **89**(1983)551-558.
2. Golben P.M., Multi-stage hydride-hydrogen compressor, *Proc. 18th Intersociety Energy Conversion Engineering Conf.* (A.I.Ch.E., New York 1983) pp. 1746-1753.
3. Qidong Wang, Jing Wu and Changpin Chen, Development of new mischmetal-nickel hydrogen storage alloys according to the specific requirements of different applications, *Z..Phys.Chem. NF* **164**(1989)1293-1304.
4. Ming Au and Qidong Wang, Rare earth-nickel alloy for hydrogen compression, *J. Alloys Comp.* **201**(1993)115-119.
5. da Silva E.P., Industrial prototype of a hydrogen compressor based on metallic hydride technology, *Int. J. Hydrogen Energy* **18**(1993)307-311.
6. Bowman R.C. Jr., Freeman B.D., Ryba E.L., Spjut R.E., Liu E.A., Penso J.M. and Lynch F.E., Performance testing of a vanadium hydride compressor, *Z. Phys.Chem.* **183**(1994)245-250.
7. Changpin Chen, Zhou Ye, Jing Wu and Qidong Wang, The properties and some applications of the hydride hydrogen-compression alloy $(CaMmCu)(NiAl)_5Zr_{0.05}$, *Z. Phys. Chem.* **183**(1994)251-258.
8. Solovey V.V., Ivanovsky A.I., Kolosov V.I. and Shmal'ko Yu.F., Series of metal hydride high pressure hydrogen compressors, *J. Alloys Comp.* **231**(1995)903-906.
9. Zhan Feng, Bao Deyou, Jiang Lijun, Zhang Liang, Yu Xiaoyu and Zhou Yiming, Metal hydride compressor and its application in cryogenic technology, *J. Alloys Comp.* **231**(1995)907-909.
10. Mordkovich V.Z., Baichtok Yu.K., Dudakova N.V., Mazus E.I. and Mordovin V.P., Equilibria in the hydrogen-intermetallics systems with high dissociation pressure, *J. Alloys Comp.* **231**(1995)498-502.
11. Bin-Hong Liu, Dong-Myung Kim, Ki-Young Lee and Jai-Young Lee, Hydrogen storage properties of $TiMn_2$-based alloys, *J. Alloys Comp.* **240**(1996)214-218.
12. Klyamkin S.N., Verbetsky V.N., Interaction of intermetallic compounds with hydrogen at pressures up to 250 MPa: the $LaCo_{5-x}Mn_x$-H_2 and $CeNi_5$-H_2 systems, *J. Alloys Comp.* **194**(1993)41-45.
13. Klyamkin S.N., Verbetsky V.N. and Demidov V.A., Thermodynamics of hydride formation and decomposition for $TiMn_2$-H_2 system at pressure up to 2000 atm, *J. Alloys Comp.* **205**(1994)L1-L2.
14. Klyamkin S.N., Verbetsky V.N. and Karih A.A., Thermodynamic particularities of some $CeNi_5$ -based metal hydride systems with high dissociation pressure, *J. Alloys Comp.* **231**(1995)479-482.
15. Mitrokhin S.V. and Verbetsky V.N., Titanium based Laves phase hydrides with high dissociation pressure, *Int. J. Hydrogen Energy* **21**(1996)981-983.
16. Mitrokhin S.V. and Verbetsky V.N., Titanium-based Laves phase hydrides with high dissociation pressure, *Int. J. Hydrogen Energy* **22**(1997)219-222.
17. Osumi Y., Suzuki H., Kato A., Oguro K., Sugioka T. and Fujita T., Hydrogen storage properties of $Ti_{1+x}Cr_{2-y}Mn_y$ alloys, *J. Less-Common Met.* **89**(1983)257-262.
18. Bernauer O., Töpler J., Noréus D., Hempelmann R. and Richter D., Fundamentals and properties of some Ti/Mn based Laves phase hydrides, *Int. J. Hydrogen Energy* **14**(1989)187-200.
19. Hagström M.T., Lund P.D. and Vanhanen J.P., Metal hydride hydrogen storage for near-ambient temperature and atmospheric pressure applications, A PDSC study, *Int. J. Hydrogen Energy* **20**(1995)897-909.
20. Hagström M.T. and Lund P.D., Pressure DSC studies on the formation and reproducibility of double peaks in the sorption of $LaNi_5$-H_2 during thermal cycling, *Thermochimica Acta* **3243**(1997)1-7.

COMPATIBILITY OF STAINLESS STEEL TYPE 316L WITH MOLTEN LiH UNDER HYDROGEN PRESSURE

R. ADINBERG and A. YOGEV
Solar Research Facilities Unit
Weizmann Institute of Science
Rehovot 76100, Israel

1. Introduction

Lithium hydride is an attractive candidate for high temperature thermal energy storage in space solar power devices. This phase change material has a high heat of fusion per unit mass, 2.58 Mj/kg, at a melting point of 688.6 °C. Thermodynamics of LiH in the liquid state is described by the reaction of decomposition

$$LiH_{(liquid)} \Leftrightarrow Li_{(liquid)} + 1/2\ H_{2\,(gas)},$$

and mutual solubilities of the components (Veleckes, 1979). Potential problems of the system "LiH - Li - H_2" compatibility with the containment vessel are a strong corrosion attack toward almost all conventional structural materials, except the refractory metals, and a high rate of hydrogen loss by permeation into the environment. According to the life time tests presented in the literature (Dunn and Reay, 1991, Steiner, 1976), low-cost austenitic stainless steels can be acceptable for systems destined for operating at temperatures not exceeding 800 °C.

The aim of the present work is to estimate short term (e.g., several months) compatibility of type 316L stainless steel to molten LiH under operating conditions of a solar thermal system being designed. The experiments were conducted at a storage temperature 800 -820 °C under pressure of hydrogen 2.0- 2.3 bar used to prevent extended dissociation of LiH.

2. Experimental Setup

The experimental setup schematically shown in Fig. 1 was dual-purpose system destined to conduct both the compatibility tests and hydrogen permeation experiments. By making small changes in the assembling it was possible to switch from one experiment

T. O. Saetre (ed.), Hydrogen Power: Theoretical and Engineering Solutions, 371–376.

to the other. The main components of the apparatus were all made of type 316L stainless steel. The gauge section of permeation specimens had the form of a closed-end hollow cylinder machined from a solid rod. The membrane thickness of the specimens was 1.2 mm. Each plate-shaped material sample had dimensions of 38.0 (length) x 15.0 (width) x 2.7 (thickness) mm with as-polished surface. The crucibles were 70 mm long with 17 mm of an internal diameter to hold approximately 5 g of lithium hydride. According to the task of experiment, either a permeation specimen or a crucible with the material sample inside could be positioned into the vessel.

The LiH used in this study was purchased from Fluka Chemie AG with prescribed purity grade 97% (NT). Cover gases, high-purity argon and hydrogen, were both of research purity grade (99.999%), as received from Gordon Gas Ltd. The test facility was equipped with an evacuable glove box for handling LiH under some excessive pressure of argon.

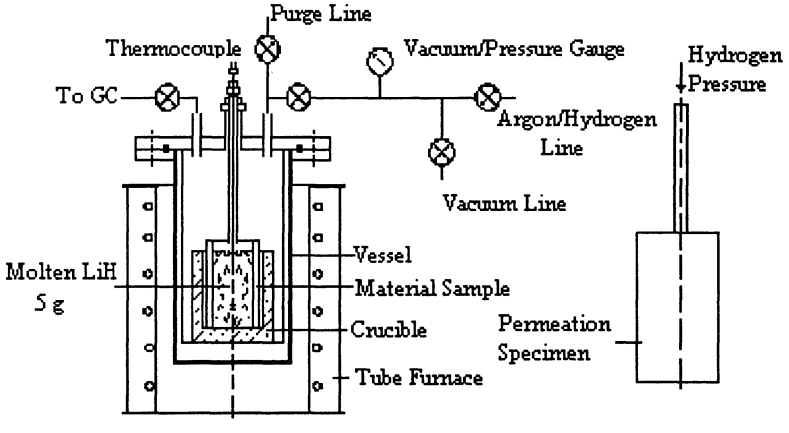

Figure 1. Apparatus to study both the compatibility of materials and H_2 permeation.

Thermocouples of type K were used to measure temperatures in several points inside the vessel. The pressure changes due to hydrogen permeation were measured using an absolute pressure transmitter having a full-scale reading of 10 bar and a resolution of 0.01 bar. The outputs of the thermocouples and pressure transmitter were connected to a computer to record and process the results.

3. Hydrogen Permeation Study

Knowledge of the hydrogen transport in austenitic stainless steels is very important in regard to structural applications for the storage systems operating at high temperatures. The temperature and pressure variations of the permeability of hydrogen through the steels have been reported in many works (Forcey et al., 1988, Katsuta and Furukawa, 1981, Sun et al., 1989) covering the temperature range 240-920 °C and pressure range

0.01-1.0 bar. The permeation rate was shown to be dependent on the half-power of the pressure, suggesting diffusion-limited conditions of the process:

$$J = \frac{\Phi}{d}(p_h^{1/2} - p_l^{1/2}), \tag{1}$$

where J is the rate of gas permeation per unit area of material of thickness d; Φ - coefficient of permeation, p_h and p_l are the gas pressure on the high and low pressure sides respectively. For commercial type 316L austenitic steel the permeability Φ is well represented by the following equation (Forcey, 1988):

$$\Phi = 1.80E\text{-}7exp(-64030/RT) \tag{2}$$

However, deviations, due to surface effects (mainly oxides), are noted in the literature with pressure exponents between 0.5 and 1.0 often being observed (Katsuta and Furukawa, 1981). A linear relationship $J \sim p_h$ would be expected if slow surface reactions are controlling the process of permeation (Steiner, 1976). Influence of the oxidation state or the polishing preparation of the exit surface on steel is not yet recognized. In general, the objective of the present study was to establish a sound experimental base required for determining the surface effects with account for testing some ceramic coatings in the future.

Experimental. The gas permeation technique described above has been employed to measure the permeability of hydrogen in the type 316L stainless steel over the pressure range 0 - 2.5 bar at temperatures 800-850 °C. In the present experiment no electroplate coating was used as a means preventing oxidation. Thus, a passive layer might be formed on the exit side if linked to an oxidizing atmosphere.

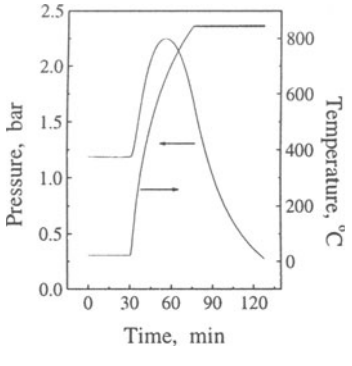

Figure 2. Temperature and pressure variations in the gauge section

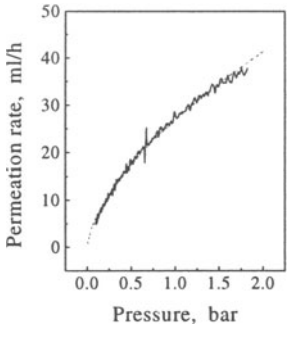

Figure 3. Permeation rate as a function of hydrogen pressure in experiments with vacuum on the exit side.

Hydrogen was introduced to the interior of the specimen and the permeation rate was measured with respect to the vessel interior exposed either to vacuum or to the air atmosphere. Measurements were made for the sequences of gas pressure, p_h, and specimen temperature, T, upon time of heating up the specimen to a given temperature, including the followed period when the temperature was kept constant. Data on the pressure and temperature obtained during the typical run of heating up the specimen to 840 °C with vacuum on the exit side are shown in Fig. 2. These data demonstrate that at beginning of heating due to relatively low temperatures the pressure changes in direct ratio to a temperature rise, approximately up to 300 °C. At higher temperatures, permeation of hydrogen becomes strong enough to predominate over the effect of gas expansion. This effect turns the residual pressure from elevation to go down till a real vacuum inside the specimen is reached.

Since the volume was calibrated prior to the measurements, the rate of pressure variation could be converted into an amount of gas (in moles) permeating through unit area of the sample wall per second:

$$J = V_0 T_0 P_0^{-1} \left(p_h T^{-1}\right)_\tau', \tag{3}$$

where τ is time and V_0, P_0, T_o are consecutively the volume, pressure, and temperature of the gauge section before the heating started. This expression considers only pressure of hydrogen on the entrance side, since the exit side pressure is negligible in comparison, $p_l \approx 0$.

Experiments with vacuum on the exit side of the specimens demonstrated good repeatability in series of up to 5-6 runs with the same specimen. Fig. 3 presents the permeation rate dependence on the hydrogen pressure for the results given in Fig. 2. According to these results, the permeation rate $J \sim p_h^n$ is best fitted by the power n=0.62 (dash line), which is close to that stated by eq. (1).

Fig. 4 presents the permeation rate dependence on the hydrogen pressure for experiments carried out under the exterior conditions of the air atmosphere. After testing, some layered oxide was observed on the surface of the specimens. In this case the permeation rate J is found consistent with direct proportionality to p_h, n=1.

From the given results follow that the passive layer formed on the exit side acts as a barrier for hydrogen permeation, reducing the rate of hydrogen release to the environment. However, the evolution of this barrier so depended on time and conditions of the surface that stationary conditions could not be obtained.

4. Compatibility Testing

Several patterns of austenitic stainless steels were tested by Pawel (1993a,b) in molten LiH at 715 - 850 °C under argon-hydrogen atmosphere. Progressive growth of the ferrite layer at extended exposure time due to selective leaching of nickel and carbon from the near-surface regions of the steels has been considered the primary mechanism of corrosion in molten LiH.

In the present tests samples of type 316L stainless steel were exposed to molten LiH for duration of about 200 h in the same temperature range of 800 - 850 °C as in the former work, but at much higher pressure of hydrogen, 2.0-2.3 bar. The experimental procedure used is in general similar to that suggested by Pawel (1993 a, b).

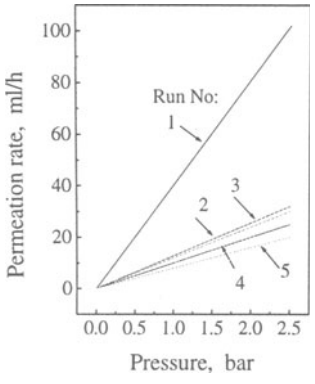

Figure 4. Permeation rate as a function of hydrogen pressure for a series experiments with the same specimen

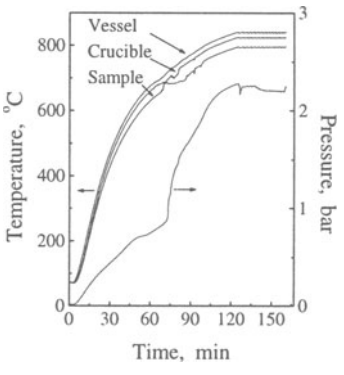

Figure 5. Temperature and pressure variations in the reaction vessel

Experimental. Three test runs, each time with a new sample, crucible and portion of LiH, were carried out at the conditions specified above. After the furnace reached the desired temperature of 850 °C, a sample was inserted into the melt by shifting down the holder through the sliding fitting at the vessel lid. At the end of each experiment the sample was withdrawn from the melt up into the gas pad; then the furnace was turned off with following exchange of the cover gas from hydrogen back to argon at a room temperature. The samples were cleaned and weighed, and then taken for metallographic examination.

Typical variations of pressure and temperatures in the reaction vessel through the period of heating up are shown in Fig. 5. The plateau found on the *sample* curve at the time of 75 - 80 min corresponds to melting of the LiH, that in the present experiment occurred at a temperature of 685 °C. It can be compared to the melting point of 688.6 °C given in JANAF Thermochemical Tables (1985). As expected, on reaching the temperature of the melting point, the reaction of LiH decomposition is going strongly up that is clearly seen in a steep pressure rise as the heating continues.

Initial inspection of the samples undergone the test showed no sign of corrosion and no dimensional changes to a detection limit of 0.01. Polished and etched sections of the samples were subjected to metallographic examination by means of UNITRON Series N Metallograph. The pictures observed appear essentially identical to those described by Pawel (1993 b) for 316L stainless steel disk-shaped coupons following exposure to LiH at 800 °C. The similarity includes the presence of a surface layer which Pawel identified as a ferrite layer using X-ray diffraction and microprobe analysis.

However, the qualitative similarity in metallographic features does not extend to quantitative comparison of weight loss. In our tests weight changes measured for the samples show losses scattered in the range of 30 - 50 g/m^2. This result is about a factor from 2 to 3 greater than in the referred experiment (~15 g/m^2) for the same exposure of 200 h. The only reason that can be thought responsible for increased corrosion attack of the austenitic steel in the present work is the high pressure of hydrogen (2 - 2.3 bar) over molten lithium hydride. In the other researches discussed the cover gas was argon containing 10 - 30 % hydrogen at the total pressure (usually not specified) just a little above an atmospheric pressure. Accordingly, a concentration of hydrogen dissolved in the steel samples tested was remarkably higher, at least as a factor $\sqrt{10}$, than that in the compared experiments.

The effect of hydrogen presence on corrosion and mechanical properties of austenitic stainless steels in the liquid lithium hydride environment, particularly, grain boundary diffusion of hydrogen in the structural material needs further detailed investigation.

5. Summary

In order to define the corrosion behavior and gas permeation characteristics of potential structural materials for solar energy storage designs employing high heat flux conditions at the elevated temperatures, an experimental program has been initiated, in which type 316L austenitic stainless steel is the candidate containment material. Several samples of stainless steel type 316L have been tested at 800 - 850 °C in the environment of molten LiH and hydrogen, as a cover gas. Gas analyses and metallographic examinations were carried out at the termination of the corrosion tests. The main conclusion concerning the compatibility of materials is that high pressure of hydrogen can be a factor significantly enhancing the corrosion rate of stainless steel under molten lithium hydride operational conditions.

6. References

Dunn, P. D. and Reay, D. A. (1991) *Heat Pipes*, 4th edition, Pergamon Press.

Forcey, K. S. et al. (1988) Hydrogen transport and solubility in 316L and 1.4914 steels for fusion reactor applications, *J. Nucl. Mater.*, **160**, 117-124.

JANAF Thermochemical Tables (1985) *J. Phys. Chem. Ref. Data*, **14**, Suppl. 1.

Katsuta, H. and Furukawa, K. (1981) Hydrogen and deuterium transport through type 304 stainless steel at elevated temperatures, *J. Nucl. Sci. and Tech.*, **18** (2), 143-151.

Pawel, S. J. (1993a) Type 304L stainless steel corrosion in molten lithium hydride as a function of temperature, *J. Nucl. Mater.*, **200**, 184-199.

Pawel, S. J. (1993b) Compatibility of potential containment materials with molten lithium hydride at 800 °C, *J. Nucl. Mater.*, **207**, 136-152.

Steiner, D. (1976) Materials requirements for fusion power, in Chi. Stein (ed), *Critical Materials Problems in Energy Production*, Academic Press, Inc., pp. 39-86.

Sun Xiukui, Xu Jian and Li Yiyi (1989) Hydrogen permeation behavior in austenitic stainless steels, *Mater. Sci. Engineering*, **A114**, 179-187.

Veleckis, E. (1979) Decomposition pressures in the (α + β) fields of the Li-LiH, Li-LiD, and Li-LiT systems, *J. Nucl. Mater.*, **79**, 20-27.

MECHANICAL ALLOYING AND CHARACTERISATION OF NANOCRYSTALLINE Mg_2Ni

J. KESKINEN AND P. RUUSKANEN
VTT Manufacturing Technology, Technical Research Centre of Finland
P. O. Box 17031, FIN-33101 Tampere, Finland

Abstract

Nanocrystalline Mg_2Ni absorbs hydrogen at considerably lower temperatures than the same material possessing crystals of larger size. In this study Mg_2Ni was produced by mechanical alloying in a planetary ball mill using elemental magnesium and nickel powders as the starting materials, as well as MgH_2. Palladium powder was added to the mechanically alloyed material to catalyse the reaction between Mg_2Ni and hydrogen.

1. Introduction

Magnesium and magnesium compounds have great potential as hydrogen storage materials because they can store relatively high percentages of hydrogen: MgH_2 contains 7.6 wt. % of hydrogen and Mg_2NiH_4 3.6 wt. %. In many applications the problem with magnesium is that the temperature and pressure required for the absorption of hydrogen are high and that hydrogen desorption also needs high temperatures. The reaction kinetics are also relatively low. Mg_2Ni absorbs and desorbs hydrogen in less-demanding conditions. Typical conditions for the absorption of hydrogen by Mg_2Ni are temperatures of the order of 300 °C and pressures of 10 bar (Reilly 1977).

It has recently been discovered that a nanocrystalline structure results in a remarkable improvement in the hydriding of Mg_2Ni (Zaluski *et al.*, 1995A). Also, mechanical alloying (MA) has emerged as a novel technique for alloy formation. Mechanical alloying is a solid state process in which powders are processed in a high energy ball mill. This process causes repeated fracturing and cold welding of the powders and can achieve mixing at atomic scale. Mechanical alloying can be used to produce crystalline, nanocrystalline and amorphous alloys and compounds. It has been employed by several research groups in the preparation of Mg_2Ni compounds (Singh *et al.* 1995, Zaluski et al., 1995A, Orimo *et al.*, 1996, Chen *et al.*, 1996). The results achieved have been very promising, indicating that mechanical alloying results in nanocrystalline Mg_2Ni which exhibits improved properties when compared with

T. O. Saetre (ed.), Hydrogen Power: Theoretical and Engineering Solutions, 377–382.

material having a larger crystal size. Palladium has been used to catalyse the reaction between Mg_2Ni and hydrogen (Zaluski *et al.* 1995B).

This study deals with the synthesising of nanocrystalline Mg_2Ni powders by mechanical alloying and characterisation work on the resulting material in order to determine optimal parameters for the preparation of the compound, and to understand the behaviour of mechanically alloyed Mg_2Ni with hydrogen.

2. Experimental details

The mechanical alloying of magnesium and nickel was performed in a hydrogen atmosphere. The hydrogen atmosphere is necessary because it prevents the agglomeration of the constituent powders on the walls of the milling vials. The initial particle size of the magnesium powder was 45 - 200 μm and that of the nickel powder 2.5 - 3.5 μm. When MgH_2 was used instead of elemental magnesium the powders did not stick over-severely to the walls of the vials and it was possible to perform the milling operation in an argon atmosphere. The palladium powder used to catalyse the hydrogen reaction had a particle size of <50 μm.

A planetary type ball mill was used. The milling vials and balls were of hardened steel. The powders were loaded into the vials in an argon-filled glove box. Each batch of powder weighed 20 g, and 200 g of 10 mm diameter balls were used. In most cases the milling time was 80 hours. Samples 0.25 g in size were removed from the vials after 2, 5, 10, 20 and 40 hours of milling. At the beginning and after removal of the samples the milling vial was filled with hydrogen gas (at 4 bar). After 80 hours of milling, palladium doping was achieved by adding 1 wt. % Pd to the milled powder. Milling was then continued for one hour.

The microstructure of the powders was studied using scanning electron microscopy. The crystal structure was defined by X-ray diffractometry (XRD) using Mo-K_α radiation and by transmission electron microscopy (TEM). Hydrogen absorption properties were examined in an instrumented pressure chamber. A thermogravimetric analyser (TGA) was used to characterise the desorption of hydrogen.

3. Results and discussion

3.1 MICROSTRUCTURE

The particle size and shape of the Mg_2Ni powder after 80 hours milling is shown in Figure 1. The particle size is in the range 0.5 - 5 μm. As is usual after mechanical alloying, the shape of the particles is irregular.

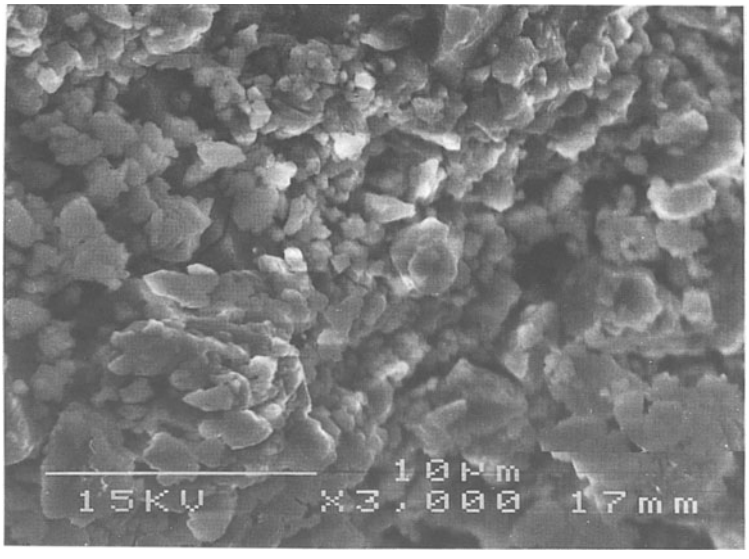

Figure 1. Scanning electron micrograph of mechanically alloyed nanocrystalline Mg_2Ni powder.

3.2 CRYSTAL STRUCTURE

The X-ray diffraction results showed that magnesium and nickel powders milled for periods of up to 20 hours consisted of elemental Mg and Ni phases (see Figure 2). After 40 hours of milling a transformation from the mixture of elemental Mg and Ni phases to nanocrystalline Mg_2Ni phase had taken place. Because of the overlapping of the peaks corresponding Mg_2Ni and its hydrides it is difficult to determine the quantities of these phases or the crystal size. Although the powder was nanocrystalline in form after 40 hours of mechanical alloying, the material milled for 80 hours was chosen for use in the hydrogen absorption tests. The reason for this was that the XRD curves still showed traces of elemental Ni in the powders which had been milled for 40 hours.

The crystal size of the material was estimated by using transmission electron microscopy. After 80 hours of milling the crystal size was generally in the range 10 - 30 nm. Some crystals 50 - 100 nm in size were found.

When magnesium hydride, MgH_2, and nickel were used as the starting materials, the corresponding diffraction peaks in the associated XRD curves disappeared during milling. After prolonged milling, diffraction peaks corresponding to Mg_2Ni-based hydrides appeared. The main difference when these results are compared with the 80 hour curve shown in Figure 2 is that the relative amount of hydrides was higher. It must be noted, however, that the XRD curves are difficult to interpret because the compounds in question have overlapping peaks which are relatively wide because of the nanocrystalline structure. The width of the peaks indicate that the crystal size was of the same order as that in the sample consisting of elemental Mg and Ni. Because it is important to avoid grain growth in the material, the crystal structure was defined after heating the samples at temperatures up to 300 °C. After heat treatment at 300 °C

the diffraction peaks did not exhibit any further broadening, indicating that the crystal size had increased above 100 nm.

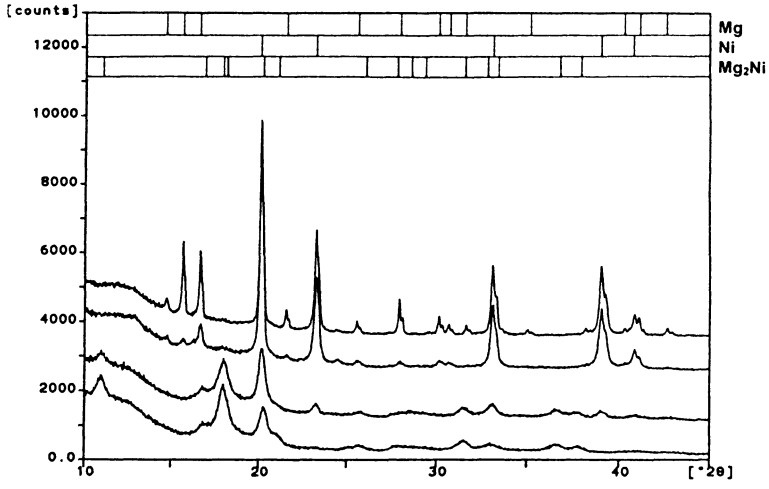

Figure 2. X-ray diffraction patterns measured after 2, 20, 40 and 80 hours of milling.

3.3 THERMOGRAVIMETRIC ANALYSIS OF THE MECHANICALLY ALLOYED POWDER

Thermogravimetric analysis (TGA) showed that the amount of absorbed hydrogen was about 1.8 wt. % after 80 hours of mechanical alloying in hydrogen. The hydrogen content increased during the milling process as shown in Table 1.

TABLE 1. Hydrogen content and the energy required to liberate hydrogen as a function of milling time.

Milling time (h)	Hydrogen content (wt. %)	Energy bound in hydrogen desorption (J/g)
5	0.46	69
20	1.15	108
40	1.62	149
80	1.77	178

Figure 3 presents the combined thermogravimetric and differential thermal analysis curves for a nanocrystalline Mg_2Ni sample milled for 80 hours. The desorption of hydrogen begins slowly at a temperature of about 205 °C. The peak in the DTA curve indicates that energy is bound during the desorption process.

3.4 HYDROGEN ABSORPTION

When 1 wt. % palladium was added to mechanically alloyed Mg_2Ni it was found that the compound absorbed hydrogen at room temperature. The amount of absorbed hydrogen at room temperature was measured to be 2 - 2.2 wt. %, the theoretical maximum for Mg_2Ni being 3.6 wt. %. Without the addition of palladium the

compound absorbed only about 0.5 wt. % hydrogen, which is more than would be absorbed during the formation of $Mg_2NiH_{0.3}$. According to the literature, $Mg_2NiH_{0.3}$ is formed when Mg_2Ni is exposed to hydrogen at low temperatures (Reilly 1977). Figure 4 shows absorption curves for samples with and without the addition of palladium.

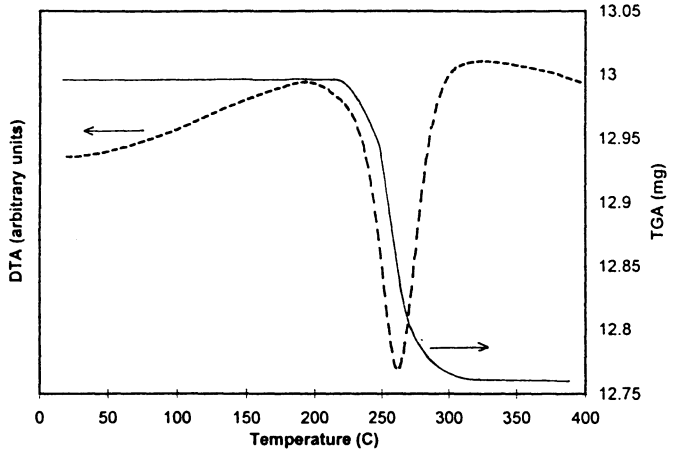

Figure 3. Thermogravimetric and differential thermal analysis data of Mg_2Ni sample milled for 80 hours. The curves show the desorption of hydrogen when the sample was heated at a rate of 10 °C/min.

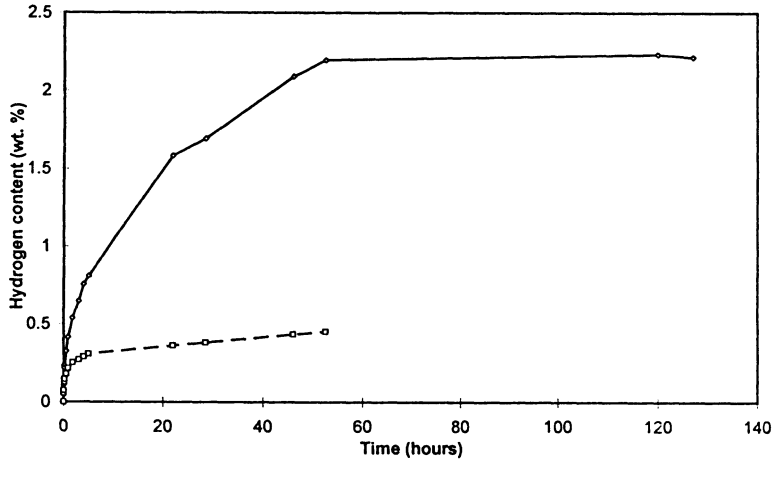

Figure 4. Hydrogen absorption in palladium-doped Mg_2Ni (solid line) and Mg_2Ni without added palladium at room temperature.

In the TG analysis it was found that the material made from MgH_2 and Ni required temperatures greater than 300 °C to desorb all the hydrogen. For this reason, absorption tests were carried out on Mg_2Ni after desorbing hydrogen at 300 °C. After

this heating process the absorption rate of hydrogen at room temperature decreased. This is most probably the result of changes in the crystal structure. Thus, if MgH_2 were to be used as a starting material, it would be necessary to determine how to prevent these changes.

The absorption of hydrogen by the palladium-doped material was also determined at temperatures of 100, 150, 200 and 250 °C. Higher temperatures were not employed in order to avoid the deterioration in low temperature absorption properties. Between 150 °C and 250 °C changing the temperature did not result in any clear change in the hydrogen absorption properties, the quantity of hydrogen being absorbed was about 2.6 wt. %. At 100 °C absorption of hydrogen was approximately 2.1 wt. %.

4. Conclusions

Nanocrystalline Mg_2Ni was produced by a mechanical alloying process. Magnesium, nickel and MgH_2 were used as starting materials. When magnesium and nickel were milled in a hydrogen atmosphere, nanocrystalline Mg_2Ni was formed. The hydrogen content of this compound increased during milling. The addition of palladium improved hydrogen absorption properties at room temperature, 2-2.2 wt. % hydrogen being absorbed. At temperatures ranging between 150 °C and 250 °C hydrogen absorption of about 2.6 wt. % was achieved.

Acknowledgements

This research work was financed by Technology Development Centre (TEKES), AGA Ab and the Technical Research Centre of Finland.

References

Chen J., Dou, S.X. and Liu, H.K. (1996) Crystalline Mg_2Ni obtained by mechanical alloying, *J. Alloys Comp.*, **244**, 184-189.

Orimo S. and Fujii H. (1996) Hydriding properties of the Mg_2Ni-H system synthesized by reactive mechanical grinding, *J. Alloys Comp.*, **232**, L16-L19.

Reilly, J.J. (1977) Metal hydrides as hydrogen storage media and their applications, in K.E. Cox and K.D. Williamson, Jr. (eds.), *Hydrogen: Its technology and Implications, Volume II, Transmission and Storage*, CRC Press, Cleveland, pp. 13-50.

Singh, Arvind K., Singh, Ajay K. and Srivastava O.N. (1995) On the synthesis of the Mg_2Ni alloy by mechanical alloying, *J. Alloys Comp.*, **227**, 63-68.

Zaluski, L., Zaluska, A. and Ström-Olsen J.O. (1995A) Hydrogen absorption in nanocrystalline Mg_2Ni formed by mechanical alloying, *J. Alloys Comp.*, **217**, 245-249.

Zaluski, L., Zaluska, A., Tessier, P., Ström-Olsen J.O. and Schulz R. (1995B) Catalytic effect of Pd on hydrogen absorption in mechanically alloyed Mg_2Ni, $LaNi_5$ and FeTi, *J. Alloys Comp.*, **217**, 295-300.

OPERATING EXPERIENCES OF A TWO-STAGE METAL HYDRIDE HYDROGEN COMPRESSOR

K. Bonhoff, H. Barthels
Institute of Energy Process Engineering (IEV)
Research Centre Jülich, P.O. Box 1913, D-52425 Jülich, Germany

Abstract - The performance of a two-stage metal hydride hydrogen compressor has been investigated. The two reactors of each stage are filled with 5 kg $TiMn_2$-based metal hydride material each. In the first stage hydrogen is absorbed at 10 °C and 5 bar. Desorption takes place at 100 °C and pressures up to 125 bar. The hydrogen flow of the present experimental setup varies between 0.47 $m_n^3{}_{(H2)}$/h at 83.4 bar and 0.3 $m_n^3{}_{(H2)}$/h at 125.6 bar for a desorption time of 20 minutes. The specific heat consumption varies between 2 kWh/$m_n^3{}_{(H2)}$ (at 83. bar) and 2.9 kWh/$m_n^3{}_{(H2)}$ (at 125.6 bar).

1. Introduction

The PHOEBUS project at the Research Centre Jülich demonstrates the autonomous solar electric supply of a large building. The seasonal energy storage is realized in a system consisting of an electrolyser, hydrogen and oxygen storage and a fuel cell (Barthels *et al.*, 1996). At present one third of the plants energy losses are due to the pneumatic piston compressors for the high pressure gas storage. The sorption characteristics of metal hydrides offer the possibility to compress hydrogen using low temperature thermal heat. Exchanging the piston compressor for a hydride hydrogen compressor, which is supplied by solar thermal energy, raises the overall plant efficiency by 5.2 % (Bonhoff *et al.*, 1996).

The theory of operation of a multi-stage hydride-hydrogen compressor has been described by Golben (1983). The minimum number of stages needed to achieve high pressures depends on the metal hydrides used and the temperature levels available. For the application in PHOEBUS $TiMn_2$-based metal hydrides have been chosen to compress the hydrogen up to 120 bar in two stages. The experimental setup of the testing device, the process of operation and the hydrogen flow as well as the specific heat consumption are presented.

2. Experimental setup

2.1. $TiMn_2$-BASED METAL HYDRIDES

T. O. Saetre (ed.), Hydrogen Power: Theoretical and Engineering Solutions, 383–388.

The experiments have been carried out with the $TiMn_2$-based metal hydrides Hydralloy® C15 (Ti 24,6 %, Zr 8.3 %, Mn 48.1 %, V 13.9 %, Fe 3.4 %, Ni 1.8 %) and C0 (Ti 30 %, Mn 52 %, V 14.5 %, Fe 3.5 %). Figure 1 shows the van't Hoff-Plots for desorption and absorption of these alloys.

Taking into consideration the plateau slope of the metal hydrides the hydrogen can be compressed in two stages from 5 to 120 bar having temperature levels of 10 °C for absorption and 100 °C for desorption available.

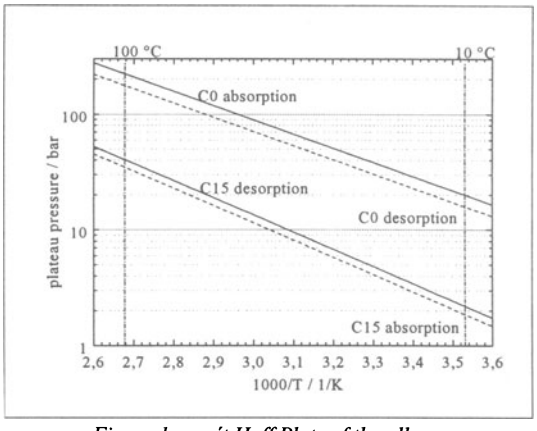

Figure 1: van't Hoff Plots of the alloys Hydralloy® C0 and C15

2.2. SYSTEM CONFIGURATION

Figure 2 shows the system configuration of the testing device allowing absorption of low pressure hydrogen (5 bar) in the first stage (reactors I.1 and I.2) and desorption of hydrogen at high pressures (125 bar) out of the second stage (reactors II.1 and II.2) on the

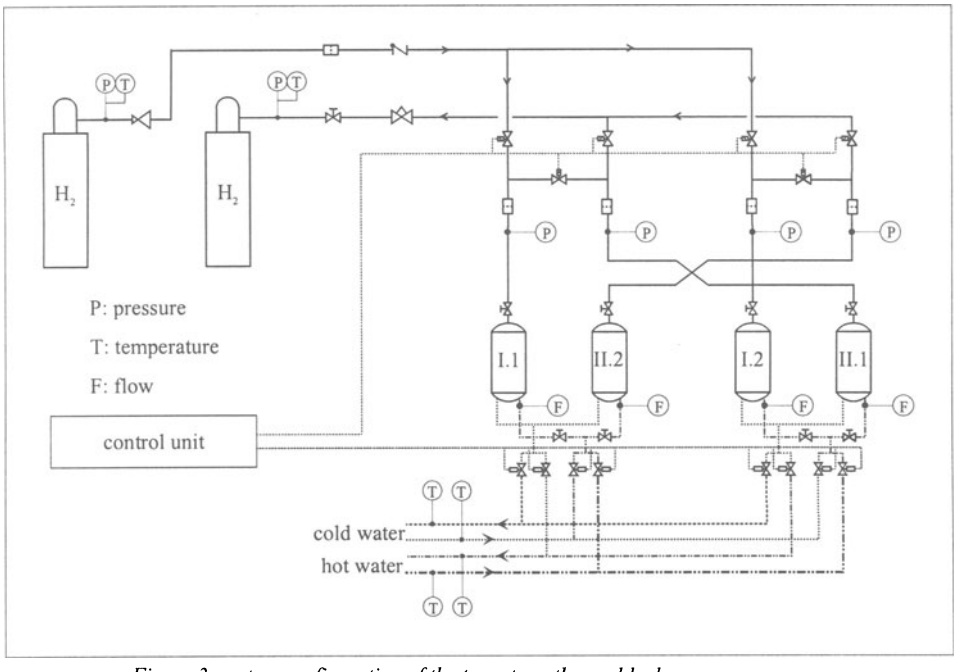

Figure 2: system configuration of the two-stage thermal hydrogen compressor

one hand and desorbing hydrogen out of the first stage into the second stage at a medium pressure on the other hand.

The heat for desorption is supplied by hot water (100 °C) and cold water (10 °C) is used to cool the reactors while absorbing the hydrogen. Automatic operation is provided by a control unit. The temperatures and pressures of the hydrogen and the temperatures of the water are registered by a data aquisition system.

2.3. METAL HYDRIDE REACTORS

With regard to an effective hydrogen compression fast sorption times as well as low costs are the main requirements the reactor has to fulfill. However, mechanical requirements due to the high hydrogen pressure must not be neglected. This means that the walls of the pressure vessels need to have a certain thickness. From this point of view the heat transfer from outside through the reactor walls seems not to be suitable for high pressure metal hydride reactors. To provide an effective heat transfer an inner heat exchanger has been applied with an active heat transfer area of 0.27 m².

Figure 3 shows the design of the metal hydride reactors used. The volume of the reactor is 2.5 l and the total weight is 14.5 kg.

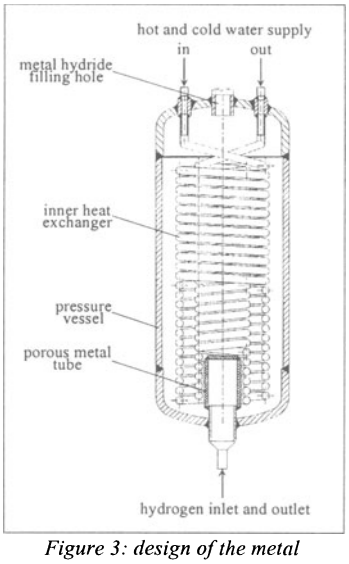

Figure 3: design of the metal hydride rectors

3. Operation of the two-stage thermal hydrogen compressor

The operation of the two-stage thermal hydrogen compressor can be divided in two phases. In the first phase the first stage is cooled and the second stage is heated. This phase is characterized by a pressure rise in the second stage from the medium pressure up to the final desorption pressure. When this high pressure is reached hydrogen is desorbed out of the reactor. At the same time hydrogen is absorbed in the first stage leading at first to a pressure drop and then to a hydrogen flow into the reactor at a constant low pressure. In the second phase the first stage is heated and the second stage is cooled leading to a pressure rise in stage one and a pressure drop in stage two. As soon as the pressure in stage one is higher than the pressure in stage two the valve between the reactors opens and hydrogen will flow from the first into the second stage.

Since each stage is equipped with two reactors (Figure 2) a continous hydrogen flow can be obtained if one reactor of the stage is cooled while the other one is heated.

4. Experimental results

With the system described above experiments have been carried out compressing hydrogen up to a pressure of 125 bar. The absorption of the hydrogen took place at a temperature of 10 °C and a pressure of 5 bar. The desorption temperature was 100 °C. The experiments were performed in order to investigate the influence of the desorption pressure of the second stage and of the desorption time on the overall process. The hydrogen flow as well as the specific heat consumption of the two-stage thermal hydrogen compressor were analysed.

4.1. HYDROGEN FLOW

The hydrogen flow depends on the time needed for the pressure shift in stages one and two as well as on the reaction rates for absorption and desorption. From the amount of hydrogen that is compressed per cycle the hydrogen flow of the overall system can be calculated:

$$\dot{V}_{H_2} = \frac{V_{H_2}}{2 \cdot t_{des}} \tag{1}$$

$\dot{V}_{H_2}$: hydrogen flow,

V_{H_2}: compressed hydrogen (per cycle with two reactors per stage),

t_{des}: desorption time.

Figure 4 shows the hydrogen flow as a function of the desorption time for different desorption pressures.

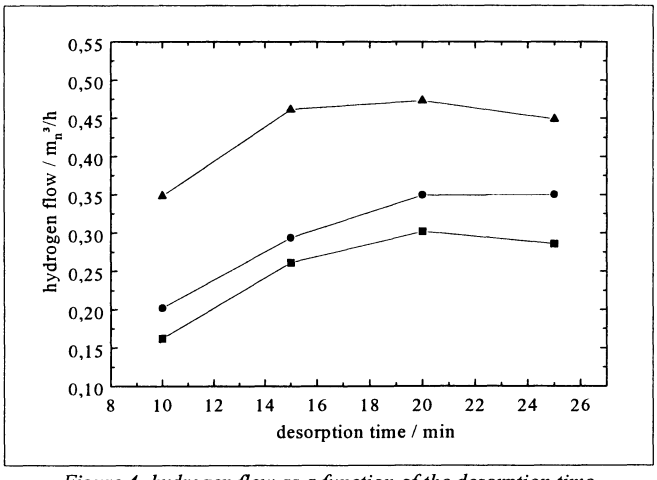

Figure 4: hydrogen flow as a function of the desorption time
absorption temperature: 8 °C; absorption pressure: 5 bar
desorption temperature: 100 °C
desorption pressure: -■- 125.6 bar; -●- 108.8 bar; -▲- 83.4 bar

The influence of the time needed for the pressure shift in the reactors leads to a low hydrogen flow at short desorption times. On the other hand the kinetics get slower the longer the desorption time lasts. Therefore a desorption time can be found where the hydrogen flow is at its maximum. With the current setup a hydrogen flow from 0.47 m_n^3/h at 83.4 bar to 0.3 m_n^3/h at 125.6 bar can be obtained when realizing a desorption time of 20 minutes.

4.2. SPECIFIC HEAT CONSUMPTION

The heat supplied during operation can be derived from the temperature difference between the hot water inlet and outlet:

$$Q = \dot{m}_w \cdot c_{p,w} \cdot \int_0^{2 \cdot t_{des}} \Delta \vartheta(t)\ dt \tag{2}$$

Q: supplied heat (per cycle),
$\dot{m}_w$: mass flow of the hot water,
$c_{p,w}$: specific heat capacity of the hot water,
$\Delta \vartheta(t)$: temperature difference between the hot water inlet and outlet.

The specific heat consumption q is:

$$q = \frac{Q}{V_{H_2}}. \tag{3}$$

Figure 5 shows the specific heat consumption as a function of the desorption

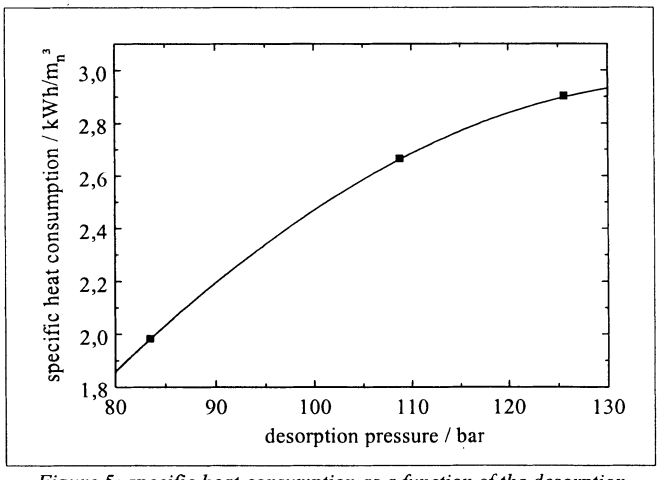

Figure 5: specific heat consumption as a function of the desorption pressure;
absorption temperature: 8 °C; absorption pressure (first stage): 5 bar;
desorption temperature: 100 °C; desorption time: 20 minutes

pressure. The values have been calculated for a desorption time of 20 minutes. The specific heat consumption raises with higher desorption pressures. The values range from 2 kWh/m_n^3 at 83.4 bar to 2.9 kWh/m_n^3 at 125.6 bar.

5. Conclusion

The performance of a two stage metal hydride hydrogen compressor has been investigated. Using a total metal hydride mass of 20 kg ($TiMn_2$ based alloys Hydralloy® C0 (stage 2) and C15 stage 1)) a maximum hydrogen flow of 0.3 m_n^3/h can be obtained at a desorption pressure of 125 bar. In order to optimize the system the influence of the void fraction and of the reactor design on the hydrogen flow needs to be investigated.

The high specific heat consumption needed for the compression is mainly due to the temperature change of the reactor as well as of the metal hydride during cycling. From the energetic point of view it becomes obvious that the low temperature thermal heat needs to be supplied either by solar thermal energy or by industrial waste heat.

6. References

Barthels, H., Brocke, W.A., Bonhoff, K., Groehn, H.G., Heuts, G., Lennartz, M., Mai, H., Mergel, J., Schmid, L., Ritzenhoff, P. (1996) An autonomous energy supply system comprising photovoltaics, electrolytic hydrogen, fuel cell, *Proc. 11th World Hydrogen Energy Conference*, pp. 1005-1015, Stuttgart, Germany, 23-28 June 1996

Bonhoff, K., Barthels, H., A thermal hydrogen compressor based on metal hydrides for an autonomous solar power plant, *Proc. 11th World Hydrogen Energy Conference*, pp. 1323-1328, Stuttgart, Germany, 23-28 June 1996

Golben, P. M. (1983) Multi-stage hydride-hydrogen compressor, *Proc. 18th IECEC '83*, Orlando, Florida, Aug. 21-26, 1983

HYDROGEN ABSORPTION-DESORPTION AND CRYSTALLOGRAPHIC CHARACTERISTICS OF $CeNi_{5-x}Zn_x$ ($x = 0.3 \div 0.85$) INTERMETALLICS

W. IWASIECZKO, I.M.OPAINYCH*, V.V.PAVLYUK*, O.I.BODAK* AND H.DRULIS
W.Trzebiatowski Institute of Low Temperature and Structure Research Wroclaw, Poland
**Department of Inorganic Chemistry, State University Lviv, Lviv, Ukraine*

The hydrides of the $CeNi_{5-x}Zn_x$ ternaries with $0 < x < 0.85$ were prepared and studied as a function of composition, temperature and hydrogen pressure. X-ray diffraction investigations were made. It was found that whereas the pure $CeNi_5$ phase is not a hydrogen absorber its intermetallic solid solutions with a Zn take-up hydrogen effectively. After hydrogenation of $CeNi_{5-x}Zn_x$ alloys their hexagonal $CaCu_5$ -type structure is preserved. The equilibrium pressures measured at room temperature for hydrides with maximum hydrogen content were higher than 0.1MPa .The hydrogen capacity changes almost linearly with Zn concentration in the range studied.

1. Introduction

The hydrides of the intermetallic compounds with a general chemical formula of REB_5 - H (RE -is rare earth elements , B - 3d transition metals like Co and Ni) have been an object of many studies mostly from their application point of view [1]. The most known system among them is the $LaNi_5$ [2]. The partial substitution of lanthanum atoms by much cheaper cerium element in the $La_{1-x}Ce_xNi_5$ system causes the increase of hydrogen content and modifies the equilibrium pressure in the range of the plateau [3]. Unfortunately, the increase of Ce concentration over $x > 0.8$ results in so high equilibrium pressure that it is reasonable to state that stoichiometric $CeNi_5$ compound does not absorb hydrogen at all [4]. In spite of such pessimistic experiences with the materials based on cerium , further works were continued [5] mainly because the cost of cerium as a starting material which is lower than that of the other rare earth . The interesting observation has been made, for instance, that after partial substitution Co for Ni, in the $La_{0.4}Ce_{0.6}Ni_2Co_3$ system, the equilibrium hydrogen pressure can be lowered from 15 to 0.5 MPa [3].
Boring it in mind, we undertook the effort to open the inert $CeNi_5$ compound for hydrogen gas absorption throughout the substitution of Zn metal for Ni . In the investigation of the phase diagram of the Ce- Ni- Zn system the limited solid solution on the base of $CeNi_5$ binary compound has been observed [6] . In this paper we are

T. O. Saetre (ed.), Hydrogen Power: Theoretical and Engineering Solutions, 389–393.

presenting the hydrogenation processes and the pressure-composition isotherms taken for intermetallic solid solution of $CeNi_{5-x}Zn_x$ system with $0 < x \leq 0.85$.

2. Experimental

The intermetallic $CeNi_{5-x}Zn_x$ alloys were prepared by arc melting in argon atmosphere and annealed in quartz ampoules under vacuum at 470 K for 400 h. The purity of starting metals was better than 99.9 %. The powder X-ray diffraction patterns of alloys were obtained by using powder diffractometer DRON-4 (CuKα- radiation). Lattice parameters and crystal structure refinement were calculated by LATCON and Rietveld Analyses Program . Boundary of the solubility of Zn in the $CeNi_5$ was determined from the change of lattice parameters. The structural data together with the structural changes associated with hydrogen absorption will be shown in Table I in the next section.

The synthesis and PTC measurements were performed in quartz ampoules contained in stainless steel chambers of volume 5 cm^3 . The hydrogen gas of the highest purity was obtained from $LaNi_5$ hydride storage. Every sample have been activated first through the vacuum ($p = 5 * 10^{-6}$ Tr) pumping at temperature 670 K for about 4 hours. For each sample studied the initial hydrogenation reaction has been performed at 650 K and at a hydrogen pressure of 2.5 MPa. Prior to the P- T -C readings the samples were generally subjected to five absorption-desorption cycles. After such treatment the samples were able to absorb hydrogen at room temperature. The time needed to reach complete equilibrium in the desorption procedure depended on the sample composition and changed from a few to several minutes. The amount of hydrogen absorbed /desorbed was determined by volumetric method. Honeywell electronic tensometric transducer has monitored the pressure . The X-ray diffraction analysis has been carried out for partly discharged samples only (with H/f.u.$\sim$ 0.4) since the equilibrium pressure at room temperature was too high to perform such experiments for samples with maximum hydrogen content.

3. Results and discussion

The results obtained in this study are collected in Table 1 and Figs.1-3 where the pressure-composition isotherms for samples $CeNi_{5-x}Zn_x$ with x = 0.3 ; 0.6 and 0.85 are presented.

Both *a* and *c* lattice constants determined for the initial intermetallic alloys show a steady increase with Zn content increasing. As it has been proposed by Lundin et al. [4] there should be a correlation between the stability of ternary hydrides and the size of the interstitial holes present in the original intermetallic compounds. For isostructural compounds the trend in the hole size will be similar to that in the unit cell volumes. Therefore, in Table 1 we have also collected the unit cell volumes of the compounds investigated. The X-ray diffraction patterns taken for partly discharged hydrides were indexed in the hexagonal $CaNi_5$ -type unit cell as the uncharged compounds.

Analyzing the pressure-composition data it is seen that there is no plateau pressure in the range considered in these investigations. We can not exclude that the plateau exists in the range of compositions lower than x = 0.4. The composition-pressure isotherms shown in Figs. 1-3 fulfill the Sieviert's law ($p \approx c^2$) characteristic for the interstitial solid solution of the hydrogen in metallic lattices. Nevertheless, the results obtained indicate that the doping of $CeNi_5$ system with Zn leads to the material,

TABLE 1. Hydrogen absorption behavior of $CeNi_{5-x}Zn_x$ alloys.

Alloys	Hydride	lattice constants		V
	H/Me [a]	uncharged	charged [b]	$Å^3$ uncharged
$CeNi_5$	--------	a = 4.875	-	83.0
		c = 4.010	-	
$CeNi_{4.7}Zn_{0.3}$	0.5 (1.5 MPa)	a = 4.901	a = 4.901	83.6
		c = 4.023	c = 4.022	
$CeNi_{4.4}Zn_{0.6}$	0.9 (1.5 MPa)	a = 4.908	a = 4.923	84.4
		c = 4.037	c = 4.053	
$CeNi_{4.15}Zn_{0.85}$	1.3 (1.5 MPa)	a = 4.911	a = 4.919	85.5
		c = 4.053	c = 4.108	

[a] The H/Me ratio correspond of the hydrogen pressure shown in parentheses.
[b] The lattice constants in Å are room temperature values obtained after charging and exposing to normal pressure .

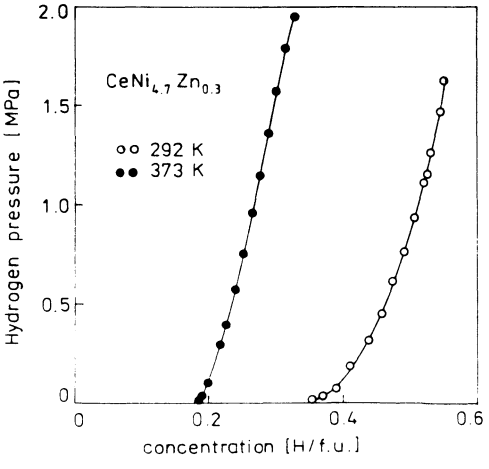

Figure.1.Pressure-composition isotherms of the hydrogen desorption in $CeNi_{4.7}Zn_{0.3}$

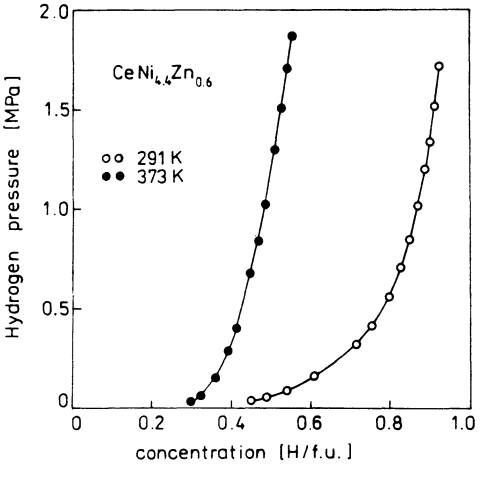

Figure 2.Pressure-composition isotherms of the hydrogen desorption in $CeNi_{4.4}Zn_{0.6}$

which is effectively opened for absorption of hydrogen gas. The dependence of hydrogen capacity on Zn concentration at room temperature is shown in Fig.4 .

The hydrogen absorption capacity almost linearly increases with Zn content and follows the unit volume changes of the initial alloys. The trend shown is consistent with the Lundin's correlation idea that is, the larger the cell volume , the larger hydrogen capacity and lower equilibrium pressure of the corresponding hydride.

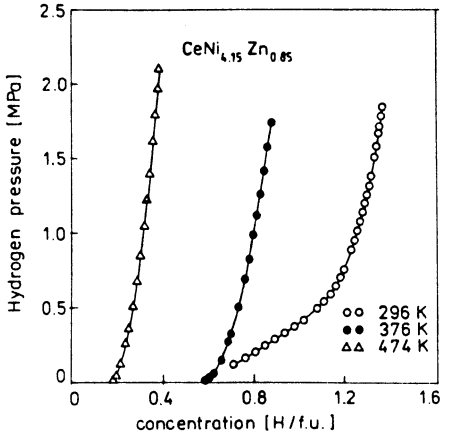

Figure 3. Pressure-composition isotherm of the hydrogen desorption in $CeNi_{4.15}Zn_{0.85}$

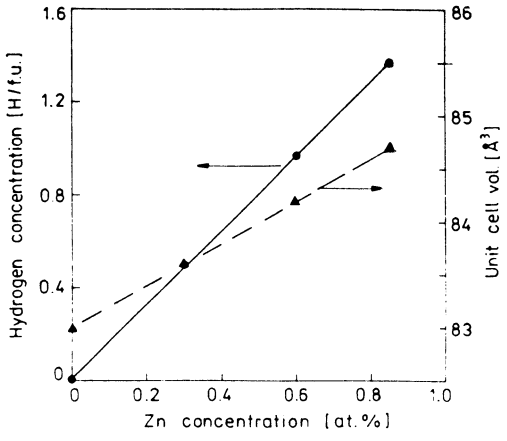

Figure 4. Hydrogen capacity and unit cell volume as a function of Zn content

4. Conclusion

The stability of hydride in a series is mainly controlled by lattice dimensions it is perhaps unwarranted to conclude that the more size of the interstitial site available to hydrogen is the determining parameters in $CeNi_5$ system.

Acknowledgment

This work was partly supported by the Committee for Scientific Research , Grant no.KBN 2 P03B 021 10

5. References

1.Percheron-Guegan, A., Achard, J.C., Sarradin, J., and Bronoel, B.: in Anderson, A.F., and Maeland A.J., (eds.), Proc.Int.Symp.Hydrides for Energy Storage, Geilo, Norway, Pergamon, Oxford, 1978 ,p.485

2. van Vucht, J.H.N., Kuijpers, F.A., and Bruning, H.C.A.: Philips Res.Rep., 25 (1970) 133

3. Huang, Y.C., Tada, M., Watanabe, T., and Fujita, K.: in Veziroglu, T.N., and Seifritz, W.

(eds.), Proc.2nd World Hydrogen Energy Conference, Zurich, Pergamon Press, Oxford, 1979, p.1613

4. Lundin, C.E., Lynch, F.E., and Magee, C.B.J.: J. Less-Common Met., 56 (1977) 19

5. Sinha, V.K., and Wallace, W.E.: J.Less-Common Met., 96 (1984) 283

6. Bodak, O.I., (1997) : (will be published)

THE IMPORTANCE OF SAFETY IN ACHIEVING THE WIDESPREAD USE OF HYDROGEN AS A FUEL

F. J. EDESKUTY
Los Alamos National Laboratory (retired)
Los Alamos, NM, USA

Abstract

The advantages of hydrogen fuel have been adequately demonstrated on numerous occasions. However, two major disadvantages have prevented any significant amount of corresponding development. These disadvantages have been in the economics of producing sufficient quantities of hydrogen and in the safety (both real and perceived) of its use. To date, work has mostly been properly centered on solving the economic problems. However, a greater effort on the safety of new hydrogen systems now being proposed also deserves consideration.

To achieve the greatest safety in the expansion of the use of hydrogen into its wide-spread use as a fuel, attention must be given to four considerations. These are, obtaining knowledge of all the physical principles involved in the new uses, using that knowledge to put in place the regulations that allow the safe interfacing of the new systems, designing and constructing the new systems with safety in mind, and the training of the large number of people that will become the handlers of the hydrogen.

Existing organizations that produce, transport, or use hydrogen on a large scale have an excellent safety record. This safety record comes as a consequence of dedicated attention to the above-mentioned principles. However, where these principles were not closely followed, accidents have resulted. Some examples are cited.

As the use of hydrogen becomes more wide-spread, there must be a mechanism for assuring the universal application of these principles. Larger and more numerous fleet operations with hydrogen fuel may be the best way to begin the indoctrination of the general public to the more general use of hydrogen fuel. Demonstrated safe operation with hydrogen is vital to its final acceptance as the fuel of choice.

T. O. Saetre (ed.), Hydrogen Power: Theoretical and Engineering Solutions, 395–405.

1. Introduction

Hydrogen as a portable fuel is the inevitable replacement for fossil based fuels. A more general introduction of hydrogen fuel should begin soon for three reasons: First, it is necessary to alleviate the continuing insult to the environment caused by present use of fossil fuels. Second, fossil fuels will eventually be exhausted. There is general agreement on this point, but not on the time that the supply will be exhausted. However, fuel supply problems become difficult to accommodate long before the time when fossil fuels are exhausted. The time of peak production capability occurs much earlier than total exhaustion of the source. When the production capacity begins to decrease, then the inequity of distribution of the decreasing supply and competition for what is left become disruptive to society in several ways. Third, the longer the time available for a change-over to a new fuel, the less disruptive and less expensive will be the transition.

2. Barriers to the Large-scale Introduction of Hydrogen Fuel

In the past there have been two major barriers to the large-scale introduction of hydrogen fuel. The first barrier is that of economics. Hydrogen does not naturally occur in its free form to any significant degree. Currently, most hydrogen production is from fossil fuel, which is not a long-term solution to the energy problem. To offer a long-term solution the hydrogen must be produced in a different manner, which is usually at the expense of more energy being used in its production than will be generated in its combustion. To date, most of the work on hydrogen fuel is being expended on finding more economical ways to produce hydrogen, and this effort continues to be useful and necessary.

The second barrier is that of safety. There is a wide-spread apprehension about the safety of hydrogen as a fuel. Probably most of the people at this meeting have personal experiences of the existence of this distrust. I have experienced this distrust of hydrogen on numerous occasions, and the literature continues to mention this concern.[1,2]

As with any fuel, there are legitimate reasons to be concerned about the safety of a new and different fuel. However, by its very nature, any fuel can cause accidents, and a strong case can be made that hydrogen is no more dangerous than any other commonly used fuel. Much of the fear is an over-reaction to past accidents with the consequence that the perceived fear is greater than can be justified and is therefore somewhat irrational. In spite of that fact, the barrier still exists and the successful introduction of the wide-spread use of hydrogen fuel will require education of the general public, a task that can only be effective if the safe handling and use of hydrogen as a fuel are convincingly demonstrated.

3. The Fear of Hydrogen and the Possible Effect upon Future Developments

Until about a half-century ago hydrogen fuel was accepted without any great trepidation. City gas, containing roughly equal portions (by volume) of hydrogen and carbon monoxide, was produced by the action of steam on coke and then the "city gas" was delivered by pipeline to many homes, offices, and commercial establishments for lighting, water heating and cooking purposes. The home of my youth was one such house. Because of the toxicity of carbon monoxide, a case might be made that its presence in the city gas caused more harm than did the hydrogen, by causing deaths both inadvertently and intentionally by suicides by "taking the gas pipe". In any case there was no wide-spread fear of this energy source, and it was universally accepted.

However, one spectacular, high profile accident that was reported in a very emotional manner was that of the airship, Hindenburg. Recently, Bain[3] has made a convincing argument that hydrogen was not the primary cause of that accident. However, the fear lives on. The publicity for that accident, plus references to a "hydrogen bomb", have led to the general public distrust of hydrogen being used as a fuel. The common response to our own work with hydrogen fueled vehicles clearly demonstrated that this distrust still exists.

A similar accident[4] with liquefied natural gas (LNG) in Cleveland, Ohio in 1944 is often blamed for a 20 to 40 year set-back in the development of LNG storage and transport. If the development of hydrogen's use as a fuel is to occur in a timely manner, it can ill afford a further set-back caused by public reaction to any future accidents. Safety, or at least the perception of safety must still be regarded as a barrier to the implementation of a successful hydrogen fuel program. Thus, safety must be a primary concern in all phases of the development of any hydrogen utilization project. The continuing demonstration that hydrogen can be used safely is necessary so that the general public will eventually accept hydrogen fuel as a benefit rather than as a feared hazard.

4. Conditions for Safe Operation with Large-scale Use of Hydrogen Fuel

To achieve the highest degree of safety in a hydrogen operation there are four major considerations that must be taken into account.

4.1. FUNDAMENTAL UNDERSTANDING OF SAFETY REQUIREMENTS

First, for each new application, all of the pertinent physical principles and potential hazards involved in the production, transport, storage, and use of the fuel must be understood. As new uses are proposed, or as applications change, they must be examined to see if new, or different physical principles become important. In some cases, additional experimental investigation could be required.

Incomplete knowledge of the operation of a system is an invitation to disaster. Pilatre de Rozier's experience of combining a hydrogen balloon with a Montgolfier (hot air) balloon provides an example of the problem that can arise from having only a

partial understanding of the physical principles involved in a given situation.[5] De Rozier believed that by having the hydrogen balloon placed above the Montgolfier, thus at a higher elevation than that of the flame of the Montgolfier, there would not be the problem of a fire if the hydrogen were to leak. The lower density of the hydrogen would cause it to rise and travel further away from the flame. It is true that hydrogen's buoyancy is a faster mechanism for the dispersion of the hydrogen than is diffusion. However, convection currents and atmospheric winds can be much more potent dispersion forces then either of the previously mentioned mechanisms. The lack of realization of this fact made de Rozier its victim when there was a hydrogen fire and the balloon crashed, killing De Rozier and his fellow passenger. Thus for the use of hydrogen fuel to become universal and safe, it is first necessary to understand, for each system, all of the physical principals that are involved and also the various ways in which accidents can occur for the specific systems being used. Where the lack of operating data or experience is encountered, further safety research will be required.

4.2. SECOND, REGULATIONS

For safe operation involving different organizations and different nations it will be necessary to have internationally accepted regulations in place that give guidelines for safe design and operation. An important reason for the existence of regulations is to ensure the safety of interfacing one system with another. Systems must be built to be capable of safe interaction between different organizations and across national boundaries. Although there may be more than one safe way to operate an isolated system, for most cases it is necessary that each system be compatible with the other systems with which it must interface.

4.3. THIRD, SYSTEM DESIGN AND CONSTRUCTION

The entire system must be designed and constructed with due consideration to its safety of operation and its compliance with the regulations mentioned in section 4.2. Thus, safety must be the primary consideration from the initial design stage through the entire process of final design, construction and testing of the finished product. Design reviews must be made by people knowledgeable in the possible hazards that can accompany the wide-spread use of hydrogen, and that are not directly involved with the promotion of that particular project. For each new system the application of the techniques of failure modes and effects analysis, or HAZ-OP investigations will be necessary. The degree to which the approach to producing a safe system has been achieved will depend upon the knowledge and understanding developed in the requirement described in section 4.1. In reaching the goal of producing a "safe system" it must be realized that this is a necessary, but not necessarily a sufficient condition for safe operation. The belief that one has built a "fool-proof" device fails to take into account the "ingenuity of fools".

4.4. FOURTH, EDUCATION AND TRAINING

It is necessary to educate, or train the producers, transporters, users, and accident response personnel in the safety of their respective operations. Training must be an ongoing, continuous part of operation. Also training must not merely rely upon each new employee being trained by the current workers. A necessary part of the training must be from a primary source, designed for the particular application. If training is merely passed on from one employee to the next, after several iterations of this procedure there can be great departures from the established safe procedures. On-the-job training can be a valuable part of training, but must be reinforced by fundamental training involving an exposure to the principles that are basic to the safety practices.

Once the general public becomes involved, safety training becomes more difficult. One can see examples of the type of attempt now being made to educate the public in safe operation. One might see a label attached to a ladder stating that the user should not stand on either of the top two steps because "you might lose your balance and fall". This simple solution might be adequate for such an unsophisticated application. However, as the degree of complication, and possible hazard increases, a more significant effort will be required. A more technical example can be found in the widespread sale of automobiles with anti-lock brakes. Experience shows that very little is said to the purchaser of a new automobile about the proper method to apply the brakes under slippery conditions, and that this method is different from previous practice. Lack of such information has led to accidents, and has made it necessary to try to educate the public with television programs. Actually, a better training method would involve instruction to the prospective buyer followed by giving him the opportunity to try out the braking system in a safe way before a panic stop becomes necessary. In the case of hydrogen, it is of particular importance to convince prospective users of the necessity of properly maintaining the hydrogen system. A look at many of the vehicles entering the average self-service gasoline refueling stations gives one cause for concern over what to expect for the maintenance of a hydrogen system.

5. What Can Be Done to Meet These Requirements

5.1. UNDERSTANDING SAFETY REQUIREMENTS

Safety problems continue to exist and as new applications of hydrogen fuel arise, new problems will also arise and require further investigation to understand the potential hazards that the new application of hydrogen fuel might present. Although it is possible to anticipate some facets of the safety of handling hydrogen that need further investigation, it must be remembered that new applications must each be examined to look for additional safety problems that a specific new use of hydrogen might entail. Different applications will favor the use of different types of hydrogen storage. Probably all forms of hydrogen storage will be used in one case or another.

In some cases it will be necessary to examine the effect of hydrogen embrittlement on new materials involved in structural applications in systems using gaseous and/or hydride storage systems. A number of research laboratories are still pursuing the study of hydrogen embrittlement. Problems that might be encountered with systems using liquid hydrogen include cold embrittlement of new structural materials that are subjected to cold temperatures. For each specific system, appropriate purging techniques must be developed for refilling operations as well as for the performance of any maintenance operation requiring disassembly of the system. Inadequate purging procedures have been responsible for a number of hydrogen accidents.[6]

The possibility and consequence of hydrogen leakage should be studied for each new application. Zalosh and Short[6] analyzed over 400 accidents that involved hydrogen. Most of these accidents occurred in industrial facilities during the period from 1965 to 1977. They report that 25% of these accidents were caused by undetected hydrogen leakage. Thus, undetected leakage is one of the most important causes of the accidents that have occurred with hydrogen. The development of inexpensive, and reliable systems for the detection of leakage of hydrogen is important. Several new detection systems are now under development at US National Laboratories and appear promising.[7]

Theoretical studies have been made of the consequences of hydrogen releases.[5,8] Swain[9] has studied experimentally the distribution of hydrogen leakage and the consequent size of a combustible plume that results. The spread of hydrogen after liquid spills has been investigated experimentally by Witkofsky[10] and Schmidchen.[11] These studies are all valuable, and give a good indication of the way hydrogen will disperse after being spilled, or vented into open spaces and also into semi-confined spaces. However each new application might introduce new and different circumstances so that this work can not be considered to be complete.

Because of the ease of ignition of hydrogen and the lack of visible evidence of a hydrogen fire, an investigation should be made of the available fire detection devices and their suitability for the various applications of hydrogen being proposed. An obvious, yet important, consideration is that the detection devices not be a source of ignition themselves. In an unconfined atmosphere the ignition of a hydrogen-air mixture as a simple combustion (or deflagration) generally does not cause much damage to anything not directly in the flame area. Overpressures that result usually are not very high. However, if confined, very destructive pressure can be produced even from a simple deflagration. Zalosh and Short[6] found that hydrogen explosions have been more serious than other hydrogen accidents when considering casualties, property damage, and number of incidents. The destructive power of a hydrogen explosion becomes much greater if the combustion occurs as a detonation. The conditions necessary for the transition from deflagration to detonation are understood. However, the environment through which the flame will travel can influence the progress of the flame as it encounters obstructions that could induce turbulence in the flame and thus increase its velocity and tendency for transition from deflagration to detonation.

5.2. REGULATIONS

There are numerous safety guidelines, codes, standards, and regulations that address, either directly or indirectly, the safe handling of hydrogen. In the USA, the overriding safety requirements for hydrogen are in the Code of Federal Regulations (CFR). In some places the CFR specifically addresses hydrogen, and in other places the inclusion of hydrogen is by inference. In some places sections of various standards, such as those of the ASME or the ANSI, are written into the code. In other places these standards are included by reference. The individual states, or even cities or other localities can have additional restrictions, but this is not too common. Other countries have similar regulations that are suited to their particular needs.

Hydrogen applications have already become international in character. Fortunately the International Organization for Standardization (the ISO) has already begun the process of writing the international standards that must be available to ensure safety in the pursuit of international projects by forming a technical committee, ISO/TC 197, Hydrogen Technologies. The Bureau de Normalisation du Quebec, on behalf of the Canadian ISO member, the Standards Council of Canada, has taken over the responsibility of secretariat and the scope of the committee has been expanded to include "Standardization in the field of systems and devices for the production, storage, transport, measurement and use of hydrogen". The committee wishes to ensure that all countries become aware of, and become interested in its work because the final standards will have world-wide influence. Twelve countries are members with active participation including the right to vote, to attend meetings, and to appoint experts for the working groups that will prepare drafts of the standards. Sixteen other countries are also committee members as observers with the right to attend meetings and give comments.

To date, six working groups (WG) have been formed and are formulating standards addressing hydrogen safety. WG-1/2 consists of 12 experts appointed by members from Canada, Germany, Japan, Switzerland, and the USA. These groups are convened by Dr. Robert Hay of Canada. WG-1 has been working on Standard #13984, Liquid Hydrogen - Land Vehicles Fuelling System Interface and on Standard #13985, Liquid Hydrogen - Land Vehicle Fuel Tanks. WG-2 is working on Standard #13986, Tank Containers for Multimodal Transportation of Liquid Hydrogen. WG-3 consists of 7 experts appointed by members from Canada, Japan, Republic of Korea, and the USA and is convened by Mr. Addison Bain of the USA. WG-3 is working on Standard #14687, Hydrogen Fuel - Product Specification. WG-4 consists of 6 experts appointed by members from Canada, Germany, Japan, and The Russian Federation and is convened by Mr. Norbert Rostek of Germany. WG-4 is working on Standard 15594, Airport Hydrogen Fuelling Facility. WG-5 will be convened by Mr. James Hansel of the USA and will work on Hydrogen and Hydrogen Blends Vehicular Fuel Systems. WG-6 will be convened by Mr. Robert Zalosh of the USA and will work on Gaseous Hydrogen Vehicle Fuel Tanks. One more working group, WG 7, has been proposed to consider the topic of Basic Requirements for the Safety of Hydrogen Systems. [12,13]

It takes about three years to process a standard, so it is fortunate that these present efforts are underway.

5.3. SAFE DESIGN OF SYSTEMS

A great deal of advice that is helpful to the designers of new systems is available in the literature.[4,5,14-16] Safety must be considered and be a part of any new proposal for the production, storage, transport, or use of hydrogen. Safety analysis must be done anew to specifically address each new system. Such techniques as failure modes and effects analysis, or HAZ-OP methods must be included. There is a need to understand the causes and consequences of accidents and design the system to avoid accidents and to allow remedial actions to mitigate their consequences. Where two or more competing systems are proposed to solve the same problem, a safety analysis can give valuable guidance to assigning priorities for their development.

5.4. EDUCATION AND TRAINING

The importance of education and training of the workers that handle the hydrogen can not be overemphasized. The cause of the accidents to be discussed in section 6 can be directly attributed to the lack of training of the workers involved.

Ordin[17] analyzed 96 accidents and incidents involving hydrogen that occurred at the US National Aeronautics and Space Administration (NASA) facilities and those of NASA contractors. In 80 of these incidents there was some release of either gaseous of liquid hydrogen. In 25 of these releases there was no ignition of the hydrogen. Of the total accidents, about half were attributed to causes that were procedural or operational. Examples of these causes include such actions as failure to follow established procedures, not having proper procedures, and improper purging. In most cases better training of the operators might have prevented these accidents. Ordin suggested the requirement that operation must be based on knowledge of the potential hazards of hydrogen and personnel education in these potential hazards as well as technical knowledge of the system.

Careful attention to training of personnel can result in safe operation. An example of effective training is that used by Air Products and Chemicals, Inc.[18] Their standard practice for drivers that deliver liquid hydrogen is 18 hours in the classroom, 3 hours of video training, and about two months of on-the-job training. This is supplemented by systematic retraining and review programs. The excellent safety record of their transport and distribution of liquid hydrogen testifies to the success of this training.

In principle, fleet operation of hydrogen vehicles should also be able to attain an excellent safety record. The question must be asked, what can be done to assure similar care in operation by the general public if the use of hydrogen fuel is to become universal? Perhaps the best way to start is the publicizing of the precautions being taken in successful and safe fleet operations. Once there is a widespread general knowledge of the safe practice of using hydrogen fuel, the training of users before they take possession of a system should be mandatory. Additional measures might be necessary for controlling the resale of hydrogen powered vehicles. The large percentage of hydrogen accidents that is caused by hydrogen leakage makes it important that all potential users become aware of the requirement for excellent

maintenance of hydrogen containing systems. Obviously the methods of assuring safe operation and satisfactory maintenance of hydrogen powered vehicles used by the general public require thorough investigation.

6. Hydrogen Accidents

Although the large-scale handling of hydrogen has an excellent safety record, some accidents have occurred. Frequently these accidents can be attributed to inexperience of operators, or in their failure to follow established procedures.

In one laboratory with very little experience in handling hydrogen, workers were investigating the Charpy impact strengths of metal specimens at liquid hydrogen temperature (20 K or -253 °C). They carried out the experiment by starting with the specimen immersed in an open Dewar of liquid hydrogen. As the pendulum was released but before it had fallen far enough the contact the test specimen, the Dewar was lowered to expose the sample to the path of the pendulum. The workers did not realize that the open Dewar would allow solid air to condense in the liquid hydrogen, and that as the cold specimen was exposed to the atmosphere it would also liquefy air that would then drop into the liquid hydrogen. An explosion resulted, injuring the technician that was performing the experiment. The consequences could have been much worse.

In another case a shed had its sides blown off when a valve was opened into a line from a gas storage container containing hydrogen gas at 225 atm (2.25 MPa) pressure. Upstream of the valve that was opened there were two other closed valves also believed to be closing off the high pressure hydrogen. However, these valves had leaked hydrogen into the intervening line in large enough quantity that when flowing into the shed it could create a combustible atmosphere. There were numerous ignition sources within the shed and an explosion resulted. There were several people working inside the shed at the time of the explosion, but fortunately, the injuries were limited to some ruptured ear drums and one broken heel.

In another case, an inexperienced operator connected a hydrogen tube trailer to the same manifold as an oxygen tube trailer. This was followed by a series of errors that led to oxygen (coming from a tube at a pressure of 120 atm, or 12 MPa) flowing into the hydrogen tube (initially at a pressure of 15 atm, or 1.5 MPa). The resulting deflagration transited to a detonation, rupturing the tube and throwing fragments of the vessel as far as 350m. Fortunately, no injuries were caused by the fragments, but two workers suffered serious burns.

Adequate training and the existence of well understood procedures would have prevented all of the above accidents.

7. Conclusion

There is no question that hydrogen can be handled safely. In spite of the above-mentioned incidents, the overall safety record of hydrogen production, transport and usage attests to the fact that the above conditions for safe operation are well met at the present scale of handling hydrogen.

An example can be found in the liquid hydrogen transportation industry.[18] Air Products and Chemicals, Inc., the largest distributor, has not lost any liquid in over 25 years, in spite of the fact that vehicle accidents have occurred. The company delivers annually about 250 million standard cubic meters (9 billion cubic feet), 92% of which is as liquid, involving 14,000 deliveries. Their trucks cover about 8 million miles per year, and on a given day there are about 70 trucks en route.

However, in industrial operation the number of people involved is limited, the operators are well trained, and rigid maintenance schedules are followed. What will happen as many more people become involved in the use of hydrogen? Some proposals for hydrogen fuel involve non-technically trained, average citizens being able to produce hydrogen in a garage and then use it to fuel a personal automobile. One could imagine parking structures with hundreds of such vehicles in closed areas. The previously cited accidents show that often people do not wait to learn what dangers exist before acting. Improvising remedies for unexpected situations can be especially disastrous, and the importance of good maintenance is paramount.

Conditions for the introduction of a new technology are different now from what they were when gasoline fuel was introduced. It would be interesting to try to anticipate the difficulty of introducing gasoline as a fuel today if it were not already accepted and in use. Many of the hydrogen accidents that have occurred can be attributed to inexperience of operators, or in their failure to follow established procedures. If future users are sufficiently well trained and if they are dedicated to following well established safety practices, the acceptance of hydrogen fuel can be more easily and quickly accomplished. Major incidents that cause injuries and property damage will delay the much needed impact of hydrogen fuel on our energy systems.

The record shows that hydrogen can be handled safely, although this has not always been the case. Will it be safely handled in the future? The successful transition to its larger scale use as a fuel depends upon how safely it is used. Obviously it will first be necessary to introduce hydrogen fuel to fleet operations where there can be better control, better training of operators, and better adherence to maintenance schedules. If such operations can demonstrate a sufficient degree of safety for a long enough period of time, then these safety principles will diffuse into the public consciousness and a more general usage can be attempted.

In conclusion, for hydrogen to be widely accepted as the fuel of choice to replace gasoline and other fossil based fuels, the new hydrogen systems must be safe, and also must be convincingly demonstrated to be safe.

8. References

1. Schmidtchen, U., Gradt, Th., and Wursig, G. (1933) Safe Handling of Large Quantities of Liquid Hydrogen, *Cryogenics*, **33**, No. 8, 813-817.
2. Cannon, J. S. (1996) Safety First! H_2's Double Standard, *NHA Advocate*, **1**, No.3, 1-3.
3. Bain, A. (1997) The Hindenburg: Separating Myth from Reality, National Hydrogen Association Press Release, Washington, DC.
4. Zabetakis, M. G. (1967) *Safety with Cryogenic Fluids*, Plenum Press, New York.
5 Edeskuty, F. J. and Stewart, W. F. (1996) *Safety in the Handling of Cryogenic Fluids*, Plenum Press, New York.
6 Zalosh, R. G. and Short, T. P. (1978) Compilation and Analysis of Hydrogen Accident Reports, Factory Mutual Research Corporation Report FMRC J.1 4A7NO.RG to the US Department of Energy.
7 Haberman, D. (1997) Advances in Sensor Technology May Expand Hydrogen Applications, *NHA Advocate*, **2**, 1-2.
8 Hansel, J. G., Mattern, G. W., and Miller, R. N. (1993) Safety Considerations in the Design of Hydrogen-Powered Vehicles, *Int. J. Hydrogen Energy* **18**, No. 9, 783-790.
9 Swain, M. R. and Swain, M. N. (1992) A Comparison of H_2, CH_4, and C_3H_8 Fuel Leakage in Residential Settings, *Int. J. Hydrogen Energy* **17**, No. 10, 807-815.
10 Witcofski, R. D. and Chirivella, J. E. (1984) Experimental and Analytical Analysis of the Mechanisms Governing the Dispersion of Flammable Clouds Formed by Liquid Hydrogen Spills , *Proceedings of the World Hydrogen Energy Conference IV*, Pergamon Press, Elmsford, New York.
11 Schmidtchen, U., Marinescu-Pasoi, L., Verfondern, K., Nickel, V., Sturm, B., and Dienhart,B. (1994) Simulation of Accidental Spills of Cryogenic Hydrogen in a Residential Area, *Cryogenics* **34**, 401-404.
12 Bain, A. (1997) personal communication
13 Allard, D. (1997) personal communication
14 Timmerhaus, K. D. and Flynn, T. M. (1989) *Cryogenic Process Engineering*, Plenum Press, New York.
15 Barron, R. F. (1985) *Cryogenic Systems*, Oxford University Press, New York.
16 Scott, R. B., Denton, W. H. and Nicholls, C. M., eds. (1964) *Technology and Uses of Liquid Hydrogen*, Pergamon Press, Oxford.
17 Ordin, P. M. (1974) Review of Hydrogen Accidents and Incidents in NASA Operations, NASA Technical Memorandum NASA TM X-71565, NASA Lewis Research Center, Cleveland, Ohio.
18 Ringland, J. T. (1994) Safety Issues for Hydrogen Powered Vehicles, Sandia Report SAND94-8226, Sandia National Laboratories, Albuquerque, NM.

AN ECONOMICAL HYDROGEN DETECTOR FOR PASSENGER VEHICLES

P.L. SPATH
National Renewable Energy Laboratory
1617 Cole Blvd.
Golden, CO 80401 USA

D. BENSON
National Renewable Energy Laboratory
1617 Cole Blvd.
Golden, CO 80401 USA

A cost-effective hydrogen detector system is needed for detecting leaks associated with hydrogen fueled passenger vehicles. Work at the National Renewable Energy Laboratory (NREL) involves the development of a reversible, thin-film, chemochromic hydrogen sensor that can be applied to the end of a polymer optical fiber but is likely to have other applications. The sensor is being designed for use in hydrogen fueled passenger vehicles. Currently available hydrogen sensors require electrical wiring and any electrical fault at the location of a sensor could cause ignition when a hydrogen leak occurs. The current NREL sensor consists of a thin-film reflector at the end of a low-cost polymer optical fiber, thus eliminating electrical wiring and thus, an ignition source.

A prototype is being developed which will demonstrate the overall fiber-optic hydrogen detector system. Light from a central source will be transmitted along a fiber to the sensor and reflected back to a detector. The presence of hydrogen at the sensor causes a decrease in the reflected light signal which is proportional to the concentration of hydrogen in the vicinity of the sensor. A novel optical design provides a reference signal that is unaffected by any hydrogen at the sensor. The ratio of the hydrogen signal and the reference signal is used to provide a stable indication of the presence of hydrogen, and is virtually unaffected by changes in the transmission characteristics of the optical fiber and its couplings or by changes in the light source. The signal will then be used to close a valve(s), sound an alarm, light a warning light, turn on a fan etc. in the event of a hydrogen leak. The response(s) required will be determined by the location and concentration of the hydrogen leak. An initial estimate of the overall cost of this fiber-optic hydrogen detector system in a passenger vehicle was completed in 1996 and updated in 1997. A discussion of the fiber optical hydrogen detector system and the resulting economics are presented.

T. O. Saetre (ed.), Hydrogen Power: Theoretical and Engineering Solutions, 407–412.

1. Introduction

This work involves the development of a reversible, thin-film, chemochromic hydrogen sensor. The sensor is being designed for use in hydrogen fueled passenger vehicles. Currently available hydrogen sensors require electrical wiring and any electrical fault at the location of a sensor could cause ignition when a hydrogen leak occurs. The current NREL sensor consists of a thin-film reflector at the end of a low-cost, multi-mode, polymer optical fiber, thus eliminating electrical wiring and the possibility of a fire. A light beam is transmitted along the fiber to the sensor then reflected from the end of the fiber back to a light detector. The presence of hydrogen at the sensor causes a decrease in the reflected light signal indicating the presence and concentration of hydrogen in the vicinity of the sensor. Chemochromic films have been prepared by thermal evaporation onto glass and polymer substrates. Work with these substrates has progressed in optimizing the speed of response and the hydrogen selectivity in the presence of hydrocarbon gases. The optimized coating design of the substrates is being applied to the ends of polymer optical-fiber sensors.

A prototype is being developed which will demonstrate the overall fiber-optic hydrogen detector system. Light from a central source is transmitted along a fiber to the sensor and reflected back to a detector. A novel optical design provides a reference signal that traverses the length of the optical fiber, but is unaffected by any hydrogen at the sensor. The ratio of the hydrogen signal and the reference signal is used to provide a stable indication of the presence of hydrogen. The ratio is virtually unaffected by changes in the transmission characteristics of the optical fiber and its couplings or by changes in the light source.

2. Analysis

An initial estimate of the overall cost of a fiber-optic hydrogen detector system in a passenger vehicle was completed in 1996 and the analysis was updated in 1997. The system design is based on the initial prototype that is currently being constructed at NREL. The design of the hydrogen detector system and its components are depicted graphically in Figure 1. The following production scenarios were examined: 6 sensors/vehicle and 20 sensors/vehicle for a production rate of 5,000 vehicles/year and for 3 million vehicles/year. The actual number of sensors required per vehicle will depend on the size of the vehicle and the layout of the hydrogen fuel system. Two microprocessors, with different cycling speeds, were also examined; it is anticipated that the low cost microprocessor will be adequate for monitoring hydrogen detection. The initial cost estimate showed the light source to be the largest cost driver in all scenarios studied ranging from 27.4% to 58.9% of the overall detector system cost. Therefore, in 1997 the analysis was re-done using light emitting diodes (LEDs) instead of a halogen light source. The only difference between the two system designs is that in the original design one 20 W halogen light supplied light for all of the sensors in the vehicle and now the halogen light is replaced with one LED per sensor. The halogen light source including the housing reflector array, and regulating circuitry costs $40/vehicle for each of the 4 scenarios studied. However, by using LEDs

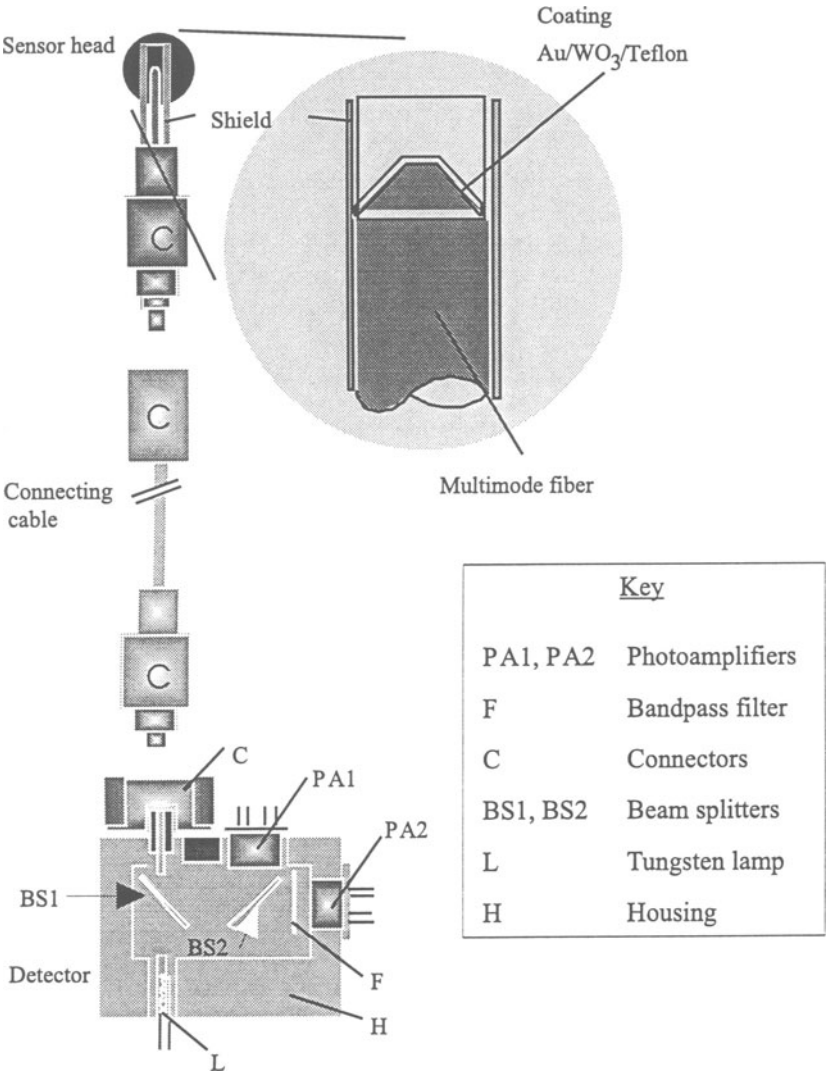

FIGURE 1. Prototype Fiber-Optic Hydrogen Gas Detector

the cost for the light source and any necessary circuitry such as switching transistors is reduced to $3 - $10/vehicle.

2.1 EQUIPMENT REQUIREMENTS

The equipment required for coating the fiber ends includes a polisher to produce a flat edge on the top and angles on the side of the plastic optical fiber and a thermal evaporator to coat thin films on the polished fiber. The current NREL sensor design consists of a thin layer of gold, followed by a layer of transparent, amorphous tungsten oxide covered by a very thin reflective layer of palladium. Cost estimates were made using these three metals and the following coating thicknesses: gold, tungsten oxide, and palladium at 50 nm, 10 nm, and 1 nm, respectively. It should be noted that these thickness have not been optimized and it is possible that palladium may not be required or that a different protective coating will be used on the end of the fibers.

The thermal evaporator used in this analysis is the Temescal BJD-1800 Vacuum Deposition System. It is anticipated that this thermal evaporator will be able to coat 2,700 fibers at a time at 1 hour per cycle. The parts and accessories required for the thermal evaporator include: a vacuum chamber (18" diameter), instrumentation, a standard mechanical pump, a cryopump and controls, an electron beam sweep controller, an electron beam power supply, a film deposition controller, an electron beam source (triple crucible for coating three materials consecutively), and two fiber optic holders each holding a minimum of 2,700 fibers.

For this analysis, it was assumed that one polisher could polish 25 fibers at a time at a rate of 25 fibers per 30 minutes. This is based on a mass production polisher by Nanometer Technologies which has recently become commercially available. The initial cost estimate performed in 1996 assumed that only 10 fibers could be polished at one time. This basis was used at that time because most of the fiber polishers available from manufacturers could typically polish only 1 fiber at a time with the possibility that a maximum of 12 fibers could be polished simultaneously with some adaptation to the machine.

2.2 COSTS USING LEDs AS LIGHT SOURCE

The following two tables summarize the overall detector system cost using LEDs as the light source for each scenario studied and a break down of the component costs. Note that these costs are the costs of manufacturing and assembling the system i.e., a profit or return on investment is not included. Table 1 shows the total costs for the 4 production scenarios studied and includes the cost reduction from the initial design which utilized the halogen light source and polishing of only 10 fibers per machine. Table 2 summarizes the cost of all the individual components used to build the overall fiber-optic hydrogen detector system.

TABLE 1. Total Detector Cost Using LEDs

detectors/ vehicle	microprocessor	5,000 vehicles/year	% cost change	3 million vehicles/year	% cost change
6	low cost	$11.68/detector $70.10/vehicle	-34.55	$5.53/detector $33.20/vehicle	-52.99
	high cost	$13.18/detector $79.10/vehicle	-31.87	$6.85/detector $41.12/vehicle	-47.90
20	low cost	$7.04/detector $140.80/vehicle	-22.72	$4.30/detector $86.00/vehicle	-25.62
	high cost	$7.54/detector $150.80/vehicle	-21.54	$4.65/detector $93.00/vehicle	-24.12

TABLE 2. Breakdown of Component Costs

Component	**Cost**
light emitting diodes and circuitry	$0.50/ sensor
1 x 2 splitter (2 per sensor)	$0.50 each
connectors (1 at the end of each sensor)	$0.20
silicon photodiodes (2 per sensor)	$0.40 - 0.75/ two
multiplex and support circuitry (for a set of 2 photodiodes)	$0.60 - 1.00
module housing and module printed circuit board (cost includes soldering)	$2.00 - 4.00
plastic optical fiber (average of 10 feet of fiber in three pieces/sensor)	$0.90 - 1.50/ three pieces
microprocessor	$1.00 - 2.00 (low) $8.00 - 13.00 (high)
sensor cost	$0.04 - 2.34/ sensor

In the system design, one LED per sensor dispenses a light signal through the plastic optical fibers to one sensor. The light reflected back from each sensor is split into two portions (wavelengths) based on the flat top and angled sides design at the end of the fiber. The sensor sends back the following two reflected light beams: one from the flat part of the sensor head which is the reference light beam and one from the angled part which is the hydrogen detection light beam. These two beams are separated and sent to two different photodiodes. The two voltages from the photodiodes will be ratioed to obtain a stable hydrogen response signal. The ratio of the two signals cancels the variation in transmission along the fiber path producing a stable indication of the presence of hydrogen. This detection will then be used to close a valve(s), sound an alarm, light a warning light, turn

on a fan etc. in the event of a hydrogen leak. The response(s) required will be determined by the location and concentration of the hydrogen leak.

Two pie charts are presented in Figure 2 for the production scenario of 6 sensors/vehicle for 3 million vehicles/year for both the initial design (Halogen light and polishing 10 fibers) and the updated design (LEDs and polishing 25 fibers). The cost breakdown for each of the components shown in the pie charts is a percentage of the total detector system cost. The relative sizes of the two pie charts demonstrate the cost difference in the overall detector costs of the two systems.

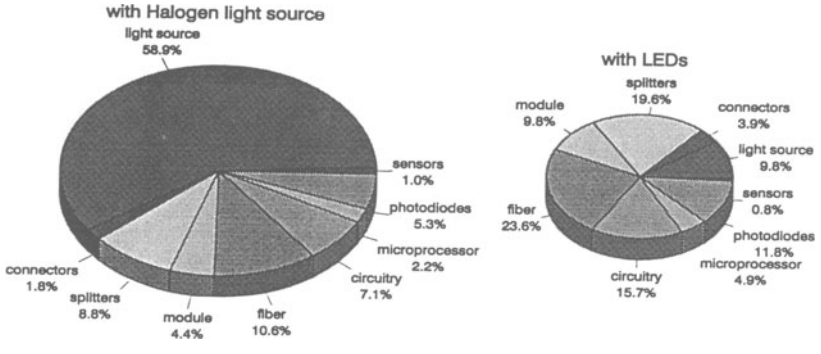

FIGURE 2. Breakdown of Detector System Costs
for 6 sensors/vehicle @ 3 million vehicles/year

3. Conclusions

The initial analysis performed in 1996 showed that the light source was the largest cost driver in all scenarios studied ranging from 27.4% to 58.9% of the overall detector system cost. This cost was reduced by replacing the halogen light with one LED per sensor. The analysis was re-done in 1997 to include the costs for the new light source as well as increasing the fiber polishing from 10 fibers per machine to 25 fibers per machine. The costs are now more evenly distributed among the various components: light source, microprocessor, fibers, module, circuitry, photodiodes, connectors, splitters, and sensors. The total system costs for the 4 scenarios studied (6 sensors/vehicle and 20 sensors/vehicle for a production rate of 5,000 vehicles/year and for 3 million vehicles/year) range from $4.30/detector to $13.18/detector and $33.20/vehicle to $150.80/vehicle. This cost range is still much lower than the cost of existing hydrogen sensing devices which range from $27 - $3,900/sensor and these are the sensor costs only. They do not include additional costs required for an integrated system.

4. References

Mann, M.K., Spath, P.L., and Kadam, K. (1996) *Technoeconomic Analysis of Renewable Hydrogen Production, Storage, and Detection Systems*. Proceedings of the 1996 U.S. DOE Hydrogen Program Review. Volume I. May 1-2, 1996. Miami, Florida.

SET-UP OF HY-TU VIEW APPARATUS FOR HYDROGEN TURBULENT FLAME STUDY - FIRST EXPERIMENTS[1].

M. CARCASSI, G. GIUSTI, F. PILO

Dipartimento di Costruzioni Meccaniche e Nucleari - Università di Pisa
Via Diotisalvi 2, 56126 Pisa - Italy
Tel +39-50,585254 Fax +39-50,585265 E-mail carcassi@ing.unipi.it

1. Introduction

In last 20 years at the Department of Mechanical and Nuclear Construction (DCMN) of the University of Pisa, many theoretical and experimental research investigations have been done in the area of hydrogen risk in nuclear power plants [1,2,3,7].

Experimental investigations have been performed relative to the study of hydrogen distribution in closed volumes, hydrogen combustion behaviour in confined and in vented volumes, the influence on combustion of some different parameters, such as internal fans, spray, igniter positions.

In addition, theoretical studies have been performed which are related to the development of computer codes able to study the behaviour, in volumes with venting, of the combustion and to permit some evaluation of turbulent combustion velocities observed during tests [4,6].

Recently, the European Community has accepted two different projects, where the DCMN is coordinator: the first one is named HYMI (Improved Modelling of Turbulent Hydrogen Combustion and Catalytic Recombination for Hydrogen Risk Mitigation), and the second one is named VOASM (Validation of A Simulation Methodology for Hydrogen Mixing, Catalytic Recombination and Deliberate Combustion).

An important objective of the HYMI project is to define the mono-dimensional relation of flame propagation with interactions between turbulence and chemical reactions which are present during combustion.

In particular, the new facility HY-TU VIEW permits the observation of all flame propagation which occurs inside the two compartments of the vessel during a hydrogen deflagration.

2. HY-TU VIEW facility

The HY-TU VIEW facility (Figure 1.) has been designed and built to study deflagration of hydrogen-air mixtures, and in particular, to understand turbulent flame

[1] Work performed under contract FI4S-CT96-0017 of the EU and MURST contribution.

T. O. Saetre (ed.), Hydrogen Power: Theoretical and Engineering Solutions, 413–418.

propagation, including slow deflagration, turbulent flame acceleration, and flame-obstacle interaction.

The new apparatus is similar to previous one (LargeVIEW[4,5]), but with some improvements.

The most important parts are: the vessel, the internal homogenizer system, the hydrogen concentration monitor system, and the LDA measurement system.

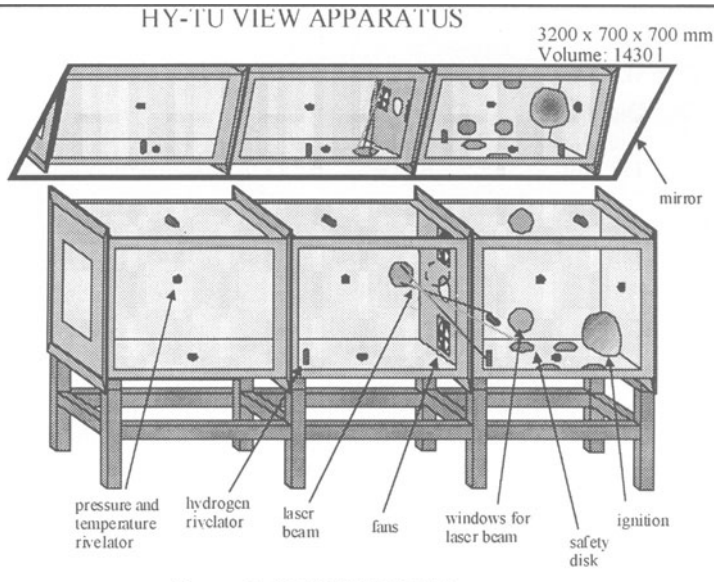

Figure 1. HY-TU VIEW Apparatus

The vessel has been built to withstand a maximum overpressure of 300 kPa.

The frontal and upper panels are made of high strength multi-stratified glass (with a thickness of 40 mm); the other panels are made of reinforced steel.

One of the lateral plate is provided of a large opening to permit discharge of burned gas during deflagration.

A steel screen has been employed to divide vessel in two parts.

The screen has a ventilator system to homogenize the vessel mixture, also it has a central hole to connect the chambers and permit the flame to pass from the first to the second chamber.

A very important problem is to obtain a homogenized hydrogen-air mixture prior of ignition; in fact a non homogenized hydrogen-air mixture can cause flame acceleration not foreseen in the theoretical models and codes used to study this combustion transient in the nuclear reactor field.

Two fans, fixed in the central screen, with opposite rotation directions, have been used in order to obtain a forced circulation of the mixture inside the vessel as shown in Figure 2.

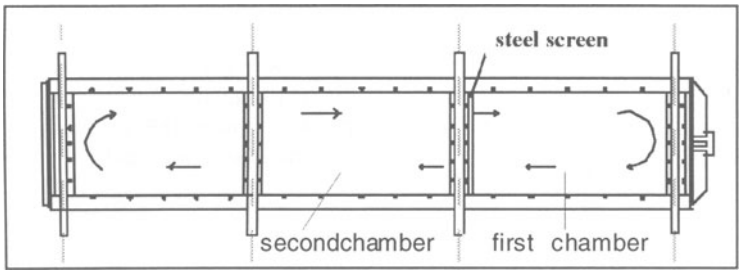

Figure 2. Recirculating paths induced by fans inside the apparatus

To increase the safety level during tests with the HY-TU VIEW facility, a hydrogen monitor system is planned. In particular, six gas rivelators have been built and are placed inside the vessel in the two chambers.

The rivelator's behaviour is based on differences in the thermal exchange coefficient between stainless steel heated by electrical current and the external environment.

Signal variations permit determining the hydrogen concentration inside the vessel and, in particular, to understand if the hydrogen concentration is uniform and homogeneous in all parts of the vessel.

An example of gas rivelator signal is indicated in Figure 3. where is possible distinguish the following phases:

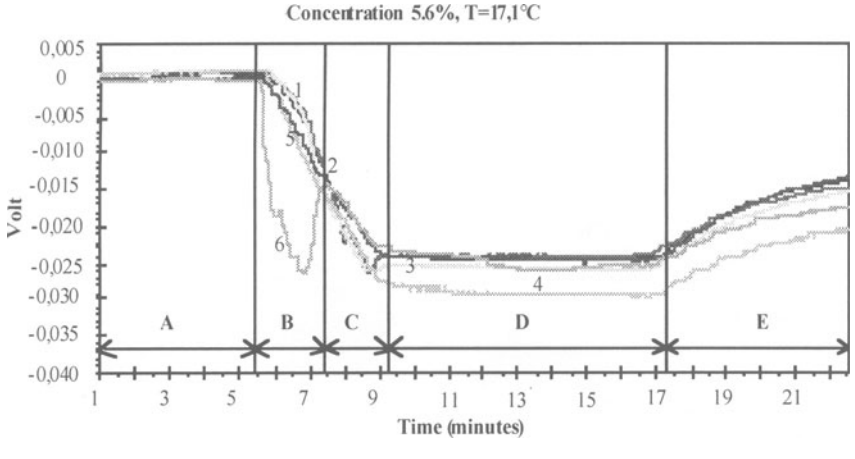

Figure 3. Signal behaviour of the six hydrogen rivelators during the immission phase

A Initial equilibrium condition without hydrogen
B First chamber hydrogen immission
C Second chamber hydrogen immission
D Equilibrium concentration with active ventilation system
E Equilibrium condition without ventilation system

Similar signal behaviour from all rivelator during the phase D and E indicate quite uniform concentration inside vessel hydrogen.

The first chamber of the vessel has four windows to permit use of an LDA system. In particular, an argon laser is used to measure flame turbulence.

Four laser beams are concentrated at a specific point of the internal volume; at this point are measured velocities and relative variations of NaCl and TiO particles along the horizontal and vertical axes.

3. Experimental programme

To date, about 140 tests has been performed with the HY-TU VIEW facility. Parameters which are changed during tests are: hydrogen concentration (9, 9.5 and 10%), ignitor position and optic position for LDA measurements.

Test analysis is still in process. Therefore, presented here are the results of one test (test 30T) as an example of flame behaviour analysis.

Test 30T conditions are: hydrogen concentration 10%, ignitor position E.B.(End Bottom), laser position in the upper part of the first chamber.

Figure 4. shows four frames of the flame behaviour during the test.

Pressure behaviour during the test inside the chambers is illustrated in Figure 5.

In this test, jet-ignition phenomena cause a rapid pressurization of the second chamber, which produces a new pressure increase inside the first chamber (recoil phenomena).

Figure 6. provides some first results about particles velocities measured by LDA.

From a preliminary analysis is possible to measure the increase of the velocity of particles along the main flame development direction.

In particular it is clearly showed the time where the flame reach the laser beam; in this time the NaCl particles disappears and the LDA measure only the TiO particles.

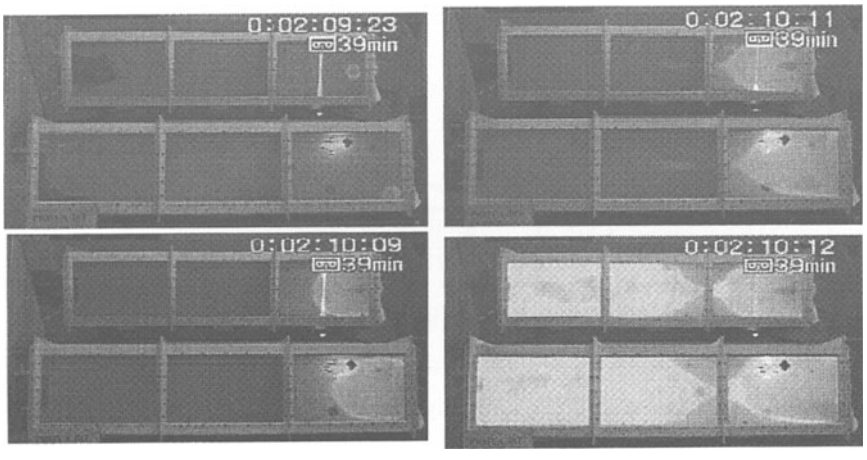

Figure 4 - Some frames of test 30T (10% H_2)

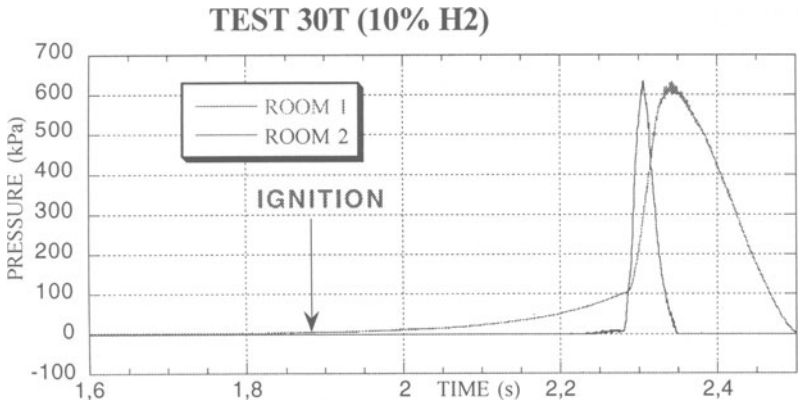

Figure 5. Pressure traces on Test 30T

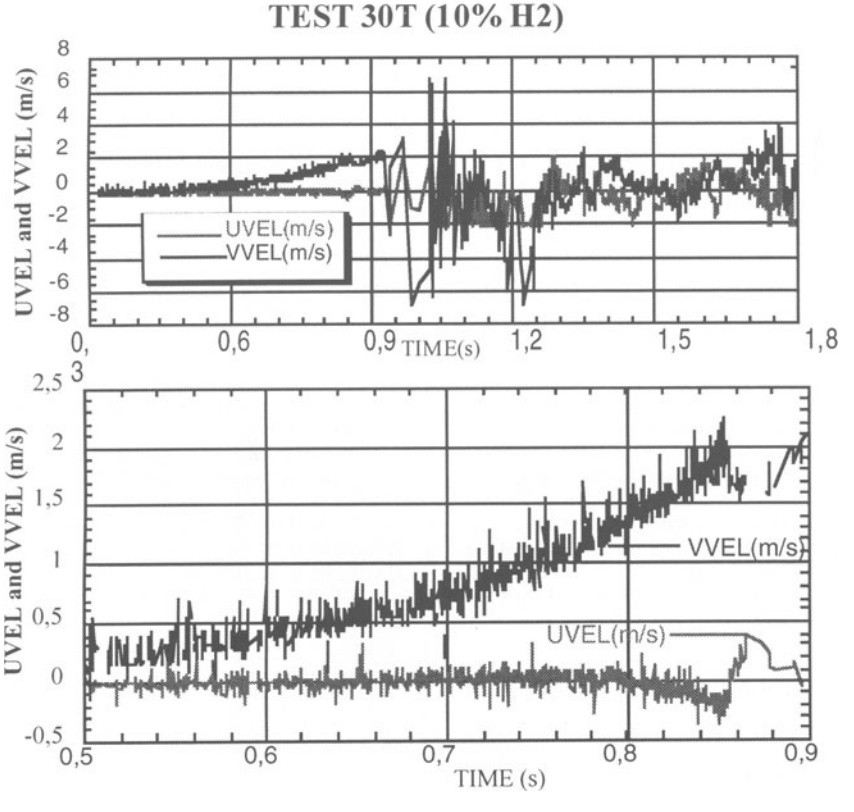

Figure 6. LDA measurement rough data of Test 30T

4. Conclusions

The experiments conducted with the HY-TU VIEW apparatus have demonstrated generally satisfactory behaviour of the new facility; in particular, the apparatus has been shown to sustain high overpressure during the tests (i.e., some experiments developed more then 180 kPa).

Furthermore, we are now sure that the hydrogen concentration inside the vessel prior the ignition is uniformly distributed.

The apparatus confirmed some important phenomena, such as the jet-ignition and recoil observed in the previous facility.

Another important result is the capability of the apparatus to permit good measurements with LDA in transient conditions.

For the main objective of the apparatus, i.e., the measurement of turbulent burning velocity, the analysis of the tests are still in process.

Some modifications are planned to introduce inert gas (like carbon dioxide) prior to the test to study the influence of these gas on the general behaviour of turbulent hydrogen combustion.

5. References

1. Carcassi M., Fineschi F., Lombardi G. (1987) Air-Hydrogen Deflagration Tests at the University of Pisa, *Nuclear Engineering and Design*, 104 241-247.
2. Carcassi M. (1992) Deflagration Tests of an Air-Hydrogen-Steam Mixture with Steam Nonuniformly Distributed *International Conference of CEC, IAEA, KIAE on Hydrogen Behaviour and Mitigation in Water-Cooled NPPs, Brussels, Belgium, 4-8 March 1991, Proceedings edited by E. Della Loggia*, EUR 14039 EN
3. Carcassi M., Carnasciali F., Fineschi F.(1988) Flammable Gas Mixtures and Containment Integrity during Severe Accidents in Nuclear Plants, *Proceedings of an Int. Symposium IAEA-OECD on Severe Accidents in Nuclear Power Plants (Sorrento, 21-25 March 1988)*, **2**, IAEA-SM-296/42P (Austria, Sept.1988) 659-667.
4. Carcassi M., Fineschi F. (1993) A theoretical and experimental study on the hydrogen vented deflagration, *Nuclear Engineering and Design*, **145** , 355-364.
5. Carcassi M., Fineschi F., Lanza S. (1994) Flame Propagation in Hydrogen-Air Mixtures in Partially Confined Environments, *Proceedings of the International Conference on "New Trends in Nuclear System Thermohydraulics", Pisa, Italy, May 30th - June 2nd 1994* , **2**, 125-132.
6. Carcassi M., Fineschi F., et alii, (1995). Combustion Phenomena in Nuclear Reactor Containments, *Proceedings of the FISA-95 Symposium - EU research on severe accidents, Luxembourg, Ed. G. Van Goethem et alii,* EUR 16896EN, 20-22 November 1995
7. Pilo F., (1997) Degree Thesis Progettazione e Prove di una Apparecchiatura per lo Studi Sperimentale di Miscele Gassose, Atti Università di Pisa .

CATALYTIC MIXED PACKING FOR H_2 - O_2 RECOMBINATION AT LOW TEMPERATURE

GHEORGHE IONITA and IOAN STEFANESCU

Institute of Cryogenics and Isotopic Separation
P.O.BOX 10, Rm. Valcea Cod 1000, Romania; 040 - 050 - 732746

1. INTRODUCTION

The hydrogen combustion is very important both in chemical industry for the purification of gases but especialley in nuclear energetics in next processes:

- the recovery of deuterium in CANDU off-gas systems
- removal of hydrogen from pressurised water reactor off-gas systems
- elimination of hydrogen evolved in wet-spent nuclear fuel storage containers
- removal of oxygen from steam or cooling water to reduce corrosion in heat exchanger
- purification of hydrogen and oxygen streams from water electrolysis cells
- removal of large volumes of hydrogen evolved in chemical processes or nuclear accidents. The majority of enrichment and separation tehnologies of the hydrogen isotopes based on isotopic exchange includes for hydrogen isotopes a step of catalytic conversion to water. The hydrogen combustion may be achieved by:

a) combustion flame [1]

b) catalytic combustion on:

- hydrophilic catalysts [2] at high temperatures, the reactants mixtures beeing out off flamability limit, requires large volume of inert gas (Ar, He)
- hydrophobic catalysts [3,4] at temperatures below 100°C using water as cooling agent, flowing directly on catalysts. The last proceeding offers the next advantages:
  - the diminution of hot points appeareance in the catalyst's mass.
  - diminution of thermic degradation of the catalyst

Due to the developpment of the nuclear energetics national programe, the burning of the hydrogen is very present but very dangerous because explosion or detonation risck for hydrogen and oxygen stoichiometric mixtures. For protium and deuterium in mixture with oir or oxygen the flammability limits are presented in table 1. For the radioactive isotope, tritiu, speciality reference is poor in dates, but recently [5] , the posibility of the conversion tritialed hidrogen on heated metal surfaces was, been observed.

Negative value of the Gibbs energy for hydrogen - oxigen reaction, suggests the great thermodinamycs probability to take place the process. Both for flamme combustion of hydrogen and for catalytic burning on metallic catalysts a radicalic or Eley - Rideal reaction mechanism is admited, the reaction beeing first order related to oxygen.

T. O. Saetre (ed.), Hydrogen Power: Theoretical and Engineering Solutions, 419–424.

Table 1 The characteriscs of protium and deuterium combustion in air or oxygen

Mixture type the characterisc		Natural hydrogen-air	Deuterium -air	Natural hydrogen-oxigen	Deuterium - oxygen
Flammability Limit (% Vol)	Inferior	4	6,7	4	5
	Superior	74,5	79,6	94	95
Detonation Limit (% Vol)	Inferior	18,3	15,8	15	16,3
	Superior	59	59,7	90	92,3
Minimum burning point (°C)		570	-	560	-
Deflagration velocity (M/S)		2,65	-	14,36	-
Detonation velocity (M/S)		2050	-	2821	-
Maxim pressure of explosion at P_i = 1Bar, T = 20°C (Bar)		7,4	-	8,2	-

2. EXPERIMENTAL

2.1. DESCRIPTION OF THE INSTALLATION

For the experimental study of catalitic combustion an experimental installation was performed (figure 1), to allow the testing in deplin safety.

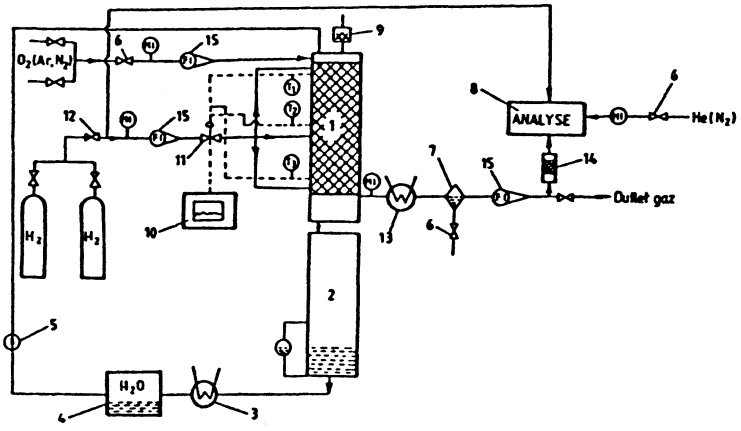

Fig. 1. EXPERIMENTAL INSTALLATION FOR HYDROGEN - OXYGEN RECOMBINATION.

This contains: the catalytic recombiner (1), the cooling water circuit, the hydrogen and oxygen circuit and control and measure system of work parameters. The main installation's component, catalytic recombiner has a cylindrical shape (90 x 400 mm) is made off stainless steel and by ××three gas distributors is feeded with hydrogen. The feeding with oxygen and cooling water is made on upper side. This feeding mode ensures both the simultaneous contact of reactants with the whole catalytic mass and a uniform distribution of them due to the positions and variable dimensions of distribuitor's perforations. For the safety of the combustion process, the recombiner is

forseeded with a double protection against pressure (over 3 at) and temperature's growth (over 70°C). Snapshat, the hydrogen and oxygen (2%) in excess, reacts in recombiner, the heat of reaction beeing assumed by cooling water. The cooling water circuit includes: water reservoir (4), pump (5) vas of gathering (2) and heat of exchanger (3). The cooling water flow is direct relation to the reactants flow and the develloped reaction heat, so that the temperature of outlet water must be below 70 °C. When, the deuterium is burned, the used cooling water must be heavy water with the same deuterium's concentration. The reactants circuit includes: connected oxygen and hydrogen botles to a distribution system which allows the continueously feedind of the recombiner, taps (6) recombiner (1), heat exchanger (13), electrovalve (11), phase separator (7), trap with molecular sieve (14) and chromatografic analyse system(8).Three thermocouples, flowmeters (15), the recording system of temperatures and pressure, form the measure and control system of work parameters. When the temperature grows over 70 °C, the thermic protection system closed the feeding with hydrogen by electrovalve (11).

2.2. PREPARATION AND CHARACTERISATION OF CATALYTIC PACKINGS

By applying an original preparation method [6] a platinum on carbon and teflon (Pt/C/PTFE) hydrophobic catalyst was prepared. This has Rashig ring shape and very good flowing properties compared with its surface area, high mechanical strength and low pressure drop during use. The main physical-structural characteristics of the catalyst determined by clasical methods are shown in table 2.

Table 2. The physico-structural characteristics of Pt/C/PTFE catalyst

Testure	Measure Unit	Value
Active metal content	%	0,44
Active metal area	m^2 / g	152
Platinum particle size	Å	13
Specific surface area	m^2 / g	10
Pores volum	cm^3 / g	0,15
Mechanical strength	Kg f /ring	5
Density	g / cm^3	1,60
Termic stability	°C	320

Due to its hydrophobic nature, this catalyst repels liquid water, but allows a surrounding envelope of gas to be retained on the catalyst surface. Gaseous reactants and theirs resultant products, difusse easly through this gas layer to and from the active catalytic centres. The Pt/C/PTFE wetprooafed catalyst is therefore able of achieving reaction rates comparable to those for conventional catalysts operating in dry environment. Unfortunely, with so hydrophobic catalyst the cooling water, flows nonuniform through the recombiner, preferential on the walls, the appearance of some hot points in the catalytic mass beeing very possible. To improve water distribution and to prevent the growth of locale temperature, the catalyst isn't used alone but mixed

with hydrophitic component. The selection of the nature and composition of mixed catalytic packing, able to ensure the hydrogen combustion with high efficiency and in safety for a long time was the purpose of this study. Six mixed catalytic packings differents as nature and composition was prepared as Table 3. If the first three packings are different as nature and composition, the next three tells one from the other only by presentation mode of the catalyst:

- common catalytic Rashig rings for A type packing.
- catalytic rings having exterior surface coated with stainless steel net for B type packing.
- catalytic rings having the whole surface coated with stainless steel net as Figure 2.

3. RESULTS AND DISCUSSIONS

Equal volume of packings in the next experimental conditions was tested:

- reaction temperature: - 50 °C
- presure: 45 - 50 mm H_2O;
- cooling water flow: 80 - 100 l/h
- H_2: O_2 raport - stoichiometryc with 2% oxigen excess.

After evry experiment masic balance was calculated, the outlet gas composition chromatografic gas analysed, the physical state and the possible loss in weight of the catalysed was pursued: The resuts of the testing on the six packings are presented in Table 3.

Table 3. The results of the testing mixed catalytic packing to hydrogen combustion

Packing's nature and composition	Burned hydrogen volume (l/h)	Burning time (h)	Loss in weight of catalyst (%)	Catalytic activity (mol/g · h)
25% catalyst + 75% glass rings	18500	92,5	16	55
10 % catalyst + 90 % glass rings	21900	109,5	8,3	149
10% catalyst + 90% ceramic rings	14900	74,5	5	152
10% catalyst (A) + 90% stainless steel net rings	31200	150	5,1	170
10% catalyst (B) + 90% stainless steel net rings	18300	91,5	1,4	1 78
10 % catalyst (C) + 90 % stainless steel net rings	43400	217	-	182
	20400	102	-	186
	34200	171	-	184

For the first packing the hydrogen combustion was complete but after 93 hours, the catalyst is partial burnt, a part from catalytic rings are united beetwen them and the total loss in weight was 16%. This fact shows there are hot points in catalytic mass (over 330 °C) which determined termic degradation of the catalyst. The modification of packing's composition by growth to 90% of the glass rings determined twice reduction of the loss in weight for an experimental time twice greater. The change hydrofilic component's nature by use ceramic rings hadn't a great influence on eficciency and stability of packing. The use of the stainless steel net rings thermochimic activated by original method [7] in the same propprtion as 2 or 3 packings, improved the performances of the packing. Though catalytic activity was greater, the loss in weight of the catalyst was still observed. To ensure the complete wetting of evry catalytic ring with a water thin layer (which must take over the produced reaction heat), the lateral surface of rings with stainless steel net was coated (packing B). In this mode the loss in weight lowered until 1.4% while the catalytic activity grew. Subsequent, the whole surface of rings was coated with stainless steel net as Figure 2 achieving C packing type and the thermic degradation of catalyst was total reduced. After the repetition of experiments for longer time, the complete combustion and the high catalytic activity of C type packing was confirmed. After 60 days none explosion or diminution of the catalytic activity wasn't observed (figure 3).

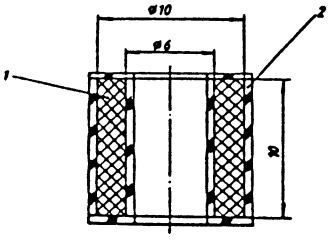

Fig. 2 PYC/PTFE CATALYTIC RING (1) COATED WITH STAINLESS STEEL NET (2).

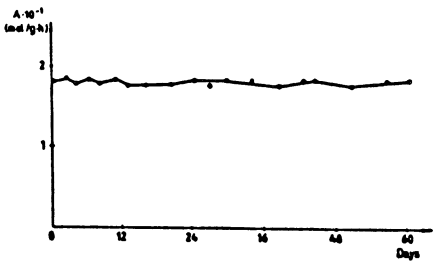

Fig. 3 THE STABILITY OF MIXED CATALYTIC PACKING.

The isotopic composition analyse of the process water resulting by mixing cooling water of 144 ppm deuterium with reaction water of 50 ppm deuterium, showed the value of 80 ppm deuterium, in accordance with the theoretical value from isotopic balance. Physico-chemical analyse for process water shows important modifications for the packing in which the degradation of the catalyst was produced and the keeping of water's quality for C type packing. This fact may be pursued in Table 4.

Table 4. The quality of waters from H_2 - O_2 recombination process

Analyse type / Water type	pH	Conductivity ($\mu S/cm^3$)	Turbidity ($^\circ SiO_2$)	$KMnO_4$ Consum (mg/l)	Fe^{2+} (mg/l)	Mg^{2+} (mg/l)	Cl^- (mg/l)	F^- (mg/l)
Cooling water	6,8	15,2	0,01	4,6	< 0,1	0,2	0,39	-
Process water from A type packing	4,6	180	0,02	140	1,3	0,2	1,5	22
Process water from C type packing	7,0	17,1	0,01	3,9	< 0,1	0,2	0,44	-

The quality of process water is similar to cooling water so that C type packing may be used and in the separation and enrichment of hydrogen isotopes in nuclear energetics. This packing was chosen for hydrogen - oxygen recombination in a pilot plant for detritiation of heavy water puts into service in this year to Rm. Valcea (figure 4).

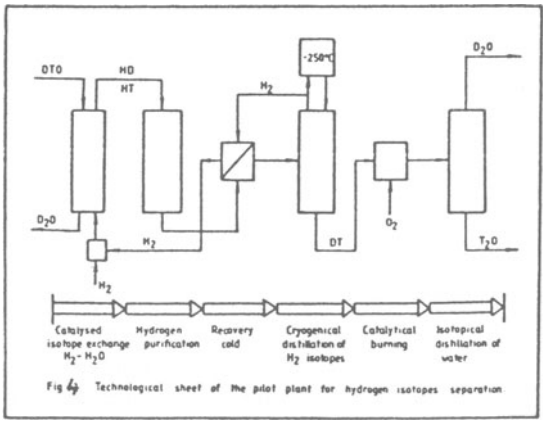

Fig 4 Technological sheet of the pilot plant for hydrogen isotopes separation

4. CONCLUSIONS

Six catalytic mixed packings consisted by hydrophilic component and a Pt/C/PTFE hydrophobic catalyst have been tested in identical condition in hydrogen's combustion process. The best catalytic mixed packing which provides complete combustion at low temperature and in deplin safety, was the packing consisted by 90% stainless steel rings, thermochimic activated and 10% Pt/C/PTFE rings having the whole surface coated with stainless steel net.The catalytic activity of packing was 180 mol/g · h and its stability is greater then 60 days. This packing was chosen for hydrogen oxygen recombination in a pilot plant for heavy water detritiation puts into service in this year in Romania.

5. REFERENCES

1. Ruchert Friedrich (1989) - Procede et dispositif pour la combinaison d'hydrogen avec de l'oxygen natamment pour un enrichissement en tritium,*Demande de Brevet d'Invention*, **2628728**, France
2. Tatcher D. R. P, Chuang K. T., Quaiattini R. J. and Rolston J, H, (1986) - The separation of tritium from heawy water in trickle bed reactors *AECL Report*, **8714**
3. Chuang T. Carl et Roett F. Maurice (1981) - Procede et appareil pour la combustion d'hydrogene et d'oxygene gazeux. *Demande de Brevet d'Invention*, **8115625**
4. Seddon W.A., Chuang K.T., Holtslander W.J. and Butler J.P, (1984) - Wet proofed catalysts: A new and effective solution for hydrogen isotope separation and hydrogen/oxygen recombination, *AECL Report*, **8293**
5. Dikson R.S., (1993) - Conversion of tritiated hydrogen on heated metal surfaces *AECL Report*, **10866**
6. Ionita Gh. and M. Peculea, (1994) - The proceeding for preparation of hydrophobic catalysts preparation, *Patent*, **107842**,Romania
7. Ionita Gh. and M. Peculea, (1995) - The combustion of H_2 - O_2 stoichiometric mixtures, *Romanian Revue of Chemystry* **5**, 448 ÷ 454

WE-NET : THE NATIONAL HYDROGEN PROGRAM OF JAPAN VISION AND STATUS

KAZUKIYO OKANO
WE-NET Office
Engineering Advancement Association of Japan
CYD Bldg. 1-4-6, Nishi-Shinbashi, Minato-Ku,
Tokyo, 105 Japan

Abstract

The WE-NET (World Energy Network) Program is a project that has been conducted by the New Energy and Industrial Technology Development Organization (NEDO) since FY1993 as part of the Japanese government's New Sunshine Program. The WE-NET Program aims to secure new energy sources and maintain the global environment in good condition by building an international network for hydrogen energy. Over the past four years, steady progress has been made and superb results obtained in R&D activities of each subtask on hydrogen production, transportation, storage and utilization systems.

1. Introduction

The WE-NET Program is a large-scale project aimed to give comprehensive solutions to two global problems of energy and environment. With the goal of laying the foundation for building a large-scale hydrogen energy network system, research and development work have been carrying out since FY1993.

The overall system comprises three basic processes, hydrogen production, hydrogen transportation, storage and hydrogen utilization. Besides technology development total system design and analysis have been conducted. The program is being proceeded in cooperation with government, industry and academia.

T. O. Saetre (ed.), Hydrogen Power: Theoretical and Engineering Solutions, 425–432.

2. Japan's Response to Protect the Global Environment

Developing measures to prevent global warming accompanying the increase in energy demand is a common issue faced by countries throughout the world. Although the world energy demand is predicted to rise, the increase in Asia is expected to be particularly striking. In its midterm report issued in June 1995, the Advisory Committee for Energy of the Ministry of International Trade and Industry (MITI) predicts that energy demand in 2010 will be double the 1992 volume. The CO_2 emissions volume in the Asia region will also approximately double accompanying this rising energy demand, and Asia's CO_2 emissions will come to account for 25 percent of the world volume. Refer to Figure 1.

To control air pollutant and CO_2 emissions, Japan drafted the action program to arrest global warming in 1990 and has been endeavoring to develop new energy technologies.

The WE-NET program was started in FY1993 as a large scale international project of the New Sunshine Program, and MITI and NEDO commenced a long-term technological development project to create an international network for hydrogen energy.

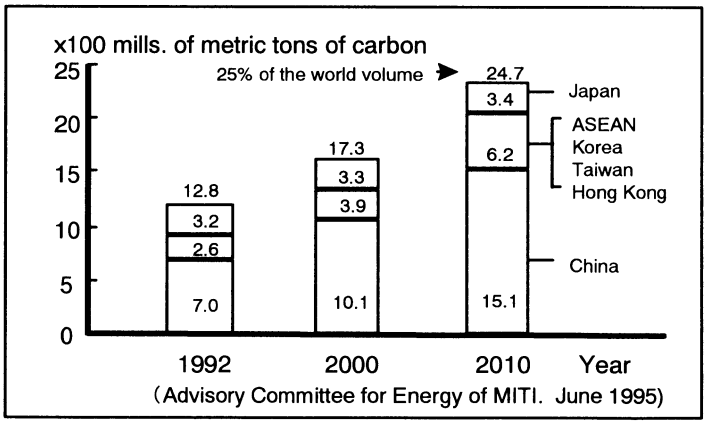

Figure 1. Estimated CO_2 emissions in the Asia region

3. Outline of the World Energy Network

The WE-NET program proposes to convert hydropower and other renewable energy, that are available in abundant quantities and not being used at the present in various part of the world, into hydrogen through water electrolysis

and other appropriate processes, and transport hydrogen to the countries in demand. The transportation of hydrogen would be carried out by ships in the form of liquefied hydrogen. Hydrogen would be stored in the energy consumption areas and used to generate electricity by means of hydrogen combustion turbines and in other forms of application such as hydrogen vehicles and fuel cells etc.

The WE-NET program proposes to carry out international cooperation for developing the core technologies required to build the international network making it possible to materialize the energy utilization scheme described above, as well as the optimum design of the network system.

Should a clean secondary energy system of this kind utilizing hydrogen is realized, the special and chronological imbalance between the supply and demand of energy in global scale could be eliminated and it would be possible to expect the simultaneous solution of both energy problem and environmental problem. Goals of the WE-NET program are as follows.

- To establish global, clean-energy network using hydrogen produced by renewable energies
- To improve air quality and reduce CO_2 emissions
- To assure adequate future energy and fuel sources

4. WE-NET Program Structure

The project term is divided into three phases extending over a 28 year period from 1993 to 2020. Phase 1 of the project is from FY1993 to FY1998. An evaluation has been done at the end of FY1996 (March 1997) on the R&D results up to that date. R&D plan for FY1997 and thereafter will then be drawn up based on the evaluation. The whole program is financially supported by MITI / NEDO. The total budget is 300 billion yen (US$ 2.4 billion) for 28 years. The budget of Phase 1 period is about 10 billion yen.

5. Organization of the WE-NET Program

Under the WE-NET program, a wide range of R&D activities is being conducted on every aspect of hydrogen energy technologies by pooling the efforts of Japanese industry, government, and academia and receiving the cooperation of research institutes and corporations in overseas countries .
Under the guidance of the Agency of Industrial Science and Technology

(AIST) of MITI, NEDO oversees the overall WE-NET program while the individual R&D subtasks are supervised by other organizations that serve as subtask managers. A committee is set up for each subtask to determine R&D topics, follow research progress, and evaluate research results. These committees are composed of the subtask managers as well as representatives from universities, national research institutes, corporations and organizations. The actual R&D work is performed by leading Japanese corporations in various industries as well as foreign participants. The organization and the subtasks for the project are outlined in Figure 2 and 3.

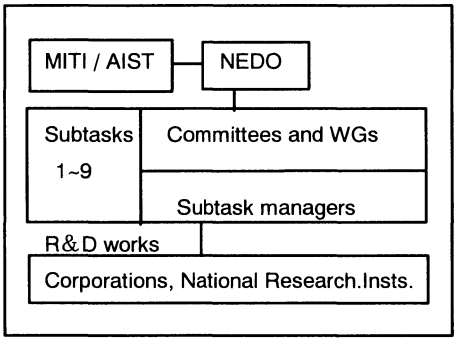

Figure 2. Organization

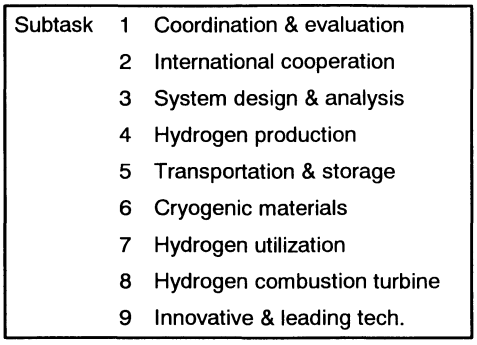

Figure 3. Subtask structure

6. Research and Development in the WE-NET Phase 1 Period [1]

Activities in Phase 1 period have been focused on the basic research and system studies. The main system flow and the target capacity of each unit plant are shown in Figure 4.

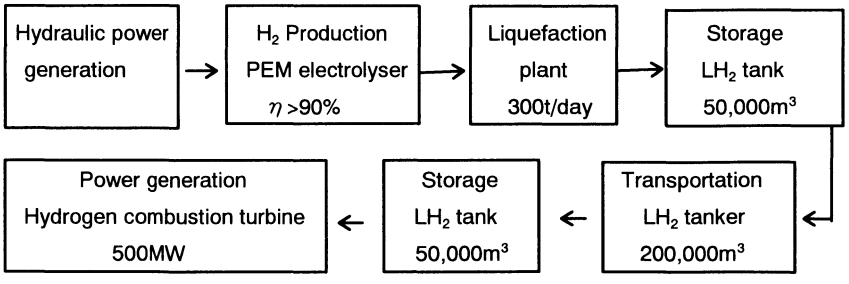

Figure 4. The main system flow and target capacity of plants

6.1 SYSTEM ANALYSIS

6.1.1 *Conceptual Design of the Total Systems*

The total system, the efficiency, the economy and the technical feasibility have been studied and evaluated. In case of hydrogen production using 1000MW electricity and hydrogen transportation of 5000km by a tanker, energy losses in the processes of hydrogen production, liquefaction, transportation and storage are about 30%. The total system efficiency which is output electric power from hydrogen combustion turbine by input hydraulic electric power is 37.7%. System studies on methanol and ammonia as an energy carrier, and comparison of those systems with hydrogen system were conducted.

6.1.2 *Analytical Evaluation on Introduction of Hydrogen Energy*

Analytical evaluation on introduction of hydrogen energy using modified GREEN model was conducted for the global market and Japanese market.

6.1.3 *Other Assessment*

National level and city level energy estimation and assessment, and safety measures and assessment have being conducted.

6.2 HYDROGEN PRODUCTION

High efficiency and large scale water electrolyser plant using solid polymer electrolytes are being developed. Target of 90% energy efficiency at 1A/cm^2 was achieved by 50 and 200 cm^2 test cells. Development of 2500cm^2 large size cells has been started from FY1997 and finally 10000cm^2 class cells will be developed. Chemical plating method and hot press method will be applied for production of large sized and high performance cells. Besides these cell development higher temperature polymer membrane has being developed to raise energy conversion efficiency of water electrolysis.

6.3 HYDROGEN TRANSPORTATION AND STORAGE

6.3.1 *Hydrogen Liquefaction Plant*

Hydrogen Claude and Helium Brayton cycles have being studied for the 300t/day liquefaction plant of over 40% process efficiency. Research and development of major components of a plant such as a compressor and an

expansion turbine will be conducted in the next stage of the development.

6.3.2 *Liquid Hydrogen Tanker*

Conceptual design of 200,000m^3 tankers with prismatic tanks and spherical tanks was carried out. Testing of insulation structures will be started to know the characteristics of the tank insulation at cryogenic temperature from FY1997. Specification of a tanker is shown in Table 1.

TABLE 1. Specification of a liquid hydrogen tanker

Tank capacity : 200,000 m^3	Ship speed : 25 knots
Ship length : 290~320 m	Type of ship : Twin hull ship
Ship width : 48~56m	B.O.G. rate : 0.2~0.4%

6.3.3 *Liquid Hydrogen Storage*

Development of the liquid hydrogen storage equipment comprises the design of the entire system for storage and research of the storage equipment. The conceptual design of the 50,000m^3 storage tanks such as spherical, cylindrical, and in-ground tanks was carried out. A test equipment for insulation structures will be installed in FY1997 and the testing of insulation structures will be conducted at liquid hydrogen temperature. Also liquid hydrogen pumps will be developed for handling of liquid hydrogen for storage tanks and hydrogen combustion turbines.

6.3.4 *Metal Hydrides*

Application of metal hydrides for transportation and stationary storage have been studied, and development of higher performance alloys has been started from FY1997 to achieve the target of 3wt% absorbing capacity at 100°C.

6.4 CRYOGENIC MATERIALS

A mechanical test equipment which can be used for evaluation of mechanical properties and hydrogen embrittlement of structural materials in liquid hydrogen atmosphere was installed. Material tests for mother plate and weld metal of stainless steel and aluminum alloy have been started from FY1997.

6.5 HYDROGEN UTILIZATION

The following hydrogen utilization systems are being studied and evaluated to propose the technology development and demonstration.

6.5.1 *Hydrogen/Oxygen Fueled Diesel Cogeneration Systems*

Zero-emission closed cycle diesel engine cogeneration systems of 600~1000kW were studied. The system is perfectly clean and high electrical efficiency of 45~50% (LHV) is expected. Development for main components of a diesel engine such as a hydrogen injector and an igniter has been started.

6.5.2 *Hydrogen Vehicles*

Hydrogen engine hybrid system for a wagon and PEM fuel cell hybrid system for a bus have being studied. Conceptual design of these vehicles will be conducted till the end of FY1998 using metal hydrides storage system for a wagon and liquid hydrogen tank system for a fuel cell bus.

6.5.3 *Fuel Cells*

The following PEM fuel cell power plants were studied.

(1) Hydrogen/Oxygen fueled 5000kW dispersed power plant
(2) Hydrogen/Air fueled 200kW onsite power plant
(3) 20kW power system for vehicles

In case of 5000kW PEM fuel cell power plant, very high electrical efficiency of 56% (HHV) can be achieved. Conceptual design of these plants will be conducted till the end of FY1998.

6.5.4 *Oxygen Production Systems*

Small scale oxygen production systems utilizing cryogenic heat of liquid hydrogen have being studied for diesel cogeneration systems and 5000kW fuel cell power plant. Air separation plant method (Cryogenic method), PSA-combined general condensation method and V-PSA method were examined to evaluate system efficiency, and economics will be studied in FY1997.

6.5.5 *Hydrogen Distribution Systems*

A medium-size city in Japan was selected as the candidate model city. The energy supply and demand situation in the city was investigated in the case of entire energy demand, and the feasibility of converting hydrogen energy in the city was analyzed. The necessary infrastructure for a hydrogen distribution and supply systems in a city will be examined, and the design of hydrogen storage systems and refueling systems will be conducted.

6.6 HYDROGEN COMBUSTION TURBINES

Hydrogen combustion turbine system will be one of the most effective system for large-scale and centralized power generation. The evaluation to select the optimum turbine cycle and conceptual design of a 500MW power generating plant were conducted. Electrical efficiency was proved about 61% (HHV), and gas inlet temperature is 1700℃. R&D subjects in Phase 1 period for developing elemental technologies are as follows.

(1) Combustion control technology
(2) Turbine blades, rotors and other major components
(3) Major auxiliary equipment
(4) Super-pyrogenic materials

6.7 STUDY OF INNOVATIVE AND LEADING TECHNOLOGIES

This project aims to study, review and assess innovative and leading technologies as well as existing technologies in order to identify promising technologies and to propose them for addition to the WE-NET project as new R&D areas or subjects. Subtask 9 is always open for new proposals.

7. OUTLOOK OF THE WE-NET PROGRAM

The WE-NET Program is an effective plan to prevent air pollution and global warming. However to achieve this program the understanding and support of countries throughout the world, government and industry partnership to introduce hydrogen, long term government support of hydrogen technology commercialization and reliable technology development by industry are indispensable for the success of this program.

The international conference on climate change (COP3) will be held in Kyoto Japan on coming December、 and the target of CO_2 reduction will be decided at the conference. That will be a potential significant driver for the development of CO_2-free clean energy systems. The WE-NET Program should be promoted vigorously with the international cooperation as one step in overcoming problems of global environment.

Reference

(1) New Energy and industrial Development Organization (NEDO) (1997), The midterm Report of the WE-NET program Phase 1.

THE EURO-QUEBEC HYDRO-HYDROGEN PILOT PROJECT (EQHHPP)

Rationale, Concept, Realisation

Dr.-Ing. JOACHIM GRETZ
European Commission, Joint Research Centre, Ispra, Italy

Gesellschaft zur Einführung des Wasserstoffs in die Energie - Wirtschaft, Hamburg, Germany

1. Introduction

Back in 1985 it was the European Commission's intention to demonstrate on rather large scale the provision of clean and renewable energy with hydrogen as energy vector and fuel.

The cheapest and technologically available form of renewable electricity, the primary energy for electrolytic hydrogen, is hydropower. Most of the hydroenergy sources are oversea's. The World's topologically and technically exploitable hydroenergy potential is estimated to be in the order of 20.10^3 TWh/y, i.e. 0.0057% of the hydraulic cycle energy. Today's hydroelectricity generation is ~ 2500 TWh/y i.e. ~ 21% of the World's electricity generation. Québec's installed hydroelectricity is 33.5 GW, its residual potential is 50 GW or 190 TWh/y and 285 TWh/y, respectively (load factor 0.65).

The construction of hydropower installation is rather clean. The construction of La Grande at James Bay with an installed rating of 10.7 GW used 23 TWh/y of energy for fuel, steel, iron and cement production with an energy payback of 4 months emitting 2 g CO_2/kWh over a 50 years operation (coal and natural gas fired plants emit ~ 800 and 400 g CO_2/kWh, respectively).

2. The Euro-Quebec Hydro-Hydrogen Pilot Project

The concept of a hydrogen-based, clean, renewable energy system, was conceived by the Joint Research Centre Ispra of the Commission of the European Communities in 1986. It is currently being investigated by European and Canadian Industries and coordinated by the JRC-Ispra of the Commission of the European Communities and the Government of Québec.

T. O. Saetre (ed.), Hydrogen Power: Theoretical and Engineering Solutions, 433–446.

2.1 THE CONCEPT

The 100 MW (el) pilot project is to demonstrate the provision of clear and renewable primary energy in the form of Canadian hydropower converted via electrolysis into hydrogen and shipped to Europe, where it is to be stored and used in different ways: electricity/heat cogeneration, vehicle and aviation propulsion, steel fabrication and hydrogen enrichment of natural gas for use in industry/households (Figure 1), [1].

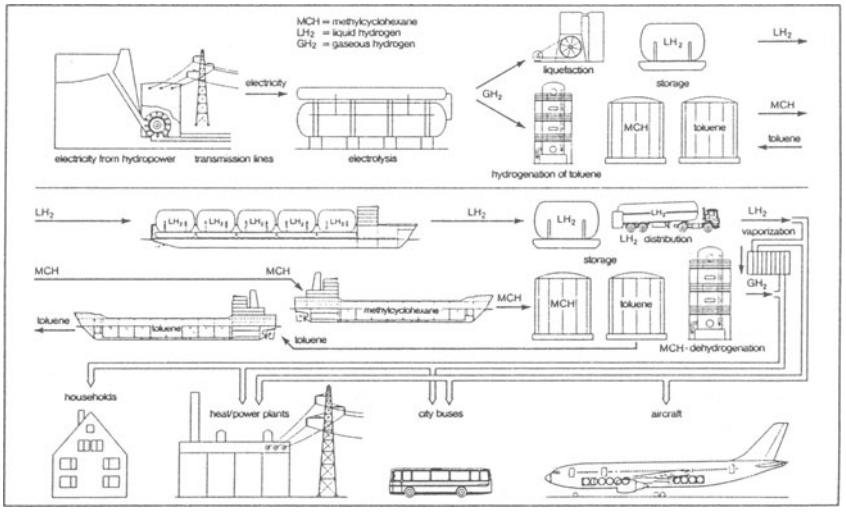

Figure 1. EQHHPP concept.

2.2 MILESTONES

The project was foreseen to be carried out in 4 Phases:

- Phase I : Assessment; completed by March 1987.
- Phase II : Detailed system definition, 01.01.1989-31.03.1991.
- Phase III,0 : Hydrogen application demonstration programme; 1991-1997.
- Phase III : Detailed engineering & specifications; planned to last 1-2 years.
- Phase IV : Construction; planned to last 4-5 years.

With Phases III e IV of the project - detailed engineering & specifications and construction in suspension - the project is presently in its Phase III.0 i.e.; "Hydrogen applications demonstration projects" in fields where the use of hydrogen exhibits its attractiveness.

2.3. ASSESSMENT (PHASE I).

An assessment of the hydro-hydrogen concept has been undertaken in 1986 by some twenty German interested companies under the leadership of the Commission of the European Communities and the overall management of the DECHEMA, the Deutsche Gesellschaft für Chemisches Apparatewesen, Chemische Technik und Biotechnologie e.V. [2].

The scope of the investigation was to establish the main characteristics of the system and components and to give first indications of costs of a complete system.

2.4. DETAILED SYSTEM DEFINITION (PHASE II) [3].

In Phase II of the project the Phase I results have been updated, cost calculations refined, environmental analyses undertaken and questions of safety and regulations investigated.

2.4.1. Vectorisation

Originally, three modes of vectorisation have been considered namely ammonia (NH_3), methylcyclohexane (C_7H_{14}) and liquid hydrogen (LH_2).

NH_3 has been excluded at the very beginning because of it's toxicity.

For reasons of thermodynamic properties, availability of technology and end use, two different modes of vectorization have been investigated namely liquid hydrogen (LH_2) and methylcyclohexane (MCH) in order to have hydrogen in both forms, liquid and gaseous, available for the end use requirements.

Weighing the pros and cons of the LH_2 vector vs. the MCH vector, i.e. considering the advantages of MCH:

- unlimited storage period
- transport and storage in existing normal oil product ships and containers

against its disadvantages:

- the energy intensive dehydrogenization and the liquefaction is done at the user's site whereas the energy intensive liquefaction of LH_2 is done with abundant hydropower in Québec
- MCH as well as toluene are petrochemical products and therewith environmentally less avantageous than LH_2
- its product (GH_2) is not adapted to the user's profile, about 80% of hydrogen use being in form of LH_2

the decision was taken to retain LH_2 as vector for the realization of the project.

The MCH concept is described under 3.2.

2.4.2 Barge Carrier for Liquid Hydrogen Transport

The new component in Phase II is the LH_2 ship. The LH_2 is transported in 5 vessels, containing 3000 m^3 LH_2 each, fixed on barges which are loaded on a barge carrier, thereby transporting altogether 15.000 m^3 LH_2, Figure 2. The containers are super-

insulated with no boil-off for 50 days. The floating barges permit individual towing on the waterways from the arrival sites to the users.

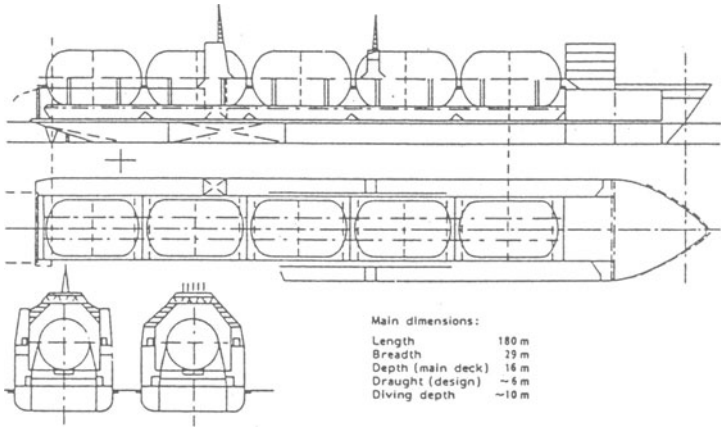

Figure 2. Barge carrier for liquid hydrogen (LH_2) transport.

2.4.3. *Main Characteristics.*
For the reference case, i.e. the LH_2 vector, the main characteristics are:

- hydropower : 100 MW;
- electrolysis (net) : 74%;
- load factor : 95%;
- hydrogen delivered in Hamburg : 74 MW = 614 GWh/y;
- hydrogen transmission efficiency : 74%;

2.4.4. *Costs and economics*
The cost of liquid hydrogen, produced with hydropower at 2 $cents_{ECU}$/kWh, shipped to Europe and stored in the port of Hamburg would be about 15 $cents_{ECU}$/kWh. These costs are pictured in Figure 3 together with the gasoline prices in Europe (average of the 12 EC countries, August 1990) of 8,5 $cents_{ECU}$/kWh which are made up of 3 $cents_{ECU}$/kWh for the crude oil itself, its transportation, refinement, handling and distribution and of 5,5 $cents_{ECU}$/kWh for taxes (1991). Including the submerged costs of protection/repair of the damaged environment resulting from the use of fossil fuel (the value of 2,5 ¢/kWh is the average of different litterature investigations), hydrogen would be competitive with today's latest container shipped liquid hydrogen price of 8 ¢/kWh (9 vs. 11 ¢/kWh).

2.4.5. *The Partners.*
The investigations have been carried out by 46 industrial partners and Universities from 5 countries (CH, CND, D, E, I):

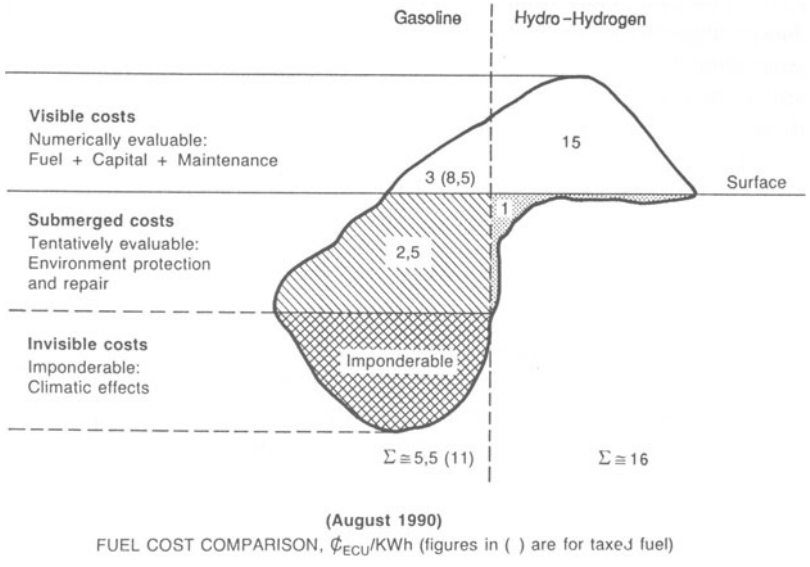

Figure 3. Cost iceberg.

2.5. DEMONSTRATION PROJECTS

The project actually in its Phase III.0, where demonstration projects have been launched on the utilization of hydrogen in five fields where the use of hydrogen exhibits its attractiveness. These projects are executed by industry on the basis of contracts following a tender action by the European Commission with a cost sharing of al least 50% by the industrial partners [4]. All projects foresee the construction of the components/systems and a two year's demonstration.
Since early 1992, demonstration activities started focusing on the following technologies and concepts:

- city bus with internal combustion engine and liquid hydrogen storage, Belgium
- city bus with internal combustion engine and liquid hydrogen storage, Germany
- city bus with membrane fuel cell drive and liquid hydrogen storage, Italy
- two hythane city buses, Montréal
- passenger transport boat with electric drive powered by a membrane fuel cell and LH_2 storage, Italy
- development, manufacturing, testing and commercialization of advanced 40 and 80 feet super-insulated transport containers for LH_2, Quebec
- safety tests for LH_2 vehicle tanks (approx. 125 l) and for a down-scaled maritime barge transport container (approx. 180 m^3), Germany

- low NOx conception and-emission testing on sectors of LH_2 adapted combustors of Airbus jet engines for low NOx emissions, Germany and North America
- cogeneration plant with a piston engine, Belgium
- cogeneration plant with a phosphoric acid fuel cell, Germany
- study on rules and regulations, safety and acceptability of hydrogen
- study on socio-economic effects of reduced emissions by hydrogen buses and airplanes compared with conventional technology investigated for 3 metropolitan areas
- study activities on LH_2 transport containers
- several smaller study activities.

An important fact supporting early application of hydro-hydrogen systems is that most of the involved components already exist, virtually no engineering breakthroughs are required and real scale pilot/demonstration project can be built and operated already today or in the foreseeable future and are needed in order to gain valuable systems experience.

2.5.1. *Some Selected Projects*

In the period 1992 to 1994, VCST-Hydrogen Systems (Belgium) and Messer Griesheim (Germany) completed as the first in Europe a proof of concept liquid Hydrogen city bus. The original diesel engine was modified by VCST-Hydrogen Systems into a hydrogen driven Ottocycle engine. According to the European 13-mode drive test, NOx emissions were as low as 0.25 g/kWh at $\lambda = 2{,}13$. A commercial prototype of a 100% low floor Midi Bus (type Van Hool-A308) having a capacity of 70 passengers is planned to be demonstrated by the bus exploitation company De Lijn in the ancient city of Gent mid 1998, Figure 4.

Figure 4. The Belgian VAN HOOL bus.

The MAN SL 202, 92 passenger 140 kW floor city bus, operating on liquid hydrogen, is Europe's first hydrogen city bus licensed for general use by fare-paying public, Figure 5. It operates since May 96 in Erlangen and Munich and has covered in the meanwhile more than 15.000 km transporting more than 60.000 persons with no incidents or breakdowns whatsoever. The NOx emissions are 0,4 gr/kWh at $\lambda = 1$ Figure 6.

Figure 5. The MAN bus.

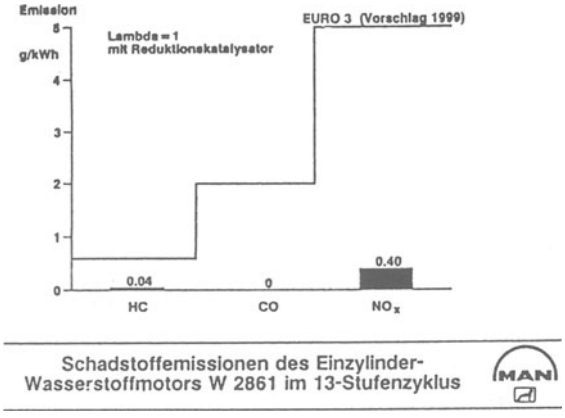

Figure 6. MAN bus emissions.

In Montreal two city buses are operating on hythane since several months. The NOx emissions of the 20% hydrogen - 80% natural gas mixture operated buses are 44% less than with natural gas and 60% less than with diesel. The operating costs are 32,5 $¢_{can.}$/km vs. 32,9 with diesel fuel.

A hybrid fuel cell - battery passenger boat will be operating on the Lago Maggiore by the end of this year. The boat has an electric power output of about 100 kW, of which 30-50 kW will be covered by a PEM fuel cell whereas the peak demand will be provided from a battery pack. In operating modes with low power demand the fuel cell will charge the batteries.

An experimental project establishing the NOx reduction potential in an aircraft combustion chamber operated with hydrogen is to provide design guidelines for later development of a real flight engine combustor. A test series with different injection nozzles has been conducted, the results are given in Figure 7. In Figure 8 the potential of hydrogen combustion is situated with respect to NOx emissions.

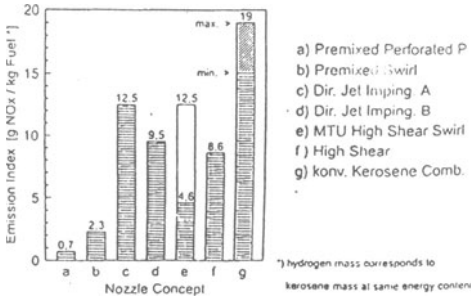

Figure 7. NOX emissions with different nozzle figurations.

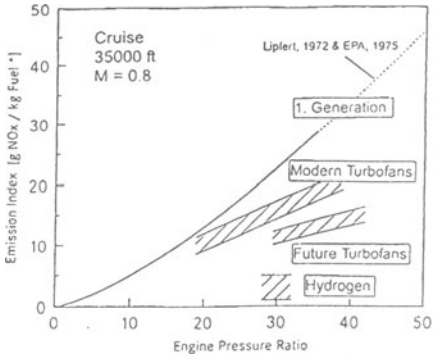

Figure 8. NOx emissions hydrogen vs. kerosene.

3. Other Techniques of Hydrogen Vectorisation.

3.1. IRON REDOX CYCLE

Oversea's hydrogen vectorisation can be done by an iron redox cycle, Figure 9. Iron oxyde would be reduced with hydrogen at the hydrogen production site, the iron then be

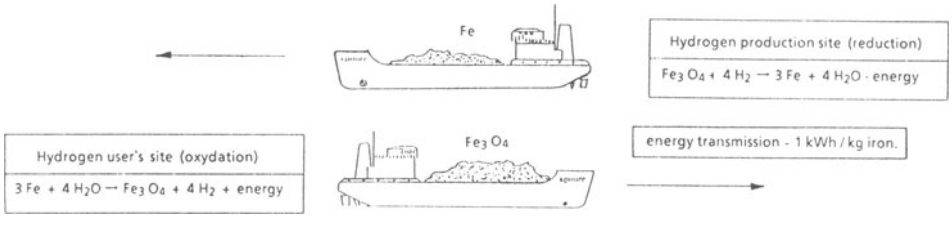

Figure 9. Oversea's transportation of hydrogen by iron redox.

shipped to the hydrogen user's site where it would be oxydized with steam. The resulting oxyde would then be shipped back to the hydrogen production site. The rather costly and complicated cryotechnical transport would therewith be replaced by the more simple iron/iron ore bulk carrying. The energy transmission capacity would be in the order of 1 kWh/kg iron. A bulk carrier of 200.000 DWT could carry 100 GWh/y of energy. The back-shipping of the iron oxyde would require a 280.000 DWT ship. In the EQHHPP for instance, the 15 round trips per year with a LH_2 carrier would be substituted by about 6 trips by an iron bulk carrier. Compared with LH_2 transport, about the same amount of energy would be required for the iron oxyde reduction as for liquefaction, with the difference that the latter requires electricity (energy) whereas the reduction requires thermal energy. The "price" of this kind of vectorization is that gaseous hydrogen will be arriving at the user's site.

The iron redox reaction technique is not that new, though. An iron redox generator in which 50 kg of iron cuttings have been exposed to steam and which produced 170 m^3 of hydrogen was sent to Egypt with General Bonaparte for filling up his army observation balloons during his campaign in Egypt (unfortunately, the ship carrying the hydrogen generator sunk at the entrance of the port of Alexandria where it is still lying).

3.2. METHYLCYCLOHEXANE (MCH)/TOLUENE CYCLE

Originally also the MCH/toluene cycle has been considered as chemical hydrogene carrier within the EQHHPP. The MCH technology is a process more or less known to the chemical industry. Methylcyclohexane (MCH) is liquid at ambient pressure and temperature and can, in its consistence and specific weight very similar to crude oil, be stored and transported in existing oil tanks and ships. This is important in view of smooth energy system infrastructure transition. The synthesis of toluene and hydrogen to MCH is an exothermic reaction.

$$C_7H_8 + 3H_2 \rightarrow C_7H_{14} - 205 \text{ kJ/mole}$$

releasing heat at 440°C which can be used as process heat. The dehydrogenation requires heat input of the same amount as the heat freed at its synthesis. 3 moles of hydrogen being conveyed per 205 kJ/mol, the losses would be 28% of the energy contained in the hydrogen.

In a solar MCH system, the ~ 450°C heat for dehydrogenisation would be provided by a solar energy, Figure 10.

3.3. HYDROGEN-METHANOL-CO_2 CYCLE

With the H_2 - CH_3OH - CO_2 cycle, hydrogen oversea's transport and permanent deep sea disposal of CO_2 is effectuated with methanol as vector, Figure 11, [5].

Methanol, generated from renewable hydrogen and stack or atmosphere extracted CO_2 would be transported in standard marine tankers from its production site to the user site, e.g. Canada to Europe or Japan, where methanol reforming would liberate hydrogen for use and the CO_2 for solidification and transformation for permanent ocean disposal.

The proposed system would provide a simplified transport vector for hydrogen as well as carbon dioxide and a permanent disposal mechanism for this anthropogenic waste.

The storage in deep ocean sediments is based on free-fall penetrator technology with the penetrators being made out of solid carbon dioxide. It has been shown that permanent storage can be envisaged by using sequestration of carbon dioxide in deep marine geological sedimentary formations (carbonate or silicate rich sediments) at oceanic sites having depths between ~ 1-4 km. Once emplaced, the carbon dioxide will slowly react with the surrounding pore water to form a solid clathrate. The formation of carbon dioxide clathrates (hydrates) has been observed in deep marine sediments as well as large formations of the natural stable analogue methane clathrate.

The efficiency of the cycle including the energy for CO_2 extraction, electrolysis, methanol synthesis and reforming and CO_2 solidification would be 35% for the stack separation case and 30,5% for the case of atmospheric extraction.

Carbon-based liquid energy carriers for the vectorisation of renewable energies are attractive alternatives to liquid hydrogen even more so if it is combined with CO_2 disposal.

4. Generalities

4.1. MASSIVE USE OF HYDROGEN

The only emissions from fuel cell/hydrogen energy systems being water, the question arises whether massive use of hydrogen would be harmful, water vapour being a strong greenhouse gas. The worldwide water evaporation from the oceans and rivers is ~ 5 x 10^{14} m^3/year. If mankind's total energy consumption of 11 TW were to be effected by hydrogen, its yearly water emission would be 2.5 x 10^{10} m^3, i.e. about 1/20000 of the natural evaporation, Figure 12. Water vapour contributing with some ~ 65% to the overall natural greenhouse effect of 34 K, the additional heating of a hydrogen powered society would be ~ 0,001 K, supposing proportionality. All the worldwide ~ 450 Mio automobiles, if fuelled with hydrogen, would emit ~ 1 billion (10^9). To of water per year and would have a heating effect of ~ 0,00004 K, local effects not considered.

4.2. SQUARING THE CIRCLE BY ADVANCED TECHNOLOGY

A look into the future shows a rather perturbing situation. Today mankind consumes some 12 TWy/y of energy, 88% of which is of fossile origin. Realistic predictions indicate that by the year 2030 mankind will consume about the double with some 75-80% fossile's share, if ever. Are the intentions to reduce the CO_2 emissions within the next 30 years a squaring-the-circle enterprise? The question arises whether there are solutions to this situation which, by the way, was already pictured somehow by Malthus a hundred years ago for the food problem. I would not know of any patent solution, probably nobody does. But one thing seems to be clear and that it is advanced technology that could help may be not to master but at least to bear the future. Almost all computer analyses indicate this, see Figure 13, [6].

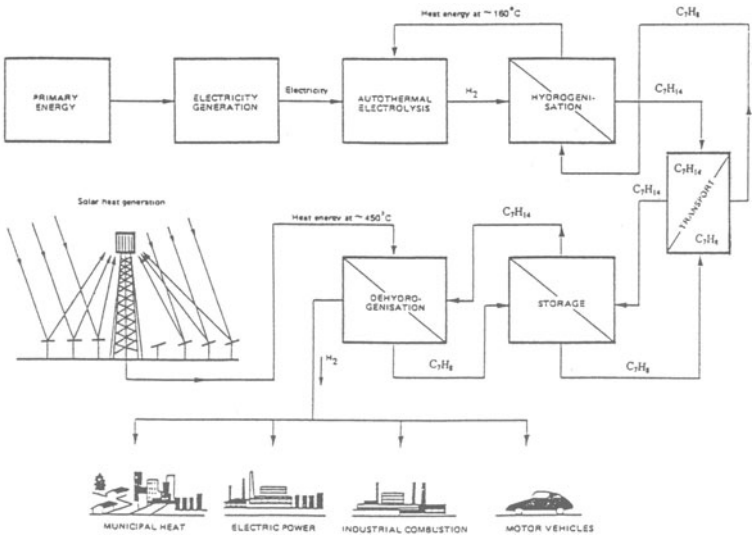

Figure 10. Solar energy operated MCH cycle.

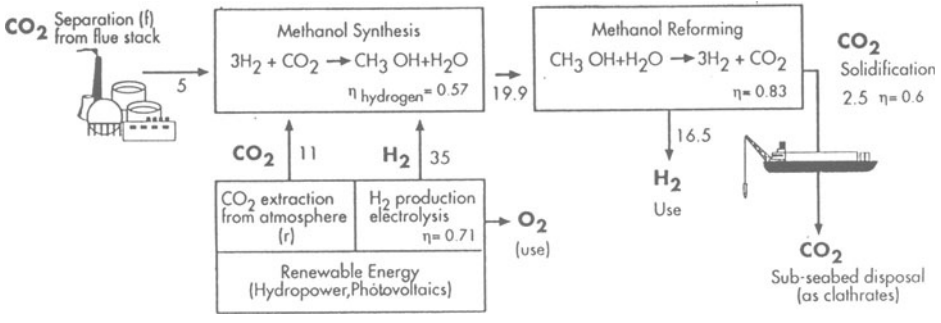

The efficiency (η) is defined as the available energy for use (clean hydrogen, minus solid CO_2 disposal) divided by the renewable energy input plus the energy for extraction of the CO_2 from the atmosphere or from the stack flue gases. Energy in MJ/kg of methanol, LHV. (f) = fossil energy, (r) = renewable energy.

$$\eta_{stack} = \frac{(19.9 \cdot 0.83) - 2.5}{5 + 35} = 35\% \qquad \eta_{atmos.} = \frac{(19.9 \cdot 0.83) - 2.5}{11 + 35} = 30.5\%$$

Figure 11. Hydrogen-Methanol-CO_2 cycle.

World energy consumption of 11 TW with H2 ⟶ 2,4 X 10^{10} m^3 H_2O/a

World ocean & river water evaporation ⟶ 5 X 10^{14} m^3 H_2O/a

H2 use/natural evaporation ⟶ 50 ppm ⟶ 0,001 K increase

Worldwide ~450 Mio automobiles ⟶ 2 ppm ⟶ 0,00004 K increase

A passenger car operating 100km/day
would generate ~ 20 ltr water/day

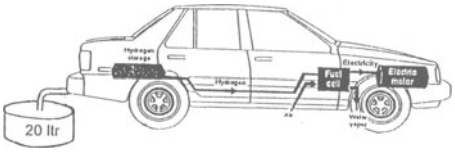

Figure 12. Clima effects of massive use of hydrogen; water generation.

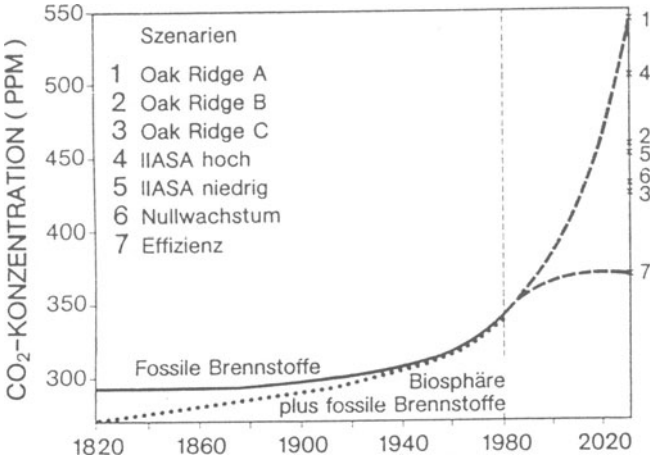

Figure 13. CO_2 concentrations for different scenarios.

Let alone the absolute values on the ordinate and the gradients of the different curves, what matters is the qualitative pattern of scenario 7. The thing to be done is to pursue R&D on the leitmotives of modern concepts and technologies like fuel cells, co-generation, condensing boilers a.o. Renewable hydrogen by itself is only one answer to the challenge and not necessarily the solution by itself.

5. Outlook

Figure 14 shows the remaining time of CO_2 in the atmosphere of 30% per century after its emission. This leads to the perturbing for not to say alarming situation pictured in Figure 15, [7]. For a 1-2 K temperature rise by the year 2050, continuous CO_2 emission reduction should have started by 1980 resulting in a maximum CO_2 concentration delayed by 35 years.

These delays dictated by atmospheric chemistry are treacherons. Whatever we undertake for reducing the negative influence of fossil fuel burning should be done the earlier the better. Time is a precious raw material.

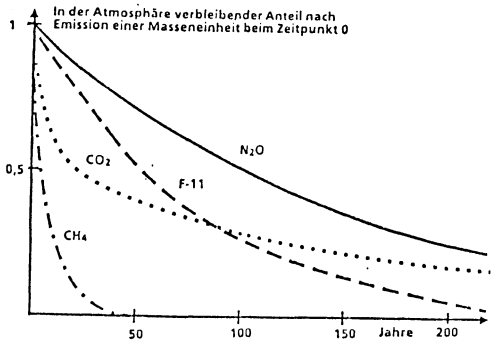

Figure 14. Remaining time of CO_2 in the atmosphere.

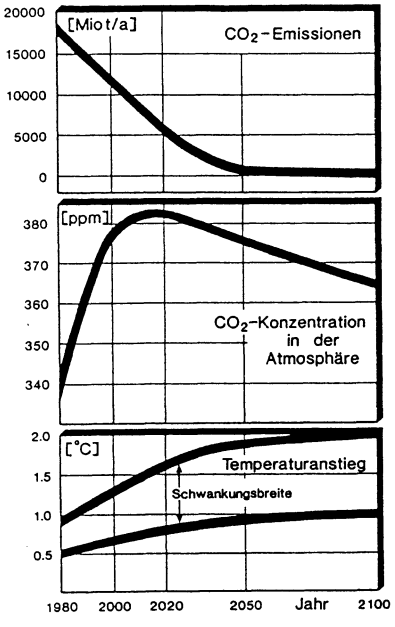

Figure 15. CO_2 emissions concentrations and temperature rise.

6. References

[1] Gretz, J., Wendt, H.,Reh, L. and Baselt, J.P., *A 100 MW Hydrogen Pilot Project, Proc. ISES World Congress,* Hamberg (Sept. 1987).

[2] Final Report of the DECHEMA/CEC contract No. EN 35-0024-D(B). *Investigations on the production, intercontinental transport and use of the clean energy vector hydrogen on the basis of abundant and cheap hydropower* (1987).

[3] EQHHPP Phase II Feasibility Study Final Report, prepared by the Joint Management Group Ludwig-Bölkow-Stiftung/Hydro-Québec, March 1991.

[4] Drolet, B., Gretz J., Kluyskens, D., Sandmann, F., and Wùrster, R., The Euro-Québec Hydro-Hydrogen Pilot Project (EQHHPP): Demonstration Phase, Proceedings of the 10th World Hydrogen Energy Conference N. 10 Cocoa Beach, Florida, U.S.A., June 20-24, 1994.

[5] Murray, C.N., Gretz, J., Specht, M., and Bandi, A., H_2-Methanol-CO_2 Cycle: Storage of CO_2 in Deep Marine Sediments using Methanol as a H_2 Transport Vector. Proceedings of the IEA Intern. Conference Technologies for Activities Implemented Jointly, May 1997, Vancouver, Canada.

[6] Bach., W., Wasserstoff als Chance zur Entschärfung des CO_2 - Klimaproblems (1987), Serie Piper.

[7] Flohn, H., (1983): Das CO_2-Klima-Problem, in: Geogr. Rundsch. 35 (5).

INTERDISCIPLINARY PERSPECTIVES TOWARD PROVIDING RENEWABLE, HYDROGEN-BASED ENERGY TO ISOLATED COMMUNITIES WORLDWIDE

GLENN RAMBACH
Desert Research Institute
Energy and Environmental Engineering Center
P.O. Box 60220
Reno, NV 89506

DAVID HABERMAN
DCH Technology, Inc.
14241 Ventura Blvd.
Suite 208
Sherman Oaks, CA 91423

CATHERINE GREGOIRE PADRO
National Renewable Energy Laboratory
Hydrogen Program
1617 Cole Boulevard
Golden, CO 80401-3393

ADDISON BAIN
National Aeronautics and Space Administration
Kennedy Space Center, FL 32899

Abstract

The United States Department of Energy (DOE) has identified isolated communities as a viable opportunity for demonstrating the practicality of hydrogen-based power systems. These DOE-led initiatives are pertinent to meeting the energy needs of isolated communities worldwide. The technological building blocks of a hydrogen energy system have reached a state of maturity that permits responsible planning. Implementation of such systems does not require scientific breakthroughs but rather is an engineering, fiscal and public policy challenge. The State of Alaska is a candidate for such integrated demonstration projects because of its exceptional vulnerability to fossil fuel price fluctuations, and its energy infrastructure logistics and environmental challenges. The DOE laboratories have been leaders in documenting and analyzing the technical progress in several disciplines and industries toward the

T. O. Saetre (ed.), Hydrogen Power: Theoretical and Engineering Solutions, 447–452.

creation of a stable hydrogen energy systems engineering methodology. These efforts are complemented by the broad experience of the National Aeronautical & Space Administration (NASA), one the world's largest users of hydrogen as an energy carrier. Universities and their research institutions have played a key role in the development of hydrogen technologies and in the fundamental knowledge base that is the critical forerunner of integrated energy system prototypes. Recent advances in hydrogen sensing technology, licensed by private industry from the DOE National Laboratories, now offers highly reliable situational awareness of hydrogen system efficiencies and safety. These new sensors overcome the previous inhibitors to progress by enabling the implementation of safe, insurable systems in proximity to populations. The combination of systems engineering, parametric analyses, standards adherence and product development disciplines will be applied toward a presentation of the art of the possible in designing, optimizing, building and operating renewable hydrogen-based energy systems to service isolated communities worldwide.

1. Introduction

Over the past two decades many of the technologies needed for a sustainable energy economy have evolved considerably, and are at the brink of commercialization. Renewable technologies such as wind and solar have proven to be technically viable sources of power. Wind power production costs are competitive with conventional sources, while solar power is expected to be competitive within a decade. There are certain markets where the value of electricity is several times higher than the electricity price in large power grid markets. For example, dozens of communities in Alaska pay $.25 - .75/kWh for diesel-powered electricity, where the national average is less than $.10/kWh. Many of these regions have an abundant wind resource. Other regions of the world where these conditions exist include remote Canadian, Russian, and other communities, insular islands, isolated military installations, isolated mines, and remote autonomous devices. These high-value power markets are where renewable technologies are making their commercial entry.

Increased use of renewables in these markets will accelerate economy-of-scale cost reductions, and broaden the market base. Most of the developed world has a well established electrical power infrastructure in place, providing electricity at relatively low cost. In regions where electricity is ubiquitous, its value is defined by the combination of its functionality and its availability. Where electricity is rare, or nonexistent, its value is defined by its functionality, and its lack of availability dramatically increases the value. About 1/3 of the world's six-billion population has yet to benefit from the use of utility electricity, therefore it is environmentally and strategically prudent to foster the use of renewables in developing regions.

Intermittent renewable power systems integrated with adequate energy storage can provide a steady supply of electricity to an isolated community, and be competitive with fossil power alternatives. The energy storage component provides power to the load when the renewable source is quiescent. Examples of energy storage methods are: batteries, pumped hydroelectric, compressed air, hydrogen-fuel cell systems, hydrogen-

engine-generators, halogen-fuel cell systems, Zn-air-fuel cell systems, Zn-FeCN-fuel cell systems and flywheels. Where compressed air and pumped hydroelectric are not practical, hydrogen systems show the most promise.[1]

Renewable energy production with hydrogen can be deployed under two main conditions: in regions where there is the need for a steady source of electricity and no grid is available, or where the renewable source is grid-connected but not phased with the peak price. Here a large pricing differential can justify the cost energy storage.

The key element for providing uninterruptable power from an intermittent, renewable source is the energy storage component. Heretofore, the availability of energy storage media was confined to pumped hydroelectric or batteries. Pumped hydroelectric can economically provide for long storage periods and can be utilized where the appropriate topography is available, if permitting for site construction is not a barrier. Battery storage is effective for small installations or where the load is small.

2. Hydrogen technologies available to isolated communities

A narrow set of criteria creates the favorable situation for deploying renewable energy systems with hydrogen storage in isolated communities, but that still creates the opportunity for numerous systems which would be technically and economically viable today. The main criteria are: commercial availability of all the necessary components in sizes that meet the needs of isolated communities; and communities with adequate renewable resource whose electricity costs are high enough to permit hydrogen systems to be competitive. Isolated communities are already benefiting from the installation of wind, solar and small hydroelectric power systems in stand-alone or diesel hybrid configurations. The additional technologies necessary for hydrogen energy storage; electrolyzers, storage vessels, compressors and fuel cells (or hydrogen ICE motor-generator sets) are all commercially available in sizes that are adequate for most isolated communities. They have yet, however to be integrated in a system in this way.

Making hydrogen technology available to an isolated community will first require an understanding of the current status of a community's knowledge, relationship, applications, if any, regarding hydrogen energy or related energy aspects. This process will help define a program suitable for the particular community and address technical needs and shortcomings. A demonstration can be made with the most evolved technology that can be leveraged from current, available commercial technology adaptable to the regional situation. The variety of hydrogen technologies that can be drawn from NASA as well as other international hydrogen-based space programs should be maximized. Such aspects as training, maintenance and operational support can be assessed as to the need for internal (regional) or external arrangements. The impact of adapting to different or local languages and cultures would require consideration for technical instructions and procedures. The NASA worldwide educational exchange program by satellite may assist in this endeavor.

Two key products that will result from the development of such a prototypical, uninterruptable, renewable power system are: 1) A generic design optimization algorithm that matches an arbitrary renewable energy source profile with an arbitrary

community load profile with the right amount, and type of storage. This can be generalized for any energy storage process and medium, and 2) A generic control system optimization algorithm that provides electricity to the customer at the lowest cost, and highest quality and reliability, based on temporally varying source and load conditions. The control system, as well as the overall power system design will strongly benefit from advanced, mesoscale meteorological forecasting, which can aid in optimizing the system and help drive down the capital and operating costs.

3. Current initiatives to use hydrogen in communities

Environmental issues continue to be the primary drivers behind the use of hydrogen as an energy alternative. Efforts to reduce pollution in urban areas in California have resulted in legislation that may pave the way for the introduction of hydrogen-fueled vehicles. In addition, a number of cities in the U.S. have tested, plan to test, or are continuing to test hydrogen-powered buses as part of the Clean Cities initiative of the USDOE.

Government-led initiatives focused on the reduction of power costs to isolated communities are also important for the introduction of hydrogen into the energy infrastructure. Renewable hydrogen utility power systems will initially be intrinsically expensive, compared to conventional, combustion power systems. However, in regions such as remote Alaska it is expected that the cost of electricity from an integrated hydrogen/renewable power system can be initially competitive with some of the higher electricity costs from conventional, isolated power plants. As more renewable hydrogen systems are deployed, their costs will decrease, making them more competitive, and opening broader market opportunities for installations of fully renewable power installations for communities worldwide. In Alaska, there is also a new requirement to remediate the environmental damage caused by prior, non-standard storage of diesel fuel used to power the numerous isolated communities. Estimates of the total remediation cost run well above $100 million.

4. Design criteria

Conditions at numerous sites worldwide would lead to the selection of hydrogen as the best choice for energy storage. Once a specific site is selected, the hydrogen storage loop design is basically a series of an electrolyzer, a compressor, pressure vessels and a fuel cell (or ICE motor-generator set). Variations on this would be for additions such as hydrogen distribution for a local vehicle fleet, for local space heating from waste heat, or for thermal integration of the hydrogen production and utilization components

The implementation of energy storage systems to provide a buffer, permitting steady state power to be derived from an intermittent, renewable energy supply requires a broad range of technical, economic and integration considerations. Because if a high degree of variability in source and load conditions, climate, economics and system

component properties, the system design and control optimization is a complex, multivariable process.

5. System Elements

5.1 PRIMARY POWER PRODUCTION OPTIONS

The primary power production installation must be "over built" in peak capacity to permit simultaneous load following and stored energy production.

Wind turbines are mature and permit small-scale, and incremental installation. Quiescent periods may last for days to weeks. Arctic rated turbines are commercially available.

Solar photovoltaic capital costs are several times higher than wind turbines, but are expected to be competitive in 5 - 10 years. Under certain conditions, PV can be the technology of choice. Quiescent periods would generally follow a diurnal cycle.

Micro- or low-head hydroelectric can be appropriate where an adequate, intermittent flowing water resource is available.

5.2 ENERGY STORAGE OPTIONS

All hydrogen energy storage systems require three basic elements:
1) a primary power-to-hydrogen conversion system (hydrogen production),
2) a hydrogen storage system (storage), and
3) a hydrogen-to-electricity conversion system (electricity production).

For hydrogen production:

Potassium hydroxide (KOH) electrolyzers are commercially available in low-pressure, unipolar and intermediate-pressure, bipolar designs. Both are attractive methods of hydrogen production for isolated power systems. The bipolar system can provide hydrogen at elevated pressure, reducing the requirement on the compressor.

Solid polymer electrolysis is an emerging, solid state method of hydrogen production whose capital costs should evolve similar to PEM fuel cells. As the costs decline, this will be an attractive method of hydrogen production.

For hydrogen storage, the size of the required container is directly proportional to the maximum credible quiescent period of the renewable resource, and the average load. This makes hydrogen storage more attractive than batteries in isolated, renewable applications with long quiescent periods, because the power conversion and energy storage hardware are separate, requiring only the size of the hydrogen storage hardware (generally least costly) to fit the quiescent power production conditions.

Intermediate-pressure, 100 - 500 psi, gas vessels are a good choice for most small community power systems, where expected costs and system volumes are reasonable.

For electricity production an electric generator driven by an internal combustion engine (ICE), with a high compression ratio and lean operation can produce electricity with efficiencies similar to a fuel cell, at a reasonable capital cost. This power

production system needs to have an efficient turn-down ratio that matches well with the temporal load profile. The primary environmental concern would be the slight NOx emission from nitrogen fixation.

Three hydrogen fuel cell options are also possible for electricity production. The phosphoric acid fuel cell (PAFC) is currently available in 200 kW units integrated with a natural gas reformer (not necessary for hydrogen energy applications). Its operating temperature in excess of 150C permits cogeneration of utility heat, but also requires long start up times. Long start up times mean that the PAFC would have to "idle" even while stored electricity is not necessary.

The proton exchange membrane fuel cell (PEMFC) in 205 kW units has been integrated into buses for use with hydrogen. A hydrogen PEMFC could operate with short (several seconds) start-up and shut-down times. The primary issue for including a PEMFC in a isolated, stationary power application is the capital cost.

Solid polymer regenerative fuel cells (RFC) are devices that electrolyze water when current is applied to the electrodes, and produce electricity when hydrogen and air are applied to the electrodes. Current, costs are high and sizes are small, but if RFCs can be manufactured at a lower combined cost than electrolyzers and conventional fuel cells, then this would be the preferred technology.

6. Current status of international cooperation

The International Energy Agency (IEA) serves as a local point for international cooperative efforts in the advancement of hydrogen technologies. The IEA Hydrogen Implementation Agreement, with twelve member countries, has three active tasks to examine photoproduction of hydrogen, storage of hydrogen in metal hydrides, and development of design guidelines for integrated hydrogen demonstrations. In addition to design guidelines, this third task includes the development of a modeling tool that will provide a library of subsystem models that can be integrated, using the simulation platform (ASPEN Plus®), into the system of interest. Subsystem models include production (biomass pyrolysis; biomass gasification; coal gasification; steam methane reforming; PV/electrolysis; wind/electrolysis; grid/electrolysis), storage (metal hydrides; compressed gas; liquifaction), distribution/delivery (pipeline), and end-use (all fuel cell designs; gas turbine). The task includes the collection of operating data from existing hydrogen demonstrations to validate the subsystem models and the integrated system modeling result.

7. References

1. Rambach, G. and Haberman, D, (1997) Uninterruptable, Renewable, Hydrogen-Based Energy for Isolated Communities Worldwide, *Advocate of the National Hydrogen Association*, **2**, 2, 6-7. Presented to 8th Annual U.S. Hydrogen Meeting, Washington, DC, March 1997.

EVALUATION TOOL FOR SELECTION AND OPTIMIZATION OF HYDROGEN DEMONSTRATION PROJECTS

C.E. GREGOIRE PADRÓ
National Renewable Energy Laboratory
1617 Cole Blvd.
Golden, CO 80401 USA

T.H. SCHUCAN
Paul Scherrer Institute
CH 5232 Villigen PSI, Switzerland

E. SKOLNIK
Energetics, Inc.
501 School St. S.W.
Washington, D.C. 20024 USA

M. BRACHT
Netherlands Energy Research Foundation ECN
P.O. Box 1
1755 ZG Petten, The Netherlands

As part of the International Energy Agency Hydrogen Implementing Agreement, an evaluation tool to assist in the design, operation, and optimization of hydrogen demonstration facilities is under joint development. Using commercially-available software (ASPEN Plus®), this tool is being designed to provide a comprehensive data base or library of component models and an integrating platform through which these models may be linked. This tool, in conjunction with data collection, will be used to develop design guidelines for integrated demonstrations.

Component models are included in the initial test platform, including several production, storage, transport, and end-use modules. Production models include biomass gasification and pyrolysis, natural gas steam reforming, and water electrolysis. Storage technologies consist of metal hydrides, chemical hydrides, liquefaction, and compressed gas. Transport models include high and low pressure pipelines, truck transport, and a refueling station. End-use technology models include several types of fuel cells and a gas turbine. It is anticipated that users of this tool will select production, storage, transport-distribution, and end-use models from the library of component models, or will use one or more of their own models in conjunction with the library models. Component models are then linked, using the integrating platform, into an overall hydrogen system.

T. O. Saetre (ed.), Hydrogen Power: Theoretical and Engineering Solutions, 453–458.

Situational analyses of two potential integrated hydrogen demonstrations were performed to illustrate the use of this tool. Configuration and selection of the subsystems are addressed in the context of the design of a hydrogen demonstration facility.

1. Introduction

Around the world, a number of hydrogen demonstration facilities currently exist or are in the planning stages. These facilities, developed for a variety of reasons, can provide important operating data for future commercial systems. Evaluation of the performance of these demonstrations can provide important insight into the design, configuration, and operation of future demonstration facilities, as well as for future commercial enterprises.

In a cooperative effort under the auspices of the International Energy Agency Hydrogen Implementing Agreement, representatives from seven countries (Canada, Italy, Japan, Spain, Switzerland, the Netherlands, and the United States) have been collecting, evaluating, and using data and models to develop a tool for the design and optimization of existing and future demonstration projects. This effort includes the development of process models for individual production, storage, transport, and end-use applications, followed by integration of these component models into overall hydrogen system models. The component models that have been developed include PV-electrolysis, biomass gasification, compressed gas storage, metal hydride storage, high pressure pipeline transport, fuel cells, and gas turbines, among others. A strict developmental methodology was instituted to ensure that integration into an overall hydrogen system could occur with minimal effort.

To demonstrate the use of this tool, two integrated systems of potential interest have been evaluated: a stand-alone, grid-independent power system for electricity production; and a decentralized renewable system for transportation applications. The stand-alone power system consists of an intermittent renewable energy source (PV or wind) with water electrolysis, storage as a compressed gas or in a metal hydride system, and electricity generation in a fuel cell or gas turbine. The decentralized system consists of production from biomass via gasification or pyrolysis, transport by pipeline or truck, storage of liquid or compressed gas hydrogen, and dispensing at a refueling station. Behavior of the individual component models and of the integrated systems provides insight into the usefulness of the design tool for evaluation of hydrogen demonstrations.

2. Data Availability and Collection

A survey of the participants was conducted to determine the location and configuration of existing or planned hydrogen demonstration facilities, from which data could be obtained. This canvas identified a number of PV-electrolysis facilities, with compressed gas and/or metal hydride storage systems, where data are available. In addition, other systems were identified, including wind-electrolysis; hydroelectric-electrolysis; and a number of commercial facilities based on steam methane reforming. Additional subsystem demonstrations were also identified, where future hydrogen projects might be possible with

the integration of additional components. These included several types of biomass gasifiers, coal gasifiers, chemical hydride storage systems, and a number of fuel cell sites.

Collection of configuration and operation data was initiated for existing and potential demonstrations. These data are used to validate results of component model simulations.

3. Component Model Development and Evaluation

Using the ASPEN Plus® process simulator as the basis for model development, individual component models were created. These models are used to develop an understanding of the important design and operation parameters for the individual components. While it is not possible to foresee all potential applications for the subsystem models, care has been taken to address the most likely engineering design for each component model.

Table 1 describes the subsystem models that are available through this effort. A short description of the models is included.

4. Integrated System Modeling

There are additional interactions between components in an integrated system that require simulation of combinations of subsystems. Although determination of overall system efficiency and performance is important in the evaluation of a proposed hydrogen demonstration project, specific attention must be given to the practicality of the chosen system. Important considerations for the integration of these component models include internal versus external heat integration, flow of materials, purity, temperature and pressure of interfacing streams, and availability of utilities.

4.1 STAND-ALONE, GRID-INDEPENDENT POWER SYSTEM

As an illustration of a stand-alone, grid-independent power system, a series of cases were modeled: PV-electrolysis/compressed gas/gas turbine and PV-electrolysis/metal hydride storage/PEM fuel cell. Important integration issues in these systems are: the identification of the operating point for the PV-electrolyzer subsystem; the temperature and pressure of interfacing streams; and the power demands that must be satisfied by the gas turbine or fuel cell. Although a number of systems can be configured using these subsystem components, only a few combinations result in practical engineering systems.

The characteristics of the PV-electrolysis subsystem in this study were obtained from the demonstration project operating in the Los Angeles, California (USA) area. The solar insolation for this region is 858 W/m^2, and the 40 kW (nominal) PV system consists of 36 cells in series per module, and 37 modules in parallel. The system has a short circuit current of 70.4 amps per assembly, voltage at maximum power point of 16 volts, and an open circuit voltage of 20.9 volts. The electrolyzer, supplied by Electrolyser Corporation, operates at atmospheric pressure and produces 10 Nm^3 of hydrogen per hour (nominal) from approximately 10 liters of water per hour.

TABLE 1. Component Model Development

	Technology	Description	Resources
Production	PV/Electrolysis Wind/Electrolysis	PV or wind turbine characteristics to find operating pt for interfacing renewable resources with electrolyzer; calculates production rate.	Spain, U.S., Canada
	Biomass Pyrolysis	Decentralized production of bio-oil; liquid shipped to processing facility (near market). Centralized steam reforming of bio-oil; shift, PSA purification. Produces H_2, high quality steam.	U. S.
	Biomass Gasification: - Indirect-heated, low pres, fast-fluidized	All processes occur in a centralized location. Both types of gasifiers produce syngas, which is then steam-reformed, shifted, and PSA-purified. Produces H_2 and high quality steam.	U. S.
	- Air-blown, high pres, fluidized-bed		Netherlands
Transport and Distribution	High-pressure pipeline	Calculates pressure drop and heat transfer as a function of segment length; location of compressors based on allowable pressure drop.	U. S.
	Distribution pipeline	Includes pressure reduction valves for end-use distribution	U. S.
	H_2 refueling station	Model considers heat maintenance, pressure relief, and fuel losses. Considers both compressed gas and liquid H_2.	U. S., Canada
Storage	Metal hydrides	Hydride identity and characteristics are user-specified. User-supplies Van't Hoff equations for ad- and desorption. Calculates round trip efficiency and energy requirements for storage and recovery.	U. S.
	Compressed gas	Considers unit operations to compress H_2 to user-specified pressure.	Canada, Netherlands
	Liquefaction	Calculates liquefaction energy requirements.	Japan
End-use	Hydrogen gas turbines	Uses existing natural gas turbine system models modified for H_2.	U. S.
	Fuel cells	Calculates electrical power produced by PEM or phosphoric acid fuel cells.	U.S., Spain, Canada

Electrolyzers operating at elevated pressure (30 bar) produce hydrogen at high pressure. For a gas turbine, the production of high-pressure hydrogen is an important system consideration; compression prior to the combustor could be eliminated if the hydrogen were to be produced at a pressure that is appropriate for the turbine subsystem.

For compressed gas storage, the hydrogen is compressed to 100-300 bar in a multistage compressor. The final storage pressure depends on end-use requirements and on the available storage area (allowable tank size) and compressor costs. In our study, the gas turbine requires an inlet pressure of approximately 25 bar; selection of storage pressure is primarily driven by allowable storage tank volume and compressor capital costs.

The metal hydride selected for this study was Mg_2Ni, a high temperature hydride, with a hydriding temperature of 256°C at 4 bar, and a dehydriding temperature of 281°C at 2 bar. Hydrogen desorption from the metal hydride bed is accomplished by reducing the pressure and supplying the necessary heat. The low-pressure hydrogen can be fed into the fuel cell operating at atmospheric pressure, but would have to be pressurized to 25 bar for the gas turbine application. Additionally, the high temperature of the released hydrogen could damage the PEM fuel cell, and temperature control may be required.

4.2 DECENTRALIZED RENEWABLE TRANSPORTATION SYSTEM

The decentralized system for transportation applications examined biomass gasification/ high-pressure pipeline transport/liquefaction/refueling station. The important integration issues in this system include temperature, pressure, and composition of the interfacing streams. As in the above case, special attention must be given to the requirements of the individual subsystems when integrating into an overall system.

The selection of gasification technology depends on a number of interrelated parameters. A low-pressure, indirectly-heated gasifier produces a syngas stream with relatively high concentrations of CO and H_2, but requires compression of the syngas prior to reforming and water-gas shift. The high-pressure circulating fluidized bed gasifier, on the other hand, requires an oxygen plant to reduce the dilution of the syngas stream, or processes to recover hydrogen from the dilute stream generated in an air-blown system. Several biomass gasifiers exist and could be integrated into hydrogen production facilities.

Hydrogen purification following the low-temperature shift reactor is generally accomplished in industry by pressure swing adsorption. Since the resulting hydrogen stream is at a relatively low pressure following this process, a compressor will be needed to increase the hydrogen pressure to the pipeline pressure (50-65 bar). The hydrogen is delivered to the refueling station storage field for further compression to 250 bar for on-site storage. Another possible system configuration includes liquefaction of the hydrogen, with truck transport to the refueling station. Comparison of capital and operating costs for these options are important in the selection of the subsystems, with special attention required in calculating the transportation distances.

Flexibility in on-board storage technologies may require an equal flexibility in available hydrogen from the refueling station. In other words, the refueling station may need to be able to service a number of potential configurations for on-board storage. High-pressure and metal hydride on-board storage can be handled by the compressed gas

stationary storage system, whereas liquid and metal hydride on-board storage can be handled by the liquid stationary storage system.

5. Development of Design Guidelines

Guidelines will be developed to assist in the design of future demonstration plants to meet operating and user requirements, and to facilitate the systematic integration of hydrogen into the world's energy system. Validation and optimization runs conducted on integrated systems, such as those described above, will serve as the basis for optimization of existing hydrogen systems and for guidelines for new, promising, and desirable hydrogen systems.

The requirements for the development of a design include information on the integration of components in real systems, sizing of facilities, optimization of performance, and methods for calculating overall system efficiency. The guidelines will also assist the designer in selecting the best system for various applications, and will give design criteria for inclusion of externalities such as CO_2 sequestration/mitigation.

The important measures of performance to be included in the design guidelines are: emissions; availability of energy source (biomass, wind resources, solar insulation); comparative efficiency; size; cost; quality/purity of output; comparative storage capacity and availability; and safety and acceptance. The IEA activity will include development and quantification of these measures of performance for hydrogen demonstrations.

6. Evaluation and Optimization of Hydrogen Demonstrations

Using the library of subsystem models, an integrated system can be evaluated for any of the measures of performance discussed above, or additional measures specified by the user. Optimization of individual subsystems is instructive for developing operating curves, but the optimum operating point for an individual subsystem may not be the optimum operating point for an integrated system.

The ASPEN Plus® platform is structured to permit optimization of complex systems, with a graphical user interface that is designed for interactive setup and evaluation of results. The library of subsystem models will be made available to interested parties with access to the ASPEN Plus® software. Arrangements may also be made for evaluation of cases through interactions with the participants in this activity.

7. Acknowledgments

The authors wish to acknowledge the following contributors to this effort: Matthew Fairlie (Canada), Makoto Akai (Japan), Felipé Rosa (Spain), Arend deGroot (Netherlands), Hajo Ribberink (Netherlands), Margaret Mann (USA), Johanna Ivy (USA), Pamela Spath (USA) and Joseph Badin (USA). This IEA task-shared work is funded by agencies and industrial entities within each participating country.

PUBLIC DEMONSTRATION OF PEM FUEL CELLS AS MINIATURE HOUSEHOLD CO-GENERATION PLANTS IN MUNICH

U. BÜNGER, E. KRAUS
Ludwig-Bölkow-Systemtechnik GmbH
Daimlerstraße 15
D-85521 Ottobrunn
e-mail: buenger@lbst.tnet.de

TH. SCHMALSCHLÄGER
Stadtwerke München / Energieservice
Kapellenweg 4 - 6
D-80287 München

1. Introduction

We are currently observing rapid changes in international local energy market structures. The general trend towards competitiveness can be subsummized under terms like *liberalization*, *deregulation* and *privatization* [1]. Starting in the U.S. with the Public Utility Regulatory Policies Act in 1978 various European countries like the UK and Norway followed. Restructuring the energy system will eventually lead to a unification of large electricity and gas suppliers, and to efficient small energy service companies installing decentral, flexible and low cost energy conversion technologies.

With a growing awareness of the costly dependency on oil imports from politically instable regions [2] and that its resource depletion may happen faster than generally believed [3] we now observe a trend to natural gas as a power generation fuel. Currently the world natural gas demand is projected to be doubled by 2030, annually increasing by 2.1 - 3.5% until 2010 [4]. This facilitates small decentralized power plants often operated by flexible independent power producers (IPP), free trade of the grid energy carriers natural gas and electricity and rising numbers of natural gas operated cogeneration systems.

Furthermore, the trend towards gaseous energy carriers will eventually lead to renewable hydrogen as the most versatile non-carbon based fuel. Its widespread application is no longer a vision, but is accepted as a reasonable means of reducing global CO_2-emissions [5], although the time for its advent is still heavily debated [6].

T. O. Saetre (ed.), Hydrogen Power: Theoretical and Engineering Solutions, 459–465.

All developments together foster the introduction of energy savings and conversion, storage and supply technologies for stationary small scale high efficiency power supply. Fuel cells (FCs) are known for their fuel flexibility. As their operation with hydrogen results in highest efficiencies they are a key component to a non-fossil era.

2. General Trends Concerning the Use of Residential FCs

In Europe an obvious trend in residential electricity and heat supply in new buildings points towards significant energy savings. For existing residential buildings new directives will further tighten reduction goals for heating demand. E.g. in Germany a new law expected for 1999 will require that so called low energy houses with 50 - 70 kWh/m² a be built. In these houses low temperature distribution systems with 40/60°C will ease the introduction of low temperature heat generating systems like PEMFC.

Other trends are the application of electric heat pumps and local district heating grids. Whereas the electric heat pump is a direct competitor for the FC technology, consuming electricity for heating instead of co-producing it locally, district heating and FC cogeneration systems could harmonize well. Furthermore, first attempts have been undertaken to evaluate the advantages of combining renewable energy technologies and FCs [7]. As the discussion is in progress general conclusions can not be drawn yet.

As only small quantities of renewable hydrogen may be available the next 10 - 20 years for economic reasons most sensitive FC fuel alternatives are natural gas and methanol. Natural gas is available from a dense distribution grid in many European countries, methanol can replace oil for remote applications. Both fuels however require efficient fuel converters, currently being developed [8, 9]. Small FCs cogenerating heat and electricity can flexibly supply valuable peak power, capable of eventually changing the electric heat pump energy supply strategy for buildings to „gas in - electricity out".

3. Technology of Natural Gas Operated PEMFC for Cogeneration

Among the five known FC technologies – mainly characterized by their operating temperature – proton exchange or polymeric electrolyte membrane FCs (PEMFC), phosphoric acid FCs (PAFC) and, for widely unmodulated operation, also solid oxide FCs (SOFC) are suitable for small scale residential heating. PEMFC typically operate at 40 – 80°C with high total efficiencies of ≥ 85 % in hydrogen and 65 - 80% in natural gas operation, resulting in electrical efficiencies of 45% (31%). Thus, PEMFC are ideal for low temperature cogeneration of heat and electricity in individual single family homes or small district heating grids. They can also be used for remote power generation as e.g. in developing countries. FCs are the core of these cogeneration systems. However, the techno-economic adaptability of FC systems for individual applications is determined by the layout and performance of the tailored subsystems.

3.1. PRIMARY FUEL REFORMER

In carbon-fuel operated FCs fuel converters are responsible for producing hydrogen from a variety of fuels like natural gas, methanol, ammonia, LPG etc.. The reformer/purification unit must be customized to the individual operating requirements (load dynamics). For dynamic PEMFC especially with small fuel converters the problem is their complexity with subsystems like desulphurizer, reformer, CO shift-reactor and CO removal system ($\leq$ 10 ppm), which can be Pd-membranes or selective oxidizers. For 10 kW_{el}-class PEMFC systems miniaturized natural gas reformer technologies are described in more detail in [10]. For large applications the specific reformer costs for natural gas operated PEMFC systems will be about 2/3 of the stack costs themselves [11], in small units they will probably approximate the stack costs.

PAFC are much more tolerant to CO than PEMFC, decisively lowering the degree of fuel converter complexity. SOFC may not require a fuel converter at all as it can be integrated into the high-temperature ($\approx$ 600°C) stack [12]. For an optimization towards uninterrupted FC operation it may be necessary from case to case to consider a hydrogen buffer storage system.

3.2. GAS AND HEAT FLOW SUBSYSTEMS

PEMFC can be characterized by their operating pressure level. The lowest secondary energy demand is necessary for unpressurized systems. The highest energy densities and material intensity can be reached with pressurized systems. The pressure is typically below 3 bar, resulting in relatively simple hydrogen/air blowers. The exhaust gases have to be removed from the system confinement, however no over-the-roof ventilation stack will generally be required in residential systems. The heat generated will be taken out by a circulating flow of water, which can also be stored in conventional warm water storage equipment, thus lowering system complexity.

3.3. DC / AC CONVERTER AND SYSTEM CONTROLS

In grid connected residential FC systems the electricity has to be transformed to the grid quality and safety specifications. The development of FC integrated inverters will eventually require least costs, which can only be reached by a highly integrated single-chip-design of power and control logics within the system controller. Specific inverter investment costs, which can be as low as 400 DM/kW_{el} [13] today, may well reach 50 DM/kW_{el} when mass produced in the future [14].

3.4. SAFETY COMPONENTS

For small residential FC cogeneration systems, generally installed in the basement of single family residences, special attention must be paid to safety. Preliminary results of a German inspection authority require a forced ventilation of about 5 h^{-1} either by

natural or forced convection. An alternative is the installation of cheap customized sensors at locations of highest possible hydrogen concentrations, requiring customized low maintenance sensors as under development in Europe [15] and the U.S [16].

4. Operating Modes of Small 10 kW_{el} Class Household PEMFC

In a follow-up project to previous hydrogen related studies of the Stadtwerke München (municipal utility owned by the city of Munich) and Ludwig-Bölkow-Systemtechnik [17] an analysis of three operating modes (see table 1) for small natural gas operated PEMFC was carried out in comparison to a conventional calorific gas burner [18]. A flow diagram of the system is sketched in fig. 1.

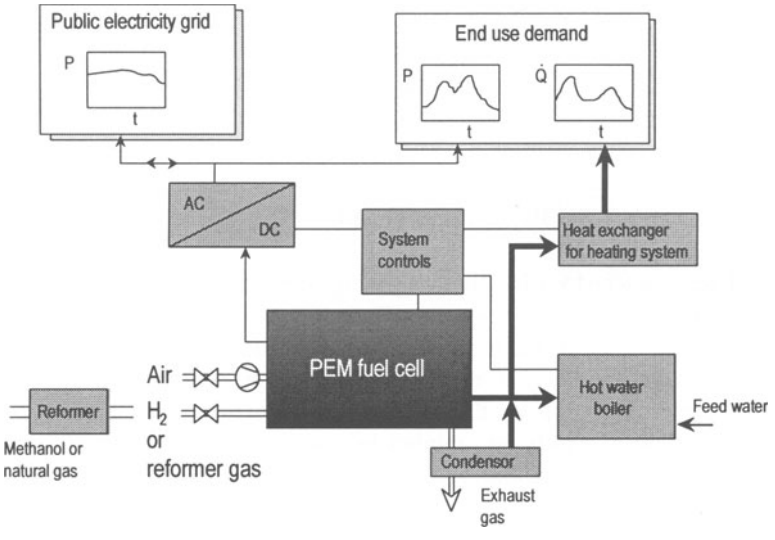

FIGURE 1. Flow diagram of a small natural gas residential co-generation PEMFC (Siemens)

The specific operating conditions (local climate, electricity and gas tariffs, etc.) of Munich were considered. The techno-economic PEMFC development goals of the industry involved were anticipated. The system was expected to be operated priorizing heat production in winter and electricity production in summer. During summer the decision about the time and period of operation lies within the responsibility of the local utility. As the period for maximum electricity demand in the grid can coincide with the warm water demand of the individual household by means of a warm water storage system (e.g. 150 l) the utility can now flexibly levelize its electricity production capacities within the grid, hence improving overall system economy.

The economic evaluation of the system was based on a complex simulation model (see table 2) and a consecutive sensitivity analysis.

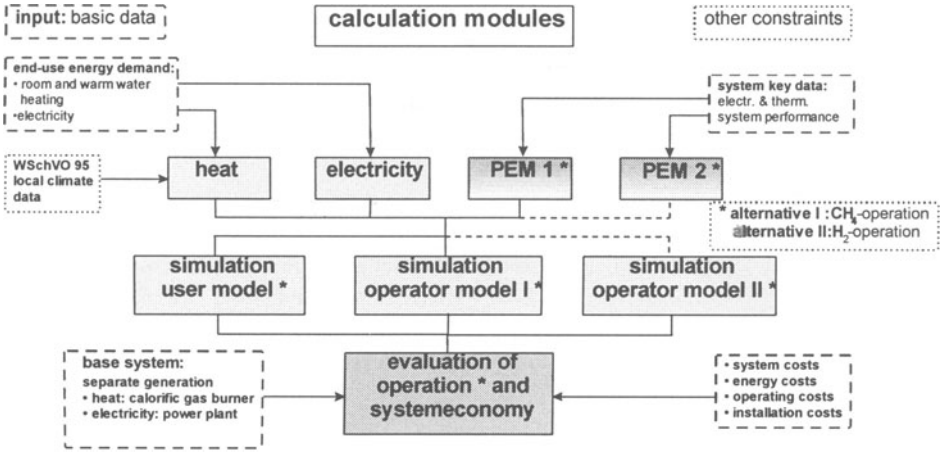

FIGURE 2. Functional entities of the PEMFC simulation tool [18]

The conclusions can be summarized as follows.

- local emissions can be reduced to a minimum, the reduction of global CO_2-emissions depends on the total efficiency and operating mode, but is decisively lower than from other conventional technologies
- electric and total efficiencies are as high as 31 and 73%$_{lhv}$ in cogeneration mode
- part load characteristics are favorable
- low noise and low maintenance system

Although the techno-ecological determinants are highly favorable the commercial chances for the proposed system are limited to specific operating conditions (table 1).

TABLE 1. Commercialisation chances for different small PEMFC operating modes

Owner / Operator	Evaluation
Private	• not competitive if connected to the electricity grid • small systems possibly competitive if grid-independent
Energy service company	• currently not competitive
Utility	• competitive by replacing peak power (typically at noon)

The utility option currently seems to be most promising for small natural gas and electricity supplying communities, because only then the operational flexibility of small decentralized heat and electricity generation systems can be utilized.

For larger 200 kW_{el}-class FCs (PEMFC, PAFC) a recent study revealed that when reaching their investment cost development goals both technologies may not only be

competitive with natural gas fired boilers, but also with gas engine cogeneration plants [7]. The next years of intensive development efforts and pilot projects such as the first 250 kW_{el} PEMFC for Berlin [19] will unveil verifyable development potentials.

5. Conclusions and Recommendations for Further Work

Further techno-economic studies are necessary to study the economic chances for PEMFC and SOFC in the 10 kW_{el}-class, and for 200 kW_{el}-class PAFC or PEMFC district heating systems. Among the specific topics to be examined are

- best fit studies of various FC and gas converter technology combinations,
- in depth techno-economic evaluation of small 10 kW_{el}-class FCs (PEMFC, SOFC) with 200 kW_{el}-class district heating systems (PEMFC, PAFC) and
- gain-to-investment ratio (emissions, efficiency, simplicity, etc.) of system combinations like PV/FC, solar thermal systems/FC or biomass/FC.

In the current development stage practical experience from pilot and demonstration projects is necessary. A first small PEMFC co-generation project is planned for the city of Munich during the next years, others will hopefully follow in the not too far future.

6. References

1. Schmitt, D.: Europäische Elektrizitätswirtschaft und EU-Binnenmarkt. 10 Thesen. Proc. *Energieinnovation als Wirtschaftsfaktor*, Ed. Kurt Friedrich and Wolfgang Wallner, Vienna, 1996, pp. 37 - 42.
2. Riva, J.P.: World oil production after year 2000: business as usual or crises? U.S. Congress report 35-925 SPR, 18 August 1995.
3. McKenzie, J.J.: Oil as a finite resource: When is global production likely to peak? Paper *by World Resources Institute*, Washington, March 1996.
4. Study of the International Gas Union, Presented *at 20th World Gas Conf.*, Kopenhagen, 8 - 13 June 1997.
5. Decarbonisation of fossil fuels. Report PH2/2 by Foster Wheeler for Statoil and IEA-GHG, March 1996.
6. Nitsch, J.; Dienhart, H.; Langniß, O.: Entwicklungsstrategien für solare Energiesysteme - Die Rolle von Wasserstoff in Deutschland, *Energiewirtschaftliche Tagesfragen*, 47(1997), No. 4, pp. 223 - 229.
7. Blandow, V.; Bünger, U.; Eckstein, U.; Loerbroks, A.; Maier, S.; Niebauer, P.: Die Bedeutung von Energiespeichern in zukünftigen Niedrigenergiehäusern. Report *Ludwig-Bölkow-Systemtechnik*, April 1997.
8. Jones, R.; von Waveren, T.: Novel compact steam reformer for fuel cells with heat generation by catalytic combustion augmented by induction heating. To be published in *Catalysis Today*, 1997.
9. Product brochure of the Fraunhofer Institute for Solar Energy Systems, Freiburg, April 1997.
10. Weindorf, W.; Bünger, U.: Verfahren zur Reinigung von Wasserstoff aus der Erdgasdampfreformierung für den Einsatz in Brennstoffzellen. To be published in *Brennstoff-Wärme-Kraft*, 7/8 1997.
11. Gavalas, G.R., Voecks, G.E.; Moore, N.R.; Ferrall, J.F.; Prokopius, P.R.: Fuel cell locomotive development and demonstration program - phase I: systems definition. Report to *SCAQMD*, California, 1995, p. 4-12.
12. Barp, B.; Dienhart, R.: Solid oxide fuel cells for small scale cogeneration. Conf. Proc. *Eurogas* Trondheim, 3 - 5 June 1996.
13. Rasch, H.: Untersuchung zum Einsatz von Frequenzumrichtern für Photovoltaikanwendungen. Thesis FH München, FB Elektrotechnik, Oktober 1996.
14. Schwab, M.; Reismayr, D.; Fechner, U.: Concept and cost degression potential of PV-inverters at very high mass production. Conf. Proc. *EuroSun '96*, pp. 876 - 878.
15. Sensorsystem mit minimalem Energieverbrauch basierend auf gasempfindlichem Feldeffekttransistor zur Wasserstoffdetektion. Project proposal for the Hydrogen Initiative Bavaria (WIBA), 1996.

16. Haberman, D.: Advances in sensor technology may expand hydrogen applications. *NHA Advocate*, newsletter of *National Hydrogen Association*, Vol. 2, No. 1, 1997, pp. 1 - 2.
17. Bünger, U.; Zittel, W.; Schmalschläger, T.: Hydrogen in the public gas grid - a feasibility study about its applicability and limitations for the admixture within a demonstration project for the city of Munich. Xth World Hydrogen Energy Conf., Cocoa Beach 1994, pp. 173 - 183.
18. Kraus, E.: Einsatz und Betreibermodelle kleiner stationärer Brennstoffzellen-Blockheizkraftwerke im Versorgungsgebiet der Stadtwerke München. Thesis FH München, FB Versorgungstechnik, April 1997.
19. Das Brennstoffzellen-Blockheizkraftwerk im Bewag-Heizwerk Berlin-Treptow. Unpublished description of the first 250 kW_{el} PEMFC in Berlin, June 1996.

Role of the NHA in Strategic Planning for the Hydrogen Economy:
An International Initiative

Robert L. Mauro
Karen I. Miller
The National Hydrogen Association

The NHA, in conjunction with the U.S. Department of Energy, is defining the path to a hydrogen energy industry. The NHA has produced a draft document titled *Strategic Planning for the Hydrogen Economy: The Hydrogen Commercialization Plan*, which was officially adopted by the membership at the *8th Annual U.S. Hydrogen Meeting*, in March of this year. Much of this paper is based on the objectives of the plan, and describes existing activities which support these objectives.[1,2]

1. PARTNERSHIPS

The NHA believes that the journey along the path to a sustainable hydrogen energy future will only be successful by working together in partnerships. These partnerships include industry, government, and other organizations, and must span national borders. The plan states that:

> "Industry has the expertise and financial resources to bring new products to the marketplace. But industry must respect the bottom line and the demands of its stockholders to provide short-term return on investment. Industry cannot finance long-term societal goals such as clean air and reduced dependence on foreign oil."
>
> "On the other hand, governments are responsible to protect their citizens and the environment from the excesses of individuals or corporations pursuing their own economic self-interest. Government alone has the long-term staying power and the mission, acting on behalf of all citizens collectively, to develop and promote new

[1]Much of this Activity was performed under an NHA cooperative agreement with DOE.

[2]The authors would like to acknowledge the editorial contributions of Beth Cole.

T. O. Saetre (ed.), Hydrogen Power: Theoretical and Engineering Solutions, 467–474.

> technology and new policies that will achieve societal objectives. Working together, government can provide the marketplace savvy and the large capital investment, once the hydrogen technology development comes within industrial planning horizon time scales."
>
> "The primary objective of the plan is to obtain commitments from both industry and government to begin implementing the hydrogen energy industry. Such joint commitment will require an economically and[1] technically feasible roadmap on how to get from here to there. Industry must be convinced that it can eventually make a return on investments in hydrogen technology. Government must be convinced that its investments will leverage larger societal benefits in the form of reduced health costs, reduced oil imports, and improved international competitiveness over time. In short, the hydrogen commercialization plan must point to a credible benefit/cost ratio for all participants."

1.1. INDUSTRY/GOVERNMENT PARTNERSHIPS

Both the NHA and HTAP are partners with the DOE. The NHA represents domestic companies with business or market interests in the US, and supports International Energy Association (IEA) objectives.

1.2. ORGANIZATION PARTNERSHIPS

Both HTAP and the NHA currently have efforts underway to implement the commercialization plan for hydrogen. HTAP and the NHA compliment each other in the common purpose of helping DOE reach its objectives of advancing technologies critical to the development of sustainable hydrogen energy systems which will be environmentally benign, and economically viable. The NHA is also actively establishing technical and policy alliances with other organizations, particularly in the area of codes and standards, leading toward national and international acceptance of hydrogen standards. In fact, two draft standards developed by working groups in the NHA for hydrogen containers and refueling stations were accepted as ISO TC/197 work items in Toronto on May 27, 1997.

1.3. INDUSTRY PARTNERSHIPS

Cooperation between industries is also critical to success. Industry partnerships are the key elements required to implement the Commercialization Plan. Committees composed of NHA and HTAP members, must advance technologies and lower barriers to create a hydrogen future. The DOE is interested in cost-sharing projects with industry, with industry paying an increasing share of the cost as each technology approaches market viability. To this end, industry members of the NHA are forming coalitions, such as the California Hydrogen Business Council (CHBC), to plan and implement near term projects in support of continued growth in hydrogen based technology and business. This type of coalition provides local synergy for focused

action to realize common DOE-NHA-HTAP goals embedded in the drive to the Commercialization of Hydrogen. The first CHBC meeting was held in Long Beach, California on June 4, 1997. The meeting drew over 30 business, agency, and government representatives who are committed to building hydrogen cluster, while increasing hydrogen business for their employers. The combined resources of the CHBC provides a synergism that is required to take the hydrogen industry to the next level; enabling consumers to use hydrogen in a market which is safe, economical, and sustainable. The CHBC works with the DOE and NHA with implementation and commercialization by organizing business teams to conduct demonstrations of equipment in the Western region of the United States. Groups such as this are being encouraged in other regions as well.

2. CORRIDORS

The NHA works with the DOE an industry to coordinate and promote hydrogen activities. This occurs through the Codes and Standards Workshops, NHA web page information and publication of two newsletters: the NHA Advocate and the H2 Digest. In addition, the NHA hold annual meetings. The Annual Hydrogen Meeting, NHA's signature event, is recognized world wide for it's importance in bringing together a diverse group with a common interest in hydrogen energy technology. The objective is to promote the exchange of information relevant to the development of the commercial use of hydrogen as an energy source within the hydrogen community. Held each year in the Washington, DC area, the meeting draws high level hydrogen policy decision makers, hydrogen and fuel cell industry leaders, research institutions, academics, policy makers and press from around the world. The meetings have been sponsored every year by the U.S. Department of Energy and NASA: other sponsors include DOT/FTA, SCAQMD, and EPRI.

The DOE supports a Corridors Program which promotes the concept of industry partnership and cooperation to identify and solve niche-market opportunities to develop clusters around sites that already need or use hydrogen, which will lead to hydrogen corridors. In this way the hydrogen infrastructure will evolve in response to the end use needs of hydrogen and the hydrogen activities and infrastructure are less likely to disappear when Government funding is reduced or eliminated. Meetings have already been held on the West Coast and the East Coast of the United States. The following is a step by step development of infrastructure and map of flexible paths for the development of these hydrogen corridors.

2.1. DEVELOPMENT OF CORRIDORS

Existing industries using hydrogen applications in their embryonic stages grow, attracting other industries with hydrogen activities. These industries develop into clusters because of their geographical proximity. As more and more hydrogen applications grow at geographically separate sites, there will evolve a natural need for commercial interaction in the form of corridors. Need will trigger placing additional hydrogen-related businesses and hydrogen dispensing stations along the route to serve

both markets. There is a desire on the part of industry and government to jump start this process with demonstrations focused around existing hydrogen users and systems easily modified to accommodate hydrogen.

2.2 EXISTING HYDROGEN APPLICATIONS

The first step in this development process is to identify existing hydrogen applications. Hydrogen sites exist throughout the U.S. Many are at NASA facilities, DOD sites and national laboratories. Sandia, Los Alamos, Sacramento, WSRC, Nevada Test Site, many military facilities and Kennedy Space Center are all potential sites around which clusters could develop.

Along the Gulf Coast are a series of industries linked by four different hydrogen pipelines owned by hydrogen gas producers connecting various plants that produce and consume hydrogen. Some pipelines are over 100 miles long and connect dozens of industrial facilities that range from chlor-alkali plants to petrochemical plants. Such a cluster of facilities which uses hydrogen for industrial purposes is well on its way to becoming a corridor of industrial users in a crescent from Houston, Texas to Pensacola, Florida. These pipelines carry hydrogen primarily for use as a chemical feedstock. There is widespread use of hydrogen as a chemical feedstock or for industrial processing in chemicals, fertilizer, and methanol, as well as steel, electronics and food processing. Hydrogen use in these industrial sectors is increasing at between 8% and 10% a year. In addition NASA makes extensive use of liquid hydrogen for rocket propulsion and engine testing.

Additional hydrogen clusters exist in Southern California where environmental concerns make clean energy use a high priority. The aerospace industry in Southern California has on-site hydrogen in order to conduct fuel-based tests for engines, fuel cells and to create hydrogen environments for processing. Their familiarity with hydrogen and environmental concerns make them logical candidates for various types of hydrogen demonstrations.

2.3. DEVELOPING OTHER HYDROGEN APPLICATIONS

There are several applications that industry believes might offer cluster opportunities. These applications can be located near existing industrial hydrogen users or producers. The following are applications identified at a recent meeting of the California Hydrogen Business Council:

2.3.1. *Municipal Solid Waste*

Municipal Solid Waste can be gasified to produce a hydrogen gas stream that, when cleaned, can provide hydrogen for power generation, fuel for fleet vehicles or a chemical feedstock. In theory such a project coupled with recycling would virtually eliminate the need for landfills. A project of this type is being considered for Los Angeles' landfill.

2.3.2. *Airport Vehicles*

Airport Vehicles are all fleet vehicles. The shuttle buses, vans and on-field vehicles can all be hydrogen powered and refueled from a central facility. This would eliminate the diesel pollution from airports such as LAX and open the door for fleet use of hydrogen. Munich airport is planning on putting hydrogen based shuttle vehicles in service.

2.3.3. *Indian Reservations*

Indian Reservations are another possible application, large portions of which often do not have electric power. The cost of line extensions to serve individual customers or villages is prohibitive. Hydrogen energy systems provide a means of supplying reliable power and bringing an improved quality of life to native peoples in remote locations. These systems could be direct solar based in the Southwest and wind based in the Plains States. This is a similar concept to remote applications for Alaska villages.

2.3.4. *Buses*

Buses represent a major early market for hydrogen. Many urban bus systems service communities in non-attainment areas for particulates. Hundreds of these communities exist throughout the United States. Diesel exhaust is a major contributor to small particulate emissions which EPA has identified as the most hazardous to human health. Hydrogen power conversion systems are contributors to a solution. Hydrogen fuel cell buses will be running in Chicago this fall and an engine based hydrogen bus will soon begin revenue operation in Augusta, Georgia.

2.3.5. *Power Generation*

Power Generation is another use of hydrogen. Early applications are likely to be remote sites with renewably produced hydrogen. However, landfill or biomass gasification to produce hydrogen for multiple purposes including on-site power generation is also an early potential use.

In addition to these applications, there is the need to consider hydrogen vehicles in the context of ZEV requirements on the 2002 time frame, and fleet vehicles for major corporations, utilities and governments at all levels.

2.4 IDENTIFYING FUTURE CORRIDORS

Corridors develop out of the need to connect clusters either to provide chemical feedstock needs or a desire for hydrogen transportation between clusters. The DOE has tasked Sandia National Laboratory to develop the corridor concept in partnership with industry and DOE.

The first corridor opportunity would be presented in California. Existing sites between the Los Angeles Basin (which has both production and hydrogen use facilities) and Sacramento could be connected. The PVUSA facility at Davis, California tests photovoltaic (PV) systems for power production. Electrolyzers could be added at the facility to test different types of electrolyzers with different PV systems. The hydrogen produced at the facility could be used to refuel Sacramento urban buses or a Clean Air

Now facility which refuels converted hydrogen vehicles. With an existing hydrogen production facility in the area, the ability exists to expand beyond the limitations of renewably based hydrogen that the PVUSA site could provide. Hydrogen buses could also potentially run between Los Angeles and Sacramento.

There is another opportunity to expand a second corridor by developing a hydrogen site in Las Vegas. The goal would be to have hydrogen powered buses run between Los Angeles and Las Vegas with a hydrogen dispensing station in Las Vegas. This station could also be used to refuel hydrogen buses that regularly operate between the Nevada Test Site and Las Vegas. Hydrogen based transportation around the test site could also be instituted. Additional bus service could also be extended between Las Vegas and Phoenix. The final link in this initial chain would be installing dispensing stations and providing hydrogen buses that operate from Phoenix to Albuquerque. Hydrogen buses could also be operated between the Sandia, Los Alamos and Albuquerque and on-site at each of the National Laboratories. Beyond these sites, clusters and then corridors could extend to Salt Lake City and Denver.

A third corridor could be developed in the Southeast. Environmental issues are of increasing concern in Florida. Miami in particular provides the opportunity for using hydrogen buses for urban transport. The Kennedy Space Center already extensively uses hydrogen as does Warner Roberts Air Base in Georgia and the Westinghouse Savannah River Site in South Carolina. By connecting these sites by regular bus service from Miami to Augusta through Jacksonville and Atlanta, a corridor could be created with hydrogen dispensing stations for buses and on-site hydrogen powered vehicles.

2.5. NEAR TERM ACTIVITIES

Extensive planning is required for the successful expansion of existing applications into clusters and from clusters into corridors. It is easy to envision refueling stations up to 400 miles apart which operate on different hydrogen production technologies. These hydrogen production technologies might include partial oxidation, small size methane steam reforming, electrolysis from the grid and with various renewables, and plasma production of hydrogen. Transportation is provided by converting hybrid vehicle platforms to operate on hydrogen. There would also be interest in using DOT's Advanced Transportation Transit Bus for this project.

The first phase of this effort might include:

- A study of the best approach for corridor development
- Support of the formation and development of hydrogen business councils and integration of current hydrogen industry interests with those of government and community interests (to build interest, financial and other support for involvement in this effort.)
- Initiate development of dispensing facilities in Los Angeles, Las Vegas, Sacramento and Nevada Test Site
- Develop plans to continue concept to Phoenix and Albuquerque

- A study of the corridor concept for the Southeast and Gulf Coast

The scope of phase 2 depends on the study results in phase 1 and the availability of funds. The second phase of the program might include:

- The installation of facilities at Los Angeles, Las Vegas, Sacramento and Nevada Test Site;
- The acquisition and conversion of buses;
- Finalizing of plans for corridor concept for Phoenix to Albuquerque, Southeast and Gulf Coast.

This approach provides for the infrastructure to grow with and tailor itself to the application. Infrastructure and use of the corridor will grow at the same pace without massive infrastructure investments outstripping demand. For success, industry involvement is essential. The NHA anticipates working with DOE, the California Hydrogen Business Council, the National Laboratories and other participants to play a role in providing support for the cluster development and organizing industry interest in obtaining the results anticipated.

2.6. FOLLOW ON ACTIVITIES

The remaining phases would involve operation of bus service in each of the corridors. This is likely to be a 5 year effort. Underlying the bus application is the use of hydrogen in many of these facilities for other purposes. The establishment of a network of refueling stations and buses leads naturally to consideration of fleets of hydrogen vehicles. This could then be followed by both public refueling at selected fleet centers and the addition of hydrogen dispensing at existing service stations. The NHA, with DOE support, is currently working through ANSI with the International Standards Organization Technical Committee 197 on hydrogen vehicular fuel systems and on-board hydrogen storage. Both items proposed by the NHA have been accepted as work items by ISO with the United States as the convener and at least 5 member countries of ISO TC 197 are serving on these two work groups.

3. INTERNATIONAL PARTNERSHIPS

In addition to all of these activities, there are international partnerships which play an important role in the communication of hydrogen systems. The United States, with the participation of other TC 197 member countries, is in a position to set the terms for the performance standards for these systems for purposes of international trade. The expertise and experience of these demonstrations will help us better define the terms of the dispensing facility and for an automobile on-board fuel system. Many of these same questions will be faced by industrialized nations throughout the world.

The Canadian government recently announced it will support Ballard to develop a Fuel Cell Engine for Ford. Ballard fuel cells are also being developed for Daimler-Benz, General Motors, Hitachi, Honda, Volkswagen, Volvo and GPU International. These

industries from all over the world should be congratulated for integrating the best hydrogen technologies from all over the world to create effective, pertinent demonstrations of hydrogen energy systems and their infrastructure.

4. SUMMARY

The Hydrogen Commercialization Plan includes both long term goals and short term action items that will start us down the road toward the hydrogen energy industry. The most important short-term activity is the development and demonstration of a viable, cost-effective hydrogen fueling infrastructure. This goal can only be achieved by the hydrogen community working together to form a safe, economical, and sustainable hydrogen future.

5. REFERENCES

National Hydrogen Association, (November, 1996), Strategic Planning for the Hydrogen Economy: the Hydrogen Economy; The Hydrogen Commercialization Plan.

Lloyd, A. Ph.D. (1995) The Role of Hydrogen in Meeting Southern California' Air Quality Goals.
Hoffman, A. R., (March 1997)Office of Utility Technologies, U.S. Department of Energy, Presented at the NHA's 8th Annual US Hydrogen Meeting.

Mauro, R., Serfass, J. A., Leach, S. (1996)A Bridge to a Sustainable Hydrogen Energy Future: Reassessing the Transition, Presented

---

Raman, V., Miller, K. (1997) US Hydrogen Program Industry Perspective: Increasing Cooperation Between the DOE, NHA, and HTAP. Presented at the 8th Canadian Hydrogen Workshop.

Gronich, S. (1997) Hydrogen Program Perspectives. Presented at the 1997 DOE H2 Program, Hydrogen R and D Program US Department of Energy.

RENEWABLE ENERGY SOURCES (RES) ACTION PLAN IN ROMANIA

Prof. Dr.LAURENTIU FARA
National Agency for Renewable Energy (NARE)
c/o Phys. Dept., Bucharest Polytechnic University, 313, Splaiul Independentei,
sector 6, Ro-77206, Bucharest, ROMANIA

Abstract

A PHARE project entitled "Strategy on RES in Romania" was elaborated by LDK (Greece), COWI (Denmark), AGIPLAN (Germany), CRES (Greece) and NARE (Romania). On this basis an *Action Plan on Short Term*, as well as *on Medium and Long Term for RES implementation* was proposed [1].
The main characteristics of the *Short Term Action Plan* are: the involvement of the private sector; the transfer of technology; elaboration and issue of a legislative framework; elaboration and establishment of an institutional framework; fiscal and financial issues to support and develop RES applications; creation of industrial activities and joint ventures; orientation of R & D activities in RES and elaboration of a programme.
At the same time, it is important to stress that there is a need to promote and undertake a number of demonstration projects and rehabilitation of existing installations. The demonstration projects will prepare the ground for large scale applications in the medium and long term period. These actions may be co-financed by the European Commission or other Organisations and the Romanian Government.
RES Action Plan will determine several important benefits for the country (economical, social and environmental advantages).

1. Present Situation

Romania has a population of 22.8 millions with an area of 238.000 km^2. About 12.4 million Romanians (55%) live in cities, whereas 10.4 millions are considered as rural population. About 25% of the Romanian population live in small communes, where the population is between 2000 and 5000 inhabitants, while 16% live in communes with a population between 5000 and 10000 inhabitants. The total rural population, together with the urban population living in medium-sized towns (population less than 50000

T. O. Saetre (ed.), Hydrogen Power: Theoretical and Engineering Solutions, 475–483.

inhabitants) will be considered as the primary market segment for RES applications, as these populations (about 61% of total) live close to the resources, and possibly do not have the same options and the same diversity of energy supply as the urban population [2].
It is also important to stress that RES can constitute an additional revenue for the rural population in a time when the transition towards market economy generates drawbacks and scarcity of means. Combining the quality of energy producers and energy consumers could be one of the main objectives of the strategy in the rural areas.
The total primary energy supply in Romania reached a peak of 68 Mtoe in 1989, fell to 44 Mtoe by 1992, to recover in the following years. Romania's domestic energy production from coal, lignite, oil, gas and hydropower, covers at present about 60% of the energy needs. Romania has been a relatively large producer of oil and gas but production has declined. Nuclear power will be added from a CANDU plant being built at Cernavoda. Electricity interconnection with the UCPTE system through Hungary will enable Romania participate in power exchanges. Connections exist with Bulgaria, Serbia and Ukraine.
Natural gas is still the main primary energy source, followed by the oil product and coal-lignite.
A growth of the final energy demand will result in a growing dependency on imported energy, which is presently delivered at a very low price (Russian gas, low price for coal and oil on the world market). This situation with cheap primary energy source is precarious. One of the challenges for RES development is to reduce this dependency and consequently the level of future bills for imported primary energy.
The industrial sector is the most energy intensive in Romania, due to the importance of large industries. About 53% of all primary energy consumption takes place in this sector. The domestic sector has presently a relatively modest share (16%) of primary energy consumption, reflecting the scarcity in energy supply and/or the purchasing power while a low share of about 3% refers to the agriculture sector. Efforts are presently launched in the industrial sector and in the centralised energy system (gas, power and district heating schemes) in order to improve the supply situation, reduce losses and modernise the management of these sectors. Therefore, efforts within the RES and RET sector will primary focus on decentralised systems having domestic energy demand as their primary target.
At present, the contribution of RES is the following:

- *solar thermal* 0.14 PJ/y, solar passive and solar PV negligible
- *hydro* 12.8 TWh, from which 0.4 TWh SHP (44.64 PJ/y large hydro, 1.44 PJ/y SHP)
- *wind* negligible
- *biomass* 49.3 PJ/y
- *geothermal* 1.1 PJ/y

Taking into account primary energy consumption in the country, the share of RES is 5.3 % (excluding large hydro is only 2.9%). The contribution of each RES sector at present is shown in the Fig.1.

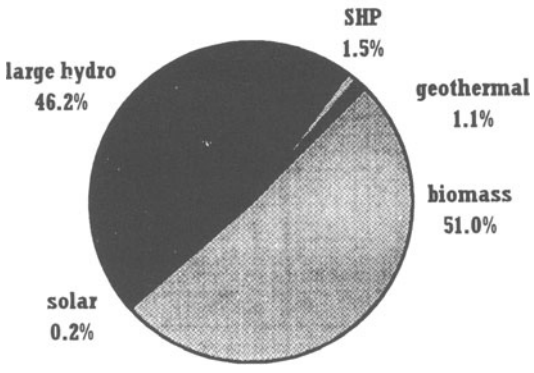

Figure 1 Present RES Contribution in Romania (Total RES 96.6 PJ/y)

2. Priorities of RES in Romania

2.1 THERMAL ENERGY

Besides and complementary to the priority granted to energy conservation for thermal applications, the challenge to be faced and the priorities set according to the competitiveness of the RES sector are the following:

- displace fossil fuels in existing district heating (DH) schemes (geothermal energy, and wood chip)
- enhanced use of RES in the industrial sector (mainly geothermal and wood chips)
- improved use of RES (geothermal energy and biomass) for new DH schemes in small towns and villages
- use of straw and other agricultural by-products in appropriate biomass boilers for heat supply of farms and small villages
- continuous use of wood for individual dwellings in the countryside
- use of solar collectors for domestic hot water production.

2.2 POWER GENERATION

Future power generation and supply cost in Romania will be of great importance for the competitive penetration potential of RES. Private investments for independent power producer will accelerate the penetration of RES. Prerequisite to this action is the adoption of a legislative framework setting up the rules as well as the fair selling tariff to the electric utility. The most promising applications are:

- *Small Hydro Power (SHP).* The rehabilitation of existing SHP and the construction of new are competitive alternatives to fossil fuel power generation.
- *Wind Energy* applications depends highly on the future power generation cost, on a strong political commitment to develop a Romanian wind industry or to use wind energy as an element within the country's environmental policy.
- *Combined Heat and Power (CHP)* applications utilising biomass could be considered in the medium and long term for several cases.
- *Stand-Alone Applications* for rural electrification can be developed incorporating small solar Photovoltaic (PV) systems, wind converters and very small hydro considered as economically reliable solutions.

3. Recommended Targets for RES Applications

The developing of RES requires a set of specific targets to be achieved for each of the economic feasible renewable energy applications for the short, medium and long term. Beside the economic feasibility of the RES applications, the targets take into account the underway energy sector restructuring process as well as the technological ability of the sector to adopt new methods of resource exploitation, the socio-economic and the environmental aspects associated with each particular application. It should be noted that these targets coincide with the recommendations of the ALTENER EC Programme for RES contribution (7.8% of total energy consumption including large hydro by the year 2005) [3-4].

TABLE 1. Milestones for the Development of RES in Romania

Time Horizon	***% of primary energy consumption***		***% of power generation***		***% of heat supply***
1995 (current level)	5.3 *	(2.9)	23.0 *	(0.7)	10.9
2000	5.5 *	(3.2)	22.0 *	(1.6)	13.2
2005	6.3 *	(4.0)	21.7 *	(2.0)	17.3
2010	6.9 *	(4.8)	21.0 *	(2.8)	21.5

* *including contribution of large hydro power plants*
1995: 12.4 TWh, 2000: 13.5 TWh, 2005: 14.8 TWh, 2010: 15.4 TWh
( ) *excluding large hydro power plants*

The actual targeted electricity and thermal energy production from RES for the time period 1995 - 2010 is presented in the Fig. 2

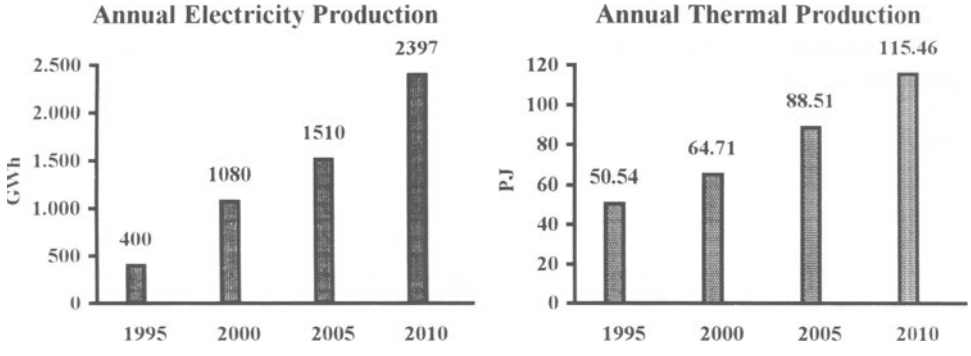

Figure 2 Targeted Annual RES Production (large hydro excluded)

TABLE 2 Recommended RES Targets in Romania and Required Funding
(for power generation GWh/y and heat production PJ/y)

Time Horizon	Production		Total Budget	Public Funds*
	GWh/y	*PJ/y*	*MECU*	*MECU*
actual	400	50.54		
present to 2000	680	14.17	314.1	87.7
2000	**1080**	**64.71**		
2001 to 2005	430	23.80	363.5	93.0
2005	**1510**	**88.51**		
2006 to 2010	887	26.95	591.0	40.0
Total by 2010	**2397**	**115.46**	**1268.6**	**220.7**

* The public funds are considered to contribute partly the total budget

The contribution of RES by the year 2010 represents 10% of the country's current primary energy consumption almost three times the today primary energy consumption in the agricultural sector. The overall RES investments (excluding large hydro) till the year 2010 (15 year time horizon) is estimated at 1269 MECU. The public funds required to promote and support the development of RES applications has been assessed to be in the order of 220 MECU (about 20 MECU/year until the year 2005).
It is recommended that these targets are adopted by the Government of Romania. The expected benefits of RES development for the country can be summarised as:

- *by the year 2005*

An additional amount of 42 PJ/y is expected from RES (if the recommended targets are reached). This figure represents an avoided expenditure for imported oil (without taxes) of about 200 MECU/y by developing RES for power generation and heat production.

Primary energy consumption 2340 PJ/y (forecasted)
contribution of RES by 6.3% (recommended, large hydro>10 MW are included)

power generation (total 75 TWh/y) heat production (total 510 PJ/y)

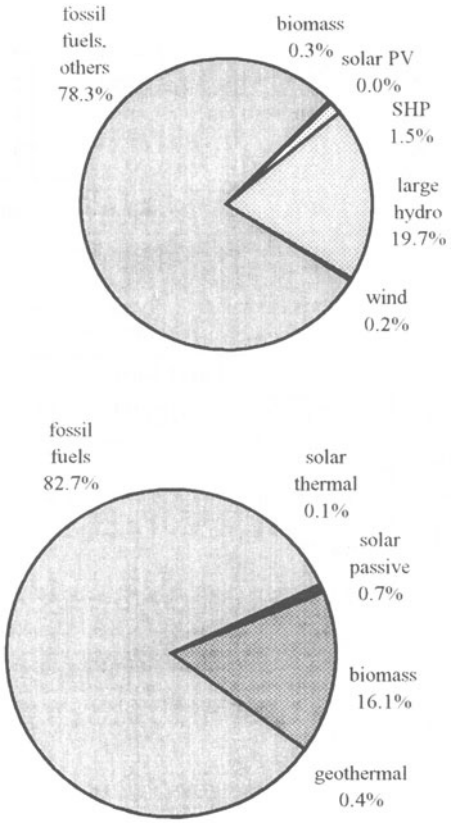

Figure 3 Recommended RES Contribution by the Year 2005

- *by the year 2010*

An additional amount of 72 PJ/y is expected from RES. The figure represents an avoided expenditure (without taxes) of about 350 MECU/y by developing RES for power generation and heat production.

The expected yearly turnover from the recommended activities in RES in the country for power generation and heat production is at the same level, with additional benefits to the national economy from the activities developed (industry, SMEnterprises, new jobs, agriculture) and from the environmental improvements.

The penetration of renewable energies producing clean energy with zero emissions contributes to avoiding about 11 million tonnes CO_2 emissions per year by 2010 (large hydro excluded).
Therefore, the recommended public funds in the form of grants and subsidies to promote and support RES, constitute one of the best investments in the national economy as well as a contribution to the improvement of the environment.
The above targets on RES development have to be translated into a clear operational strategy, expressing specified goals dedicated for each RES sector. Some goals can be directly related to energy production and consumption (substantial participation of a specific RES to heat and/or power production). Other goals can consider energy as a secondary target, while the primary goals can be related to environmental and/or industry development policies, for instance: development of an industrial sector (wind turbine, solar collector) for a national and regional market, and/or use of RES as a tool for local development (added value and labour creation).

4. RES Implementation Legislative and Organisational Framework

The RES promotional policy measures have to be translated into concrete legislation providing the necessary framework into which the sector will operate with transparency and open competitiveness. The legislative actions needed are the following:

- Legislate an independent power production and central DH production law geared towards RES and cogeneration
- Legislate RES promotional incentives for all RET according to strategic targets.
- Establish an investment support programme for RES providing the necessary financial support.
- Establish a common evaluation and project selection process that should be applicable to all energy projects.

One of the key policies to RES strategy is to organise a flexible and efficient scheme for the implementation of the policy adopted by the Ministry of Industry. Taking into account the European model, it seems that the long term energy supply activities in Romania will be dominated by individual, competitive and efficient producers and suppliers. This requires a new structure and regulation of the RES sector as well, as a part of the changes in the structure of the energy sector. The institutional framework has to support the development of a dynamic process for the promotion of RES which shall take place at the interface of the institutional system on one side (Ministry of Industry) and the market force (the institutional or private users and the operators like the institutes, the manufacturers and the financial and banking system).

5. Short Term Action Plan

As a first step towards the commercialisation of RES, a short term action plan needs to be implemented for achieving the set forth long term objectives. The success of the

short term action plan will provide the experience necessary to undertake the investment obligations necessary. The short term action plan includes promising projects for the demonstration of technologically and economically viable applications in each RES sector. The main characteristics of the short term options aim towards:

- the involvement of the private sector
- the transfer of technology
- elaboration and issue of a legislative framework
- elaboration and establishment of an institutional framework
- fiscal and financial issues to support and develop RES applications
- creation of industrial activities and joint ventures
- orientation of R+D activities in RES and elaboration of a programme.

Co-operation with European companies experienced in the field and financial contribution within EC, World Bank and other programmes should be incorporated. The gained experience from this short term programme will substantially contribute to a large scale programme leading to successful applications, [5].

The specific institutional, legal, financial, information and technology transfer action to be undertaken during the short-term period should include the following:

- *Introduce legislative framework.* Increase confidence in RES leading towards less risk and therefore longer time horizon for return on investment.
- *Create organisational framework.* A flexible and efficient organisation contributed by specialised institutes and experts to manage and support the implementation of the programmes.
- *Promote R&D activities.* Mostly applied to RES technology, international co-operation, to support the renewable technologies leading in reliable plants, high efficiency, cost effective applications, social and environmental benefits.
- *Promote training and information campaigns.* Information for decision makers and training of the people involved may lead to an increased confidence.
- *Establish environmental protection legislation.* Targets to reduce CO_2 and other emissions which will support the development of renewable energies and attract the investors.
- *Introduce financial issues, incentives, subsidies.* Gradually adjust energy prices to reflect their long term marginal cost so that renewable energies could penetrate with high share to the energy balance of the country. Given the capital investment requirements, priorities should be given and long term programmes should be established. Therefore, goals and targets have to be set very carefully for a better use of the available budget.

Along with the above soft measures and action, it is important to stress that there is a need to promote and undertake a number of demonstration projects and rehabilitation of existing installations. The demonstration projects will prepare the ground for large scale applications in the medium and long term period. The overall capital requirements for the short term period actions and measures sums up to 15.0 MECU. This actions may be co-financed by the European Community or other Organisations and the Romanian Government.

The above estimated budget includes financial support from EU relevant programmes and other financial sources, as well as domestic sources. Other projects like energy efficiency project may have a separate budget and any competition with RES development is not considered as a strategic approach in this study.
In the short term and especially during the transition period, activities on RES for commercial projects should be promoted and supported, attracting the involvement of the private sector. Mainly during this period, a shorter time of about 10 years for capital amortisation and a discount rate of 10% should be considered in the investment of RES and the assessment of the production cost.

6. Medium and Long Term Strategy

The actions to be promoted in the medium and long term period, beyond the year 2000, involve mass applications of RES exploitation aiming towards the targets set in §3. The implementation of these applications will be designed according to the experience gathered from the short term action. It should be noted that the completion of the legislative, institutional and organisational framework is a prerequisite for the launching of the medium and long term action plan.
The promising medium and long term projects will mostly be undertaken by the private sector and therefore financial support will have to be provided. Considering that a part of these investments will be made in the power sector, characterised of capital intensity, generous economic support is needed. The financial support could be in the form of grants, soft loans subsidy on RES production.
Commercial investments in RES exploitation will contribute to the country's balance of payments as well as towards the environmental protection. Therefore, these actions may be supported through a special national fund specially designed for RES and energy conservation investments. This fund will be formed by a bill that will result from an environmental penalty or tax that could be imposed on fossil fuel use. However, care should be taken in imposing this tax so that the competitiveness of the Romanian industry is not be affected. In similar cases in Europe, such public funds are supported by environmental tax on fuels.

References

[1] (1996) *Strategy on Renewable Energy Sources in Romania*, Final Report, PHARE Programme
[2] (1996) Romanian Statistical Yearbook
[3] (1994) The Declaration of Madrid, *An Action Plan for Renewable Energy Sources in Europe*, Madrid
[4] (1994) The European Renewable Energy Study, *Prospects for Renewable Energy in the European Community and Eastern Europe up to 2010*, Main Report and Annex I, II, III; ALTENER Programme
[5] Laponche, B. (1992), *Energy Consumption in the Central European Countries*, ICE, National Solar Energy Colloquium, Bucharest, 11-13 November 1992

INTRODUCING HYDROGEN ECONOMICALLY TO CITY CENTRES
Environmental externality adders

DAVID HART[†] AND NIGEL LUCAS
Imperial College Centre for Environmental Technology,
48, Prince's Gardens, London SW7 2PE, UK
DAVID HUTCHINSON
London Research Centre,
81, Black Prince Road, London SE1 7SZ, UK

1. Introduction

Over the centuries there has been a transition in fuel use, from solid, high-carbon fuels (wood, coal) to liquid or gaseous high-hydrogen ones (oil, natural gas). This trend follows a set of curves which, when extrapolated, suggest the potential for an overwhelming use of pure hydrogen as a fuel by the year 2050 (Cannon, 1995). In the past the change has been encouraged by increased ease of use and efficiency gains and to a lesser extent by cleanliness; now the thrust is environmental. With the growing acceptance of potential problems caused by global warming, and urban pollution increasingly problematic in many areas, the potential for a clean fuel should be enormous. However, at present the use of hydrogen in transport and power generation is limited to a few pilot plants and test schemes. One significant reason for this may be an odd reluctance to place a value on environmental benefits.

A large number of studies has been carried out on the externalities associated with polluting emissions (Kågeson, 1993; Pace, 1990; Pearce et al., 1992; Eyre, 1997). The values these studies ascribe to various pollutants vary significantly, though these differences can be partly explained by geographical influences, methodological variations and the consideration of different effects. Some weaknesses in externality costing methodologies have been analysed by Stirling (1995). However, all of the studies show that the impacts of pollution can be expressed as a monetary value – a potential externality 'adder'.

Applying these adders to fossil fuel prices or subsidising cleaner technologies such as renewables by an equivalent margin has not been carried out directly in practice, although some use of adders has been made in relation to new electricity investment decisions by public utility commissions in some states in the USA (EIA, 1995). This

[†] To whom correspondence should be addressed

T. O. Saetre (ed.), Hydrogen Power: Theoretical and Engineering Solutions, 485–491.

study therefore is an initial attempt to categorise the polluting effects of emissions from fossil fuels in London and the possible monetary benefits associated with replacing those fuels by hydrogen. The calculations for the scenarios have been made using the highest and lowest values for externality costs found in the literature, in order to give a feeling for the wide variation in estimated externality values.

2. Externality costing and calculating the 'premium' for hydrogen

Externality costing is a methodology that attempts to attach monetary values to costs that are otherwise not considered in an economic analysis. For example, particulate emissions in urban areas may be linked to increased instances of breathing difficulty, in turn resulting in increased hospital admissions, healthcare costs and personal experience of ill-health. By following the trail backwards it may be possible to disaggregate the costs sufficiently to be able to estimate the 'cost' of particulates in $/kg or £/tonne (e.g. Pace, 1993). Using these cost figures in conjunction with emissions factors it is possible to evaluate the amount of avoided pollution and thus monetary benefit resulting from the introduction of hydrogen. By comparing this value with the cost of the technology and infrastructure changes required to bring the hydrogen to the user, it is possible to assign a 'premium' to the amount of hydrogen used, in $/GJ or equivalent. Equation 1 shows how this can be done:

$$Premium\ (\$/GJ) = \frac{value\ of\ avoided\ \ pollution\ (\$) - cost\ of\ introducing\ hydrogen\ (\$) + corr.*}{amount\ of\ hydrogen\ (GJ)} \quad (1)$$

**corr. denotes a correction for efficiency which will influence the amount of energy and emissions for each technology*

This 'premium' is intended to represent the value of the hydrogen within the city, and may be offset against the cost of producing hydrogen, but the cost of supplying it from the city boundary has already been included in the analysis. The calculation allows for a timespan considered appropriate to the technology under investigation, e.g. 20 years, and discounts using a suitable rate. This enables the investigation of a longer-term scenario.

3. The Reference Scenario

The analysis presented here is based upon comprehensive energy and emissions data compiled for Greater London by the London Research Centre (Chell and Hutchinson, 1993). The data are sufficiently disaggregated to allow the investigation of the effects of specific fuel substitution within small areas of London (down to 1km square), both on energy use and emissions characteristics. The analysis is conducted under the auspices of the Japanese WE-NET project – a Japanese Government supported hydrogen programme. It has been set at a convenient point in the future – far enough that it is conceivable that hydrogen could have been introduced into the energy supply

infrastructure, yet near enough that energy demand and usage patterns can be regarded as being largely unchanged from today. The nominal date is 2015.

In order to reduce the amount of data in the computation it was decided to divide London into 'central', 'inner' and 'outer' regions and analyse a representative sample from each. An area of nine square kilometres was chosen to be representative and the full calculation was carried out only using this region.

To focus on the supply and demand infrastructure of the city, and the environmental issues associated with urban air pollution, it is assumed that pure hydrogen is available at the urban boundary. At this stage there is no cost associated with the hydrogen. The analysis seeks to associate a value with its use by first investigating the infrastructure requirements of moving the hydrogen to where it is demanded, and the technology requirements of using it. The costs related to these elements can then be offset against the potential environmental benefits associated with reduced urban pollution by using externality adders.

The analysis is based upon cost-benefit analysis of energy and emissions scenarios. Alternative scenarios representing different methods of introducing hydrogen into the energy infrastructure of the city are assessed against a reference scenario. This reference scenario is based on expectations of energy demand in the year of 2015 but includes some assumptions that are time-frozen – in particular the fact that some levels of demand-generating activity remain the same as present (passenger-kilometres, building floorspace, etc.). For the purposes of the modelling, however, this is unimportant, as the scenario provides a 'level playing field' against which to compare the alternatives.

The goal of the scenario is for hydrogen to provide 10% of the energy demand of the city, and for some scenarios it has been necessary to consider more than one option for hydrogen in order to achieve this. For example, adding hydrogen to methane for use in internal combustion engines is beneficial for an energy content of about 5%, but emissions benefits tail off above that level (Fulton and Lynch, 1996). It may therefore not be sensible to continue to add hydrogen until the 10% overall target has been attained. Instead, an alternative market may be considered.

4. The Alternative Scenarios

The long-term aim of this study is not only to provide information on the most cost-effective ways of introducing hydrogen into an urban area, but also to propose transitional strategies for achieving hydrogen penetration. At present, it seems that the most likely uses of hydrogen are in niche market areas that exhibit some specific cost or emissions advantage, so these areas have been investigated with a view to assessing their strategic promise in addition to their hydrogen capacity. The alternative energy supply scenarios have therefore been designed to target particular niche areas for the use of hydrogen. These niches include decentralised power generation using fuel cells, fuel cell buses and the mixing of hydrogen with natural gas for both vehicles and power generating equipment.

The first two scenarios considered were the 'Hythane‡' and the 'Niche Market' scenarios. In the former, 5% of the energy content of the natural gas use in London is replaced by hydrogen – a 15% replacement by volume. This gas is distributed using the existing pipeline network to the existing stock of appliances and vehicles, with the minor modifications required assumed to be carried out as part of general maintenance. Using hydrogen in this way results in low introduction costs but relatively high reductions in polluting emissions.

In the niche market scenario the hydrogen is used in its pure form, but only used in technologies where it is considered that the environmental benefits may be large – for example in emissions-free fuel cell buses. In this case the infrastructure required to provide the hydrogen and the technology required to use it must both be costed and the environmental benefits offset against these costs. Discounted cash flow analysis has been applied to enable a longer-term view of the scenarios.

5. 'Distributed Hythane'

The distributed Hythane concept has been explained as a mixing of 5% hydrogen by energy with the natural gas supply to London. Taking the reference scenario as a base, it is possible to calculate the emissions reductions brought about by using the Hythane mixture. The reduction in volume of a pollutant emitted is then multiplied by an externality cost to give the potential reduction in external costs brought about by reducing emissions. Values for each pollutant (NO_x, SO_x, CO, etc.) are then added to produce the total monetary value of emissions reduction. The final results are strongly influenced by the choice of externality adders, as these vary widely both geographically and methodologically. In order to give some indication of the spread of values each calculation has been repeated using both high and low estimates of externality costs. Table 1 shows the results obtained for central, inner and outer London using a discount rate of 8%.

Table 1: The Premium on Hydrogen used in Hythane by Area and Cost

Value (95$/GJ)	***Area of London***		
Externalities	*Central*	*Inner*	*Outer*
High	**48**	**44**	**36**
Low	**7**	**5**	**4**

It is apparent from the table that there may be significant benefits attached to the use of hydrogen mixed with the natural gas supply in urban areas. According to the analysis, there are benefits for pollution reduction in central London ranging between seven and 48 $/GJ of hydrogen. To add some perspective to this, natural gas costs about $2/GJ at the beach. It is thus apparent that there may be a cost-effective case for mixing small amounts of hydrogen with natural gas.

---

‡ 'Hythane' is a registered trade mark of Hydrogen Consultants, Inc.

6. The 'Niche Market'

In the niche market scenario the hydrogen is not used in a mixture but in its pure form, and targeted at specific market areas. These areas are chosen primarily on the basis that they contribute a significant amount of urban pollution and that the introduction of hydrogen could thus benefit them in particular. Other areas that may be initial markets for hydrogen, such as combined heat and power schemes using fuel cells are also considered.

In the niche market scenarios the amount of pollution coming from any one unit of production is reduced to almost zero. The overall effect on pollution will be determined by the take-up of the technology. For example, replacing all local buses with fuel cell buses may have a significant effect on local particulate emissions, but replacing only one bus would not. Also, infrastructure costs associated with the introduction of a particular technology will be amortised better with a larger technological penetration. Building a hydrogen pipeline to supply one home is not efficient; the same pipeline supplying 200 or 2,000 homes may be. The results for selected cases are shown in Table 2.

Table 2: Premiums on Hydrogen in Niche Markets

	Technology			
Premium (95$/GJ)	**Gas Turbines**	**PAFC**	**FC Bus**	**ICE Taxi**
High Externalities	***12***	***3***	***4***	***1***
Low Externalities	***2***	***0***	***-23***	***-6***

PAFC- Phosphoric Acid Fuel Cell; FC – Fuel Cell; ICE – Internal Combustion Engine

Again, the results suggest that there may be instances where it is economic to introduce pure hydrogen into an urban energy supply system. However, it is also apparent that the infrastructure and technology costs associated with some areas are likely to be expensive in comparison with the expected benefits of hydrogen.

7. Targeting Hythane

Further analysis of the Hythane scenario suggested that the majority of the emissions reductions were occurring in the transport sector, and that it might be valid to investigate the targeting of Hythane rather than its indiscriminate distribution to all natural gas users. As part of the wider aims of the WE-NET Project are the eventual use of pure hydrogen and strategies for its introduction, it was decided that pure hydrogen would be fed to the point of use (assumed to be refuelling stations) for natural gas vehicles. It would be mixed with methane at this point for refuelling vehicles, though there would also be an option for using it in pure hydrogen vehicles or other modes.

By combining some of the techniques used for the previous two scenarios and introducing further estimated infrastructure costs, it was possible to analyse a targeted Hythane scenario. Table 3 shows the results obtained.

Table 3: The Premium on Targeting Hythane by Area and Cost

Value (95$/GJ)	***Area of London***		
Externalities	*Central*	*Inner*	*Outer*
High	**211**	**173**	**-124**
Low	**-23**	**-50**	**-292**

These results suggest that the extra infrastructure costs required for the introduction of targeted Hythane are only worthwhile in the case of high externality costs, and even then only in central and inner areas. This is because the central area is more densely populated than others are and thus proportionally lower investment is required to bring the technology to a large market. It is also the central areas that suffer most from pollution episodes. The large difference in values suggests the variation in externality cost estimates is more of a factor here than in some of the other scenarios.

8. Conclusions

The work presented here is a first attempt to introduce the concept of externality costing to a cost-benefit analysis of hydrogen introduction in an urban area. The analysis suggests that it may be valuable in pure economic terms to introduce hydrogen into a city in order to reduce pollution and associated effects. The value associated with pollution reduction varies considerably from place to place and with different methodological approaches and thus a particular geographical area needs to be examined in some detail before specific recommendations can be made.

The results suggest that it is valuable to mix hydrogen with natural gas and deliver it indiscriminately to all users of natural gas, but that targeting pure hydrogen may not be as cost-effective in the short term because of the high costs associated with developing a hydrogen infrastructure. Targeting the hythane mixture may be valuable, partly as it can be cost-effective in its own right and partly because it may allow a transitional strategy towards the use of pure hydrogen to evolve. It should be noted that targeting hythane will effectively 'cherry-pick' the most polluting technologies, making it pointless to then distribute hythane on a wider basis.

For future work it is intended to refine the analysis as new data are received on all aspects of the model. The city of Tokyo, amongst others, will be subjected to the same procedures to verify the transferability of some of the underlying methodologies in the analysis. Further scenarios and transitional strategies will be developed.

9. References

Cannon, J.S. (1995) *Harnessing hydrogen – the key to sustainable transportation*, INFORM, Inc., New York

Chell, M. Hutchinson, D. (1993). *London Energy Study*, London Research Centre, London.

EIA (Energy Information Administration) (1995) *Electricity generation and environmental externalities: case studies*, DOE/EIA-0598, Department of Energy, Washington, D.C.

Eyre, N (1997) *External costs: what do they mean for energy policy?*, Energy Policy, **25(1)**, pp. 85-95.

Fulton, J., Lynch, F. (1996) *Leveraged use of hydrogen in internal combustion engines*, Hydrogen Consultants, Inc., 12420 N. Dumont Way, Littleton, CO 80125.
Kågeson, P. (1993) *Getting the prices right. A European scheme for making transport pay its true costs.* European Federation for Transport and Environment (T&E), Stockholm.
Pace. (1990) *Environmental costs of electricity*, Oceana publications, New York.
Pearce, D., Bann, C. and Georgiou, S. (1992) *The social costs of fuel cycles*, Centre for Social and Economic Research (CSERGE), University College, London.
Stirling, A. (1995) *Some practical and theoretical difficulties with attempts to place monetary values on the environmental effects of electricity generating technologies*, ENER Bulletin 17.95, European Network for Energy Economics Research, pp. 126-166

THE SOLAR ENERGY CONVERSION STUDIES AND SYSTEMS IN THE REPUBLIC OF ARMENIA

VLADIMIR M. AROUTIOUNIAN
Yerevan State University
1 Manoukian Str., Yerevan 375049 ,Republic of Armenia

1 . INTRODUCTION

The prospect of direct conversion of solar energy to electricity or storage fuel, namely hydrogen, is attractive[1-3]. It is reported here about investigations in Armenia in the field of the solar - hydrogen photoelectrochemical conversion by use of semiconductor electrodes. When a semiconductor is immersed in a solution (for example, in the water), the charge transfer occurs at the interface, space charge regions at the surface of the semiconductor and in an electrolyte are formed. Radiation is absorbed at the semiconductor interface, electrons move towards the bulk of the n-type semiconductor and holes move towards the surface and injected into the electrolyte [2, 4, 5]. A wire connect the semiconductor with second electrode. The latter could be metal or another type (p-type) semiconductor. The combination of two such electrodes immersed in the electrolyte solution comprises the basis of a photoelectrochemical cell. Photogenerated holes may cause the oxidation of the semiconductor surface therefore the stability and regime of work of electrodes can be attained by suitable choice of the solution and redox-couple and by the electrode surface [2, 4, 5]. Influence of these factors and recombination processes is important to take into account in the process of calculations and of an analysis of the current-voltage characteristics of photoelectrochemical electrodes (see, in particular Ref. [6]). As materials for the photoelectrode it is possible to use both single crystalline and polycrystalline as well as ceramic semiconductors which are resistant to photocorrosion.

2. FABRICATION OF ELECTRODES

As starting materials for manufacturing of the electrodes in our laboratory TiO_2 , ZnO, Fe_2O_3 , $SrTiO_3$ and other oxides and materials powders have been selected. Of course, we are dealing with good insulators in this case. In order to minimize ohmical losses in a circuit, it is often necessary in the process of manufacturing of polycrystalline and ceramic electrodes made of powders to increase the conductivity by factor of 10^{10}-10^{14}. In Yerevan State University different technological methods of manufacturing of ceramic, thin film and polycrystalline photoelectrodes covered more than 10 USSR patents are proposed and investigated. The alloying of semiconductor oxides and solid

T. O. Saetre (ed.), Hydrogen Power: Theoretical and Engineering Solutions, 493–498.

solutions was usually carried out at high temperatures in the CO or He medium or in vacuum, fully adequate for the partial reduction of semiconductors. The same procedure was undertaken when we added some impurity atoms in an oxide or a solid solution. [7-10]. New technologies of manufacturing of thin film photoelectrodes with large. "working" area were patented by us also.

The following samples have been synthesized and investigated in our University: TiO_2 <Ta, Mo, W, Nb, Re ,Cr, V, Fe, Mn, Al etc.>, Fe_2O_3 <Sn, Ge, Zn, Hf, Nb, Ti, Ta etc.>, ZnO<Al, Y, Sn etc.>, $SrTiO_3$ <Zn, Ta, Cr ,La, I etc.>, TiO_{1-x} , TiO_2 - MnO and ZnO - CdO solid solutions etc. InSe, GaSe, GaTe, and $CuInSe_2$ were grown and investigated and InP and CdTe single crystals were studied also. We manufactured and studied also Y- Ba -Cu -O and Bi - Sr- Ca- Cu- O high temperature superconductive (HTSC) ceramics with different compositions containing Cs, K, Al, Cl, Cr, Na, Fe, Li, Ni etc.[11].

3. EXPERIMENT

We have investigated electrical, photoelectrochemical, photoelectric, optical, luminescence, reflection, electroluminescence, electroreflection, photocorrosion and other properties of photoelectrodes. Corresponding references can be find in my review - papers [4, 5]. Some interesting results are listed and discussed below.

The photosensity of the majority of semiconductors investigated is considerable only at short wavelength region of a spectrum. This is the main reason of rather low efficiency of the solar energy conversion encountered in the photoelectrolysis of the water. We have carried out investigations of a possibility of photoanode sensitization to visible light. It was established that the doping of semiconductor electrodes altered the spectral dependence of photocurrent for the case involving TiO_2 with chromium, vanadium and manganese and ZnO with aluminum. We noted that photoelectrodes made of TiO_2 doped with Cr are sensitive up to 600 nm, and ones doped with vanadium - up to 800 nm (see Fig.1).This is important for a shifting of the sensitivity region of the photoelectrodes closer to the maximum of the Sun spectrum.

When a n-type photoanode was supplied by a positive bias, the value of the photoelectrochemical conversion efficiency increases and the maximum of photocurrent spectrum shifts towards the longer wavelengths region. A fall of the conversion efficiency at short wavelengths is the result of the influence of surface recombination processes. These latter become important with an increase of the charge carriers velocity and decrease of the band bending potential. With an increase of the electrical field intensity the spatial separation of electron-hole pairs generated by light will be more effective and the influence of the surface recombination processes will be less effective.

At present our solar to hydrogen conversion efficiency for ceramic electrodes equals 1.5 - 2 % for TiO_{2-x} , TiO_2 <Mg>, TiO_{2-x} <Re>, ZnO_{1-x} , ZnO <Al> etc., 1% for Fe_2O_3 <Sn or Ta>, and $SrTiO_3$ <La>. The efficiency for single crystal CdTe <In> photoelectrode was 12 %.

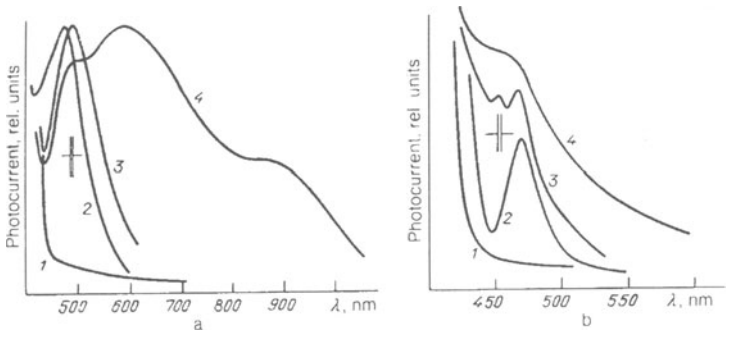

Fig.1.Photocurrent spectra of polycrystalline TiO_2 doped with : a) Al (curve 1), Cr (curve 2), Mn (curve 3),and V (curve 4); b) Cr in concentrations of 0 at. % (curve 1), 0.1 at. % (curve2), 1.0 at. % (curve 3), and 2,5 at. % (curve 4).

One of the modern approach to the conversion efficiency improvement is the Pt counter electrode replacement by a semiconductor photocathode. In such a cell two illuminated semiconductor photoelectrodes are used. It is more difficult to choice of p-type materials for creating of the photocathode than of n-type materials for the photoanodes. We have investigated the properties of HTSC materials. It was shown that the forbidden gap of the Y-Ba-Cu-O and Bi - Sr - Ca - Cu - O samples investigated is about 1,38 eV which is very attractive for applications in the photochemistry. The photocurrent values for the Y- Ba- Cu - O photoelectrodes were smaller than the values for the InP cathodes [5, 7]. Photocurrents in the cell with two ceramic electrodes could be 45-65 % of the photocurrents when a Pt counter-electrode is used in the same cell. The higher photocurrents were obtained in the cells with the pair of Y - Ba - Cu - O <Fe and Cl> or Bi-Sr-Ca-Cu-O electrode with $SrTiO_3$, TiO_{2-x} and TiO_2 <Nb> photoanodes [11].

It is known that investigations of the semiconductor - electrolyte interfaces allows to get valuable information about different parameters of semiconductors such as the energy bandgap, concentration of impurities and its energetic distribution in the forbidden gap, flat band potential , diffusion lengths of carriers , quantum yield, direct or indirect optical transitions existence, etc. An investigation of spectral dependence of optical absorption coefficient of semiconductors used for electrodes was carried out. For example, the spectral dependence for rutile was obtained in a wide spectral range where above-mentioned coefficient varied from 1 up to 10^6 . The results of investigations demonstrated the occurrence of indirect optical transitions at 3.037 eV and direct ones at 3.57 eV. In case of $Fe_2 O_3$ <Zr> -photoelectrode in addition known indirect transition at 1.95 eV direct transition at 2.68 eV and indirect one at 2,17 eV were observed. Capacitance - voltage characteristics were discussed in Ref.[8]. Impedance of such a system was calculated and compared with experimental curves measured together with Dr. G. Lorentz (Germany) [9]. It allowed to find the quantities of all components in rather complicated correct equivalent circuit for this interface for the case of $SrTiO_3$ and other photoelectrodes. If in the semiconductor there is only one type of impurity

centers, we observe usually the Mott - Schottky relationship. Investigations carried out in collaboration with Dr. J. Turner from NREL (Golden , Colorado) on our specimen of $Fe_2 O_3$ doped with different impurities have shown that such a simple relationship does not exist in this case. Our calculations used the model with two types of donor centers which has shown that it is possible to estimate the concentration of donor centers, their energetic positions in the forbidden gap from the capacitance - voltage characteristics measurements [8]. Investigations of the impedance characteristics of the Fe_2O_3 samples are continuing now in the framework of the CRDF award AE1-373.

The existence of the high electric field region at the semiconductor - electrolyte interface opens up the possibility of using it as a light source also. The high electrical bias at the electrode and the field intensity in the depletion layer lead to a high probability of photons emitting outside of the semiconductor into the electrolyte via radiative recombination of free and captured charge carriers. So, it is easy to realize the electroluminescence effect without a p-n junction manufacturing. The brightness-voltage characteristics can be described by the same formula as in the case of the solid-state light sources with p -n - junction or heterojunctions [4, 5].

Our measurements of the photocurrent, photoconductivity, photocapacity, and photoluminescence spectra of ZnO and other materials with the direction diagrams for various emission lines have shown that peculiarities observed near the fundamental absorption edge of the semiconductor were connected with the formation of quasi-two dimensional and two dimensional excitons [4, 5, 12-14]. Increasing of the band bending can leads to the field dissociation of surface excitons. Under definite conditions it initiates remarkable absorption shift to long wavelengths which contribute to increase of photocurrent and correspondingly the efficiency of conversion. The theoretical model and corresponding calculations were reported in Ref.[13]. Influence of surface potential, electron and exciton states is discussed in detail in Ref.[14]. For understanding of the physical phenomena created at the semiconductor - electrolyte interface it is important also to investigate above-mentioned interface at low temperatures and smooth changing of the surface potential. This is carried out by us for the ZnO, InSe and other photoelectrodes. It is shown that phenomena following by the involvement of the surface states, volume and surface excitons can take detectable part in the efficiency of the photoelectrochemical conversion of solar energy. Such situation were observed by us for the 12 % - efficiency photoelectrochemical cells made of the CdTe single crystal as well as on the InSe electrodes. Spectral dependence of the quantum efficiency of the photoelectrodes made of CdTe is shown in Fig.2. This photoanode was characterized by an increase in the quantum efficiency in the fundamental absorption region of CdTe at 810 nm and at 865 nm when the anode bias was increased. Valuable information about properties of semiconductors was obtained from electroreflection measurements [5, 6].

A plant with personal computer for industry allowing make non-destructive control of different parameters of silicon and GaAs was developed. Plant allowed to obtain a distribution of the surface photovoltage on a semiconductor wafer and other valuable information about surface of solid state without special electrical contacts preparing.

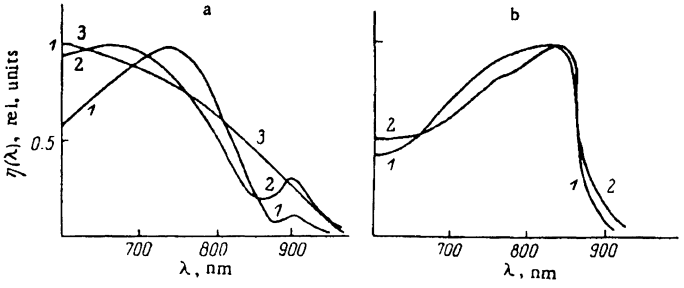

Fig.5 Spectral density of the quantum efficiency of photoanodes made of indium-doped CdTe: a) $n = 10^{17}$ cm^{-3}, V_{ext} = - 0.5, -1.5 and 3V (curves 1,2, and 3, respectively); b) $n = 2.5x10^{17}$ cm^{-3}, V_{ext} = 0 and 1.5 V (curves 1 and 2, respectively).

PHOTOELECTROLYSIS PLANTS

In order to obtain hydrogen and investigate the efficiency of the solar energy conversion three versions of the photoelectrolysis setups have been created and tested in the Yerevan State University [5, 7].

In the first equipment hydrogen had been obtained at photoelectrodes with small area (1,5 - 2sq. cm) under high concentration of the solar radiation (up to 50 W/sq. cm).The equipment had a concentrator in the form of a parabolic mirror with the area of 0,2 sq. m, having a photoelectrolysis cell in its focus. This equipment with photoelectrodes made of reduced and (or) doped TiO_2 allowed to get 0.04 l/h hydrogen. However such equipment despite lower cost of photoelectrodes, may be, is not economically profitable because of using of rather expensive parabolic mirror and a tracking system . Besides, an additional water - cooling system is necessary to add at such concentrations of solar radiation.

In one of other three photoelectrolysis setups a matrix of photoelectrodes with common area up to 550 sq. cm was used. Equipment had not any concentrator, in second one double concentration of the solar radiation had been released by means of the parabolic-cylindrical concentrator. Other proposed by us technologies allow to manufacture large area electrodes by use of metallic sheet covered by powder of semiconductor by using of a conductive glue or by the method of the layer - by - layers covering of a metal substrate by oxide powders. These setups do not require a complicated tracking system. The engine, placed in the lower part of the equipment, was switched on several second each our to make the equipment turn across the vertical axis for 15 grad. With this equipment supplying by the parabolic - cylindrical concentrator and the rutile electrodes matrix with area of about 100 sq. cm equipment productivity was equal to O.046 l/h of solar hydrogen, without concentrator - 0,028 l/h. As in this equipment solar radiation was about 80 mW/ sq. cm, the electrolyte and matrix of

photoelectrodes were heated to temperature not more than 60 C. That is why a necessity in a cooling system did not arise. In the equipment with the Fresnel lens and rutile photoelectrodes reported in Ref. [15] production of hydrogen was 7 l/h, the size of equipment (in mm) was 3600 x 2300 x300, size of one photoelectrode was 1 sq. cm. Weight of this solar- hydrogen setup is about 80 kg, mean efficiency of solar energy conversion to hydrogen was less 3 %.Cheap nickel electrodes were used. It opens the necessity in compensating of an overpotential by use of silicon photoelectric cells illuminated through the Fresnel lens also. Polycrystalline rutile photoelectrodes were manufactured by the technique of layer-by-layer sintering patented by us.

New type of photoelectrochemical converters - aerobic one was discussed in Ref. [16]. The equipment for effective production of hydrogen by means of use of a silicon photovoltaic array and an electrolyser was reported by us in Ref. [17]. The silicon photocells array had the area about 950 sq. cm and efficiency 9 %. The electrolyser with a solid polymer electrolyte had the efficiency of conversion equal 80 %.In result we had the efficiency of the solar-hydrogen conversion more than 7 %.

I express my deep gratitude to all my co-authors, the U. S. Civilian Research and Development Foundation and "Open Society" Institute for support.

REFERENCES

1. Fahrenbruch, A. and Bube, R. (1983) Fundamentals of solar cells, Academic Press, New York.
2. Energy resources through photochemistry and catalysis, Gratzel M., (ed.),(1983)Academic Press , New York.
3. Ogden, J. and Williams, R. (1989) Solar Hydrogen: Moving beyond fossil fuels, World Resources Inst., USA.
4. Arutyunyan, V. M. (1989) Physical properties of the semiconductor-electrolyte interface, Sov. Phys. Uspekhi **185**, 521-542.
5. Aroutiounian, V. M.(1991) Optical phenomena in semiconductor photocatalysers and possibilities of its applications, in: Photocatalytic conversion of solar energy, Zamaraev K. and Parmon V.,(eds.), Nauka, Novosibirsk (in Russian).
6. Aroutiounian, V. (1993) Current-voltage response of an electrochemical photosensor, Sensors and Actuators B **13-14**, 632-634.
7. Harutyunyan, V.M. et al. (1988) Water electrolysis by use of semiconductor oxide anodes, Hydrogen Energy Progress **1**, 515-521, Pergamon Press, London.
8. Sarkissyan, A. et al. (1989) Photoelectrochemical characteristics of the $SrTiO_3$ / electrolyte interface, Sov .Electrochemistry, **25**, 78-81.
9. Sarkissyan, A. et al. (1988) Influence of deep levels on capacitance-voltage characteristics of the semiconductor-electrolyte interface, ibid.,**24**, 515-521.
10. Shahnazaryan, G. et al. (1994) Study of quantum efficiency of doped Fe_2O_3 ceramic photoelectrodes, ibid.,**30**, 610-614.
11. Sarkissyan, A. et al. (1992) Photoelectrochemical characteristics of photocathodes made of high-temperature superconducting ceramics, Solar Energy Materials and Solar Cells, **28**, 217-221.
12. Harutyunyan, V. et al. (1989) Surface excitons in ZnO crystals, J .Phys. Condensed Matter, **1**, 847-854.
13.Aroutiounian, V. et al. (1994) The influence of exciton field dissociation on the efficiency of photoelectrochemical production of hydrogen, Int .J. Hydrogen Energy **19**, 209-213.
14. Aroutiounian, V. et al. (1993) Effect of surface potential on the physical processes in photoelectrochemical converters of solar energy, Appl. Solar Energy **29**, 8-15.
15. Vardapetian, T. et al. Solar photoelectrochemical station with hydrogen carriers, see [5], 294-315.
16. Arutyunyan, V. et al. (1983) Aerobic converter of regenerative type, Appl. Solar Energy, **19**, 1-5.
17. Pleskov, Ju. et al. (1985) A device for obtaining hydrogen by electrolysis of water, ibid, **21**, 77-81.

APPLICATION OF HYDROGEN ENERGY IN THE TOURISM DEVELOPMENT STRATEGY OF THE CROATIAN ISLANDS

RANKO VUJČIĆ
Brodosplit-Institute
Put Supavla 21, 21000 Split, Croatia

ŽELJKO JOSIPOVIĆ
Chroatian Chamber of Economy, County Chamber Split
Obala A. Trumbiœa 4, 21000 Split, Croatia

FRANO MATEJČIĆ
The County of Split and Dalmatia
Vukovarska 1, 21000 Split, Croatia

Abstract

Croatian islands represent the most valuable resources of Croatian tourism. The recently adopted Development Strategy of the Croatian Tourism Sector contains the basic terms of reference for the formulation of a quality island tourism development concept. For a such development program it is imperative to establish new, environmentally compatible power system suitable to ensure sufficient quantities of high quality power. One of the viable possibilities to ensure sufficient quantity of quality power is a hydrogen power system based on renewable energy sources (solar and/or wind energy).

1. Introduction

Interdependence of "energy" and "human activities" is soimportant that the energy can be consider as primary element of socio-economic development of the certain region. It is especially important for Croatian islands which are represent most certainly, extremely delicate natural, cultural, economic and ecological systems, [1].

Croatian islands represent the most valuable resources of Croatian tourism. In a same time they had prospects of development of agriculture, fishery, shipbuilding and other maritime related industries based on a small-scale economy. The recently adopted Development Strategy of the Croatian Tourism Sector offers guidance for a long-term development of the tourism (at islands) on a ecotourism as an advanced form of tourism. In order to take advantage of the natural beauties of the numerous Adriatic islands and

T. O. Saetre (ed.), Hydrogen Power: Theoretical and Engineering Solutions, 499–504.

islets as an economic potential, the adopted Strategy offers also a small autonomous tourist resorts which are featured by flexibility, modularity and comprehensiveness.

Proposed development program requested as an imperative a new, environmentally compatible power system that is enables to ensure sufficient quantities of high quality power. The hydrogen energy system based on the harnessing of wind and solar energy represents a realistic possibility for meeting the insular energy supply needs and moreover it is the environmentally completely acceptable, [2,3].

2. Basic Characteristic of Adriatic Islands

For the finding out a suitable power supply system for Croatian islands, and according to that for a tourism resort, it is necessary to take into consideration all their specific qualities. Therefore, a brief account of its geographic and demographic characteristic, as well as of its economic structure, consumption of energy and resources of the islands, are given bellow, (Table 1, [4, 5]).

Table 1 The basic geographical and demographically data (1991 census) of inhibited Croatian Islands

Group and Island area (km^2)	No. of islands	Area (km^2)	Length of the coastline (km)	No. of inhabitant	No. of settlements
Kvarner Islands : A > 100	2	814.2	437.0	19640	97
10 < A < 100	3	182.3	252.0	17420	15
A < 10	4	11.4	37.6	407	4
Σ	9	1007.9	726.6	37467	116
North Dalmatian Islands : A > 100	2	399.0	439.9	10842	21
10 < A < 100	10	264.9	413.5	18290	30
A < 10	10	52.2	147.6	4355	15
Σ	22	716.1	1001.0	33467	56
Middle Dalmatian Islands: A > 100	2	694.3	429.3	25283	46
10 < A < 100	4	134.4	216.6	11900	25
A < 10	4	14.4	38.8	79	4
Σ	10	843.1	684.7	37262	75
South Dalmatian Islands : A > 100	2	376.4	313.0	17888	31
10 < A < 100	2	62.7	74.5	1728	5
A < 10	4	10.3	38.7	512	4
Σ	8	449.4	426.2	20128	40
Σ	***50***	***3016.5***	***2838.4***	***128324***	***287***

Croatian archipelago that is consists of 641 islands and of 467 cliffs and reefs represent extremely delicate natural, economic and ecological systems. According to the 1991 census there are 126,447 inhabitants in 303 settlements on 67 permanently and 15 seasonally inhabited islands.

By way of their natural characteristics they are predominantly rocky features and Karst soil. The islands of Kvarner are located close to the mainland and their winter climate is colder than that of the Dalmatian Islands. The islands, especially those located farther

from the mainland, have a mild Mediterranean climate (long, hot and drought summer period and mild, cooler winter periods with abundant precipitation).

According to their natural characteristic and limited of economic resources Croatian islands had a very limited prospects of development. Namely, they had, until the era of tourism their main economic activity was agriculture, fishing, small shipbuilding ant other maritime related industries.

They are characterised by scarcity of energy resources. The energy reserves at islands are limited to non-conventional renewable sources such as the sun and wind. Such situation with resources has, up to the present, directed the development of an energy supply system based on the exploitation of liquid fuels (≈55%) and electric energy (up to 40%, P_{peak}= 107.2 MW; E = 38 GWh/year) from the continental power grid by means of submarine cables, [6]. The rest demand for energy satisfies with fuel wood (in household) and LPG (dominantly for cooking in households and hotels).

3. Tourism on Croatian Islands

From an economic point of view, due in the main to their natural characteristics and resources structure the Croatian islands represent the tourist and agriculture areas. The relevant development of tourism at Croatian islands really began some twenty years ago. Accommodation capacities on Adriatic islands according to regions and type of accommodation are given in Figure 1, [7].

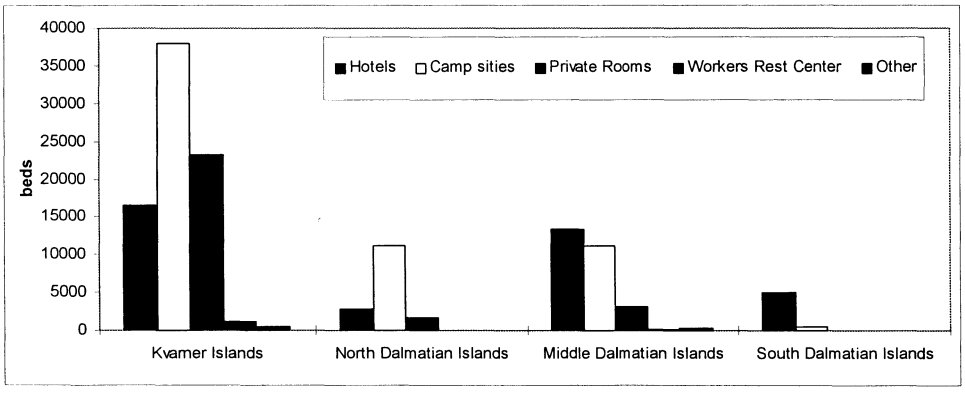

Figure 1. Accommodation capacities on Croatian islands

The island basic accommodation structure (29.3%) is significantly less adequate then its counterpart on the coastal part of the Adriatic sea (34.1%). The Kvarner and North Dalmatian islands hold almost 75% of the accommodation capacity of Adriatic archipelago. On the northern Croatian islands the number of campsites and rented rooms and apartments is above average, while the share of hotels and similar accommodation is lower than the overall island average.

The analysis of tourist sector development on the islands leads to the conclusion that this development was, for the most part, random and similar to tourism development in the coastal zone of Croatia. Such development resulted in the mass tourism during peak summer seasons. This kind of mass tourism has largely contributed to the prosperity of the islands, but taking into consideration all aspect of such development, in the long run, done the islands more harm than good. The above mentioned facts lead to the conclusion that the future concept of tourism development on Croatian islands would be primarily directed to:

- restructing and modernisation of the existing offer in order to adapt it to market demands
- complete valorisation and continually protection of non-renewable resources of the islands
- creating a new identity based on their uniqueness and special qualities.

Long-term sustainable development of the islands (especially tourist sector) must be predominantly based on a small-scale economy that is environmentally friendly and desirable to the local population. Furthermore, in order to take advantage of the natural beauties of the numerous Adriatic islands and islets as an economic potential, the proposed development of tourism take in consideration an construction of small autonomous tourist resorts, [3]. Ecopansions, autonomous tourist resorts will be designing to enhance the cultural, historic, architectural and natural heritage of islands.

For a programmed development of the tourism on islands, it is imperative to establish a new, environmentally compatible power system suitable to ensure sufficient quantities of high quality power. One of the viable possibilities is a hydrogen power system based on renewable energy sources such as the sun and wind. As the first the potential of wind and solar power, bellow will be discus.

4. Wind and Solar Power Potential

The use of renewable energy sources at Croatian islands is looked as a necessity and represent a fundamental condition for a their sustainable development. Namely, the Croatian islands have a great potential for wind and solar energy, [2, 8, 9]. Taking into account the actual circumstances and the benefits of the transformation of wind and solar energy into electric and/or thermal energy, Croatia throughout National Energy Program (SUNEN and ENWIND) fully supports the development such power plant, especially on islands.

According to the published data the northern area ranks as the high wind energy potential area (200-300 W/m^2 at altitude of 10 m above ground and 3000-6000 kWh/m^2 at 50 m), while the southern area ranks among the medium wind energy potential areas (100-200 W/m^2 at 10 m and 500-4500 kWh/m^2). The specific wind energy of the

southern remote islands rates from 1500 to 4500 kWh/^{2}. The annual mean wind speeds on the macrolocations at islands, Table 2 [9], vary from 4 to 8 m/s.

Table 2. Annual mean wind speeds at islands seasons

Island group	annual mean wind speed (m/s)
Kvarner Islands	6.0 - 8.0
North Dalmatian Islands	5.5 - 7.0
Middle Dalmatian Islands	5.5 - 6.5
South Dalmatian Islands	5.5 - 6.5

Table 3. Average sun radiation hours by

	Kvarner Islands	Dalmatian Islands
spring	500 - 600	600 - 700
summer	900 - 1000	> 1000
autumn	400 - 500	> 500
winter	200 - 300	> 300

Geographical situation of Croatian islands (N 45°30'; E 13°30' and N 42°22'; E18°32') offers very good possibilities of harnessing of solar energy. The average yearly amount of insolation to the horizontal plane ranges from 1450 to 1600 kWh/m^2 per year, i.e. from 3.55 to 4.35 kWh/m^2 per day. The average sun radiation hours per year on the coastal area are range from 2000 to 2500 hours and on the remote islands are 3000 hours. Tables 3 and 4 shows the basic data about sun radiations and insolations on Croatian islands.

Table 4. Average daily insolation on horizontal plane by month (Wh/m^{2}day)

	Kvarner Islands	Dalmatian Islands - inside	Dalmatian Islands - remote
January	1100 - 1350	1550 - 1750	1750 - 1850
February	1600 - 2000	2250 - 2450	2450 - 2650
March	3000 - 3450	3500 - 3850	3800 - 4100
April	4200 - 4750	5000 - 5300	5350 - 5650
May	5300 - 6000	5750 - 6200	6200 - 6500
June	6000 - 6250	6150 - 7000	7000 - 7250
July	6050 - 6400	6400 - 7450	7400 - 7750
August	5200 - 5700	5750 - 6500	6600 - 7000
September	3750 - 4550	4750 - 5000	5000 - 5250
October	2550 - 3100	3250 - 3400	3300 - 3500
November	1350 - 1650	1750 - 1850	1850 - 2000
December	900 - 1000	1100 - 1350	1300 - 1500
Year	3400 - 3700	3750 - 4150	4250 - 4350

5. HYDROGEN ENERGY SYSTEM

The hydrogen energy system based on the renewable sources of energy, represents a realistic possibility for meeting the insular energy supply needs. The Fig. 2 illustrates a model of hydrogen energy system for small autonomous tourist resorts that would be located on islands. These resorts should be created in a manner compatible with their surroundings, and in a same time they should meet all requirements for elite tourism. The required energy will be provided by renewable sources such as the sun and/or wind, whereas the drinking water will be provided by desalinisation plants.

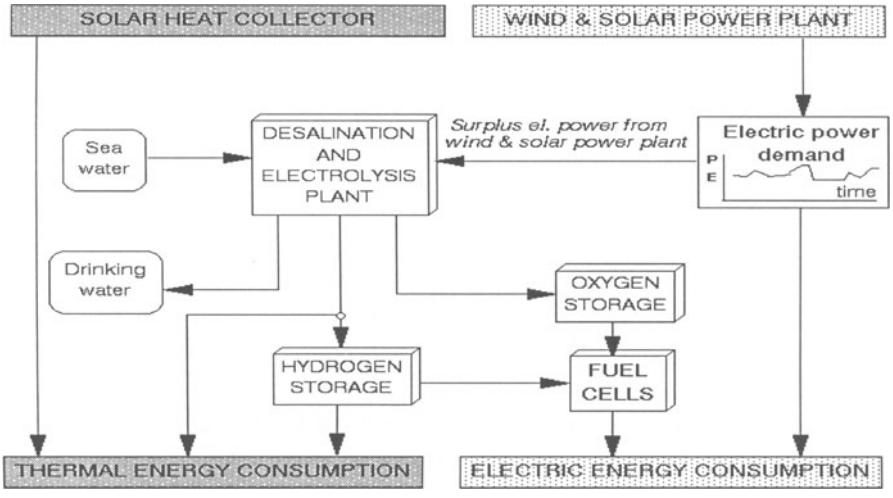

Figure2. Model of hydrogen energy system for autonomous tourist centres at small Adriatic islands

6. CONCLUSION

The hydrogen energy system based on harnessing of solar and wind energy as primary sources, represents the realistic possibility for Adriatic islands to reach a good quality energy supply. The high share of electric in the total energy consumption implies the possibility of setting up of a considerably rational energy system in which the hydrogen, besides being a substitute for fossil fuel, might replace a significant part of the electric energy. The construction of commercial pilot centres is proposed. The objective is to gain a necessary experience insight to further set up the system.

REFERENCES

[1] *Strategy of a Sustainable Development of Croatian Islands (1994).* University of Split, Faculty of Economy, Croatia

[2] Vujčić, R (1995). Solar/Wind Hydrogen Energy System for Adriatic Islands. *Energy, Environment And Economics International Symposium*, Melbourne, Australia

[3] Vujčić, R and Ž. Josipović (1996). Hydrogen Energy System - Role in Power Supply of Autonomous Tourist Centres on the Adriatic Islands. *World Renewable Energy Congress* , Denver, Colorado, USA

[4] Mikačić, V (1987). The Population of Croatian Islands. PZ (25), 1987, 57-63.

[5] National Program of Croatian Islands, 1996

[6] Neve. ćanin, J. (1994). Electric Supply Scenario for Dalmatia - up to 2020., Croatian Electroenergy Corporation, Split, Croatia

[7] Kunst, I. (1996). A Conceptual Framework For Tourism Development on Croatian Islands, Tourism, 9-10/1996, 207-227

[8] Poje, D. and Cividini, B. (1988). Assessment of wind energy potential in Croatia. *Solar Energy. Vol. 41. No. 6*

[9] Pilić, Lj. and Sansević, M (1993). Possibilities of Economical Exploitation of Wind Power System in Dalmatia. *J. Solar Energy Science and other Alternative Energy Sources Vol. 14.* No. 1 pp. 27-31

A STEAM CYCLE WITH DIRECT COMBUSTION OF HYDROGEN AND OXYGEN AND AN ISOTHERMAL EXPANSION

S. P. CICCONARDI, E. JANNELLI, A. PERNA, G. SPAZZAFUMO
Industrial Engineering Dept. - University of Cassino
Via G. di Biasio, 43- 03043 Cassino (FR) - Italy

Abstract

A new thermodynamical cycle characterised from an isothermal expansion has been examined from a theoretical point of view. In the real cycle the isothermal expansion could be approached by means of mixing re-heatings. The high temperature steam for mixing is produced in a direct steam generator burning a stoichiometric mixture of hydrogen and oxygen. The theoretical analysis has shown that the reference cycle allows an efficiency very close to the efficiency of a Carnot cycle evolving between the same extreme temperatures. The ratio between the two efficiencies can approach 90%.

1. Introduction

Since a long time the steam plants have reached a great technological development. For a such reason it is difficult to change the thermodynamical cycle and achieve further improvement to the plant performance. Currently only hypercritical steam cycles are considered in power-plants designing. It is not a simple way to increase efficiency and it also involves significant capital costs.
Among all the partial efficiencies that contribute to the plant efficiency, the only ones which have values significantly different from the unity are the steam generator one and especially the thermodynamical cycle one. From a general point of view, two possible chances exist for increasing the thermodynamical cycle efficiency:
$\Rightarrow$ to approach the cycle to the Carnot one;
$\Rightarrow$ to widen the gap between the extreme temperatures of the cycle.
Since the birth of the Rankine cycle up to date significant steps in both the directions were made. The use of a steam condenser allowed to lower the minimum temperature of the cycle down to a value close to the environment one. This is usually a limit for the minimum temperature. On the other hand, the maximum temperature of the cycle raised thank to the use of a super-heater. In this case the upper limit for the heat source is higher than the level currently reached for steam. This is due to the criticality of the super-heater which, having the task to allow heat exchange, operates under high tem-

T. O. Saetre (ed.), Hydrogen Power: Theoretical and Engineering Solutions, 505–510.

peratures on both its faces. The materials currently used do not allow steam temperatures over 550÷600 °C. Actually materials with better characteristics exist, but their cost is very high. At this level the turbine does not constitute a limitation to a superior temperature: it is not a component for heat exchange and therefore it is possible to adopt cooling techniques, like in gas turbines technology. In Japan an international plan denominated WE-NET (World Energy Network) has started: a target of this plan is the realisation within the 2020 of turbines able to accept "steam" at temperatures in the range of 1500÷1700°C and pressures up to 10 MPa [1, 2].
About the approach to the Carnot cycle, the more meaningful step was the introduction of the heat regeneration. The super-heating is unfavourable, but subsequent re-heatings have a positive effect since, like the regeneration, they approach the average admission temperature of the heat to the maximum temperature of the cycle. These favourable interventions have a limit in the complexity of the plant. In particular, due to a re-heating the steam must return into the boiler: this is a complication of the plant lay-out and of the steam generator geometry and therefore causes heat and pressure losses. This is why re-heatings are not more than 2 or 3.

2. Mixing re-heating

Since more than 10 years in Germany and more recently in Japan and in Russia, the study and testing of direct steam generators is developed [3, 4, 5, 6]. In Italy a prototype has been realised at the Department of Energetic of the University of Pisa [7]. Such device is essentially made up of a combustion chamber followed by a mixing cylinder. Hydrogen and oxygen in stoichiometric ratio burn in the combustion chamber producing very high temperature steam. This steam is then cooled by water injection and the steam temperature is adjusted to the required value.
Replacing the cooling water with steam to be re-heated, in the opportune rate, the direct steam generator is modified in a mixing re-heater (schematically shown in fig.1).

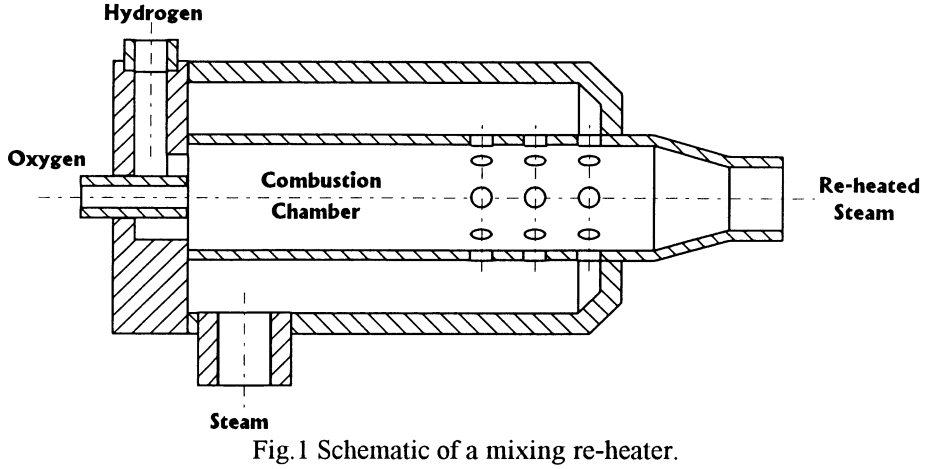

Fig.1 Schematic of a mixing re-heater.

With respect to a surface super-heater more expensive materials, usually employed in the rocket technology, are required. However the re-heater is very compact and much less material is necessary (see tab.1). The system for combustion control is very critical and could be the most important for mixing super-heater cost evaluation.

Table 1. Characteristics of the traditional and direct steam generators [8]

Type	Traditional	Direct (H_2/O_2)
Fuel	Natural gas, Oil, Coal	H_2
Oxidant	Air	O_2
Equivalence ratio	>1,1	<1,1
Steam maximum temperature (°C)	535÷600	1000÷1700
Burner specific power (MW/m^3)	0,1÷1	1.000.000
Heat transfer method	Allothermic	Mixing
Wall temperature of generator (°C)	600÷850	200 (water film cooled) 500÷1000 (steam cooled)
Combustion efficiency	0,9÷0,94	0,98÷0,995

Thank to the use of such a re-heater will be possible to increase the maximum temperature of the cycle: the limit currently imposed by the steam generator will be transferred to the turbine, exactly like happens for a gas turbine system. Moreover the steam returning into boiler will be avoided and therefore it will be possible to increase the re-heatings number and to approach more closely an isothermal expansion: the re-heatings number will find a limit connected to economic or fluidodynamic (perturbation of the steam flow at each injection) aspects.

The new steam cycles which could be designed with mixing re-heaters would have at the same time the characteristics of a traditional steam cycle, at low temperatures, and of a gas cycle, at high temperatures. The high temperature section of the cycle would supply heat to the low temperature one by means of regeneration: therefore these cycles, e. g. the Jericha cycle [9], could be considered combined cycles working with only one fluid.

Finally the possibility to realise a quasi-isothermal expansion (fig.2) could allow further performance improvements. This type of cycle requires a new reference cycle proposed by Spazzafumo: this cycle has some characteristics of a Rankine cycle and some characteristics of an Ericsson cycle.

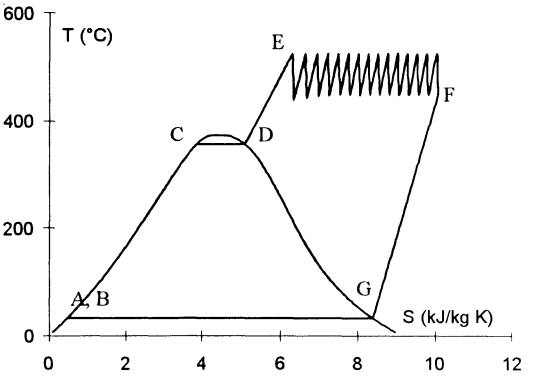

Fig.2 A steam cycle with a quasi-isothermal expansion [10]

3. The reference cycle

The reference cycle, with p_{max}=18 MPa and T_{max}=600 °C, is shown in fig.3. This limit cycle is followed by a real fluid (water-steam-gas) evolving in an ideal machine able to exchange heat during an isothermal expansion. The area between the abscissas axis and the F-G transformation represents an amount of totally recoverable heat.
Relationships (1)÷(7) are the basic thermodynamical relationships for the reference cycle. The subscripts NR and R means "Not Regenerated" and "Regenerated"; the other symbols are conventional ones.

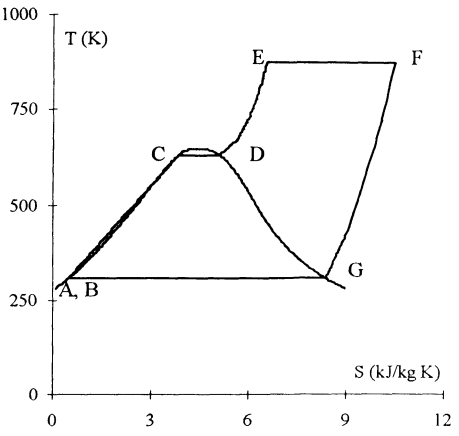

Fig.3 Reference cycle

$$Q_{1NR} = m \cdot \left[T_E \cdot (s_F - s_E) + (h_E - h_B)\right] \tag{1}$$

$$Q_{2NR} = m \cdot (h_A - h_F) \tag{2}$$

$$L_{NR} = L_R = m \cdot \left[T_E \cdot (s_F - s_E) - (h_F - h_E) - (h_B - h_A)\right] \tag{3}$$

$$\eta_{NR} = \frac{T_E \cdot (s_F - s_E) - (h_F - h_E) - (h_B - h_A)}{h_E - h_B + T_E \cdot (s_F - s_E)} \tag{4}$$

$$Q_{1R} = m \cdot \left[T_E \cdot (s_F - s_E) + (h_E - h_B) - (h_F - h_G)\right] \tag{5}$$

$$Q_{2R} = m \cdot (h_A - h_G) \tag{6}$$

$$\eta_R = \frac{T_E \cdot (s_F - s_E) - (h_F - h_E) - (h_B - h_A)}{T_E \cdot (s_F - s_E) + (h_E - h_B) - (h_F - h_G)} \tag{7}$$

The following performance indexes, when varying the maximum temperature of the cycle, being p_{max}=18 MPa and p_{min}=0.005 MPa, are shown in fig. 4a):

⇒ efficiency of the Carnot cycle (η_C);
⇒ efficiency of the not regenerated cycle (η_{NR});
⇒ efficiency of the regenerated cycle (η_R);
⇒ ratio between the efficiencies of not regenerated cycle and Carnot cycle;
⇒ ratio between the efficiencies of regenerated cycle and Carnot cycle.

The same performance indexes, when varying the maximum pressure of the cycle, with T_{max}= 600 °C MPa and p_{min}= 0.005 MPa, are shown in fig.4b).

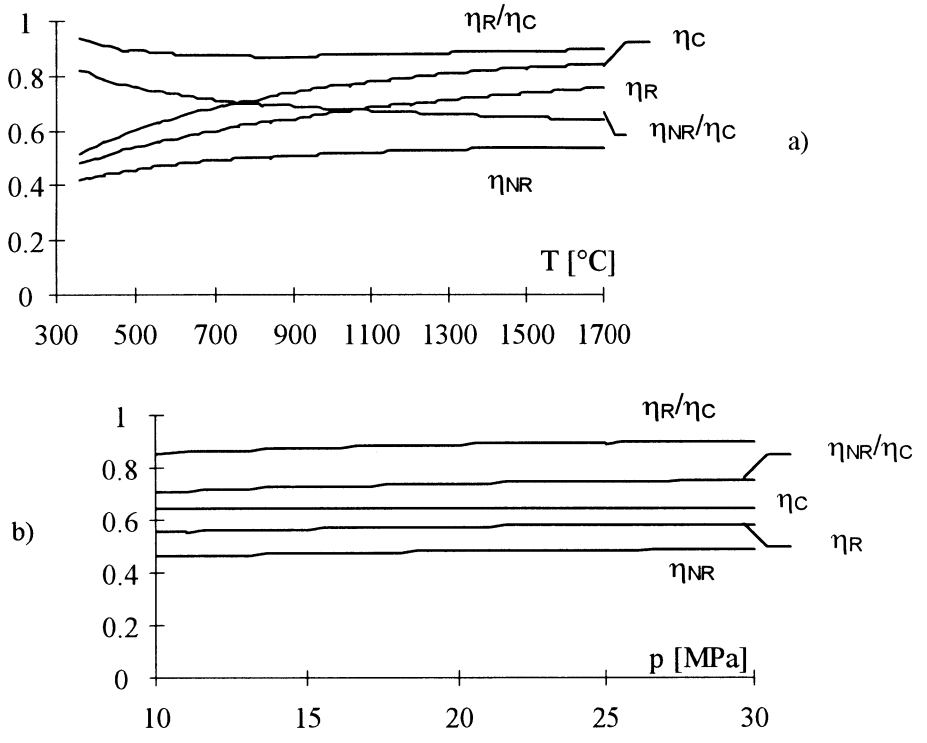

Fig.4 Performance indexes.

If the maximum temperature of the cycle increases, the gap between the efficiency of the not regenerated cycle and that of the Carnot cycle increases too. For the case considered in fig.4a) their ratio drops from 0.81 to 0.64. But the efficiency of the regenerated cycle is able to follow very closely the efficiency of the Carnot cycle. Actually, for the case considered in fig.4a) the ratio between the two efficiencies ranges from 0,93 to 0,89 with a minimum of 0,87. The existence of the minimum in the relationship between η_{SR} and η_C is due to the effect of the maximum temperature of the cycle on the regeneration: until regeneration interests the preheating and evaporation the heat admission average temperature grows very slowly when compared with the maximum one.

The effect of the maximum pressure is more regular: both not regenerated and regenerated cycle efficiencies rise slightly with the pressure (about +2% from 10 MPa to 30 MPa) and therefore also their ratios with the efficiency of Carnot cycle rise. The positive effect of the pressure is connected with the reduction of the evaporation heat.

It is important to observe that, in the case of hydrogen/oxygen systems, these values of efficiency almost coincide with the efficiency (HHV) of the system, being nearly unitary the efficiency of the steam generator.

REFERENCES

1. Chiba M., Arai H., Fukuda K. (1996) "International and national program and project Hydrogen Energy Technology Development in Japan: New Sunshine Program", XI World Hydrogen Energy Conference, June 1996, Stuttgart (Germany), page 13.

2. Yamawaki S., Maya T., Yasu S. (1996) "Study of film cooling with shaped holes for a hydrogen combustion turbine blade", XI World Hydrogen Energy Conference, June 1996, Stuttgart (Germany), page 1905.

3. C. J. Winter, J. Nitsch (1988) "Hydrogen as an energy carrier - Technologies, systems, economy", Springer-Verlag Berlin 1988.

4. Haidn O.J., Fröhlke K., Carl J., Weingartner S. (1996) "Improved combustion efficiency of a H2/O2 steam generator for spinning reserve application", XI World Hydrogen Energy Conference, June 1996, Stuttgart (Germany), page 1418.

5. Hashimoto T., Koyama K., Yamagishi M. (1996) "Hydrogen combustion characteristics in a model burner with a coaxial injector", XI World Hydrogen Energy Conference, June 1996, Stuttgart (Germany), page 1493.

6. Volkov A.G., Bebelin I.N., Gryaznov A.N., Malyshenko S.P. (1996) "Development and testing of experimental H2/O2 steam generators", XI World Hydrogen Energy Conference, June 1996, Stuttgart (Germany), page 1913.

7. Dini D. (1995) "Test installation for an already built 20 bar hydrogen-oxygen-water combustion chamber", paper presented at HYPOTHESIS, Hydrogen Power Thermal and Electrochemical Systems International Symposium, June 1995, Cassino-Gaeta (Italy).

8. Malyshenko S.P. (1996) "Hydrogen combustion systems in power production", paper presented at the XI World Hydrogen Energy Conference, June 1996, Stuttgart (Germany).

9. Jericha H., Wilplinger H., Perz E. (1987) "A Novel High Efficiency Steam Cycle", ASME Cogen Turbo, Montreaux.

10. Cicconardi S.P., Jannelli E., Spazzafumo G. (1996) "A thermodynamic cycle with a quasi-isothermal expansion", paper presented at the XI World Hydrogen Energy Conference, June 1996, Stuttgart (Germany). Currently in press on Int. J. of Hydrogen Energy.

A Study of Advanced Hydrogen/Oxygen Combustion Turbines

H. SUGISHITA and H. MORI
Takasago R&D Center, Mitsubishi Heavy Industries, Ltd
2-1-1 Shinhama Arai-cho, Takasago, Hyogo Pref. 676 Japan

K. UEMATSU
Takasago Machinery Works Mitsubishi Heavy Industries, Ltd
2-1-1 Shinhama Arai-cho, Takasago, Hyogo Pref. 676 Japan

ABSTRACT

Mitsubishi Heavy Industries Ltd. have proposed the advanced hydrogen/oxygen combustion turbine system which is an inter-cooled topping recuperation cycle as part of a Japanese government sponsored program WE-NET ("World Energy Network"). The efficiency of this cycle reaches more than 60% (HHV), not (LHV), with a power capacity of 500MW. This cycle is formed by a compressor, turbines, a combustor and heat exchangers. The combustor burns hydrogen/oxygen to make high temperature (1700 °C) steam.

As a result of MHI research in 1994 [1], the topping extraction cycle (A) designed by Jericha et al. [2] was found to be the best cycle. MHI also designed the inter-cooled topping recuperation cycle (BI) in 1995 which modified cycle (A) to be suitable for a high combustion temperature (1700 °C).

This paper presents the details of the comparison between the above mentioned cycles. The investigation shows that cycle (BI) is considered to be better than cycle (A) from the point of view of both the thermal efficiency and the feasibility of manufacture.

1 INTRODUCTION

WE-NET, a part of "New Sunshine Project", is a Japanese government program aimed at solving energy and environmental problems in the world. WE-NET, which began in 1993 and is expected to last for 30 years, has the aim of constructing a clean energy network throughout the world; firstly by producing Hydrogen by electric dissolution of water using hydro-electric-power, solar energy, geothermal energy, wind energy, etc. and then transporting, storing and generating electricity using this produced Hydrogen. In this paper some evaluation of "Hydrogen/Oxygen Combustion Turbine Cycles", which is a sub-task of "World Energy Network", is presented.

In 1994, three different closed hydrogen combustion turbine cycles, were evaluated [1]. These are the Bottoming Reheat Cycle, the Topping Extraction Cycle (A) designed by Jericha et al. [2] and the Rankine Cycle. Results of this study showed the Topping Extraction Cycle (A) to be the best cycle.

Subsequent to this research, further work was undertaken to design a highly efficient and highly feasible cycle adapted to high combustion temperature (1700 °C) - the Topping Recuperation Cycle

T. O. Saetre (ed.), Hydrogen Power: Theoretical and Engineering Solutions, 511–516.

(B). Cycles with an inter-cooler between low pressure and high pressure compressors in cycles (A) and (B) have also been investigated which are the Inter-cooled Topping Extraction Cycle (AI) and the Inter-cooled Topping Recuperation Cycle (BI).

2 CYCLE CONFIGURATIONS

The Inter-cooled Topping Extraction Cycle (AI) shown in Figure 1 is a kind of gas turbine combined cycle whose working fluid is steam. The topping cycle is a Brayton cycle comprising of low pressure compressor 1, high pressure compressor 2, turbine 4 ,heat exchanger 5,6, and combustor 3. The bottoming cycle of cycle (AI) is a Rankine cycle. Steam is extracted from between heat exchanger 5 and 6, is expanded by turbine 6, and condensed by condenser 8. The same flow rates as the hydrogen fuel and stoichiometric oxygen are discharged, the rest of the steam is pumped up by pump 12 and 13. The steam is economized by feed water heaters 10 and 11, recuperated by heat exchanger 5 and 6, expanded by turbine 9 and mixed with the topping steam in the outlet of compressor 2. The water to be inter-cooled is extracted after being condensed in condenser 13, and pumped up in pump 17. It is mixed with the the topping steam in the outlet of compressor 1. The Topping Extraction Cycle (A) is same as non-inter-cooled one of cycle (AI).

The Inter-cooled Topping Recuperation Cycle (BI) shown in Figure 2 is also a kind of gas turbine combined cycle like cycle (AI). Cycle (BI) has added heat exchangers 14 and 15 compared with cycle (AI). The heat exchanger 14 recuperates the heat from the exhaust of turbine 4 to the exit of compressor 2.

3 ASSUMPTIONS CONDITIONS

The investigations are carried out preliminarily in the operating conditions in Table 1 and the component efficiencies in Table 2. Table 1 shows the operating pressures and temperatures of each component (such as turbines, compressors, and heat exchangers) which are assumed to be the almost the same values in cycle (A), (AI), (B) and (BI). The values in Table 1 and 2 are expected in the near future. Because of these assumptions, the thermal differences of the cycles can be clarified. The total output of all cycles is a constant 500MW. Combustor outlet temperatures are assumed to be both 1700 °C and 1500 °C, because the firing temperatures of current high efficiency industrial gas turbines have already reached 1500 °C. Cooling steam flow rate ratio is 0%, and 15%. The outlet pressure downstream of the condensers is fixed at 0.05bar(10^5Pa). As the components' assumptions and conditions above are almost the same, the manufacturing realization of the components (turbines ,heat exchangers, compressors, combustors and so on) should be nearly equivalent.

The paramatric studies based on the above investigations are carried out to assess the characteristics of pressure ratio and the inlet temperature of turbine 4. The pressure ratio should be selected carefully if the operating temperature is decided because a lot of factors are affected by the pressure ratio. The merits and demerits of increasing the pressure ratio are displayed in Table 3. From Table 3, it would be beneficial to achieve a high cycle thermal efficiency at the lowest possible pressure ratio.

4 PERFORMANCES AND FEASIBILITY OF COMPONENT

Cycle calculations for cycle (A), (AI), (B) and (BI) were carried out to estimate the performance of the cycles. The typical results of cycle calculations, assuming that combustor outlet temperature is 1700

°C and cooling steam flow rate ratio is 0% are shown in Table 4. Comparison of cycle (A) and (BI) shows the thermal efficiency of cycle (BI) to have a relative change of 4.0% higher than cycle (A). The first vane height of the high pressure, high temperature turbine of cycle (BI) has a relative change of 7% higher than cycle (A). The exhaust temperature of the turbine 4 and the maximum operating temperature of the heat exchanger in each cycle are almost the same at 800 °C . The compressor outlet temperature is about 700 °C in cycles (A) and (B) and 550 °C in cycles (AI) and (BI). Therefore, cycle (BI) is judged to be the best cycle from the point of view of the feasibility of the components. The results of other cases are shown in Table 5.

The results of the parametric studies are shown in Figure 3 and 4. The results show that the pressure ratio for the maximum thermal efficiency is about 130 in cycle (A) and 50 in cycle (BI). The thermal efficiency of cycle (BI) is higher than cycle (A) for a pressure ratio of less than 70. If the pressure ratio becomes higher, a lot of problems shown in Table 3 are anticipated. Cycle (BI), therefore, has an advantage in terms of thermal efficiency at a more feasible pressure ratio. The pressure ratio should ,therefore, be set to 50.

The thermal efficiency of cycle (BI) is higher than cycle (A) when the turbine 4 inlet temperature is more than 1500 °C. Cycle (BI) is, therefore, suitable for the high operational temperature cycle of more than 1500 °C. The features of the Inter-cooled Topping Recuperation Cycle are shown in Table 6.

5 CONCLUSIONS

1) The thermal efficiency of cycle (BI) is 62.2%(HHV), which is a relative change of 4.0% higher than cycle(A).

2) The cycle (BI) has a relative change of 7% larger first stage turbine vane height than cycle (A), and the advantage from the point of view of both the manufacturing of the complex cooling passage inside the vane and the turbine aerodynamic efficiency. It is especially important to have high aerodynamic efficiency of the high temperature turbines in each cycle to achieve higher overall thermal efficiency.

3) The pressure ratio for the maximum thermal efficiency is about 50 in cycle (BI), which is lower than that of cycle (A) at 130. Cycle (BI), therefore, has an advantage of high thermal efficiency at a more feasible pressure ratio.

4) Cycle (BI) is suitable for a high operational temperature cycle of more than 1500 °C.

5) The inter-cooled topping recuperation cycle (BI) in Figure 2 is considered to be the best cycle from the view point of the thermal efficiency and the feasibility of manufacturing.

References

[1] H.Sugishita, H.Mori and K.Uematsu "A Study of Thermodynamic Cycle and System Configurations of Hydrogen Combustion Turbines", 11th World Hydrogen Energy Conference, Stuttgart Germany, June 23-26,1996, pp1851-1860.

[2] H. Jericha, R.Ratzesberger, "A Novel Thermal Peak Power Plant", ASME Cogen-Turbo Nice France August 30 - September 1 ,1989.

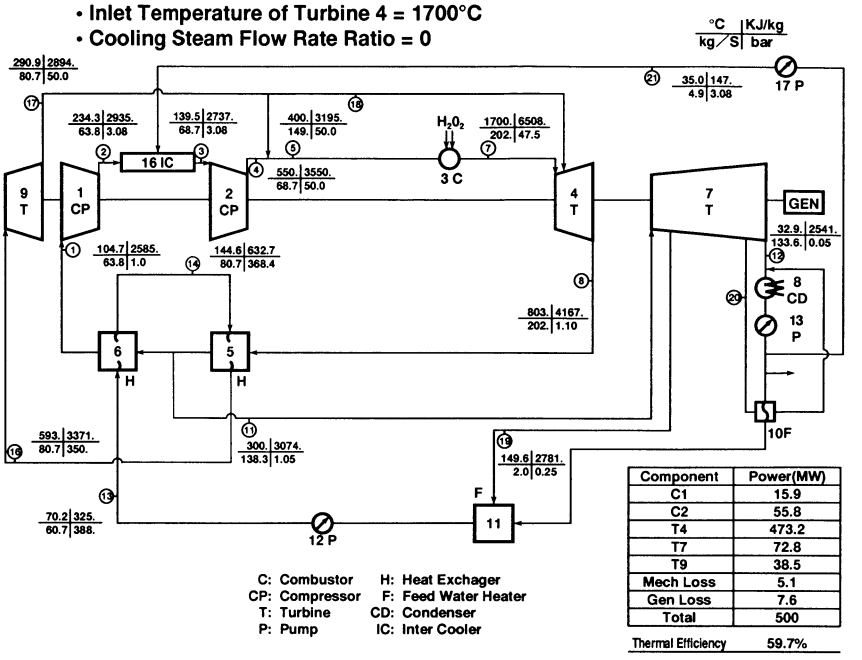

Fig.1 A Typical Calculation Result of Intercooled Topping Extraction Cycle(AI)

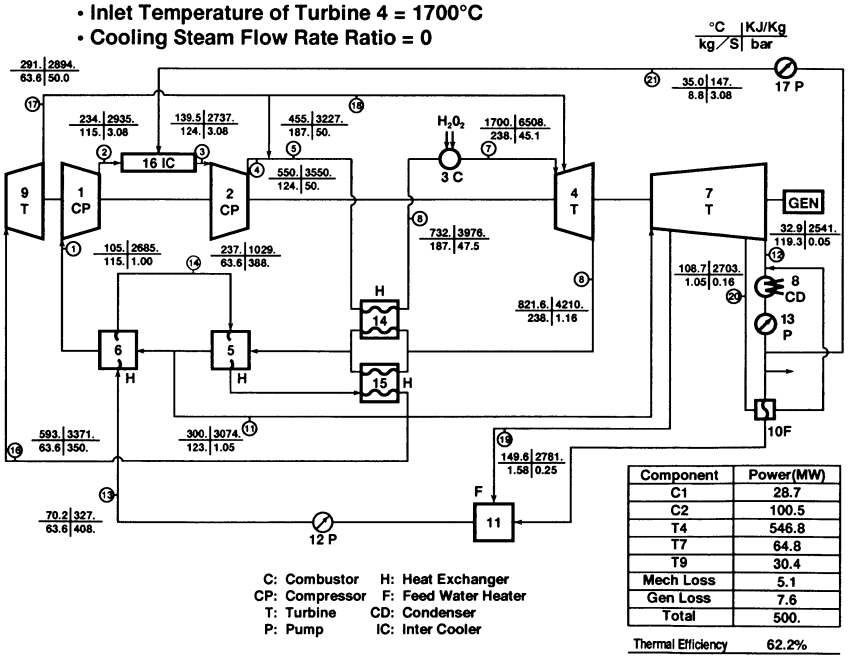

Fig.2 A Typical Calculation Result of Intercooled Topping Recuperation Cycle (BI)

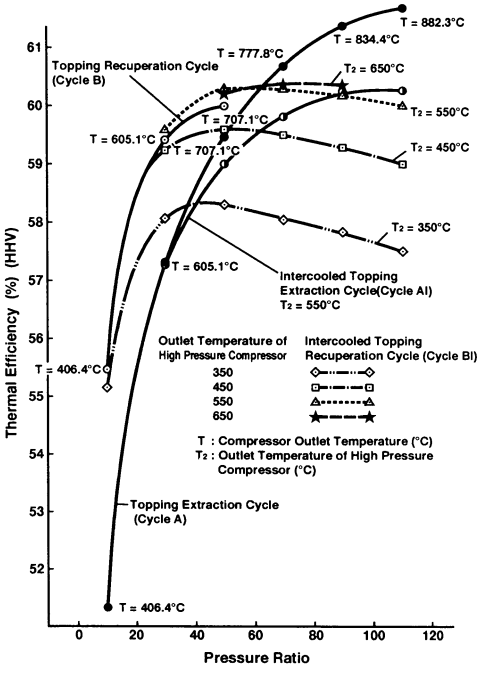

Fig.3 Effects of Topping Pressure Ratio

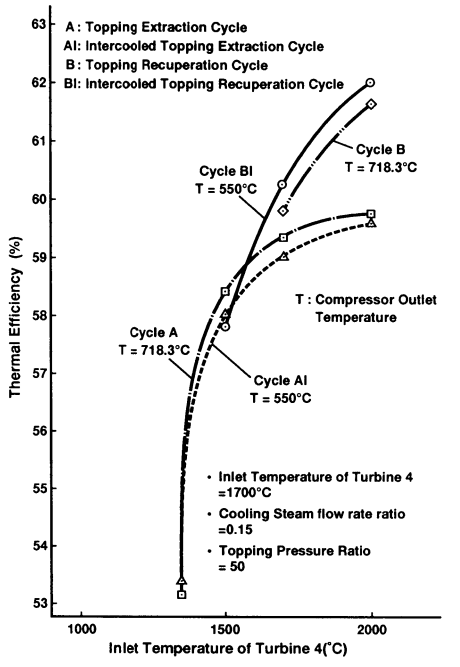

Fig.4 Effects of Inlet Temperature of Turbine 4

Table 1 Operating Conditions

• Compressor Inlet Pressure	1.0 bar
• Compressor Inlet Temperature	+5°C of a Saturated Temperature
• Compressor Outlet Pressure	50.0 bar
• Compressor Outlet Temperature	550°C (With inter-cooled)
• Turbine 4 Inlet Temperature	1700, 1500°C
• Cooling Air Flow Rate Ratio of Turbine 4	0, 0.15
• Turbine 4 Outlet Temperature	Less than 870°C
• Turbine 9 Inlet Temperature	593°C
• Turbine 9 Inlet Pressure	350 bar
• Maximum Operating Temperature of Heat Exchanger	Less than 900°C
• Temperature Efficiency of Heat Exchanger	Less than 0.85
• Total Output	500 MW

Table 2 Components Efficiency

Compressor Efficiency	0.89
Turbine Efficiency	0.93
Combustion Efficiency	1.0
Combustor Pressure Loss	5% of inlet pressure
Heat Exchanger Pressure Loss	5% of inlet pressure
Pump Loading	0
Mechanical Efficiency	0.99
Generater Efficiency	0.985

Table 3 Merits and Demerits by increasing Pressure Ratio

Merits
• Higher Thermal Efficiency
Demerits
• Increase the number of stages of turbines and compressors
• Increase the leakage flow rate
• Higher compressor exhaust temperature
• Thicker casing of compressor outlet and combustor chamber
• Higher heat transfer coefficient on the surface of blades
• Higher energy to pump up a fuel
• Lower height of first stage turbine vanes

Table 4 Comparison of Results

	Thermal Efficiency (%)	Relative Change of Thermal Efficiency	Relative Change of First Stage Turbine Vane Height of Turbine 4	Compressor Outlet Temperature (°C)	Exhaust Temperature of Turbine 4 (°C)	Maximum Operating Temperature of Heat Exchanger (°C)
Cycle A	60.0	1	1	707	803	803
Cycle AI	59.7	0.995	0.98	550	803	803
Cycle B	62.4	1.04	1.09	707	822	822
CycleBI	62.2	1.04	1.07	550	822	822

• Inlet Temperature of Turbine 4=1700°C
• Cooling Steam flow Rate Ratio=0

Table 5 Results of Cycle Calculations

		Topping Extraction Cycle								Topping Recuperation Cycle							
Cycle		(A)				(AI)				(B)				(BI)			
Pressure ratio		50				50				50				50			
Inlet temperature of turbine 4		1700		1500		1700		1500		1700		1500		1700		1500	
Cooling Flow rateratio		0	0.15	0	0.15	0	0.15	0	0.15	0	0.15	0	0.15	0	0.15	0	0.15
Compressor Outlet Temperature	Low	707.0	707.0	707.0	707.0	234.3	234.3	234.3	234.3	707.0	707.0	707.0	—	234.3	234.3	234.3	234.3
	High					549.8	549.8	549.8	549.8					549.8	549.8	549.8	549.8
Inlet temperature of Turbine 4		803.1	699.4	672.7	578.2	803.1	699.4	672.7	579.8	821.6	716.8	689.6	—	821.6	716.8	689.6	595.7
Flow rate of Turbine 4		209.15	223.35	267.68	289.84	202.11	211.44	252.06	266.42	246.35	241.10	290.65		237.95	236.88	279.83	275.63
Thermal Efficiency (%)		60.0	59.5	59.6	58.2 (T15=538°C)	59.7	59.0	59.1	58.0	62.4	60.0	60.3		62.2	60.3	60.3	57.8 (T15=566°C)

Table 6 Features of Cycles

	Inter-cooled Topping Extraction Cycle (AI)	Inter-cooled Topping Recuperation Cycle (BI)
1. System Configurations	• Combined Cycle	←
2. Recuperation from Turbine Outlet to Combustor Inlet	×	○
3. Characteristic of Pressure Ratio	• Optimized Pressure Ratio is about 130	• Optimized Pressure Ratio is about 50
4. Characteristic of Temperature of Turbine 4 Inlet	• Higher Efficiency in less than 1500°C	• Higher Efficiency in more than 1500°C
5. Steam Flow Rate of Turbine 4 Inlet	• Small	• Large (Easier to construct complicated cooling passages)

LIQUID HYDROGEN TECHNOLOGY

PRESENT STATE AND FUTURE FUEL APPLICATION

W. PESCHKA
German Aerospace Research Establishment
DLR Stuttgart

Abstract

The initial large scale application of liquid hydrogen was as a high energy rocket propellant. In the past procedures for large scale liquefaction, storage, transportation and handling were generally developed in the U.S. and is state of the art there. More recently in Europe similar activities are being conducted in France and in Germany. Similar activities are also under progress in Canada and Japan.
As a result of its storage and transportation characteristics liquid hydrogen offers possible advantages in the supply of energy in general and as an alternative fuel. It is unequalled for environmental compatibility in aviation as well as in ground transportation. Earthbound vehicles will continue for a long time to use primarily internal combustion engines, while electric drives with batteries or hydrogen-air fuel cells will be limited to special applications. In addition to the preferred use of liquid hydrogen due to its range per tank filling and low amount of mass for storage in the vehicle, the cryogenic characteristics of hydrogen provide significant advantages. Additional aims of more intense R&D work relate to internal mixture formation and improved engine roadability as well as utility vehicle application including trucks and buses.
The main reason to support hydrogen as a fuel lies in the foreseeable problems regarding the CO_2 emissions into the Earth's atmosphere due to the unrestrained use of fossil energy. While combustion of currently used, or feasible hydrocarbon fuels releases about the same amount of CO_2 per amount of heat produced, even hydrocarbon fuels with a greater hydrogen content do not lead to substantial improvement in this regard. Hydrogen represents the only practical, technically feasible, carbon free fuel. With respect to fuel costs there will be an increased demand in developing hydrogen production free from CO_2 emissions even from fossil energy sources such as crude oil or natural gas. All these applications to be implemented in the first decades of the next century offer important contributions toward substantially more complex applications in the future.

T. O. Saetre (ed.), Hydrogen Power: Theoretical and Engineering Solutions, 517–528.

1. Introduction

Hydrogen was liquefied for the first time by *Dewar* in 1898. For more than half a century its use was basically limited to laboratory scale experiments for the generation of low temperatures and the measure of the specific heat of solids down to approximately 13.8 K, the lowest possible temperature attainable with liquid hydrogen. In addition to these tests, primarily carried out by *Simon* in Oxford with the objective of proving *Nernst's* theorem, work on the free energy of chemical bonding in the temperature range from liquid hydrogen to ambient temperature was later carried out by *W. F. Giauque* from 1920 to 1930.
Due to the theoretical work in quantum-theory by *E. Schrödinger* and *W. Heisenberg*, the latter was able to prove that the two forms of the hydrogen molecule, ortho-hydrogen with parallel nuclear spins and para-hydrogen with anti-parallel nucelar spins were responsible for the unusual behavior of the specific heat of hydrogen at low temperatures. This is important in the long-term storage of hydrogen to avoid additional excessive evaporation.
Following pioneer work by *Herrick L. Johnston* at the Cryogenic Laboratory of the Ohio State University from 1940-1950, the National Bureau of Standards (now National Institute for Standards and Technology, NIST) established a laboratory in Boulder, Colorado in 1952 (commissioned by the U.S. Atomic Energy Commission) with the goal of technical applications. Included among these applications were primarily the liquid hydrogen bubble chambers for nuclear research, the first of which was built at the Lawrence Radiation Laboratory (LRL) in 1959, as well as nuclear and chemical rocket propulsion.
Nuclear thermal rocket propulsion systems that were tested successfully from 1960 to 1970 have still a great potential to be used for interplanetary missions. Compared with low thrust electrical propulsion systems the mass required for the electrical power conversion system and the radiator for waste heat release can be avoided. Liquid hydrogen as a rocket fuel has been developed intensively since 1959. The first successful launch of a hydrogen-oxygen rocket from Cape Kennedy on the 27th of November 1963- the upper stage of a NASA Centaur rocket with an Atlas booster-led to the NASA Apollo program and the Space Shuttle./2/.

2. Future LH_2- Application

As a result of its storage and transportation characteristics it offers superior advantages even as an alternative fuel. It is unequalled for environmental compatibility in aviation as well as in ground transportation. Although the latter will surely not be the first to be implemented on a large scale, they already have provided important contributions toward substantially more complex applications in the future. In the following chapters more emphasis is given to the small scale applications.

2.1 LARGE SCALE SYSTEMS

The large-scale application was essentially influenced and promoted by space technology requirements. It also includes projects and development work related to subsonic and supersonic aircraft. /1, 2, 3/. While technical problems at intermediate scale for the flying apparatus aircraft components are not insurmountable, the required huge capital investments for airport ground installations such as fuel supply, storage and handling, represents a primary hindrance to successful political-economic decisions.
Hydrogen seems to be made for the supersonic range. Higher flight altitudes are attainable so that effects of the sonic boom practically can be eliminated. Further development will finally lead to aero-space vehicles which can use conventional runways. Due to foreseeable developments of air breathing hybrid propulsion systems liquid hydrogen and even slush hydrogen will be an universal fuel for aircraft and transatmospheric vehicles. /2, 3/.

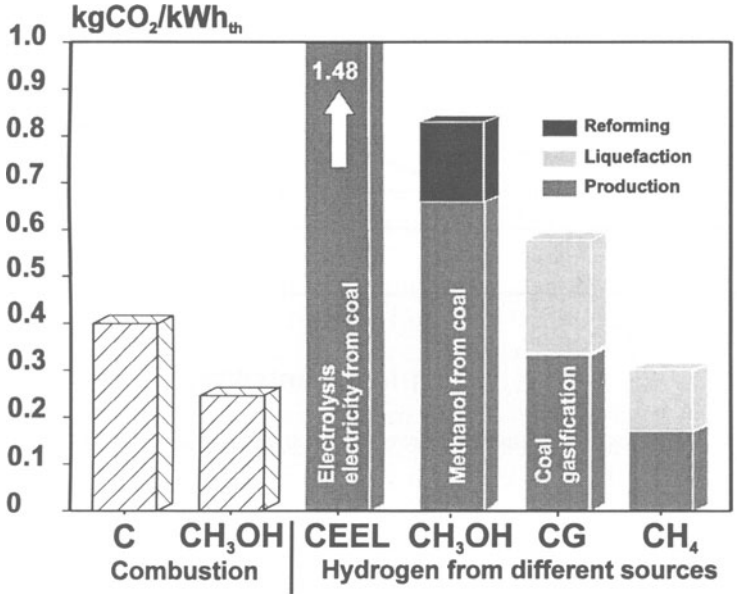

Figure 1. Total CO_2 emissions from combustion and hydrogen.

2.2 SMALL SCALE SYSTEMS

The small scale end is represented by application of liquid hydrogen as an alternate fuel in ground transportation. It still requires development of miniaturized components such as valves, pumps for onboard fuel storage, handling and fuel conditioning for the propulsion system.
Earthbound vehicles will continue for a long time to use primarily internal combustion

engines, while electric drives with batteries or hydrogen-air fuel cells will be limited to special applications. The clear superiority of the internal combustion engine is obvious as well as the considerable limitations which battery or fuel cell powered vehicles are subjected with respect to range and acceleration. No realistic way can be seen, to improve this situation substantially. Even more significant are comparisons of the mass fractions of the energy storage like fuel and batteries, the drive motor as well as of the structural mass and the payload./1, 5, 14, 18/.

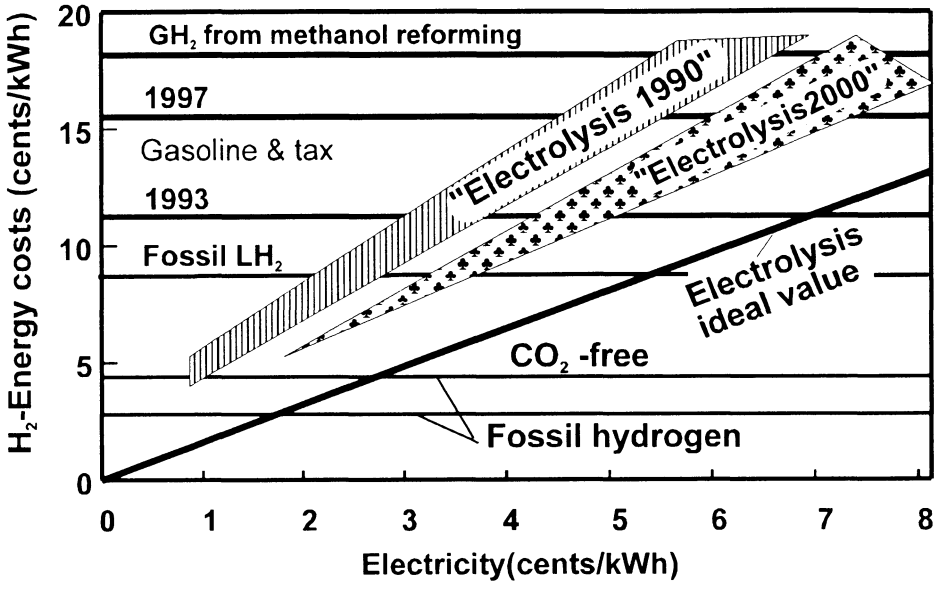

Figure 2. Hydrogen and gasoline energy costs. LH_2 from fossil sources (80 cents/gal.)

3. Production

The main reason to support hydrogen as a fuel lies in the foreseeable problems regarding the CO_2 emissions into the Earth's atmosphere due to the unrestrained use of fossil energy. While combustion of currently used, or feasible hydrocarbon fuels releases about the same amount of CO_2 per amount of heat produced, even hydrocarbon fuels with a greater hydrogen content do not lead to substantial improvement in this regard. Hydrogen represents the only practical, technically feasible, carbon free fuel (see *fig. 1*).
Depending upon the production method, hydrogen from electrolysis, liquefied and primary energy of liquefaction included, contains roughly from 25% to 40% of the primary energy /6/. The use of hydropower can increase this fraction up to 70%. The cost of electrolytic hydrogen is comparable to synthetic hydrocarbon fuels, and about

three times as expensive as hydrogen from fossil fuel sources (*fig.2*).
Liquid hydrogen from fossil fuels made from steam reforming or partial oxidation contains about 37% of the expended primary energy (process waste heat and primary energy for liquefaction included) /6/. Liquid hydrogen from methane contains a fraction of primary energy slightly less than gaseous hydrogen made from the well known methanol reforming. /17/. Neglecting economics (see *fig.2*) the latter presently was taken in consideration again for fuel cell drives. Some car manufacturers obviously maintain the objection that hydrogen and especially liquid hydrogen has to be rejected from energetic reasons and that it would be a tall order for the customer and have no sufficient warrant in expecting him to accept hydrogen as a fuel. But this objection cannot be justified from the fraction of primary energy contained in the fuel when hydrogen is made from methane or from hydropower and electrolysis (see *fig.3*). Even catalytic decomposition (cracking) of methane will become more important in the future./4, 5, 6/. In accordance with the reaction $CH_4 \rightarrow C + 2H_2$, in addition to elementary carbon, hydrogen is set free, where about 60% of methane's heat value is available from the hydrogen. In this case liquid hydrogen contains about 29% of the fossil primary energy, whereas 19% are stored in form of elementary carbon. /5/. The required process heat at a temperature level in the range between 700°C to 980°C could be provided by combustion of the carbon byproduct or from some other, CO_2 free energy. Reaction kinetics could be substantially improved with excitation of molecular vibrations by means of available highly efficient semiconductor infrared lasers.

4. Liquefaction

Several procedures for hydrogen liquefaction are state of the art, encompassing the range from laboratory equipment to large scale plants.
In case of large scale plants the Claude process is the most economic one. (see/1/). In the best case it attains for liquefaction work about 11 kWh/kg (36% Carnot) in comparison to the ideal value of 3.92 kWh/kg.
State of the art are liquefaction plants with capacities of 25 to 60 tons per day. Larger plants up to about 250 tons per day and more could be achieved by modular design. Further reduction of liquefaction work to about 9.8 kWh/kg corresponding to about 40% Carnot is possible through the development of improved componente in accordance to the best results attained for some plants of smaller size.(see/1/).
In case of small scale liquefaction and refrigeration units especially the Stirling refrigerator offers an important alternative in general and also for hydrogen. Even small scale systems (several kilograms LH_2 per day) having high thermodynamic efficiency can be realized.
Magnetocaloric refrigeration can be seen as a variant of the Stirling process. It uses isentropic demagnetization of a ferromagnetic material near its Curie point temperature as a refrigeration procedure. Here a ferromagnetic material, (also a paramagnetic at very low temperatures) i.e., a solid body, takes over the role of the working fluid. As further possible application magnetic cooling could be applied in the final stage of large scale liquefiers instead of Joule-Thomson expansion (see references in /1/).

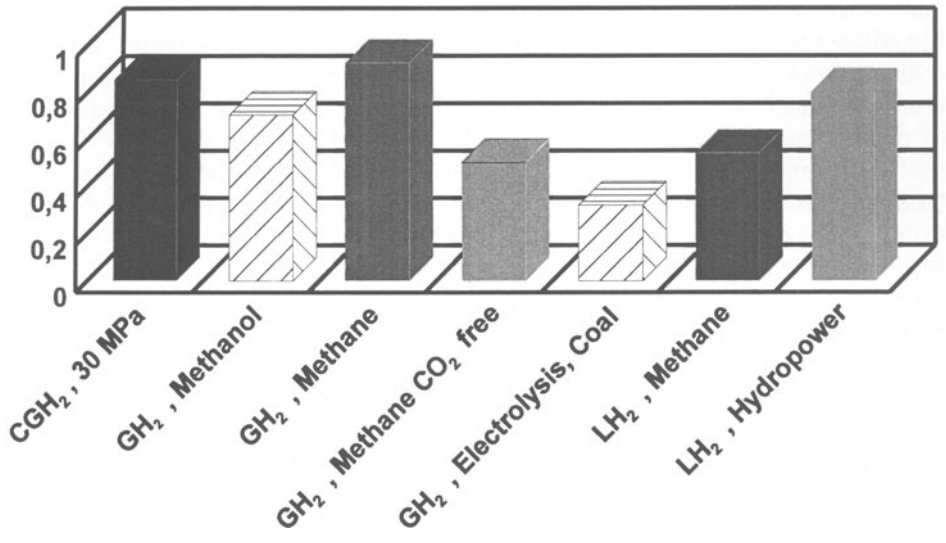

Figure 3. Hydrogen, fraction of primary energy in gaseous and liquid hydrogen from different sources

5. Transport and Storage Technology

The storage and safe handling of large amounts of liquid hydrogen is state of the art./see /1/). At the smaller scale of automotive application development of liquid hydrogen fuel tanks in Germany was originally started in 1974 and has been continued since 1982 by the cryoindustry /1/. Presently tanks with a capacity of up to approximately 150 Liter (33 Liter gasoline equivalent), are available from industrial manufacturers. They supply either cryogenic gaseous or liquid hydrogen using automatically controlled instrumentation, valves, safety valves, tube systems, and heat exchangers. First development steps have begun for tank forms similar in shape to flat prisms, which are required for conventional vehicles /1/. Further zero ventilation tanks are feasible by integrating of a pulse tube refrigerator with the tanks thermal insulation./14/.

6. Handling and Refueling

Fully automatic filling stations that can be safely operated even by non technically trained people have been developed, tested and demonstrated /1/.
A total of three filling stations were built and tested within the scope of different projects, the first two in somewhat simplified versions. (German DLR Pat. P 33 44 770). One was used for refueling test vehicles in a joint project between the Los Alamos National Laboratory and DFVLR. /1,7/. The third filling station which was finished and

successfully demonstrated already in 1986 served as the basis for all the further development done by the cryoindustry (see /1/, p. 225, footnote) and by car manufacturers. With systems working according to this principle, since 1986 already at DFVLR a total refueling time (line cooldown included) of between 4 and 4.5 minutes for a cold 140 Liter fuel tank was state of the art which agrees well with the required amount of time for refueling with conventional fuel /1, 5, 15/. Fifteen minutes were required for filling the tank at ambient temperature including cooldown. No similar success was reported by the cryoindustry and by car manufacturers until 1993.
Also no vent refilling has been demonstrated at DLR for a cold LH_2 fuel tank since 1989 successfully. (German Pat. P 41 29 020). /14/.
Measuring the amount of hydrogen drawn is still a problem in small scale systems, which has not yet been solved with satisfaction. Volume flow meters, turbine flow meters, which are used in cryo-technology, lead to excessive measurement error for the small mass flow rate (up to about 30 g per second), which occurs when refueling a vehicle, where it is seemingly impossible to avoid vapor formation within the flow. A solution to this problem is expected to be a direct mass flow rate measurement which is either based on inertial effects (axial flow or gyroscopic transverse momentum mass flow meters), the anemometer principle (heat transfer) or proton spin resonance, for which considerable development work could not be finished anymore, when cryogenic high technology R&D activities were abandoned. /14/.

7. Mixture Formation and Engine Operation

The extreme physical properties of ambient and cryogenic hydrogen are of beneficial influence on combustion as well as on mixture formation. The smaller volumetric heat value of the stoichiometric hydrogen-air mixture (2890 J/L) results in a corresponding power loss at the engine compared to conventional fuel (3900 J/L). The wide flammability range of H_2-air mixtures enables quality governing and very lean operation with substantially reduced NO_x emissions. Also hydrogen offers a considerable reduction of air throttle and cylinder charge intake flow losses. In this point hydrogen differs considerably also from other gaseous fuels such as natural gas or propane.
The 745i test vehicle of Figures 9, 10, 11, shown in /15/, was designed in 1983/84 in a joint effort between the DFVLR and BMW (see /1/). Sequentially timed external mixture formation with air precharging was applied for the turbocharged three liter six cylinder engine. As a successor of the first european liquid hydrogen test vehicle of 1978 (see /1/) it was the first LH_2-vehicle in Europe that was licensed for liquid hydrogen operation. Besides of hydrogen operation, both test vehicles have permitted backup gasoline operation.

7.1 ENGINE OPERATION WITH CRYOGENIC HYDROGEN

The advantages of liquid hydrogen concerning on board storage have been recognized for a long time and have been widely demonstrated /1, 7, 9, 10/. Hydrogen is mainly used as cold gas (boiling point 20.4 K) and can be used close to its critical state (33 K, 1.28 MPa). As a result of the low mass flow rate and correspondingly small vaporization enthalpy (440 J/g) it is practically impossible to inject the hydrogen into the com-

bustion chamber of small automotive engines in the liquid state. Without further investigation this cannot be excluded for large stationary engines or naval engines.

7.1.1. Cryogenic Internal Mixture Formation

When choosing injection start at about the beginning of the compression stroke (early injection) backfiring into the intake manifold cannot take place. However uncontrolled preignition during the compression stroke can be eliminated only with a low power to piston displacement ratio by means of a very lean fuel-air mixture. In that case economic operation requires strong supercharging of the engine./21/. The cryogenic version of early internal mixture formation does not offer any significant advantages over ambient hydrogen. Primarily, uncontrolled preignition and thus torque failure under partial load cannot be eliminated or circumvented in this manner without excessive supercharging. According to current experience, cryogenic internal mixture formation with late start injection at about 5° b.t.d.c. (before top dead center), via mechanically or hydraulically actuated cryogenic injectors is the most promising method to develop hydrogen I.C. engines which, with respect to driving culture, correspond to conventional Otto-cycle and Diesel engines /1,9, 10, 12/. The very short time available for late injection require an injection pressure between about 15 MPa to 20 MPa and more. On one hand this is to provide a greater initial density to the H_2-flow that leaves the injector at sonic speed and thus a larger impulse. On the other hand this is to keep the volume of the gas that has to be injected as small as possible in order to utilize small injector orifices and thus small moving masses. Cryogenic injectors for cryogenic hydrogen are available for 20 MPa since 1988. /11, 14/.

7.1.2. Hybrid Mixture Formation

The cylinder is first filled by means of a sequential intake manifold injection of hydrogen (pressure below 0.4 - 0.5 MPa) with a lean mixture (fuel-air equivalence ratio $\varphi <$ 0.6) and is ignited at about 40° b.t.d.c. This mixture does not exhibit any tendency toward uncontrolled preignition nor does it result in any substantial NO_x formation. Cryogenic hydrogen at a pressure of 20 MPa is then injected into the flame front at about 5° b.t.d.c. The existing flame front promotes turbulence and mixing, and the injection rate controls the rate of pressure rise /1,3,19/. It appears possible that this process of hybrid mixture formation for hydrogen enables stoichiometric combustion in time average with very low NO_x emissions. (German Pat. P 37 31 986). The advantage of this kind of advanced mixture formation can be seen from the fact, that the standard characteristics obtained for conventional fuel could be demonstrated even with hydrogen. /12,13,14/. Because lack of car manufacturers activities in cryogenic high pressure injection no similar success could be reported from there as yet. Following the late success in fast LH_2 refueling obviously the high technology gap of cryogenic high pressure injection still has to be closed there. Obviously also from this reason in succeeding hydrogen projects of car and engine manufacturers external ambient mixture formation with large piston displacement engines at poor economy was preferred. /19, 20/.

7.2. FUEL CONDITIONING SYSTEM

Depending on the type of mixture formation, the fuel conditioning system has to provide either gaseous hydrogen at ambient temperature at a pressure of 0.3-0.5 MPa (external mixture formation), cryogenic hydrogen between 40 and 100 K and approximately 0.3--0.5 MPa (external cryogenic mixture formation) or cryogenic hydrogen between 20-40 K at high pressure for internal mixture formation (direct injection). For Otto-cycle - engines and two stroke engines with injection during the early part of the compression stroke, pressure between 1 and 3 MPa is necessary, whereas for late start injection (approximately 5° b.t.d.c.) a pressure of considerably more than 10 MPa must be provided.

7.2.1. Cryogenic Fuel Conditioning System

With external mixture formation the pressure necessary for the injection, is either already available in the fuel tank or can be produced by a small piston or diaphragm pump that is integrated into the tank. More sophisticated systems result for internal mixture formation with late injection start. LH_2 as boiling liquid, tends to form vapor. Measures need to be taken in order to guarantee proper filling during the intake phase. DFVLR development led to LH_2 reciprocating pumps separated from the LH_2-tank. Pistons were provided, with two sleeves made of PTFE graphite that compensate for radial expansion. Developments at Cryomec-AG Basel /10,14/ lead to small compact high pressure piston pumps for liquid hydrogen that could be installed primarily in vehicles like trucks and buses.

The most effective cryogenic fuel conditioning system for hybrid mixture formation, was realized with two stage pressurization./1, 13, 14, 18/. An intermediate pressure pump is located close to the LH_2 tank and delivers liquid hydrogen at a pressure of about 1.5-2.5 MPa is. The pressurized liquid becomes warmed up slightly above critical temperature (33 K) whithout deteriorative liquid/vapor phase transitions. Finally this fluid supercritical cryogenic hydrogen becomes pressurized to injection pressure level without phase transitions by a high speed multicylinder high pressure cold compressor driven by the vehicle´s engine.

Gaseous hydrogen, evaporating from the fuel tank and from losses in the intermediate pressure pump can feed a small fuel cell, which charges the starter battery of the vehicle at rest and could totally replace the alternator when the vehicle is operating. Therefore emission of evaporated hydrogen into the atmosphere is completely prevented during driving as well as during parking phases.

8. Conclusion

Application as aviation and rocket fuel, transatmospheric vehicles and supersonic traffic represent the large scale applications of liquid hydrogen. Economic large scale liquefaction is state of the art, further scaling up of present liquefaction plants is feasible. Future plants with respect to investments and costs can best be compared to chemical processing plants and petrochemical plants.

Earthbound vehicles will continue for a long time to use primarily internal combustion engines, while electric drives with batteries or hydrogen-air fuel cells (see *fig.4.*) will be limited to special applications. Even more significant are comparisons of the mass fractions of the energy storage like fuel and batteries, the drive motor as well as of the structural mass and the payload /5, 18/. The hydrogen/air mixture formation in internal combustion engines can considerably improve engine operation by use of cryogenic hydrogen. In addition to the preferred use of liquid hydrogen due to its range per tank filling and low amount of mass for storage in the vehicle, the cryogenic characteristics of hydrogen provide significant advantages. Cryogenic characteristics of hydrogen such as high density and a considerable cooling effect favor the fuel injection, the mixing process and thus the combustion process. Hydrogen as an "unorthodox fuel" leads to somewhat costly (but by far not so expensive as low cost fuel cells) systems for fuel conditioning, which according to the latest developments in cryotechnology research, can be designed for highly redundant operation.

Hybrid mixture formation, a combination of external and internal mixture formation with hydrogen, will be very attractive with respect to power and torque flow under steady and intermittent operating conditions.

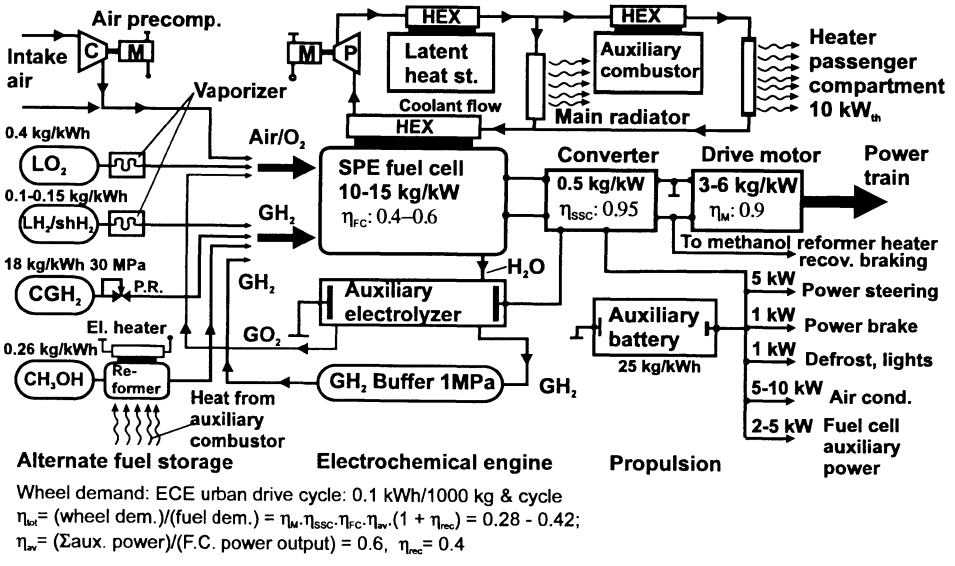

Figure 4. Alternate fuel storage and energy management concepts of fuel cell drives. (See /18/).

Of fundamental interest is a variation of hydrogen production from natural gas and hydrocarbons using a process which is based on the catalytic cracking of hydrocarbons under heat input at temperatures ranging between 700-980° C. This method of producing

hydrogen from fossil energy carriers such as natural gas and crude oil fractions is potentially more cost effective as water electrolysis which can be only minimally improved. This method is also well suited, to introduce CO_2 free fuel combustion techniques in vehicle propulsion even for fossil energy carriers. In spite of the fact that no short term exhaustion of the oil supply is in sight, the development potential provided here can not be overestimated. Furthermore, with this method also it is basically possible to convert natural gas delivered over long distance gas lines into hydrogen and to use it for heat production free from CO_2 emissions. If the real existence of gashydrate sites can be proved, huge ressources of methane would be available in the future./16/.
CO_2 free hydrogen from fossil raw materials permits the use of the indispensable sources of fossil raw materials with their powerful global supply structure. CO_2 free fossil hydrogen as a fuel combines the interests and advantages of the globally established fossil energy and raw material supply system along with the interests of environmental protection in the face of increasing global traffic.
It is a fact, that, thanks to venturesome industrialists of high responsibility, all presently used processes of power generation and of energy storage - nuclear power excepted- already were established in the last century. If one considers the immense investments for prospecting and tapping new oil reservoirs, even oil companies or also synthetic fertilizer manufacturers would most be able to act as a decisive factor in hydrogen energy technology.
Obviously- besides of warfare technology- a similar spirit of free enterprise or social responsibility hardly can be seen in this century, that often has to be proven as simple minded and very cautious in initializing decisive steps. Obviously the present period of profit seeking neo-liberalism suffers from lack of understanding to rank those qualities as first order attributes. Future may change that again.

9. Acknowledgments

The author still shows great gratitude to his former colleagues and coworkers especially to *O. Goldschmitt, G.Schneider, H. Böhringer, J.Schilling, C.Carpetis*, for successful cooperation in the field of highly advanced cryogenic technology and for a brilliant feat of engineering. Their engagement and technical skill shown over a three decades period was substantial prerequisite to venture ambitious high R&D work on miniaturized systems of liquid hydrogen as a cryofuel. The accomplishments of this crew are appreciated almost everywhere.
The author further wishes to express his thanks to all the numerous individuals and institutions, who *really* have contributed, supported and promoted his work, ideas and initiations on terrestrial and space energetics within the past forty years.

10. References

1. Peschka, W. (1992) *Liquid Hydrogen Fuel of the Future*, Springer, Wien-New York
2 Sloop J.L. (1978), *Liquid Hydrogen as a Propulsion Fuel*, The NASA History Series

3 Barthelemy R.R. (1990), The National Aero-Space Plane Program, in Univ. of Hawaii ed., *Proc. Symp. on National Aero-Space Plane and Space Applications*, Hawaii Natural Energy Institute

4 Pohlenz J.B. and Stine L.O.(1962), New process promises low cost hydrogen. *Oil and Gas J.*, 60, p. 82

5 Peschka W. (1992), The use of hydrogen for vehicles -Wasserstoff als Kraftstoff für bodengebundene Fahrzeuge (paper in English), in *VDI Report Nr. 1020, VDI* Verlag, Düsseldorf

6 Stewart W.F. (1986), Hydrogen as a vehicular fuel, in K.D. Williamson Jr., F.J. Edeskuty, ed., *Recent Developments in Hydrogen Technology, Vol.2*, CRC Press, Cleveland, Ohio

7 Peschka W. (1990), Liquid hydrogen pumps for automotive application, *Int.J.Hydrogen Energy*, 15, p. 817

8 Furuhama S. (1989), Hydrogen engine systems for land vehicles, *Int.J.Hydrogen Energy*, 14, p. 907

9 Takiguchi M. and Furuhama S. (1987), Combustion improvement of liquid hydrogen engine for medium duty trucks, *SAE-Techn. paper 870535*

10 Peschka W. (1992), Cryogenic fuel technology and elements of automotive propulsion systems, in *Adv.in Cryogenic Eng.*, Vol. 37, Plenum Press, New York

11 Ninomiya Y., and Furuhama S. (1992), NO_x control in LH_2-pump high pressure hydrogen injection engines, in *Proc. 9th World Hydrogen Energy Conference, Vol.2*, p.1295-1304, Paris, France

12 Koyanagi K., Hiruma M., Hashimoto H., Yamane K., Furuhama S. (1993), Low NO_x emission automobile liquid hydrogen engine by means of dual mixture formation, *SAE Technical Paper* 930757

13 Peschka W. (1994), Hydrogen cryofuel in internal combustion engines; in *Adv.in Cryogenic Eng.*, Vol . 39, Plenum Press, New York

14 Peschka, W. (1996), Hydrogen: The Future Cryofuel in Internal Combustion Engines, in DECHEMA ed., *Hydrogen Energy Progress XI*, DECHEMA, Frankfurt/M, pp. 1453-1482

15 Gaudernack, B., and S. Lynum, S. (1996), Hydrogen from natural gas without release of CO_2 to the atmosphere; in DECHEMA ed., *Hydrogen Energy Progress XI*, DECHEMA/IAHE 199643, Frankfurt/M, pp. 511-525

16 Førrisdahl O.K., Kvamme B., Haymet A.D.J. (1996), Methane Clathrate Hydrates: melting, supercooling and phase separation from molecular dynamics computer simulations, *Molecular Physics*, 89, p. 819-834
see also: Stern, L.A., Kirby S.H., Durham W.B. (1996), Peculiarities of methane clathrate hydrate formation and solid-state deformation, including possible superheating of water ice, *Science 273*, p.1843
see also: Harvey D. (1996), Potential Feedback Between Climate and Methane Clathrate, Univ. of Toronto, Department of Geography, Toronto, Ontario, Canada, Internet Com.. Dec. 1st.1996, http://www.gcrio.org/ASPEN/scienceleoc94/EOC2/EOC2-5.html

17 Rothfleisch, J.E. (1964), Hydrogen from Methanol for Fuel Cells, *SAE Technical Paper 935C*, New York

18 Peschka, W. (1997), *Wasserstoffantrieb für Kraftfahrzeuge. Sollen hier reale Chancen für die Zukunft vertan werden?*, Österr. Verein für Kraftfahrzeugtechnik (ÖKV), Wien

19 Knorr H., Held W. and Prümm W. (1996), The MAN Hydrogen Propulsion System for City Buses, in DECHEMA ed., *Hydrogen Energy Progress XI*, DECHEMA, Frankfurt/M, pp. 1611-1620

20 Reister D., Strobl W. (1992), Current Development and Outlook for the Hydrogen-Fueled Car, Hydrogen Energy Progress IX, Int.Ass. for Hydrogen Energy, pp. 1201-1213

21 Digeser S., Jorach R. et al. (1996), The Intercoooled Hydrogen Truck Engine with Early Internal Fuel Injection- a Means of Achieving Low Emission and High Specific Power Output, in DECHEMA ed., *Hydrogen Energy Progress XI*, DECHEMA, Frankfurt/M, pp. 1537-1546

Fore more detailed and comprehensive references see /1,5,14/.

SEA TRANSPORTATION OF HYDROGEN

Present status and future aspects

F.J. SANDMANN
Managing Partner
CONOC Continental Contractors GmbH
Hamburg

Abstract

The specific technical characteristics of hydrogen having an impact on its sea transportation are outlined and the related requirements for LH2 vessels are defined.
After a brief review of past development and present state of the art, future concepts of large scale liquid hydrogen sea transportation are described and evaluated.
This includes the provision for a defined consumer profile as integrated part of the EURO-QUÉBEC HYDRO HYDROGEN PILOT PROJECT (EQHHPP), a joint German system development for world wide transportation of liquid hydrogen and the Japanese studies on the same subject, conducted within the WE-NET (world energy net-work) research programme as part of the new 'Sunshine Project'.
As a first attempt of commercial application under present market conditions, a Canadian project is described based on newly developed jumbo containers for multi modal transportation.
The technical comparison of the various concepts is supplemented by economic calculations, wherever possible.

1. Introduction

Hydrogen, being a secondary energy (an energy vector) has to be generated by a primary energy source. In order to produce 'clean hydrogen', e.g. neither direct nor indirect by utilisation of fossil fuels, solar energy or hydro-electricity as indirect solar energy source have to be used.

The world-wide distribution of both primary energy sources is determined by nature and not by human beings and their industrial needs, as Fig. 1 shows [1].

T. O. Saetre (ed.), Hydrogen Power: Theoretical and Engineering Solutions, 529–542.

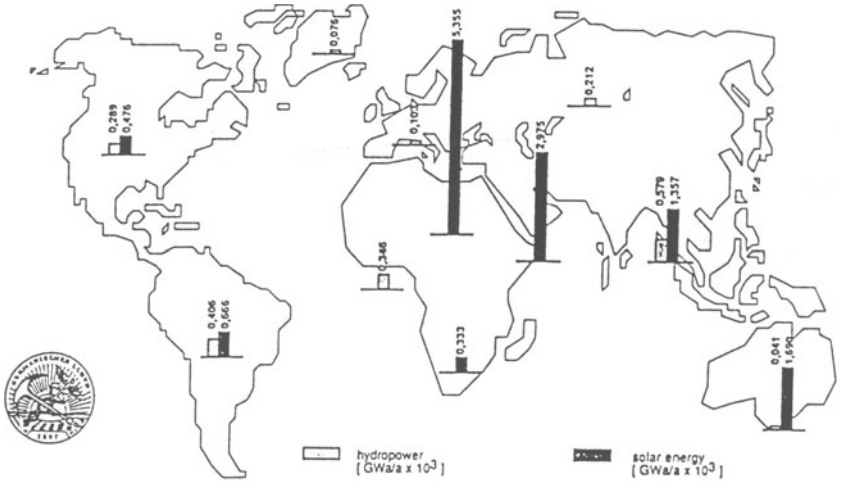

Fig. 1 Distribution of hydropower and solar energy (source Germanischer Lloyd)

Solar energy is centred around the equatorial belt and hydro-electricity produced in mountain areas, far away from its industrial utilisation. It is clearly documented that both, the industrial centres of Europe to a very large extent and Japan entirely, depend on energy import via shipment.

Therefore has storage and sea transportation of hydrogen been frequently the subject of extensive research and development;

as a system component in the frame of the EURO-QUÉBEC HYDRO-HYDROGENE PILOT PROJECT (EQHHPP) [5],

as the main task of product development within a German research project for world wide sea transportation of liquid hydrogen [2],

as part of the WE-NET (world energy net-work) research programme of the New Sunshine Project promoted by the Japanese Ministry of Trade and Industry [4],

only to mention three examples.

The background and driving force behind, however, was and still is different:

The 100 MWa EURO-QUÉBEC project had its first centre of utilisation in Hamburg, Germany, and was based on 'clean hydrogen' exclusively, which had to be imported.

The German research project was initiated jointly by a major German shipyard and Germanischer Lloyd as product development for a future market.
The Japanese WE-NET finally, as the most ambitious one, is targeted to secure the energy basis for the entire country when fossil resources start to be in short supply.

All a.m. projects are based on the transportation of liquid hydrogen (LH_2) as it was found to be the most suitable for maritime transportation in a less polluting and economically acceptable energy system.

2. Specific characteristics and its implication

When comparing the properties of hydrogen with those of natural gas and crude oil there are three characteristics which have an impact on either the ships design or its cargo space:

- The density of the liquid state,
- the mass related energy and
- the heat of vaporisation per unit mass.

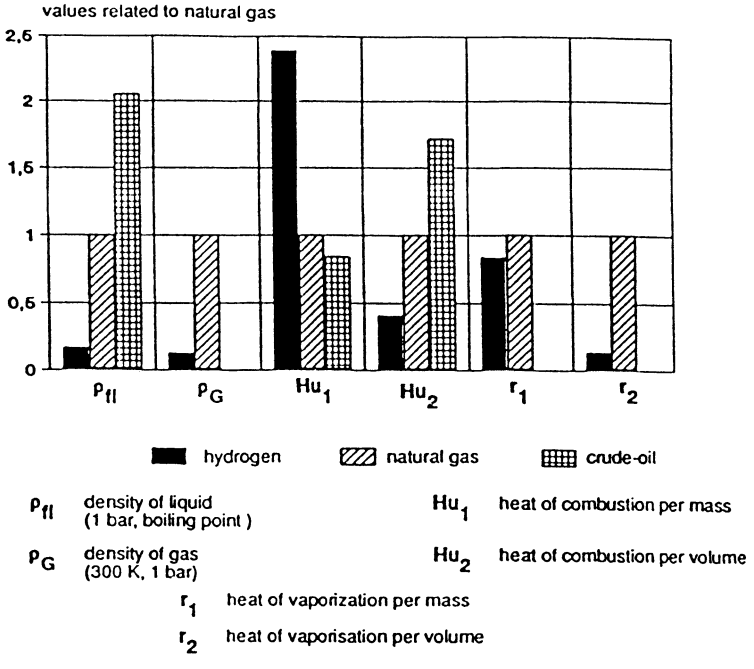

Fig. 2 Properties of hydrogen compared with natural gas and crude oil (Source: Germanischer Lloyd)

The low density of liquid hydrogen affects the design of the LH_2 carrier. In order to obtain adequate stability, the vessel has to take considerable water ballast in the double bottom and side tanks. The resulting large metacentric height will cause strong accelerations in heavy seas for which the hydrogen tanks have to be dimensioned.

In sea-borne transport is the cargo volume the key design factor. As *Fig. 2* shows, can compared to LNG only 40 % of the energy be transported in the same volume with LH_2 as cargo. Moreover, since a large tank has a lower boil-off rate than a small tank with the same insulation, have large ships to be designed with high tank capacities.

The rated heat of vaporisation is another feature with important implications for the design of LH_2 tanks and in particular their insulation. As it can be seen from *Fig. 2* is the heat of vaporisation for hydrogen and natural gas of a similar order of magnitude, while the volumetric heat of vaporisation of hydrogen is only 14% of the corresponding value for natural gas. Therefore only 1/7 of the energy needed to evaporate natural gas is required for the evaporation of hydrogen. In order to avoid a pressure rise during transportation and storage above acceptable limits, need hydrogen tanks to be of vacuum-insulated double shell design.

3. The sea transportation concept of the EQHHPP

The shipment of LH_2 from Sept Isles, Canada, to Hamburg, Germany, represents only a system component within the entire cycle covered by this pilot project as *Fig. 3* shows [5].

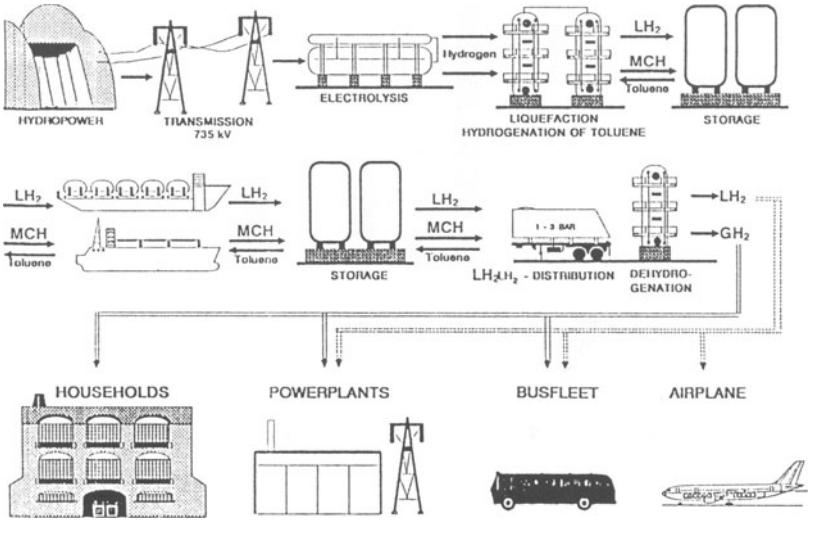

Fig. 3 Flow diagram EQHHPP

The size of the ship was determined by the production rate in Canada and the consumer profile in Europe. 100 MWa input of hydro electricity resulted in an overall production of 15,916 t/a which were split into 16 roundtrips per year. *Fig. 4* shows the calculation scheme and mass flow [5].

At the beginning of investigations it was assumed, to derive the design of the LH_2-carrier from existing LNG-ships. Due to the specific requirements of liquid hydrogen transportation this assessment turned out to be impractical.
A barge carrier concept has eventually been chosen in order to achieve the necessary efficiency, flexibility and safety of the transportation system. The vessel and its docking system is shown in *Fig. 5* and *Fig. 6*.

Production		Transport	
production rate	48 t/d	operating days	380 d
overall production	15918 t/a	speed	18 kn
		duration for ocean transit	11 d
roundtrips per year		18	
volume per voyage	14050 m^3	total transport capacity	15236 m^3
volume per tank and voyage	2810 m^3	capacity per tank	3047 m^3
		boil-off-rate	10,5 kg/h
		return volume per tank	150 m^3

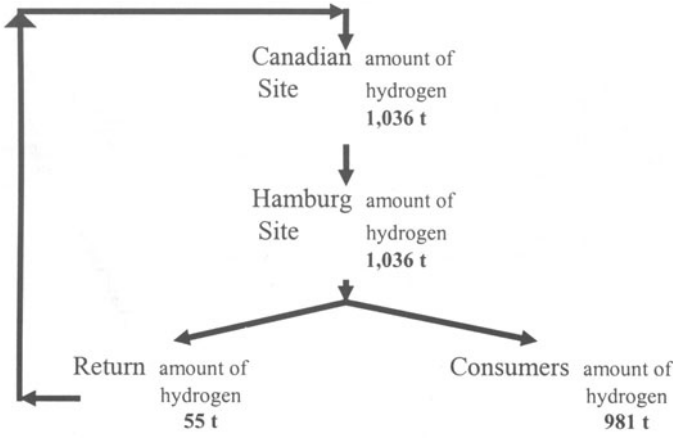

Fig. 4 System conditions and LH_2 mass balance (source EQHHPP Phase II Final Report)

The hydrogen tanks are designed as type C tanks according to the IGC Code. The design criteria ensure that cracks cannot penetrate through the entire wall. It is hence not necessary to provide a second containment around the cargo tanks.

The design philosophy of the barge carrier system can be summarised as follows:

- Barges are loaded/unloaded from carrier by docking procedure - float in/out.
- Cargo tanks on the barges are in open atmosphere.
- No void spaces inside carrier or barges to be inerted (mandatory for integrated tanks).
- Short discharge and loading time in port due to float in-/out-principle.
- Reliable logistics because of the modular system (mal-functioning of one barge will not endanger the systems operation).
- Lowest probability of tank damage in a collision, increased tertiary safety in case of major accident (it is unlikely that more than one tank is damaged in a damage case).

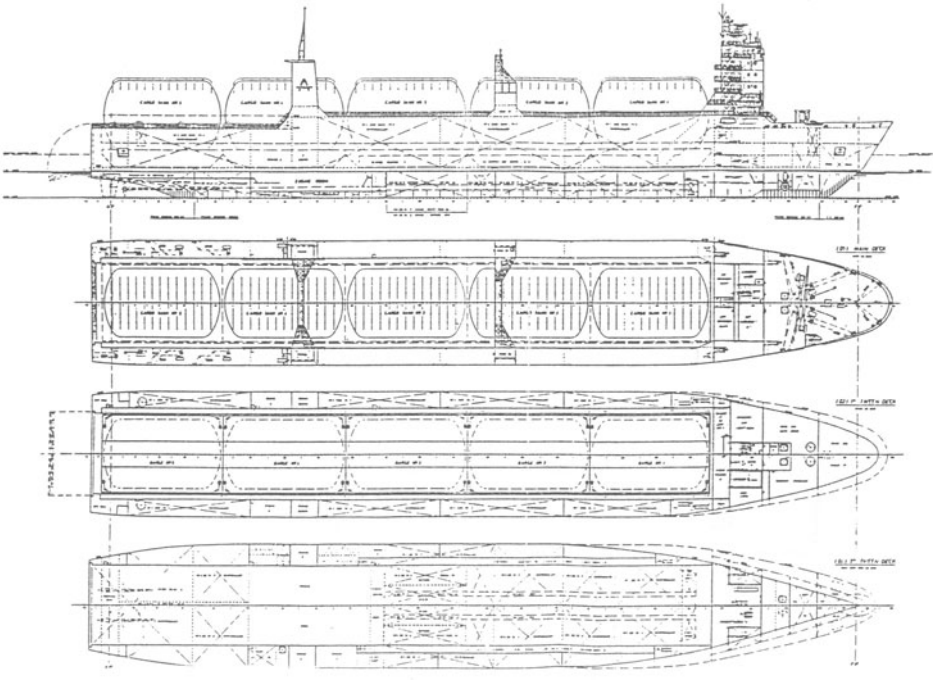

Fig. 5 General Arrangement Plan of EQHHPP Barge carrier (source Thyssen Nordseewerke)

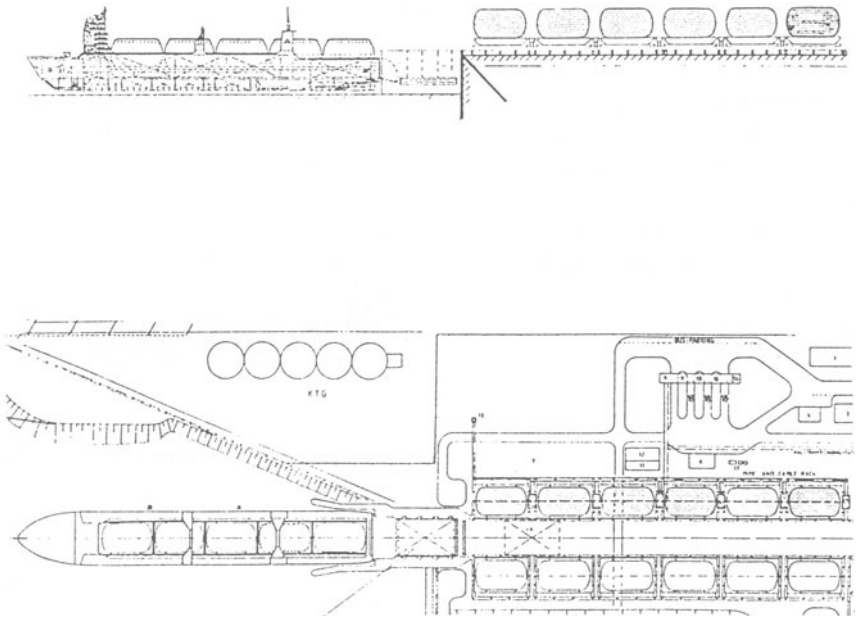

Fig. 6 Discharge and docking procedure of EQHHPP Barge Carrier (source Thyssen Nordseewerke)

4. Large scale sea transportation of LH_2

For the world-wide transportation of large quantities of LH_2 have Germanischer Lloyd (GL), Howaldtswerke Deutsche Werft (HDW) and Noell-LGA executed a study, supported by the German Ministry of Research and Technology [2].

Based on a capacity of 8150 t LH_2 (equivalent to appr. 116,000 m^3) were two transport concepts studied:

Dock ship,
SWATH ship.

4.1 Dock ship

The design principle is similar to the EQHHPP transportation scheme. Five double shell spherical tanks with an outer diameter of ~40m are mounted on floating barges, which are towed in or out of the semi-submerged barge carrier.

Main dimensions	
Length overall	318 m
$Breadth_{WL}$	62 m
$Draught_{CWL}$	10 m
Displacement	134 400 t
$Power_{mcr}$	36 000 kW
Trial speed	16 kn

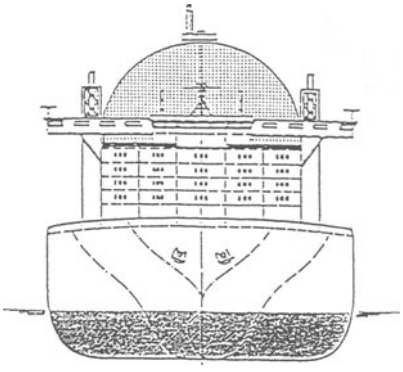

Fig. 7 Dock ship

4.2 SWATH ship

The ships hull is again designed as a carrying platform without any integrated cargo space. The spherical LH_2 tanks are single mounted on supporting steel structures as standardised handling platform.
Discharge and loading is performed by ballasting and deballasting of the vessel. The system requires a special docking facility with a receiving- and intermediate storage-area equipped with a rail-based handling system.
Both designs, dock ship and SWATH ship, reflect the experience of the involved shipyard gained during construction of LNG carrier.

Main dimensions	
Length overall	322 m
$Breadth_{WL}$	65 m
$Draught_{CWL}$	14 m
Displacement	104 000 t
$Power_{mcr}$	36 000 kW
Trial speed	17,5 kn

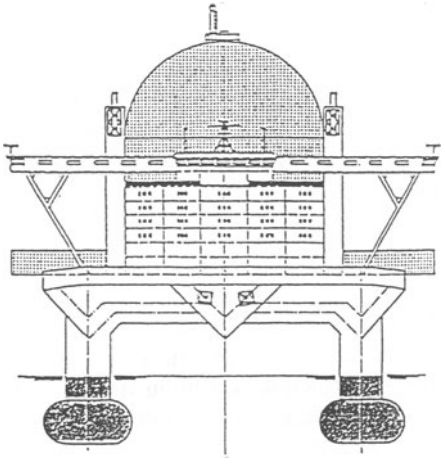

Fig. 8 SWATH ship

4.3 The WE-NET hydrogen tanker programme

The most comprehensive approach to the challenge of world-wide sea transportation of hydrogen is definitely the Japanese WE-NET programme, consisting of 9 subtasks where subtask 5 is assigned to the research of storage and transportation technology of liquid hydrogen [4].
As part of subtask 5 exists the tanker research team consisting of four major shipyards being the builder of large LNG carrier as licensee of SPB prismatic tank system and Moss Rosenberg (Kvaerner) spherical tank system.

The principal particulars for the ship design were set as follows:

Consumption		Transport	
1,000 MW power plant		Duration of round trip	20 d
LH_2 consumption rate	1,200 t/d		
		Number of ships	2
		Loading and discharge period every	10 d
		Total LH_2 capacity*1)	14,000 t
		Endurance [nautical miles]	6,000
		Speed	20-25 kn

*1) including transportation loss

The cargo capacity of 14,000 t LH_2 represents a volume of 200,000 m^3 compared to the average size of 125,000 m^3 for LNG carrier presently in operation.

The required ship speed allowed the application of a normal mono-hull, in addition has a twin hull ship been developed. In order to apply both alternatives of tank configuration, four ships had to be designed:

Spherical tank - (1) mono-hull
(2) twin hull
Prismatic tank - (3) mono-hull
(4) twin hull

As the most severe problem of both designs is the insulation of the LH_2 tanks considered. Three alternative combinations are under further detailed investigation:

- PUF panel in vacuumed or non-vacuumed hold space
- Vacuum panel insulation in vacuumed or non-vacuumed hold space
- Super insulation in vacuumed hold space.

Fig. 9 and *Fig. 10* show the conceptual designs of the twin hull ship for spherical and prismatic tank design with 4 and 2 LH_2 tanks respectively.

Main dimensions	
Length overall	345 m
Breadth	64 m
Draught	14 m
Tank capacity	200,000 m³
Power	2x40,000 hp
Speed	20-25 kn

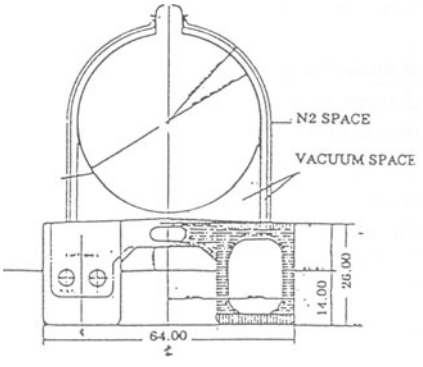

Fig. 9 Spherical tank design
(source IHI, KHI, MHI, MES Japan)

Main dimensions	
Length overall	330 m
Breadth	56 m
Draught	14 m
Tank capacity	200,000 m³
Power	2x40,000 hp
Speed	20-25 kn

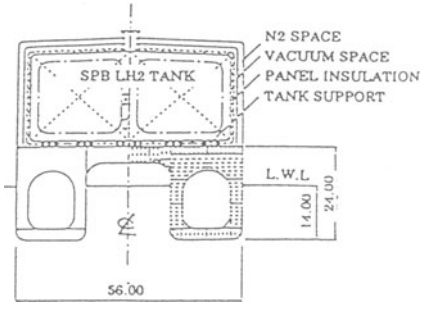

Fig. 10 Prismatic tank design
(source IHI, KHI, MHI, MES Japan)

5. Containerised sea transportation of LH_2

A world-wide market for LH_2 which justifies the operation of large carriers as described under 4.1 - 4.3 is unlikely to develop before 2015-2020 at the earliest. However a steadily increasing volume has to be transported overseas for which container transportation is most suitable.

There are presently three types of ISO-LH_2-transportation containers existing [6]:

Characteristic	Manufacturer		
	L'Air Liquids	L'Air Liquide	Gardner Cryogenics
Type	CNT 12 LH2	CNT 12 LH2 Long Autonomy	11,000 Gallon LH2-Tank
Length [mm]		12,192	
Width [mm]		2,438	
Height [mm]		2,591	
Weight, gross [kg]	23,000	26,000	21,219
Volume, geometric, warm [m³]	45.0	41.6	43.5
Filling limit [%]	90	90	89
Weight of LH_2 (90%) [kg]	2,800	2,620	2,710
Rate of evaporation [%/d]	0.5	0.05	0.076
Max. working pressure [bar]	12	12	4.4
Stand alone time[d]	30	60	60
Material inner vessel	SA 240-304 stainless steel	SA 240-304 N stainless steel	SA 240-304 stainless steel
Material framing	carbon steel	SA 516-60	SA 516-70

This containers can be shipped on standard container ships as deck cargo without specific arrangements.
Their present disadvantage is the unfavourable ratio weight of LH_2 versus gross weight which varies between 10.1 and 12.8.
The first attempt to overcome this problem was a French feasibility study (L'Air Liquide, Louis Dreyfus & Cie.) for an open hatch container ship carrying 54 'Jumbo' container, 360 m³ each at a filling rate of 85%. With a total capacity of 16,500 m³ was the design of similar size as the EQHHPP barge carrier [3].
The project did not materialise for logistic reasons. The infrastructure on shore can economically not be adapted for handling and on-going transportation to the consumers site.

A more practical approach has recently been launched as a joint European-Canadian project, on the European side as part of Phase IV of the EQHHPP [7]. The target is the development of an ISO LH_2 40' and 80' container as prototypes for series production with minimised weight and maximised cargo capacity.
For this purpose will the outer shell be made of composite material.

The work packages are distributed as follows:

Project Management	Canada: Hydro Québec Europe: EU-Joint Research Centre Ispra ARGE LBST/CONOC
Engineering and fabrication of test specimen and prototype	Econoden Inc. Canada
Classification	Germanischer Lloyd (GL)
Fire test and crash test	Bundesanstalt für Materialforschung und -prüfung (BAM), Germany
Certification	GL, BAM

It was expected that the composite outer shell results in a smaller gross weight and thereby improves the payload/gross weight ratio. This did not materialise for the 40' container as the comparison with L'Air Liquides long autonomy container shows:

Characteristic	Manufacturer	
	L'Air Liquide	H2T / Cryonor
Weight gross	26,000 kg	27,000 kg
Volume, geometric, warm	41.6 m^3	41.0 m^3
Filling limit	90 %	95 %
Weight of LH_2	2,620 kg	2,800 kg
Rate of evaporation	0.05	0.02
Stand alone time	60 d	60 d
Material outer shell	SA 516-60	composite
Ratio weight LH_2/weight gross	10.1 %	10.4 %

The achieved figure of 10.4 % shows no significant difference to the already existing containers.
It does improve for the planned 80' container with 38,000 kg estimated gross weight and a payload of 5,600 kg resulting in a ratio of 12.8 %. This 80' container, however, shows economic advantages only during handling and ongoing transportation onshore, not during sea transportation (double payload covers double container storage area).

6. Economic comparison

The specific cost distribution of the EQHHPP as shown on *Fig. 11* can be considered as being typical for a LH_2 production, transportation, receipt and storage system [5].

Ship plus receipt and storage represent 27.7 % of the overall cost and require therefore the same attention as liquefaction and electrolysis.

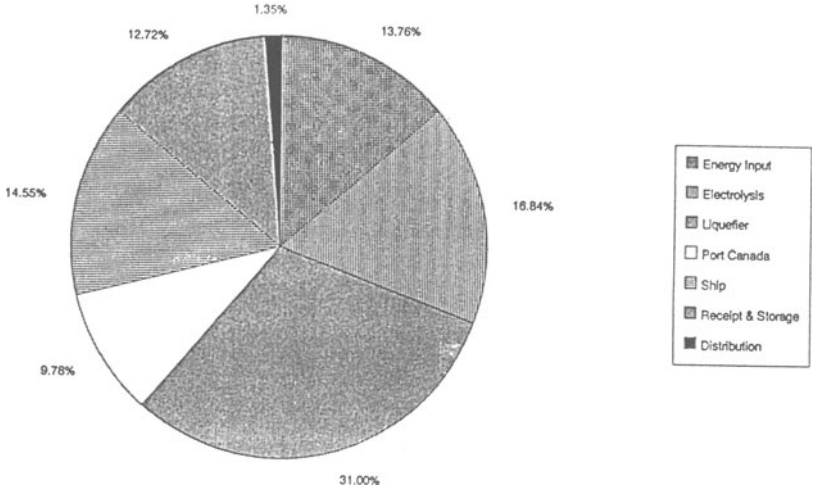

Fig. 11 LH_2 PATH: specific cost at distribution output (source EQHHPP)

The subsequent comparison of sea transportation systems, *Fig. 12,* includes the EQHHPP barge carrier, the dock ship as described under 4.1 and container transportation on standard container ships without any special arrangements.

Characteristic	EQHHPP Barge carrier	Dock ship	Container ship with 2x40' cont.
Service speed [kn]	18	16	18
Roundtrips per year	16	20	8
Specific transportation cost [mio DM/year]	26,722	195,260	0,460
System cost (incl. financing of investment) [mio DM/year]	50,080	288,750	0,460
Transported LH_2 [t]	16,800	337,700	44.8
System cost per ton LH_2 [DM]	2,981	855	10,267

Fig. 12 System cost comparison

EQHHPP assumes an interest rate of 8% and a capital payback period of 15 years with a constant annuity of 11.7% (interest and depreciation).

GL and HDW have calculated the dock ship capital cost with an interest rate of 10% and 12 years capital payback period.

H2T/Cryonor finally made the following assumptions:

Maintenance cost per container (including material)	1,000 Can$/yr
Cost of sea transportation of a standard 40' Container	15,000 Can$/container
Cycle time per container	46 d
Rent per container	700 Can$/d

The Canadian consortium expects a local purchase price per ton LH_2 of 3,000 Can$ and a sales price in Europe of 9,000 Can$/ton LH_2 [7]. The difference of 6,000 Can$ corresponding to 7,500 DM (exchange rate 1.25) does not cover the system cost of 10,267 DM and leaves a loss of 2,767 DM per ton LH_2 delivered c.i.f. European port.

The cost comparison, even if based on a number of assumptions, shows clearly

- the need to design large ships with high tank capacities,
- to increase the payload within given ISO dimensions for container transport.

References

[1] Krapp R., Petersen U. and Würsig G.:
Design and safety considerations for large scale sea-borne hydrogen transport.
Proceedings of the 9th World Hydrogen Energy Conference, Paris, France, 22-25. June 1992

[2] Howaldswerke Deutsche Werft AG, Noell LGA Gastechnik, Germanischer Lloyd (Publ.):
Entwicklung eines Seetransportsystems für Flüssigwasserstoff.
BMFT Schlußbericht MTK 0462, Hamburg 1990

[3] Giacomazzi G. and Gretz J.:
Hydrogen Transport: Status and perspectives. Liquid hydrogen.
Publications of the Joint Research Centre of the European Union in Ispra, Italy, 1993

[4] Abe A., Nakamura M., Sato I., Uetani H. and Fujitani T.:
Studies of the large scale sea transportation of the liquid hydrogen.
Proceedings of the 11th World Hydrogen Energy Conference, Stuttgart, Germany, 23.-28. June 1996

[5] Hydro Québec, Montreal, Canada, Ludwig-Bölkow-Stiftung, Germanischer Lloyd, Holinger Umwelttechnik and Thyssen Nordseewerke, all Germany:
Euro-Quebéc Hydro-Hydrogen Pilot Project (EQHHPP), Phase II Feasibility Study, Final Report.
Joint publication of the Government of Québec and the Commission oft the European Communities.

[6] Sandmann F., Kölling M.:
Harminisation standardisation of hydrogen storage and transportation.
EQHHPP Phase III.0-4 Final Report, CONOC Continental Contractors, Hamburg, Germany

[7] Kluyskens D., Legrand B. and Shama E.:
Container Project.
Econoden, FRE Composites, Hydro Québec, Montreal, Canada, 1994

INVESTIGATION INTO THE OPERATING BEHAVIOUR OF 61 CUM LIQUID HYDROGEN TANK

U. PETERSEN
Germanischer Lloyd
Hamburg, Germany

G. WÜRSIG
Germanischer Lloyd
Hamburg, Germany

AND

N. WÖHREN
Germanischer Lloyd
Hamburg, Germany

1. Summary

The tank concept developed for the Euro–Quebec Hydro Hydrogen Pilot Project (EQHHPP) assumes that the hydrogen produced in Canada should be avaliable in Europe in liquid form. The tank pressure is allowed to increase during transportation as a result of the inevitable heat input. With a safety margin the design of the tank must guarantee a stand alone period of more than 25 days, which is required during normal operation (Germanischer Lloyd, 1990). Nevertheless the design is fundamentally different from existing principles for liquefied gas transport where the pressure is kept within the design values for infinite periods of time (Würsig *et al.*, 1997). This was the main reason to examine the thermal behaviour of a 61 m^3 model of the 3600 m^3 EQHHPP tank. Germanischer Lloyd performed a test series with this model tank from July 96 to January 97. The tank was operated by the German Institute for Material Research and Testing (BAM) at their test site in Horstwalde 50 km south of Berlin. Initial results are presented in this paper.

T. O. Saetre (ed.), Hydrogen Power: Theoretical and Engineering Solutions, 543–550.

2. Experimental Study

The program included three different types of tests:

- Open evaporation at constant pressure:
  The energy input from the surroundings to the tank was studied during these tests. In addition, open evaporation periods were necessary between pressurization tests to obtain nearly stationary starting conditions at the time of tank closing.
- Self pressurization:
  The tank was closed and the heat input from the surroundings caused a pressure build–up in the tank. These are the conditions during sea transport. Aim of these tests was the verification of theoretical models for the pressure build–up in the closed tank.
- Pressure build–up with heat exchanger R01 (Fig. 1):
  At the beginning of these tests the pressure was increased with the heat exchanger to approx. 2.5 *bar g*. Subsequently the heat input from the surroundings resulted in an additional pressure increase up to the releaving pressure of 3.6 to 3.9 *bar g*. These tests gave additional information about the pressure build–up behaviour by including an external heat source.

All tests were performed for different filling levels to examine the influence of different liquid and gas volumes on pressure build–up and open evaporation behaviour. The test results are presented in the following sections.

3. Boil–Off–Rate and heat flux to liquid and gas

The Boil–Off–Rate (BOR) is a characteristic design value for cryogenic liquid tanks. It indicates the thermal performance of the tank by giving the loss of liquid per day caused by the heat input from the surroundings. In the given case the geometrical tank volume of $V_T = 61\ m^3$ was used for BOR calculations. The design value for the 85% *vol* filled tank was $0.5\%/d$.

The approximation for BOR and the measured values are given by Fig.2. It demonstrates that the Boil–Off–Rate is not a constant value but changes with filling level. The BOR for a filled tank is significantly higher than the BOR for a partly filled tank. For the test tank the BOR for the tank filled to 50% *vol* was by the factor of two below the value for the 90% *vol* filled tank. Therefore, a given BOR is valid for a special filling level only. The design value of $0.5\%/d$ was reached during the tests at filling levels below 10% *vol*.

The calculation of BOR by use of the temperature sensors sets the BOR equal to the mass evaporated from the liquid surface. Defining the BOR as the loss of liquid per day this method is a direct BOR measurement. An alternative BOR definition by measuring the gas flow from the tank as it is done by use of the gascounter FT31 includes an additional gas flow $\dot{m}_g$ which is caused by the temperature rise in the gas space. For high filling levels this effect can be neglected, but the temperature rise in the gas space accelerates with decreasing filling level. For Example at 16% *vol* the measured BOR was 41% higher than the value calculated with the assumption of negligible gas space influence.

4. Influence of the steel

Energy absorbed by the warming up of the steel has a substantial influence on the BOR. The mass of the inner tank (12 t) and its heat capacity reduce the BOR. During pressure build up the energy absorbtion extends the time required for pressure build up.

The temperature of liquid hydrogen is nearly constant during open evaporation. The part of the steel wetted by liquid is not warmed up and therefore has no influence on the BOR.

The temperature in the gas space increases with time as the liquid level falls. Hence, the steel in contact with the gas absorbs a part of the energy transmitted into the tank. For an estimation of this effect, the large change in steel heat capacity at low temperatures must be taken into account. The heat capacity changes between 0 and 100 K from nearly zero to about 250 $J/(kg \cdot K)$. Consequently, the influence of tank steel for high filling levels is much smaller compared to the influence at low filling levels. This effect explaines to some extent the reduction in BOR with decreasing filling level.

Assuming that the tank wall temperature is equal to the gas temperature and excluding condensation simplifies the energy balance.

$$\dot{Q}_{g,tot} = \dot{U}_g + \dot{Q}_{St} + \dot{m}_g \cdot (h''(T_fg) - h_g) \tag{1}$$

The heat entering the gas space ($\dot{Q}_{g,tot}$) is warming up the boil off gas ($\dot{m}_g \cdot (h''(T_{fg}) - h_g)$), the steel ($\dot{Q}_{St}$) and the residential gas ($\dot{U}_g$). Stationary conditions can be assumed because changes in liquid level and temperatures are very slow.

At the end of the test period a reference test was performed with a liquid free, cold tank. For this purpose the tank was closed just after the

liquid had completely evaporated. From this test the heat input into the tank can be calculated taking into account the above factors.

It is concluded that the influence of the steel is negligible for a filled tank. On the other hand it reduces the BOR and extends the stand alone time with decreasing filling level. At levels below 20% *vol* filling, approx. 1/3 of the heat flux is absorbed by the steel.

5. Self Pressurization Tests

Aim of the tests was the verification of theoretical studies of the pressure increase for a closed tank. The pressure increase depends on (i) heat transport from ambient to gas and liquid space and (ii) on mass transport from the liquid to the gas space.

A very simple model to calculate the limits for pressure increase assumes a heat input into the gas only for the upper limit and into the liquid only for the lower limit. Both calculations assume a constant temperature equal to the boiling temperature at the given pressure. For the upper limit it is assumed that the mass to the gas space is constant and that the heat input into the tank is completely absorbed by the gas. The liquid remains at the temperature it had at the time of tank closing. The result of the calculation is illustrated by curve A in Fig.3. The lower limit (C) is calculated by assuming that the complete heat flux is absorbed by the liquid. The liquid temperature is assumed to be at saturation temperature to the tank pressure.

The real behaviour shown by curve B in Fig.3 is not reflected by these often used simplifications. The main factors which should be included in a model to predict the tank pressure are mass flux from liquid– to gas space, temperature distribution in the gas space and the heat absorbtion of the tank material.

At the moment of tank closing after stationary open evaporation conditions, the complete liquid phase is at boiling temperature. No temperature variation in the liquid was observed during open evaporation tests.

Caused by the heat flux into the closed tank, pressure and temperature in the tank are increasing. At any time the temperature at the liquid surface is equal to the boiling temperature corresponding to the tank pressure. The rate of evaporation for a closed tank is reduced to values between 10 and 50% of the BOR before tank closing.

The heat flux into the liquid leads to a temperature rise of the liquid close to the tank wall. Thermal conduction and convection transports the heat to the phase boundary. The liquid beneath the boundary is heated up and forms a layer of increased temperature compared to the bulk liquid which becomes subcooled (comp. (Dietzler, 1995), (Huntley, 1960), (Liebenberg *et al.* , 1964)).

The temperature profile in liquid and gas phase at the beginning and end of a test is shown in Fig.4. The extension of the temperature layer in the liquid during the test illustrated by Fig.4 was approx. 700 *mm*. The mass of liquid in the layer was approx 27% of total liquid content. Temperature increase of bulk liquid was about 2 K. Given a boiling temperature of 27 K at 4.9 *bar*, the bulk liquid was subcooled by 5 K.

During a series of pressurization tests it was observed that the rate of pressure increase varied strongly with the tank filling level. For low and high filling levels the pressure build up time was found to be smaller than for a 50% *vol* full tank. Fig.5 shows experimental data for pressurization tests up to 4 *bar* and compares the data with an approximation based on the following theoretical considerations:

The ratio of tank surface in contact with liquid hydrogen (A_f) to liquid volume (V_f) is proportional to the rate of temperature increase of the bulk liquid. The temperature increase in turn is directly proportional to the mass flux evaporated from the liquid ($\dot{m}_{fg}$), hence

$$\dot{m}_{fg} \sim \frac{A_f}{V_f} \tag{2}$$

The rate of pressure increase is directly related to the ratio mass flux/gas mass

$$\frac{\Delta p}{\Delta t} \sim \frac{\dot{m}_{fg}}{m_g} \tag{3}$$

Assuming a constant density in the gas phase yields

$$\frac{\Delta p}{\Delta t} \sim \frac{A_f}{V_f \cdot V_g} \tag{4}$$

where V_g is the gas volume. In Fig.5 the left hand axis denotes the inverted pressure build up factor $V_f \cdot V_g / A_f$, while the right hand axis shows the time needed to reach a pressure level of 4 *bar*. The theoretical approximation makes use of assumptions and simplifications, most notably by neglecting

the influence of the liquid/gas interface area, however it captures the correct qualitative behaviour.

6. Conclusions

The consequences of self pressurization tests can be summarized as follows:

- The major factor for pressure increase is the mass transfer from liquid to gas. Therefore simplifications disregarding the evaporation of liquid are not suitable to predict the pressure increase.
- Pressure increase can only be calculated if the mass balance in the gas space is determined correctly. Since the mass is strongly related to temperature a single average temperature in the gas space is not sufficient.
- Evaporation takes place even when the tank is closed.
- The time for pressure increase depends on the filling level. For the filled test tank and the test tank filled to approx. 20% *vol* the times required for pressure increase are similar. Between these levels a maximum time for self pressurization exists.
- The steel of the tank absorbes an increasing amount of heat with falling liquid level. As a trend, the steel extends the time of pressure increase with falling filling level. This effect is more relevant for small and less relevant for large tanks.
- A strong temperature gradient near the liquid surface was observed during the pressure build up tests. This is a major difference to open evaporation where no temperature difference in the liquid was observed.

References

U. Dietzler. Zur Auslegung von Bereitstellungssystemen für Flüssig-Wasserstoff. (Dimensioning of supply systems for liquid hydrogen) Doctoral work, mechanical ngineering department of Hannover University, published 1995.

S.C Huntley. Temperature–Pressure–Time Relationship in a Closed Cryogenic Container. In *Advances in Cryogenic Engineering*, Proceedings of the 1960 Cryogenic Engineering Conference; Library of Congress Catalog, 1960.

D.H. Liebenberg and F.J. Edeskuty. Pressurization Analysis of a Large Scale Liquid–Hydrogen Deware. In *Advances in Cryogenic Engineering*, Proceedings of the 1964 Cryogenic Engineering Conference; Library of Congress Catalog Card No.: 57–35598, 1964.

G. Würsig and U. Schmidtchen. Flüssig–Wasserstoff sicher transportieren (Safe Transport of Liquid–Hydrogen). *Technische Überwachung*, 38(4):S. 26–30, 1997.

Germanischer Lloyd, editor. *Rules for Classification and Construction; I–Ship Technology; Part 1–Seagoing Ships; Chapter 6 Liquefied Gas Tankers.* Germanischer Lloyd, Hamburg, 1997.

N.N. EQHHPP-Phase II: WP-080 Maritime Transport Europe; Final Report. Germanischer Lloyd, Hamburg, 1990.

International Maritime Organization, editor. *International Code for the Construction and Equipment of Ships Carrying Liquefied Gases In Bulk*, volume 3. IMO, London, 1993.

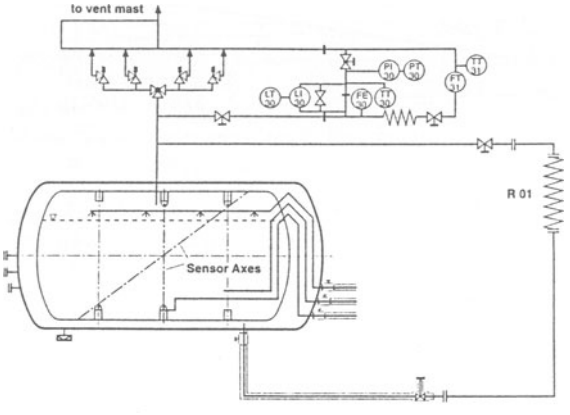

Fig. 1 Simplified flow chart for test tank

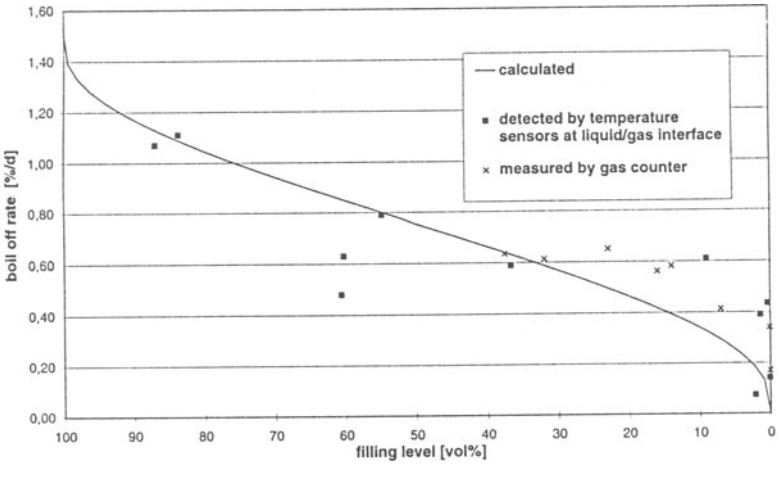

Fig. 2 Comparison of calculated and measured boil off rates

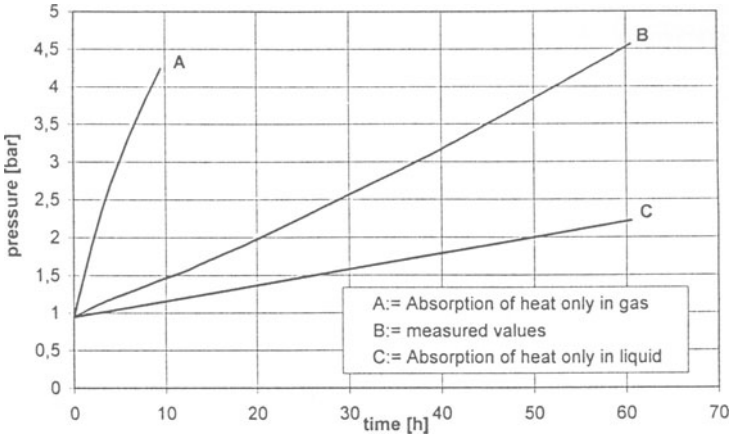

Fig. 3 Comparison of pressure increase observed at 83% vol with theoretical limits

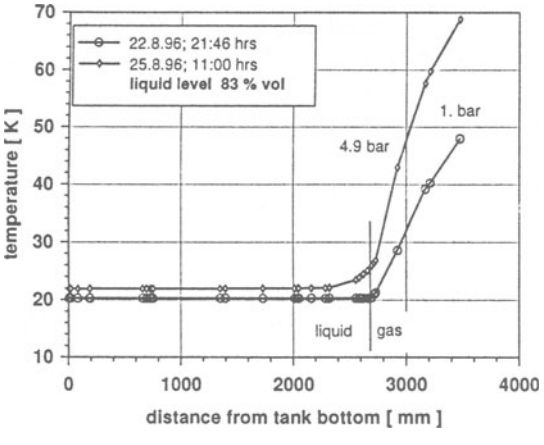

Fig. 4: Typical temperature distribution before and at the end of a self pressurization test.

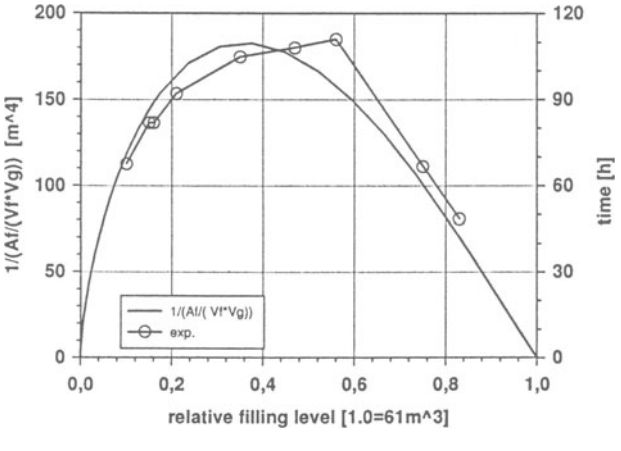

Fig. 5: Approximation of pressure build up time compared with test results.

AN EXPERIMENTAL FEASIBILITY STUDY OF A CRYOGENIC FLUID PISTON PUMP OPERATED BY A LINEAR OSCILLATORY ACTUATOR INSTALLED IN A CRYOGENIC LIQUID TANK

YAMANE, K., NAKAGAWA, K., ABE, Y.* , AOKI, A.*,
EBIHARA, D.*, NAKAJIMA, Y. AND FURUHAMA, S.
*Hydrogen Energy Research Center and *Department of Electric and Electronic Engineering, Musashi Institute of Technology*
1-28-1 Tamazutsumi, Setagaya-ku, Tokyo 158 Japan

1. Introduction

It is necessary to pressure liquid hydrogen(LH_2) to deliver it to an engine on a hydrogen (H_2) vehicle. There are two methods of the pressurization. One is to pressure the LH_2 in a tank by the gaseous H_2 evaporated in the tank[1], [2], [3]. The other is to pressure the LH_2 by a pump[4], [5], [6]. The former method needs a heavy tank because of the structure proof against the pressure. To make the matter worse, some part of LH_2 in the tank evaporates when the pressure in the tank reduces to the atmospheric pressure for refuelling[7]. The latter method does not need the pressurization. However, it is necessary to have a pump driving system(PDS) outside the tank because it is impossible for the PDS to be operated in an extremely low temperature of LH_2. Therefore, a large heat flows into the tank through the PDS outside the tank and a duct through which the pump is steeped into the LH_2 in the tank. As a result, the LH_2 in the tank evaporates. When the engine stops, the evaporated H_2 gas will be a dead loss. Both methods suffer some dead loss anyway. Especially the pump method suffers a large amount of evaporation loss due to the way of the pump installation in the liquid tank .

To minimize the evaporation loss, an experimental feasibility study was carried out by using a cryogenic fluid piston pump operated by a linear oscillatory actuator(LOA) installed inside the tank. This pump is installed at the bottom of the inner tank without any path of heat inflow from the outside of the tank except for the electric wires and a delivery pipe to the outside of the tank. For as easy availability, liquid nitrogen(LN_2) was used as the operating fluid. It was found in the actual operation that the cryogenic piston pump was feasible for LN_2.

This paper describes the pump structure, the operation principle, the specifications, the experimental results obtained by using LN_2 such as the pump performance and the heat generation in the LOA due to the energy loss and the prospects for the application to liquid hydrogen, LN_2 and liquid natural gas(LNG) as cryogenic fluids.

2. Structure and Operation of a LOA Pump

The LOA pump consists of a stationary piston body, a mover and a stator. The piston

T. O. Saetre (ed.), Hydrogen Power: Theoretical and Engineering Solutions, 551–556.

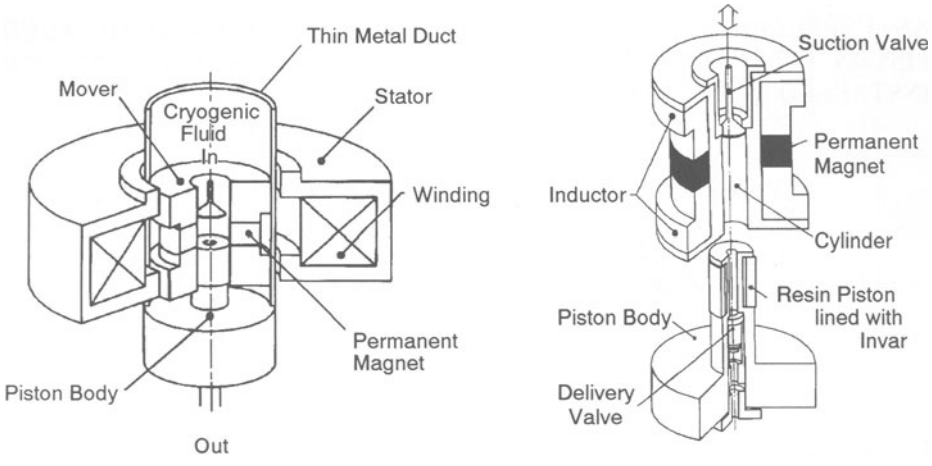

Figure 1. Structure of the linear oscillatory actuator pump

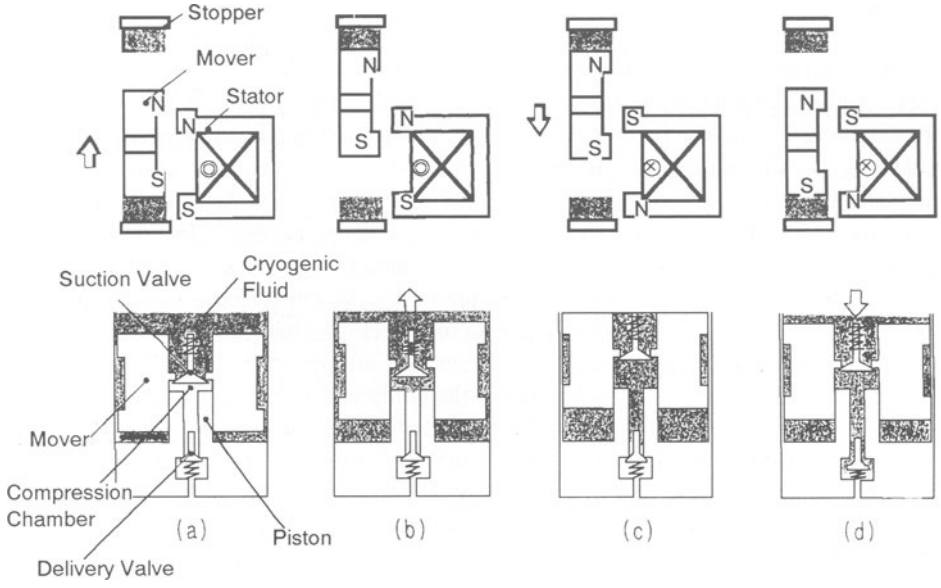

Figure 2. Operation of the linear oscillatory actuator pump

body is composed of a piston and a outlet path with a delivery valve installed midway. The mover is composed of a cylinder, a permanent magnet, inductors and a suction valve. The stator is composed of a core with a winding inside. The piston has a two-layer structure to fit the thermal expansion rate to that of the cylinder in order to obtain the same radial clearance between the piston and the cylinder even at room temperature and cryogenic temperature because a precise clearance control is necessary. Figure 1 shows the structure of the LOA pump. The pump is operated one by one as shown in (a), (b), (c) and (d) in Fig. 2 as follows.

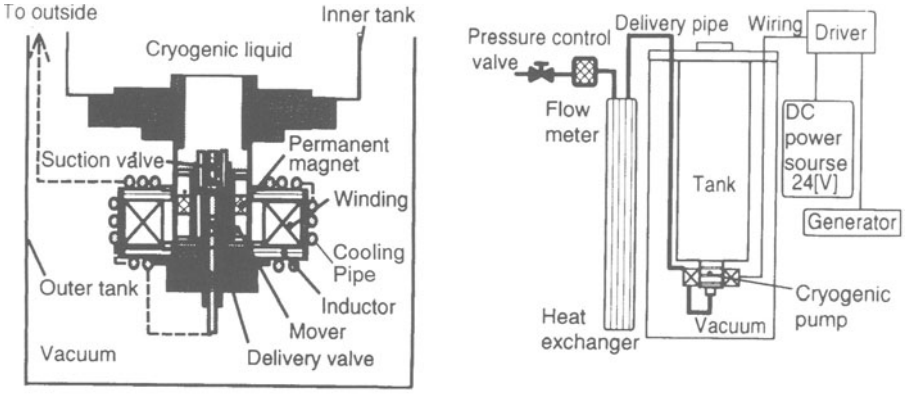

Dimensions and Materials

Stator Size	ϕ 152 x 48 (mm)	Inductor	Iron Steel(SS41)
Mover Size	ϕ 58 x 42 (mm)	Permanent Magnet	Nd-Fe-B
Piston Bore x Stroke	ϕ 15 x 15 (mm)	Cylinder	Stainless Steel
Max. Magnetmotive Force	5000(A)	Piston Body	Stainless Steel
Resistance(RT)	0.18(Ω)	Piston	Resin
Gap Length	1 (mm)	Cooling Pipe	Copper ϕ 6-4

Figure 3. Experimental Installations

(a) and (b): The mover at the bottom is moved up by magnetic repulsion between the mover and the stator. While moving up, cryogenic fluid comes down into the compression chamber and the suction stroke takes place. The mover stops by the upper stopper which limits the stroke of the pump.

(c) and (d): To the contrary, when the magnetic poles change by the reverse current, the mover at the top is moved down by magnetic attraction. While moving down, the suction valve closes and the cryogenic fluid in the compression chamber is pumped out through the delivery valve at the set pressure. And the mover stops by the lower stopper at the bottom.

3. Experimental Installations

The LOA pump was installed to the bottom of the inner tank thermally insulated by vacuum 10^{-6} torr. A cooling pipe was soldered on the three surfaces of the stator to cool down the surfaces to the boiling temperature , aiming to decrease the radiant heat emitting from the surfaces. The right figure in Fig. 3 is the schematic diagram of the PDS and the devices to measure the flow rate of a cryogenic liquid. There also appear the dimensions and the materials in Fig. 3. The pump was operated by the PDS, controlling the amount of electric current and changing the electric current direction. The LN_2 was pumped out, gasified and warmed up in a heat exchanger. The flow rate of the N_2 was measured by a laminar flowmeter.

4. Experimental Results

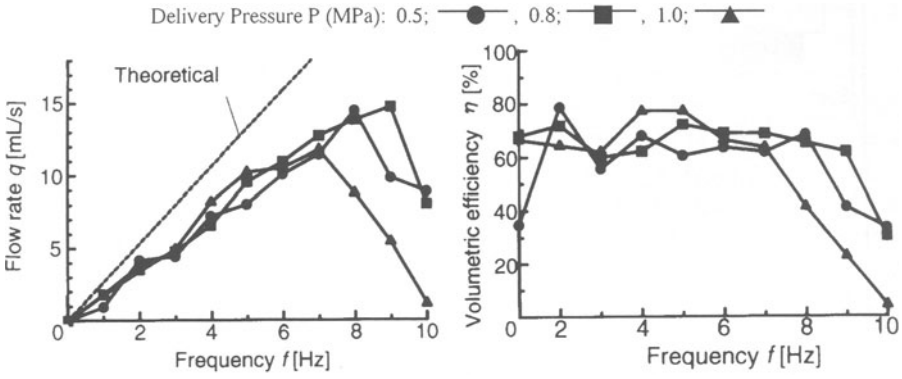

Figure 4. Pump performance in flow rate and volumetric efficiency

4.1 Pump Performance

As the cryogenic fluid, LN_2 was used because of its easy availability. The pump was operated at the delivery pressures(DP) of 0.5, 0.8 and 1.0 MPa respectively, changing the operation frequency in the cryogenic tank filled with LN_2. Figure 4 shows the results of the pump performance . It is found that the pump could deliver LN_2 at the pressures with a volumetric efficiency of around 70 %, which seems to be a little smaller than expected. This may be attributed to a clumsy motion of the suction valve. In any case, the flow rates of the three DPs all fell down at a high frequency; about 8 Hz for the DP of 0.5 MPa, 9 Hz for 0.8 MPa and 7 Hz for 1.0 MPa. As the pump operation was carried out to a higher frequency, the striking sound caused by the bump of the mover to the two stoppers was heard more irregularly and the irregularity was

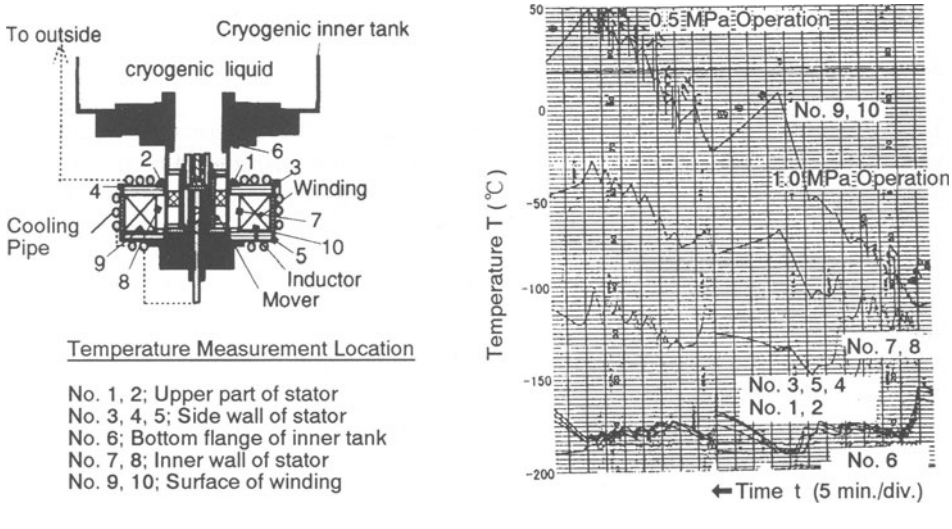

Figure 5. A result of temperature measurement

more noticeable. This implies that the mover could not move in the full stroke.

4.2 Temperature Measurements on the Pump

The surfaces of the stator was cooled down by the LN_2 pumped out from the inner tank to the outside. Figure 5 shows the locations of temperature measurement and a typical results of the temperature change in time at the PDs of 1.0 and 0.5 MPa. It is found that the temperatures measured on the surfaces of the stator No. 1, 2, 3, 4 and 5 decreased while the LN_2 was pumped out and they increased while the pump stopped. The temperature at the bottom of the cryogenic inner tank No.6 remained almost the same at -185 ℃ but the temperature was higher than the boiling temperature of LN_2 of -197 ℃ by 12 ℃ . This shows that the insulation especially against radiant heat was very poor. To the contrary, it is found that the temperatures on the surface of the winding No.9 and 10 and on the inner wall of the stator No.7 and 8 increased while the pump was operated and decreased while the pump stopped. The temperature No. 9 and 10 reached 50 ℃ . It is conceivable from these results that the heat transfer from the winding to the surfaces of stator was very poor. To overcome this problem, a new cooling system design is required.

5. Discussion

Though the pump could pump out the LN_2 at the set pressures, the temperature on the surface of the winding and on the inner wall of the stator increased to a large extent while the pump was operated, which showed that the heat transfer of this design was very poor. But, it is very important to evaluate whether the heat of evaporation of the LN_2 can overcome the heat generation in the winding of the stator. By using the flow rate of LN_2 shown in Fig. 4, the electric resistance of the winding measured at different temperatures and the electric current measured during the operation, the calculation was made in single cycle for the comparison between the heat of evaporation and the heat generated by the copper loss which is said to contribute to a large part of the generated heat.

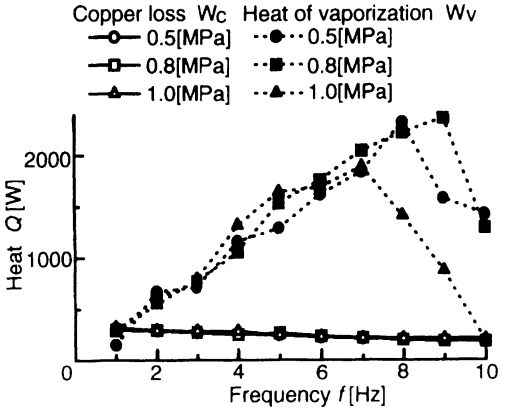

Figure 6. Comparison between copper loss and potential heat of evaporation

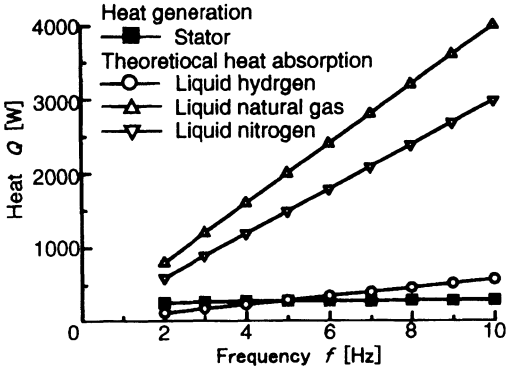

Figure 7. Margin between heat of evaporation and heat of loss

Figure 6 shows the result. It is found that the difference between the heat of evaporation and the heat of the copper loss increases as the frequency increases and that the heat of evaporation is about 9~10 times as much as the heat of the copper loss at the frequency of 7 Hz. This implies that the LN_2 pumped out can absorb the heat of the copper loss and the temperature of the winding can be decreased to a large extent if a proper design is made to cool down the winding.

A calculation was made to know the margin between the heat of evaporation and the heat of the loss of the winding when LH_2, LN_2 and LNG are used as the cryogenic liquid respectively. Figure 7 shows the result. It is found that there is a large margin in cases of LN_2 and LNG, but almost no margin in case of LH_2. This implies that it is very difficult to apply this pump operated by the LOA unless the efficiency of the LOA is improved to a great extent in addition to the good design of the cooling system.

6. Conclusion

A cryogenic fluid piston pump operated by the LOA was design, build and experimentally studied for the feasibility of the application for a LH_2 pump. It is found that it is very difficult to realize the pump for LH_2 unless the efficiency of the linear oscillation is improved to a great extent in addition to a good design of the cooling system.

7. References

1. Furuhama,S., Hiruma, M. and Enomoto, Y.: Development of a liquid hydrogen car, Int. J. Hydrogen Energy 4, 1978, 171-192
2. Stewart, W. F. : Operating experience with a liquid-hydrogen fueled Buick and refueling system, Int. J. Hydrogen Energy 9, 1984, 525-538
3. Rödlger, H.: Design characteristics and performance of a liquid hydrogen tank system for motor cars, Cryogenic 32, 1992, 327-329
4. Furuhama, S., Enomoto, Y. and Kobayashi, Y. : Liquid hydrogen car with two-stroke fuel injection spark ignition engine, The 14th Int. Congress Refrigeration, A3-22, Sep. 1979, 1-7
5. Peschka, W. : Liquid hydrogen pumps for automotive application, Int. J. Hydrogen Energy 15, 1990, 817-825
6. Furuhama, S., Hiruma, M. and Koyanagi, K. : The power system of a computer controlled hydrogen car — GH_2 injection and spark ignition engine with LH_2 tank and pump, C430/028 IMechE, 1991, 179-188
7. Tachtler, J. and Szyszka, A. : Car fueling with liquid hydrogen (Neunburg Von Wald solar hydrogen project: experience and results of first project phase, concept for second phase), Int. J. Hydrogen Energy 19, 1994, 377-385

STUDIES ABOUT THE SEPARATION OF MOLECULAR SPECIES OF HYDROGEN'S ISOTOPES BY CRYOGENIC DISTILLATION IN A PLANT FOR HEAVY WATER DETRITIATION

I. CRISTESCU, IOANA CRISTESCU, M. PECULEA
Institute of Cryogenics & Isotope Separation
P.O.BOX 10, 1000 Rm. Valcea, Romania

Cryogenic distillation is the main industrial method for separating hydrogen's isotopes, because it presents the advantage of high separating factors and also the possibility of processing great quantities of gases.

In the case of multicomponent mixtures the determination of transport for molecular species between the two phases is very difficult owing to the particularities of physical characteristics of each component from the mixture. The transport of molecular species is also strongly influenced by the hydrodynamics of two phases, in strong connection with the dimension of the interface between the vapor and liquid phase. The characteristics of the interface depend on the type and geometry of the separation area: plates or package. The traditional methods of analysis for exchange processes use the concept "theoretic plate", a physical entity for which the values of concentrations for vapors and liquid that leaves the plate are in thermodynamic equilibrium at the pressure and temperature from the plate for all the components of the mixture. Actually in cryogenic distillation for some determined value of concentrations, the equilibrium is not simultaneously attained for all the components [6]. This paper tries to establish the ranges of concentrations where these phenomena appear and to compute the values of deviation from equilibrium in this case.

For solving the problem we considered that in a distillation column of Kuhn type, the transfer between the vapor and liquid phase can be expressed in the frame of elementary theory of transport phenomena.

Referring to the interaction potential that characterize the collisions between two molecules, for hydrogen and it's isotopes the most adequate one is an attractive-repulsive potential of Lennard-Jones type [1]:

$$\varphi(r) = 4\varepsilon[(\sigma / r)^{12} - (\sigma / r)^{6}] \qquad (1)$$

ε represents the maximum value of attraction energy and σ the r value foe which $\varphi(r)=0$. For hydrogen and it's isotopes the values are $\sigma = 2.93$A, $\varepsilon/k = 37$ K [1],[4].

T. O. Saetre (ed.), Hydrogen Power: Theoretical and Engineering Solutions, 557–562.

1. Multicomponent coefficients of diffusion for mixtures of hydrogen's isotopes

For a bicomponent mixture, the binary diffusion coefficients can be expressed as [1]:

$$\mathcal{D}_{ij} = \frac{3(m_i + m_j)kT}{16 n m_i m_j} \frac{1}{\Omega_{ij}^{(l,1)}} \tag{2}$$

where Ω_{ij} represents the collision integrals and for potential of Lennard-Jones type and their values are tabulated [1].
In the same theory, the multicomponent coefficients of diffusion for a ternary mixture are:

$$D_{12} = \mathcal{D}_{12}\left[1 + \frac{c_3\left(\frac{m_3}{m_2}\mathcal{D}_{13} - \mathcal{D}_{12}\right)}{c_1\mathcal{D}_{23} + c_2\mathcal{D}_{13} + c_3\mathcal{D}_{12}}\right] \qquad D_{23} = \mathcal{D}_{23}\left[1 + \frac{c_1\left(\frac{m_1}{m_3}\mathcal{D}_{12} - \mathcal{D}_{23}\right)}{c_1\mathcal{D}_{23} + c_2\mathcal{D}_{13} + c_3\mathcal{D}_{12}}\right]$$

$$D_{13} = \mathcal{D}_{13}\left[1 + \frac{c_3\left(\frac{m_2}{m_1}\mathcal{D}_{23} - \mathcal{D}_{13}\right)}{c_1\mathcal{D}_{23} + c_2\mathcal{D}_{13} + c_3\mathcal{D}_{12}}\right] \tag{3}$$

By their shape (3) the ternary coefficients of diffusion are functions of binary coefficients of diffusion and concentrations.

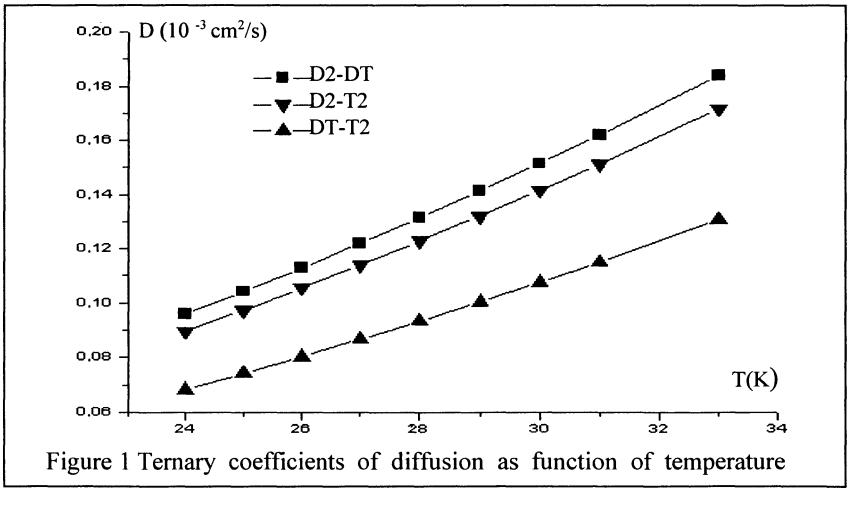

Figure 1 Ternary coefficients of diffusion as function of temperature

We computed the ternary coefficients of diffusion for mixture D_2-DT-T_2 as functions of temperature and concentrations of components from the mixture. Their variation with temperature is shown in figure 1. The concentrations are D_2: 0.8; DT: 0.15; T_2: 0.05.

2. Model for separation of a ternary mixture based upon elementary theory of transport phenomena

Corresponding to elementary theory of transport phenomena, the composition and temperature gradients are the causes of mass transport. In this case the mass flux of molecules of j type is:

$$\vec{j}_j = m_j \int f_j \vec{V}_j d\vec{V}_j = n_j m_j \vec{V}_j \tag{4}$$

The diffusion velocity of chemical species i is function of coefficients of diffusion [1]:

$$\vec{\bar{V}}_i = \frac{n^2}{n_i \rho} \sum_j m_j D_{ij} \frac{\partial}{\partial \vec{r}} \left(\frac{n}{n_j} \right) \tag{5}$$

From Enskog equation for mass conservation:

$$\frac{\partial n_i}{\partial t} = - \frac{\partial}{\partial \vec{r}} \left(n_i \left(\vec{v}_0 + \vec{V}_i \right) \right) \tag{6}$$

If in equation (6) we introduce the velocity of diffusion given by (5), and we divide with the total number of molecules we obtain:

$$\frac{\partial c_i}{\partial t} = - \frac{\partial}{\partial \vec{r}} \left[c_i \vec{v}_0 + \frac{1}{\rho_c} \sum_j m_j D_{ij} \frac{\partial c_j}{\partial \vec{r}} \right] \qquad i = 1..n \tag{7}$$

where ρ_c is the density of the system defined as:

$$\rho_c = \sum_i c_i m_i \tag{8}$$

In equation (7) we assumed that we can neglect the influence of exterior forces, the temperature gradient and the pressure variation. These conditions are fulfilled in a cryogenic distillation column where the pressure variation is small and the terms consisting the temperature gradient is a few orders lower then the one containing the concentration gradient.

The concentrations must also satisfy the evident equality:

$$\sum_i c_i = 1 \tag{9}$$

Having in view the axial symmetry of the problem, for solving system (7) we choose cylindrical co-ordinates. The system was applied to a ternary mixture D_2-DT-T_2 and it was solved with finite differences.

3. Boundary and initial condition

We considered that the diffusion process is much more important in the vapour phase. For describing more accurate the phenomena occurring in a Kuhn column, the geometry and initial distributions of concentration are presented in figure 2 a.

At the interface for a very small thickness we considered that the vapour is in thermodynamic equilibrium with the liquid.

Condition 1: $c_1^L(z) = \frac{\left(c_1^L(HTP) - c_1^L(0)\right)}{HTP} + c_1^L(0) \qquad c_2^L(z) = \frac{\left(c_2^L(HTP) - c_2^L(0)\right)}{HTP} + c_2^L(0)$

$c_i^L(z)$, $c_i^L(0)$, $c_i^L(HTP)$ represents the concentration of component i in liquid phase at a height z, 0, HTP respectively.

Referring to the behaviour of concentration on z direction, it was considered that the point z=0 is corresponding to the bottom of the theoretical plate, and the concentration values on liquid phase at this point are known. At the point z=HTP (height of the theoretical plate) the concentration on liquid phase is in equilibrium with the one from z=0, condition required for total re-flux ratio. It was considered that the variation of concentration on liquid phase is linear.

For simulating the motion on Oz axis, it was considered that after a time t the vapours advance a distance equal to:

$$z=t \bullet v_z \tag{10}$$

v_z is the stream velocity on Oz axis and it is a process characteristic.

Condition 2: $\mathbf{c_1[r_{col},z]=c_{1c}(z);\ c_2[r_{col},z]=c_{2c}(z)}$

c_{1c}, c_{2c} are concentrations on vapour phase corresponding to equilibrium with the liquid phase of concentrations $c^1_L(z)$, $c^2_L(z)$ determined by condition 1.

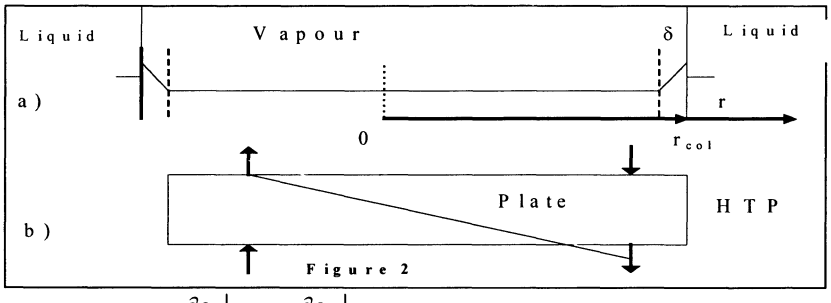

Figure 2

Condition 3: $$\left.\frac{\partial c_1}{\partial r}\right|_{r=0} = \left.\frac{\partial c_2}{\partial r}\right|_{r=0} = 0$$

Condition 3 expresses the axial symmetry of the problem.

Condition 4: $\bar{c}_1[r,0] = c_1^I(0)$ $\quad$ $\bar{c}_2[r,0] = c_2^I(0)$

At initial moment the average concentrations of the components on vapour phase on Or direction at the bottom of the plate are equal with the concentrations of the components on liquid phase. This condition simulates the equality of concentrations on liquid and vapour that leaves the theoretical plate at total reflux ratio (as it can be seen form figure 2.b). The average is given by:

$$\bar{c}_i[z] = \frac{1}{\pi r^2_{\max}} \sum_r \pi r^2 c_i[z] \tag{11}$$

Condition 5: c1[r-δ,0]=const; c2[r-δ,0]=const

The initial distribution of concentrations on Or direction at the bottom of the plate vary from the equilibrium values ($c_{1c}[0]$, $c_{2c}[0]$) in a thick layer (δ~5% radius of vapour phase) until a constant value, in such a way that condition 4 is also satisfied.

The numerical method considered the special shape of equation (7). As it can be seen the time derivatives are separated from the spatial derivatives. This fact allows to

compute the spatial distribution of concentrations at time t+δt as a function of spatial distribution of concentration at time t.

4. Numerical model

Input data

-geometrical parameters of distillation column (radius of vapour phase, value of thick layer δ, height of theoretical plate); pressure, stream velocity of vapour phase; the value of concentrations of liquid phase at the bottom of the theoretical plate.

Structure of the program

1. Compute the temperature and the equilibrium values of concentrations of components on vapour phase corresponding to pressure and concentrations on liquid phase.
2. Compute the initial spectrum of concentrations of components on vapour phase at the bottom of the plate.
3. Compute the distribution after z of the concentrations of components on liquid phase.
4. Compute the binary coefficients of diffusion.
5. 1. Compute the ternary coefficients of diffusion
5. 2. Compute the distribution of concentrations on Or direction at a moment t=t+δt.
5. 3. Compute the average of concentrations in planes of z=cst.
5. 4. Compute the deviation from equilibrium as:

$$EQL(z) = \frac{average\ \ concentration\ \ \ on\ vapour\ phase\ (z)}{concentration\ of\ \ liquid\ (z)} \qquad (12)$$

5. 5 The new boundary value for concentration on vapour phase is the one correspondent to equilibrium with liquid phase at a height given by (13).
6. if z=HTP then stop, else return to 5.1.

Output data

The distribution of concentrations' $c_1(r,z)$,$c_2(r,z)$, $c_3(r,z)$ and EQL (HTP).

5. Results

In figure 3 it is shown the variation of EQL with the value of T_2 concentration on liquid phase at the bottom of the theoretical plate, at the same value of DT concentration 0.01% . It can be seen that at low values of T_2 concentration in the feed current (100 ppm) T_2 attained only 20% from the concentration correspondant to equilibrium. At higher values of T_2 concentration in the feed current(>2%) T_2 attained about 85-90% from the correspondent value to equilibrium. D_2, DT attained 99%, 90% respectively of their equilibrium values on all the range considered. This fact explains why D_2 and T_2 have different values for equivalent height of theoretical plate in a multicomponent mixture.

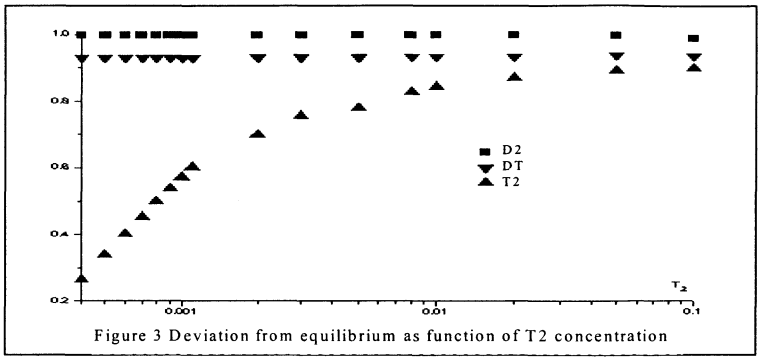

Figure 3 Deviation from equilibrium as function of T2 concentration

The knowledge of distributions' $c_1(r,z),c_2(r,z),c_3(r,z)$ allowed the calculus of mass flux vector of the components. From the analysis of axial and radial components of mass flux vectors, we can assess the phenomena of retro-diffusion (which is the diffusion in the opposite direction of the global movement of vapour phase). In figure 4 are represented the variations of the ratio between the axial and radial components of mass flux vectors (J_r/J_z) for D_2,DT,T_2 as function of T_2 concentration in the feed current. It can be seen that for T_2 the values of this ratio are lower than for D_2, which means that the diffusion on Oz direction (and having an opposite sense then the stream velocity) is much stronger for T_2 then for D_2, DT. This fact explains the low values for T_2 equilibrium presented in figure 3.

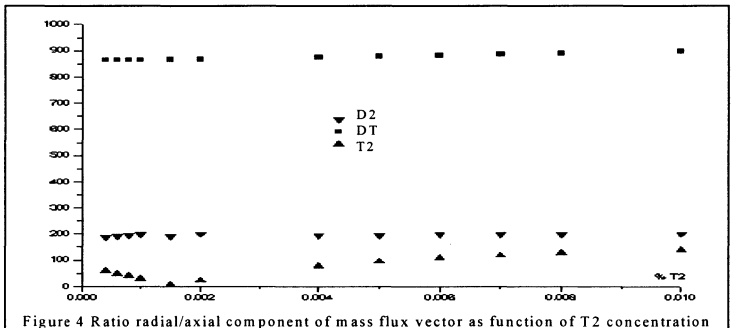

Figure 4 Ratio radial/axial component of mass flux vector as function of T2 concentration

6. References

1. J. Hirschfelder, C. Curtiss, R. Bird (1954)- *Molecular Theory of Gases and Liquids*, John Wiley & Sons,
2. K. Lucas (1991) - *Applied Thermodynamics,* Springer Verlag
4. Landolt-Bornstein (1967) - *Zahlenwerte und Funktionen, aus Physik -Chemie -Astronomie - Geophysik und Technik, Band IV 4.Teil Warmetechnik*, Springer Verlag
5. H. M. Mittelhauser, G. Thodos (1964) - Vapour Pressure Relationship up to the Critical Point of Hydrogen, Deuterium and their Diatomic Combinations, *Cryogenics,* **6,** 368-373
6. A. Coulon, G. Simonet, L. Stouls, (1961) - Distillation des Melanges d'Isotopes de l'Hydrogen et Applications, *Supplement au Bulletin de l'Institute International du Froid, Commsission 1*, **Annexe 1961-5**, 45-63

APPLICATION OF SMALL SCALE FUEL CELLS IN COMBINED HEAT/POWER COGENERATION

J. GARCHE
Center for Solar Energy and Hydrogen Research Baden-Württemberg,
Energy Storage and Energy Conversion Division
Helmholtzstr. 8, D-89081 Ulm, Germany

1 Introduction

In order top reduce CO_2 emissions world-wide, more efficient energy technologies are required in the future. Combined heat and power generation has a considerable higher fuel efficiency than conventional technologies. Today, mostly internal combustion engines are used for this purpose. The use of fuel cells will introduce further benefits due to their higher electrical efficiency and their negligible emissions of other pollutants.

Although the H_2-O_2 fuel cell was discovered in 1839 by W. Grove, about 20 years before the first lead-acid battery was built, no real introduction into the market has taken place up to now, except for space applications. Nevertheless, different applications are currently under development:

a - mobile application - electric vehicle propelling, power sources for small equipment
b - stationary application - electric power generation, electric power/heat cogeneration

In recent years considerable progress has been achieved in the development of electric vehicles powered by polymer electrolyte fuel cells (PEFC) (e.g. Daimler-Benz, Ballard, Toyota). For stationary applications 200 kW PAFC units manufactured by ONSI are commercially available. Even portable fuel cells based on the PAFC system [1] and the PEFC system [2,3] have been demonstrated.

In this paper stationary applications of fuel cells will be discussed. for combined heat and power generation. Particular emphasis will be given to residential fuel cells having comparatively low total power.

T. O. Saetre (ed.), Hydrogen Power: Theoretical and Engineering Solutions, 563–574.

2 Stationary fuel cell application

2.1 BASICS OF THE STATIONARY FUEL CELL APPLICATION

Electric power generation in stationary fuel cells is in competition to thermal processes where the maximum energy efficiency is given by the CARNOT cycle.

The theoretical electrical efficiency (η_{el}^{*}) for the electrochemical and the thermal processes are as follows:

fuel cell

$$\eta_{el}^{*} = \frac{\Delta G}{\Delta G + T\Delta S} \tag{1}$$

CARNOT cycle

$$\eta_{th}^{*} = \frac{T_2}{T_2 - T_1}. \tag{2}$$

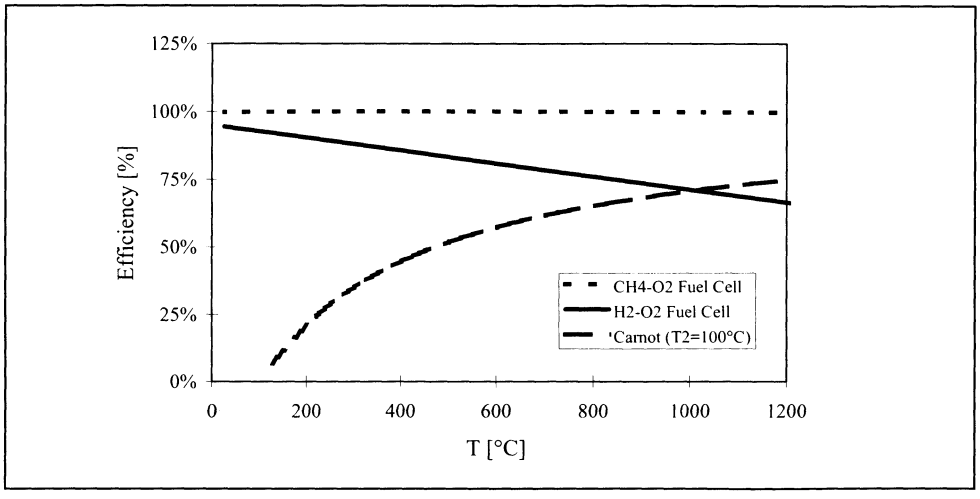

Figure 1. Temperature dependence of the energy efficiency of fuel cells and the Carnot cycle

The theoretical electrical efficiency values will be reduced in reality by additional process losses. In fuel cells they are mainly caused by internal resistive losses producing so called JOULE heat

Therefore, thermal energy in fuel cells (Q_{FC}) is generated as reversible heat Q_R ($T\Delta S$) and as JOULE heat Q_J.

$$Q_{FC} = Q_R + Q_J \tag{3}$$

As shown in figure 1, the amount of reversible heat Q_R in H_2-O_2 fuel cells is relatively low at temperatures below 100 °C. Nevertheless, it becomes more important at higher temperatures. At approximately 1000 °C the theoretical efficiency of a H_2-O_2 fuel cell system is equal to the efficiency of the carnot cycle. For this reason, pure hydrogen not the best fuel for high temperature fuel cells. Direct conversion of methane would result in dramatically reduced reversible heat losses.

The quotient of the electrical energy and usable thermal energy is an important operating parameter of the fuel cell system. This α quotient is defined as follows:

$$\alpha = \frac{P_{el}}{Q_{th}} \tag{4}$$

It depends strongly on the fuel cell type and on the electrical load.

At lower electrical load (IFC) less JOULE heat is generated. Therefore with decreasing load not only the electrical efficiency η_{el} will increase but due to reduced resistive losses α increases as well.
In practice, however, at very low load, η_{el} is decreasing again, caused by electricity consumption of auxiliary aggregates (e.g. pumps).

Nevertheless, it has to be stressed that the emissions of atmospheric pollutants such as NO_x, particulates, CO etc., which in fuel cell systems are caused by the conversion of fossil fuels into H_2, are dramatically reduced as compared to conventional technologies. If the fuel cell system is powered by hydrogen produced from regenerative energies, the total system can be considered as emission free.

2.2 EXAMPLES OF STATIONARY FUEL CELL APPLICATION

Fuel cells are classified according to their operating temperature and the electrolyte used. Table 1 shows a compilation of the different technologies currently under development. The different fuel cell technologies require different fields of applications. Low temperature systems (T_{op} < 200 °C) show comparatively high electrical efficiency, however, heat is released at a low temperature level thus the thermal energy can only be used in the immediate vicinity of the fuel cell system. Intermediate and high temperature systems (MCFC and SOFC) can convert CH_4 directly additionally, they allow further use of the thermal energy e.g. by using gas and steam turbines for the conversion of excess heat into electricity. Furthermore, process heat e.g. for chemical processes can be generated this way.

From these technical data, it is evident, that low temperature systems are most suitable in mobile applications and in small scale decentralized power stations or combined heat and power applications. Intermediate and high temperature systems are most efficiently used for larger power plants and combined heat and power applications.

Table 1. Characteristic data of different types of fuel cells

Type	Operating temperature	Electrolyte	Fuel	Application	Efficiency
Alkaline fuel cell (AFC)	50-90 °C	aqueous KOH	hydrogen	aerospace	50-65%
Polymer electrolyte membrane fuel cell (PEFC)	60-90 °C	acidic polymer ion exchanger membrane	reformate hydrogen,	vehicles, aerospace, combined heat and power (CHP)	40-60%
Phosphoric acid fuel cell (PAFC)	200 °C	phosphoric acid	reformate, hydrogen	stationary power plant, CHP	35-45%
Molten carbonate fuel cell (MCFC)	650 °C	alkali-carbonates	methane, reformate	stationary power plant, CHP	45-60%
Solid oxide fuel cell (SOFC)	850-1000 °C	stabilized zirconia	methane, reformate, coal gas	stationary power plant, CHP	50-60%

In figure 2, typical plant sizes are shown for the different fuel cell and conventional power plant technologies.

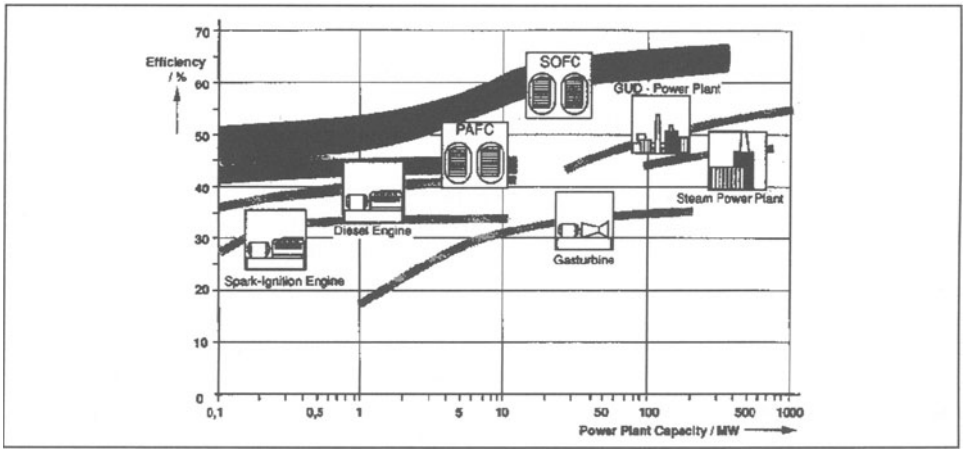

Figure 2. Practical electrical efficiency of different generation processes vs. power plant size

In conventional large scale stationary applications (>50MW), the highest energy efficiencies (>55 %) are achieved using a combined gas and steam turbine (GUD)

generation scheme which is currently installed in several locations. However, its efficiency can further be enhanced (η_{el} = 60....70 %) if the this already existing GUD process is used as a thermal topping cycle for SOFC power plants. Because the SOFC technology is still in a developmental stage (stack sizes <25 kW), fuel cell applications are concentrated in the region of < 50 MW.

The MCFC is now in a relatively advanced state of development. Energy Research Corp. (USA) has build last year a 2 MW_{el} MCFC power station in Santa Clara and a 2.85 MW_{el} unit is planed for 1999. In Germany the MTU a Daimler Benz daughter is currently constructing a 300 kW unit.

The state of development of PAFC systems is at the edge of market introduction. Ready to use systems are commercially available however at rather high system costs. The American company ONSI is producing now the ONSI 25 C. This decentralized FC power station has about 200 kW of electrical and 226 kW thermal power. The system includes a fuel processor, it can fueled directly by natural gas. About 100 systems are currently installed worldwide.

The PEFC also has a relatively high development level. BALLARD has developed stationary units of 30 kW including methane reforming. 250 kW is the largest PEFC system. The strong effort to develop an inexpensive (< 200 DM/kW) PEFC for the vehicle market will also lead to significant cost reductions for PEFC for stationary applications.

Although alkaline fuel cells are in a rather advanced state of development, their use will most probably remain restricted to aerospace applications since they are typically operated on pure hydrogen and pure oxygen.

2.3 Fuel Cell Size

The size of the fuel cell unit is determined by the necessary electrical power and the heat requirements of the user. Fuel cells could mainly be used in

a - electric power generation	peak load	5 - 250 MW
	middle load	50 - 250 MW
	basic load	100 - 1000 MW
b - electric combined heat and power generation	industry	1 - 50 MW
	trade	20 - 1000 kW
	household	2 - 20 kW

For low power (2-5 kW) combined heat and power generation (2...20 kW) only low temperature systems are suitable, since downscaling of high temperature systems causes thermal management problems.

For high temperature fuel cells (SOFC, MCFC) a power of about 10...20 kW is necessary to maintain the operating temperature. The size of high temperature reactors, e.g. fuel cells or reformers, is limited by the size, where the thermal energy loss of the reactor is equal to the energy input into the reactor.

The thermal losses are depending especially on the reactor isolation and its size. These losses are large at small sizes (surface/volume ration is high). The following figure is showing the curve were the equilibrium between energy input and energy loss is reached. This curve is going back to standard furnace manufacturers (e.g. NABER company) for the temperature region of 650 °C. That means this curve is valid for the MCFC [6]. This curve can be less steep if better isolation is used.

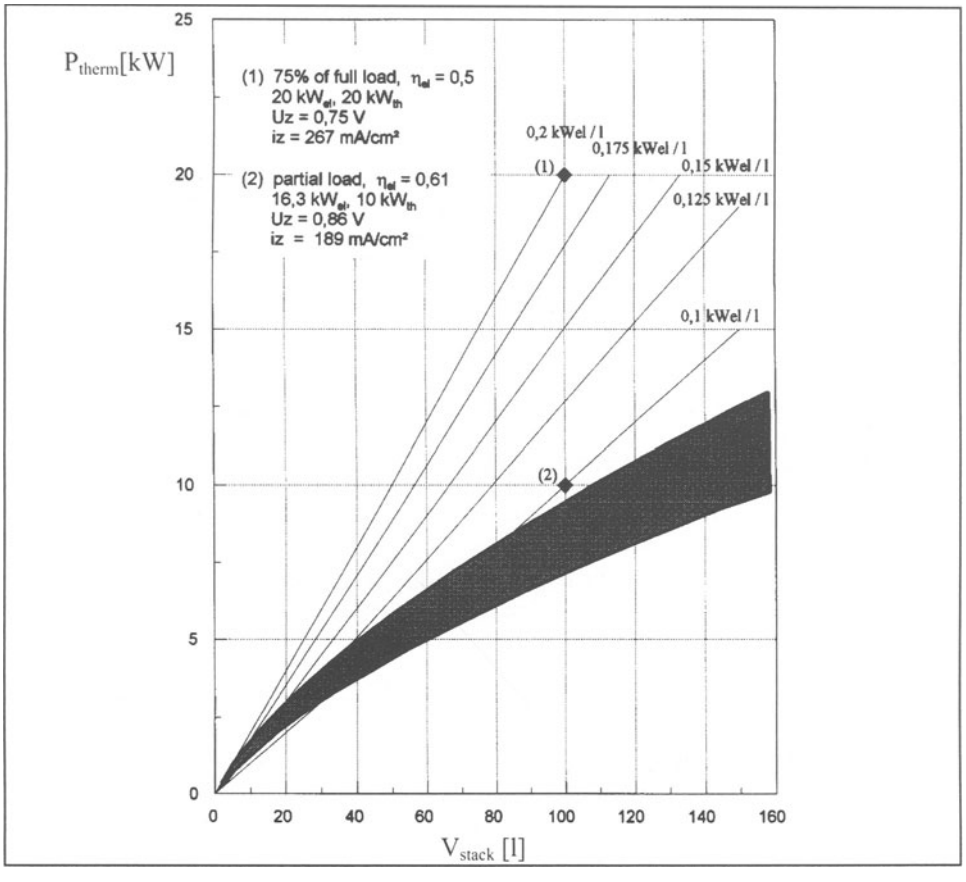

Figure 3. Fuel cell size vs. electrical power of MCFC for heat conducted operation

The heat in fuel cells is mostly generated by JOULE heat. The specific power of the fuel cell is given in W/cm². Approximately it is possible to estimate the volumetric power density (p[mW/cm^2] ≈ p[kW/l]). Therefore one can harvest thermal energy only

if the heat input (JOULE heat) is above of the equilibrium curve. For a 100 l fuel cell with a practical specific energy of 250 mW/cm² ≈ 0,25 kW/l the stack power must be above 25 kW in order to produce useable heat.

For combined heat and power generation using fuel cells, a large number of auxiliary aggregates are necessary. These aggregates can't be reduced in size infinitely, especially the reformer. If for example the reformer is to small (surface/volume ration is high), the efficiency decreases. Large scale CH_4 reformer have an efficiency of about 80...85 %. In small scale CH_4 reformers (10 kW) the efficiency is reduced to 65..70 % [5]. Additionally the size is influenced by the catalyst efficiency, which is measured by the volume of reacting gas in litre per litre catalyst per hour. For the different reactors included in the fuel processor, these figures are as follows [5]:

methanol reformer	- 20,000 h^{-1}
CH_4 reformer	- 10,000 h^{-1}
shift reactor	- 2,000 h^{-1}

Furthermore, the electrical load and heat profile of a typical household shows relatively large daily changes and not every fuel cell system can follow this load profile (see figure. 4). Especially a system start up from room temperature is critical for high temperature fuel cells (see table 3). The following consequences are expected when the fuel cell system is operated dynamically under varying load conditions.

SOFC A load decrease is leading to a higher η_{el} which is coupled to reduced JOULE heat production which causes a reduction of the operating temperature. The consequences of this are local temperature differences causing mechanical stress leading to micro cracks especially in the interface area. At temperatures > 900 °C a self-healing of the cracks is observed. Therefore SOFCs are best operated at a constant temperature above 900 °C in order to prevent this effect.

MCFC The same arguments as for SOFCs hold for MCFCs. In these systems, cracks are generated mostly by cooling the stack below the melting point of the electrolyte.

PAFC With decreasing load the potential of the cathode is increasing. At higher potentials the oxidation rate of the carbon catalyst support is increasing, as well. Therefore the PAFC operation should be preferably at maximal load and not lower than 40 % of the full load [4].

PEFC No major lifetime reducing problems are known associated with operation under partial load and start up.

Table 3. Operating conditions of different fuel cells

FC type	T_{stack} [°C]	start-up time	size [kW]	operation
PEFC	80	1–3 sec	1–50	discont. 10–100 % rat. power
PAFC	180	3–5 h	250–600	perm. 50–100 % rat. power
MCFC	650	1–3 d	300–500	permanent ratedpower
SOFC	900	1–3 d	2–100	permanent rated power

Therefore most fuel cell systems are best operated at constant load. Only smaller changes are possible. A further development of materials with nearly equal thermal extension coefficients can reduced these problems associated with high temperature fuel cells.

2.4 COMBINED HEAT AND POWER GENERATION USING PEFC

As it is evident from table 3, dynamic load profiles can be followed by PEFCs and - to a limited extend - by PAFCs. Therefore, the following discussion will be limited to the behavior of PEFCs in combined heat and power applications.

The electrical efficiency of PEFCs is influenced by the fuel stoichiometry and various other operating conditions. To study the influence of these operating condition a hydrogen fueled model system containing a 700 W stack made from 20 cells having an active area of 100 cm^2 (figure 4) has been constructed. This system contained a control unit for fuel and oxidant flow. Furthermore a cooling and a gas humidification system was included. The electrical parameters as well as the coolant inlet and outlet temperatures were continuously monitored. Furthermore, the test rig contained a DC/AC-converter. Fuel and oxidant stoichiometries were kept constant under varying load. The electrical current was used to control the power output of the stack. The stack was well insulated in order to avoid thermal losses.

Figure 5 shows a typical current-voltage curve for this stack. From current-voltage curves under different operating conditions, optimized parameters for combined heat and power generation have been derived.

It is evident that the electrical efficiency is decreasing with increasing load. At 40% nominal load an electrical efficiency of 60% is achieved, which reduces to 40% at 75% nominal load.

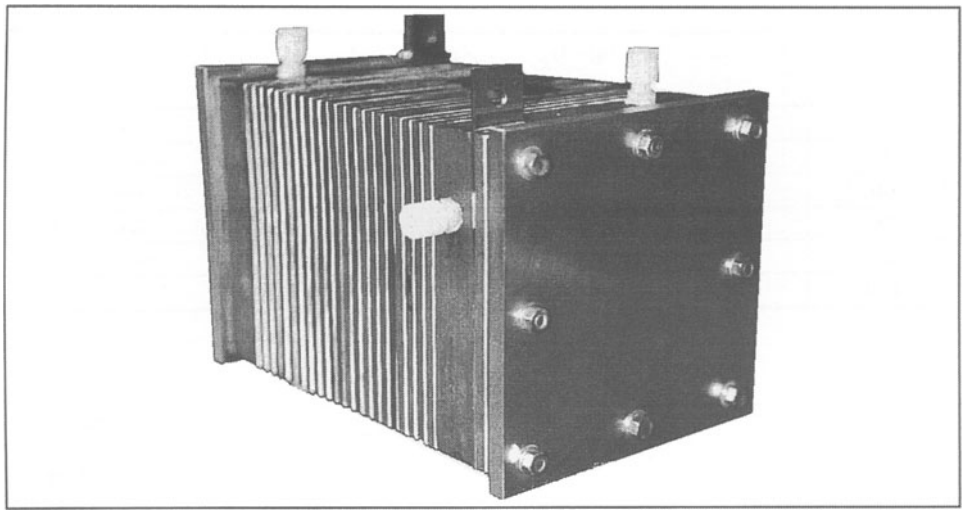

Figure 4. 20 cell PEFC model stack

From the current-voltage curves the electric power and the heat generation can be calculated. In figure 6 these values are shown depending on the stack current and the operating temperature. Numerical values are compiled in table 4.

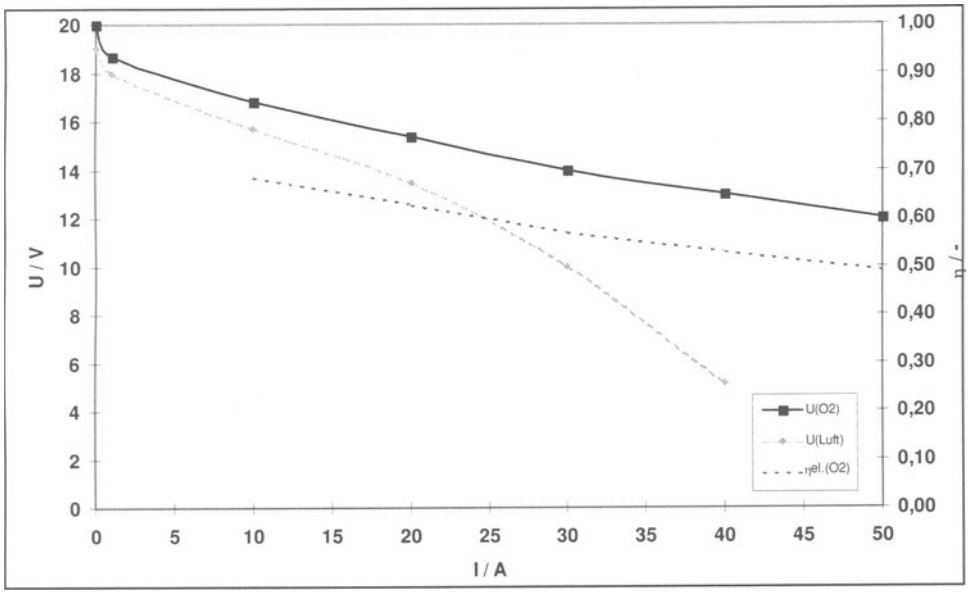

Figure 5. Current-voltage curves for the 20 cell PEFC model stack
active area 100 cm^2, H_2-consumtion 85%, air consumption 30%
T_{stack}: 42°C....79°C, η_{el} with respect to the lower heating value

Table 4. Heat and electricity production of the 20 cell model stack

% P_{max}	i / $mAcm^{-2}$	P_{el} / W	$\dot{Q}_{el}$ / W	% $\dot{Q}_{max}$	$T_{vorlauf}$ / °C
20	**100**	**140**	**130**	**12,5**	**42**
40	**200**	**281**	**250**	**23,8**	**49**
60	**300**	**425**	**360**	**34,3**	**55**
75	**430**	**525**	**527**	**50,2**	**63**
85	**(500)**	**(595)**	**(625)**	**(59,5)**	**(67)**
100	**(700)**	**(700)**	**(1050)**	**(100)**	**(72)**

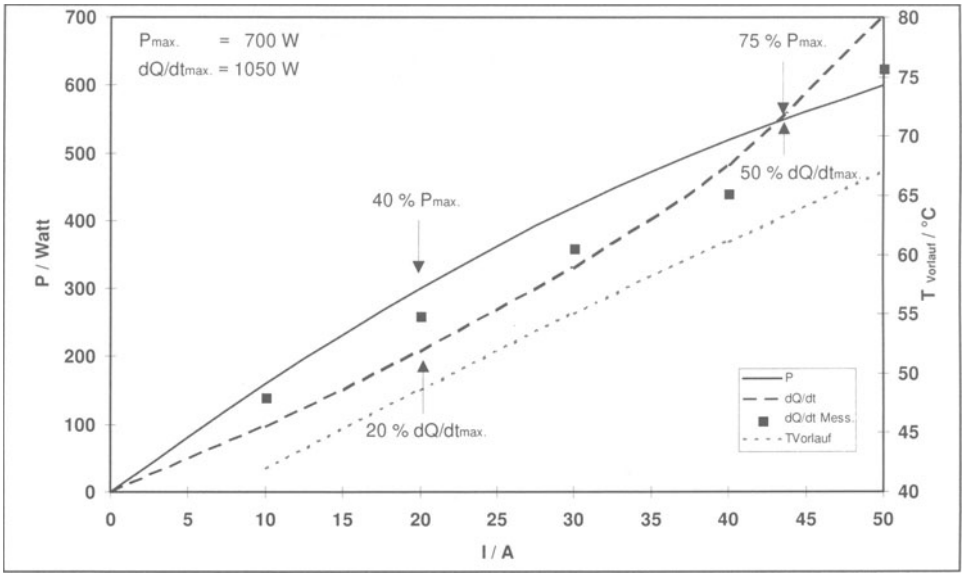

Figure 6. Characteristic curves P_{el}-I and dQ/dt-I curves for the 20 cell stack

It can be seen from figure 6 and table 4 that useable heat is produced above 40% nominal load of the fuel cell. At 75% nominal load already 50% of the maximum heat production is achieved.

The heat production below an operating temperature of 60 °C is above the values calculated theoretically from the lower heating value of hydrogen. This is caused by the condensation of water vapor inside the stack. Above 60 °C water condensation occurs mostly outside the stack. In total 89...92% of the thermal energy generated in the fuel cell could be recovered by the model system.

2.5 COMBINED HEAT AND POWER GENERATION FOR FALILY HOMES

In figure 7 a typical load profile for a family home during wintertime is shown. Combined heat and power generation by a 5 kW PEFC system is assumed. It is evident that the fuel cell follows the electricity demand. However, the heat demand is considerably larger than the electricity demand under these operating conditions. Therefore an extra heater will be required to supply the additional thermal energy which is required. The differences between electrical and thermal power requirements are much smaller during summertime.

Based on the thermal load profile shown in figure 7 and experimental data measured with the model system, it can be calculated that combined heat and power generation using a PEFC- module can cover 100% of the electricity demand of a typical family home. However, by this electricity demand drive operation only 40% of heat demand are covered by the fuel cell. Therefore, for economic reasons the fuel cell will typically be operated in the heat conducted mode during wintertime. Surplus electricity will be fed into the grid.

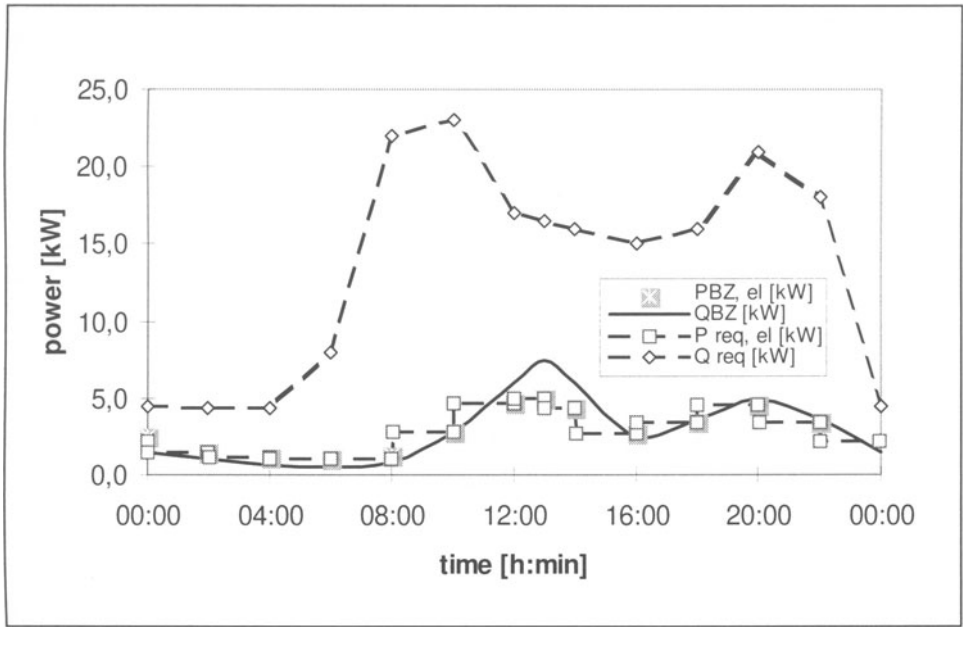

Figure 7. Daily electric power and heat requirements of a family home during wintertime

Economical fuel cell operation driven by the electricity demand will be possible if specific system costs are below 2000,- DM/kW

2.6 REQUIREMENTS FOR FURTHER DEVELOPMENT

The most challenging task for PEFC introduction in combined heat and power generation in family homes will be a dramatic reduction of the system cost. This can be achieved by the following improvements:

- the fuel cell stack — the use of less expensive materials for membranes and bipolar plates and the simplification of the flow field geometry, will allow considerable cost reductions.
- fuel processing — improved gas processing e.g. by improved reformer-shift converter modules combined with CO-cleaning inside the stack leads to a considerable simplification of fuel cell control and operation.
- integrated control — construction of integrated PEFC-heating modules will reduce the number of components used thus leading to significant cost reductions..

3 Acknowledgements

Support from the colleagues at ZSW Ulm especially Dr. habil. Bernd Rohland, Dr. Joachim Scholta, and Dr. Ludwig Jörissen is gratefully acknowledged.

4 Literature

[1] N. Nhishizawa, K. Naktoh, Development of small-capacity fuel cell systems Kagaku Kogyo 47, (1996) 183-189

[2] H. Maeda, H. Fukumoto, K. Mitsuda, H. Urushibata, M,. Enami, K. Takasu Development of PEFC for Transportable Applications, Fuel cell seminar 12/96

[3] anonymous: H Power Sets Up Quebec Subsidiary for Low Power PEM Fuel Cells Hydrogen&Fuel Cell Letter 12(6) (1997)1

[4] J. Scholta, B. Rohland, Operation of a 2 kW PAFC Demonstration Unit and Investigation of the Heat Conducted Operation Mode, Proc. 7th Ann. Meeting of the Canadian Hydrogen Association, 5th-7th June, 1995, Abstracts, p. 1161-169

[5] K. Ledjeff-Hey, A. Heinzel: Membranbrennstoffzellen-Erste Pilotanlagen, Symposium Fuel Cells, ACHEMA 97, Frankfurt/M. , 10 June 1997, lecture

[6] B. Rohland, V. Plzak, U. Jantsch, Stand der Komponentenentwicklung der MCFC, Battery-Meeting , 7 November 1997, Essen, lecture

DYNAMIC MODELLING OF A CATALYTIC METHANOL-STEAM REFORMER FOR FUEL-CELL HYDROGEN PRODUCTION

J.C. AMPHLETT, J.C. FORSYTH, R.M. HOLLAND, R.F. MANN, B.A. PEPPLEY
Department of Chemistry and Chemical Engineering
The Royal Military College of Canada
Kingston, ON K7K 5L0

1. Introduction

The development of a catalytic methanol-steam reformer for the production of a hydrogen-rich gas for fuel cell applications presents a number of unique challenges. Some of the most difficult to achieve requirements include fast start-up, load following, compactness and high selectivity for hydrogen. A methanol-steam reformer simulation has been developed that accurately predicts the steady-state operation of such reactors and can be used in the optimisation of new and novel designs with respect to compactness and selectivity (Amphlett *et al.*, 1996). A major obstacle still to be overcome, however, is the dynamic response of the system to changes in load. A comprehensive dynamic reactor model makes it possible to evaluate reactor design concepts in an economical and logical fashion.

This paper presents the results of the second phase (dynamic modelling) of our methanol-steam reformer development efforts. A previous paper (Amphlett *et al.*, 1996) has reported the details of the steady-state model.

2. Model Development

A tube-and-shell methanol-steam reformer was chosen as the basic modelling configuration due to its simplicity. This design consists of an inner cylindrical tube containing the catalyst bed and reacting gases, and an outer cylindrical shell containing the heating fluid that runs in parallel with the reacting gases. Such a reformer is also effective for obtaining heat transfer information about catalysts.

The following assumptions have been made with respect to the dynamic methanol-steam reforming process:

a. Any change in the inlet feed rate is propagated through the reformer as an instantaneous change in volume flow rate, as opposed to a change of concentration of the reformate gas (i.e. incompressible flow assumed)
b. Time-domain changes in flow rates can be ignored in the conservation of energy equations.

A steady-state model, previously described in Amphlett *et al.* (1996), was used as a starting point in the development of the dynamic model and hence the basic assumptions used in the development of the steady-state model also apply to the dynamic model.

T. O. Saetre (ed.), Hydrogen Power: Theoretical and Engineering Solutions, 575–580.

2.1 CHEMICAL REACTIONS AND KINETICS

Mann *et al.* (1993) have shown that the three overall reactions which describe the process of methanol-steam reforming are the reaction of methanol and steam to CO_2 and three-H_2 (Referred to as Reaction *a*), the direct decomposition of methanol to CO and two-H_2 (Referred to as Reaction *b*) and the water-gas shift reaction. Over most of the range of methanol conversions of interest the water-gas shift reaction has a negligible effect on the composition of the product gas, therefore, the kinetics can be adequately described by the first two reactions.

Fractional conversion defined as:

$$X_j = \frac{\text{moles of methanol consumed by reaction 1j}}{\text{moles of methanol initially}} \tag{1}$$

has been adopted to track the amount of methanol conversion by Reactions *a* and *b*, with the total conversion calculated as the sum of the individual conversions. Kinetic parameters for the $Cu/ZnO/Al_2O_3$ catalyst used in this study have been previous reported (Amphlett *et al.*, 1996; Mann *et al.*, 1993):

2.2 MASS AND ENERGY BALANCES

Using conversion and conservation of mass concepts for methanol and water yields (Amphlett *et al.*, 1996; Alatiqi *et al.*, 1987):

$$\frac{dX_a}{dt} = \dot{V}\left(-\frac{dX_a}{dV} + \frac{r_a}{F_{1,0}}\right) \tag{2a}$$

and:

$$\frac{dX_b}{dt} = \dot{V}\left(-\frac{dX_b}{dV} + \frac{r_b}{F_{1,0}}\right) \tag{2b}$$

where X_a and X_b are fractional conversion of methanol for Reactions *a* and *b* respectively, $\dot{V}$ is the volume flow rate of reformate gas, dV is the incremental volume of fixed bed, $F_{1,0}$ is the inlet flow rate of methanol, and r_a and r_b are the reaction rates for Reactions 1a and 1b respectively.

Conservation of energy for the reformer wall to reacting gas reveals (Fogler, 1986):

$$\frac{\partial T}{\partial t} = \frac{Ua\left(T_W - T_R\right) - \sum_{i=1}^{n} F_i Cp_i \frac{\partial T}{\partial V} - \sum_{j=a}^{c}\left(r_j\right)\left[\Delta H_{Rj}(T)\right]}{\sum_{i=1}^{n} C_i Cp_i} \tag{3}$$

The first term in the numerator describes the heat transfer from the reactor wall to the reacting fluid, the second term describes the temperature profile in the reactor, the third term represents the heat of reaction. The denominator is the heat capacity of the reacting fluid. Subscript *i* denotes species while subscript *j* denotes the reaction. Corresponding equations can also be written for the heating fluid to reformer wall, reformate gas to catalyst, and inter-catalyst particle heat transfer.

2.3 HEAT TRANSFER TERM

Since heat transfer was a critical aspect of the overall model, the heat transfer term was calculated for each element of the reactor, relating it to fluid/solid temperature, thermophysical properties, and interface conditions. This was necessary as the presence of large amounts of hydrogen in the reformate greatly changes the heat transfer characteristics of the reacting fluid. In order to accomplish this, the initial steady state conditions were re-evaluated for each step in the time-space-domain as flow rates, temperatures, and thermophysical properties changed.

3. Solution Procedure

The general solution procedure is:

1. Establish steady state - Using steady-state model from Amphlett *et al.* (1996).
2. Apply new inlet conditions - New flow rates or temperatures of methanol/water mixture or heating fluid.
3. Calculate space-domain derivatives - Use finite difference to determine space-domain derivatives of temperature and conversion.
4. Determine time-domain derivatives - Use fourth-order Runge-Kutta-Gill solution procedure to determine simultaneously the time-domain derivatives of temperature and conversion, using Equations 2a, 2b, and 3.
5. Determine new conversion profile and temperature profile - Given old values of temperature and conversion, and time-domain derivatives, determine new values of temperature and conversion.
6. Increment time and return to step 2, or end.

The methanol-steam reformer modelled in this simulation measured one meter in length and was divided into 100 elements for the finite difference solution. Equations 2a, 2b, and 3 were simultaneously numerically integrated for each element in the reactor. The inlet conditions of temperatures, partial pressures, flow rates, and thermophysical properties were fed into the fourth-order Runge-Kutta-Gill method. As time was incremented, the full set of elements in the reactor was solved for local conversion and temperature.

4. Simulation Results

The simulation presented here tracks the dynamic response from an initial steady-state through a step change in feed rate. The initial conditions are: methanol flow rate 10.0 mol/hr (plus 20.0 mol/hr of steam), steam-to-carbon ratio 2.0, feed temperature 265°C, heating fluid flow rate 0.2 kg/sec, and heating fluid inlet temperature 265°C. The step-change dictated a steady-state inlet methanol flow rate of 20.0 mol/hr (with a corresponding change in steam flow rate to maintain the same steam-to-carbon ratio). All other inlet conditions as stated above were unchanged (Amphlett *et al.*, 1996).

To test the dynamic simulation, the initial steady-state conditions were fed into the dynamic program, which was then allowed to settle for 25 seconds. After this, the new feed rate (20.0 mol/hr of methanol, 40.0 mol/hr of steam) was fed into the dynamic program as a step change; no other inlet conditions or operating parameters were

changed. The results were tracked until the dynamic program settled at a final steady state.

The results of the simulation indicate that the dynamic model and the steady-state model are in agreement at the beginning and the end of the transient. Data for the validation of the dynamic simulation, however, are very limited. Thérien and Tessier (1987) carried out a limited study of the dynamic behaviour of a methanol-steam reformer. Energy Research Corporation (1990) also reported temperature-time profiles for a few transients of their methanol-steam reformer design. The time constant for the reformer design simulated in this work is approximately ten to twenty times less than that for the other reformers. This is approximately proportionate to the ratios of their thermal masses.

The predicted dynamic response of the reformer is shown in Figure 1 (Temperature), and Figure 2 (Hydrogen Flow Rate and Conversion).

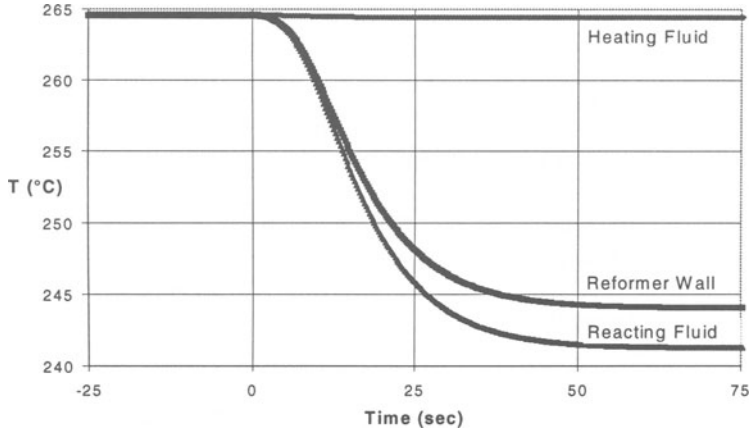

Figure 1: Response of temperature at exit to a step change in inlet flow rates.

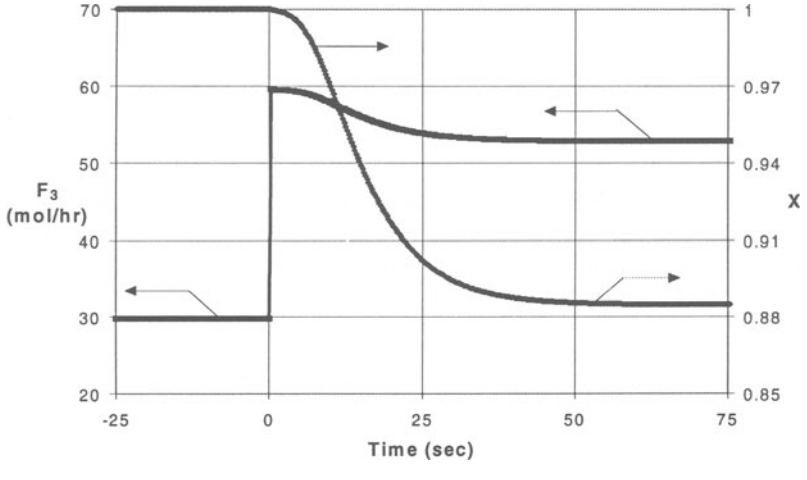

Figure 2: Response of H_2 flow rate and overall conversion to a step change in feed rate.

These two figures demonstrate the dynamic response of the reformer to a step change in feed rate of methanol-steam mixture. Two observations can be made concerning the overall response of the reactor: first, the step change in feed rate results in an immediate step change in outlet flow rate of reformate gases, and second, the temperature (and conversion) response of the reformer to changes in inlet conditions is much slower. The overall response time of the reformer for this case appears to be on the order of 50 seconds, as dictated by the thermal response, at which time the reactor has reached a new steady-state.

The thermal response of the reformer indicates that the reactor may have a relatively large overall thermal capacitance when compared to the energy exchanges that take place. If fast thermal response times are desired for the reactor, efforts should be made to limit the mass or heat capacity of the overall reactor, and/or to improve its heat transfer properties.

The general response of the overall conversion is very similar to that of temperature, confirming that outlet conversion and temperature are strongly linked. This may suggest that, if one assumes the reaction rates to respond instantaneously to local changes in temperature, flow rates, and thermophysical properties, they may be assumed to be in quasi-equilibrium with respect to the local temperature and reformate gas composition of the reactor (Thérien and Tessier, 1987).

Reformate gas flow rate response may be seen as a function of two factors: feed rates and conversion. The initial flow rate response is attributable to the step change in inlet flow rate, in which a step change in the feed rates of the methanol/steam mixture dictates a corresponding immediate step change in the outlet flow rates of reformate gases. Initially, the conversion remains quite high. However, as the conversion slowly responds to a new, lower overall conversion, the outlet reformate gas flow rate also responds to reflect this change.

Overall the flow rate reactor seems to respond instantaneously to changes in feed rates, but there is a substantial lag in the thermal response of the system. This would suggest that any dynamic situation requiring a large thermal (and conversion) response would be quite slow, but that changes where thermal and conversion response is not a large factor (i.e. small flow rate changes for hot operation) could be considered quite fast.

5. Conclusion - Generalisation of Model

To date, limited dynamic data have been located which can be used to verify the accuracy of the dynamic model. The dynamic model presented in this work agrees quite well with the previously-reported steady-state model on the initial and final states of a step input change to the reformer. Additionally, it appears that the dynamic response or the reformer is a function of two factors: heat transfer capability, and thermal capacitance or inertia. Reformer designs which maximise heat-transfer clearly are needed. The development of catalyst systems which minimise thermal inertia could also result in a significant improvement in reformer performance.

Acknowledgement: Support for this work by the Canadian Department of National Defence through funding supplied by the Chief of Research and Defence is gratefully acknowledged.

REFERENCES

Alatiqi, I.M., A.M. Meziou, and G.A. Gasmelseed "Modelling, Simulation and Sensitivity Analysis of Steam-Methane Reformers" Int. J. Hydrogen Energy, Vol. 14, No. 4, pp. 241-256, 1989.

Amphlett, J. C., R. M. Holland, R. F. Mann, and B. A. Peppley, "Modelling a Catalytic Methanol-Steam Reformer for Reactor Development and Design" Emerging Energy Technology Symposium, Houston, Texas, Jan/Feb 1996.

Energy Research Corporation, "Research and Development of a Fuel Cell/Battery Powered Bus System, Phase 1 Final Report" U.S. Department of Energy Contract DOE-AC08-87NV10714, 1990.

Fogler, H. Scott Elements of Chemical Reaction Engineering Prentice-Hall, Inc, Toronto, 1986

Mann, R. F., J. C. Amphlett, and B. A. Peppley "A Fuel Conditioning System for a Methanol-Fueled PEM Fuel Cell Power Generator", Proceedings of the First International Conference - New Energy Systems and Conversions, pp. 613-618, Yokohama, Japan, June 1993.

Thérien, N., and P. Tessier "Modélisation et simulation de la décomposition catalytique du méthanol dans un réacteur à lit fixe" The Canadian Journal of Chemical Engineering, Vol. 65, pp. 950-957, 1987

NOMENCLATURE

a	=	Heat exchange area per unit volume (m^{-1})
C	=	Molar concentration (mol m^{-3})
C_p	=	Gas heat capacity (J mol^{-1} K^{-1})
F	=	Molar flow rate (mol s^{-1})
ΔH_R	=	Heat of reaction (J mol^{-1} of methanol reacted)
r_j	=	Rate of reaction j (mol s^{-1} [kg of catalyst]$^{-1}$)
T	=	Temperature (K)
U	=	Overall heat transfer coefficient (W m^{-2} K^{-1})
X	=	Conversion of limiting species (methanol

Subscripts

i	=	Species (1 - Methanol (CH_3OH), 2 - Water (H_2O), 3 - Hydrogen (H_2), 4 - Carbon Dioxide (CO_2), 5 - Carbon Monoxide (CO), T - Total)
j	=	Reaction (*a* - Reforming, *b* - Decomposition, *c* - Water-Gas Shift)
0	=	Initial conditions, at inlet

HYDROGEN UTILIZATION EFFICIENCY IN PEM FUEL CELLS

R. METKEMEYER, P. ACHARD, L. ROUVEYRE, D. PICOT
ECOLE DES MINES DE PARIS, CENTRE D'ENERGETIQUE
B.P. 207, F- 06904 SOPHIA ANTIPOLIS
FRANCE

Summary

In this paper, we present the work carried out in the frame of the FEVER project (Fuel cell Electric Vehicle for Efficiency and Range), an European project coordinated by Renault, joining Ecole des Mines de Paris, Ansaldo, De Nora, Air Liquide and Volvo.

For the FEVER project, where an electrical air compressor is used for oxidant supply, there is no need for hydrogen spill over, meaning that the hydrogen stoechiometry has be as close to one as possible.

To determine the optimum hydrogen utilization efficiency for a 10 kW Proton Exchange Membrane Fuel Cell (PEMFC) fed with pure hydrogen, a 4 kW prototype fuel cell was tested with and without a hydrogen recirculator at the test facility of Ecole des Mines de Paris .

Nitrogen cross over from the cathodic compartment to the anodic compartment limits the hydrogen utilization of the fuel cell without recirculator to 97.4 % whereas 100% is feasible when a recirculator is used.

1. Introduction

Most fuel cells use pure hydrogen as a fuel and ambient air as the oxidant.
On the air side, normally an air stoechiometry between 1,5 and 2,0 is often advised. On the H_2 side, we want a stoechiometry as close to one as possible. In this case we have 100 % fuel efficiency and highest energy efficiency. However, mainly for waterdraining reasons a stoechiemetry of 1,2 to 1,5 is advised. If we neither recycle this excess hydrogen nor use it in an auxiliary, like a hydrogen turbine, unacceptable fuel efficiency will result.

This leads to the choice to either operate the fuel cell with a recirculator or in a so called " dead end mode ". Pure Hydrogen is fed via an internal distributor to the upper part of the single cells as schematically depicted in figure 1. A collector is located on the bottom part of the single cells.

The hydrogen supply is guaranteed by a fuel cell upstream pressure regulator. The bottom collector is connected to the fuel outlet of the fuel cell stack.
In the "dead end" mode, this outlet is closed by means of an electrovalve. Accumulated water is evacuated by gravity via another electrovalve .

In the "recirculator" mode, the outlet and the inlet of the fuel cell are connected via a recirculator. Liquid water is mainly stripped in the water separator.

In the frame of the FEVER programme, an 1 kW, a 4 kW and a 10 kW PEM fuel cell from De Nora spa were tested in a "dead end" mode and in a "recirculator" mode at the Ecole des Mines de Paris's test facility. During these tests it appeared that nitrogen, which

T. O. Saetre (ed.), Hydrogen Power: Theoretical and Engineering Solutions, 581–590.

diffuses through the membranes from the cathodic compartment into the anodic compartment, determines largely the strategy of operation of a power module containing a fuel cell running on pure hydrogen.

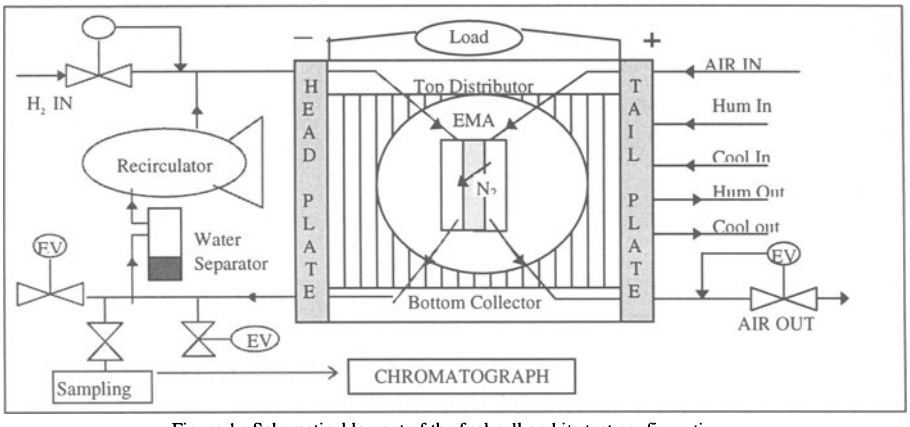

Figure 1 : Schematical lay out of the fuel cell and its test configuration

2. Theory

In the fuel cell, the fuel compartment and the oxidant compartment are separated by an Electrode Membrane Assembly (EMA). Oxygen from air diffuses into the cathodic electrode in which it is electrochemically reduced to water.
The same for hydrogen which diffuses into the anodic electrodes to be oxidized to hydronium ions, which migrate through the membrane to the cathode.
Air contains about 80 vol% of nitrogen whereas the hydrogen on the other side of the membrane is a pure gas. Therefore, the nitrogen will tend to diffuse through the membrane and accumulate in the anodic gas chambers.
The chances that hydrogen accumulates in the cathodic compartment are negligible. Hydrogen escaping from oxidation on the anode will diffuse towards the cathode and once in contact with the cathode immediately be oxidized.
For the same reasons oxygen accumulation in the hydrogen compartments can be neglected : oxygen escaping from reduction on the cathodes will be immediately reduced once in contact with the anode.
Nitrogen however is electrochemically inactive and will thus not be stopped by the electrochemical barriers which are the electrodes.
So, the anodic compartment will during functioning be fed by hydrogen which is electrochemically consumed and by nitrogen which is permeating through the membrane. Nitrogen is not consumed and will therefore accumulate in the anodic compartment.

This nitrogen diffusion through the membrane can be described by the following equation :

$$Jn = Pe*A*(Pnc - Pna)/\delta \quad [moles/s] \qquad (1)$$

Jn	=	molar flux of nitrogen through the EMA	[moles/s]
Pe	=	permeability coefficient	[moles.cm/cm^2.Pa.s]
A	=	EMA surface	[cm^2]
δ	=	membrane thickness	[cm]
Pna	=	partial nitrogen pressure in the anodic gases	[Pa]
Pnc	=	partial nitrogen pressure in the cathodic gases	[Pa]

By knowing the volume of the anodic compartment and by assuming ideal gas behaviour, we can derive the following equation describing the partial pressure of nitrogen in the anodic compartment as a function of time :

$$d\,Pna(t)/dt = (Pe*A*R*T/\delta*Va)*(Pnc - Pna(t)) \quad (2)$$

Va	=	volume of the anodic compartment	[m3]
T	=	absolute temperature	[K]
R	=	ideal gas constant = 8,31	[J/mole.K]

By putting Pna = 0 at t = 0, equation (2) can be integrated to yield :

$$Pna(t) = Pnc*(1-\exp(-k*t)) \quad (3)$$

in which

$$k = Pe*A*R*T / (\delta*Va) \quad (4)$$

What we are most interested in is the nitrogen fraction appearing in the anodic gases due to this nitrogen cross-over. The nitrogen fraction can be calculated by the following equation:

$$Xna(t) = Pna(t) / Pta \quad (5)$$

in which Pta = total pressure of the anodic compartment [Pa]

In fuel cell operation it is good practice to have a slight overpressure of air with respect to hydrogen. Often humidification reasons are quoted. The air pressure needs to be as high as possible in order to minimize the kinetic losses due to the sluggish electro-oxydation of oxygen and to minimize the losses due to oxygen diffusion hindrances.
On the anodic side we do not have these problems but we encounter another problem : During the electrochemical reaction the anodes are drying and therefore the gases have to be humidified. This humidification is carried out by an external humidification section in which hydrogen is humidified before entering the fuel cell. At low pressures hydrogen can absorb more water than at high pressures.
So, common practice is to keep the hydrogen pressure somewhat lower than the air pressure (The pressure difference is limited by mechanical parameters and is mostly lower than 1 bar).

However, we have to point out here, that during our tests we have inversed this pressure difference (e.i hydrogen pressure superior to the air pressure) and we have not noticed the slightest influence (the amount of liquid water found at the exit of the anodic compartment did not change from one situation to the other, nor did the performance).

By combining equations (3) and (5) we get for the nitrogen fraction in time

$$Xna(t) = (Pnc/Pta)*(1-\exp(-k*t)) \quad (6)$$

For the partial nitrogen pressure in air (Pnc)we can write the following equation

$$Pnc = Xmean,nc * Ptc \quad (7)$$

in which Xmean,nc = mean nitrogen fraction in the cathodic compartment
Ptc = total pressure in the cathodic compartment

Air enters the fuel cell with 20 vol.% of oxygen and will leave the fuel cell with a lower concentration, depending on the oxygen utilization rate, which is determined by the air stoechiometry.

Air stoechiometries of 2 are common practice and this corresponds to 50 % of oxygen utilization : The exiting air will roughly contain only 10 % of oxygen and the mean nitrogen fraction in the cathodic compartment can be fairly estimated at 0,85. So, for the nitrogen fraction in the anode gases we finally obtain :

$$Xna(t) = Xmean,nc*\Pi*(1-exp(-k*t)) \quad (8)$$

in which Π = (Ptc/Pta)

This function is plotted in figure 2 for various anode-cathode pressure ratios, for a 10 kW De Nora fuel cell stack (45 cells 900 cm^2 each, Nafion® 115, Va = 7 dm^3, T = 343 K, for Pe a value of 10^{-16} moles.cm/cm^2.Pa.s was chosen) .

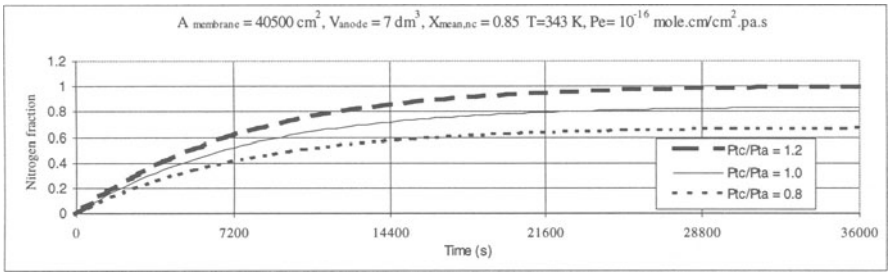

Figure 2 : Nitrogen fraction as function of time according to equation 8 for the 10 kW De Nora Stack

For the case where Π =1 (Pta=Ptc), we see that after a certain time of functioning an equilibrium concentration of 85 % of nitrogen in the anode compartment is reached. This equilibrium concentration can either be influenced by oxygen enriched air or by inversion of the pressure difference between anodes and cathodes. Here we limit the discussion to ambient air.

For cases where Π > 1 (Ptc > Pta) we notice that after a certain time the nitrogen concentration attains 100 % and the fuel cell will extinguish.

For cases where Π< 1 (Ptc < Pta) the equilibrium concentration that will be reached will always be lower than Xmean,nc. For the case Π =1,2 we may hope to operate the fuel cell continuously, without purging at all because fuel cells accept homogeneous hydrogen nitrogen mixtures as fuel with nitrogen concentrations up to rather high concentrations as will be shown in the experimental part of this paper and as has been shown elsewhere [1].

These high nitrogen concentrations are acceptable only if the mixture remains homogeneous. In the experimental part however, we will notice that if no recirculator device is installed, nitrogen stratification occurs which leads to undesirable effects.

3. Experimental

The experimental set up on which our results were obtained is schematically depicted in figure 1 and consist of the following main items.

1) Fuel cell; De Nora spa :
Nominal power 4 kW (12,4 V; 333 A) 18 single cells of 900 cm^2 each.
Air pressure 3,0 bara, stoechiometry 2.0
Hydrogen pressure 2,7 bara ; volume anodic compartment = 4 dm^3

Operating temperature 45°C for the cooling section, 70°C for the humidification section.

2) Air supply subsystem with a fuel cell downstream pressure regulator.
3) Hydrogen supply system with a fuel cell upstream pressure regulator, a water trap, a hydrogen recirculator and three electrovalves (EV) : one for purging purposes, one for liquid water removal and one for gas sampling.
4) Power dissipation section.
   An electronic MOS FETT piloted load (400 A max, 100 V max) capable of testing the fuel cell in a current or voltage mode.
5) Cooling and humidification loop.

The bench is monitored by a data acquisition unit containing 200 channels measured once a second and the control is guaranteed by some programmable single board computers. Hydrogen samples were analysed by a gas-chromatograph [Hewlett Packard 5890-II, Column PoraPack N, 3,3 m, carrier gas He ; TCP detector].

The fuel cell has been tested in a "dead end" mode and in a "recirculator mode" for low, medium and high currents : 100, 200 and 300 A respectively.

4.Results

In figure 3, we present the results concerning the nitrogen accumulation in the anodic compartment as function of time. The points in this graph represent experimental results for both the so called "dead end" mode and "recirculator" mode. The lines in this graph are the best fitted curves for equation 8 for various permeability coefficients (for the recirculator mode only) For this fitting the following set of parameters has been chosen and which reflects the 4 kW fuel cell (18 cells of 900 cm^2 each) and the experimental conditions.

δ	=	125	(micrometre)[Nafion® 115]
Va	=	$4*10^{-3}$	(m^3)
T	=	343	(K)
Pair/Phydrogen	=	3,0/2,7	(bara/bara)
SFair	=	2.0	(-)

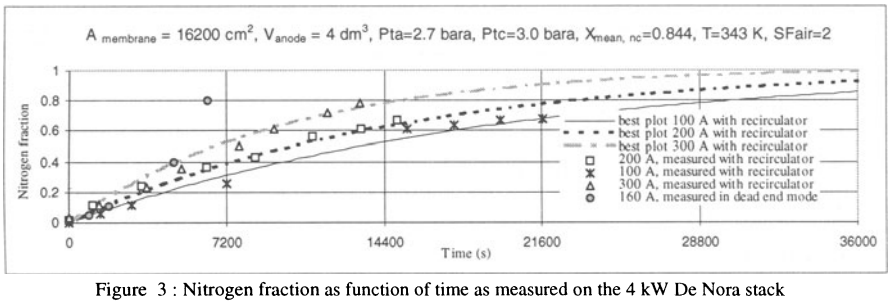

Figure 3 : Nitrogen fraction as function of time as measured on the 4 kW De Nora stack

From figure 3, it appears that the nitrogen permeation coefficient is a function of current (or current density) and that the absolute value of this coefficient can be evaluated according to the equations at the following values :

Pe (100 A) = $5,50*10^{-17}$ (mole.cm/cm2.Pa.s)
Pe (200 A) = $7,20*10^{-17}$ (mole.cm/cm2.Pa.s)
Pe (300 A) = $10,5*10^{-17}$ (mole.cm/cm2.Pa.s)

Another important point to remark in figure 3 is that the nitrogen concentration in "dead end" (i.e. without recirculator) increases very rapidly with time.
This leads us to think that nitrogen stratifies in the bottom part of the fuel cell where we have taken the gas samples.
This leads to very specific problems concerning the stability of fuel cell functioning, which is single cell extinction. By single cell extinction, is meant a single cell which voltage goes to zero volt due to some reason. The main reasons which are often forwarded are bad fuel feeding, bad cooling, or bad water removal. We clearly notice here that nitrogen accumulation also plays an important role.

This single cell extinction should be avoided and either the fuel cell has to be purged and /or the current has to be cut in order to avoid inversion of polarity of the cell. Very low voltage or inversed polarity leads to excessive heat production and this leads to irreversible damage to electrodes and membrane. These inevitable purges determine the fuel utilization efficiency of the system.

5. Discussion

The experimental values obtained for the nitrogen permeability correspond quite well to data we can find in literature [2] who give results for the nitrogen permeability for dry and humidified Nafion® for various temperatures.
Their results lead to the conclusion that Nafion® exposes a nitrogen permeability coefficient ranging from $1*10^{-17}$ to $20*10^{-17}$ moles.cm/cm^2.Pa.s for a completely dry and a completely humidified membrane in the temperature range from 0 to 50 °C. The permeability increases with the level of hydration and with temperature.

Comparison of the experimentally obtained permeability data to the above mentioned literature data shows good agreement and a simple model as exposed in the theoretical part of this paper is thus rather close to reality. However, the reasons that the permeability coefficient changes with current are more academic.

According to the above mentioned literature data, water is playing an important role in the nitrogen permeability for the Nafion® membrane in question.
Their results have been obtained with typical sorption measurements without the existing electrochemical regime witch occurs in EMA's. Other studies, dealing with humidification problems in fuel cells, show that the water balance in the membranes (or more specifically EMA'S) is a rather delicate problem. The results reported by [3] show that hydration of the membrane in fuel cell functioning depends on many parameters. It depends first of all on membrane thickness and temperature and in a lesser extent on parameters such as air pressure, hydrogen pressure and gas humidification level .

Without going too much into detail, it is quite evident that the membrane temperature will rise with increasing current to temperatures which may deviate considerably from the cooling temperature which is often taken as reference. Increasing temperature increases the permeability coefficient of nitrogen. In this paper, the temperature increase will be held responsible for the observed increase in permeability. A more precise discussion taking also into account the waterbalance is under preparation and will be published elsewhere [4] [5].

To come back to the point, which is nitrogen accumulation, in the "recirculator mode", nitrogen which is entering the anodic compartment by permeation is homogeneously mixed by the recirculator. This homogeneous mixture permits us to operate the fuel cell for very long periods without major problems. In the "dead end mode" a problem appears which is created by nitrogen stratification. Nitrogen stratification leads

quite rapidly to blanketing of the bottom part of the anodes. This may lead to inhomogeneous current distribution from membrane to membrane and inhomogeneous potential distribution along the membrane.

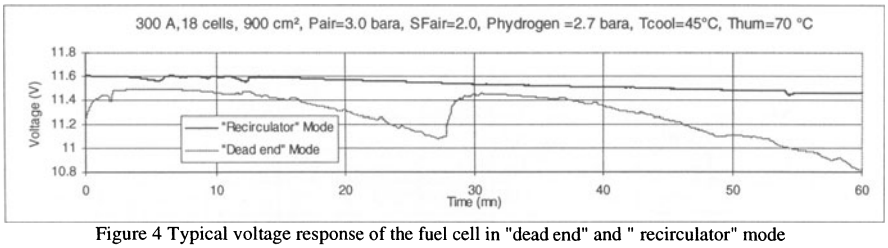

Figure 4 Typical voltage response of the fuel cell in "dead end" and " recirculator" mode

To show the practical impact of the above discussed phenomena we show in figure 4 the voltage response of the fuel cell in a "dead end mode" and in a "recirculator mode" for 300 A. The typical voltage jumps from 11.1 to 11.5 V correspond to a purge. These experimental results show that the fuel cell in the "dead end" mode has to be purged at least every 25 minutes with a *certain amount of fuel* , whereas the fuel cell operated in the recirculator mode could be kept operational for more than four hours without purging at all.

The *certain amount of fuel* depends on the mode of functioning : "dead end" or "recirculator" mode. To replenish the fuel content of the fuel cell, we theoretically need to replenish only once the contained volume of the anodic part of the fuel cell and eventually the volume of the recirculator.

This theory was adopted for the recirculator mode where the recirculator is guaranteeing a homogeneous mixture and we see that we can stand for four hours before purging one volume.(the nitrogen concentration went up as high as 80 % ! cf. figure 3) By purging one volume the nitrogen concentration drops to 40 % and we end up with a stable regime in which the fuel cell needs to be purged every two hours.

In the dead end mode however, we are obliged to purge approximately every 25 minutes and the amount we have to purge to keep the fuel cell in good shape appears to be approximately 2 times the contained volume of the anodic compartment.

To explain and to prove this amount, we show in figure 5 a sequence of pictures obtained by modelisation showing qualitatively a stratified nitrogen layer leaving the anodic compartment of the fuel cell via the purge valve. This clearly shows that if we purge the contained volume only one time, the single cells in the extremities of the fuel cell stack will continue to accumulate nitrogen, leading to undesirable effects such as single cell extinction. The pictures shown in figure 5 only have a qualitative interest and can not determine the amount of gas to purge.

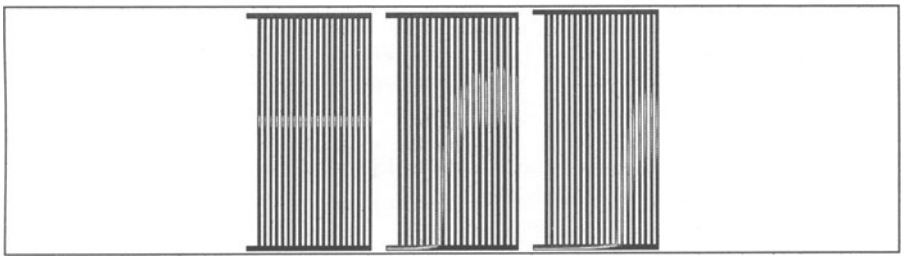

Figure 5 Numerical simulation of an hydrogen purge with a stratified nitrogen layer (dead end mode).
(Colour Blue : Nitrogen ; Red : Hydrogen)

To quantify the amount, we show in figure 6 the voltage rise of the fuel cell in "dead end" mode being purged with consecutive discrete purges (each purge contains 0,7 dm3).

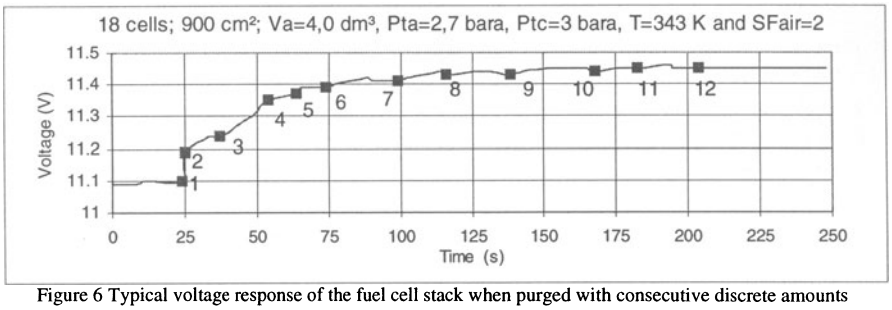

Figure 6 Typical voltage response of the fuel cell stack when purged with consecutive discrete amounts

From this figure we can conclude that for our fuel cell about 12 discrete purges are necessary to bring the performance fully back to the initial value. 12 discrete purges correspond in our case (2,7 bara; 0,7 dm3) to a purge of 12*(2,7-1)*0,7 = 14,3 Ndm3 of gas. The anodic fuel cell compartment of the fuel cell stack has been evaluated at 2,8 liters. Working at 2,7 bara it contains 7,6 Ndm3 of gas.
This leads to the necessity to purge at least every ten minutes 1,9 times the contained volume.

Simple comparison of the "recirculator" and "dead end" mode leads to the conclusion that the hydrogen spill over due to purging is far more important for the "dead end" mode than for the "recirculator"mode :

"dead" end	: every 25 minutes	1,9 volumes
"recirculator"	: every 120 minutes	1,0 volume

In the "dead end" mode, we have to purge roughly 10 times more than in the "recirculator mode". These results hold for our operating mode, i.e. 2,7 bara for the anodic gases and 3,0 bara for the cathodic gases and showed surprisingly hat the fuel cell functions stablely with 70 -80 % of nitrogen in the anodic gases up to nominal currents of 333 A.

Now if it were possible to increase the hydrogen pressure to levels equal to or higher than the air pressure, it can be concluded from fig 2 that in these cases the maximum nitrogen concentration in the anodic compartment will be limited to approximately 65 %. This means that we can operate the fuel cell as long as we like without only one single purge, and that we will have 100 % fuel utilization !

To find the energetical optimum amount for the purges we will have to find the optimum for energy efficiency. The energy efficiency can be expressed by the following equation

$$\eta_{energy} = \left(I \int_0^t U(t)dt \right) / \left(\left(\frac{qit}{nF} + Jp \right) HHV \right) \qquad (9)$$

t	= time between purge	[s]
I	= current	[A]
u(t)	= Voltage evolution as function of time as depicted in fig. 3	[V]
HHV	= Higher Heating value of Hydrogen	[J/mole]
q	= number of single cells in series	[-]
n	= number of electrons transferred in the oxidation reaction	[-]
F	= Faraday constant	[F/eq]
Jp	= Amount of hydrogen purged	[mole]

Jp is the amount of hydrogen purged and has to be put at 1,9 times the volume content of the anodic part of the fuel cell working in "dead end" mode and can be put at once the volume (anodic compartment) for the fuel cell working in a "recirculator" mode.

The results in terms of Energy efficiency are presented in figure 7 for two currents, 200 and 300 A. From Fig. 7 it can be seen that the optimum purging time laps varies with current. The higher the current, the lower the time laps. Next it can be concluded that with the "recirculator mode" the optimum time laps is higher than for the "dead end" mode. However, in the recirculator mode it is not quite necessary to respect this optimum time because the decay in efficiency is only marginal compared to the efficiency decay in the dead end mode. Further it can be concluded that the efficiency in the "recirculator mode" is always higher than in the "dead end mode"

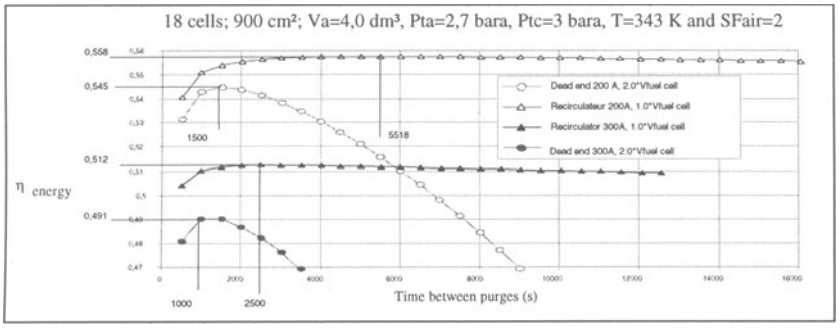

Figure 7 Energy efficiency as function of time between purges for the tested fuel cell

The necessity of purging determines the fuel utilization and the size of the associated catalytic combustor. Fuel efficiency is expressed by the following equation :

$$\eta_{FUEL} = \frac{\frac{qIt}{nF}}{(\frac{qIt}{nF} + Jp)} \qquad (10)$$

The graphical representation of this equation is presented in figure 8. Figures 7 and 8 are resumed in table I.

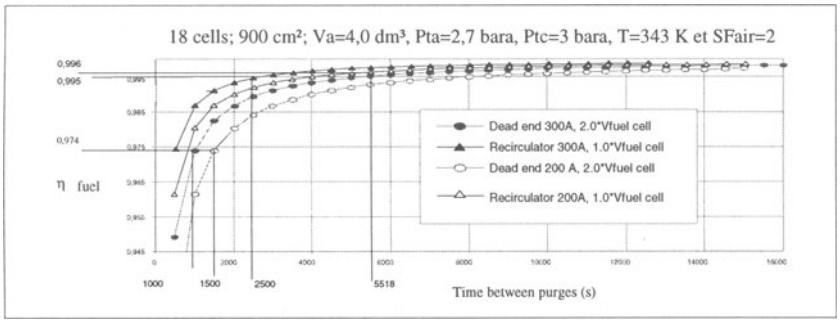

Figure 8 Fuel utilisation as function of time between purges for the tested fuel cell

TABLE 1 Resulting energy and fuel efficiencies of the tested fuel cell stack

	Optimal time (s)		Energy efficiency (%)		Fuel efficiency (%)	
I (A)	With	Without	With	Without	With	Without
200	5518	1500	55.8	54.5	99.6	97.4
300	2500	1000	51.2	49.1	99.5	97.4

From table I it can be concluded that energetically seen, we can gain about 2% in fuel by using a recirculator device.

In the frame of this study we have tested a recirculator device, designed by l' AIR LIQUIDE for the RENAULT LAGUNA which consumes approximately 50 to 100 W_e for a system generating 30 kW_e . So energetically seen the hydrogen recirculator can be justified !

What is more important, is that the stability of the fuel cell with recirculator is far better than without recirculator and that a recirculator permits to operate the fuel cell without purging at all, thus reaching 100 % of fuel utilization efficiency.

6. Conclusion

Nitrogen permeation plays an important role in PEM fuel cell operation strategy.

Maximum obtainable fuel utilization efficiencies in the "dead end" mode are determined by premature single cell extinction due to nitrogen stratification and can be evaluated at 98 % for the fuel cell tested in this study.

A hydrogen recirculator facilitates a fuel cell system to reach 100 % of fuel utilization without losing in energy efficiency. To reach 100 % hydrogen utilization, it is preferable to have a hydrogen pressure higher than the air pressure. This will keep the maximum nitrogen fraction in the anodic compartment as low as possible .

Energetically seen, the benefit of a hydrogen recirculator has been proven in this paper.

It should be born in mind that in this paper only the nitrogen crossover has been analysed and that hydrogen and oxygen cross over may considerably influence the figures quoted here, especially in the low current density regions for which the oxygen and hydrogen concentration at the membrane/electrode interphase reach high values. Preliminary estimations show that fuel efficiency may drop to 80 % for low currents.

7. References

[1] Metkemeyer, R., Thesis Ecole des Mines de Paris, Sophia Antipolis February 1994
[2] Thomas, M., Thesis Univesité "Claude Bernard" Lyon I, Lyon November 1989
[3] Nguyen, T.V., White, R.E., J. Electrochem. Soc., vol. 140, n°8, 1993
[4] Picot, D., Thesis Ecole des Mines de Paris, Sophia Antipolis, to be presented December 1997
[5] Picot, D., Metkemeyer,R., To be presented elsewhere.

ADVANCED CO TOLERANT ANODES FOR POLYMER ELECTROLYTE FUEL CELLS (PEFCs)

F. LUFRANO, E. PASSALACQUA, G. SQUADRITO, A. PATTI
CNR - Institute for Transformation and Storage of Energy
Via Salita S.Lucia sopra Contesse n.39, 98126 S. Lucia - Messina, Italy

Abstract

The experimental results of a study on CO tolerant anodes for PEFC are presented. Anodes prepared with different carbon supported platinum alloys were tested in a 50 cm^2 single cell, using as cathodes low platinum loading (0.1 mg/cm^2) electrodes. The obtained results indicate that the performances are temperature dependent, and they have a remarkable increase in the range from 70 to 90°C. The carbon supported Pt-Ru alloy with atomic ratio 1:1 seems to be the most promising anode catalyst for H_2/CO fuel in PEFCs at low temperature.

1. Introduction

In recent years polymer electrolyte fuel cells (PEFCs) have attracted enormous interest as promising power sources for low or zero emission vehicles. They have many advantages such as quick start-up, stable operation at low temperature, high energy efficiency and high power density.

Actually, the most probable fuel is hydrogen coming from reformed gases, that with proper treatments can contain not less than 100 ppm of CO. However, the presence of few parts per million of CO causes a nearly complete loss of cell performance due to poisoning of platinum catalyst. At the present, specific gas clean-up systems should be used to decrease CO content less than 100 ppm [1, 2], but this would result in additional stages in the fuel cell gas reforming system. For this reason the development of anodes with improved CO tolerance becomes an important goal to render PEFCs more interesting for electrical vehicles [3].

In this paper, the behaviour of anodes prepared with different commercial carbon supported platinum-ruthenium (Pt-Ru) and platinum-tin (Pt-Sn) alloys was evaluated in a PEFC single-cell. The performance of the platinum alloys in presence of hydrogen containing 100 ppm of CO was compared with pure hydrogen and the effects of the cell temperature and anode catalyst composition were analysed.

T. O. Saetre (ed.), Hydrogen Power: Theoretical and Engineering Solutions, 591–596.

2. Experimental

All the electrodes were prepared by a brushing method [4]. For the active layer the electrocatalyst was blended with the ionomer Nafion® by using a 20wt% Pt/Vulcan XC-72 for cathodes and several commercial (purchased by E-TEK) Pt-Ru (by varying the atomic ratio) and Pt-Sn alloys supported on Vulcan XC-72 for the anodes preparation. A platinum loading of 0.1 mg/cm^2 was used for cathodes, while the platinum loading in the anodes catalyst layer was maintained constant at about 0.6 mg/cm^2. The gas diffusion backings consisted of a carbon (Vulcan XC-72) layer containing an hydrophobic agent (Teflon®) brushed on a carbon paper sheet (Toray TGPH090).

The membrane/electrodes assemblies (MEAs) were prepared by hot-pressing the electrodes onto the Nafion® 117 membrane at 130°C. The performance was evaluated in a 50 cm^2 single cell (GlobeTech Inc.) in both H_2/air (H_2 op.) and H_2+100 ppm CO/air (CO op.) operation mode in the temperature range from 70 to 90°C, at fixed absolute pressure of 2.5/3.0 bar for anode and cathode side respectively.

Data extracted from the equilibrium polarisation curves and from time tests at constant cell voltage were used to compare the anode performances.

3. Results and Discussion

At the first, a comparison in pure H_2/air between the Pt-Me/C and Pt/C anodes at different temperatures was carried out and the obtained results were used as reference to evaluate the performance in presence of 100 ppm of CO. The CO tolerance of the different catalysts was evaluated using the voltage loss percentage at a current density of 0.5 A/cm^2 between H_2 op. and CO op., as reported in Tab.1.

TABLE 1. Cell voltage (mV) at 0.5 A/cm^2 current density, for T= 70 and 90°C, and relative voltage loss, obtained for the different Pt alloys.

Anode catalysts	T=70°C			T=90°C		
	H_2/air	H_2+ CO /air	Loss	H_2/air	H_2+ CO /air	Loss
20% Pt/C	640	110	80%	670	200	70%
20% Pt-Ru/C (1:1)	592	391	34%	621	545	12%
20% Pt-Sn/C (3:1)	566	269	52%	584	355	39%
20% Pt-Ru/C (3:1)	630	204	68%	657	476	27%
20% Pt-Ru/C (7:3)	614	140	77%	650	444	32%
30% Pt-Sn/C (3:1)	603	317	47%	610	412	32%
40% Pt-Ru/C (1:1)	649	415	36%	674	611	9%

From the data in Table 1 it seems evident that the performance of Pt-Me anodes in H_2/air is generally lower if compared with Pt/C catalyst, but the cell voltage increases

by increasing the Pt:Ru atomic ratio. The high performance in pure H_2 obtained for 40% Pt-Ru (1:1) electrocatalyst could be attributed to the higher platinum loading in the active layer respect to our standard low platinum loading anode (0.1 mgPt/cm^2) and to a thinner catalyst layer thickness respect to the 20% Pt-Ru anode with the same atomic ratio.

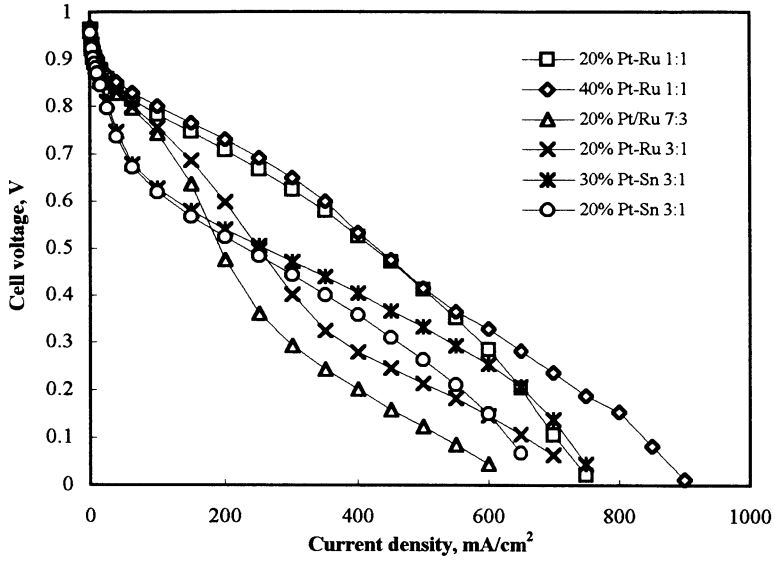

Figure 1. Cell voltage vs. current density in H_2+100 ppm CO/air at 70°C for several Pt-Me/C anodes.

In Fig.1 a comparison between the behaviour of the anode catalysts in presence of 100 ppm of CO at 70°C is shown. Our results indicate that between the different Pt-Ru compositions and Pt-Sn anodes both the two Pt-Ru catalysts (20 and 40 wt%) with atomic ratio 1:1 have the best CO tolerance. The difference between Pt-Ru and Pt-Sn becomes more evident at 90°C, while for the various examined Pt-Ru alloys this difference is reduced by increasing the temperature, as shown in Tab. 1. Besides in the curves for Pt-Ru alloys there is an inflection point corresponding to a cell voltage of about 0.4 V. This inflection point is not observed at 90°C. A similar behaviour was reported from other authors [5, 6].

The steady state performance of the MEAs prepared with CO tolerant anodes was evaluated in a short time test to verify the effect of the poisoning in the time. Tests for several Pt-Me catalysts were carried out by recording the current density at a fixed cell potential of 0.5 V by varying the cell temperature. In Fig. 2 the plot of time-test for the 40 wt% Pt-Ru (1:1) anode is reported. After the introduction of H_2+100ppm CO at 80°C the cell performance decreases quickly and reaches the equilibrium in about 20 minutes and the potential remains constant for 90 min.. At this time the current density

increases as a consequence of a rise in temperature up to 90°C. The replacement of pure H_2 causes a complete recovery of the initial performance in less of an hour.

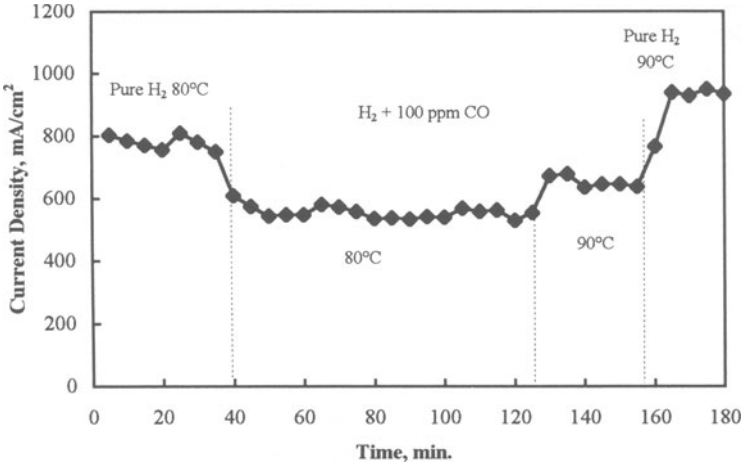

Figure 2. Plot of a time test performed at 80 and 90°C with a 40% Pt-Ru (1:1)/C anode.

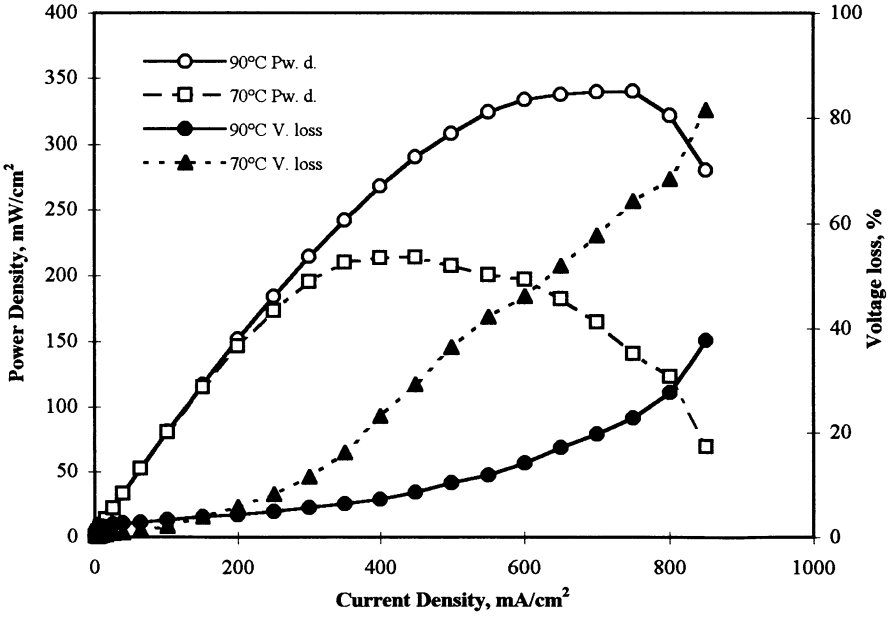

Figure 3. Voltage loss and power density for 40% Pt-Ru(1:1)/C anodes at 70 and 90°C in CO operation.

In Fig. 3 the voltage loss at 70 and 90°C for 40% Pt-Ru (1:1) is reported. As can be seen the decrease in the cell voltage is lower than 20% at current density less than 0.4 and 0.7 A/cm^2 at 70 and 90°C respectively, and is highly dependent on current density. This behaviour could be seen as a consequence of hydrogen consumption that increase the CO coverage of the Pt reaction sites. In the same figure the power density in CO op. at the two investigated temperatures is reported, a power of 305 mW/cm^2 was obtained at 90°C and 0.5 A/cm^2 that render this catalyst promising as CO tolerant anode if compared with platinum catalyst operating in pure H_2.

4. Conclusions

The performance of a PEFC with Pt-Ru and Pt-Sn anode catalysts was evaluated at 70-90 °C in single cell using as fuel H_2 or H_2 containing 100ppm of CO, and air as oxidant. In this low temperatures range Pt-Ru/C and Pt-Sn/C alloys show CO tolerance as compared to Pt/C catalyst.

The Pt-Ru alloy with atomic ratio 1:1 appears to be a promising catalyst for electroxidation of H_2/CO fuel in the investigated temperature range. From experimental results the CO tolerance is enhanced at 90°C, and a power of about 340 mW/cm^2 in H_2 op. and 305 mW/cm^2 in CO op. were obtained at this temperature.

A steady-state cell voltage vs. current density behaviour was reached within the 30 min of operation, after this time the performance becomes stable and the poisoning appears fully reversible.

5. Acknowledgement

This work was financial supported by a contract from the Italian Agency for New Technology, Energy and Environment (ENEA).

6. References

1. Amphlett J. C., Mann R. F. and Peppley B. A.: On board hydrogen purification for steam reformation/PEM fuel cell vehicle power plants, Int. J. Hydrogen Energy **21**(1996), 673-678.
2. Gottesfeld S. and Pafford J.: A new approach to the problem of carbon monoxide poisoning in fuel cells operating at low temperatures, J. Electrochem. Soc. (accelerated brief communication) **35**(1988), 2651-2652.
3. Kawatsu S., Aoyama S. and Iwase M.: PEFC R&D technology at Toyota, 1996 Fuel Cell Seminar, Book of Abstracts, p. 262-265, 17-20 November 1996, Orlando, Florida (USA).

4. Passalacqua E., Lufrano F., Squadrito G., Patti A., Giorgi L.: Optimization of polymer electrolyte fuel cells electrodes, International Conference on Applications of Conducting Polymers: Electrochromics, Supercapacitors and other Devices, Book of Abstracts, p. 82-84, 13-16 April 1997, Rome (Italy).
5. Iannello R., Schmidt V. M., Stimming U., Stumper J. and Wallau A.: CO adsorption and oxidation on Pt and Pt-Ru alloys: dependence on substrate composition, Electrochimica Acta **39**(1994), 1863-1869.
6. Oetjen H.-F., Schmidt V. M., Stimming U. and Trila F.: Performance data of a proton exchange membrane fuel cell using H_2/CO as fuel gas, J. Electrochem. Soc. **143**(1996), 3838-3842.

MATHEMATICAL MODEL OF PEM-FUEL CELL CATALYTIC LAYER

V.Fateev, I.Baranov, A.Sysoev, M.Tsypkin
Professor Doctor Doctor Doctor
HEPTI RRC Kurchatov Institute, Kurchatov sq., Moscow, 123182,
Russia

1. INTRODUCTION

The electrochemical behavior of fuel cell catalytic layers is rather complicated and influenced by many parameters and components of the cell. That is why that optimization of the fuel cell catalytic layer is a very important but complicated problem.

In PEM-fuel cell catalytic layer is based on catalytic particle dispersion in solid polymer electrolyte (SPE) with hydrophobic agent. Such layer has some peculiar properties which are quiet different form the properties of the «traditional» catalytic layers (electrodes) used in liquid solutions. The probability of electric contact between catalytic particles is not equal to 1 and the electronic resistivity may be comparable with ionic one; total porosity of the layer does not quiet determines the active surface area (area of the catalyst-SPE surface) at the fixed pressure as there are pores of two types: «gas» pores - traditional pores which can be filled by gas or water in dependence of their diameter and gas pressure and pores filled with SPE (SPE distribution is not influenced by pressure as strong as water distribution); and active surface may be the function of the distance from current collector, electronic and ionic resistivity also may be the function of the distance (the latter because of water transport). Some other differences also may take place.

2. EXPERIMENT

The experiments were carried out in a standard three-electrode glass cell and in a two compartment cell described in [1] which permitted to investigate catalytic layer in a contact with a gas phase. Also experiments in a PEM-fuel cell with the electrode surface ~ 10 cm2 were done. As SPE the modified membrane MF-4SK was used. The catalytic layers were based on platinum and platinized carbon, colloidal Teflon particles and colloidal solutions of the polymers (same type as in the membrane) with different exchange capacity.

For numerical investigation the theoretical model developed previously [2,3] for electrolyzer catalytic layer, based on percolation theory, Monte Karlo method and approaches of electrochemical kinetics was used as the basis. Taking into account also

T. O. Saetre (ed.), Hydrogen Power: Theoretical and Engineering Solutions, 597–601.

the theory of the porous electrodes [4] a computer software for calculation of the main parameters of the layer was developed.

3. RESULTS AND DISCUSSION

In PEM-fuel cell catalytic layer active catalyst particles (which are in electric contact with current collector and can participate in electrochemical processes) at low concentrations build (fig1) tree-like clusters where «trunks» are mainly responsible for electronic conductivity and the «branches» are responsible for active surface area [3]. In the case of homogeneous nonporous layer the size of clusters is increasing with the growth of catalyst concentration and percolation through the whole layer takes place at catalyst concentration higher then 33% volume when infinite cluster is build. But even up to 50% one can observe «edge effects» on the boarder with current collector and SPE-membrane. The active particle concentration reduction is produced because of cutting small «branches» from the infinite cluster by the membrane boarder. As one can see (fig.2) the active particle distribution is strongly influenced by the particle concentration and «gas» porosity of the layer. It is necessary to underline that at high pores concentration the channels for ionic and electronic transport - SPE/catalyst channels between pores - become so thin (about ten times the catalyst particle size) that «edge effects» on the boarders of these channels with «gas» pores may become significantly more important. In the latter case the reduction of active particle concentration with the distance from current collector becomes very quick as it is shown on fig.2 and must be taken into account.

It is obvious that the active particle concentration determines the active surface area (fig.3). It may provide maximum of the active surface as at the large concentrations the contact between catalyst and SPE is reduced. But in practice only some kind of "saturation" of the active surface area is reached as concentration of catalyst particles higher then 50% vol. is difficult to get. The increase of the «gas» pores concentration mainly reduces the active surface area as results in the decrease of the catalyst /SPE bulk concentration but at high pores concentrations «edge effects» also must be taken into account (fig.3) especially at concentrations lower then percolation limit. The increase of the «gas» porosity also leads to the increase of the IR (Ohmic) loses in the layer. When kinetics limitations are dominant all these factors influence significantly the position of the reaction zone, effective Tafel slopes and total efficiency of the layer.

Using experimental data on active particle concentration, resistivity and active surface area and data obtained with the method described above we calculated the potential and current distribution across the layer and the total current for the «visible» catalytic layer surface.

For catalytic layer parameters simulation the following equations were used:

$$\frac{d^2\varphi_m}{dx^2} = \rho_m(x) * I_0 * S(x) * sh\left(\frac{\alpha z F \eta}{RT}\right) + \frac{1}{\rho_m(x)} * \frac{d\rho_m(x)}{dx} * \frac{d\varphi_m}{dx} \qquad \{1\}$$

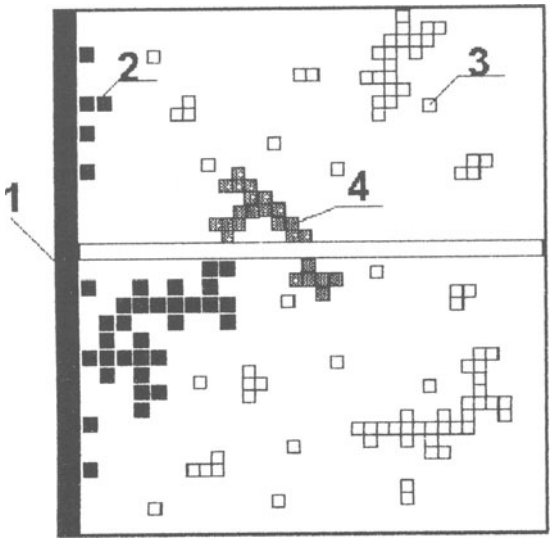

Fig.1. Schematic diagram of the model catalytic layer and characteristic form of clasters: 1 - current collector, 2 - active particle, 3 - nonactive particle, 4 - particle which became nonactive because of pores ('edge effect').

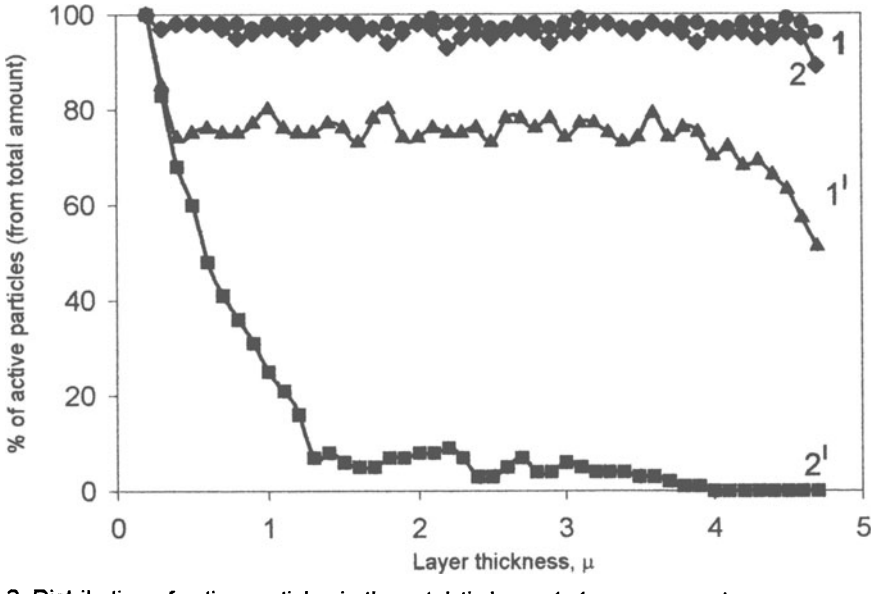

Fig. 2. Distribution of active particles in the catalytic layer: 1, 1 -nonporous layer, 2, 2^{I} -porous layer (60% pores). Concentration of catalyst particles 50 vol.% (1, 2) and 35 vol.% (1^{I}, 2^{I}).

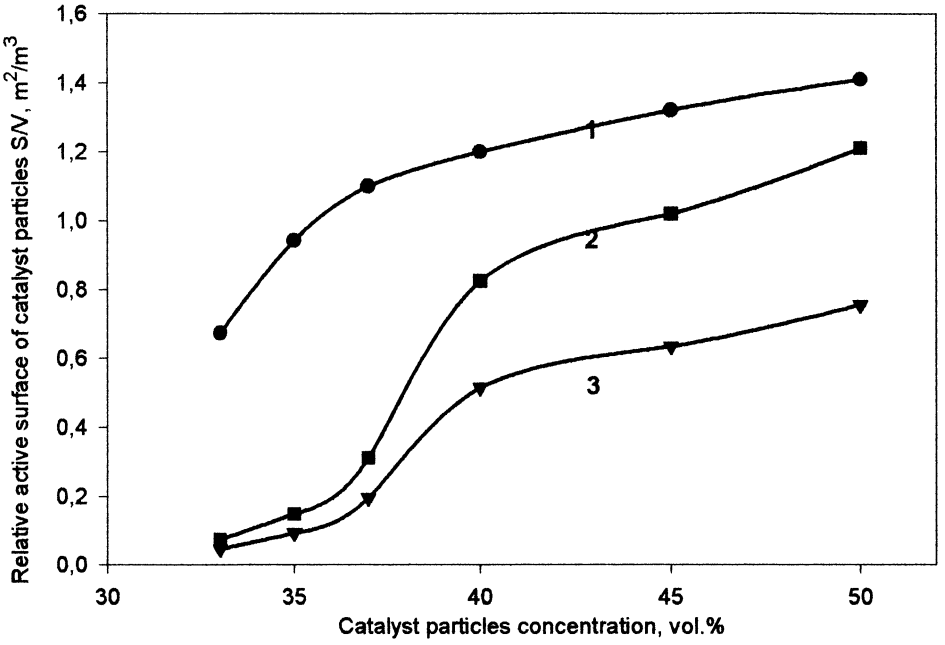

Fig. 3. Dependence of relative active surface from catalyst particles concentration
1 - nonporous layer, 2 - porosity 20%, 3 - porosity 50%.

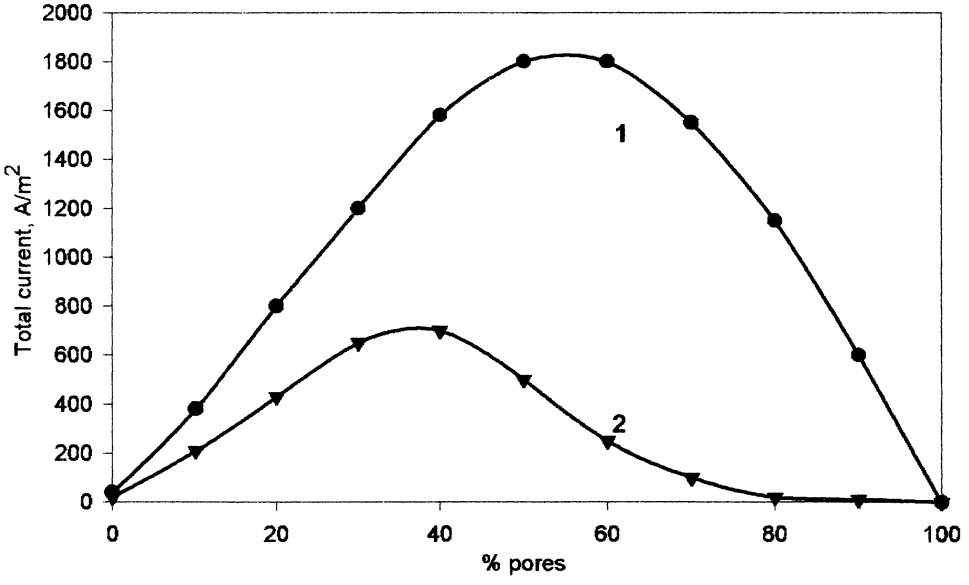

Fig.4. Dependence of total current upon porosity of the layer for different catalyst concentrations. 1 - 50 vol.%, 2 - 35 vol.%.

$$\frac{d^2\varphi_e}{dx^2} = -\rho_e * I_0 * S(x) * sh\left(\frac{\alpha z F \eta}{RT}\right)$$

where: ρ_m, ρ_e - specific resistivity of metal and electrolyte, S - specific catalytic surface (m^2/m^3), I_0 - exchange current density, $\eta = |\varphi_m - \varphi_e|$ - overpotential; φ_m, φ_e - potentials of metal and electrolyte:

Diffusion limitations were taken into account by the method described in [4].

In the case of low «gas» porosity the speed of the electrochemical processes is mostly limited by mass transport of the gas. In this case only the front surface of the catalytic layer takes part in the process and the total current is very low (fig.4). The increase of the «gas» porosity reduces mass transport limitation but because of the active surface area reduction the total current reaches maximum. If the catalyst particle concentration is less then 40% volume the «edge effects» may become so important that maximum on the curve becomes smaller and appears at lower concentrations. In real catalytic layers water may close the «gas» pores and results in total current reduction to the lowest value. Hydrophobic agent for example Teflon obviously helps water removal and «purification» of the «gas» pores but reduces conductivity and active surface. In this case the percolation takes place at higher concentrations. Maximum total current can be reached at lower porosity and catalyst concentration must be close to maximum one (about 50% volume).

So porosity, catalyst and hydrophobic agent concentrations may have rather complicated influence on active surface area and resistivity of the layer and certainly on it's electrochemical parameters.

Comparison with experimental data shows that the model can be used for analysis of the catalytic layer behavior and methods of it's optimization.

REFERENCES

1. Fateev V., Lutikova E., Amadelli R. (in press), Adsorption and oxidation of CO on composite Pt/SPE electrodes, *Russian J. of electrochemistry*.

2. Fateev V., Pakhlova E., Baranov I. et.al., (1996) Mathematical model of SPE electrolyzer catalytic layer, Proc. 11 World Hydrogen Energy Conf., Stuttgart, v.3, 2727- 2731.

3. Baranov I., Fateev V., Sysoev A., Rusanov V. (in press), Numerical stimulation of catalytic layer, *Dokladi Akademii Nauk* (in Russian) .

4. Chizmadjev A.,Markin V., Tarasevich M., Chircov Ju. (1971) *Macrokinetics in porous media*, Nauka, Moscow, pp. 228-233(in Russian) .

HIGH TEMPERATURE PROTON CONDUCTORS

Applications and Materials

TRULS NORBY

Centre for Materials Science, Department of Chemistry,
University of Oslo, Gaustadalleen 21, N-0371 Oslo, Norway

1. Liquid and Solid Electrolytes

Most of us are familiar with the use of electrolytes such as the aqueous sulphuric acid in lead accumulators and the alkaline solutions used for electrolytic production of hydrogen. Alkaline fuel cells (AFC), phosphoric acid fuel cells (PAFC) and molten cabonate fuel cells (MCFC) have been around for a few years. All these examples involve liquid electrolytes (although the liquid can be absorbed in a porous support structure). Cells with *solid* electrolytes may in principle be more compact and sturdy, easier and safer to operate, and less corrosive. Solid electrolytes carrying oxygen or hydrogen ions (or combinations) have particularly broad interest.

Solid oxide fuel cells (SOFC) and related electrolysers and electrochemical reactors are based upon yttria-stabilised zirconia (YSZ) or other oxygen ion conducting ceramics. The high activation energy of oxygen ion migration requires high operation temperatures (typically 800°) for sufficient conductivity, leading to severe degradation problems.

At the other end of the temperature scale we find a number of solid protonic conductors. These contain more or less rigidly bonded water, and many may in fact be seen as mixtures of solid and aqueous phases. The charge carriers are thus protons with varying degrees of hydration (H^+, H_3O^+, $H_5O_2^+$, etc.). Of particular interest are the proton conducting polymers, and the polymer electrolyte fuel cell (PEFC) for vehicles is now rapidly approaching commercialisation.

Polymers and other systems which rely on protonic transport on a network of water are vulnerable to dehydration due for instance to accidental overheating (overload). This leads to irreversible structural and chemical degradation of the electrolyte. As a consequence, polymers must generally be operated below 100°C so that high loads of Pt catalyst are required, and the cells become very expensive. Thus, there is interest in solid proton conductors with higher operating temperatures, i.e. without water.

Acid salts such as the classical proton conductors KH_2PO_4 and $CsHSO_4$ contain no water, only structural protons, but the thermal stability is often only marginally better than for systems with water. Furthermore, the materials are often water soluble and mechanically weak, and practical interest has been limited.

Finally, we have materials without water and nominally without protons at all. They

T. O. Saetre (ed.), Hydrogen Power: Theoretical and Engineering Solutions, 603–608.

contain protons only as randomly distributed defects, dissolved from some hydrogen-containing component in the surrounding atmosphere. These protons are strongly bonded to anions (typically oxygen ions) in the structure, and elevated temperatures are required to overcome the activation energy of proton jumps. Thus the concentration and conductivity of protons may become too low at high temperatures. But note that the structure is retained during removal of protons, such that these materials survive very high temperatures. In the following a few uses of high temperature proton conductors are mentioned, and thereafter the defect chemistry of such materials is summarised.

2. Applications of High Temperature Proton Conductors

2.1. FUEL CELLS

The principle of H_2/air fuel cells is shown in Figure 1 for a number of different charge carriers. The overall reaction produces water on the anode or cathode side, and many charge carriers require circulation of additional components. Only the high temperature H^+-ion conductor produces water at the oxidant side and requires no additional component circulation, alleviating in principle the need to circulate and dry the fuel.

The hydrogen fuel cell has been realised with different liquid and solid electrolytes,

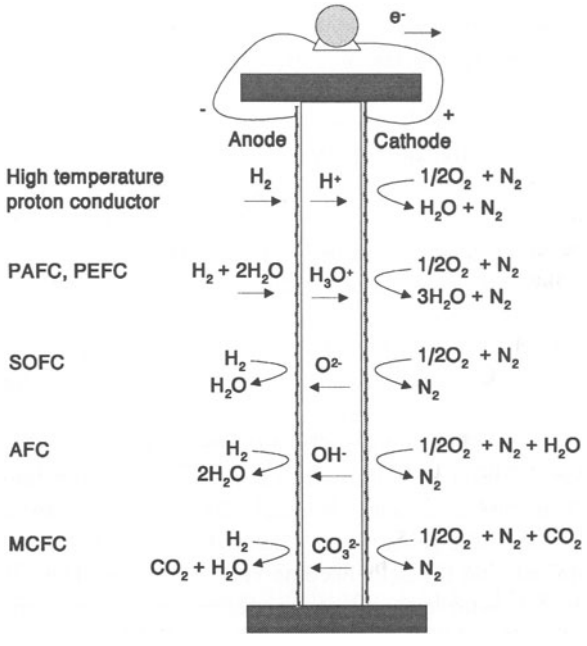

Figure 1. H_2/O_2(air) fuel cells shown for various charge carriers/fuel cell types.

but the flexibility and strength of the thin solid polymer membranes have so far put the PEFC in the lead, particularly for the near-future automobile market.

Iwahara[1] was the first to demonstrate a fuel cell and other applications with a high temperature proton conducting electrolyte; Yb-doped $SrCeO_3$. As an example of recent development, Du and Nowick[2], has demonstrated a laboratory fuel cell operating at 600°C with the new $Ba_3Ca_{1.18}Nb_{1.82}O_{9-d}$ proton conducting electrolyte. These demonstrations yield typically up to a few hundred mW/cm^2, but are only tested in small single cells. Laboratory cells with $BaCeO_3$-based electrolytes have reached higher power densities, but at temperatures where this electrolyte is probably mainly an oxygen ion conductor. It is expected that high temperature proton conductors can be equipped with electrodes which are less expensive and more tolerant to poisons and carbon containing fuels than those used in PEFCs. Unlike oxygen ion conductors, a proton conductor can in general not be used to fully oxidise a carbon-containing fuel. In this sense the mixed proton-oxygen ion conductivity of e.g. $BaCeO_3$ may be beneficial. Also for the hydrogen fuel cell it may in practice be necessary to take advantage of a minor oxygen ion conductivity to produce some water at the anode side to prevent destructively reducing conditions (although the fuel then need circulaton).

2.2. WATER VAPOUR ELECTROLYSIS

High temperature proton conductors can be used to electrolyse water vapour. However, electrolysis with aqueous electrolytes is proven technology, and solid electrolytes may not be competitive. Still, one may envisage *in situ* electrolysis of water vapour for well-controlled and safe delivery of hydrogen directly into high temperature hydrogenation processes.

2.3. ELECTROCHEMICAL REACTORS

In an electrochemical reactor we are interested in the chemical products, while electrical energy may be spent or gained in the process. With oxygen ion conductors one may, for instance, envisage partial oxidation of methane into syngas or higher hydrocarbons, e.g.:

$$CH_4 + O^{2-} = CO + 2H_2 + 2e^- \quad (1)$$

$$2CH_4 + O^{2-} = C_2H_6 + H_2O + 2e^- \quad (2)$$

The promises of the latter type of electrochemical processes have triggered many projects around the world in the last decade, but the results have been disappointing.

With proton conductors one may envisage related processes, such as dehydrogenation of hydrocarbons. The activation and selective oxidation of methane is difficult, and better results have been reached with dehydrogenation of ethane. For instance, Iwahara et al.[3] have reported the operation of a lab-scale fuel cell and a dehydrogenation pump running on C_2H_6, using a $SrCeO_3$-based electrolyte with Pt electrodes, according to the respective overall reactions

$$C_2H_6 + 1/2\ O_2 = C_2H_4 + H_2O \quad (3)$$
$$C_2H_6 = C_2H_4 + H_2 \quad (4)$$

Proton conductors may also be used for hydrogenation. While this in most cases might be performed more easily by simply mixing in hydrogen and using a proper catalyst, the use of a proton conducting membrane may allow fine dosing and electrocatalytic control of selectivity. Additionally, using electrolysis of water vapour as hydrogen source may alleviate the need for hydrogen handling.

The use of proton conducting electrolytes can even be envisaged in oxygenation processes: Water vapour may be added to the reactant and hydrogen may be extracted through the electrolyte in fuel cell or pumping mode. The water, being electrochemically stripped of protons and electrons, leaves adsorbed and activated oxygen species which may oxidise hydrocarbon fuels in catalytically specific ways.

2.4. CHEMICAL REACTORS AND FILTERS

There is increasing interest in semipermeable ceramic membranes, where, for instance, a high oxygen ion conductivity allows efficient and selective transport of oxygen, while the necessary countercurrent of electrons takes place in the same material by a high electronic conductivity without the need for electrodes or external circuitry[4]. In this way it is, for instance, possible to extract ultrapure oxygen from air by mechanical pumping or to provide pure oxygen from air directly to a reagent which undergoes oxidation. One avoids handling pure oxygen and the separation of nitrogen from the product. For instance, the production of synthesis gas by this method according to the reaction

$$CH_4 + 1/2\ O_2 = CO + 2H_2 \quad (5)$$

is promising. In comparison, the existence and application of mixed protonic-electronic conductors has hardly been investigated. If useful mixed protonic-electronic conductors emerge they may compete with Pd membranes and nanoporous filters.

2.5. SENSORS

For sensing hydrogen or humidity at high temperatures, we can use the voltage over a high temperature proton conductor in contact with the probed system and a reference system. A sensor with In-doped $CaZrO_3$ as electrolyte is now commercialised for measuring the concentration of hydrogen in molten metal[5]. There are markets for *in situ* water vapour sensors for industrial ovens and reactors. Improved pH-meters and pH-meters for high temperatures and aggressive media represent other challenges.

3. Defect Chemistry of High Temperature Proton Conductors

3.1. OXIDES

In the presence of water vapour, there is a non-zero equilibrium concentration of protons in any oxide. The protons are bonded to oxygen ions, forming OH^- ion defects. The protons move mainly by jumping between relatively stationary oxygen ions. The activation energy for the jump strongly depends on the oxygen-oxygen-distance, and an overlap between the electron clouds of the two oxygen ions is necessary to facilitate proton transfer. The lowest effective activation energies for proton migration, around 0.5 eV, are found among perovskite-related oxides such as $BaCeO_3$, $SrZrO_3$, $Ba_3CaNb_2O_9$, and $Ba_2YSnO_{5.5}$[6]. The large polarisable alkali earth cations give wider lattices, but also larger oxygen vibration amplitudes and hence temporarily shorter O-O distances.

High temperature proton conducting oxides are usually acceptor doped; protons dissolve to compensate the acceptors at the cost of oxygen vacancies:

$$H_2O(g) + V_O + O_O^{2-} = 2OH_O^- \quad (6)$$

The high energy of oxygen vacancies makes this reaction exothermic. At high temperatures it is thus driven to the left and the acceptors are compensated by oxygen vacancies (while the proton concentration increases with decreasing temperature). At sufficiently low temperatures protons attain a constant concentration compensating the acceptors, whereby oxygen vacancies become minority defects. Thus, as an example, Yb-doped $SrCeO_3$ contains oxygen vacancies at high temperatures and under dry conditions and has the nominal formula $SrCe_{1-x}Yb_xO_{3-x/2}$. At reduced temperatures and in wet atmospheres the material takes up water and becomes $SrCe_{1-x}Yb_xO_{3-x}(OH)_x$.

The transition temperature between dominance of protons or oxygen vacancies is dependent on $p(H_2O)$, acceptor level, and the thermodynamics of reaction (6). Clearly, we need to develop materials which hold protons to high temperatures, i.e., which have high negative enthalpies of reaction (6). It has been suggested that the enthalpy, through the annihilation of the oxygen vacancy, should be related to the stability of the oxide. Larring and Norby[7] have shown that this holds for rare earth oxides: The enthalpy becomes more negative with increasing enthalpy of formation of the oxide as well as with the packing density. However, this trend is broken when we go to other classes of oxides, it has been proposed that the basicity of the oxide is involved through the introduction of the two protons[6].

All in all, the development of proton conducting oxides following the above principles requires a high solubility of an acceptor dopant, a stable oxide with little tendency of formation of oxygen vacancies, and a high basicity. In addition there is a need for large, polarisable cations, to obtain high mobility. It appears that oxides with large structural oxygen deficiencies such as brownmillerites and certain complex perovskites (e.g. $Ba_2YSnO_{5.5}$) may be alternatives to ordinary acceptor-doping.

3.2. NON-OXIDE HIGH TEMPERATURE PROTON CONDUCTORS

The difficulties in finding the optimum oxide encourage investigation of other classes of materials. Phosphates are fairly basic and may support uptake of defect protons at elevated temperatures. β-$Ca(PO_3)_2$ has been demonstrated as a proton conducting electrolyte for water vapour sensors at high temperatures[8], and recently Sr-substituted $LaPO_4$ was shown to be a modestly good proton conductor up to approx. 800°C[9]. There are reports on proton conductivity also in a number of alkali metal oxyacid salts such as Li_2SO_4, K_3PO_4, and $RbNO_3$, all nominally without structural protons. The transport in these systems can be increased by dispersing insulating second phases such as alumina, and application in lab-scale fuel cells has been demonstrated[10].

4. Concluding Remarks

Solid proton conducting electrolytes have potential advantages for use in fuel cells and reactors for hydrogen exchange processes, especially if materials can be developed which operate in the intermediate temperature range (between the 100°C of the PEFC and the 800°C of the SOFC). Increased understanding of dissolution and transport of protons in oxides is leading to development of new oxides with better proton conduction, with fine balance between the demands for concentration and mobility. There are furthermore many classes of oxides and non-oxides still waiting to be examined with respect to dissolution and transport of protons.

References

1. Iwahara, H.: High temperature proton conducting oxides and their applications to solid electrolyte fuel cells and steam electrolysers for hydrogen production, *Solid State Ionics*, **28-30** (1988) 573-578.
2. Du, Y. and Nowick, A.S.: Galvanic cell measurements on a fast proton conducting complex perovskite electrolyte, *Solid State Ionics*, **91** (1996) 85-91.
3. Iwahara, H., Esaka, T., Uchida, H., Yamauchi, T. and Ogaki, K.: High temperature type protonic conductor based on $SrCeO_3$ and its application to the extraction of hydrogen gas, *Solid State Ionics*, **18-19** (1986) 1003-1007.
4. Mazanec, T.J.: Get your O_2's, *Electrochem. Soc. Interface*, **W96** (1996) 46-49.
5. Yajima, T., Koide, K., Takai, H., Fukatsu, N. and Iwahara, H.: Application of hydrogen sensor using proton conductive ceramics as solid electrolyte to aluminium casting industries, *Solid State Ionics*, **79** (1995) 333-337.
6. Kreuer, K.-D.: On the development of proton conducting materials for technological applications, *Solid State Ionics*, **97** (1997) 1-15.
7. Larring, Y. and Norby, T.: The equilibrium between oxygen vacancies, water vapour and protons in rare earth oxides, *Solid State Ionics*, **97** (1997) 523-528.
8. Greenblatt, M., Tsai, P.P., Kodama, T. and Tanase, S.: Humidity sensor with sintered β-$Ca(PO_3)_2$ for high temperature use, *Solid State Ionics*, **40-41** (1990) 444-447.
9. Norby, T. and Christiansen, N.: Proton conduction in Ca- and Sr-substituted $LaPO_4$, *Solid State Ionics*, **77** (1995) 240-243.
10. Zhu, B. and Mellander, B.-E.: Novel proton conducting ceramics for solid state fuel cells, *Electrochem. Soc. Proc.*, **93-4** (1993) 156-167.

ETHANOL FUELLED MOLTEN CARBONATE FUEL CELL: TECHNICAL FEASIBILITY EVALUATION (RESEARCH AND DEVELOPMENT)

S. FRENI*, G. MAGGIO*, S. CAVALLARO**
* *Istituto CNR-TAE, via Salita S. Lucia sopra Contesse 5, 98126 Santa Lucia (ME), Italy.*
** *Dip. Chimica Industriale, Università di Messina, P.O. Box 29, 98166 Sant'Agata di Messina, Messina, Italy.*

1. Introduction

The molten carbonate fuel cell (MCFC) technology applied to the field of electricity production is under an impressive development, but these cells, like other kinds, must employ only pure hydrogen as fuel. At present, the methane is indicated as one of the main fuels for MCFCs, even if the world fuel economy goes to meet also interest on the utilisation of oxygenated products, like alcohols, that can store and transfer H_2 as non-polluting fuel with a high heat power.

Whatever is the fuel, the first step of the process is the hydrogen production by a suitable catalytic reactor placed inside (internal configuration) or outside (external configuration) the apparatus. If the internal configuration is adopted, two ways are further practicable: direct (into anodic housing) or indirect (out of anodic housing). Each solution must take into account the temperature, the pressure and the catalyst stability, together with the fuel availability and the by-product market.

This paper presents a wide thermodynamic evaluation based on a mathematical model that simulates the behaviour of an MCFC. Equilibrium relationships and mass balances in terms of molar flows have been derived both for external and internal (direct or indirect) configuration. The results allow useful comparison between the examined configurations and provide a means of evaluation of the feasibility of such systems.

2. Modelling development

The ethanol steam-reforming can be described by the following scheme of reactions:

$$C_2H_5OH + H_2O \rightleftharpoons 4\,H_2 + 2\,CO \quad (1),$$

$$CO + H_2O \rightleftharpoons H_2 + CO_2 \quad (2),$$

$$CO + 3\,H_2 \rightleftharpoons CH_4 + H_2O \quad (3),$$

T. O. Saetre (ed.), Hydrogen Power: Theoretical and Engineering Solutions, 609–614.

whose thermodynamic equilibrium is mathematically represented by a system of non-linear equations

$$K_1 = \frac{x_{CO}^{2}\, x_{H2}^{4}}{x_{EtOH}\, x_{H2O}}\, P^4 \quad (4), \qquad K_2 = \frac{x_{CO2}\, x_{H2}}{x_{CO}\, x_{H2O}} \quad (5), \qquad K_3 = \frac{x_{CH4}\, x_{H2O}^{3}}{x_{CO}\, x_{H2}^{3}}\, P^{-2} \quad (6),$$

$$n_{EtOH} = n_{EtOH}^{in} - n_1 \quad (7), \qquad n_{H2} = 4n_1 + n_2 - 3n_3 - n_w \quad (8), \qquad n_{CO2} = n_2 + n_w \quad (9),$$

$$n_{CO} = 2n_1 - n_2 - n_3 \quad (10), \qquad n_{CH4} = n_3 \quad (11), \qquad n_{H2O} = n_{H2O}^{in} - n_1 - n_2 + n_3 + n_w \quad (12),$$

where the K_i's are the equilibrium constants, x_i's the molar fractions of the component gases, P the total pressure, n_i's the outlet flows of the gases, n_i^{in}'s the inlet flows and $n_{1,2,3}$ the converted flows associated to the reactions (1)-(3).

The term n_w is the steam molar flow produced by the cell electrochemical reaction, which can be calculated by the Faraday's equation.

Once specified the operative conditions (temperature, pressure and inlet gas flows), the outlet gas compositions relative to the anodic compartment of the cell have been determined by solving the equations (4)-(12) with an iterative method, which need an initial approximation for the reaction conversions.

The cell potential is given by the following relation:

$$V = E - (\mu_a + \mu_c) - J r \qquad (13),$$

where E is the reversible potential at open circuit voltage (derived from the Nernst's equation), μ_a and μ_c the anodic and cathodic overpotentials (derived from empirical relationships), J the cell current density and r the specific internal cell resistance.

The electrical and thermal power densities have been calculated, respectively, as

$$W_{el} = J\, V \qquad (14), \qquad W_{th} = W_{cell} + W_{comb} + W_{lat} + \frac{1}{S}\sum_{i=1}^{3} n_i\, (-\Delta H_i) \qquad (15),$$

where W_{cell} is the power density due to the electrochemical heat released by the cell and to the ohmic resistance, W_{comb} that due to the combustion of the unreacted gases (ethanol, methane, hydrogen and carbon monoxide), W_{lat} that due to the latent heats of ethanol and steam, S is the cell surface and the ΔH_i's are the enthalpies associated to the reactions (1)-(3).

The energetic efficiency of the system has also been determined as

$$\eta = \frac{W_{el} + f\, W_{th}}{W_{fuel}} \qquad (16),$$

where W_{fuel} is the power density due to the combustion of the inlet fuel (ethanol) and f the fraction of thermal power density recoverable. In particular, when f=0 the electrical efficiency is obtained.

3. Catalysts

The steam reforming reaction of the ethanol is catalysed by the presence of noble metals based catalysts, like Pt, Pd, Ir, Rh or Ru, or oxides of Cr, Mo, Co or Ni supported on ceramic materials (TiO_2, $CaO\text{-}Al_2O_3$, MgO, SiO_2, $\alpha\text{-}Al_2O_3$) [1].

The supported oxide catalysts were prepared by coprecipitation and impregnation methods. Among these catalysts, the $Ni/\alpha\text{-}Al_2O_3$ is preferred because it presents an acceptable cost and good catalyst activity. The same catalyst, supported on Si or silica/alumina/calcium oxide mixtures shows a good catalyst activity even if its mechanical properties degrade when it works at high pressure. For these catalysts it is important to modify the acidic sites of the support because they enhances the undesirable cracking reaction. This goal can be obtained by adding small amount of basic oxide, like K_2O, or supporting the Ni on MgO. An alternative way to perform the ethanol steam reforming is represented by the catalysed Pd membranes. The Pd membrane allows a continuous transfer of the hydrogen from the reactor that moves the reaction equilibrium towards the formation of further hydrogen, with yields higher than that foreseen by the thermodynamic equilibrium.

4. Results

As first, the cell voltage as a function of the current density has been determined (Tab.1) at fixed pressure (P=1 atm) and variable cell temperature. The temperatures have been chosen between a range of values (873, 923 and 973 K) that includes those usually considered as standard operative conditions for MCFCs. The influence of the temperature appears to be consistent because this parameter is strictly correlated to the partial pressure of the hydrogen generated by the reforming. In fact, the percentage of hydrogen lowers from 58.9% at 973 K to 46.8% at 873 K; at the meantime, the open circuit voltage (OCV) of the cell drops from 1115 to 1083 mV.

Fig. 1 gives the variations of the H_2 and CH_4 contents in the anodic gas vs. the temperatures at fixed values of current densities (0, 50, 100, 150, 200 and 250 mA/cm^2). In Tab.2, the outlet anodic gas composition at reference operative conditions are reported in details. From these results, it is evident that the production of CH_4 associated to the reaction (3) is not negligible mainly at low temperature. Thus, at OCV conditions, its percentage in the outlet anodic gas is 12.1% at 873 K and decreases until 6.4% at 923 K and 2.6% at 973 K. Besides, the amount of CH_4 slightly decreases when the current density increases. The reaction (1), which regulates the CO production, is favoured by the high temperature. The behaviours of the H_2O and CO_2 concentrations in the exhaust anodic gas are similar, because both are products of the cell electrochemical activity. At high current densities they are the main components of the exhaust gases. The percentage of hydrogen produced by the ethanol reforming is significantly influenced by the temperature.

TABLE 1. Cell voltage vs. current density at various T values and P=1 atm

Current density	*Cell voltage (mV)*		
(mA/cm²)	*at T=873 K*	*at T=923 K*	*at T=973 K*
0	1082.7	1099.9	1115.5
25	1009.9	1022.5	1025.7
50	938.4	957.4	958.7
75	868.3	893.9	896.5
100	797.4	829.9	835.5
125	724.7	764.1	773.5
150	649.3	695.6	709.2
170	586.6	638.3	655.3
190	521.4	578.0	598.4
200	487.6	546.4	568.4
220	416.7	479.4	504.6
240	338.5	404.2	432.1
260	240.2	307.1	336.6

The different hydrogen content practically results in the possibility to have higher current density that allows the reduction of the electrode surface and improves the system weight factor, defined as the ratio between the stack weight and the surface of the electrodes [2].

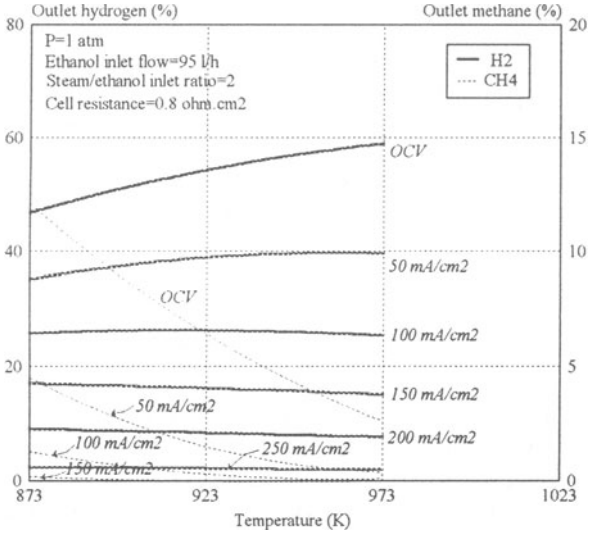

Figure 1. Outlet H_2 and CH_4 percentage vs. temperature at fixed current densities.

The degree of the system reliability to produce electricity clearly appears from the analysis of the curves reported in Fig.2 that shows the theoretical behaviour of the electrical power, of the thermal power and of the electrical efficiency released by the cell as function of the current density, at standard conditions.

TABLE 2. Outlet anodic gas composition vs. current density at T=923 K and P=1 atm

Current density	*Gas composition (%)*				
(mA/cm²)	CH_4	CO	CO_2	H_2	H_2O
0	6.4	16.8	9.1	54.3	13.4
25	3.2	17.8	15.0	46.2	17.8
50	1.5	17.2	20.7	38.9	21.7
75	0.7	15.8	26.3	32.3	24.9
100	0.3	13.9	31.8	26.3	27.7
125	0.1	11.8	36.9	21.0	30.2
150	0	9.7	41.8	16.2	32.3
170	0	8.0	45.5	12.8	33.7
190	0	6.3	49.0	9.8	34.9
200	0	5.5	50.7	8.4	35.4
220	0	3.9	53.9	5.7	36.5
240	0	2.4	57.0	3.4	37.2
260	0	0.9	59.9	1.2	38.0

Thus, the electrical power density increases with the current density, reaching 110 mW/cm^2 at 190 mA/cm^2, but this value is limited in the region characterised by high values of current density because of a lack of hydrogen. The thermal power density was calculated for f =0.5, that corresponds to the condition in which 50% of the waste energy (uncombusted fuel and sensible heat) is recovered. It shows a trend opposite to that of electrical power density, with a minimum of 107 mW/cm^2 at 200 mA/cm^2. The trend of the curve of electrical efficiency is similar to that of the electrical power density and presents appreciable values at intermediate current densities (34.2% at 190 mA/cm^2). At last, the performance of an ethanol fuelled MCFC has been compared with that of a methane MCFC, operating under similar conditions. The results of this comparison are shown in Fig. 3, where the polarization curves for both systems are reported. From these curves appears that the cell voltage results higher in the ethanol cell (+26 mV at OCV, +92 mV at 260 mA/cm^2).

5. Conclusions

The theoretical calculations demonstrated the feasibility of the studied system. Particularly, the main correlation between the operative parameters and the efficiency of the system has been explored. The main limitation of this system is the heavy influence that a temperature lowering exerts on the hydrogen production and on the electrode kinetics. For this reason, the electrical power released by the cell is limited in the region characterised by high values of current density. Otherwise, several interesting findings, like the full conversion of the raw fuel or the high electrical efficiency obtainable (34.2% at 923 K), encourage to continue the study of the applications of these systems. In this sense, the selection of a system operating at intermediate temperature (923 K), represents an interesting solution that yields acceptable efficiency and a level of problems well know in the present state of art.

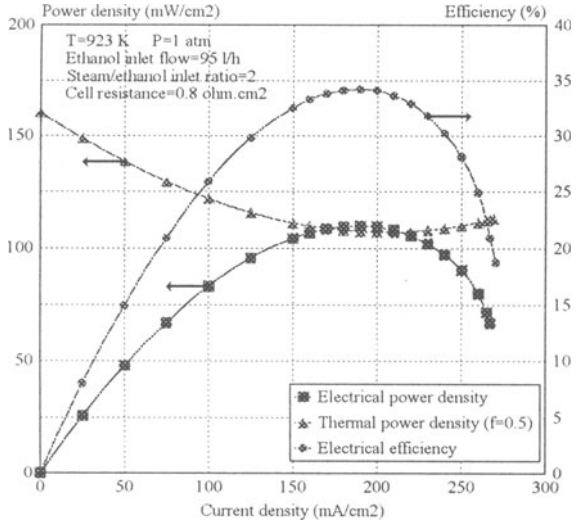

Figure 2. Power densities and electrical efficiency vs. current density.

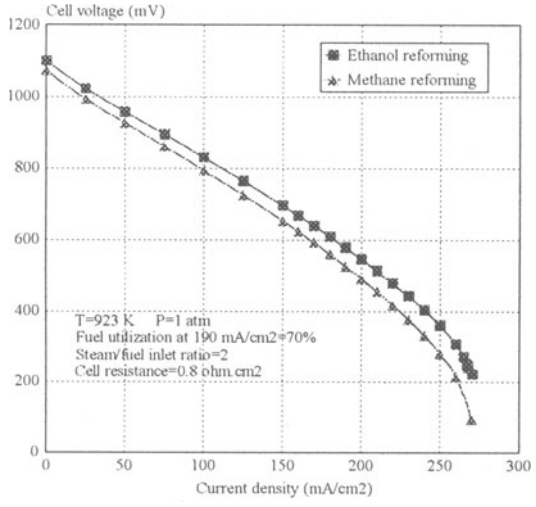

Figure 3. Comparison between cell voltages of ethanol and methane DIR-MCFCs.

6. References

1. Cavallaro, S. and Freni, S. (1996) Ethanol steam reforming in a molten carbonate fuel cell. A preliminary kinetic investigation, *Int. J. Hydrogen Energy*, **21-6**, 465-469.
2. Kinoshita, K. and Landgrebe, A.R. (1994) Analysis of power and energy for fuel cell systems, *J. of Power Sources*, **47**, 159-175.

COMBINATIONS OF CONCENTRATION AND STRAIN GRADIENT HYDROGEN DIFFUSION FACTORS IN PALLADIUM ALLOY MEMBRANES

F A LEWIS*, R V BUCUR**, X Q TONG†, Y SAKAMOTO†† and K KANDASAMY‡

* *School of Chemistry, Queen's Univ., Belfast BT9 5AG, N. Ireland*
** *Dept Inorganic Chemistry, Univ. Uppsala, S-75121 Uppsala, Sweden*
† *Dept of Chemistry, Univ. of Southampton, SQ17 1BJ, England*
†† *Dept of Mater. Science, Nagasaki University, Nagasaki 852, Japan*
‡ *Dept of Physics, Univ. of Jaffna, Jaffna, Sri Lanka*

Abstract

Utilisations of palladium and palladium alloys as membranes for hydrogen permeation have been subjects of continuing academic and technological interest. From both standpoints, certain membranes of the palladium-platinum alloy series have been particular subjects of several studies in more recent years.

Such recent series of studies have illustrated some special advantages of certain Pd-Pt alloys in providing experimental evidence of general needs of appreciation that developments of elastic strain gradients arising from lattice expansions (and contractions) produced by hydrogen entry into (and removal from) interstitial lattice sites — should be considered in combination with reliable knowledge of the pressure-composition (p-c(n)) - temperature relationships of palladium and palladium alloys in considerations of hydrogen diffusion problems.

Further, in particular, a body of results, obtained with $Pd_{81}Pt_{19}$, and $Pd_{77}Ag_{23}$ and Pd membranes, has also drawn attention to requirements for very serious considerations also to be given to concurrent time dependent developments of lattice strain gradients in conjunction with the hydrogen concentration gradients, in regard to estimations of hydrogen diffusion coefficients, D_H, including dependencies of D_H on the hydrogen contents of the membranes.

Gorsky Effects

In regard to general principles of diffusion processes, attention would seem initially to have been drawn by studies of Gorsky [1,2] to needs in conjunction with purely 'Fickian' concentration gradient considerations — for attention also to be given to possibilities of simultaneous lattice expansive strain influences arising from the diffusing species themselves.

T. O. Saetre (ed.), Hydrogen Power: Theoretical and Engineering Solutions, 615–620.

In particular reference to developments in the knowledge of permeation processes within elastic media over the past decade, studies of hydrogen permeation within membranes of palladium and selected "solid solution" alloys of palladium with platinum, silver and cerium, have provided convincing demonstrations of effects of such combinations of concentration and strain (stress) gradient operative influences [3-8]. Continuing development of understanding of these and other allied hydrogen diffusion phenomena problems, has stemmed from a wide range of observations of the initially rather unusual features [7] that had soon been descriptively classified as "Uphill Hydrogen Diffusion Effects" [8-17].

Uphill hydrogen diffusion effects

In the experimental circumstances of the initially "Uphill" hydrogen gas pressure change observations [7,8] hydrogen diffusion membranes were of $Pd_{81}Pt_{19}$ alloy composition in the form of tubes (75 mm long, 8mm internal diameter and 0.25 mm membrane wall thickness, δ) with a closed rounded lower end and with the upper end alternatively connected to vacuum and to internal hydrogen gas phase pressure measurement gauges or, eventually, other facilities [3,4].

In many studies, it has been a thermodynamic hydrogen-chemical-potential conversion requirement, that both external and internal tube membrane surfaces have been coated with a "hydrogen chemical potential transfer medium" such as palladium black, for purposes of catalytically effective equilibration of surface processes [3-10] involving

$$H^+ + e \Leftrightarrow \underset{*}{H}\ (ads) \qquad (1)$$

and

$$\underset{*}{H}(ads) + \underset{*}{H}(ads) \Leftrightarrow H_2 \qquad (2)$$

Outline descriptions of experimental observations and subsequent interpretations related to "Uphill Effects" have been broadly characterised and figuratively illustrated in Figures 1 and 2.

Breakthough Times

In Figure 1 examples of initial (and as closely similar, experimentally, as possible [7]) values of quasi-static hydrogen gas pressures p_A and p_B here represented as being initially present within tubular membranes of $Pd_{81}Pt_{19}$ [3-8,17,18], Pd [9,10] and $Pd_{73}Ag_{27}$ [11-15] — where p_A and p_B are equivalent, in turn, through p-c(n) - T relationships [3,4,7,8] to closely similar values of membrane wall hydrogen contents, $n_A \approx n_B$ (where the symbol n [7,8] has been adopted to represent hydrogen content and n = H/M (atomic ratio).

In Figure 1 the subsequent time dependent changes of hydrogen gas pressures within the tubular membranes have been produced by alternative means of increases of the hydrogen contents of *outer* surfaces, either: (i) by cathodisation [3-17] at times

indicated by p_A, or, (ii) by external hydrogen gas pressure [3-6,8,11-18] at times corresponding to p_B.

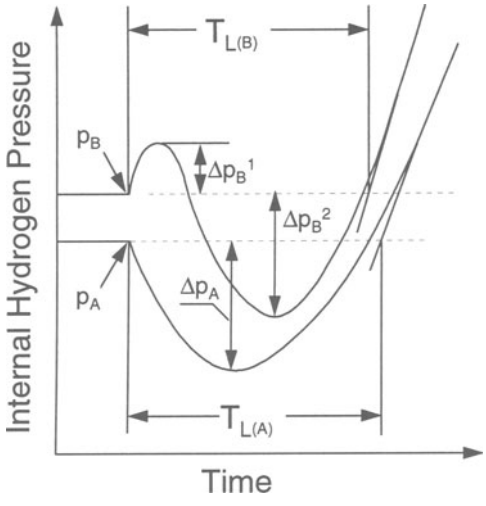

Figure 1 Comparisons of time dependent changes of hydrogen pressures within tubular membranes, following as closely as possible similar increases of hydrogen contents of external surfaces - either by electrolysis (lower curve) or by external hydrogen gas pressure (upper curve) from closely similar initial quasi static hydrogen pressures p_A and p_B respectively.

In extension of initial broadly-proposed explanations [7,8] there has now been very substantial further supporting evidence [3-5,9-12,16-18], that such significant variations in values of breakthrough times and their magnitude-dependencies on n_A or n_B were consequences of inadequate allowance being included for conjoint permeation rate contributions associated with Gorsky Effect migrations of hydrogen interstitials induced by elastic lattice strain gradients produced in the course of the overall lattice expansive processes involved [3-6]. Theoretical calculations of relative contributions of concentration and strain gradient components to overall diffusion flux $J_H(n)$, have been subjects of recent correlations with appropriate experimental data [19-23].

Permeation Process Features

In the case of the upper curve in Figure 1 originating at p_B, the first *initial increase* of pressure up to a maximum at Δp_B^1, has been satisfactorily associated [11,12,18] with initial preferred migration of hydrogen interstitials towards the inner membrane wall surface, produced by the mechanically generated lattice strain gradient resulting from abrupt increases of the external hydrogen gas pressures at p_B.

Series of further studies with tubular membranes of $Pd_{81}Pt_{19}$ [16,17], $Pd_{77}Ag_{23}$ [11-13] and solely Pd [9,10], have consistently interpreted the periods of *decreasing*

internal pressures for both curves, over $\Delta p_B{}^2$ and Δp_A respectively, in terms of initial conclusions [3-5,7] of uphill diffusion of hydrogen from inner surface regions towards the lattice expanding hydrogen entry regions.

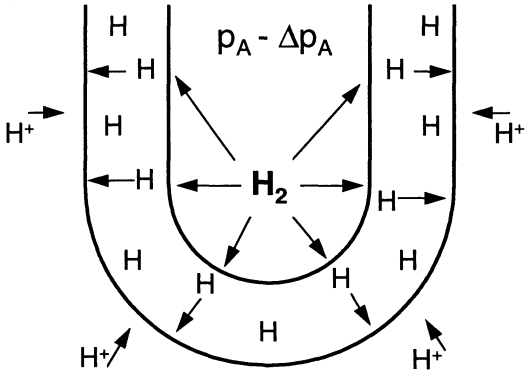

Figure 2 Representations of directions of hydrogen transfers during hydrogen permeation stages corresponding to the lower curve in Figure 1.

Hydrogen Migration Equilibria: Diffusion Parameters

In Figure 2, the "Uphill" transfer within the membrane wall of hydrogen interstitials from near to the inner surface towards the outer surface regions (near to initial hydrogen entry) is being represented (assuming conditions of highly surface active catalytic conditions [3-6]) as being compensated continuously by *entry through* the inner surface of thermodynamically equivalent numbers of surface hydrogen atoms that are being steadily contributed from hydrogen molecules already present in the interior tube volume. These secondary kinetic factors involving surface processes can clearly be expected to have influences on the conditions of final overall equilibria or in steady-state processes.

Effects on Estimations of Diffusion Parameters

Comparisons of the two curves in Figure 1 show clear time dependent differences, including the extrapolation differences between the breakthrough times $T_{L(A)}$ and $T_{L(B)}$. The value of $T_{L(B)}$ derived from the upper curve in Figure 1 is clearly lower than the value of $T_{L(A)}$ — which is characteristic of differences between analogously determined values of $T_{L(B)}$ and $T_{L(A)}$ in analogous comparisons of results for studies over wide ranges of initial hydrogen contents, n, in studies with $Pd_{81}Pt_{19}H_n$ [16,17] and $Pd_{77}Ag_{23}H_n$ [11] systems. It follows that such differences between breakthrough times will be reflected by important interferences in estimations of hydrogen diffusion coefficients D_H in membranes of thickness L, through appropriate

relationships of a generalised form [3,4,6-12,16-18].

$$D_H = \frac{L^2}{6T_L} \qquad (3)$$

Taken together with widespread acceptances [3-16] of allied dependencies of results on initial and developed hydrogen contents, these findings have encouraged conclusions, that permeation rates could be more realistically developed from qualitatively expressed relationships such as:

$$J_H(n) = f(D_H(n), \text{grad } n) - f(D(n), n_o, \text{grad } \varepsilon \text{ (Uphill)}) \qquad (4)$$

as broadly represented, qualitatively, by the lower curve in Figure 1, by initial concentration, n, and by Uphill developed strain gradients, ε [3,4,7,16,17] or

$$J_H(n) = f(D_H(n), \text{grad } n) - f(D(n) \text{ grad } \varepsilon \text{ (Uphill)}) + f(D(n), n_o, \text{grad } \varepsilon \text{ (mech.)}) \qquad (5)$$

as broadly represented by the upper curve in Figure 1.

Theoretical calculations of relative contributions of concentration and strain gradient components to diffusion flux $J_H(n)$ have been subjects of recent correlations with appropriate experimental data [19-23].

Consolidations and Extensions of Stress/Strain Gradient Related Hydrogen Permeation Studies

Additional experimental factors which modify or conceal underlying control through relations 4 and 5 have included complexities of membrane geometry and variations of surface catalytic activities [3,4] sometimes combined with important modifications of structural uniformity in courses of permeation [9,10].

In providing solutions of such problems further studies of palladium [24] and series of Pd-Ag alloy [25] membranes in the form of sheets and $Pd_{81}Pt_{19}$ membranes in the form of tubes [18,26,27] have continued to demonstrate their particular experimental material suitabilities in respect of high values of hydrogen diffusion coefficients in conjunction with sustained elasticities over wide ranges of hydrogen contents (n). Advantages of these features can in turn be valuably related to reliable knowledge of convertible possibilities between hydrogen gas pressure, p, and electrode potential, E, for appropriate uses in relation to p(E) - c(n) - T relationships over a wide range of temperature T — in conditions of high and well sustained surface catalytic activities such as can be provided by finely divided "black" surfaces of platinum, palladium or Pd-Pt co-depositions [28].

Experimental membranes of tubular forms have had important advantages in having been conveniently interchangeable between electrolytic and gas phase methods of hydrogen introductions and desorptions in precisely thermodynamic terms [3-8]. Nevertheless, very successful comprehensive series of measurements over ranges of Pd-Ag [6,25] and Pd-Ce [29] alloy compositions have recently been obtained by both galvanostatic and potentiostatic techniques with bielectrode membranes.

In addition to the majority of studies concerning immediately induced sequences of results, as in Figure 1, evidence of retained involvement of strain gradient contributions in steady state permeation conditions has been provided recently by observations of enhancements of permeation flux on interruption of flux input supply [30-32].

The increasing body of experimental observations and developing theoretical explanations of strain gradient permeation and involvement in hydrogen diffusion processes has led to expanded explanations in terms of Uphill operations of inconsistencies of directions of dependencies of hydrogen Diffusion Coefficiencies D_H on hydrogen contents n in relationships for the Pd-H System [33] and $Pd_{77}Ag_{23}H_n$ system [34].

References

1. Gorsky, W.S., Phys.Z.Sowjetunion **8** (1935), 457.
2. Cermák, J., Gardavská, A., Kufudakis, A. and Lejcek, P., Z.Physik.Chem.Neue Folge **43** (1985), 139.
3. Lewis, F.A., Tong, X.Q., Sakamoto, Y., Bucur, R.V. and Kandasamy, K., Thermochim.Acta **218** (1993), 57.
4. Lewis, F.A., Sakamoto, Y., Kandasamy, K. and Tong, X.Q., Defect Diff.Forum, **115-116** (1994), 39.
5. Lewis, F.A., Sakamoto, Y. and Tong, X.Q., Int.J.Hydrogen Energy, **20** (1995), 365.
6. Sakamoto, Y., Tanaka, H., Lewis, F.A., Tong, X.Q. and Kandasamy, K., Int.J.Hydrogen Energy, **21** (1996), 1325.
7. Lewis, F.A., McKee, S.G., Magennis, J.P. and Ssebuwufu, P.J.M, Nature, **556** (1983), 673.
8. Lewis, F.A., Baranowski, B. and Kandasamy, K., J.Less-Common Met., **134** (1987), L27.
9. Tong, X.Q., Kandasamy, K. and Lewis, F.A., Scr.Metall.Mater., **24** (1990), 1923.
10. Sakamoto, Y., Tong, X.Q. and Lewis, F.A., Scr.Metall.Mater., **25** (1991), 1629.
11. Tong, X.Q., McNicholl, R.-A., Kandasamy, K. and Lewis, F.A., Int.J.Hydrogen Energy, 17 (1992), 777.
12. Tong, X.Q. and Lewis, F.A., J.Less-Common Met., **169** (1991), 157.
13. Lewis, F.A. and Tong, X.Q., J.Less-Common Met., **179** (1992), L13.
14. Tong, X.Q., Bucur, R.V., Kandasamy, K. and Lewis, F.A., Z.Physik.Chem., 181 (1993), 225.
15. Lewis, F.A., Tong, X.Q. and Bucur, R.V., Platinum Metals Rev., **35** (1991), 138 and results to be published.
16. Kandasamy, K. Lewis, F.A., Magennis, J.P., McKee, S.G. and Tong, X.Q., Z.Physik.Chem., **171** (1991), 213.
17. Kandasamy, K., Tong, X.Q. and Lewis, F.A., J.Phys.Condens.Matter, **4** (1992), L439.
18. Dudek, D. and Baranowski, B., Polish J.Chem., **69** (1995), 1196.
19. Baranowski, B., J.Less-Common Met., **154** (1989), 455.
20. Simon, A.M. and Grzywna, Z.J., Acta Metall.Mater., **40** (1992), 3465.
21. Kandasamy, K., Int.J.Hydrogen Energy, **20** (1995), 453.
22. Simon, A.M., Int.J.Hydrogen Energy, **22** (1997), 27.
23. Kandasamy, K. and Lewis, F.A., Defect Diff.Forum (in press).
24. Sakamoto, Y., Tanaka, H., Lewis, F.A. and Tong, X.Q., Int.J.Hydrogen Energy, **17** (1992), 965; Z.physik.Che., **181** (1993) 219.
25. Sakamoto, Y., Tanaka, H., Sakamoto, F., Lewis, F.A. and Tong, X.Q., Int.J.Hydrogen Energy, **20** (1995), 35.
26. Baranowski, B. and Lewis, F.A., Ber.Bunsenges.Phys.Chem., **93** (1989), 1225.
27. Dudek, D. and Baranowski, B., Defect Diff.Forum, **129-130** (1996), 303.
28. Sakamoto, Y., Kurema, K. and Novotano, Y., J.Appl.Electrochem., **24** (1994), 38.
29. Tanaka, H., Sakamoto, Y., Lewis, F.A. and Tong, X.Q., Defect Diff.Forum, **141-142** (1997), 85.
30. Lewis, F.A., Tong, X.Q. and Kandasamy, K., Int.J.Hydrogen Energy, **18** (1993), 48.
31. Tong, X.Q. and Lewis, F.A., Int.J.Hydrogen Energy **20** (1995), 641.
32. Lewis, F.A., Bucur, R.V., Sakamoto, Y., Tong, X.Q. and Kandasamy, K., Hydrogen Energy Progress XI, Eds. T N Veziroglu, C J Winter, J P Baselt and G Kreysa, Int.Assn.Hydrogen Energy, Vol. 1 (1996), p.889.
33. Tong, X.Q., Sakamoto, Y., Lewis, F.A., Bucur R.V. and Kandasamy, K., Int.J.Hydrogen Energy, **22** (1997), 141.
34. Lewis, F.A., Tong, X.Q., Bucur, R.V. and Kandasamy, K., Defect Diff.Forum **148-149** (1997), 161.

INDEX